NASA/CP-1999-209101/PT2

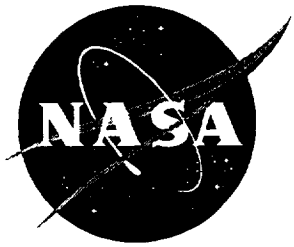

First International Symposium on Strain Gauge Balances

Edited by
John S. Tripp and Ping Tcheng
Langley Research Center, Hampton, Virginia

Proceedings of a symposium sponsored by the
National Aeronautics and Space
Administration, Washington, D.C.,
and held at Langley Research Center,
Hampton, Virginia
October 22–25, 1996

National Aeronautics and
Space Administration

Langley Research Center
Hampton, Virginia 23681-2199

March 1999

Acknowledgments

The following individuals assisted in preparation and execution of the symposium program: Thomas C. Moore, Alice T. Ferris, Risé W. Ramsey, Tammy L. Seward, Jennifer D. McCardell, Cristina L. Rector, Warren C. Higgs, Pamela J. Verniel, Mark W. Frye, Ray D. Rhew, Paul W. Roberts, Jerome T. Kegelman, and Robert A. Kilgore.

The undersigned editors wish to dedicate these proceedings to their colleague, Frank L. Wright, Boeing Commercial Airplane Group, who passed away in October 1998.

Ping Tcheng, General Chairman

John S. Tripp, Technical Chairman

Available from:

NASA Center for AeroSpace Information (CASI)
7121 Standard Drive
Hanover, MD 21076-1320
(301) 621-0390

National Technical Information Service (NTIS)
5285 Port Royal Road
Springfield, VA 22161-2171
(703) 605-6000

Executive Summary

The concept of an international strain gauge balance symposium was advocated in a technology assessment entitled "A White Paper on Internal Strain Gauge Balances." An internal document published by NASA Langley Research Center (LaRC) staff members in March 1995, this white paper was based on an international survey of internal strain gauge balances conducted under contract in 1994-1995 (ref. 1). The conclusions of the white paper were presented to a peer review panel on wind tunnel testing technology, composed of selected leaders from major commercial and government aeronautical facilities, held in July 1995 at LaRC. The panel strongly endorsed the proposed international strain gauge balance symposium, which was the first of its kind.

Based on the 1995 peer review endorsement, the first International Symposium on Strain Gauge Balances was sponsored under the auspices of the LaRC during October 22-25, 1996. Held at the LaRC Reid Conference Center, Hampton, Virginia, the Symposium provided an open international forum for presentation, discussion, and exchange of technical information among wind tunnel test technique specialists and strain gauge balance designers. The Symposium also served to initiate organized professional activities among the participating and relevant international technical communities. The program included a panel discussion (summarized in the Appendix), technical paper sessions, tours of local facilities, and vendor exhibits.

Over 130 delegates from 15 countries were in attendance, including Australia, Canada, China, Finland, France, Germany, India, Indonesia, Israel, the Netherlands, Russia, South Africa, Sweden, United Kingdom, and the United States. The program opened with a panel discussion, followed by technical paper sessions, and guided tours of the National Transonic Facility (NTF) wind tunnel, a local commercial balance fabrication facility, and the LaRC balance calibration laboratory. Vendor exhibits were also available.

The opening panel discussion addressed "Future Trends in Balance Development and Applications." The nine panel members included eminent balance users and designers representing eight organizations and five countries. Formal presentation of papers in technical sessions followed the panel discussion. Forty-six technical papers were presented in 11 technical sessions covering the following areas: calibration, automatic calibration, data reduction, facility reports, design, accuracy and uncertainty analysis, strain gauges, instrumentation, balance design, thermal effects, finite element analysis, applications, and special balances. A general overview of the past several years' activities of the AIAA/GTTC (Ground Testing Techniques Committee) Internal Balance Technology Working Group was presented. At the conclusion of the Symposium, a steering committee representing most of the nations and several US organizations attending the Symposium was established to initiate planning for a second international balance symposium, to be held in 1999 in the UK.

A Summary Report of the First International Symposium on Strain Gauge Balances, by John S. and Ping Tcheng, NASA LaRC, was presented at the 81st Fluid Dynamics Panel Symposium on Advanced Measurement Technology held in Seattle, Washington, USA, 22-25 September 1997. This paper is attached as an appendix to these symposium proceedings.

Also attached are a group photograph taken during the symposium, an index of authors, and a roster of names and addresses of the registered delegates to the symposium.

Contents

*Part 1 is presented under separate cover.

Session 5 AUTOMATIC CALIBRATION
Chair: Frank L. Wright, Boeing Commercial Airplane Group, USA

Session 6 APPLICATIONS
Chair: Robin D. Galway, National Research Council of Canada, CANADA

PART 2

Session 7 SPECIAL BALANCES II
Chair: Pieter Fuijkschot, National Aerospace Laboratory, The Netherlands

Session 8 BALANCE DESIGN
Chair: Maurice Bazin, ONERA, France

Session 9 INSTRUMENTATION, STRAIN GAUGES, AND THERMAL EFFECTS
Chair: Paul W. Roberts, NASA Langley Research Center, USA

Papers Accepted But Not Presented

Author Index

List of Attendees

International Symposium on Strain Gauge Balances
NASA Langley Research Center, October 22-25, 1996
Registered US Delegates

Name	Affiliation	Street Address	City	FAX, email
Adcock, Jerry B.	NASA LaRC	MS 267	Hampton, VA 23681	PH:757-864-5135
Arnold, Vern		624 Island View	Fillmore CA 93015	FAX:805-524-1407 PH:805-524-1407
Bader, Jon	NASA Ames	MS 227-1	Moffett Field, CA 94035	jbader@mail.arc.nasa.gov
Baker, Wink	Lockheed Martin Tactical Aircraft Systems	PO Box 748	Ft. Worth, TX 76101	wmbaker@lmtas.lmco.com PH:817-763-1987
Belew, H. W. (Bud)	Dynamic Engineering, Inc., Huntsville Div.	9172 Hwy 36	Lacey's Spring, AL 35754	FAX:205-883-8660 PH:205-883-9277
Booth, Dennis	Microcraft Technol	3050 Pacific Hwy	San Diego, CA 92101	dbooth@microcraft.com
Brewster, Rick	Sverdrop Tech.	MS 213-5, NASA Ames	Moffett Field, CA 94035	hrewster@crusher.arc.nasa.gov PH:415-604-1581
Broeren, Andy	University of Illinois	Dept. of Aero/Astro Engineering, 306 Talbot Lab, 104 S. Wright St.	Urbana, IL 61801	broeren@uiuc.edu FAX:217-244-0720 PH:217-244-3128
Burner, Alpheus W.	NASA LaRC	MS 236	Hampton, VA 23681	a.w.burner@larc.nasa.gov FAX:757-864-7607 PH:757-864-4635
Cahill, David M.	Sverdrup Technology Inc./AEDC Group	740 Fourth St.	Arnold AFB, TN 37389-6001	cahill@hap.arnold.af.mil FAX:615-454-7640 PH:615-454-6725
Clark, Edward L.	Sandia National Labs	3900 Pitt St., NE	Albuquerque, NM 87111	edlclark@aol.com PH:505-296-4541
Creekmore, Murrel	Lockheed Martin Aeronautical Systems	1055 Richardson Rd.	Smyrna, GA 30080	FAX:770-494-4790 PH:770-494-5619
Crooks, Richard S.	Microcraft San Diego	3050 Pacific Hwy	San Diego, CA 92101	RCrooks@microcraft.com FAX:619-683-8910 PH:619-683-8900 Ext 101
Davis, Tim	Modern Machine & Tool Co., Inc.	11844 Jefferson Avenue	Newport News, VA 23606	mmtool@aol.com
DeLoach, Richard	NASA LaRC	MS 236	Hampton, VA 23681	FAX:757-864-7607 PH:757-864-4657
Delcarpio, Danny	The Boeing Co.	P.O. Box 3707	Seattle, WA 98124-2207	danny.delcarpio@boeing.com FAX:206-655-1042 PH:206-655-2765
Ferris, Alice T.	NASA LaRC	MS 238	Hampton, VA 23681	a.t.ferris@larc.nasa.gov FAX:757-864-7607 PH:757-864-4702
Frisoli, Michele	National Technical Systems	Rye Canion Research, Dev., and Test Center, Building 202, 25100 Rye Canion Road, Bldg 202	Valencia, CA 91355	wndtnnl@aol.com FAX:805-257-3539 PH:805-259-8184
Garrell, Andrew F.	Calspan SRL Corporation	P. O. Box 400, 4455 Genesee Street	Buffalo, NY 14225	garrell@calspan.com FAX:716-631-4175 PH:716-631-6724
Gray, David L.	NASA LaRC	MS 236	Hampton, VA 23681	d.l.gray@alrc.nasa.gov FAX 757-864-7607
Hatten, Steven	Boeing Commercial Airplane Group	MS 1W-02, P.O. Box 3707	Seattle, WA 14225	steven.a.hatten@boeing.com FAX:206-655-0523 PH:206-655-0011
Heaman, John P.	NASA Marshall Space Flight Center	Experimental Facilities Branch, ED 34,	Huntsville, AL 35812	john.heaman@msfc.nasa.gov FAX:205-544-9358
Hemsch, Dr. Michael J.	Lockheed Martin	MS 267 NASA Langley	Hampton, VA 23681-0001	m.j.hemsch@larc.nasa.gov

Name	Affiliation	Street Address	City	FAX, email
Hertzler, Jim	Modern Machine & Tool Co., Inc.	11844 Jefferson Avenue	Newport News, VA 23606	j.a.hertzler@larc.nasa.gov FAX:757-873-8239 PH:757-873-8228
Higgs, Warren C.	NASA LaRC	MS 238	Hampton, VA 23681	w.c.higgs@larc.nasa.gov FAX:757-864-7607 PH:757-864-4706
Holmes, Harlan K.	Holmes Enterprises, Inc.	106 Normandy Lane	Newport News, VA 23606	FAX:757-930-2400 PH:757-930-2400
Hudgins, Mark	The Boeing Company	Mail Stop 1W-82, P.O. Box 3707	Seattle, WA 98124-2207	m.s.hudgins@boeing.com
Hultberg, Randy	Bihrle Applied Research	18 Research Drive	Hampton, VA 23666	FAX:757-766-9227 PH:757-766-2416
Jordan, Thomas L.	NASA LaRC	MS 237	Hampton, VA 23681	t.l.jordan@larc.nasa.gov FAX:757-864-7607
Kahng, Seun K.	NASA LaRC	MS 235	Hampton, VA 23681	s.k.kahng@larc.nasa.gov FAX:757-864-7607
Kammeyer, Mark E.	McDonnell Douglas	MC 5102-2272 P.O. Box 516	St Louis, MO 63166	
Kassaee, Ahmad	University of Maryland	Glenn L. Martin Wind Tunnel Bldg 081	College Park, MD 20742	kassaee@windvane.umd.edu FAX:301-314-9628 PH:301-405-6861
Kegelman, Dr. Jerome T.	NASA LaRC	MS 238	Hampton, VA 23681	j.t.kegelman@larc.nasa.gov FAX:757-864-7607
Kelly, Joel	Modern Machine & Tool Co., Inc.	11844 Jefferson Avenue	Newport News, VA 23606	mmtool@aol.com FAX:757-873-8239 PH:757-873-1212
Kilgore, Dr. Robert A.	CES - Hampton	P. O. Box 4006	Hampton, VA 23664-0006	RAKilgore@aol.com FAX:757-851-5212
Kilgore, W. Allen	Calspan Langley Operations	MS 267 NASA Langley	Hampton, VA 23681	w.a.kilgore@larc.nasa.gov
Kutney, John T., Sr	KCS - COS - Inc.	110 Wentworth Avenue	Cincinnati, OH 45215	FAX:513-821-3789 PH:513-821-3789
Lafferty, John F.	Naval Surface Warfare Center	10901 New Hamphire Ave.	Silver Spring, MD 20903	jlaffer@nswc.navy.mil PH:301-394-1750
Lindell, Michael C.	NASA LaRC	MS 431	Hampton, VA 23681	m.c.lindell@larc.nasa.gov
Lockwood, Chris	Calspan SRL Corporation	MS 207-2 NASA Ames	Moffett Field, CA 94035	clockwood@mail.arc.nasa.gov
Meadors, Brent G.	Modern Machine & Tool Co., Inc.	11844 Jefferson Avenue	Newport News, VA 23606	mmtool@aol.com FAX:757-873-8239 PH:757-873-1212
Mitchell, Dr. James	Microcraft, Inc.	207 Big Springs Ave, P.O. Box 370	Tullahoma, TN 37388	jmitchell@microcraft.com FAX:615-455-7060 PH:615-455-2617 Ext 213
Moore, Thomas C.	NASA Langley	MS 238	Hampton, VA 23681	t.c.moore@larc.nasa.gov FAX:757-864-7607 PH:757-864-4703
Muhlstein, Lado, Jr	NASA Ames	Mail Stop 227-4	Moffett Field, CA 94035-1000	lmuhlstein@mail.arc.nasa.gov
Ogden, Tony	NASA Ames			togden@mail.arc.nasa.gov
Paeschliman, Dan	Sandia			d.paesch@sandia.gov FAX:505-844-4523
Parker, Peter	Modern Machine & Tool Company Incorporated	11844 Jefferson Avenue	Newport News, VA 23606	peter.a.parker@larc.nasa.gov
Patel, Naresh R.	Modern Machine & Tool Company Incorporated	11844 Jefferson Avenue	Newport News, VA 23606	mmtool@aol.com FAX:757-873-8239 PH:757-873-1212
Paulk, Bob	Sverdrup Technology, Inc	760 Fourth Street	Arnold AFB, TN 37389-6001	FAX:615-454-7640 PH:615-454-3863
Pochel, Cathy	NASA Ames	Mail Stop 227-5	Moffett Field, CA 94035-1000	cpochel@mail.arc.nasa.gov
Price, Barry L.	NASA LaRC	MS 238	Hampton, VA 23681	b.l.price@larc.nasa.gov FAX:757-864-7607

Name	Affiliation	Street Address	City	FAX, email
Putnam, Lawrence E.	NASA LaRC		Hampton, VA 23681	PH:757-864-5116
Rhew, Ray D.	NASA LaRC	MS 238	Hampton, VA 23681	r.d.rhew@larc.nasa.gov FAX:757-864-7607 PH:757-864-4705
Richardson, Stan	Sverdrop/AEDC	760 Fourth Street	Arnold AFB, TN 37389-6200	RichardsonSG@hap.arnold.af.mil FAX:615-454-5432 PH:615-454-7283
Rivera, Jose A. Jr.	NASA LaRC	MS 340	Hampton, VA 23681	PH:757-864-1270
Roberts, Paul W.	NASA LaRC	MS 238	Hampton, VA 23681	p.w.roberts@larc.nasa.gov FAX:757-864-7607 PH:757-864-4704
Rock, Thomas, Lt.	NAIC/TANW USAF	2180 Watson Way	WPAFB, OH 45433	PH:513-257-8799
Rumble, Carl V.	Application Technology, Inc.	P.O. Box 9303	Hampton, VA 23670	FAX:757-722-3510 PH:757-722-6857
Sewall, J. W.	NASA LaRC	MS 373	Hampton, VA 23681	PH:757-864-4735
Shelton, P. Duane	Boeing Defense & Space Group	P.O.Box 3999 MS 86-11	Seattle, WA 98124-2499	shedp900@ccamil.ca.boeing.com
Singh, Dr. Jag J.	NASA LaRC	MS 235	Hampton, VA 23681	j.j.singh@larc.nasa.gov FAX:757-864-7607
Smith, Brooke C.	Eidetics Corporation	3425 Lomita Blvd	Torrance, CA 90505-5010	brooke@eideticscorp.com FAX:310-326-9358 PH:310-326-8228
Springfield, Robert D.	Northrop Grumman Corp.	8900 E. Washington Blvd., 9A21/GS	Pico Rivera, CA 90660-3737	FAX:310-948-8146 PH:310-942-5612
Steinle, Frank	AEDC			FRANK.STEINLE@ccmail.arnold.af.mil FAX:615-454-6317
Stewart, James R. (Rod)	Sverdrop Technology	1103 Ave B	Arnold AFB, TN 37389-1300	FAX:615-454-7741 PH:615-454-7221
Stokes, Thomas R.	Modern Machine & Tool Co., Inc.	11844 Jefferson Avenue	Newport News, VA 23606	mmtool@aol.com
Stryker, Doug	Calspan SRL Corp.	Transonic Wind Tunnel, 4455 Genesee Street	Buffalo, NY 14225	stryker@calspan.com FAX:716-631-4175 PH:716-631-6882
Suarez, C. J. ABSENT. Presented by Brooke Smith	Eidetics Corporation	3415 Lomita Blvd.	Torrance, CA 90505	eidetics@cerf.net FAX:310-326-9358
Tcheng, Dr. Ping	NASA LaRC	MS 238	Hampton, VA 23681	p.tcheng@larc.nasa.gov FAX:757-864-7607 PH:757-864-4717
Tinapple, Jon A.	U S A F , WL/FIMO	Bldg. 24C, 2145 Fifth Street, Suite 1	WPAFB, OH 45433-7005	tinappja@wl.wpafb.af.mil FAX:513-476-7652 PH:513-255-6032
Tinsley, Charles R. (Rick)	Sverdrop Technology	1103 Ave B	Arnold AFB, TN 37389-1300	FAX:615-454-7741 PH:615-454-6743
Tripp, Dr. John S.	NASA LaRC	MS 238	Hampton, VA 23681	j.s.tripp@larc.nasa.gov FAX:757-864-7607 PH:757-864-4711
Ulman, Richard J.	The Boeing Company	Mail Stop 1W-02, P.O. Box 3707	Seattle, WA 98124-2207	RICHARD.J.ULMAN@boeing.com FAX:206-655-1042 PH:206-655-4219
Van Aken, Johannes M.	Sterling Software	M/S T12-B, NASA Ames Research Center	Moffett Field, CA 94035	jvanaken@mail.arc.nasa.gov FAX:415-604-1089 PH:415-604-6668

Name	Affiliation	Street Address	City	FAX, email
Voss, Douglas J.	The Boeing Company	Mail Stop 1W-78, P.O. Box 3707	Seattle, WA 98124-2207	DOUGLAS.J.VOSS@boeing.com FAX:206-655-1042 PH:206-655-6270
Walker, Jimmy	Lockheed-Martin Aeronautical Systems	1055 Richardson Road	Smyrna, GA 30080	FAX:770-494-4790 PH:770-494-4218
Wilcox, Floyd J., Jr	NASA LaRC	MS 413	Hampton, VA 23681	PH:757-864-5593
Wilcox, Randall	Calspan Ames Operations	M/S 207-2, NASA Ames Research Center	Moffett Field, CA 94035-1000	rwilcox@mail.arc.nasa.gov FAX:415-968-8035 PH:415-604-6335
Wright, Frank L.	Boeing Commercial Airplane Group	P.O.Box 3707 MS 1W-82	Seattle, WA 98124-2207	FAX:206-655-1042 PH:206-655-4213
Yu, Dr. James C.	NASA LaRC	MS 235	Hampton, VA 23681	j.c.yu@larc.nasa.gov FAX:757-864-7607 PH:757-864-4755

International Symposium on Strain Gauge Balances
NASA Langley Research Center, October 22-25, 1996
Registered Foreign Delegates

Name	Affiliation	Street Address	City	Country	FAX/Phone
Alons, Henk-Jan	National Aerospace Laboratory NLR	Voorsterweg 31 8316 PR Marknene	1006 BM Amsterdam	THE NETHERLANDS	alonshj@nlr.nl FAX:31-527-248210 PH:31-527-248611
Baumann, Peter, H.	DLR	SM-SK, DLR Bunsenstr. 10,	D-37075 Goettinggen	GERMANY	Peter.Baumann@dlr.de FAX:49-551-709-2830 PH:49-551-709-2474/73
Bazin, Maurice	ONERA	B.P. 72,29 Avenue Division Leclere	F-92320 Chatillon	FRANCE	FAX:33-1-46-734144
Bock, Dr. Karl-Wilhelm	DLR	Abteilung Windkanaele Bunsenstr 10	D-37073 Goettingen	GERMANY	bock@gemini.wk.go.dlr.de
Bogdanov, Vasily V.	The Central AeroHydrodynamics Institute (TsAGI)	1 Zhukovsky Str.	Zhukovsky 140 160, Moscow Region	RUSSIA	buran@mx.iki.rssi.ru FAX:7-095-556-4335
Burkush, Shaya	Israel Aircraft Industries	Engineering Division	Ben Gurion Int'l Airport, Lod 70100, Dpt. 4455	ISRAEL	sburkush@engdiv.iai.co.il FAX:9723-935-4456 PH:9723-935-8570
Cheng, Yinghui	China Society for Aerodynamics, CARDC	P. O. Box 211	Mianyang, Sichuan Province	CHINA	FAX:0816-236-2490
Coulech, Vladimir	The Central AeroHydrodynamics Institute (TsAGI)	1 Zhukovsky Str.	Zhukovsky 140 160, Moscow Region	RUSSIA	Same as S. Fonov
Coulton, David G.	Aircraft Research Association, Ltd.	Manton Lane	Bedford MK41 7PF	U.K.	dgcoulton@ie.org.uk FAX:44-1234-328584 PH:44-1234-350681
Drouin, Gedeon	Defence Research Establishment Valcartier	2459 Pie-XI Blvd.	North Val-Belair QC G3J 1X5	CANADA	Gedeon.Drouin@drev.dnd.ca FAX:418-844-4502 PH:418-844-4425
Ewald, Prof. Bernd	Technical University of Darmstadt	Petersenstraße 30	D-64287 Darmstadt	GERMANY	ewald@HRZ2.HRZ.TH-Darmstadt.DE FAX:49-6151-16-2201 PH:49-6151-16-2490
Fagerstrom, Bo R.	Helsinki Univ. of Technology	Laboratory of Aerodynamics	Sahkomiehentie 4, FIN-02150 Espoo	FINLAND	Bo.Fagerstrom@hut.fi FAX:358-9-451-3418
Fariduzzaman	PUSIPIPTEK	Aero-Gas Dynamics and Vibration Laboratory (UPT-LAGG-BPPT), Serpong	Tangerang-15310	INDONESIA	itst@idola.net.id FAX:062-021-7560901 PH:062-021-7560902
Fonov, Serguei D.	The Central AeroHydrodynamics Institute (TsAGI)	1 Zhukovsky Str.	Zhukovsky 140 160, Moscow Region	RUSSIA	fonov@astris.msk.ru FAX:7-095-911-0019
Fuykschot, Pieter Herman	National Aerospace Laboratory NLR	P.O. Box 90502	1006 BM Amsterdam	THE NETHERLANDS	mahe@nlr.nl FAX:31-20-511-3210
Galway, Robert D. (Robin)	National Research Council of Canada	Institute for Aerospace Research, Aerodynamics Laboratory (Uplands)	Ottawa, Ontario K1A 0R6	CANADA	robin.galway@nrc.ca FAX:613-998-1281 PH:613-998-3410
Geldman, Chaim	Balance Technologies LTD.	MADID-DA, 46 Ben-Eliezer Street	Ramat-Gan 52290	ISRAEL	FAX:972-3-6772146
Gorbushin, Anton R.	Central AeroHydrodynamics Institute (TsAGI)	1 Zhukovsky Str.	Zhukovsky 140160, Moscow Region	RUSSIA	FAX:7-095-556-4329
Graewe, Eberhard	Daimler-Benz Aerospace	Airbus GmbH, Dep EFG	28283 Bremen	GERMANY	FAX:421-538-4999 PH:49-421-538-2215

Name	Affiliation	Street Address	City	Country	FAX/Phone
Gross, Uwe	Daimler Benz Aerospace	British Aerospace (Military Aircraft) Ltd., P.B. 801160	81663 München	GERMANY	
Gu, Xingruo	China Society for Aerodynamics, CARDC	P. O. Box 211	Mianyang, Sichuan Province	CHINA	FAX:0816-236-2490
Guo, Kaike	Beijing Institute of Aerodynamics	P. O. Box 7215	Beijing	CHINA	FAX:086-010-68374758
He, Dexin	China Society for Aerodynamics, CARDC	P. O. Box 211	Mianyang, Sichuan Province	CHINA	FAX:0816-236-2490
Hechler, Burkhard	Technical University of Darmstadt	Flughafenstrasse 19	D-64347 Griesheim	GERMANY	FAX:49- 6151-166-246 PH:49- 6151-166-210
Hufnagel, Klaus	Technical University of Darmstadt	Flughafenstrasse 19	D-64347 Griesheim	GERMANY	FAX:49-6151-16-2201 PH:49-6151-16-6200
Jermey, Chris	Aeronautical and Maritime Research Laboratory	DSTO, Air Operations Division, P.O. Box 1500	Salisbury, S. A. 5108	SOUTH AFRICA	
Johnson, Gustav Ingmar	FFA, The Aeronautical Research Institute of Sweden	Experimental Aerodynamics, P.O. Box 11021	S-161 11 Bromma	SWEDEN	FAX:46-8-253480
Joosen, Cor J. J.	Duits-Nederlandse Windtunnel (DNW)	Department of Instrumentation, P.O. Box 175	8300 AD Emmeloord	THE NETHERLANDS	cjoosen@nlr.nl FAX:31-527-24-8582
Kapoor, Kul Bhushan	National Research Council of Canada	Institute for Aerospace Research, M-10, Montreal Road	Ottawa, Ontario K1A 0R6	CANADA	FAX:613-592-7677 PH:613-990-7209
Kemppainen, Pasi	Helsinki Univ. of Technology	Laboratory of Aerodynamics	Sahkomiehentie 4, FIN-02150 Espoo	FINLAND	pasi.kemppainen@hut.fi PH:358-9-451-3429 FAX:358-9-451-3418
Kharitonov, Anatolii M.	ITAM, Russian Academy of Sciences	4/1 Instituteskaya Str.	Novosibirsk 630090	RUSSIA	khar@itam.nsc.ru
Kuzin, Alexander	Moscow Aviation Technological Institute	Petrovka 27	103737 Moscow	RUSSIA	kouzine@glas.apc.org
Lagutin, Vyacheslav I.	TSNIIMASH	Pionerskaia st. 4	Kaliningrad city, Moscow Region 141 070	RUSSIA	res@tsexp.msk.su FAX:7-095-513-4359
Lapygin, Vladimir I.	TSNIIMASH	Pionerskaia st. 4	Kaliningrad city, Moscow Region 141 070	RUSSIA	res@tsexp.msk.su
Law, Ron D.	Defence Research Agency - Bedford	High Speed & Weapon Aero. Dept., Bldg 17, Tunnel Site, DRA-Bedford	Bedford, MK41 6 AE	ENGLAND	FAX:44-1234-225-848 PH:44-1234-22-5950
Leslie G. Green	British Aerospace (Military Aircraft) Ltd.	5.5m L.S.W.T. (W175), Warton Aerodrome	Preston, Lancashire PR4 1AX	ENGLAND	FAX:44-1772-855501 PH:44-1772-852802
Levin, Dr. Daniel	Technion Israel Institute of Technology	Department of Aerospace Engineering, Technion City	Haifa 32 000	ISRAEL	aerdldl@aerodyne.technion.ac.il
Levkovitch, Michael	Israel Aircraft Industries	Engineering Division, Dept. 4451	Ben Gurion Int'l Airport, Lod 70100, Dpt. 4451	ISRAEL	mlevko@engdiv.iai.co.il FAX:972-2-9354456
Liao, Li Xin	Beijing Institute of Aerodynamics	P. O. Box 7215-14	Beijing	CHINA	FAX:086-010-68374758
Liu, Yufu	China Society for Aerodynamics, CARDC	P. O. Box 211	Mianyang, Sichuan Province	CHINA	FAX:0816-236-2490
Matheson, Neil	Aeronautical & Maritime Research Laboratory	Air Operations Divsion, GPO BOX 4331	Melbourne, Victoria 3001	AUSTRALIA	neil.matheson@dsto.defence.gov.au

Name	Affiliation	Street Address	City	Country	FAX/Phone
Murthy, H. Sundara	National Aerospace Laboratories	Experimental Aerodynamics Division, P.B. No. 1779	Bangalore 560 017	INDIA	FAX:91-80-527-3942 PH:91-80-526-4024
Panchenko, Ivan N.	The Central AeroHydrodynamics Institute (TsAGI)	1 Zhukovsky Str.	Zhukovsky 140 160, Moscow Region	RUSSIA	buran@mx.iki.rssi.ru FAX:7:095:556:4337
Pretorius, Ockert	CSIR Aerotek	PO Box 395	Pretoria, 0001	SOUTH AFRICA	opretori@csir.co.za FAX:27-12-349-1156 PH:27-12-841-4895
Quade, Matthias	Technical University of Darmstadt	Flughafenstrasse 19	D-64347 Griesheim	GERMANY	matthias@hrz2.hrz.th-darmstadt.de FAX:49-6151-16-6246 PH:49-6151-16-6208
Rajendra, G. CANCELLED	National Aerospace Laboratories	NTAF, Experimental Aerodynamics Division, P.B. No. 1779	Bangalore 560 017	INDIA	FAX:91-80-527-3942
Ramaswamy, Mathagondapally Aswathaiengar	Indian Institute of Science	Department of Aerospace Engineering	Bangalore 560 012	INDIA	maram@aero.iisc.ernet.in
Rao, Dr. Satheesh D.	Aerobalance Associate	96, 3rd Main, KEB Layout	Bangalore - 560 076	INDIA	FAX:91-80-6684937
Rebstock, Ruediger	DLR	Wind Tunnel Division, Kryo-Kanal Koln, Linder Hoehe	D-51147 Koeln	GERMANY	FAX:2203-695-961
Rosen, John T. N.	AKTIEBOLAGET ROLLAB	Box 7073	Järvstigen 5, S-171 07 Solna	SWEDEN	FAX:46-885-3632 PH:46-885-0315
Stock, J. R.	DRA Farnborough	5m Wind Tunnel, Building X80	Farnborough, Hampshire GU14 6TD	ENGLAND	FAX:01252-395275 PH:01252-395369
Vasudevan, Balasubramanian	Indian Institute of Science	Department of Aerospace	Bangalore 560 012	INDIA	vasu@aero.iisc.ernet.in
Wang, Chao-an	CAE SARI	P.O.Box 701	Shenyang 110034	CHINA	FAX:024-6520827
Yin, Liming	Changsha Institute of Techology	Automatic Control Department of CIT, Deya Road	Changsha, 410073, Hunan	CHINA	FAX:086-0731-451-8307
Zhai, Junnai	Technical University of Darmstadt	Petersenstraße 30	D-664287 Darmstadt	GERMANY	FAX:49-61-51-16-2201
Zhang, Yingpei	China Society for Aerodynamics, CARDC	P. O. Box 211	Mianyang, Sichuan Province	CHINA	FAX:0816-2362490

A WATER-COOLED SIX-COMPONENT INTERNAL BALANCE

Liao, Li Xin *and* Tao, Yu
Beijing Institute of Aerodynamics

SUMMARY

The design, calibration and use of a water-cooled six-component internal balance are described in detail, and some improvement had been gotten on the computation and heat protection methods of balances. The calibration and testing results indicate that the design of this balance is successful.

INTRODUCTION

Strain gage balances have been used widely in aerodynamic testing of various wind tunnels. The working environments of subsonic, transonic and supersonic wind tunnels are suitable for them because the flow temperature is regular. But in hypersonic wind tunnels, the flow temperature is higher than the standard case, then a series of problems may arise, such as the temperature effects of strain gage, thermocouple effects between strain gage and electrical leads, thermal strain effects of the structure, etc., all of these interfere the output signals of balances. When the environmental temperature is excessively high, the strain gages can not work normally, or be broken. In order to solve the heat protection problems, some exploratory works had been done (ref.[1,4]). In the early stage, the balance was put outside of the testing section to avoid the high-temperature environment. But the structure of this kind of balances was very complex; its performance was not satisfied. Later, various heat protection schemes of internal balances were tested, such as temperature compensation, heat protection coating, vacuum package, balance rapid injection, water cooling, etc., in which the effect of water cooling method was the best. In this paper, a water-cooled six-component balance will be introduced.

SYMBOLS

X	axial force	N
Y	normal force	N
Z	side force	N
M_x	rolling moment	$N-m$
M_y	yawing moment	$N-m$

M_z	pitching moment	$N-m$
M	Mach number	
P_0	stagnation pressure	MPa
T_0	stagnation temperature	$^{\circ}C$
α	angle of attack	degree
β	yawing angle	degree
γ	rolling angle	degree
E	modulus of elasticity	N/mm^2
β	a nondimensional function of section of beam	
G	modulus of elasticity in torsion	N/mm^2
r	rolling angle	degree
h, h_1, h_2, h_3	thickness of beam	mm
b, b_1, b_2, b_3	width of beam	mm
L	distance between median and front (rear) beam	mm
l, l_1, l_2	length of beam	mm
n	number of main beam	
n_1	number of auxiliary beam	
ρ	radius of curvature	mm

BALANCE

1. The design loading

$X: \pm 1000N$, $Y: \pm 1500N$, $Z: \pm 400N$

$M_x: \pm 8N-m$, $M_y: \pm 12N-m$, $M_z: \pm 60N-m$

2. The structure (Fig.1)

The balance has the typical compound structure, which includes front, median and rear sections. The structures of the front and rear section are the same kind of beams, which are used for measuring five components, Y, Z, M_x, M_y and M_z. The median section has been built by multi-parallel beams, which are arranged at forward, median and aft positions of the median section respectively; these beams are perpendicular to the beams of the front and rear sections, as shown in Fig.2. The median beams, used for measuring axial force (X), are called main beams, and other beams called auxiliary ones are used for supporting main beams. There are two main beams and eight auxiliary beams which are arranged symmetrically to the main beams.

The diameter of balance is 28mm, the length is 120mm, in which the length of forward and aft cones are not included.

3. The measuring principle and electrical circuits (Fig.2-3)

The measurement of every component is achieved by the correspondent element and its strain gage bridge. For a certain measuring element, it should be sensitive only to the specific one, and insensitive to the other five ones, although six components (three forces and three moments) act on it simultaneously. But the nonspecified signals can not be avoided. By arranging the bridges elaborately, the main part of the nonspecified signals can be erased, the rest part is called "interference" and can be processed during the calibration. Generally, the interference of the balances with enough rigidity is much smaller than the main signal and its linear character is perfect. The electrical circuits are shown in Fig.3

4. The computation of elements strain (Fig.4)

The calculations of balance measuring elements are as following (Fig.2-4):

(1) The strain of axial force element:

$$\varepsilon_x = \frac{30Xl}{Enbh^2} \frac{1}{1+\frac{n_1 b_1 h_1 l^3}{nbh^3 l_1^3}}$$

(2) The strain of normal force element:

$$\varepsilon_y = \frac{120Y\ LH_y}{E(2h_3^3 b_3 + h_2^3 b_2)}$$

(3) The strain of side force element:

$$\varepsilon_z = \frac{120Z\ L\ H_z}{E(2b_3^3 h_3 + 24\rho_3^2 b_3 h_3 + b_2^3 h_2)}$$

(4) The strain of rolling moment element:

$$\varepsilon_{M_x} = \frac{3h_3 M_x \times 10^3}{2l_2^2\left[\frac{G}{\rho_3 l_2}(\beta_3 h_3 b_3^3 + \beta_2 \frac{h_2}{2} b_2^3) + \frac{E}{l_2^3}(\rho_2 b_2 h_2^3 + \frac{\rho_2^2}{\rho_3}\frac{h_2}{2} b_2^3)\right]}$$

(5) The strain of yawing moment element:

$$\varepsilon_{M_y} = \frac{12M_y H_z \times 10^3}{E(2b_3^3 h_3 + 24\rho_3^2 b_3 h_3 + b_2^3 h_2)}$$

(6) The strain of pitching moment element:

$$\varepsilon_{M_z} = \frac{12M_z H_y \times 10^3}{E(2b_3h_3^3 + b_2h_2^3)}$$

5. The structure analysis (Fig.5)

The median section is the most fragile one in the three-section structure. In order to get clear signal of the axial force, the main beams must supply enough deformation when the axial force acts on the balance; at the same time, adequate rigidity must be assured. These two conditions are contradictory requirements. To solve this problem, the original cross section which is changed from circular section to semilunar section is not used (Fig.5), while uses T-shape cross section which can stiffen the structure and produce satisfied deformation. (ref.[2])

The computation method is improved, instead the original method, the optimization method is used for determining the size of the beams. For example, the computational formula for the axial force element is as following:

$$\varepsilon_x = \frac{30Xl}{Enbh^2} \frac{1}{1+\dfrac{n_1b_1h_1l^3}{nbh^3l_1^3}} \tag{1}$$

Where l, b and h are the parameters of the structure size of the element. Based on the size of strain gage and the configuration requirement of the balance, two of them may be given, then another one could be determined. In general, the parameter h, which has obvious influence on rigidity, is chosen as the parameter to be determined.

The Eq.(1) can be written as

$$\frac{n_1b_1l^3}{b\,l_1^3}\,h_1^3 = \frac{30\,Xl}{E\,b\,\varepsilon_x}\,h - nh^3 \tag{2}$$

Which represent the iso-strain curve of h_1's depending on h, as shown in Fig.6.

It can be seen that the F point is the optimum value for h_1 and h required.

Suppose

$$f(h) = \frac{30\,Xl}{E\,b\,\varepsilon_x}\,h - nh^3$$

$$\frac{df(h)}{dh} = 0$$

So

$$\frac{30\,Xl}{E\,b\,\varepsilon_x - 3\,n\,h^2} = 0$$

$$h = h_F = \sqrt{\frac{30\,Xl}{E\,n\,b\,\varepsilon_x}} \tag{3}$$

Put Eq.(3) into Eq.(2), we have

$$h_{1F} = h_F\,\frac{l_1}{l}\,(\frac{2nb}{n_1 b_1})^{1/3} \tag{4}$$

HEAT PROTECTION

Using water-cooling method to solve the heat protection problem, there are two main manners to arrange the water-cooling package's position. The first is placing the water cooling package as shown in Fig.7; in this case, the water-cooling package is a part of the model. It is difficult to avoid its interference with the force transfer, because the water supply tube will absorb some parts of forces and some additional forces will be induced by unsteady water flow, it is impossible to eliminate all of these interference during calibration.

Another method is adopted in the design of this balance, which is shown in Fig.8. The water-cooling package is set on the sting of the balance and it is a part of that. This method overcomes those above shortages, because the water-cooling package does not take part in the force transfer; besides that, the water-cooling package strengthens the sting of the balance. This method makes it easy to manufacture the water-cooling package.

It can be seen that there is a gap between the package and the balance (as shown in Fig.8), this gap must be large enough, otherwise the balance will touch the package, at the same time, it should be as small as possible in order to decrease the diameter of the package.

There is another gap located between the model bottom and the sting of the balance. This gap should be large enough to guarantee that the model does not touch the sting, while it should be as small as possible to lessen the quantity of high temperature flow which will enter the cavity of the model through this gap. In order to suit

different loading condition, several rings which can satisfy these two requirements had been prepared for this balance (ref.[3]).

A interim cage is assembled between the model and the water-cooling package. The contact area between the interim cage and the model is very small; the cavity between them is full of stagnant air whose heat conductivity rate is very low; the attachment of the balance and the interim cage is protected by a plastic sleeve reinforced with glass fiber, so the heat flux transferred to the balance is limited to minimum.

The electrical leads are protected well because the sting is cooled by the water-cooling package.

The water-cooling package has a two-layer structure which consists of inner and outer sleeves. The double-line spiral grooves are cut on inner sleeve, used as water passage. The outer sleeve is a circle one and it is assembled tightly on inner sleeve to ensure the separation between water in and out. The small amount of leakage between water passages is allowed and it is also beneficial to cool those places without grooves.

The structure is very simple and practical. The surface covered by swirl water flow is large, the cooling effect is uniform, and hydrodynamic losses are small.

CALIBRATION OF THE BALANCE

The calibration of the balance is performed on a balance calibration rig with ground-axes coordinate system; it has the loading capacity of positive or negative load. The deviation of loading coordinate system to the balance is not corrected, which will cause a system error, but in our case, this error is much small due to the adequate rigidity of the balance.

1. The balance formula

The balance formula is gotten from the component loading, also includes the interaction loading of 1st and 2nd terms.

During the calibration, the output Δn (voltage) of each component depends on the component load itself, and the interaction output from other five components, for example, the output of Y component can be written as (ref.[5]).

$$\Delta n_N = f\ (Y\ ,\ M_z\ ,\ X\ ,\ M_x\ ,\ Z\ ,\ M_y)$$

It is a multivariable function, it can be written as

$$\Delta n_y = \frac{\partial f}{\partial y} Y + \frac{\partial f}{\partial M_z} M_z + \cdots + \frac{\partial f}{\partial M_y} M_y +$$

$$\frac{1}{2}\left(\frac{\partial^2 f}{\partial Y^2} Y^2 + \frac{\partial^2 f}{\partial M_z^2} M_z^2 + \cdots + \frac{\partial^2 f}{\partial M_y^2} M_y^2\right.$$

$$\left. + \frac{\partial^2 f}{\partial Y \partial M_z} Y M_z + \cdots + \frac{\partial^2 f}{\partial Z \partial M_y} Z M_y\right) \qquad (5)$$

where, all values of the derivatives are determined for a given balance, after transformation, it can be gotten:

$$Y = K_y \Delta n_y + K_y^{M_z} M_z + \cdots + K_y^{M_y} M_y + K_y^{y^2} y^2 + \cdots$$

$$+ K_y^{M_y^2} M_y^2 + K_y^{Y M_z} Y M_z + \cdots K_y^{Z M_y} Z M_y \qquad (6)$$

Eq.(6) is a balance formula up to 2nd terms, and it includes 27 terms totally. The coefficients K are determined by the balance calibration, which are listed in Table 1.

2. The accuracy of the balance

Y: 0.10%, X: 0.41%, Z: 0.28%

M_x: 0.28%, M_y: 0.43%, M_z: 0.07%

3. The elastic deflection of the balance

$\alpha = 0.0003451\ N + 0.008708\ M_z \quad (^\circ)$

$\beta = -0.0004468\ Z + 0.01080\ M_y \quad (^\circ)$

$\gamma = 0.02075\ M_x \quad (^\circ)$

On the condition of full range, α, β, γ are 0, 9', 0.04', 0.17' respectively. The results of calibration show that the balance has a satisfied accuracy and rigidity.

WIND TUNNEL TESTING OF THE BALANCE

The cone model was tested at Mach number 5 and 8 to check the heat protection effect and repeatability accuracy of the balance. The testing conditions are:

$M = 5,\ T_0 = 100^{\circ}C,\ P_0 = 2MP_0$

$M = 8,\ T_0 = 500^{\circ}C,\ P_0 = 4MP_0$

The testing data in table 2 to table 4 indicate that the repeatability accuracy is perfect. The results show that there is no obvious temperature effect, as shown in table 5 to table 6. Three sets of data recorded at time 0, 20 and 70 seconds respectively are essentially same, the difference among them are in the error band of measured data. The temperature differences between in and out water are within $3^{\circ}C$ (for M=8 case). These show good heat protection effect.

CONCLUSIONS

1. Using improved cross section of the beams and the optimization calculation method, the rigidity of the balance is enlarged, and its performance is improved. It also provides the condition to decrease the gap between the model bottom and the sting.

2. The testing at M = 5 and 8 were done. The heat protection effect of the water-cooling package is very obvious.

3. Although the water-cooling package arranged on the sting can strengthen the sting, but it also increases the diameter of sting and the interference to base flow of model. These unfavorable effects are not serious problems relating to heat protection problems, the interference on base drag can be processed during experimental data processing.

4. In order to know the detail condition of heat protection system, it is necessary to measure the surface temperature during the wind tunnel testing. This will be done in the near future.

REFERENCES

[1] Lixin, Liao: The thermal protection problems of strain gage balance for hypersonic wind tunnel. Report of the 1st China National Conference on Wind Tunnel Balances. July 1977.

[2] A. F. Donouan, F. E. Goddard: High Speed Problems of Aircraft and Experimental Methods, P.729-732

[3] Alan Pope, K. L. Goin: High Speed Wind Tunnel Testing, John Wiley and Son, Inc 1965, Chapter 7 and 11

[4] R. J. Volluz: Handbook of Supersonic Aerodynamics, Section 20, Wind Tunnel Instrumentation and Operation, 1961, P.135

[5] Caoan, Wang and Congxin, Wang: Wind Tunnel Strain gage Balance Manual. Report, 1980.

Table 1. The main and interference coefficients of balance K_i

	Y	M_z	M_x	X	Z	M_y
Y	+.1947E+03	-.8558E-04	+.3351E-04	+.8508E-01	-.8176E-02	-.1305E-03
M_z	+.3121E+00	+.1007E+02	-.3064E-02	+.2958E+00	-.1309E-01	+.9269E-02
M_x	-.7578E+00	-.4311E-01	+.4777E+01	-.4296E+00	+.5672E+00	+.6983E-01
X	+.1219E-02	+.3201E-04	+.1665E-03	+.1780E+03	-.1626E-03	+.5179E-04
Z	+.3576E-02	+.3409E-03	-.3502E-02	-.2960E-01	-.1241E+03	+.6032E-03
M_y	+.3392E+00	-.2091E-01	-.1189E+00	+.0000E+00	-.7078E+00	+.8449E+01
Y^2	+.0000E+00	+.7760E-07	-.1865E-07	+.0000E+00	+.0000E+00	+.0000E+00
M_z^2	+.0000E+00	+.0000E+00	+.0000E+00	-.1933E-03	+.0000E+00	+.0000E+00
M_x^2	+.0000E+00	+.0000E+00	+.0000E+00	+.0000E+00	+.0000E+00	-.1442E-03
X^2	+.0000E+00	+.0000E+00	+.0000E+00	+.0000E+00	-.1836E-06	-.1206E-07
Z^2	+.5234E-05	+.0000E+00	+.0000E+00	+.1489E-04	+.0000E+00	+.0000E+00
M_y^2	+.0000E+00	+.0000E+00	+.0000E+00	+.0000E+00	+.0000E+00	+.0000E+00
YM_z	+.0000E+00	+.6393E-06	+.1988E-06	+.7256E-04	+.0000E+00	+.1176E-05
YM_x	+.0000E+00	+.0000E+00	+.5583E-05	+.0000E+00	+.2013E-03	+.7648E-05
YX	-.7133E-05	-.1357E-06	-.1823E-07	+.2246E-05	-.2009E-06	-.2242E-07
YZ	+.0000E+00	+.5433E-07	+.4937E-07	+.0000E+00	-.6046E-06	6271E-07
YM_y	+.0000E+00	+.0000E+00	-.6198E-05	+.0000E+00	+.0000E+00	-.1714E-05
M_zM_x	+.0000E+00	+.0000E+00	-.1729E-04	+.0000E+00	-.1404E-02	-.1410E-03
M_zX	-.8666E-04	+.3708E-05	+.0000E+00	+.0000E+00	-.6762E-05	+.2747E-06
M_zZ	+.0000E+00	-.1855E-05	-.8615E-06	+.0000E+00	+.0000E+00	-.1354E-05
M_zM_y	+.0000E+00	+.0000E+00	-.1505E-03	+.0000E+00	+.0000E+00	+.9157E-05
M_xX	+.0000E+00	+.0000E+00	+.5119E-05	+.0000E+00	-.2250E-04	+.0000E+00
M_xZ	-.4313E-03	+.0000E+00	+.4133E-05	+.0000E+00	+.0000E+00	+.8156E-05
M_xM_y	+.0000E+00	+.0000E+00	+.0000E+00	+.0000E+00	+.0000E+00	+.0000E+00
XZ	+.0000E+00	+.0000E+00	-.1843E-07	+.0000E+00	-.1396E-04	+.1641E-06
XM_y	+.0000E+00	+.0000E+00	+.3650E-06	+.0000E+00	+.1107E-03	+.3022E-05
ZM_y	+.0000E+00	+.0000E+00	-.1719E-05	+.0000E+00	+.7190E-04	-.4456E-05

Table 2. M=5 Normal force coefficient C_y

Run No.	Angle of attack								
	-5°	0°	5°	8°	10°	12°	15°	20°	25°
1	-0.1620	0.0024	0.1624	0.2624	0.3380	0.4122	0.5253	0.7119	0.9094
2	-0.1627	-0.0020	0.1643	0.2654	0.3356	0.4073	0.5227	0.7138	0.9031
3	-0.1642	0.0005	0.1635	0.2656	0.3351	0.4068	0.5218	0.7141	0.9072
4	-0.1607	-0.0006	0.1636	0.2661	0.3340	0.4085	0.5216	0.7141	0.9135
5	-0.1638	0	0.1610	0.2635	0.3358	0.4062	0.5290	0.7131	0.9039
$\frac{\sum C_y}{5}$	-0.1627	0	0.1630	0.2646	0.3357	0.4082	0.5246	0.7134	0.9074

Table 3. M=5 Axial force coefficient C_x

Run No.	Angle of attack								
	-5°	0°	5°	8°	10°	12°	15°	20°	25°
1	0.1477	0.1442	0.1468	0.1522	0.1580	0.1656	0.1785	0.2047	0.2379
2	0.1481	0.1456	0.1481	0.1529	0.1578	0.1653	0.1789	0.2058	0.2388
3	0.1483	0.1448	0.1480	0.1541	0.1595	0.1661	0.1782	0.2070	0.2400
4	0.1468	0.1434	0.1463	0.1539	0.1581	0.1641	0.1775	0.2052	0.2382
5	0.1470	0.1436	0.1473	0.1528	0.1581	0.1650	0.1782	0.2055	0.2389
$\frac{\sum C_x}{5}$	0.1476	0.1443	0.1473	0.1532	0.1583	0.1652	0.1783	0.2057	0.2388

Table 4. M=5 Pitching moment coefficient C_{mz}

Run No.	Angle of attack								
	-5°	0°	5°	8°	10°	12°	15°	20°	25°
1	-0.1120	0.0016	0.1118	0.1810	0.2333	0.2845	0.3626	0.4910	0.6265
2	-0.1123	-0.0014	0.1132	0.1830	0.2317	0.2813	0.3610	0.4922	0.6225
3	-0.1136	0.0003	0.1127	0.1836	0.2317	0.2812	0.3605	0.4930	0.6256
4	-0.1111	-0.0004	0.1128	0.1838	0.2305	0.2821	0.3603	0.4928	0.6297
5	-0.1132	0	0.1110	0.1820	0.2321	0.2808	0.3655	0.4922	0.6232
$\frac{\sum C_{mz}}{5}$	-0.1124	0	0.1123	0.1827	0.2319	0.2820	0.3620	0.4923	0.6255

Table 5. M=5, $\alpha=0^\circ$ each component output (mv)

	X	Y	Z	M_x	M_y	M_z
0 sec	1.3129	0.7699	0.4397	-8.1255	0.7156	3.6301
20 sec	1.3229	0.7605	0.4791	-8.1206	0.7010	3.6225
70 sec	1.3217	0.7620	0.4385	-8.1240	0.7208	3.6231

Table 6. M=8, $\alpha=0^\circ$ each component output (mv)

	X	Y	Z	M_x	M_y	M_z
0 sec	0.7899	0.8188	0.4119	-8.1749	0.7263	3.6892
20 sec	0.7916	0.8182	0.4136	-8.1755	0.7260	3.6891
70 sec	0.7920	0.8219	0.4132	-8.1743	0.7286	3.6867

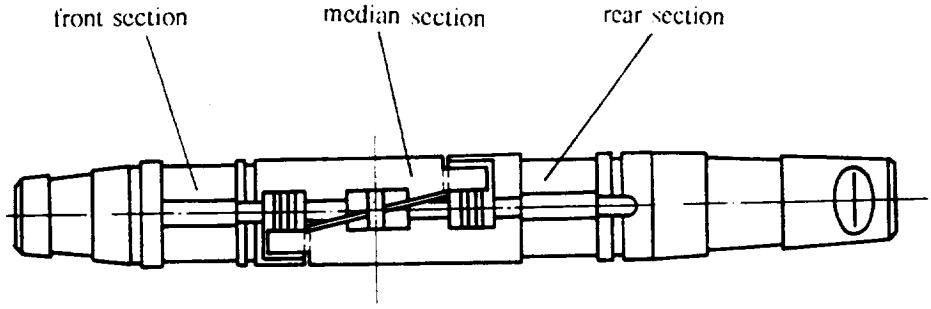

Fig.1 Construction of six-component balance

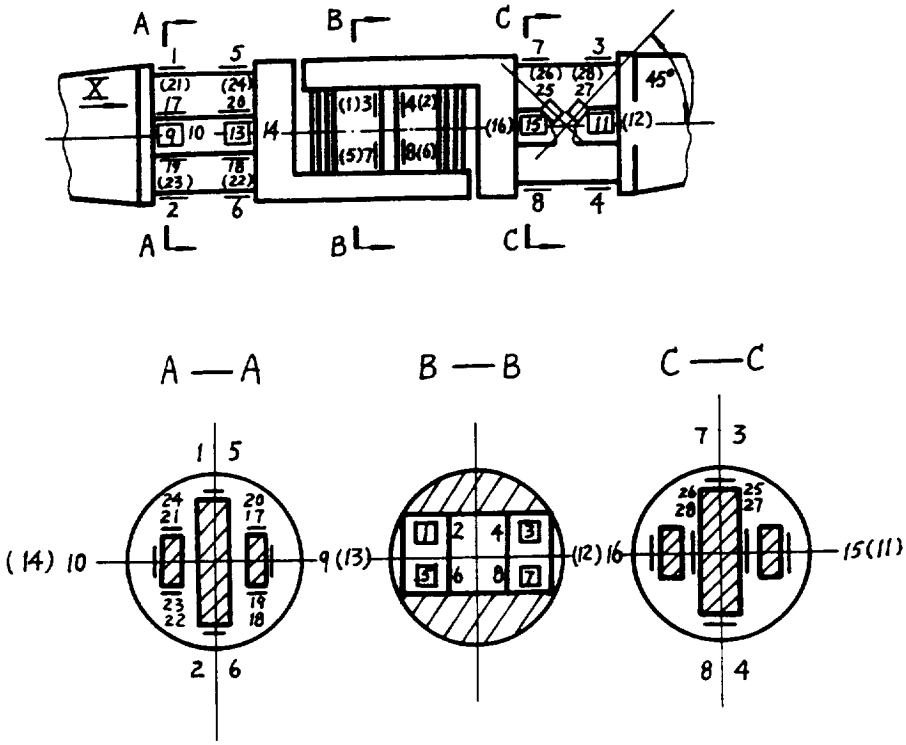

Fig.2 Installation of strain gages on the balance

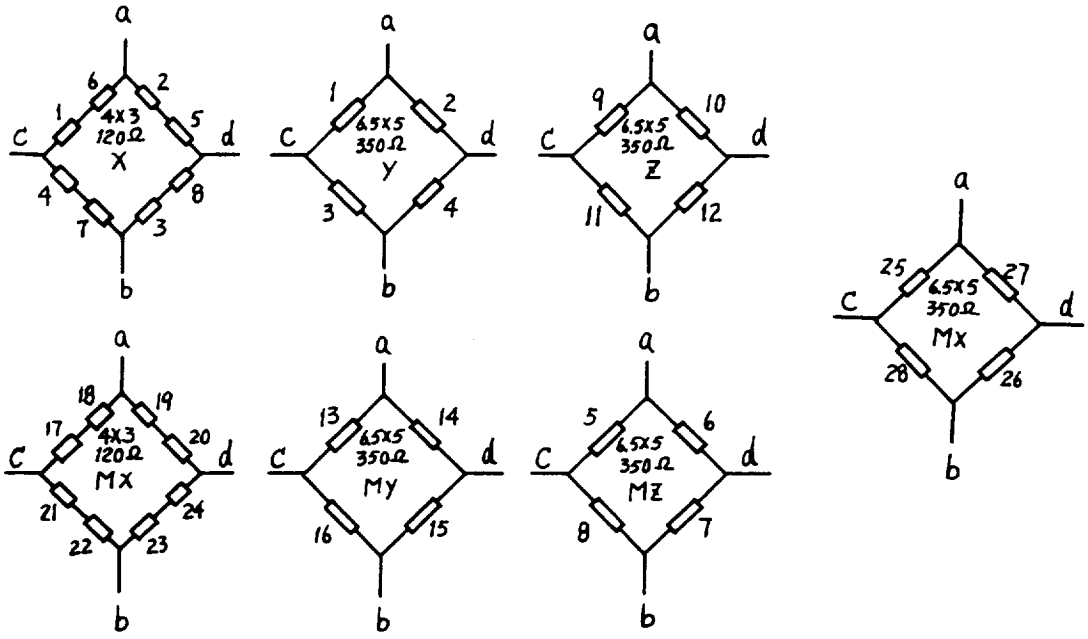

Fig.3 The electrical arrangement of strain gages in the bridge circuit

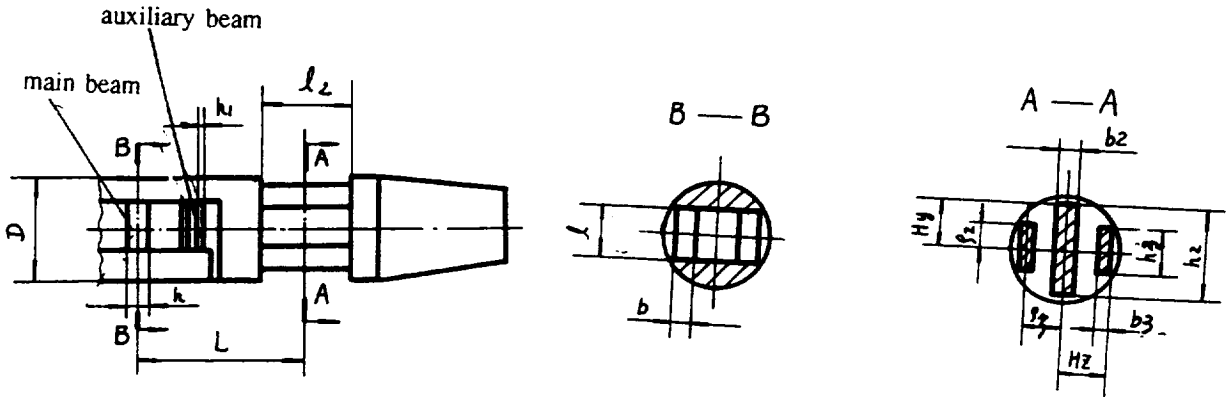

Fig.4 Dimension of the measuring units of balance

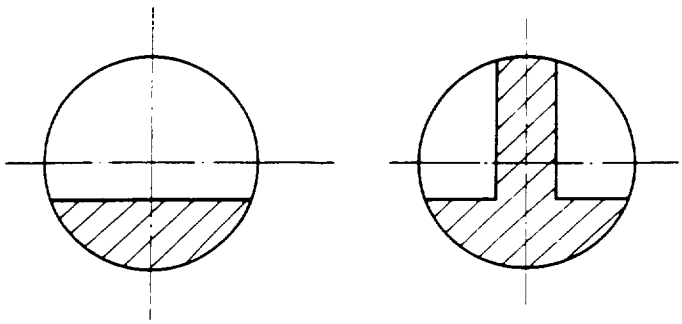

Fig.5 Modified notch section

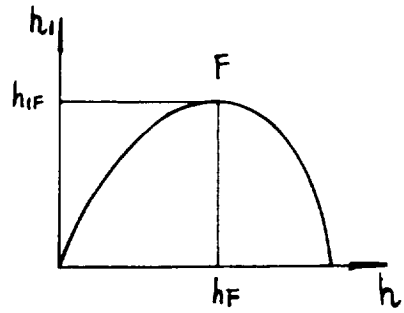

Fig.6 Iso-strain curve

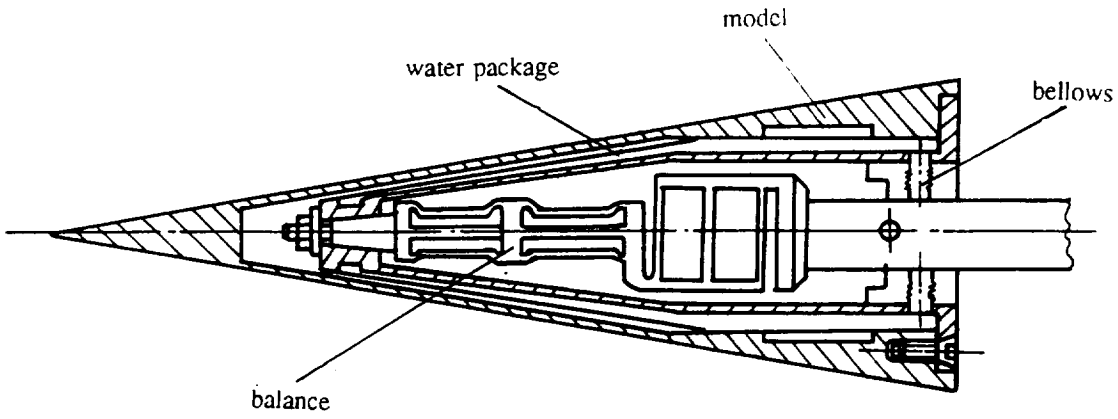

Fig.7 Construction of the heat protection of the balance water package I

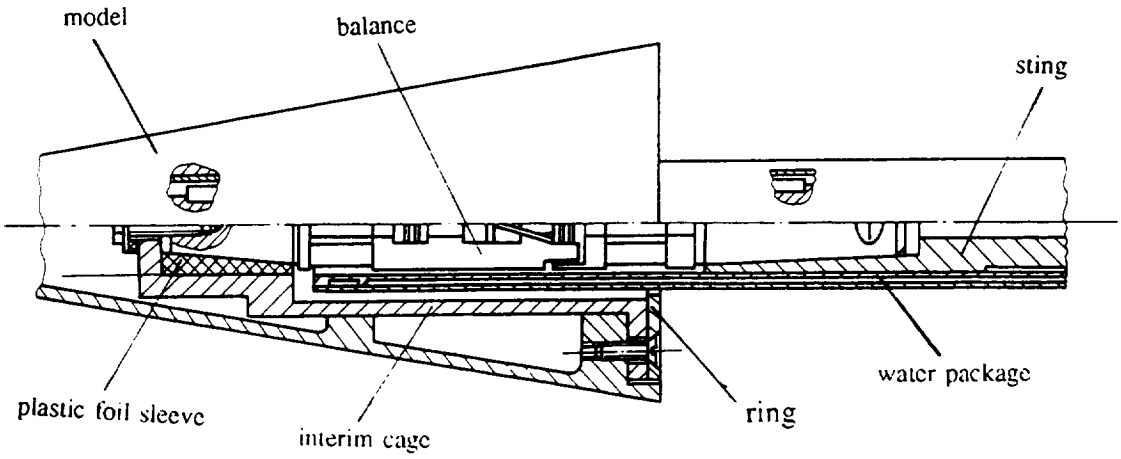

Fig.8 Construction of the heat protection of the balance water package II

SINGLE LOAD AND MULTICOMPONENT BALANCE CALIBRATION SYSTEM (SL&MBCS) OF PIEZOELECTRIC BALANCE IN SHOCK TUNNEL

Liu Hongshan Lu Zhiguo Qi Xuequn
China Aerodynamics Research and Development Center
Mianyang,Sichuan P.R.of China

SUMMARY

This paper describes a new type balance calibration system (SL&MBCS) in HAI (Hypervelocity Aerodynamics Institute) of CARDC and shows that its principle is remarkable,and its application in shock tunnel is very successful.

INTRODUCTION

YD type piezoelectric balance has been successfully used in shock tunnel in CARDC. For improving the ability and accuracy of piezoelectric balance calibration, SL&MBCS had been developed. And now, it is operating routinely in shock tunnel in CARDC. The main performance of shock tunnel and typical piezoelectric balances are shown in Table 1 and Table 2.

Table 1. Typical Piezoelectric Balances

Type	Component	Range	Sensitivity	Accuracy (%)
YD3-20B	X	2000N	100pc/N	0.85
	Y	240N	250pc/N	0.76
	Mz	530N.m	20000pc/N.m	1.1
YD3-30A	X	6000N	65pc/N	0.52
	Y	1500N	160pc/N	0.2
	Mz	2000N.m	12600pc/N.m	0.4
YD6-25A	X	3000N	96pc/N	0.17
	Y	800N	96pc/N	0.21
	Z	250N	2500pc/N	0.18
	Mx	30N.m	420000pc/N.m	0.19
	My	560N.m	110000pc/N.m	0.23
	Mz	1200N.m	5130pc/N.m	0.16

Table 2. Main Performances of Shock Tunnel

Content	Performance
Driver Pressure	≤80MPa
Mach Number	6 to 24
Reynolds Number	10^4 to 10^8 1/m
Running Time	4 to 20ms

PRINCIPLE AND FABRICATION OF SL&MBCS

Principle

Counting for the fact that the aerodynamic force acts on model can be taken as a space force vector in the model coordinate system in wind tunnel test. If a space force is applied to the balance in balance calibration, it is much better to simulate the real state of balance test. Secondly, the high resistance feature of piezoelectric balance demands the load which apply to balance should be in very short time. It is not easy to apply a few loads to balance simultaneously as strain-gauge balance calibration. Following this, SL&MBCS had been built. Its principle is described below(See Figure 1).

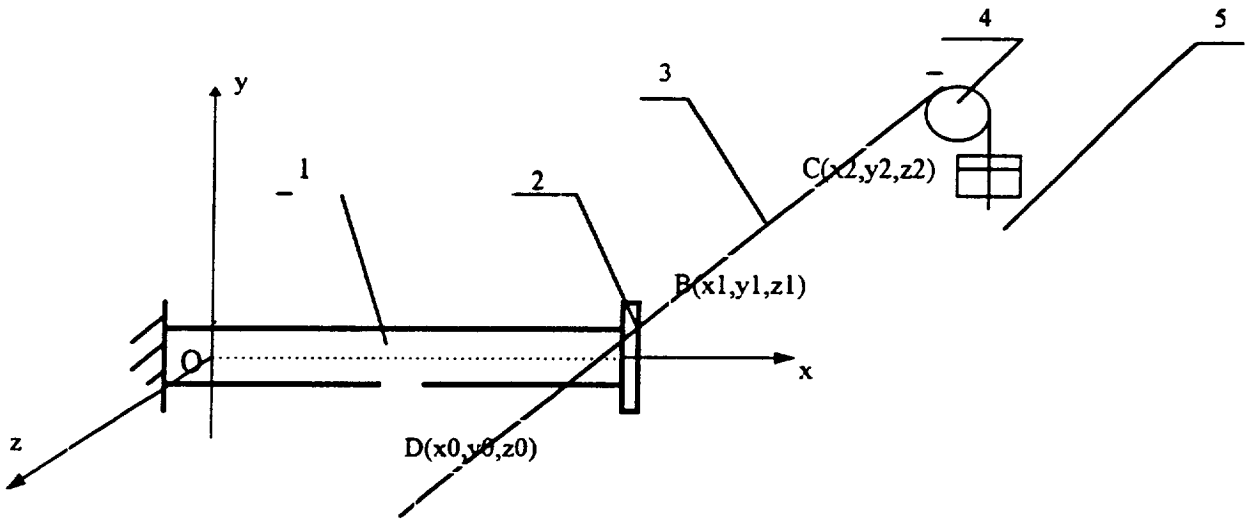

1.Balance 2.Load-sheath 3.Steel wire 4.Pulley device 5.Weights

Figure 1. Principle diagram of SL&MBCS.

In a space coordinate system, a space force vector which does not across any coordinate axis can be decomposed into 3 force components and 3 moment components of balance. So if a balance is located in a coordinate axis in a space coordinate system, every component of balance will output its signal by applying a space force. a steel wire is installed from load- sheath to a pulley device which has 2 degrees of freedom, at the end of the steel wire, some weights hung by. If the coordinates of B and C point and the weights can be measured accurately the forces and moments which apply to the balance components can be calculated by loading formulas. For the different location of pulley device and different weights, a series of equations after loads and balance outputs are acquired by the way of mathematics, the calibration results come up.

Fabrication

SL&MBCS contains 2 subsystems: Load Measurement System,Data Acquisition & Processing System. See Figure 2.

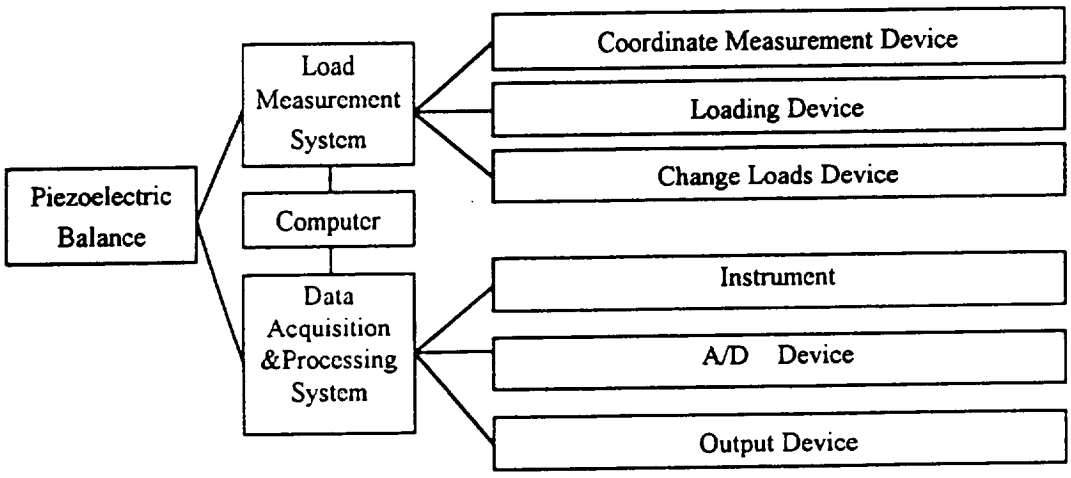

Figure 2. Block Diagram of SL & MBCS.

Load Measurement System

The main measurement device is a digital display machine tool which has 3 degrees of freedom. Its coordinates distinguishably is 5μm, measurement accuracy is 20μm. In the course of measurement,balance and pulley device was installed on the tool platform, measuring tool is installed on tool post. Moving platform and tool post, when the tool-point

contact with steel wire, the digital display device displays the point coordinates.

In order to improve the accuracy measurement, the measuring tool designed specially.

The location of steel wire changed by a pulley device which has 2 degrees of freedom. So there are different kinds of space forces act on the balance. All loads cover the full-scale range of the balance. When the load is not too large, loading is in manual mode.

Data Acquisition & Processing System

The system contains: computer, charger amplifier, high speed A/D and other instrument output devices. Every component output of balance will be managed by SSMDT software (developed by CARDC). The calibration reports are last results.

MAIN TECHNICAL SPECIFICATIONS OF SL&MBCS

a. To fit balance calibration in shock tunnel;
b. Loading accuracy: 0.5%;
c. Load ranges: Force 2--1000N;,
Moment 0.05--30N.m.

ACCURACY ANALYSIS OF SL&MBCS

Loading Accuracy

a. About dead weight and pulley friction:
- Weight accuracy: 0.001%;
- Pulley friction accuracy: 0.1%.

b. About space force decomposing accuracy:

After calculating, if the distance between B and C point (see Figure 1) is longer than 100mm, if the distance between moment vector and moment reference point is longer than 20mm, then force and moment decomposing errors are less than 0.4%.

Repeatability Accuracy

- Measuring tool accuracy: 0.01%;
- Force decomposing accuracy: 0.1%;
- Moment decomposing accuracy: 0.2%.

Data Processing Technique

Data processing technique all in SSMDT software. Main technique are:

Make Loading Table

For the needs of covering balance full-scale range in calibration, loading table must be made before operation. The table will provide some loading information, such as: how to change pulley device, what is the weight to load, and so on.

Pre-processing Output Signal

The output signal of balance is not theoretical signal, it is always affected by other periodic signals. For insuring measurement accuracy, some special data processing techniques are used.

Calibration Equation

The balance formula used in this paper is following:

$$Q_i = K_i F_i + \sum_{i=1, j \neq i}^{6} K_{i(j)} F_j + \sum_{m=1}^{6} \sum_{j=1}^{6} K_{i(mj)} F_m F_j \qquad (1)$$

where: Qi-- component i output value;
Fi-- component i load value;
Ki: coefficient.

In order to solve the equation accurately and efficiently, Regression Analysis Method was used.

APPLICATION OF SL&MBCS

Since SL&MBCS built, it has been successfully used in multicomponent balance calibration in shock tunnel in CARDC. Take a balance (Type:YD3-A) as an example, the application of SL&MBCS is described below.

Results of Calibration

All the results show that the main coefficients of balance components are much more marked, and the interaction coefficients are also show accurately. What appear in calibration equations are reasonable(See Table 3 and 4). Comparing the results which from the SL&MBCS with the results from SL&SBCD (Single Load and Single-Component Balance Calibration Device) shows that SL&MBCS is much better than SL&SBCD in accuracy and efficiency.

Table 3. Linear Interaction Calibration Equations

Component	Calibration Equation (Linear Interaction)
X	V(X)=-0.02585-0.5689X-0.00932My
Y	V(Y)=-0.00219-0.00363X+0.17923Y-0.0148My
My	V(My)=-0.01735+0.00499X-0.01753Y-0.1264My

Table 4. Nonlinear Interaction Calibration Equation

Component	Calibration Equation (Nonlinear Interaction)
X	$V(X)=0.0032-0.5653X+0.0063Y-0.0093My-0.006Y^2+0.0014MyY-0.007My^2$
Y	$V(Y)=0.0002-0.0037X+0.1794Y-0.0149My-0.0006Y^2+0.00003MyY$
My	$V(My)=-0.0098-0.1266My+0.0006X^2-0.0027XY$

Wind Tunnel Results Comparison Between SL&MBCS and Calculation

The standard model (B-2) test in shock tunnel shows that the aerodynamic coefficient-attack angle curves are good.

CONCLUSION

By the application of SL&MBCS, the conclusion are reached as following:

a. SL&MBCS is a new-type balance calibration system in China. To piezoelectric balance, SL&MBCS is suitable and its application is much better than SL&SBCD.

b. SL&MBCS has its good characteristics, such as calibration principle, fabrication, software and so on.

FREE OSCILLATION DYNAMIC STABILITY BALANCE SYSTEM

Peter A. Parker
Force Measurement Engineer
Modern Machine and Tool Company Incorporated
Newport News, Virginia USA

ABSTRACT

A dynamic stability balance system has been designed and implemented using a large amplitude free oscillation technique to determine the damping characteristics of a wind tunnel model containing a moving payload which causes changes in the center of gravity during flight. The ceiling mounted system consists of a dynamic stability balance, a variable angle of attack tunnel interface plate, a model strut which passes into the tunnel test section, and a remote operation control panel. The balance consists of four load carrying flexures and one measurement flexure. Two full strain gage bridges, a foil resistive strain gage bridge and a piezoresistive strain gage bridge, were installed on the measurement flexure. Angular deflection is collected from the foil strain gage bridge and dynamic response data is recorded from the piezoresistive bridge. The dynamic stability balance was designed with removable load carrying flexures which allows the system spring constant to be changed for transonic and subsonic testing of a model. A removable inertial disk is used in conjunction with the removable flexures to change the frequency and damping time constant of the balance oscillation. The nominal angle of attack of the model is set using the tunnel interface plate which allows for plus and minus ninety degree rotation. Operation of the balance is accomplished by remotely cocking and latching the balance to an initial angle of five degrees and then releasing the latch to begin oscillation. The damping time, frequency and amplitude are recorded with the model subjected to controlled aerodynamic conditions. Comparison of the data obtained at the various aerodynamic conditions yields the damping characteristics of the model.

INTRODUCTION

Design of a free oscillation dynamic stability balance system was requested for the testing of aerodynamic models with moving payloads which causes changes in the center of gravity during flight. Large amplitude (greater than 5°) free oscillation was determined to be the test technique utilized [1]. The balance system was designed and fabricated as a completely self contained subsystem to be incorporated into an existing transonic wind tunnel facility (figure 1). Ceiling mounting of the balance system was required in the design. A model strut which passes through a clearance hole in the ceiling of the test section and thereby into the freestream flow was also required. The model is suspended in the center of the test section by the model strut when the system is fully assembled and installed in the tunnel test section (figure 6).

Design of the balance system presented many challenging requirements. The system was to be completely self-contained and operate without hydraulic, electric, or pneumatic power. It was required to have a transonic and subsonic set of removable flexures which would provide two different system spring constants and balance oscillation characteristics. Another set of flexures was provided with a partially machined flexure area

which can be sized for future spring constant requirements. Overall size of the system was tightly constrained due to the minimal space available in the existing transonic tunnel plenum area. Model attachment was required to be simple and yet rigid enough to not effect the balance performance. An interchangeable inertial disk was incorporated into the design to allow the researcher to vary the frequency and damping time for specific model oscillation conditions. The entire balance system can also be rotated plus and minus ninety degrees in the yaw plane to provide the capability of infinite adjustment of the initial model angle of attack.

Strain gage requirements included two independent strain gage bridges which simultaneously measure the strain induced due to the applied yaw moment. A foil resistive strain gage bridge was provided for static deflection data and a piezoresistive strain gage bridge for dynamic data. Both of the strain gage bridges were installed on the same measurement flexure which was used for the transonic and subsonic configurations of the balance system.

Calibration requirements included the need to characterize the balance static deflection and dynamic response. Static calibration was required to measure the actual spring constant of the system. The static calibration was performed by deflecting the balance while recording the change in strain gage bridge outputs and measuring the deflection of the balance shaft relative to the tunnel interface plate. Weights were applied of appropriate magnitude to deflect the balance shaft in one and one quarter of a degree increments through the range of plus and minus five degrees in the yaw plane (figure 4). A dynamic calibration was performed to provide the natural frequency and the damping time of the balance system without the influences of a model attached.

This paper will focus primarily on the design and calibration of the balance. It will also address in general the fabrication and strain gaging of the free oscillation dynamic stability balance system.

BALANCE SYSTEM DESIGN

The design of the balance included a number of challenging areas which will now be discussed in detail. Those areas included a single optimized measurement flexure, a removable flexure system, frequency and damping time adjustment, a self contained manual operating system, an initial angle of attack adjustment, a model attachment strut, and an oscillation limit safety stop.

The measurement flexure is a single monolithic beam fabricated from hardened 17-4PH stainless steel (figure 2) [2]. The load path includes four load carrying flexures which can be removed to vary the system spring constant and a single strain gaged measurement flexure. The five load carrying flexures are attached to the balance housing on the non-metric end and to the balance shaft on the metric end. The balance shaft and balance housing are also monolithic components fabricated from hardened 17-4PH stainless steel [2]. Balance housing and shaft deflections were considered to be very small compared to the flexures and therefore they were considered to be infinitely rigid for the purpose of theoretical deflection analysis. It was therefore assumed in the analysis that all of the system deflection occurs due to the deflection of the five flexures (four load carrying flexures and one measurement flexure). Design of the measurement flexure needed to be optimized for the resolution of the strain gage bridge output and the load proportion of the measurement flexure relative to the entire system in both the transonic and subsonic configurations. Measurement flexure design also needed to be within the allowable stress

including an adequate factor of safety for possible unknown dynamic responses of a wind tunnel model.

The transonic configuration of the system is designed for a system spring constant of 41.4 in-lb per degree of yaw moment deflection. The flexure system installed for this configuration consists of four .099" thick, 4.00" long, and 1.000" high, load carrying flexures. The dimensions of the single measurement flexure are; .060" thick, 4.00" long and .600" high. In this condition the measurement flexure carries 3.2% of the total yaw moment load applied to the entire system. The sensitivities of the foil and piezoresistive bridges in this configuration are 1.375 mV/5V per degree and 97.564 mV/5V per degree respectively. It should be noted that although this design did not optimize the load proportion carried by the measuring beam it still obtained acceptable resolution from the strain gage bridges. The other four load carrying flexures were required due to the aerodynamic forces in the axial and side directions. These forces translated into large moments on the balance flexures due to the long transfer distance of model strut. These other forces became a predominate factor in the design thickness of the flexures [3]. The five flexures (four load carrying flexures and one measurement flexure) are mounted in a cross flexure arrangement and are distributed along the vertical axis of the balance. Flexure arrangement is designed such that the deflection of the balance is very small in all other axes except yaw which is of primary interest. Significant balance oscillation is thereby isolated to the primary component of yaw.

The subsonic configuration of the system also consisted of four load carrying flexures and the one measurement flexure. The design spring constant for this system is 3.55 in-lb per degree of yaw moment deflection. Subsonic load carrying flexure dimensions are; .025" thick, 4.00" long and 1.000" high. In this condition the measurement flexure carries 67.5% of the total yaw moment load applied to the entire system. The sensitivity of the foil and piezoresistive strain gage bridges are 1.527 mV/5V per degree and 107.973 mV/5V per degree respectively. In this configuration the load proportion of the measuring beam increased to an optimum percentage for balance measurement flexure design.

Design and installation of removable flexures presented another challenge due to the complex assembly and the cross flexure arrangement of the system which allows the balance shaft to rotate relative to the balance housing (figure 2 & 4). The non-metric end of each flexure (measurement flexure and load carrying flexures) is mounted to the balance housing with two socket head cap screws. Metric end attachment is accomplished with three socket head cap screws which firmly clamp the flexures to the balance shaft. To remove the balance shaft assembly, the non-metric end screws securing each of the five flexures are removed. Then the balance shaft with the flexures still attached at the metric end is removed by carefully lifting it vertically out of the balance housing. This removal technique required tight fabrication tolerances and a low rms surface finish in the channels which locate the flexures inside of the balance housing.

It was also a requirement of the researcher to have the ability to change the damping time and frequency of the balance while the system remained installed in the test section. To accomplish this the balance was designed with an interchangeable inertial disk which could be removed or replaced with an inertial disk of different mass or polar moment of inertia (figure 2 & 3) [4]. When the top cover of the balance is removed, the inertial disk is readily accessible. Four socket head cap screws secure the inertial disk to the top of the balance shaft. After the inertial disk is removed or replaced the balance can be operated again without the removal of the model or any access to the tunnel test section.

One of the most challenging areas of the design was the manual cocking and release mechanism requirements (figure 3 & 4). It was required that the balance would have a remote control system which could be operated from the tunnel control room. The control system could not utilize hydraulic, pneumatic or electric power. Therefore; a system which included manual levers and cables was designed. A seventy pound force was required at the moment arm to cock the balance shaft to an initial angle of five degrees in the transonic configuration. Due to this large force on the moment arm attached to the top of the balance shaft and due to the maximum allowable diameter of the balance cover, a unique shape of the cocking arm was required to achieve a suitable mechanical advantage necessary to minimize the input force from the operator (figure 2). The pivot point of the cocking arm was positioned to maximize the ratio of the input lever to the output lever on the cocking arm. A roller bearing cam follower was installed on the end of the cocking arm to minimize frictional effects which would increase the input force required from the operator. After the balance shaft is cocked to an initial angle of five degrees it is latched in place with a cylindrical pin which slides within an oil impregnated bronze bearing. After latching the moment arm the cocking arm is moved to a clear position and a rapid release of the latch will begin the balance oscillation. The control unit was designed such that minimum operator input force and motion would result in a clean and rapid release to begin the oscillation of the balance. To further encourage this release, a spherical end was machined and polished on the end of the latching pin. The latching pin and moment arm were fabricated from oil hardened tool steel to minimize wear from repeated operation of the balance. Both the cocking and the latching mechanism are operated from a single control unit which incorporates further mechanical advantage such that a minimal force is required by the operator. The cabling allowed remote operation of the balance in the tunnel control room which was twenty feet from the balance installation in the tunnel test section.

Infinite adjustment of the initial model angle of attack was required in the design. This requirement was accomplished by machining a cylindrical boss on the bottom of the balance housing which locates and maintains the axis of rotation. The boss engages a counterbore in the top of the tunnel interface plate. A pointer protrudes from the maximum diameter of the balance housing and aligns with the engraved angle divisions on the tunnel interface plate. The engraved angle divisions are provided in two degree increments and extend for plus and minus ninety degree rotation. Four socket head cap screws firmly clamp the balance housing to the tunnel interface plate after the desired model angle of attack is set. The tunnel interface plate was fabricated from 6061-T6 aluminum to minimize the possibility of galling of the rotating balance housing. Aluminum also provided an added benefit of weight reduction of the entire system.

The model strut which passes into the tunnel test section has a long tapered cylindrical shape which minimizes the disturbance of the freestream flow near the model (figure 2 & 6). Its design is also axis symmetric which maintains this cross sectional shape for any angle of attack. Model attachment is accomplished with a cylindrical fit and a set screw to lock the model onto the model strut. This simple attachment method was preferred due to the desire to move the point of attachment on a model forward and aft during a single tunnel entry.

Due to the unknown response of the wind tunnel model, it was required that the oscillation of the balance would be limited to plus and minus six degrees of yaw deflection. This safety system was accomplished with two solid dowel pins installed in the top of the balance housing. If the moment arm, which is attached to the oscillating balance shaft, exceeds six degrees of deflection it will foul into these dowels pins resulting in the limiting and damping of the balance oscillation. Stress analysis verified that the flexure system could be subjected to six degrees of deflection without a structural or strain gage failure.

Below is a summary of the design requirements of the balance system:

- Single optimized measurement flexure
- Removable load carrying flexures
- Removable inertial disk
- Manual cocking and release mechanism
- Initial angle of attack adjustment of ±90° with two degree graduation marks and capability of being locked at any angle within this range.
- Amplitude of yaw oscillation of ±5°
- Normal force capacity of ±500 pounds
- Axial force capacity of 500 pounds
- Transonic configuration stiffness of 41.4 in-lb per degree
- Subsonic configuration stiffness of 3.55 in-lb per degree
- Input voltage of 5.000 VDC
- Foil strain gage bridge with nominal output of 1.5 mV/V at 5° yaw deflection
- Piezoresistive strain gage bridge with nominal output of 100 mV/V at 5° yaw deflection
- Safety stops that will limit oscillation to ±6°

BALANCE LABORATORY CALIBRATION

A laboratory static force calibration of the balance system was completed in order to develop the relationship between the strain gage bridge output and the deflection in the yaw plane. The balance was mounted to a vertical plate which simulated the actual wind tunnel interface (figure 4). A calibration moment arm used for load application was mounted on the end of the balance shaft. The moment arm attachment simulated the actual wind tunnel attachment of the model strut to the balance shaft. A level was placed on the calibration moment arm to ensure the continued level attitude of the arm and thereby the orthogonal relationship of the applied load to the balance shaft. An inclinometer was positioned on the tunnel interface plate to measure the relative deflection of the balance shaft to the interface plate. Both positive and negative yaw moments were loaded with an incremented axial force applied at distances of 10.5" and 5.0" from the balance moment center. The effect of the axial force used to generate the desired moment and thereby the required deflection was removed from the calibration data. A calibration matrix was derived using a least square regression technique [5]. It was apparent from the static calibration plots of the transonic and subsonic balance configurations that there is a significant high order non-linear relationship of deflection versus strain gage output. Due to this non-linear behavior a third order calibration matrix was derived. Calculated system accuracies for the transonic and subsonic configurations were 4.2% and 1.0% respectively. Better accuracies could have been achieved by increasing the order of the polynomial used to derive the calibration coefficients, but the stated accuracies were deemed acceptable to the researcher. Equation (1) is used to calculate the balance deflection from the recorded strain gage signals.

$$\delta = k1\ (\theta) + k2\ (\theta^2) + k3\ (\theta^3) \qquad (1)$$

where:

δ = calculated deflection in degrees

θ = strain gage bridge output in mV/5V

k1, k2, and k3 are the calibration coefficients

The frequency and damping time of the balance system without the influence of a model installed was also measured in a dynamic laboratory calibration prior to tunnel installation. The balance system was mounted in the upright position similar to that of the actual tunnel installation. The piezoresistive strain gage bridge was monitored using a real time analog data acquisition system which provided a time based plot of the bridge signal (figure 5). The balance was cocked and latched using the remote control unit and then released to begin its free oscillation. The frequency and damping time was measured for both the transonic and subsonic configurations. It was also measured for both configurations with and without the inertial disk installed. Balance oscillation frequency and damping time were consistent with the design requirements. The logarithmic decay of the balance oscillation amplitude indicated a condition of free oscillation without any other mechanical damping or fouling occurring within the balance system. Dynamic calibration techniques and results proved to be acceptable to the researcher.

CONCLUDING REMARKS

The free oscillation dynamic stability balance system was successful in meeting or exceeding all of the design criteria. The system has been installed in the transonic wind tunnel and aerodynamic data has been successfully collected (figure 6). The system requires only minor maintenance due to its completely mechanical operation. This maintenance includes periodic lubrication and inspection of all moving parts. The installation of the free oscillation dynamic stability balance system has increased the capability and productiveness of dynamic stability wind tunnel testing techniques.

REFERENCES

[1] "General Discussion of Test Techniques," AEDC, TDR-64-99

[2] "ARMCO Advanced Materials Technical Data Manual," ARMCO Steel Corporation, Middletown, Ohio, 1974

[3] Beer, F.P., Johnston, E.R. Jr.: "Mechanics of Materials," McGraw Hill, Inc., USA, 1981

[4] Shelley, J.F.: "Engineering Mechanics, Dynamics," McGraw Hill, Inc., USA, 1980

[5] Chapra, S.C., Canale, R.P.: "Numerical Methods for Engineers with Personal Computer Applications," McGraw Hill, Inc. USA, 1985

FREE OSCILLATION DYNAMIC STABILITY BALANCE SYSTEM

BALANCE ASSEMBLY AND CONTROL UNIT

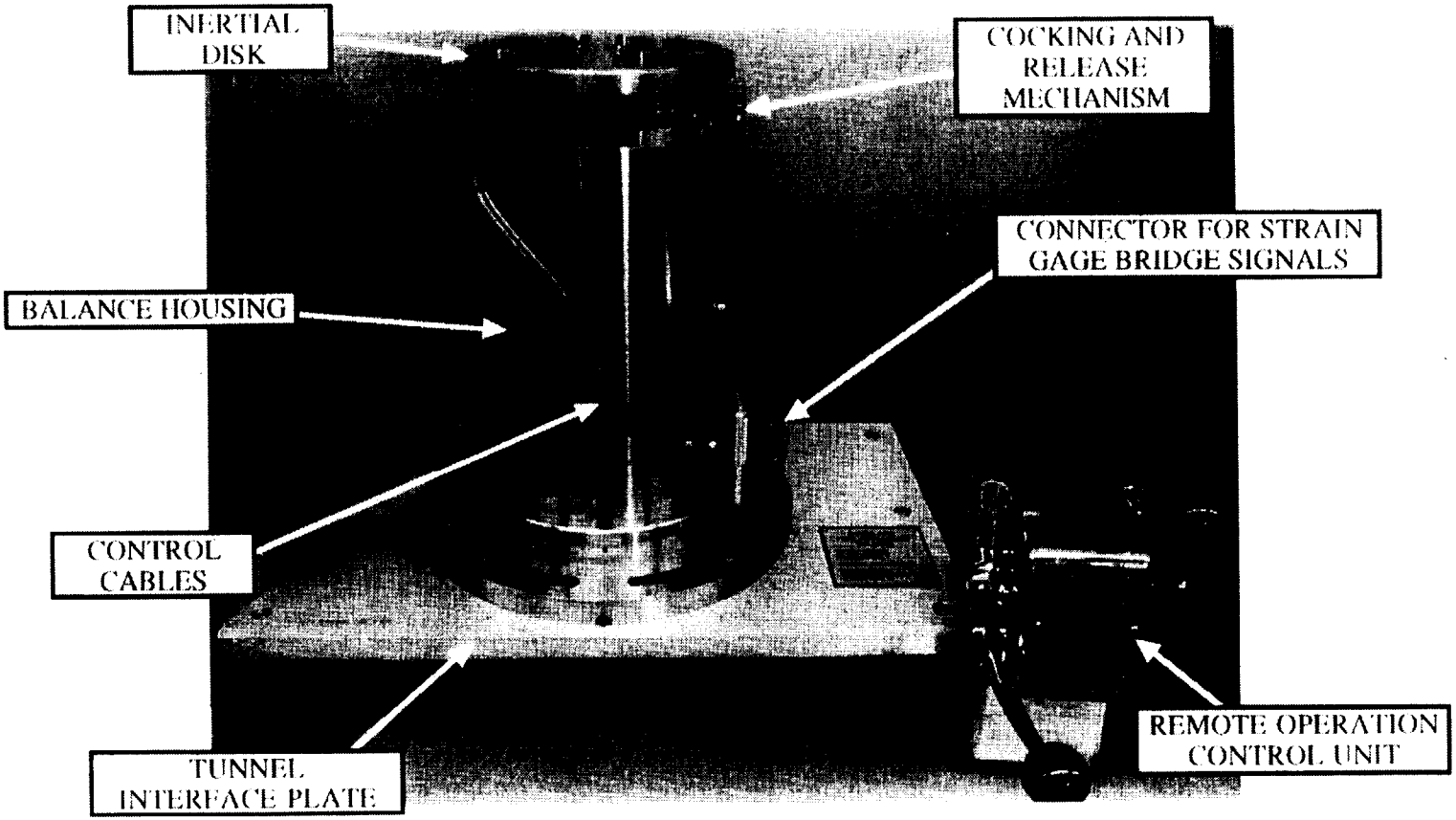

FIGURE 1

FREE OSCILLATION DYNAMIC STABILITY BALANCE SYSTEM

BALANCE SHAFT WITH FLEXURES INSTALLED

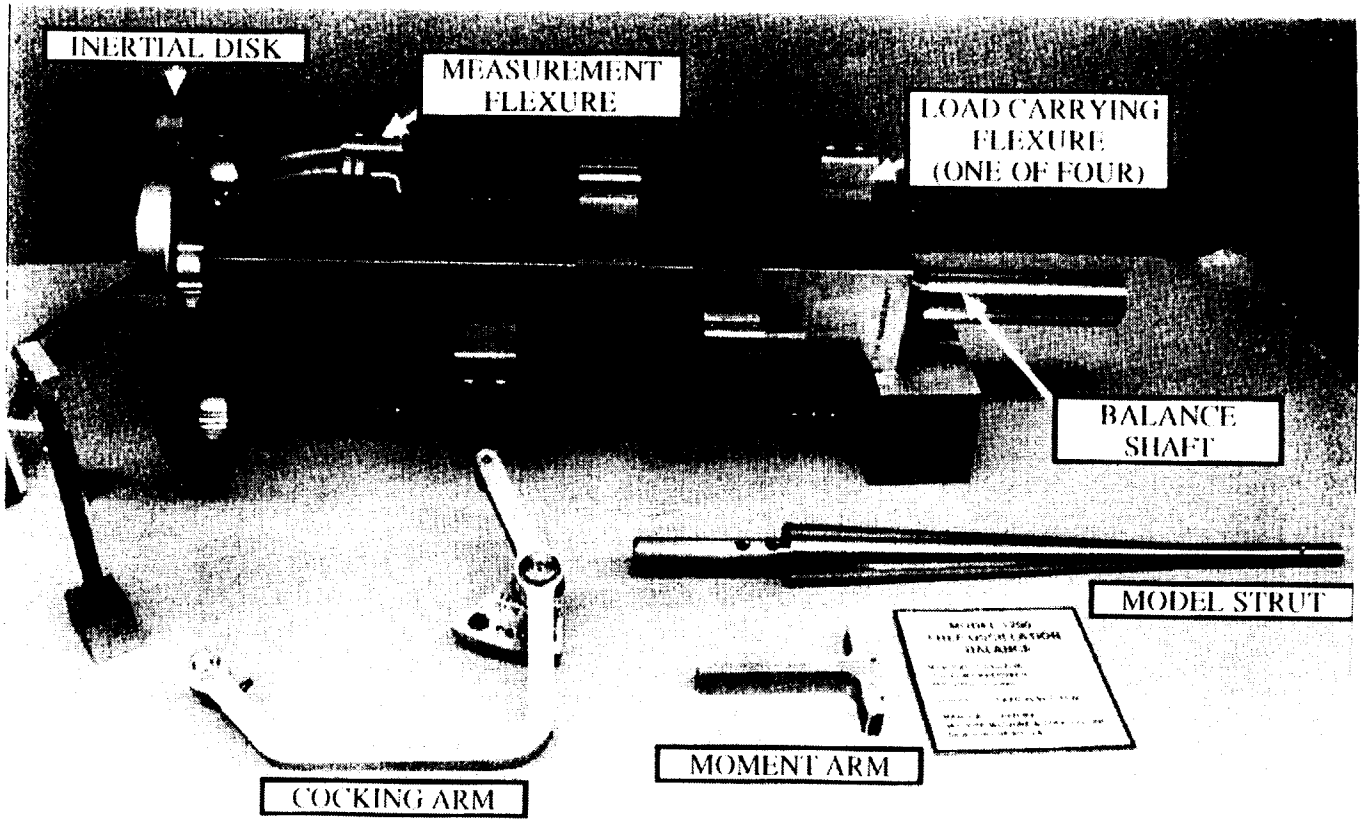

FIGURE 2

FREE OSCILLATION DYNAMIC STABILITY BALANCE SYSTEM

COCKING, LATCHING AND RELEASING MECHANISMS
(BALANCE IN LATCHED POSITION)

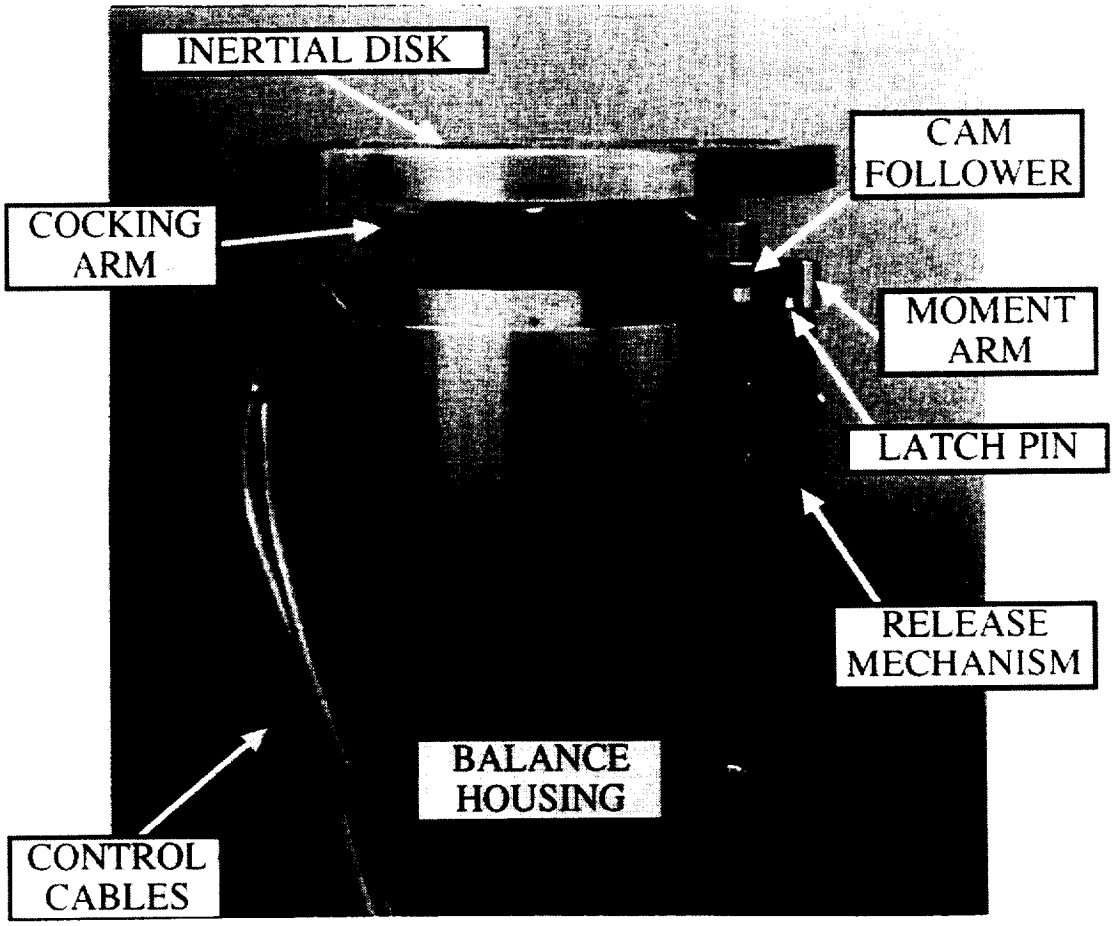

FIGURE 3

FREE OSCILLATION DYNAMIC STABILITY BALANCE SYSTEM

BALANCE STATIC DELFECTION CALIBRATION (TUNNEL INTERFACE PLATE DEFLECTED TO 5°)

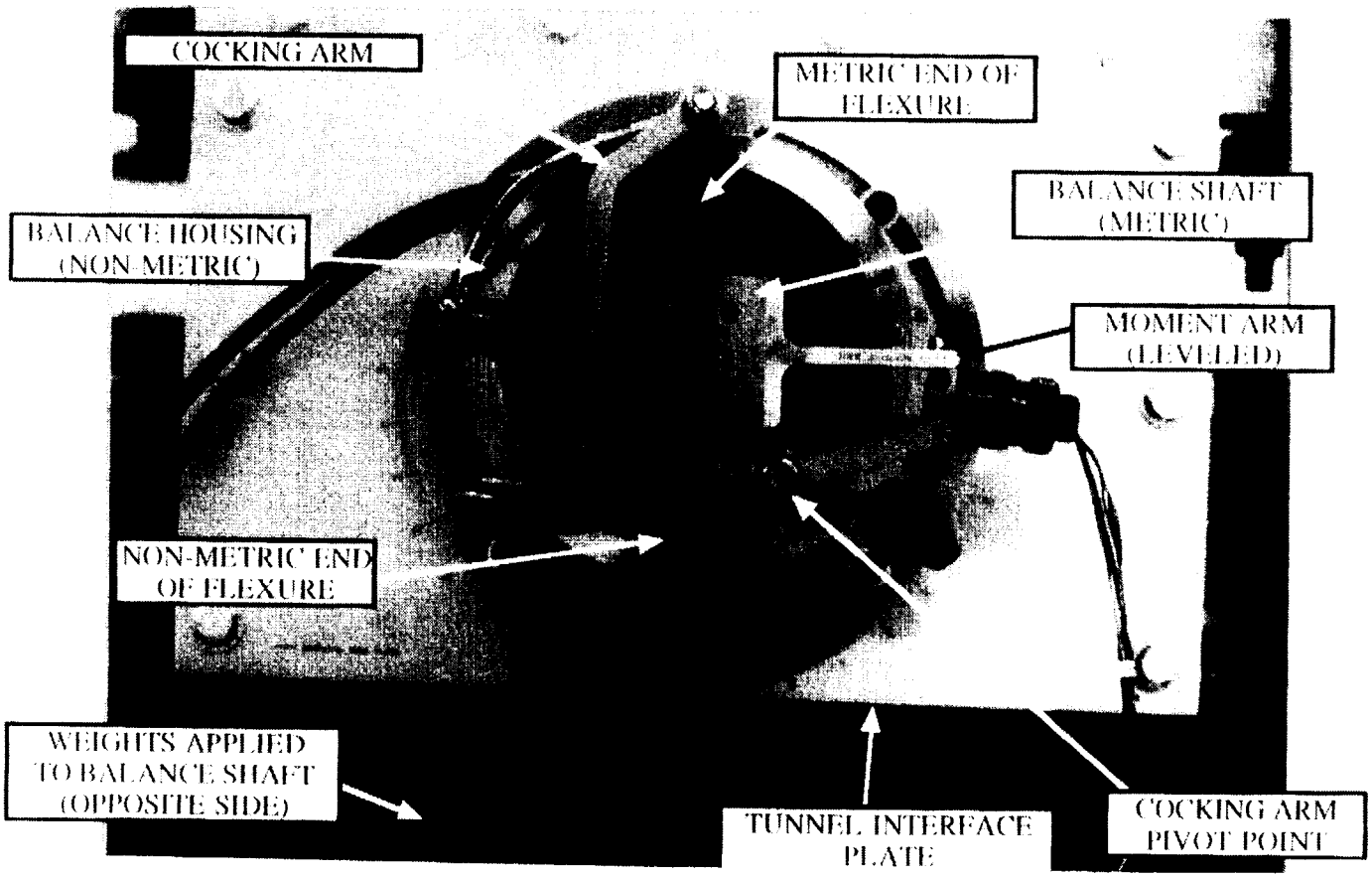

FIGURE 4

FREE OSCILLATION DYNAMIC STABILITY BALANCE SYSTEM

DYNAMIC CALIBRATION PLOT
(output of piezoresistive strain gage bridge)

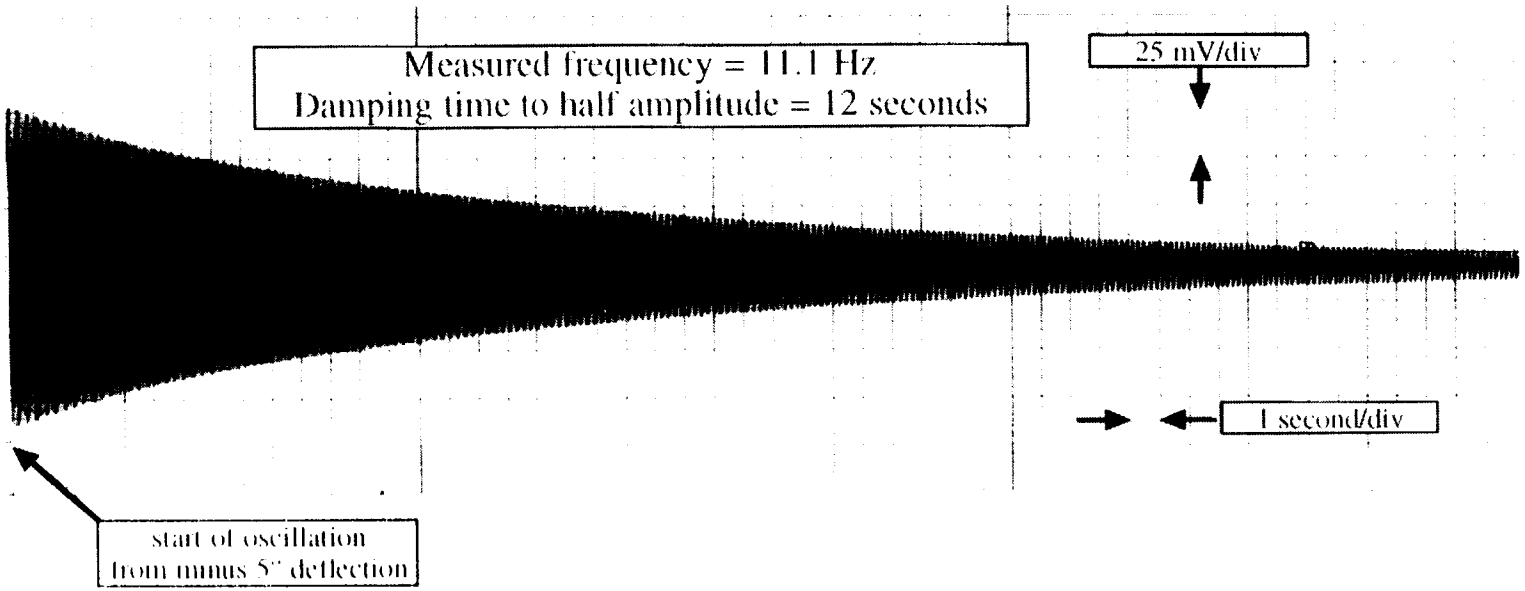

SUBSONIC CONFIGURATION WITHOUT THE INERTIAL DISK
(BALANCE OSCILLATION ONLY, NO MODEL INSTALLED)

FIGURE 5

FREE OSCILLATION DYNAMIC STABILITY BALANCE SYSTEM

TUNNEL INSTALLATION

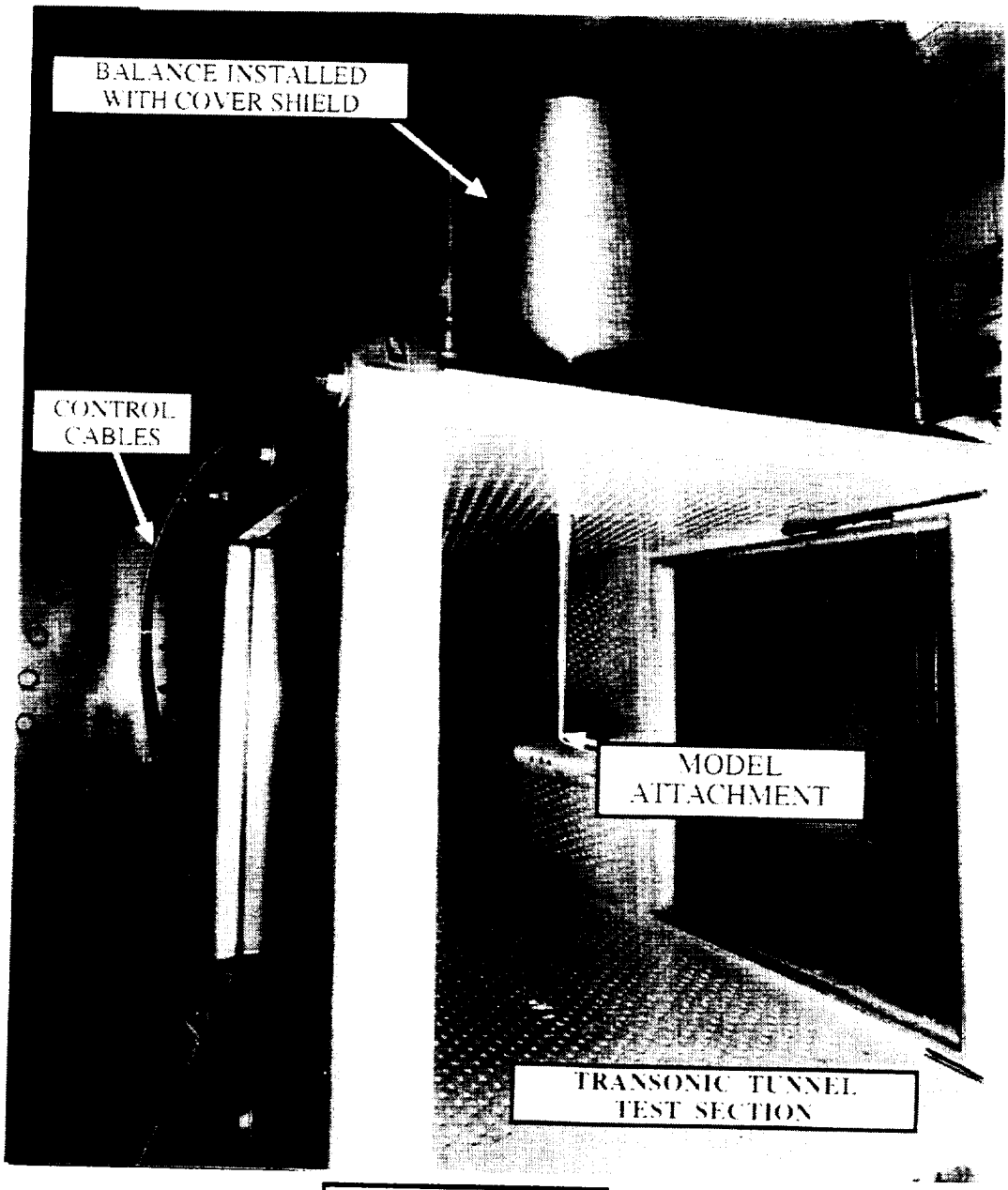

FIGURE 6

A STIFF MONOPIECE WIND TUNNEL BALANCE

Gédéon Drouin and Bertrand Girard
Defence Research Establishment Valcartier
2459 Pie-XI Blvd. North,Val-Bélair, Quebec, G3J 1X5, Canada

Ken Mackay
Martec Limited
Suite 400, 1888 Brunswick Street, Halifax, Nova Scotia, B3J 3J8, Canada

SUMMARY

Overloads generated at the start and stop of airflow in the DREV Indraft Wind Tunnel necessitated the development of strong and still sensitive aerodynamic balances. Semiconductor strain gages were considered for instrumenting the sensing structures but concerns were expressed on their sensitivity to temperature and implementation of necessary compensating circuits. A computer simulation tool was developed by Martec Ltd. to conduct statistical predictions of the effect of temperature on Zero-load balance outputs and on the sensitivity of bridges taking into account tolerances provided by component manufacturers. It can compute temperature effect compensating circuits and predict resulting performance.

INTRODUCTION

The DREV trisonic wind tunnel Fig. 1 is an intermittent indraft type operating between atmospheric pressure (atm) and vacuum. The Mach Number is continuously controllable between 0.2 and 1.5 and can take discrete supersonic values, through the use of sets of nozzle blocks, up to 4.0. The forces acting on the model are then maximum at Mach 1.4 where the dynamic pressure is 0.43 atm and minimum at Mach 4 with a pressure of 0.074 atm. A ratio of six then exists between the loads generated at these two regimes of operation. The aerodynamic balances used to measure model aerodynamic coefficients have to operate over a large range of forces and moments.

The dynamic load expected during a test must take into account not only the ± 10 to 15°- swept angle during the flow but also the flow starting and stopping load transients. Indeed when the valve controlling the flow is closed, a shock wave travels upstream with asymmetric characteristics capable of inducing efforts on our typical models which can reach values of several times those encountered during steady flow. A similar phenomenon, although less severe, occurs at the opening of the valve. Because of the physical characteristics of the DREV wind tunnel and the high aspect ratio of tested models, overloads in yawing moments are dominant. A number of balance failures were experienced in spite of the number of precursor runs conducted to determine the amplitudes of possible overloads. In some cases balances are used at 10% of rated capacity during steady flow. This results into poor resolution of measurements at minimum loading. The shock loading drives the model/sting assembly

into resonance modes which add efforts due to inertia. It is then essential that the balance be strong enough to withstand the starting/stopping transients and be sensitive enough to measure the forces and moments at minimum of loading during steady flow conditions.

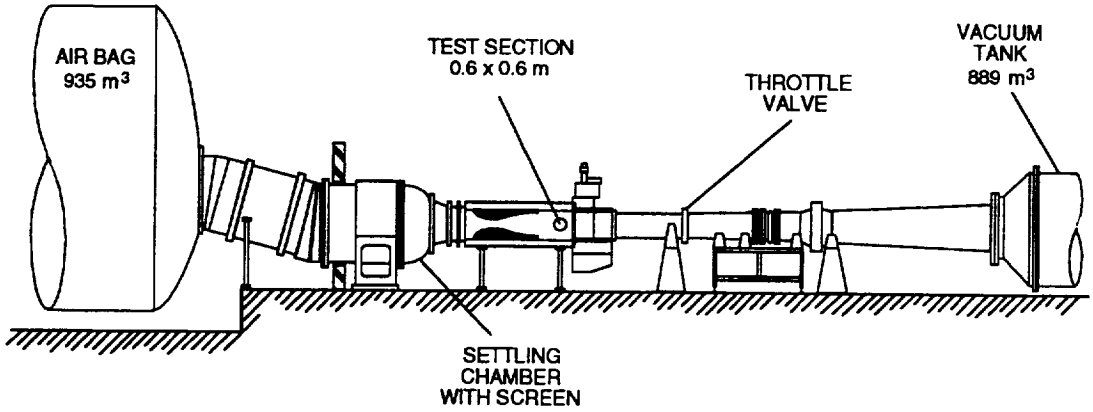

Figure 1. DREV Trisonic Wind Tunnel

Balances currently used at DREV are instrumented with metallic gages and are designed for a high level of stress at rated loads. This approach is necessary because this type of gage produces a low electrical output which must be amplified and filtered in the process of data display. At low level the signal is degraded by the electronic noise and suffers of poor resolution. The design strain level is usually selected at some 2000 microstrain ($\mu\varepsilon$) and offers little tolerance to overloads. Advantage of the full gage deformation range, which is in the order of 30,000 $\mu\varepsilon$, cannot be taken because of its incompatibility with the elasticity limits of the steel alloys used to manufacture balances. Even if it was possible to use higher elastic limits, it would not be desirable since the balance would become too flexible. The current concepts of floating frame balances use several articulated components linked by pivots, pins and screws and by design minimize interaction between effort component outputs. This further degrades the signal reliability at low level of loading because of mechanical microdisplacements and hysteresis in load transfer to sensing structures.

DREV Balance Design

It was then decided to design a 6 Degree-of-Freedom (DOF) wind tunnel balance that would be more adequate for the DREV applications. To meet most of our current needs it had to be 0.500 inch in diameter and satisfy the following specifications:

	Rated Load	Safe Overload	Limit
Normal Force (lb)	15	100	150
Side Force (lb)	10	60	90
Pitching Moment (in-lb)	15	100	150
Yawing Moment (in-lb)	8	50	75
Axial Force (lb)	10	50	75
Rolling Moment (in-lb)	3	15	25

The design involved consideration on material properties, the sensing structures and the instrumentation of sensing elements.

MATERIALS CONSIDERED

A high modulus of elasticity is required to achieve a high resonant frequency of the balance/model assembly, minimizing the chance that it can be excited under the overload transients. Good thermal conductivity is essential to allow dissipation of the heat generated at the instrumented sites. The heat generated on the small instrumented structures could cause material distortion and measurement errors. Good thermal characteristics would minimize temperature gradients in the balance assuring a constant temperature across the arms of load sensing bridges. Errors due to temperature gradients are difficult to trace and to compensate for. Other characteristics such as response linearity and absence of creep and hysteresis can be controlled by operating the balance at very low level of deformation and will be discussed later.

Once materials having undesirable characteristics have been eliminated, a short list of candidates remained. The properties of those found on top of the list are in Table I.

BALANCE STRUCTURE

For the best repeatability of the balance outputs, the response of its sensing elements must show no or negligible hysteresis. This was achieved through the manufacturing of the balance from a single piece of material and through the design for small deformations at rated loads. Joints made of welding, bonding and screws have been avoided. Mechanical connections are sources of displacements and friction, therefore of hysteresis and non-linearity. Welding can cause metallurgical effects decreasing resistance to fatigue. A foreseeable consequence of the monopiece construction is the increase of interference between loading components. Because of inherent non-linearity effects, a loading component will produce a significant output at non-intended bridges. However, this can be taken into account as long as a unique load condition can be computed for all possible vectors of balance outputs.

A schematic drawing of the new design is shown in Fig. 2. The balance is made of an instrumented core fitted on the tunnel sting through a conical attachment. The load is transmitted to the core through a covering outer shell fitting tightly into the test model.

As forces and moments are applied to the model the effort is taken by instrumented elements built into the centre core of the balance. The small yet measurable deformations measured with strain gages must be uniquely related to the 6 components of the load. As depicted on the schematic (Fig. 2) a hollow cruciform structure is machined at the forward and aft ends of the core, on which strain gages are intended to be mounted. Symmetry in deformations is used to build four-active-arm Wheatstone bridges making each bridge sensitive to the intended load component and rejecting the effects of the other components.

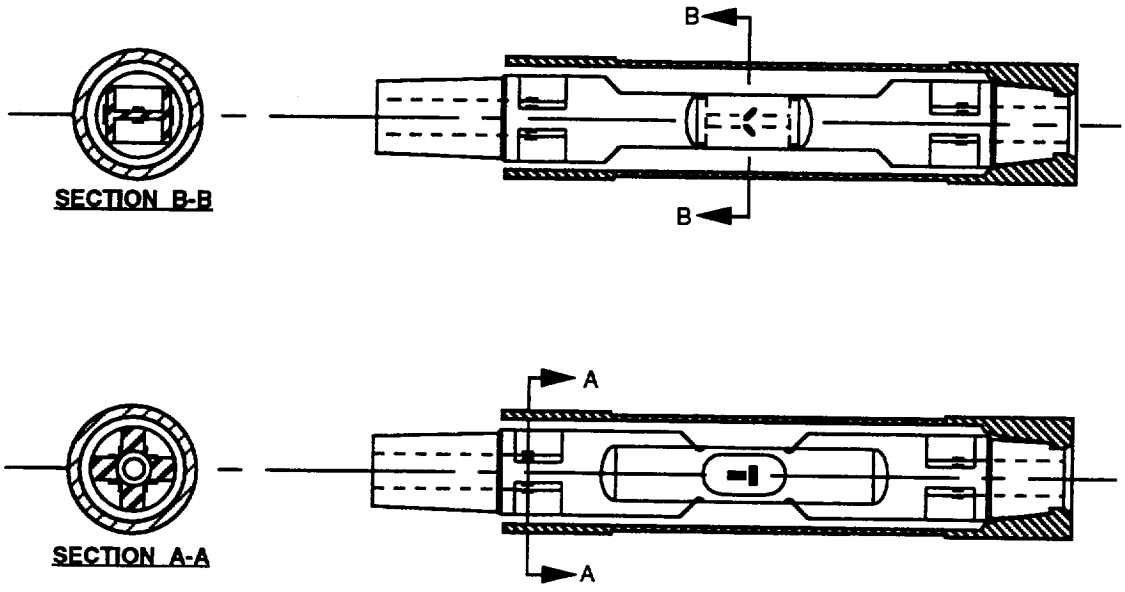

Figure 2. Monopiece Wind Tunnel Balance Sensing Structures

The forward cruciform structure senses forward normal and side forces whereas the aft counterpart provides signals proportional to the aft normal and side forces. This structure can give a relatively large local strain for a small displacement.

The third sensing structure of the core is an H-beam section sensitive to axial force and rolling moment. The axial force is determined from the axial deformation of the web and the rolling moment from the shear deformation of the flange of the beam. In the latter case gages at 45° to the centreline are mounted in a bridge to have additive contribution in the rolling mode and destructive contribution in the tension and bending modes.

Design for Overload Protection

Protection against overload is implemented by designing the sensing elements with a large safety factor with respect to the yield strength, σ_{YP}, of the material. Current transducer design uses a safety factor of 2 coupled with an overload capacity of 100% of rated load. For the present design an overload capacity of 1000% was selected. If this approach is applied to the retained list of materials, the following strain levels are obtained for the rated loads:

Material	Yield Strength (psi x 10^{-3})	Design Strain (ε) μm/m
Steel E4340	210	350
Stainless Steel 17-4PH	185	323
Stainless Steel PH 15-7Mo	220	380
Ferro-Tic	250	284

One balance of each type of stainless steel was manufactured using Electrical Discharge Machining (EDM). The centre core and the outshell were heat treated. Grinding of the conical ends was required to meet conical fixation specifications.

INSTRUMENTING THE SENSING STRUCTURES

Two types of strain gages are available for transducer instrumentation: the metallic type and the semiconductor type. It is interesting to compare their maximum elongation to the maximum elongation (σ_{YP}/E) of a commonly used steel or its commonly accepted linear range that is 50% of the elastic range:

Material	Gage Factor (G)	Maximum Strain (μm/m)
Metallic gage	2	30,000
Semiconductor gage	50-200	3,000
Typical Steel	N/A	3,550 (linear range)

It is obvious from the above that the elongation range of the metallic gage is not well adapted with the steel, being 10 times its linear range. However, the semiconductor gage is better adapted. It's elongation range is of the same range as the steel linear range.

However, the overload protection of an instrumented structure must be computed from the lower elongation permitted by the instrumenting gage and the support structure. For comparison purposes, we can compute the rated bridge output for both types of gages bonded on a steel balance. We suppose here that the resistance of each gage be 350Ω and heat dissipated be 1mW per gage.

Gage	Resistance	Heat Dissipated (mW)	G	Strain Design	Rated Output (mV)
Metallic	350	1	2	355	0.84
Semiconductor	350	1	130	300	46

The gain of using semiconductor gages is obvious and is particularly important if we consider that DREV balances are often used at less than 1% of their rated loads e.g. at Mach 4.0 and at zero angle-of-attack. The metallic gage would then give 8.4μV. At this signal level the signal to noise ratio is degraded. The amplifier manufacturer specifies the noise voltage be of 1μV at a bandwidth of

10 Hz. In the wind tunnel environment involving long lengths of cables this figure is multiplied by a small factor.

Simulation of Temperature Effects

Opting for semiconductor gages raised a lot of concerns about their response to temperature. A compromise between sensitivity and stability must be selected.

There are two basic thermal effects which apply to semiconductor strain gages: the Thermal Coefficient of Resistance (TCR) and the Thermal Coefficient of Gage Factor (TCGF). Additional thermal effects include those due to gage-substrate thermal expansion coefficient mismatch and gage self heating.

The TCR describes the change in strain gage resistance with temperature. For a full Wheatstone bridge, Fig. 3, to be balanced, the resistance, R, of each of the four arms must be equal or satisfy the condition:

$$R_1 R_3 = R_2 R_4 \tag{1}$$

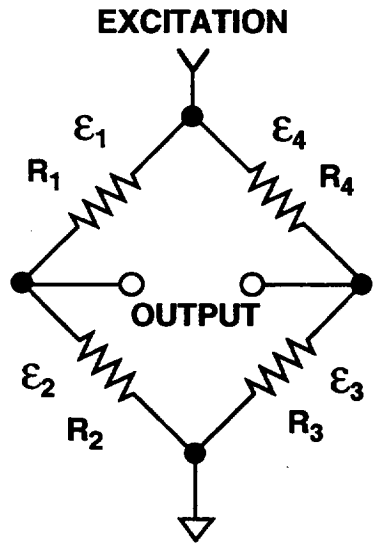

Figure 3. Wheatstone Bridge Nomenclature

If the arms of the bridge are subjected to a temperature change, the bridge will exhibit some zero-load shift unless the TCR of each arm is identical, or obeys the condition:

$$\left(1+\frac{\Delta R_2}{R_2}\right)\left(1+\frac{\Delta R_4}{R_4}\right)=\left(1+\frac{\Delta R_1}{R_1}\right)\left(1+\frac{\Delta R_3}{R_3}\right) \tag{2}$$

over the operating temperature range. Manufacturers of semiconductor gages use computer matching to produce sets of four semiconductor gages with nearly identical resistance and TCR. However, it is difficult to bond a set of four gages to a material and ensure that each gage resistance and TCR are identical. Therefore any practical bridge will display some zero-load output and thermal null shift.

The thermal coefficient of gage factor (TCFG) describes a semiconductor strain gage's variation in sensitivity with temperature. The gage factor, G, and the TCGF of a semiconductor gage are determined by the doping level of the semiconductor crystal. Unfortunately, the TCGF increases with gage factor (i.e. the greater the sensitivity of the gage the greater variation in gage sensitivity with temperature). For example, a semiconductor gage with a gage factor of 175 at 70°F will show a variation in gage factor of approximately -23%/100°F while a gage with a gage factor of 55 will exhibit a variation of approximately -2%/100°F [1].

The bonded TCR and TCGF of the semiconductor strain gages will depend on the properties of the material to which they are bonded and can be significantly different from the unbonded values. The bonded TCR of a gage can be estimated using:

$$a_b = a + (C_m - C_g)G$$

where a_b and a are the bonded and unbonded TCR of the gage, and C_m and C_g are the thermal expansion coefficients of the material and the gage respectively. The bonded TCGF of a gage can be approximated using the relationship:

$$\beta_b = \beta + \gamma$$

where β_b and β are the bonded and unbonded TCGF of the gage, and γ is the temperature coefficient of Young's Modulus (also known as the "thermoelastic coefficient").

The above equations show that the properties of the balance material will have to be considered in the simulation.

The heat, P, generated by a strain gage, is dependent on the applied voltage, V, or the applied current, I, and the resistance of the gage, R:

$$P = V^2 / R = I^2 R$$

The excitation voltage or current will be limited by self-heating considerations and therefore dependent on the surface area of the gage, the effectiveness of the balance as a heat sink, and the gage resistance.

Computer Simulation

Under contract, Martec Limited developed a computer model to simulate the semiconductor gages and accompanying circuitry required for temperature compensation of zero-load shift and sensitivity shift. The model can be used to select the strain gages and compensation circuitry necessary to meet the balance performance characteristics over the ambient temperature range. The

strain gage instrumentation must also be compatible with the existing transducer conditioning amplifiers at DREV.

The strain gage system was modeled using The MathWorks Inc. Software MATLAB with the SIMULINK toolbox [2]. SIMULINK was used to model the semiconductor strain gage systems of the balances with the MATLAB package used to analyze and present the results of the simulations. The computer simulation of the bridge circuitry takes into account the gage characteristics, the capabilities of the existing signal processing equipment at DREV, and the effect of transient temperature. The following factors are included in the models:

- Variation in gage resistance with temperature (TCR);
- Variation in gage factor with temperature (TCGF);
- Balance material (coefficient of thermal expansion, thermoelastic coefficient);
- The effect of resistive compensation circuits (zero-load and sensitivity shifts);
- Strain gage linearity;
- Strain gage resistance;
- Gage prestrain developed by curing the adhesive;
- Strain gage property tolerances;
- Compensation resistor characteristics (discrete values and TCR); and
- Excitation (constant current or constant voltage).

The model inputs include gage resistance, TCR, and TCGF, material coefficient of thermal expansion, gage prestrain, material strain at each gage location, temperature of each gage, and excitation magnitude. For each temperature step, the model outputs bridge sensitivity to strain, the zero-load and maximum strain output voltages, and the power dissipation for each gage. The model also outputs other bridge variables such as the applied bridge excitation, measured strain, total bridge resistance, and the individual gage TCR, TCGF, gage factor, resistance and temperature. The outputs that are monitored are the effective zero load bridge resistance (thermal null shift), bridge null, and gage heat output. The output data was used to calculate zero load shift, sensitivity shift, and bridge sensitivity to strain.

Two models were produced; one to simulate a full Wheatstone Bridge using constant voltage excitation; and a second simulating constant current excitation. The two computer models allow for null and zero-load shift compensation by either of two compensation methods: the method using parallel and series resistors; and the method using a pair of parallel resistors only [1,3,4]. The models also allow for three types of sensitivity compensation: one using a resistor with zero TCR [1,3,4]; a second using a resistor in parallel with a thermistor [1,3,4]; and a third using a resistor with zero TCR in series with another resistor in parallel with a thermistor [3]. For details on compensation methods the reader should consult the references.

The software was applied to the new balance design using the following specification on the resulting effects of temperature:

Operating Temperature Range (TR):	60 to 90°F (15 to 32°C)
Zero-load output shift over TR:	<0.1% of rated load output
Sensitivity shift over TR:	<0.5% of rated sensitivity
Effect of compensating circuit on bridge sensitivity to unintended load components	<5% of maximum strain output

The semiconductor gage family selected for the analysis was a series of Kulite Semiconductor Products. Properties of this series of gages and manufacturing tolerances are given in Table 2.

Simulation runs were performed to determine strain gage performance over the Operating Temperature Range. The runs were performed on both the constant current and constant voltage models in order to compare the performance of the two excitation techniques. Runs were conducted using the properties of AISI 4340 steel, Ferro-Tic and Stainless Steel 17-4PH to determine the effect of material properties. Material Properties of Table I were used.

The first step in the analysis was to determine the range of bridge performance without any compensation when the gage parameters were varied over their tolerance ranges. The variables tested during the simulation runs included gage factor, TCR, TCGF, linearity, gage resistance, average balance temperature, material strain, and magnitude of the excitation. All of the parameters mentioned have been varied over their tolerance ranges for the individual gages within a bridge. From these runs it was possible to determine the gage parameter values which gave the worst case situations with respect to zero-load shift and sensitivity shift. The next step in the analysis was to simulate combinations of the two zero-load shift compensation methods and the three sensitivity compensation methods to determine bridge performance for the worst case situations.

The results of the simulation runs were also used to determine the probability of not being able to compensate for thermal effects to within the required specifications based on the range of gage tolerances. This analysis assumed that the gage parameter values are evenly distributed over tolerance ranges.

Several assumptions were made during the simulation runs. First, the maximum strain in the balance was assumed to be 300 microstrain for the calculation of null shift and sensitivity shift. Second, prestrain in the gages was calculated based on an adhesive cure temperature of 350°F. Third, no temperature gradients exist between gages in a bridge.

Zero-load shift was determined for each 10°F temperature increment as a percentage of the average bridge output at maximum strain of 300 microstrain. Sensitivity shift over the ambient temperature range was calculated as the change in bridge output per unit strain as a percentage of the

average bridge output over the half the temperature range (this assumes that the balances would be calibrated at the middle of the ambient temperature range). The temperature Compensation Circuit Interference (CCI) was computed as:

$$CCI = \frac{\textit{Output with destructive strain effects}}{\textit{Output with additive strain effects}}$$

MODEL ANALYSIS RESULTS

Some 6561 cases were studied where the parameters were individually varied. For all cases temperature compensation circuits were simulated and zero-load output and sensitivity drifts were computed. Table 3 gives the results of the simulations for constant voltage excitation. It can be observed that the UDP and UEP gages have the lowest drift figures and best meet the specifications. Similar results were obtained for constant current excitation. Although the UDP gage gives better results than the UEP the latter is preferred because of its smaller size.

The optimum configurations were found to use constant current excitation and the zero-load shift compensation techniques using a series and parallel resistor and the sensitivity compensation technique using a single resistor in parallel with the bridge.

Table 4 shows the probability of zero-shift exceeding 0.1% for both the UDP and UEP gages. It is less than 0.4% when these gages are mounted on any of the selected materials. During the simulations conducted the maximum null shift computed was 0.16%.

Table 5 shows the probability of sensitivity shift exceeding 0.5% for a temperature change of 15°F for the selected gages on the two types of materials. This temperature change assumes that the balance is calibrated at 75°F and then used at temperatures over the ambient temperature range of 60°F to 90°F. The probability of sensitivity shift exceeding 0.5% without temperature compensation is 100% for the selected gages on the two materials and thus sensitivity compensation will be required to reduce the sensitivity shift below 0.5% for a 15°F temperature change. From Table 5 we see that the probability of sensitivity shift exceeding 0.5% for a 15°F temperature change is low (less than 0.8%) on the simulated materials with temperature compensation in place. Thus by placing a compensation resistor in the circuit for all bridges it is reasonably certain that the sensitivity shift will be less than 0.5% for a 15°F temperature change (i.e. for balance calibration at 75°F). However, as sensitivity shift improves, both sensitivity and power efficiency decrease. The sensitivity can be increased by increasing the current supplied to the circuit. Table 4 gives the excitation levels required to bring the average power dissipated by each arm of the bridge to 1 mW and the resulting sensitivity of the bridge. Note that the sensitivity values are based on the bridge output without amplification by the signal conditioning equipment. The signal conditioning equipment available at DREV is capable of gains up to 2500, thus the bridge output and sensitivities can be amplified up to 2500 times the values given (e.g. the gage bridges have a sensitivity of 0.13 mV/microstrain which can be amplified to 2500x0.13 = 325 mV/microstrain).

The probability of interactions due to compensating circuits being increased by 5% is 0.8%. This probability was determined using 324 simulation runs on each balance material. The maximum interactions for the 4340 steel and Ferro-Tic balances were 6.8% and 8.7% respectively.

FOLLOW-ON ACTIVITIES

The new balance is being instrumented by Kulite Semiconductor Products using the UEP gages. After resistance and TCR characteristics of individual gages are measured, Martec Limited will compute and install the temperature effect compensating circuits. Complete calibration at two temperatures will be necessary before sensitivity drift compensation circuit can be computed and mounted.

So far only the sensing structures were analysed on finite element analysis tools for the balance design. A complete analysis will be done to help to understand the expected interactions between the loading components and to provide information that could be useful for future versions of this balance.

CONCLUSION

The wind tunnel balances used so far in the DREV wind tunnel had to be operated during the air flow at a low level of effort with respect to the rated loads to account for existing flow start and stop transients. Pre-test runs were necessary before a model is tested to provide information on the maximum loads that could be encountered. The balance signals generated by the metallic gages were sometimes low particularly at high Mach No and low angle of attack. It is hoped that the new balance being instrumented with gages having a sensitivity which is sixty times the ones used on the present balances will provide a better signal-to-noise ratio and thereby better accuracy. The simulating tool developed by Martec persuaded of this feasibility and has been useful to select suitable gage types. It will also be used to compute resistor values required for the temperature effects compensation circuits.

REFERENCES

[1] "Kulite Semiconductor Strain Gage Manual", KSGM-3 Kulite Semiconductor Products, Inc., One Willow Tree Road, Leonia, New Jersey.

[2] "SIMULINK User Guide", The Mathworks, Inc., Natwick, Massachusetts, 1993.

[3] "Etude Theorique et Expérimentale d'un Nouveau Concept de Balance pour la Soufflerie à Aspiration du CRDV", SORENCO LTEE, Mars 1991 Volumes 1 and 2.

[4] A.L. Window and G.S. Holistor, "Strain Gage Technology", Applied Science Pub. London, 1982.

TABLE I: Material Properties				
Material	Modulus of Elasticity (E)	Yield Strength	Coefficient of Thermal Expansion	Thermal Conductivity
	psi x 10^{-6}	psi x 10^{-3}	ppm/ °F	BTU/in.h.°F
Steel E4340	30	210	6.3	1.8
Stainless Steel 17-4PH	28.5	185	6	0.94
Stainless Steel PH 15-7Mo	29	220	5	0.76
Ferro-Tic	44	250	8	0.42

TABLE 2: Kulite Gage Characteristics						
Gage Code	Resistance Ω	Gage Factor	TCR (%100°F)	TCGF (%100°F)	Linearity (%)	Thermal Expansion Coefficient (ppm/°F)
UCP-120-090	120±1%	100±2%	4±1	-6±2	±0.5	1.4
UDP-350-160	350±1%	115±2%	3±1	-8±2	±0.5	1.4
UEP-350-060	350±1%	130±2%	6±1	-10±2	±1.0	1.4
UFP-750-090	750±1%	140±2%	10±1	-11±2	±1.3	1.4
UGP-1000-060	1000±1%	155±2%	18±1	-13±2	±1.5	1.4
UHP-5000-060	5000±1%	175±2%	45±1	-23±2	±3	1.4
ULP-120-160	120±1%	55±2%	12±1	-2±2	±0.02	3.1

TABLE 3: Constant Voltage Bridge Performance Results With Power Set to 1 mW (Cm=6x10^{-6}/°F)							
Gage	UHP	UGP	UFP	UEP	UDP	UCP	ULP
Sensitivity (mV/μstrain)	0.66 ±0.06	0.26 ±0.05	0.21 ±0.03	0.14 ±0.03	0.12 ±0.04	0.06 ±0.01	0.04 ±0.00
Null (mV)	-0.44 ±0.64	-0.03 ±0.33	-0.01 ±0.09	0.00 ±0.05	0.00 ±0.03	0.00 ±0.02	0.00 ±0.02
Sensitivity Shift (%)	0.28 ±0.11	0.14 ±0.06	0.10 ±0.06	0.08 ±0.05	0.06 ±0.04	0.06 ±0.05	0.09 ±0.09
Null Shift (%)	0.24 ±0.24	0.10 ±0.10	0.07 ±0.07	0.06 ±0.06	0.04 ±0.04	0.05 ±0.05	0.09 ±0.09
Power (mW)	1.00 ±0.15	1.00 ±0.13	1.00 ±0.07	1.00 ±0.16	1.00 ±0.39	1.00 ±0.05	1.00 ±0.06
Excitation, Vi (V)	6.2	3.0	3.2	3.1	4.2	1.2	0.7

TABLE 4: Probability of Zero Load Shift Exceeding 0.1% of Maximum Output for a 10°F Temperature Change			
Gage Code	Material	Probability Null Shift›0.1% (%)	Max. Null Shift (%)
UDP-120-045	4340 Steel and Stainless Steel	0	0.08
UDP-120-045	Ferro-Tic	0.4	0.13
UEP-350-060	4340 Steel and Stainless Steel	0.4	0.11
UEP-350-060	Ferro-Tic	0.4	0.16

TABLE 5: Probability of Sensitivity Shift Exceeding 0.5% and 1.0% of Sensitivity for a 15°F Temperature Change (60 to 90°F) with Sensitivity Compensation (Gage Heat Output Set at 1 mW)						
Gage Code	Material	Compensation Resistor Ω	Prob. (%) Sens. Shift >0.5%	Prob. (%) Sens. Shift >1.0%	Excitation, Ii (mA)	Sensitivity (mV/με)
UDP-120-045	4340 Steel and Stainless Steel	200	18.2	0.3	9.6	0.07
UDP-120-045	Ferro-Tic	70	11.3	0.8	15.2	0.07
UEP-350-060	4340 Steel and Stainless Steel	400	18.2	0.3	6.5	0.13
UEP-350-060	Ferro-Tic	180	11.3	0.8	9.6	0.13

A New Master Balance for the MK15 Calibration Rig at FFA

by G. I. Johnson
FFA (The Aeronautical Research Institute of Sweden)

Abstract

The automated MK15 rig is used at FFA for calibration of wind tunnel balances with up to six components and typically a normal force of up to 50 kN.

This rig is equipped with a dedicated computer for control of calibration loads and for processing of calibration results.

For convenient production calibration the MK15 rig is optionally equipped with a master balance attached to the rig table. After an initial separate calibration of the master balance, the wind tunnel balance, here called the object balance, is installed on the master balance, whereby the two balances are coupled in series. Calibration loads are then applied to the object balance for production calibration, based on common load components as indicated by the master balance.

However, application of the master balance has implied an extension of the distance from the object balance to the calibration rig table. Accompanying long moment arms from normal and side force load lines to the plane of master balance sensors, may induce relatively strong interactions from these components leading to impaired resolution and accuracy of the balance. Similarly high parting forces may occur in the attachment joints as magnifications of normal and side forces by the moment arms. This may lead to slippage and relocation of contact forces, which would appear as hysteresis in calibration results.

It is reported here how above difficulties can be avoided by appropriate design of the master balance, with the purpose of also maintaining calibration accuracy over an extended range of calibration loads for a variety of object balances.

Brief Review on the Wind Tunnel Balance Concept

General

Wind tunnel testing is an important tool for flight performance prediction on any new or modified type of aeroplane. For this purpose it is essential to measure force and moment vectors acting on the aeroplane model suspended in the wind tunnel air stream.

The wind tunnel balance (Figure 1) meets this requirement by measuring in the general case six components, three force components and three moment components in an orthogonal coordinate system to determine the force and moment vectors.

Wind tunnel balances are distinguished as either external or internal according to their location outside or inside the model. Beside its measuring function the wind tunnel balance also serves as a link for suspension of the model in the air stream and therefore must be safe against breakage, since such a failure would be disastrous to the whole wind tunnel installation.

Design aspects

The wind tunnel balance design, commonly based on resistance strain gages, is a rather tricky business particularly for internal balances because of the requirements of strength, limited space and high strain signal output. A ratio of about 20:1 between the strongest and weakest components, usually the normal and the axial forces, makes design of balances even more tricky. In addition there is a demand for highest possible accuracy on the weak axial force since fuel economy of any projected aircraft is important.

The end result of wind tunnel balance application would be complete separation for each one of three components along given coordinate axes for resultant load vectors of the desired force and moment respectively. This is primarily obtained by mechanical design of the balance with built-in sensors, located to emphasize strain due to component loads.

However, due to such factors as limitations on available space, mechanical and electrical asymmetries, balance output signals show more or less interaction from one component to another [6].

Mechanical interactions would mean that balance strain sensors are exposed to additional loads beside the actual load for any particular component, thereby limiting resolution and accuracy of the result. Furthermore, detrimental effects on balance output may also occur due to temperature gradients and hysteresis.

The problem to obtain desired balance behavior is usually approached in three consecutive steps of development:

1. Mechanically – for basic requirements on strength and component separation with low interactions favored by symmetric balance design. Also sufficient sensor strain levels for high resolution and small temperature influence. For low hysteresis, careful attachment design and whenever applicable, the one-piece balance concept, should be used.
2. Electrically – by active and passive strain gage circuitry for further refinement of component separation, temperature compensation and signal amplification.
3. Mathematically – by application of computer software to acquired raw wind tunnel data for final result of separated components.

Calibration

Balance characteristics may be represented mathematically by a system of polynomials with signals expressed as functions of loads. Corresponding polynomial coefficient matrix is obtained by calibration with known loads in a calibration rig.

Wind Tunnel Application

Installed in the wind tunnel the balance will produce signals to be interpreted by the calibration matrix as force and moment vectors acting on the model by the air flow.

The MK15 Calibration Rig at FFA

The FFA calibration rig, designated as MK15, is of non-repositioning type with vertical roll axis. Built for flexible application it may be used for one to six component loads applied singly or in any combination [2],[3].

The rig frame consists of a rigid central cage with symmetrically located outrigger beams for attachment of loading devices (Figure 2).

Rig dimensions are 4×4×4 m and load capacity is typically 50 kN for normal force and 15 kNm for roll moment.

During calibration the object balance is installed with its model end firmly attached to the center of the cage floor. Loads are applied to the balance sting end by means of the load adapter. In this way calibration load errors due to deflection are minimized. It is noteworthy that actual calibration loads are the reaction loads on the balance model end (Figure 3).

Applied loads are generated by 14 pneumatic actuators, airbellows, attached to the outrigger beams (Figure 4). These loads are determined by means of either precision transducers (Figure 5) on the load linkage or by a master balance (Figure 6), located between the object balance and the rig frame.

Balance deflections due to applied loads are measured by eight dial indicators with digital output resolution of 0.001 mm, and used for load correction by computer.

Internal friction of the rig is kept to a minimum since the only force available to restore balance deflection to zero is obtained by the balance's own elasticity. To facilitate this repositioning, especially for smaller balances, the load linkage is equipped with vibrators.

Initial alignment of master and object balance coordinates to comply with the rig loading system is obtained optically by using a central autocollimator and crosswires in the load attachment ends of the 1.7 m long hollow linkage tubes. Angular resolution is in this way 10 seconds of arc.

Computer Control System

The dedicated rig computer takes care of the following functions (Figure 7):

* Calibration load table generation
* Calibration load application

* Acquisition of calibration load data and signals from object balance, reference balance and deflection sensors
* Computation of load corrections
* Computation of balance matrix and statistics
* Storing of data
* Report presentation

Accuracy and Resolution

Inaccuracy of calibrations in the MK15 rig must for acceptance not exceed a relative standard deviation of 0.1% referred to max load and at no point should the relative error exceed 0.5% in the calibration result.

Resolution of force is in the order of 0.5 N related to the full rig capacity of 50 kN.

Calibration Procedure

Loading tables for calibration are first generated by means of the factorial replication method to minimize the number of data points necessary for required accuracy [1].

The calibration matrix is computed by fitting acquired data points to a polynomial of type:

$$U_i = \sum_{n=1}^{6} a_{in}P_n + \sum_{n=1}^{6} b_{in}|P_n| + \sum_{n=1}^{6}\sum_{m=n}^{6} c_{inm}P_nP_m + \sum_{n=1}^{6} d_{in}P_n^3 + U_{io}$$

where U_i are the balance signals.
a, b, c and d are matrix coefficients.
P are components of resultant force or moment.

Absolute value terms |P| are used for detection of backlash and hysteresis in the balance system. These terms express the quality of balance and calibration but are not included in the matrix delivered to the wind tunnel.

Calibration Time

A typical six component wind tunnel balance calibration may be completed in one day on the MK15 rig by one man. This does not include set-up time.

Principles of the Master Balance

Use of a master balance as an option on the calibration rig is intended for more convenient and faster calibration [5].

In this case the separate master balance is first calibrated to the required high accuracy. This is to some extent facilitated since the master balance is of external type without particular restrictions on size and therefore can be made very stiff with acceptable output signals. Subsequent corrections due to balance deflections under load are small and therefore easy to control for high accuracy of calibration results.

After this precalibration of the master balance the object balance is installed in series with the master balance. Loads applied to the object balance are measured by means of the precalibrated master balance. This makes for fast production calibration since there is no need for time consuming alignment procedure of loads on the object balance. The master balance will correctly measure calibration load components no matter how loads are applied to the object balance.

When the object balance is coupled to a master balance, total calibration error (δ_i) of any balance component (i) is obtained as the square root mean from the individual errors of master and object balances (δ_m) and (δ_o) respectively.

$$(\delta_i) = \sqrt{\delta_{im}^{\ 2} + \delta_{io}^{\ 2}}$$

Master Balance Application

The master balance in use at FFA is shown in figure 6. It is made in one piece as a cylindric shell with a hub and end plate on the top. Cutouts in the cylinder shell provide four vertical beams which measure normal force, side force and roll moment. Similarly cutouts in the top end plate provide horizontal beams used to measure axial force and the moments of pitch and yaw [4].

The master balance is firmly attached to the calibration rig table with the object balance model end fixed to the hub on top of the master balance (Figure 3).

This arrangement, however, means a fairly long distance between the moment centers of the two balances. With vertical roll axis installation of the two balances, calibration loads, particularly normal and side forces, may therefore generate large parting forces in the mating surfaces between the two balances and where the master balance attaches to the rig. These parting forces are in the order of twice the corresponding component loads and may therefore cause hysteresis in the balance output due to slippage or relocation of loads in mating surfaces.

Similarly the master balance sensing elements are exposed high total strain loads. This would appear as a tendency for interactions from normal and side forces to pitch and yaw moments and particularly also to axial force. Accuracy and resolution of these components may therefore be impaired with calibrations based on the master balance.

Above drawbacks of the existing master balance would call for shorter distance between centers of object and master balances.

Accuracy in the MK15 rig with master balance is exemplified by calibration results for the diam 48 mm internal balance, I-690, as follows.

Component	T	C	N	ℓ	m	n
Load capacity (N, Nm)	1000	9000	19000	500	900	500
Inaccuracy rel std dev%	0.292	0.019	0.017	0.055	0.071	0.093

There are certain difficulties to meet required calibration inaccuracy of $< 0.1\%$ using the present type of master balance, particularly for the axial force component. As a way out calibrations often have to be complemented by using axial force data from an external separate tranducer.

The New Type of Master Balance

A new type of master balance has been suggested with a design that avoids the risk of hysteresis and high load on sensing elements. To achieve this, balance attachment to the rig table is raised to a level near the reference center of the object balance e.g. by using a bowl shaped cylindrical master balance surrounding the object balance and its load adapter (Figure 8). The bowl is fixed by an outside flange on its upper rim to the calibration rig table via a cylindrical sleeve of large diameter. The object balance is fixed by its model end to the bottom of the bowl and its sting end attached to the load adapter. Loads to the lower part of the adapter are accommodated thru holes in the sleeve and cylinder.

Sensing elements of the master balance are obtained by cutting horizontal and vertical slots in the upper portion of the bowl cylinder adjacent to the object balance center.

Application of strain gages to corresponding horizontal and vertical beams may be distributed for the various components in such a way that all measured strain signals are produced in bending.

Results of design computations

Computations were made for a master balance of the suggested type based on given dimensions and load range specifications:

New balance data

Specified dimensions

Diameter D = 600 mm
Height H = 250

In the following table load ranges and component strains are shown with distribution on horizontal (H) and vertical (V) type sensor beams.

Component		T	C	N	ℓ	m	n
Load range [N, Nm]	±	1000	2000	5000	500	500	500
Sensor strain [10^{-6}]	±	350	1050	1160	330	1160	1160
Sensor type		H	V	V	V	H	H

Discussion

Mechanical sensor strain levels are relatively low for axial force and rolling moment considering that the projected new master balance has a rather high T/N ratio. However, since total strain load for each sensor would be generally reduced by about 50 % due to absense of long moment arms and related interactions from normal and side forces, output signal levels may be raised by appropriate strain gage circuitry to acceptable resolution.

For the manufacturing of this balance relatively simple machining operations like turning, milling and drilling would suffice. The simplified design of the suggested master balance therefore means it would cost less to make. Because of large diameter and relatively low reaction forces at the rim, it may with special design precautions even be possible to make the balance in separate parts for the cylindric and bottom portions, which would considerably reduce the manufacturing cost. In similar cases with large diameter balances the experience at FFA has been that hysteresis can be avoided by concentrating the attachment bolt loads in mating surfaces to limited raised areas encircling the bolt holes.

Separate parts for bottom and cylinder would also have the advantage of fitting a broader range of object balances requiring different bottom attachments.

Since methods of calibration may differ, it would be of general interest to set up a round robin test on wind tunnel balance calibration for international comparison of results.

Conclusions

Expected advantages of the new master balance

* Reduced moment arms
  - lower interactions from normal and side forces
  - improved accuracy and resolution particularly for axial force, pitch and yaw moments
  - lower parting forces in attachment surfaces
  - less risk for hysteresis
* Closeness between balance centers
  - reduced errors in load transformation
* New master balance flexibility
  - more applicable to different object balances
  - extended use of the MK15 calibration rig
* Simplified design
  - lower manufacturing cost.

Above aspects would help to widen the applicability of MK15 calibrations, particularly into the range of smaller balances with requirements on high accuracy and resolution of the axial component.

Acknowledgment

The author is indebted to FFA personnel Johan Agrell, Sigvard Widmark and Tommy Häggblom for their support of this project, Lennart Hjelmberg and Lars Torngren for proof reading, Arne Nevlén and Birgitta Arhed for editing and typing of the report. Special thanks also to Åke Wallin, Innovationscentrum and Birgit Johansson, SUF for encouragement and economic contributions.

References

[1] Johnson, G.I., "Aspects of wind tunnel data processing at FFA". ICIASF81 Record, IEEE 1981

[2] Johnson, G.I., "Sätt att kalibrera en vindtunnelvåg jämte en kalibreringsrigg för att kalibrera en vindtunnelvåg". Swedish patent 870270-7 (457753)

[3] Han Buzhang, Wang Ming Ying, Johnson G.I., Widmark S., "A preliminary investigation of a method to calibrate wind tunnel balances by means of a reference balance". FFA TN 1990-49, 1990

[4] Häggblom, T., "Flerkomponentlastgivare för kalibrering av vindtunnelvågar". Swedish patent 9201556-8

[5] Wang Ming Ying, Danielsson, L., Widmark S., "Calibration of coupled balances". FFA TN 1992-32, 1992

[6] Fristedt K., "Mätgivare för kraft-, böj- eller vridmoment." FFA Memo 107, 1976

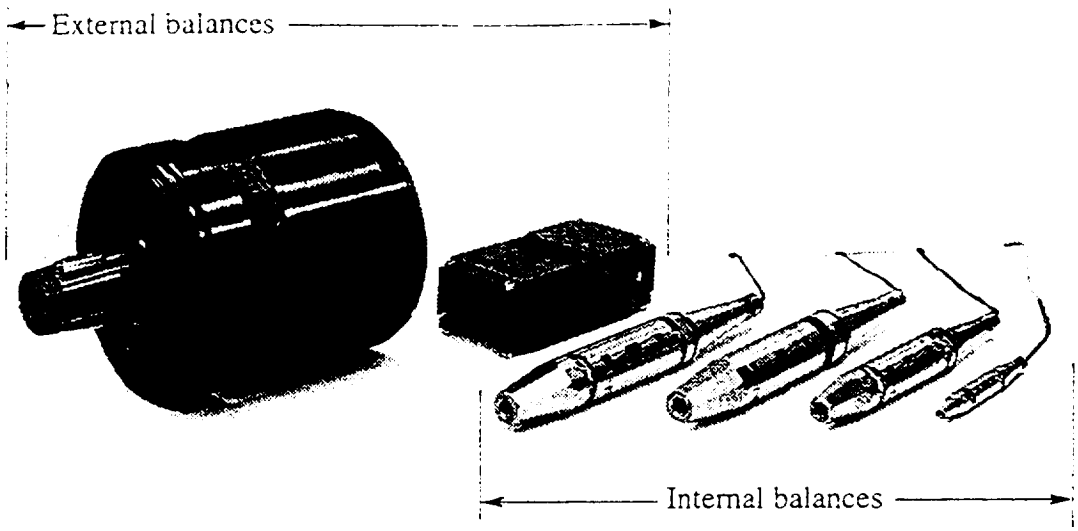

Figure 1. Various types of wind tunnel balances.

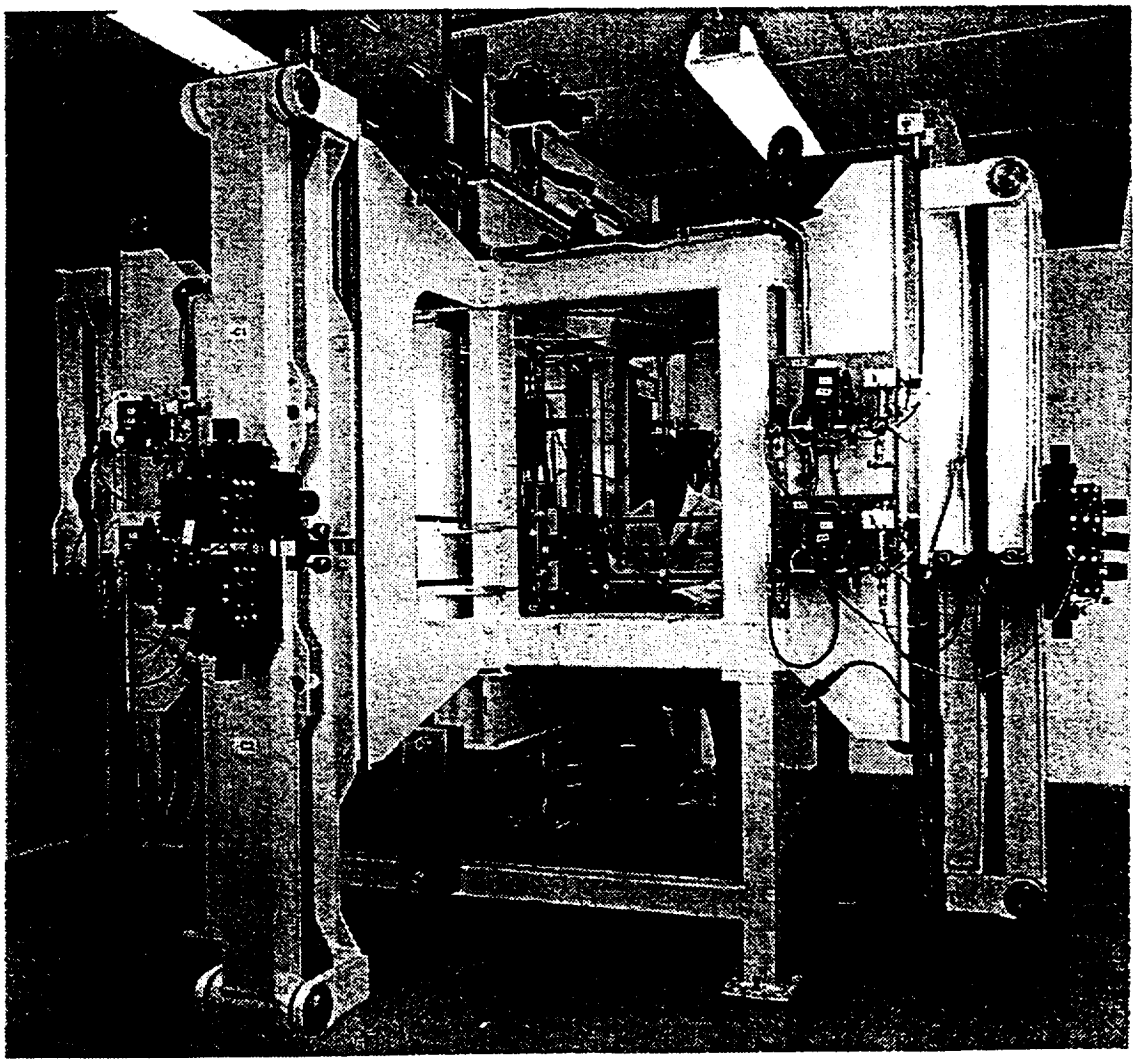

Figure 2. The MK15 calibration rig.

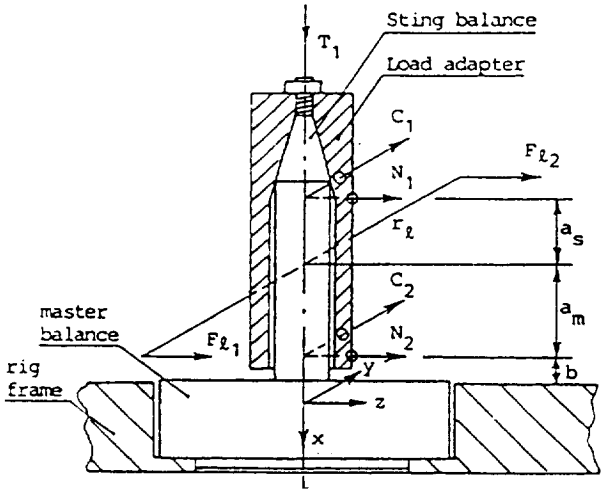

Normal force: $N = -[N_1+N_2]$
Pitch moment: $m = -[N_1(a_m+a_s+b)+N_2 \cdot b]$
Side force: $C = -[C_1+C_2]$
Yaw moment: $n = +[C_1(a_m+a_s+b)+C_2 \cdot b]$
Axial force: $T = -[T_1]$
Roll moment: $\ell = -[F_{\ell 2}-F_{\ell 1}]r_\ell$

Figure 3. Principle of load system on the MK15 calibration rig with master balance.

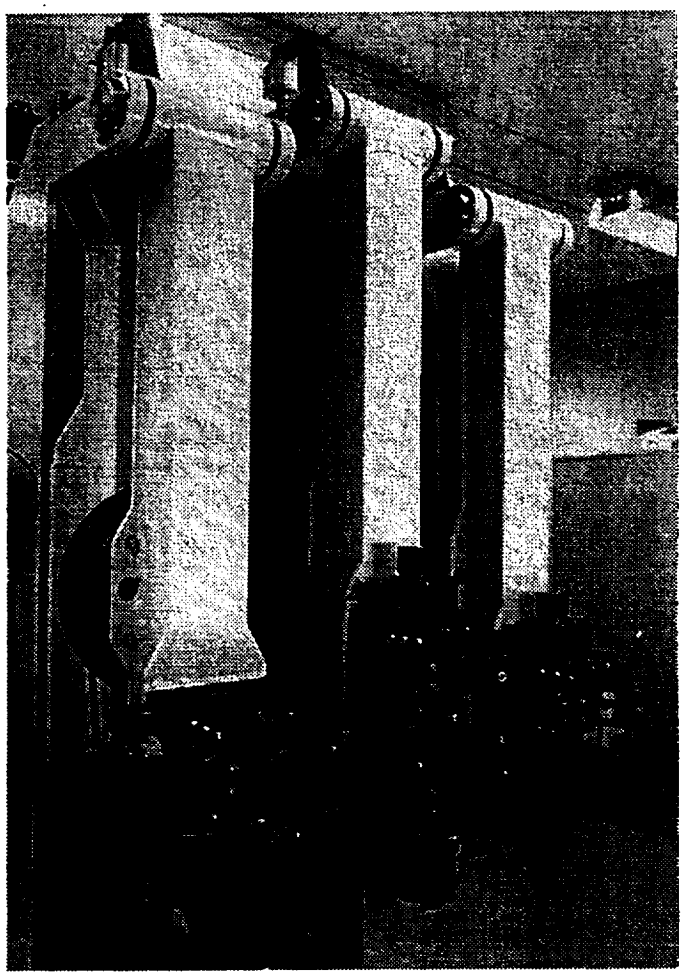

Figure 4. Pneumatic loading mechanism on the MK15 rig.

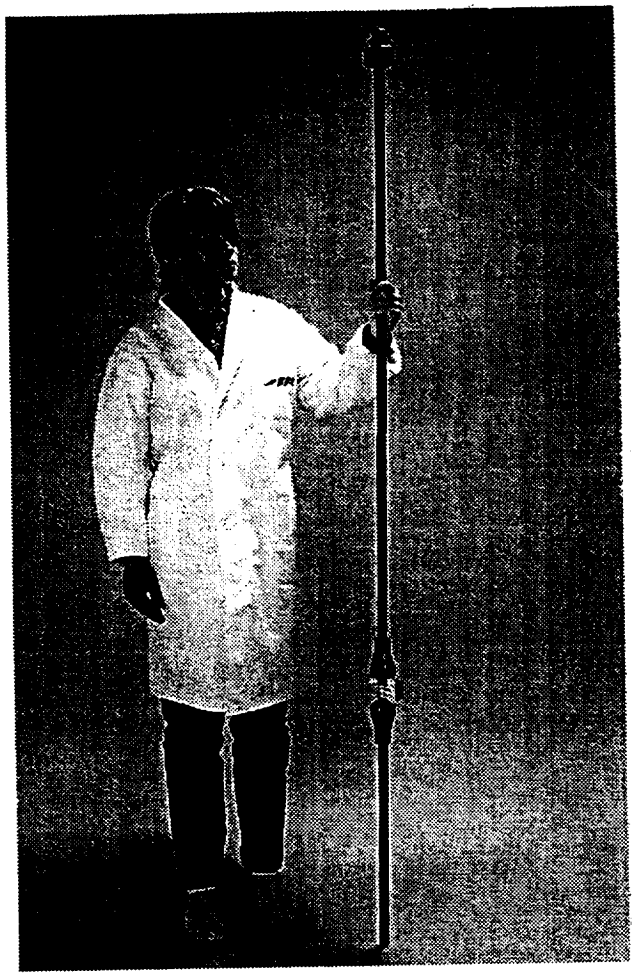

Figure 5. Load linkage with transducer.

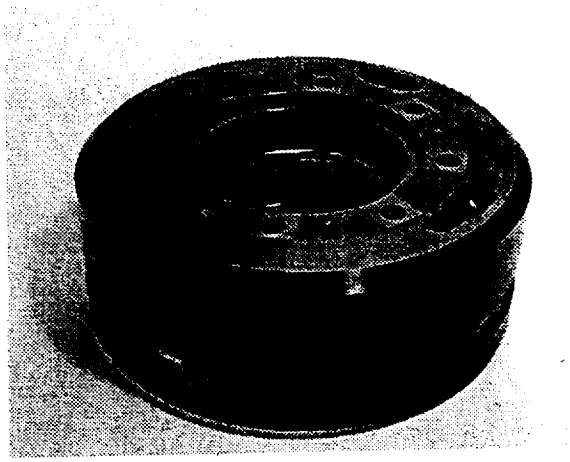

Figure 6. Master balance

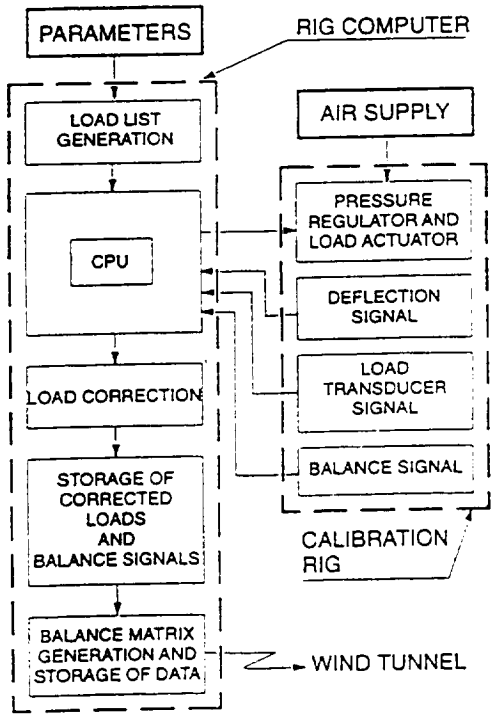

Figure 7. Computer control system

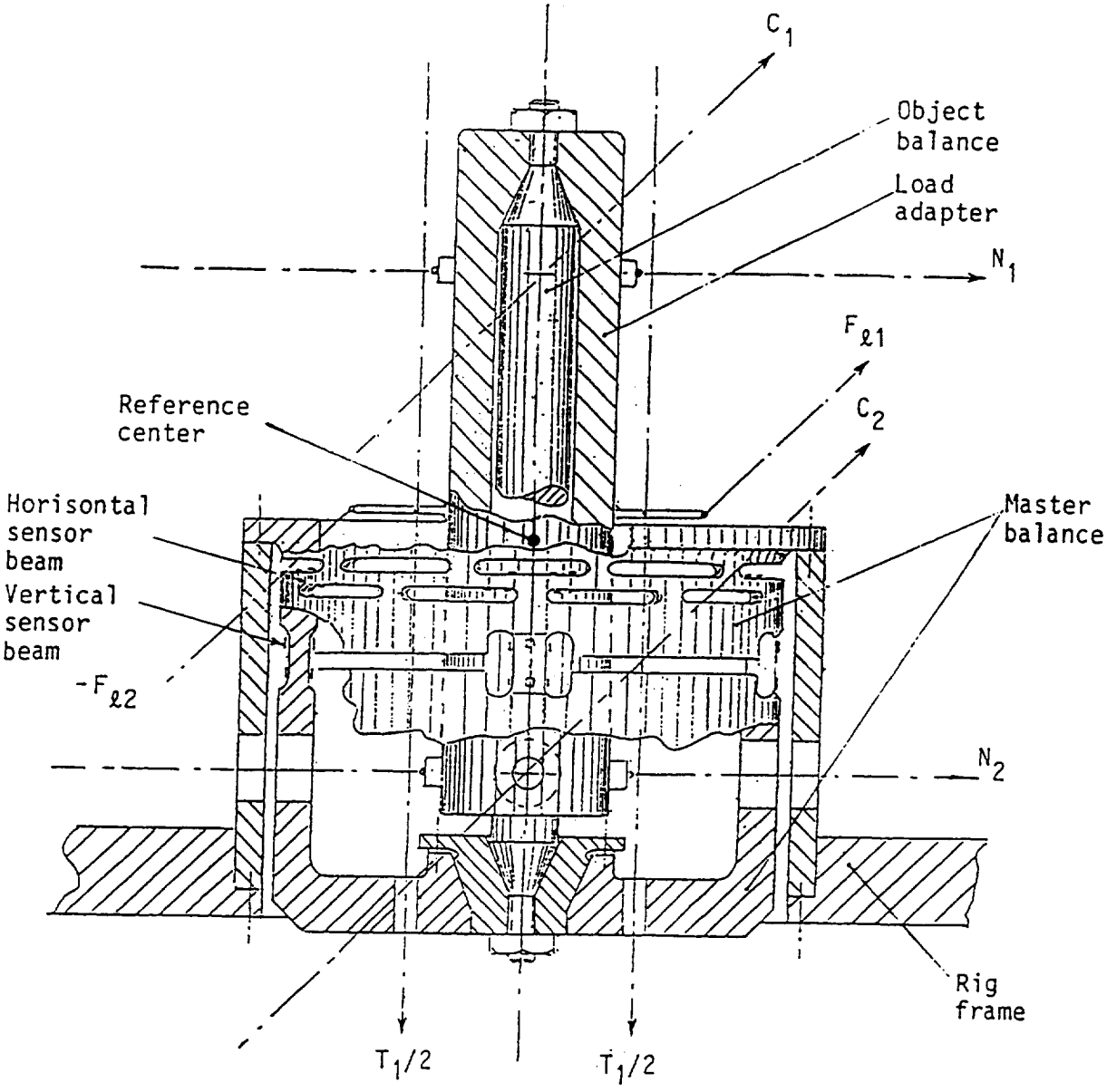

Figure 8. The new type of master balance.

DEVELOPMENT OF A FIVE COMPONENT BALANCE AS AN INTEGRAL PART OF A CONTROL SURFACE

Naresh R. Patel
Modern Machine & Tool Co., Inc.
Newport News, VA

SUMMARY

A five component balance has been designed, manufactured and calibrated at Modern Machine & Tool Co., Inc.. The balance is used to measure aerodynamic forces on wind tunnel test models. The balance was designed to measure Normal Force, Axial Force, Pitching Moment, Rolling Moment and Yawing Moment generated on a horizontal stabilizer of a wind tunnel test model. A unique feature of the balance is that the load carrying strain gaged flexures were machined as an integral part of the control surface due to space limitations. This was accomplished by using the electrical discharge machining process. The integral design eliminates mechanical joints and greatly reduces errors due to hysteresis. The five component integral control surface balance has demonstrated performance comparable to wind tunnel balances used currently in the aerospace industry.

INTRODUCTION

Historically multicomponent strain gage balances have been designed and used to measure aerodynamic loads on wind tunnel test model control surfaces. Typically on a horizontal control surface, Normal Force (vertical shear), Pitching Moment (torsional moment) and Rolling Moment (bending moment) are measured by a balance as an integral or non-integral part of the control surface. The requirements of the subject balance included the capability to measure Axial Force and Yawing Moment in addition to the other three components normally measured. Side Force is not usually measured on horizontal control surfaces. Due to physical constraints, it was not possible to install a separate balance into the control surface. Therefore, the balance had to be designed as an integral part of the test model. Measurement of a light Axial Force in the presence of other high loads also created a challenge for the designer. The challenge was to create a flexure arrangement in a very limited space with flexures being capable of resolving all forces accurately. The unique design features, use of high strength nickel steel, electrical discharge machining, precision strain gage installation and accurate calibration have resulted in a balance meeting all design requirements with very high accuracy.

This paper will discuss the design, fabrication, strain gaging, calibration and data evaluation of the five component integral control surface balance. This balance was designed to measure the aerodynamic forces generated on a horizontal stabilizer of a wind tunnel test model (Figure 1). Balance requirements for the wind tunnel tests are shown in Table 1.

DESIGN

Figure 2 shows details of the five component balance. This balance consists of a spindle with clutch teeth, flexures instrumented with strain gages, lead wires from strain gages, cover plates and mountings for a calibration fixture. The horizontal stabilizer was assembled to the fuselage by four bolts located on the clutch plate of the spindle. Clutch teeth on the spindle allowed angle of attack adjustment of the horizontal stabilizer. Cover plates blending with the mold line were designed and installed to protect the strain gage circuitry and allowed smooth air flow over the horizontal stabilizer. Precisely machined counter bores for mounting of tooling balls during fabrication were later used for mounting of the calibration fixture.

In order to provide a rigid joint and to minimize the influence of mounting stresses on flexures, the moment center of the flexure system was located 2.00 inches away from the root of the horizontal stabilizer. Also the balance moment center instead of being in line with the spindle center line was shifted aft to achieve clearance under the cover plates. Balance design loads were recomputed with reference to the balance moment center.

The most demanding challenge of this balance was to design the flexure arrangement in a very limited space and to resolve relatively high loads. Another challenge was to accurately measure 40 lb. of Axial Force in the presence of 250 lb. of Normal Force. For the design and analysis of flexures, a custom iterative computer program was developed. The dimensions of the flexures were entered into the program to compute stresses due to each component at critical points, spring constants in all directions, deflection in each direction, load sharing among flexures due to each component, stresses at strain gage locations and maximum combined stress. After analyzing these results logically, one or more dimensions of the flexures were modified and the results re-computed. This iterative process was repeated until the design met all requirements. Also, after each iteration the design was checked to verify that the machining of the flexures, strain gaging and wire routes were still possible to obtain. These computations produced an optimum balance design with a total of 22 flexures arranged as shown in Figure 3. All flexures were located symmetrically from the balance moment center in an area 2.9400 inches wide and 0.5200 inch high. The 20 central flexures were 0.0550 inch wide and 0.2200 inch high. The two outer flexures were 0.1400 inch wide (including a 0.070 inch stress riser) and 0.5200 inch high. All flexures were 1.0000 inch long. There were 0.0400 inch vertical and 0.0800 inch horizontal slots between flexures. All flexures were designed with sufficient radii at the end of flexures to reduce the stress concentration factors. The 20 central flexures were designed as load carrying flexures (secondary flexures) and the two outer flexures were designed as load measuring flexures (primary flexures). Secondary flexures were split in the middle to maximize the Normal Force load carried by the primary flexures. This design yielded 147% more Normal Force stress on the primary flexures. This stress at the primary flexures was high enough to mount strain gages to measure Normal Force. For Axial Force measurement, a unique design of stress risers was implemented. The primary flexures were designed with small additional area (0.0700 inch x 0.0700 inch) on the outside of the primary flexures and close to the horizontal centerline. These small areas are typically known as stress risers. With the implementation of stress risers, the design yielded the following results compared to one without the stress risers:

- Normal Force stiffness and stresses were virtually not affected.

- The balance was 49% more stiffer in axial direction, thereby lowering the balance deflection due to Axial Force.
- Primary flexures carried 22% more Axial Force.
- The elastic section modulus (I/C) of the primary flexures in the axial direction was lower by 7.4% and therefore exhibited higher stress due to Axial Force.
- The net result of the stress risers was an Axial Force gage stress (output) 82% higher without significantly affecting other measurements.

The geometry and positioning of the primary and secondary flexures provided an optimum design which met requirements. Gage stresses for all components except Yawing Moment were between 8,900 psi (61 MPa) and 32,240 psi (222 MPa). The measurement of Yawing Moment was least important and used only to correct any interaction effect on other prime components. Yawing Moment gage stress was 840 psi (6 MPa).

Maximum stress in the control surface balance was calculated to be 85,000 psi (586 MPa). In order to provide a safety factor greater than 2.0, it was necessary to use high strength alloy steel heat treated to a yield strength of 190,000 psi (1,310 MPa).

FABRICATION

The material selected for the balance was ARMCO PH 13-8 Mo, a martensitic precipitation-hardened stainless steel. After being heat treated to H1000 condition, the material had an excellent combination of high strength, high fracture toughness, good transverse properties and high corrosion resistance. The simple one-step heat treatment to condition H1000 resulted in a material with an ultimate tensile strength of 205,000 psi (1,413 MPa). The cover plates were fabricated using 7075-T6 aluminum.

The fabrication of the balance as an integral part of the horizontal stabilizer was vital to attain force measurements with the highest degree of accuracy. This was achieved by using electrical discharge machining or EDM. This method of fabrication, completely eliminated any mechanical joints in the load carrying portion of the balance. The fabrication process consisted of the following steps:

- Heat treating the material.
- Rough machining and some finish machining using conventional techniques like milling, turning, grinding etc.
- Electrical discharge machining (EDM) to cut flexures, slots and pockets.
- Hand polishing of flexures to a achieve a surface finish in the range of 16 to 32 μin. RMS.

The electrodes used for the EDM process of this balance are shown in Figure 4. A great deal of creativity was used in the preparation of these electrodes. All electrodes were made out of a copper-graphite composite material. By use of electrodes, the deep, thin flexures; multiple slots and pockets of

complex configurations were machined into the solid, hardened balance material. Some of these slots were cut through and others were blind slots, but all of these cuts were critical in size, shape and location to obtain flexures capable of yielding force and moment measurements with the highest degree of accuracy. The composite electrodes shown in Figure 4 were used to cut multiple narrow slots simultaneously. Flushing the cut was also a major consideration during the design and fabrication of these electrodes. As shown in Figure 4, the thin slotted electrodes were built using a diagonal groove for flushing. The diagonal grooves were machined in two different directions (one direction per side) on the thin electrodes to retain the electrode strength and to give molten particles an avenue to escape. Flushing during the EDM process is as important as having a sharp cutting tool during a conventional machining process. The combination of accuracy and creativity in making electrodes made it possible to machine the intricate flexure arrangement efficiently and with an accuracy of 0.0005 inch (0.013 mm).

STRAIN GAGING

All strain gages were precisely located on the two primary flexures as shown on Figure 5. The location of all strain gages were carefully determined so that the strain gages measured the component they were intended to measure and canceled or minimized the measurement (interactions) due to other components. All strain gages used were transducer quality and were custom made by the measurement group. These strain gages were manufactured from Karma alloy and the self temperature compensation (STC) was matched with thermal elongation properties of the balance material which minimized the no load output due to change in temperature (apparent strain output). The change in gage factor (EMC) of this gage was nearly equal and opposite to the change in modulus of PH 13-8 Mo, thereby correcting the thermal sensitivity change. These strain gages had 350 ohms resistance. The balance excitation was set at 5.0000 volts DC. All strain gages were wired using AWG #32 Teflon insulated and color coded wires. The adhesive selected for bonding the strain gages was M-Bond 610, because of its capability of forming thin, hard and void-free gluelines. It minimized creep, hysteresis and offered long term stability. M-Coat A (air drying polyurethane) was used as a moisture proofing compound. This coating provided excellent long-term stability by protecting the strain gages from moisture, chemical attack and mechanical damage. Four copper-constantan thermocouples were installed to monitor temperature distribution between the live and ground side of the balance. Thermal zero shifts of all bridges were within 0.00005 mV/V/°F. The thermal sensitivity shift also met design requirements.

CALIBRATION

As shown in Figure 6, during calibration, the spindle end (ground side) of the horizontal stabilizer was mounted to the calibration stand. The loading side (live side) of the horizontal stabilizer was attached to the calibration fixture by using the three pin holes machined into the stabilizer. The pin holes precisely located the calibration fixture with reference to the balance moment center. To minimize tare weight during calibration, the fixture was made from aluminum. There were 12 loading points machined on the fixture for load application. Additional load points were provided to facilitate specific check loads in the wind tunnel. To simplify assembly and check loads in the wind tunnel, the fixture was mounted on the

lower side of the balance. The electronic level mounted on the calibration fixture allowed leveling of the calibration fixture in the pitch and roll plane after each load application. Normal Force, Pitching Moment and Rolling Moment were applied using precision dead weights and a hanger bar with double knife edges or rod-end bearings. Axial Force and Yawing Moment were applied over a cable using a knife edge bell crank assembly. The use of bell crank assemblies made it possible to load the balance with Axial Force orthogonal to gravity and with minimal friction. The bell crank assemblies eliminated the friction problems normally encountered in "V" groove pulley systems.

The calibration approach was based on the assumption that all possible first and second order interaction exist on the balance, and therefore it was decided to perform a second order combined load calibration. Because of space limitation for mounting long moment arms, a short arm loading was considered. Primary Normal Force and its combinations with Pitching Moment and Rolling Moment were achieved by loading Normal Force at different load points on the calibration fixture. For positive Normal Force and its combination with Pitching Moment and Rolling Moment, the entire assembly was inverted. Axial Force and Yawing Moment were loaded as mentioned previously. Because of the relatively light Axial Force and Yawing Moment it was decided not to load combinations of Axial Force and Yawing Moment with remaining components. It was assumed that the effect of these interactions on the final accuracy would be minimal. All loads were applied full scale, ascending and descending, in 25% increments to establish non-linearity, hysteresis and zero shift. During calibration 168 data points were collected on each component. At the end of the calibration, a check load was performed to verify the accuracy of the derived interactions. The check loading consisted of 35 different combinations of full scale loads applied to the balance in a predetermined manner.

Angular deflection measured during calibration indicated a balance deflection of 8 minutes in the pitch plane and 50 minutes in the roll plane due to full scale loads. Assembly and disassembly of cover plates and ground side adapter did not cause any change in the balance zeros and output.

DATA EVALUATION

Least square error second order polynomials were used as a math model to evaluate the sensitivity constants and interaction coefficients of the balance. During the calibration, the balance was swept through a 180 degree rotation to establish the unloaded zero reference for all of the components. The tare weight of calibration hardware and weight of the horizontal stabilizer acting on the live side of the balance was established. The second order non-linear interactions were corrected due to tare weight. The math model yielded a 5 x 14 interaction coefficient matrix as shown on table 2.

No balance is free of interactions. Balance interactions are both linear and non-linear. These interactions are caused by deflections, machining tolerances, strain gage locations and variation in gage factors. After analyzing interactions, it was assumed that part of the 5.03 % Axial Force interaction on Normal Force was the result of being unable to locate the Normal Force gages on the neutral axis in the Axial Force direction due to the space limitations. The 8.93% pitch x roll interaction on Axial Force was believed to be caused by deflection due to the combination of the high Pitching and Rolling Moments. The interactions on the Yawing Moment as a percent of full scale are high because of its lower

381 μV/5V full scale output. The error analysis of calibration data and check loads proved that all the interactions, regardless of high or low, were repeatable and correctable with a very high degree of accuracy.

For each calibration data point, load was calculated using derived interaction matrix. The difference between the true applied load on the balance and the calculated load is called the error, and was referred to as percent of full scale of the corresponding component. The data as percent full scale were plotted versus standard loading code as shown in Figures 7 through 9. This tool gives quick view of how well the calibration data and the mathematical model are matching. Final accuracy of calibration was evaluated by reducing the check loads using the interaction matrix. The check loads consist of all five components loaded simultaneously. The error as percent full scale for check loads were also plotted as shown in Figure 7 through 9. A summary of the error analysis for calibration data and check loads is given in Table 3. The balance demonstrated standard error between 0.10% to 0.15% of full scale for calibration data and 0.11% to 0.24% of full scale for check loads for all components except yawing moment. Considering the extremely low output for yawing moment it yielded a respectable standard error of 0.28% full scale and 0.42% full scale for calibration data and check loads respectively. As shown in Table 3, the balance met the design requirements with very high accuracy.

CONCLUSION

This paper has discussed the design and performance of a five component balance as an integral part of a horizontal stabilizer. The unique design features, the creativity used during electrical discharge machining, precision strain gage installation and accurate calibration and data evaluation have resulted in a compact balance performing well within all accuracy requirements. The performance was comparable to wind tunnel balances currently used in the aerospace industry. In addition the knowledge gained from this project can and will be used to design highly accurate and compact multicomponent force transducers in the future.

REFERENCES

1. HUBBARD, R. H.; VSE MEMORANDUM "SPRING CONSTANT CORRECTION FACTOR FOR SHEARING DEFLECTION"; APRIL 5, 1968.

2. FARLEY, L. N.; VSE REPORT "EFFECTS OF TORSIONAL LOADING ON BEAMS OF RECTANGULAR CROSS SECTION WITH THE END RESTRAINED FROM WARPING"; 1969.

3. GUARINO, J. F.; "CALIBRATION AND EVALUATION OF MULTICOMPONENT STRAIN-GAGE BALANCES," NASA INTERLABORATORY GROUP MEETING, JET PROPULSION LABORATORY; APRIL 16-17, 1964.

4. SMITH, D. L.; "AN EFFICIENT ALGORITHM USING MATRIX METHOD TO SOLVE WIND-TUNNEL FORCE BALANCE EQUATIONS," NASA TECHNICAL NOTE TN D-6860, WASHINGTON DC, AUGUST 1972

5. ROARK AND YOUNG; "FORMULA FOR STRESS AND STRAIN," MCGRAW-HILL, INC., USA 1975

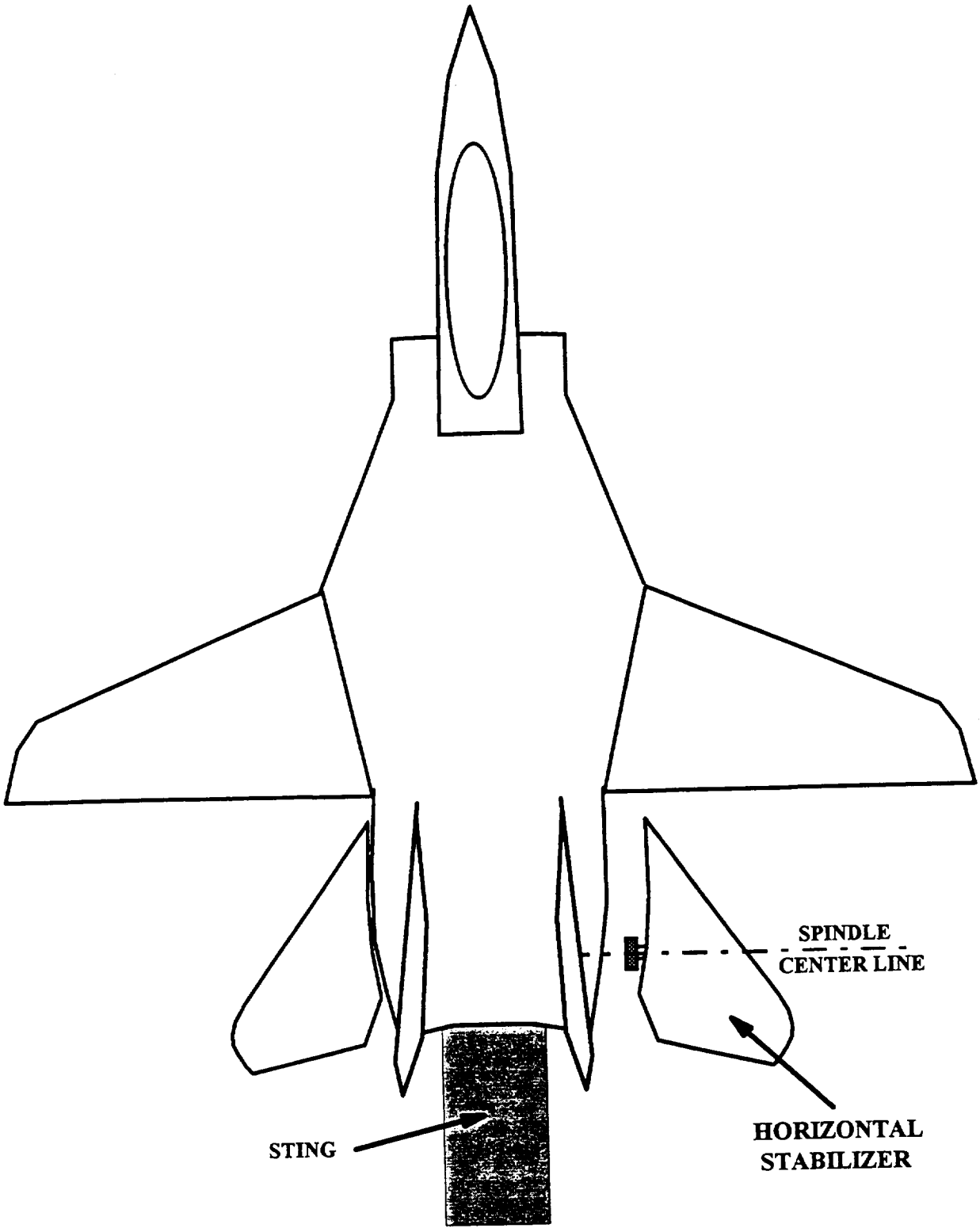

FIGURE 1

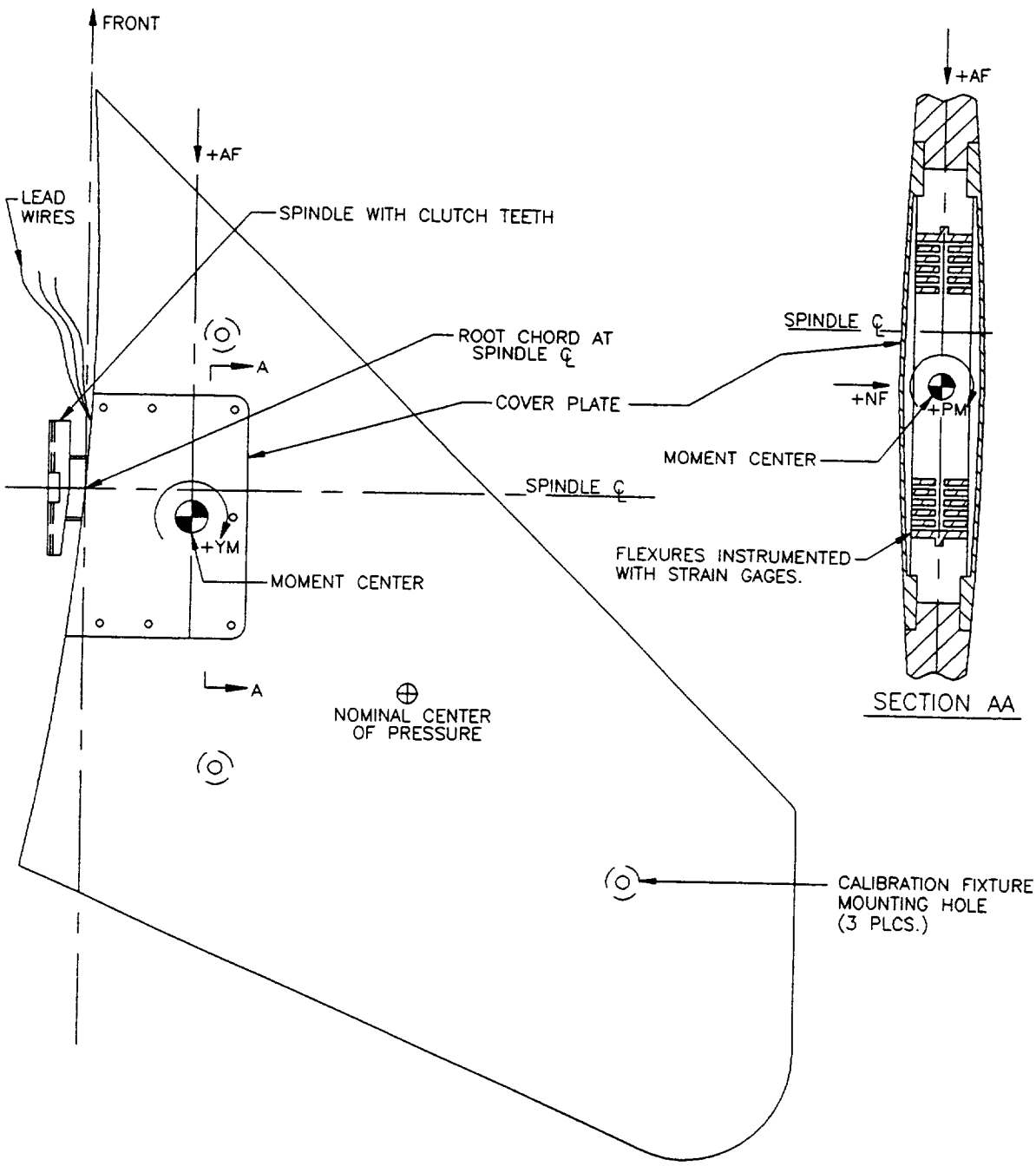
FRONT
+AF
LEAD WIRES
SPINDLE WITH CLUTCH TEETH
ROOT CHORD AT SPINDLE ℄
COVER PLATE
A
+YM
MOMENT CENTER
SPINDLE ℄
A
NOMINAL CENTER OF PRESSURE
CALIBRATION FIXTURE MOUNTING HOLE (3 PLCS.)
+AF
SPINDLE ℄
+NF
+PM
MOMENT CENTER
FLEXURES INSTRUMENTED WITH STRAIN GAGES.
SECTION AA

FIGURE–2

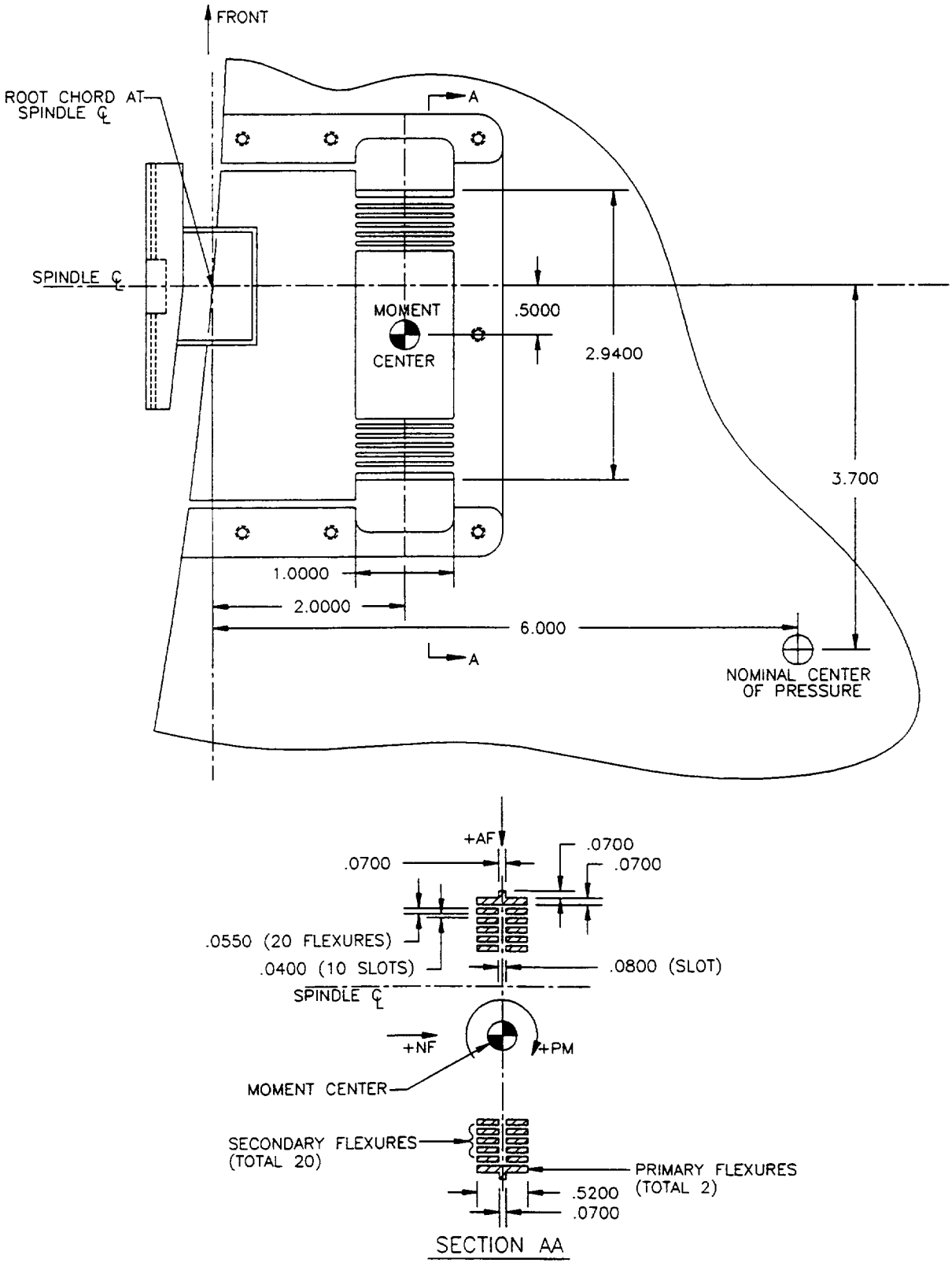
FRONT
ROOT CHORD AT SPINDLE ℄
SPINDLE ℄
A
MOMENT CENTER
.5000
2.9400
3.700
1.0000
2.0000
6.000
A
NOMINAL CENTER OF PRESSURE
+AF
.0700
.0700
.0700
.0550 (20 FLEXURES)
.0400 (10 SLOTS)
.0800 (SLOT)
SPINDLE ℄
+NF
+PM
MOMENT CENTER
SECONDARY FLEXURES (TOTAL 20)
PRIMARY FLEXURES (TOTAL 2)
.5200
.0700
SECTION AA

FIGURE–3

ELECTRODE FOR
CUTTING UNDER FLEXURES

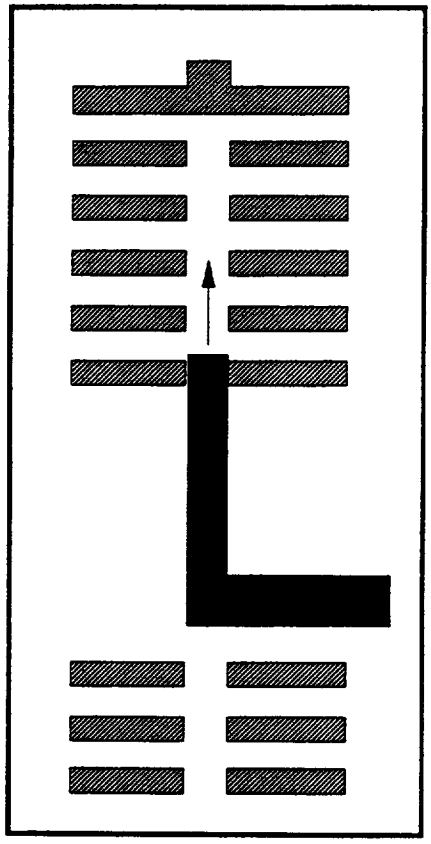

COMPOSITE ELECTRODE

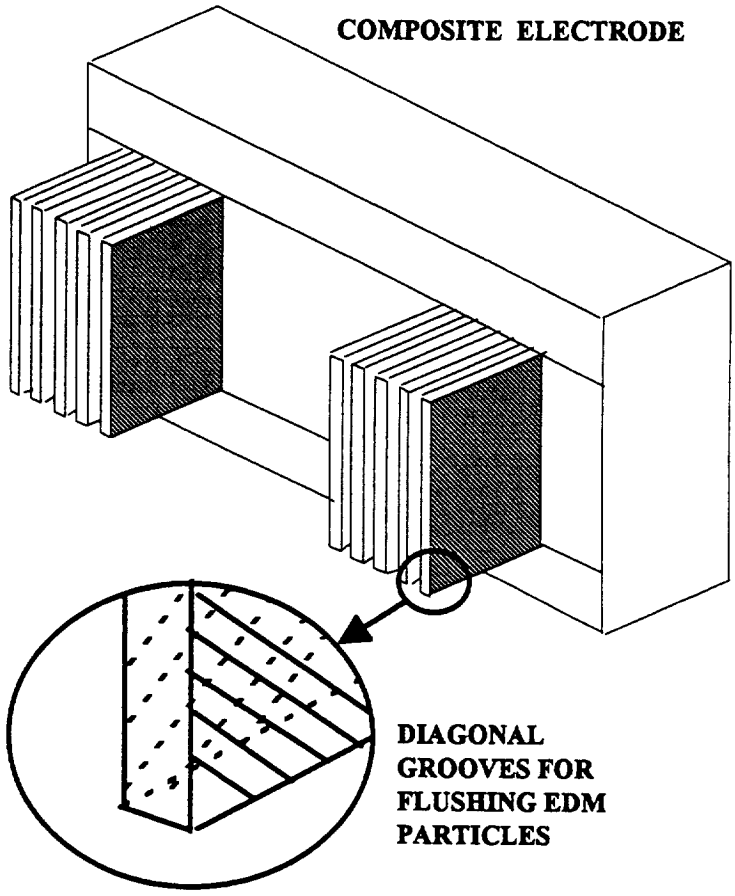

ELECTRODE FOR
CUTTING STRESS RISER FLEXURE

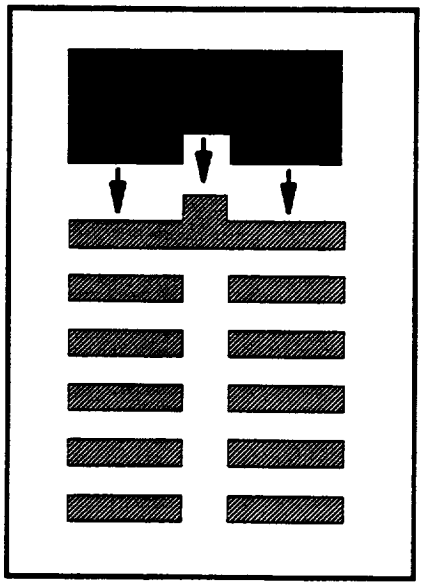

COMPOSITE ELECTRODE

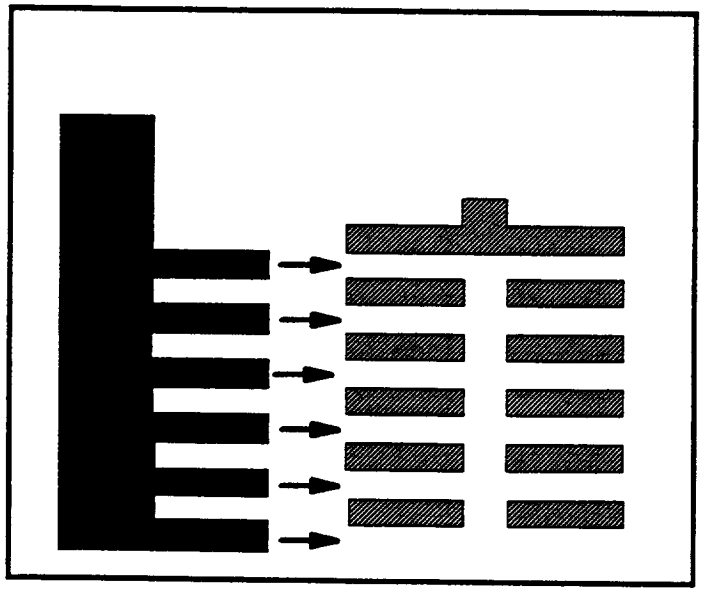

FIGURE 4

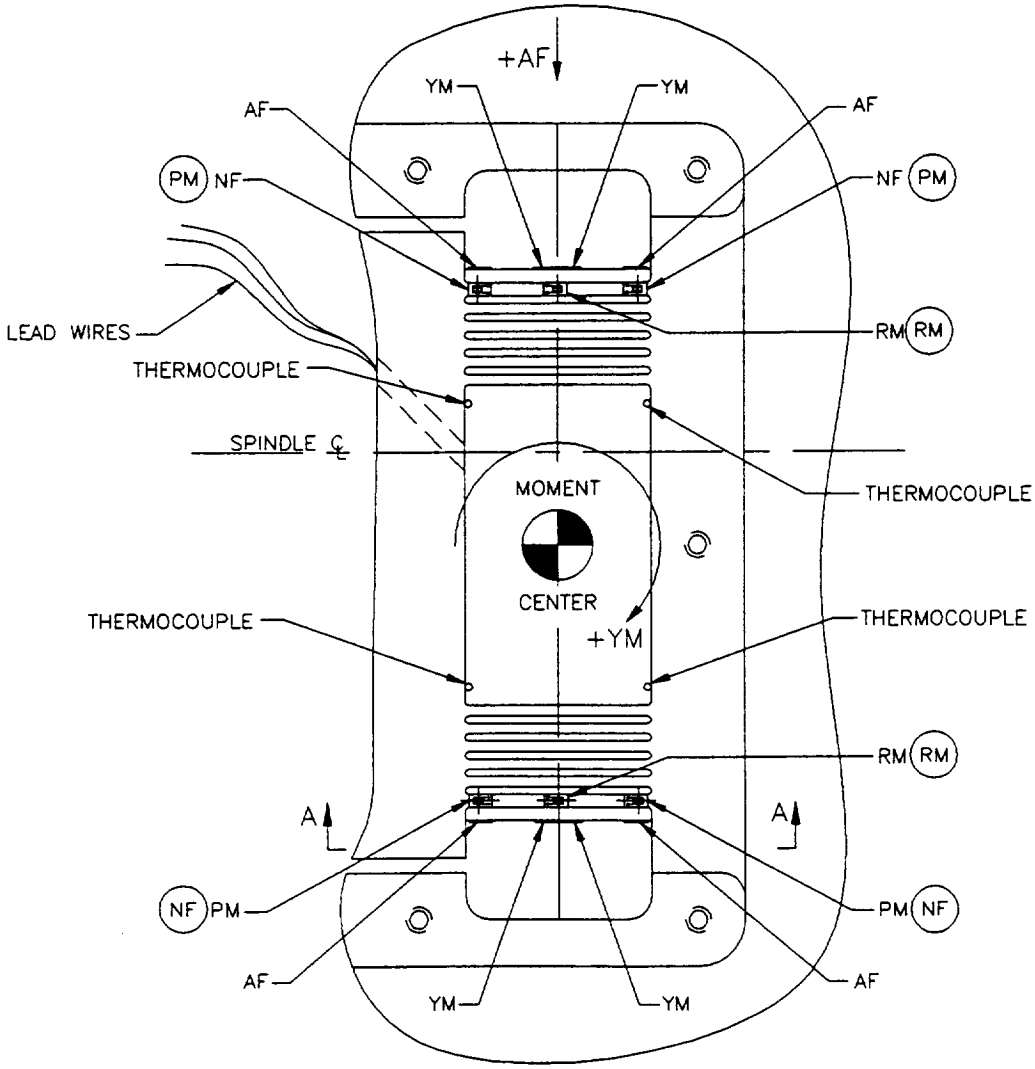

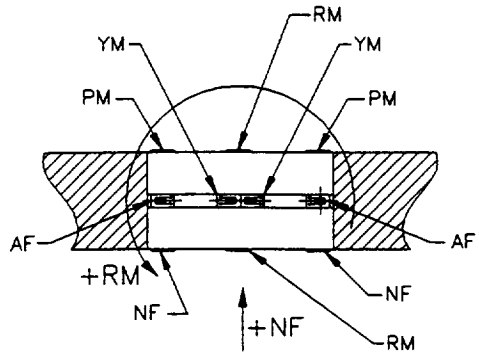

SECTION AA

FIGURE–5

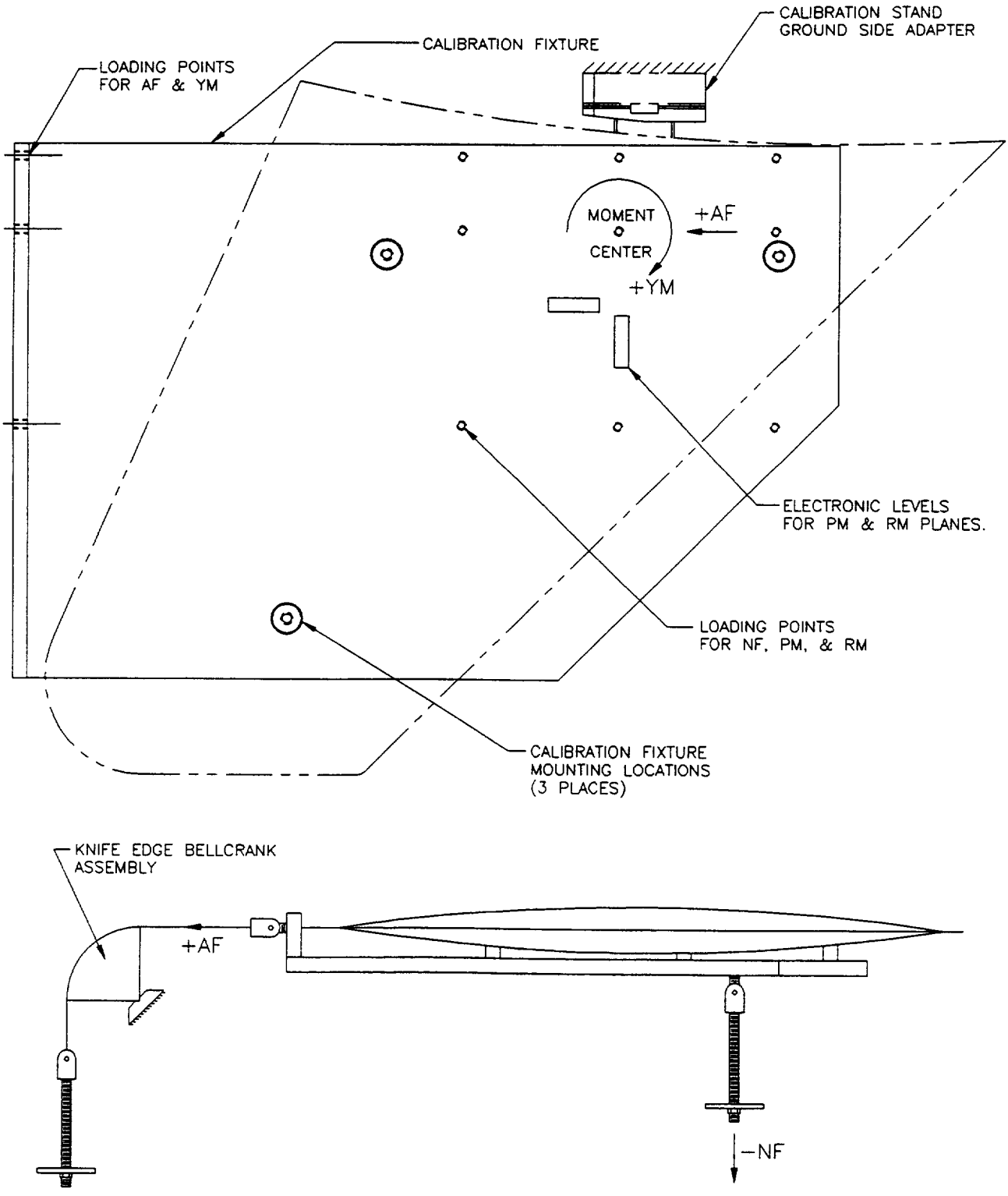
CALIBRATION STAND
GROUND SIDE ADAPTER
CALIBRATION FIXTURE
LOADING POINTS
FOR AF & YM
MOMENT
CENTER
+AF
+YM
ELECTRONIC LEVELS
FOR PM & RM PLANES.
LOADING POINTS
FOR NF, PM, & RM
CALIBRATION FIXTURE
MOUNTING LOCATIONS
(3 PLACES)
KNIFE EDGE BELLCRANK
ASSEMBLY
+AF
-NF

FIGURE–6

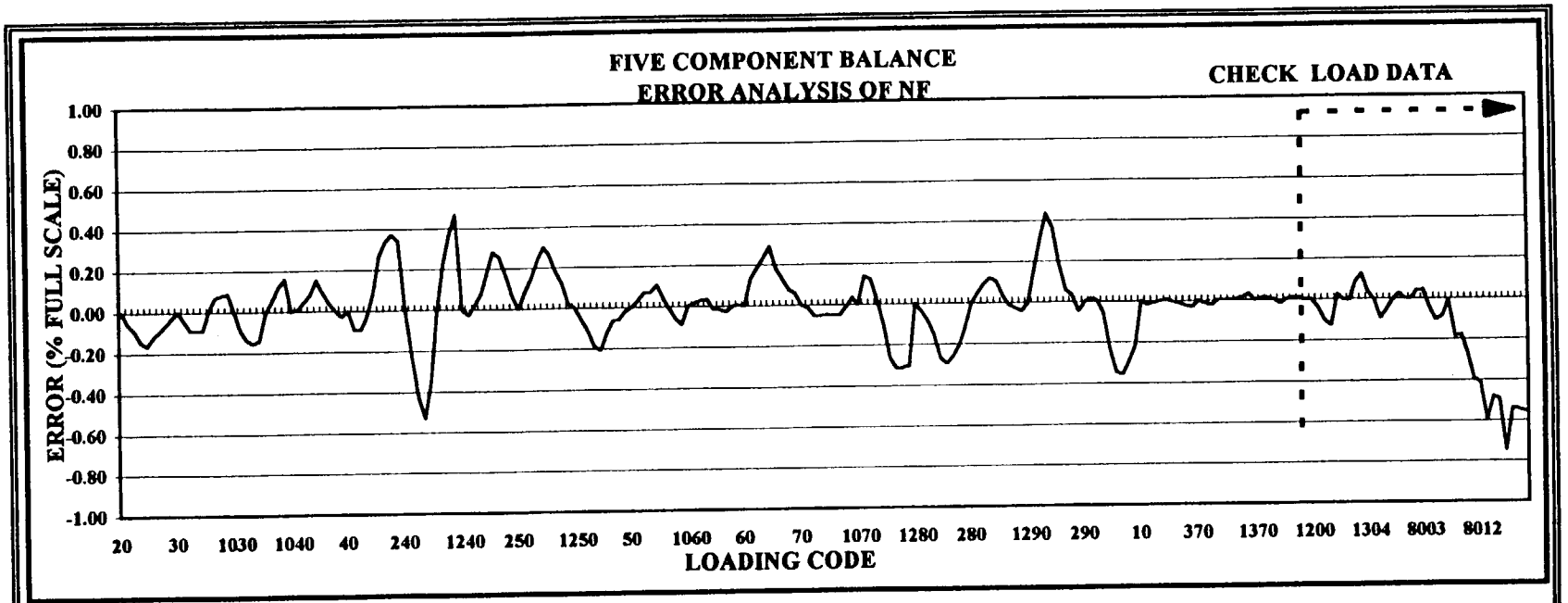
FIVE COMPONENT BALANCE
ERROR ANALYSIS OF NF
CHECK LOAD DATA
ERROR (% FULL SCALE)
1.00
0.80
0.60
0.40
0.20
0.00
-0.20
-0.40
-0.60
-0.80
-1.00
20 30 1030 1040 40 240 1240 250 1250 50 1060 60 70 1070 1280 280 1290 290 10 370 1370 1200 1304 8003 8012
LOADING CODE

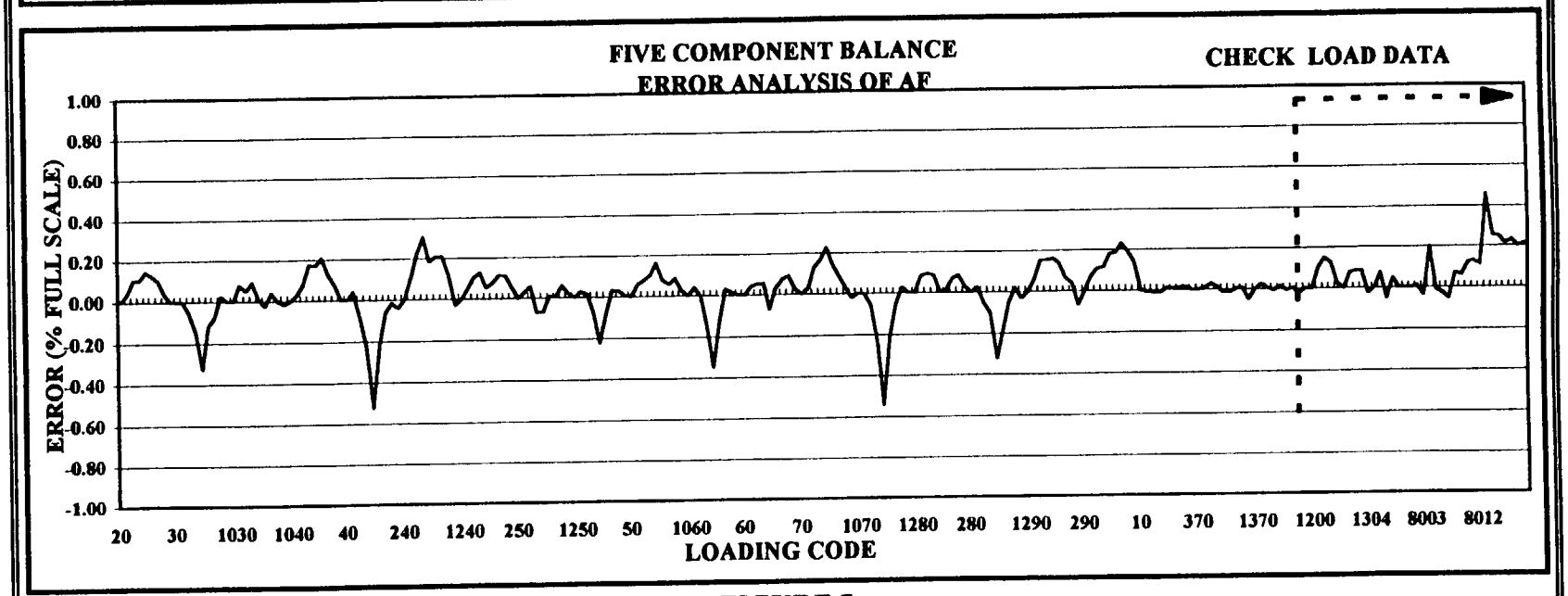
FIVE COMPONENT BALANCE
ERROR ANALYSIS OF AF
CHECK LOAD DATA
ERROR (% FULL SCALE)
1.00
0.80
0.60
0.40
0.20
0.00
-0.20
-0.40
-0.60
-0.80
-1.00
20 30 1030 1040 40 240 1240 250 1250 50 1060 60 70 1070 1280 280 1290 290 10 370 1370 1200 1304 8003 8012
LOADING CODE

FIGURE 7

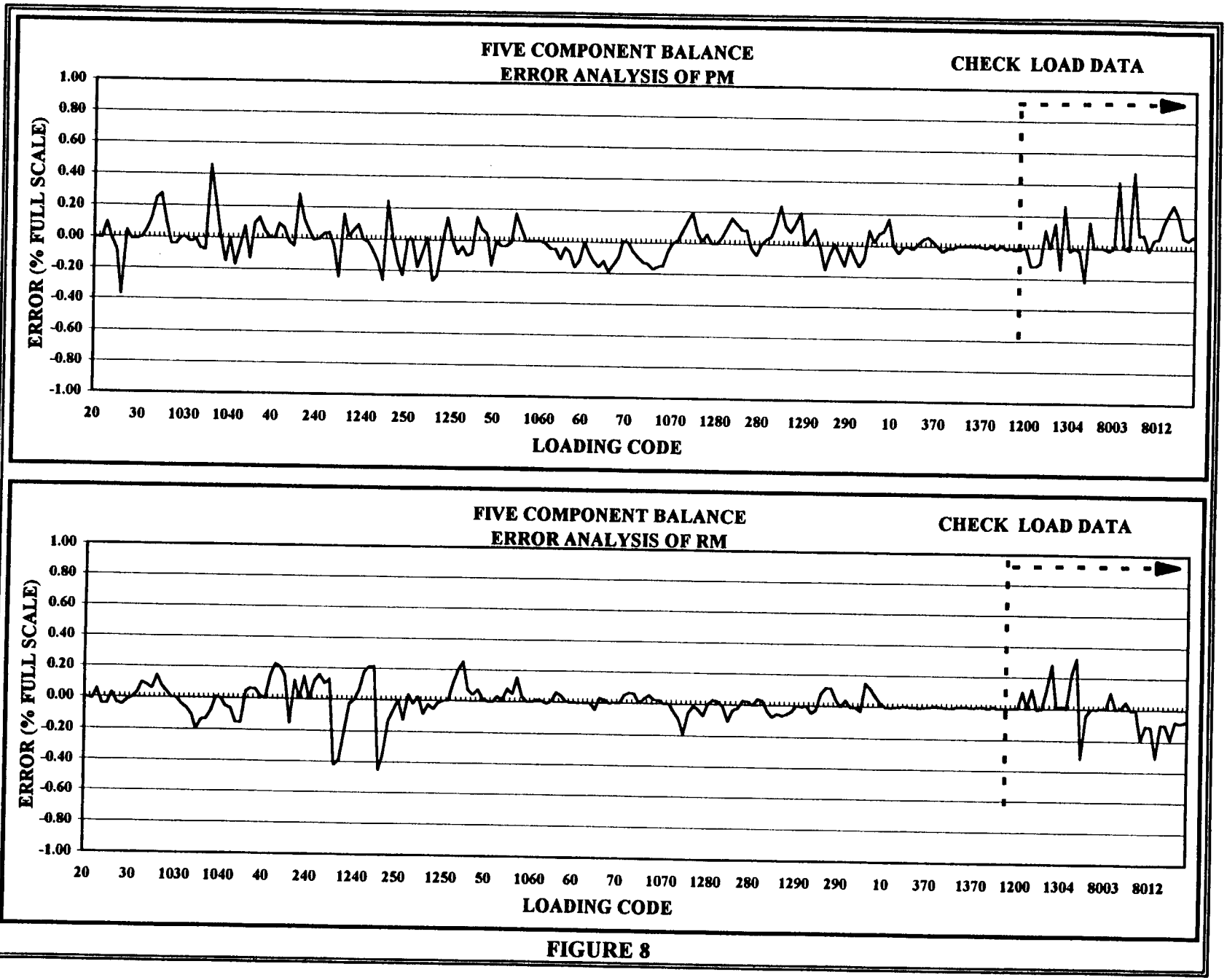
FIVE COMPONENT BALANCE
ERROR ANALYSIS OF PM
CHECK LOAD DATA
ERROR (% FULL SCALE)
1.00
0.80
0.60
0.40
0.20
0.00
-0.20
-0.40
-0.60
-0.80
-1.00
20 30 1030 1040 40 240 1240 250 1250 50 1060 60 70 1070 1280 280 1290 290 10 370 1370 1200 1304 8003 8012
LOADING CODE
FIVE COMPONENT BALANCE
ERROR ANALYSIS OF RM
CHECK LOAD DATA
ERROR (% FULL SCALE)
1.00
0.80
0.60
0.40
0.20
0.00
-0.20
-0.40
-0.60
-0.80
-1.00
20 30 1030 1040 40 240 1240 250 1250 50 1060 60 70 1070 1280 280 1290 290 10 370 1370 1200 1304 8003 8012
LOADING CODE

FIGURE 8

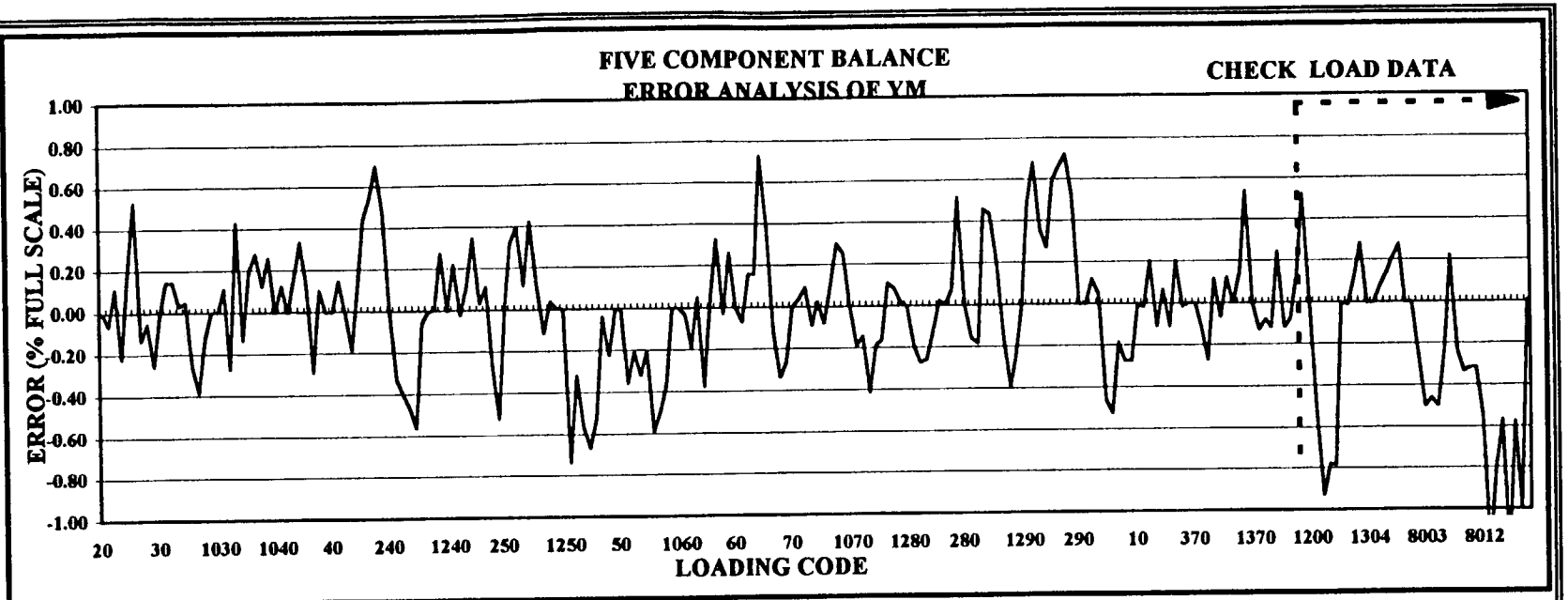
FIVE COMPONENT BALANCE
ERROR ANALYSIS OF YM
CHECK LOAD DATA
ERROR (% FULL SCALE)
1.00
0.80
0.60
0.40
0.20
0.00
-0.20
-0.40
-0.60
-0.80
-1.00
20 30 1030 1040 40 240 1240 250 1250 50 1060 60 70 1070 1280 280 1290 290 10 370 1370 1200 1304 8003 8012
LOADING CODE

FIGURE 9

COMPONENT	NORMAL FORCE	AXIAL FORCE	PITCHING MOMENT	ROLLING MOMENT	YAWING MOMENT
RATED CAPACITY @ ROOT OF HORIZONTAL STABILIZER	250 LB (1,112 N)	40 LB (178 N)	925 IN-LB (105 N-M)	1500 IN-LB (169 N-M)	250 IN-LB (28 N-M)
CALIBRATION ACCURACY (STANDARD ERROR, % OF FULL SCALE OUTPUT)	0.80	0.88	1.62	1.00	6.00
CHECK LOAD ACCURACY (STANDARD ERROR, % OF FULL SCALE OUTPUT)	1.60	1.76	3.24	2.00	12.00
OPERATING TEMPERATURE RANGE (DEGREES F)	80-160	80-160	80-160	80-160	80-160
THERMAL ZERO SHIFT FROM 80 TO 160 DEG F (MV/V / DEG F)	0.00005	0.00005	0.00005	0.00005	0.00005
THERMAL SENS. SHIFT FROM 80 TO 160 DEG F (% OF FULL SCALE / DEG F)	0.0004	0.0004	0.0004	0.0004	0.0004
EFFECT OF ASSEMBLY & DISSASSEMBLY (% OF FULL SCALE)	0.02	0.02	0.02	0.02	0.02
DEFLECTION LIMITS UNDER COMBINED LOADS	THE ROTATIONAL AND TRANSLATIONAL DEFLECTION OF THE HORIZONTAL STABILIZER SHALL BE MINIMAL				

TABLE 1 - BALANCE REQUIREMENTS

INTERACTION COEFFICIENT MATRIX

Interaction Coefficients	COMPONENTS				
	Normal	Axial	Pitch	Roll	Yaw
Full Scale Output (μV / 5 VOLT)	3,384	4,186	10,020	12,835	381
Sensitivity	7.38733E-02	9.55545E-03	7.98361E-02	7.79147E-02	6.56365E-01
Normal		7.76817E-04	-9.86909E-03	-2.73180E-02	9.91428E-03
Axial	3.14237E-01		4.83996E-02	1.81800E-03	5.30863E-01
Pitch	1.75250E-02	1.35867E-03		-2.99325E-03	-8.86830E-03
Roll	-2.17240E-02	-1.74222E-03	2.22903E-03		5.99979E-02
Yaw	1.32788E-03	-5.01002E-04	-3.59054E-03	3.05329E-04	
Normal Squared	-8.75376E-07	-2.88505E-06	-1.91600E-05	-9.86934E-06	3.78736E-06
Axial Squared	1.74952E-05	-7.17461E-06	2.54983E-04	-1.68105E-04	2.44861E-04
Pitch Squared	1.49145E-07	5.41054E-07	6.96701E-07	5.65828E-07	-2.79022E-06
Roll Squared	-2.23346E-07	-3.44517E-07	1.70325E-06	2.92997E-06	-5.61773E-07
Yaw Squared	7.54896E-06	7.44524E-08	-5.12249E-05	2.13753E-06	-2.08121E-04
Normal x Pitch	5.70118E-07	1.49467E-06	3.97871E-06	-1.71547E-07	-3.09360E-05
Normal x Roll	1.26540E-06	9.78599E-07	-8.39111E-06	-9.12903E-06	5.51769E-06
Axial x Yaw	-5.99752E-05	4.30739E-06	3.28703E-04	6.37346E-05	1.29785E-03
Pitch x Roll	4.69921E-06	4.46276E-06	-6.01548E-07	-4.11865E-07	-4.07710E-06

* ALL COEFFICIENTS ARE IN ENGINEERING UNITS

PERCENT OF FULL SCALE EFFECT

Full Scale Loads (LB OR IN-LB)	250	40	800	1000	250
Interaction Coefficients	COMPONENTS				
	Normal	Axial	Pitch	Roll	Yaw
Normal		0.49%	-0.31%	-0.68%	0.99%
Axial	5.03%		0.24%	0.01%	8.49%
Pitch	5.61%	2.72%		-0.24%	-2.84%
Roll	-8.69%	-4.36%	0.28%		24.00%
Yaw	0.13%	-0.31%	-0.11%	0.01%	
Normal Squared	-0.02%	-0.45%	-0.15%	-0.06%	0.09%
Axial Squared	0.01%	-0.03%	0.05%	-0.03%	0.16%
Pitch Squared	0.04%	0.87%	0.06%	0.04%	-0.71%
Roll Squared	-0.09%	-0.86%	0.21%	0.29%	-0.22%
Yaw Squared	0.19%	0.01%	-0.40%	0.01%	-5.20%
Normal x Pitch	0.05%	0.75%	0.10%	0.00%	-2.47%
Normal x Roll	0.13%	0.61%	-0.26%	-0.23%	0.55%
Axial x Yaw	-0.24%	0.11%	0.41%	0.06%	5.19%
Pitch x Roll	1.50%	8.93%	-0.06%	-0.03%	-1.30%

TABLE 2 - INTERACTION COEEFICIENT MATRIX

ERROR ANALYSIS SUMMARY OF CALIBRATION DATA

COMPONENT	NORMAL	AXIAL	PITCH	ROLL	YAW
MAXIMUM ERROR (%F.S.)	0.47%	0.30%	0.46%	0.25%	0.73%
MINIMUM ERROR (%F.S.)	-0.53%	-0.54%	-0.37%	-0.45%	-0.74%
STANDARD ERROR (%F.S.)	0.15%	0.11%	0.11%	0.10%	0.28%
TOTAL NO. OF DATA PTS	168	168	168	168	168

ERROR ANALYSIS SUMMARY OF CHECK LOAD DATA

COMPONENT	NORMAL	AXIAL	PITCH	ROLL	YAW
MAXIMUM ERROR (%F.S.)	0.12%	0.46%	0.47%	0.32%	0.28%
MINIMUM ERROR (%F.S.)	-0.75%	-0.05%	-0.22%	-0.31%	-1.21%
STANDARD ERROR (%F.S.)	0.24%	0.11%	0.15%	0.13%	0.42%
TOTAL NO. OF DATA PTS	35	35	35	35	35

TABLE 3 - SUMMARY OF CALIBRATION AND CHECKLOAD ERRORS

DESIGN FEATURES OF SOME SPECIAL STRAIN GAUGE BALANCES

M.A. Ramaswamy
Professor
Dept. of Aerospace Engineering
Indian Institute of Science
Bangalore - 560 012, INDIA

INTRODUCTION

Some special strain gauge balances were designed and developed in the Department of Aerospace Engineering, Indian Institute of Science, Bangalore to cater to special requirements, which could not be met using standard type of balances. Some of the special requirements, for which special balances were required are given below.

a) It was required to measure the forces and moments acting on the strut and oval body of revolution mounted on the model of an aircraft in the I.I.Sc. 14'x9' low speed wind tunnel. To meet this need a **"Special 6 Component Half Model Balance"** was designed and developed.

b) To obtain the longitudinal aerodynamic characteristics of thin slab delta wings in a 200 mm hypersonic wind tunnel of I.I.Sc. at M=8.0, without the interference effects of balance housing on the lee-side, a **"Thin 3-Component Delta Wing Balance"** was designed and developed.

c) It was found that this concept could be extended to develop a **"Thin 6-Component Delta Wing Balance"** to measure the effectiveness of control flaps (both symmetric and assymmetric deflection) on thin slab delta wings at M=8.0.

d) It was required to design a rigid 5 component balance for measuring the loads acting on the model mounted on a rotary derivative rig installed in the 14'x9' low speed wind tunnel of the IISc so that the natural frequency of the model balance combination was well beyond the maximum rotational frequency of the rig. (The model was also made of carbon-fibre composite to make it light and increase the natural frequency). To get high rigidity of the balance without unduly reducing the sensitivity of the balance, a **"Cage Type 5 Component Balance"** was designed and developed.

e) There was a requirement to measure the forces acting on a body in the IISc water tunnel using a sting type of balance. The size of the balance did not permit using encapsulated water proof gagues. Therefore an attempt was made to water proof the strain gauge bridges of a standard balance. That attempt was unsuccessful. Therefore a novel approach of enclosing the balance in a flexible rubber bellow and filling up the space within the bellow by an insulating transformer oil was tried and found to be successful. This balance is called **"Novel Bellow Type Balance for Water Tunnel"**.

In this paper, the design features of these special balances are covered. Since the "Novel Bellow Type Balance for water tunnel" is covered in detail in another paper by my colleague in the same conference, this would be only briefly touched upon here.

SPECIAL 6-COMPONENT HALF MODEL BALANCE

The schematic diagram of the mounting arrangement for the oval body strut combination on this balance is shown in figure 1. It can be seen that the balance is housed within the fuselage of the aircraft model and only the loads acting on the oval body strut combination, in the interference field of the parent aircraft model, is measured.

Design concept

A new concept of resolving the forces and moments acting on the balance has been considered in the design of the balance. The normal force Z, the pitching moment M and the rolling moment L acting on the balance is resolved into three normal forces N_1, N_2 and N_3 acting through three points located at the vertices of an equilateral triangle as shown in figure 2. The axial force X, side force Yand yawing moment N are resolved into forces P_1, P_2 and P_3 acting along the three sides of the equilateral triangle (figure 2).

From space considerations, the length of the sides of the triangle was taken to be 50 mm. Further the balance has been so designed that each of the elements measuring N_1, N_2, N_3, P_1, P_2 and P_3 are primarily subjected to their respective loads so that the interaction between elements is minimised. The manner in

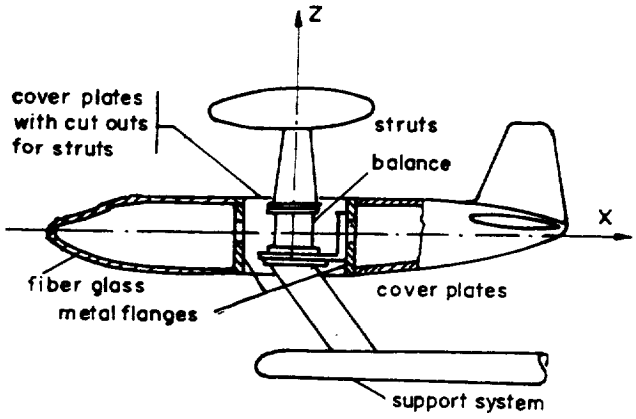

Figure 1. Schematic diagram of model mounting

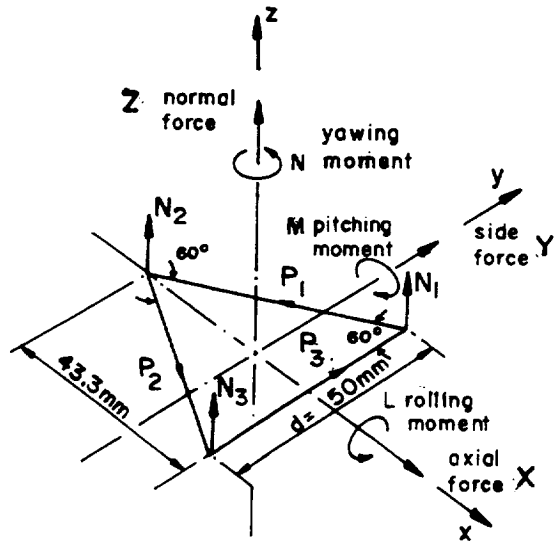

Figure 2. Resolution of force and moments

which this kind of near isolation or independence of each of the elements has been achieved, is illustrated in the isometric view of the schematic balance shown in figure 3. As illustrated in figure 3, the forces and moments acting on the top plate of the balance (which is attached to the part on which the load is to be measured) is transmitted to the bottom plate through a set of three slender vertical columns and three slender horizontal columns. The three slender vertical columns are relatively very rigid for the normal forces N_1, N_2 and N_3, but they are relatively very flexible for the planar loads P_1, P_2 and P_3. In a similar manner, the three slender horizontal columns are rigid for the planar loads P_1, P_2 and P_3, but they are very flexible for the normal loads N_1, N_2, N_3. Thus, each of the slender columns transmit essentially only one component and thus interactions are reduced to a minimum. However, interaction effects are taken into account in calibration. Each of the forces N_1, N_2, N_3, P_1, P_2 and P_3 are individually measured by strain gauge bridges mounted close to the root of the cantilever beams through which these loads are transmitted to the bottom plate.

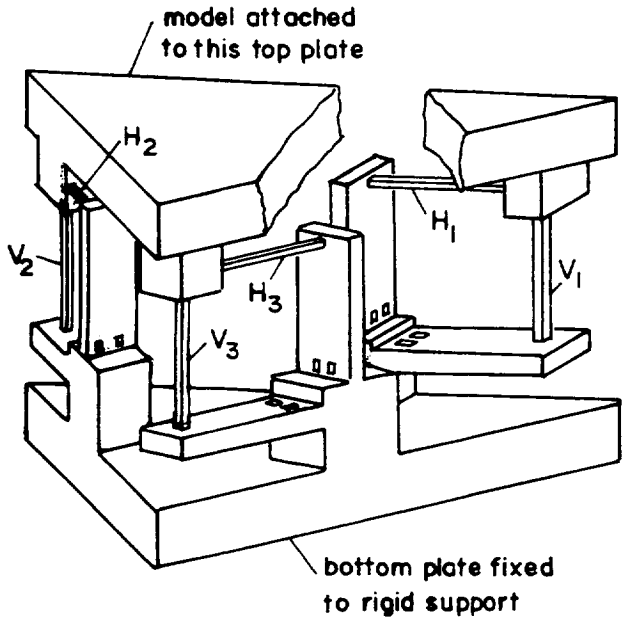

Figure 3. Isometric view of the schematic balance

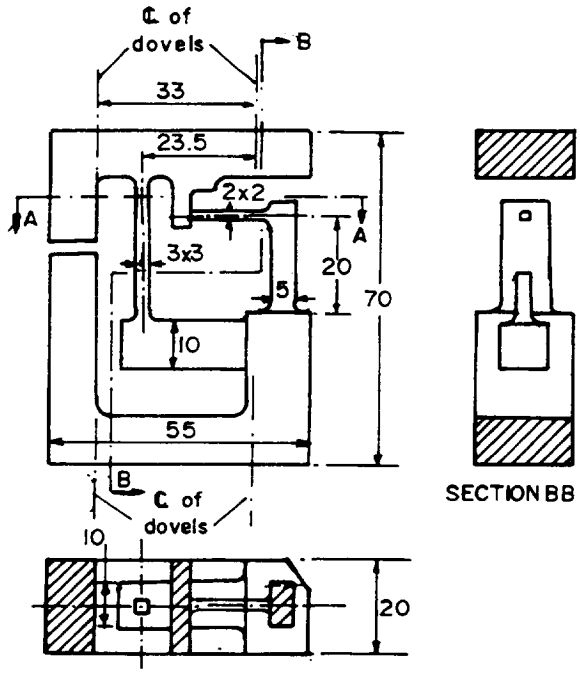

Figure 4. Details of the element of the balance

Balance details

To take the expected loads and moments on the oval body strut assembly, the balance was designed for $N_1 = N_2 = N_3 = 60$ kg and $P_1 = P_2 = P_3 = 15$ kg. Ideally, the balance should be integral with all the balance elements machined from a single block as illustrated schematically in figure 3. Though this is, in principle, feasible using spark erosion machining techniques, it was not possible to do it in India at that time because of limitations in facilities and cost considerations. Therefore, it was decided to make the balance by fabricating three elements, each of them designed for measuring one normal force and one planar force and

then assembling the three elements between two parallel plates using dovel pins and a large number of bolts as shown in figures 4 and 5. Since the design loads N_1, N_2 and N_3 were the same, and the design loads P_1, P_2 and P_3 were the same, all the three elements of the balance could be made identical.

The design of the element to take a normal force of 60 kg and a planar force of 15 kg involves the design of the slender columns to transmit these loads without buckling and the design of the cantilever beams to obtain the required strains near the root so that sufficient output from the strain gauge bridges are obtained, keeping in mind various constraints such as the space available, rigidity, etc.

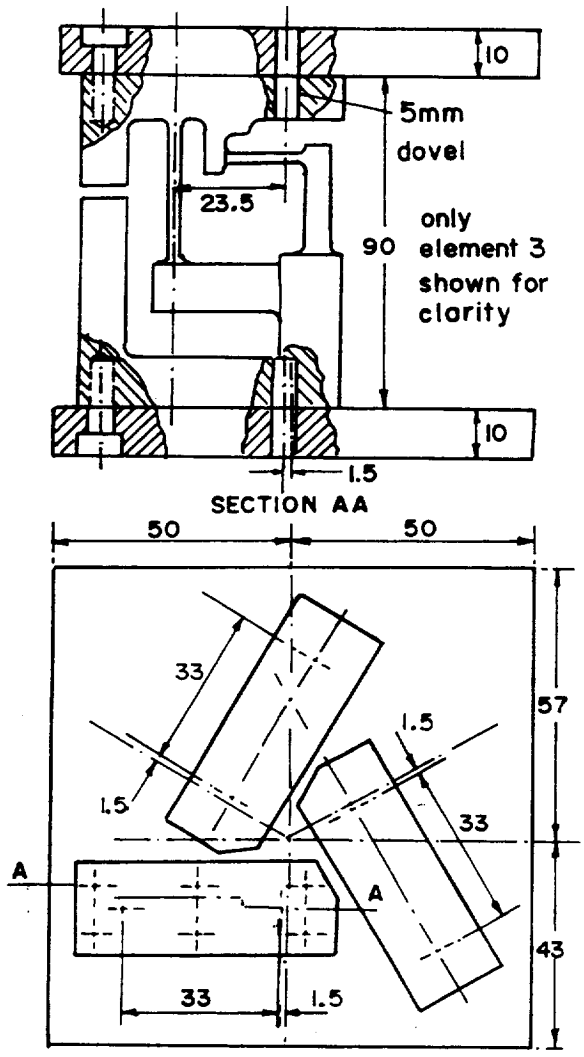

Figure 5. Details of the assembled balance

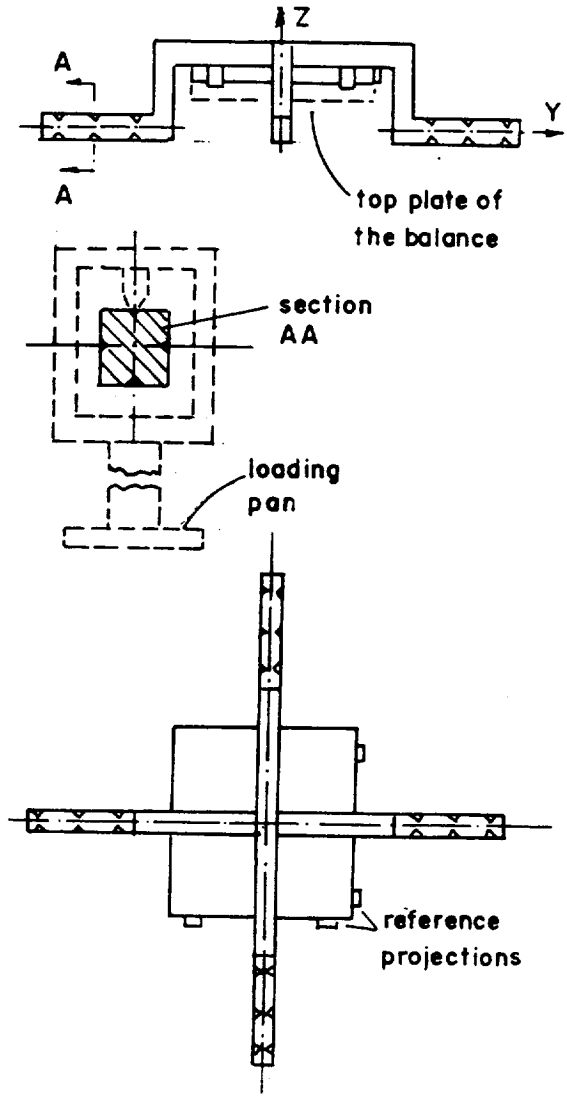

Figure 6. Calibration body for the 6-component half model balance

Calibration Concept

There are basically two concepts which can be used for calibrating this balance. One concept is to apply loads N_1, N_2, N_3, P_1, P_2 and P_3 and determine the direct and interaction outputs in each of the bridges. Then knowing the exact locations with respect to balance reference axis at which these loads were applied during calibration, the forces and moments acting on the balance with respect to the reference axes can be determined. However it may be observed that it is pretty difficult to device a calibration equipment to apply these pure loads. Also any errors in the measurement of the small distances between the balance reference axes and the points of application of the loads, would result in errors in the moments referred to the balance axes. Because of these problems an alternative concept as given below was adopted for calibration.

The forces X, Y, and Z and moment L, M and N about the reference axes are applied using a special calibration body. The calibration rig had arrangements for mounting the balance with this calibration body in the desired orientation to enable application of the desired loads and moments. Then a logical combination of outputs from N_1, N_2, N_3, P_1, P_2 and P_3 bridges as given below are taken as the corresponding outputs for the forces and moments. We denote the outputs corresponding to any generalised load or moment by the subscript 'o' attached to the symbol for the load.

$$X_0 = P_{20} - P_{10}\,; \qquad Y_0 = P_{30} - 0.5\,(P_1 + P_2)\,; \qquad Z_0 = N_{10} + N_{20} + N_{30}$$

$$L_0 = N_{10} - N_{20}\,; \qquad M_0 = 2\,N_{20} - (N_{10} + N_{30})\,; \qquad N_0 = P_{10} + P_{20} + P_{30}$$

With the above definitions, it is easily seen that X_0, Y_0, Z_0, L_0, M_0 and N_0 are primarily proportional to X, Y, Z, L, M, and N but there may be small contributions due to the others from interactions which cannot be completely eliminated. We can express the relation between the outputs X_0, Y_0, Z_0 , L_0, M_0, N_0 and X, Y, Z, L, M and N by the following matrix.

$$\begin{bmatrix} X_o \\ Y_o \\ Z_o \\ l_o \\ m_o \\ n_o \end{bmatrix} = \begin{bmatrix} C_{xox} & C_{xoy} & C_{xoz} & C_{xol} & C_{xom} & C_{xon} \\ C_{yox} & C_{yoy} & C_{yoz} & C_{yol} & C_{yom} & C_{yon} \\ C_{zox} & C_{zoy} & C_{zoz} & C_{zol} & C_{zom} & C_{zon} \\ C_{lox} & C_{loy} & C_{loz} & C_{lol} & C_{lom} & C_{lon} \\ C_{mox} & C_{moy} & C_{moz} & C_{mol} & C_{mom} & C_{mon} \\ C_{nox} & C_{noy} & C_{noz} & C_{nol} & C_{nom} & C_{non} \end{bmatrix} \times \begin{bmatrix} X \\ Y \\ Z \\ L \\ M \\ N \end{bmatrix}$$

A typical term C_{zoz} represents the out put $Z_0 = (N_{10} + N_{20} + N_{30})$ in milli volts/volt of excitation for a unit load in the z direction. Similarly C_{mon} represents the output $M_0 = (2\,N_{20} - (N_{10} + N_{30}))$ in milli volts/volt of excitation for a unit moment N about z axis.

During the calibration it was found that the outputs were quite linear with respect to applied loads and moments and interaction effects were quite small. Some combination of loads were applied and from the output, work back loads were computed and it was found that we could get the work back loads within 1%.

THIN THREE-COMPONENT DELTA WING BALANCE

Details of the thin three-component balance (reference 1) which was specially designed for this study are shown in figure 7. This balance, having a thickness of only 2.5 mm, can be housed inside a model of

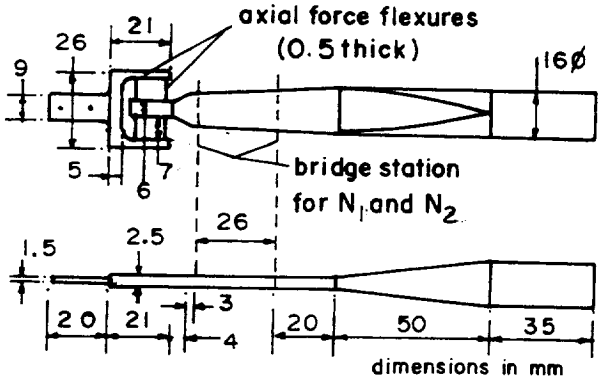

Figure 7. Details of thin three component balance

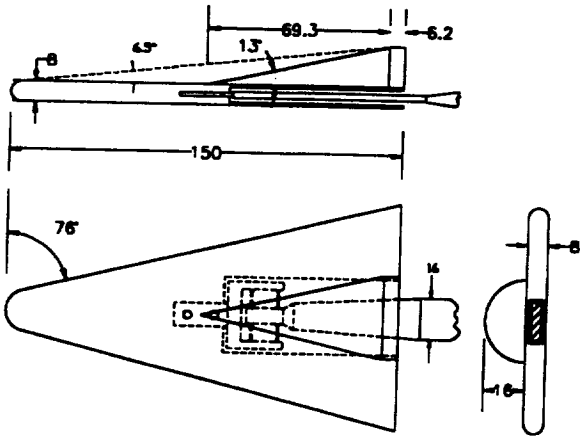

Figure 8. Details of a typical slab delta wing model with lee-side body

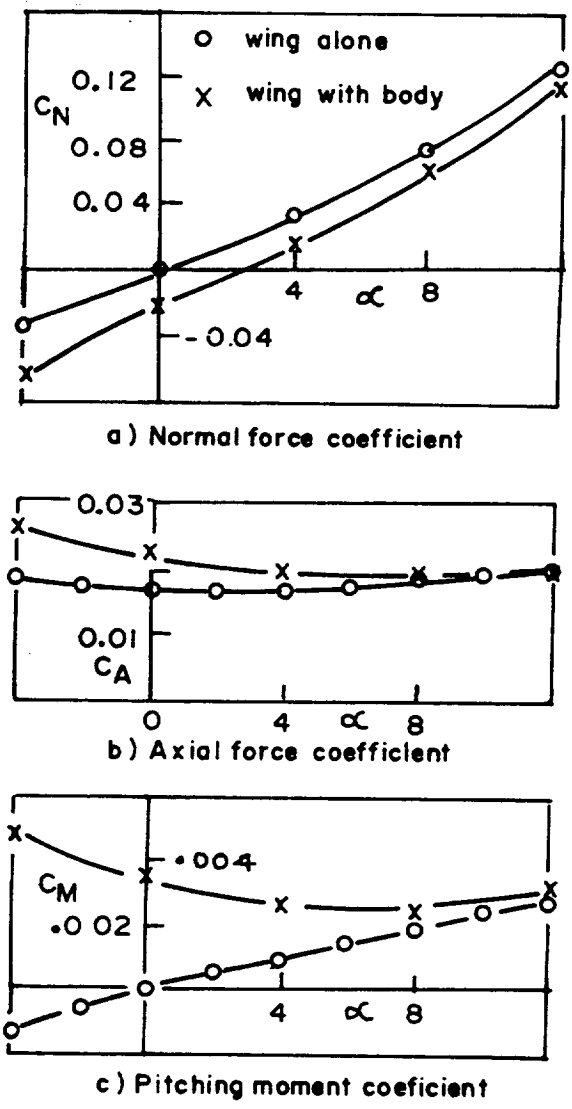

Figure 9. aerodynamic characteristics with and without lee-side body

thickness 4 mm though the delta wing thickness used in the present investigation was 8 mm. (figure 8). Aerodynamic data for wing alone and wing with different lee-side bodies could be obtained. The rear axial force flexures were gauged to obtain a four-arm active bridge. The normal force and pitching moment were measured as equivalent normal forces N_1 and N_2 acting at the two stations shown in the figure (N_1 force location is in front and N_2 force location is at the rear). The location of the balance in the delta wing was such that the 2/3 chord point, which is close to the centre of pressure for the delta wing was located at the centre of the forward and rear axial force flexures, so that the axial force flexures are not subjected to excessive twising moment. The balance was designed for a full normal force of 2 kg. This low-load design enabled accurate measurement of forces at low incidences and allowed the balance to be housed inside the delta wing. Therefore, incidence range of the test was restricted to about 12°.

It was found that the balance being flexible, second-order interaction terms in the balance calibration was important and had to be considered. The linear and non-linear second-order calibration coefficients were obtained by following the simple method of least squares given in reference 2. Knowing the bridge outputs, to determine N_1, N_2 and A an iterative technique was used. Converged values N_1, N_2 and A were obtained in 4 or 5 iterations. To check the accuracy of the calibration, typical combinations of N_1, N_2 and A were applied and from the outputs, the loads were calculated using the above iterative procedure. It was found that the calculated loads were within 1% of the applied loads. During tests, incidence correction due to deflection of the balance was applied.

Typical results and discussion

The present experiments were carried out in the 200 mm hypersonic tunnel of IISc at M=8.0. Boundary layer trip was not used in these experiments. The Reynolds number based on chord was one million. The boundary layer is therefore expected to be laminar.

Variation of the normal force coefficient C_N with incidence for the basic delta wing and for the wing with the lee-side body is shown in figure 9. It may be pointed out that lee-side body goes into aerodynamic shadow at an angle of 6.5°. It is obvious from fgure 9a, that even at $\alpha = 12°$, which is well beyond 6.5°, C_N for the delta wing with the lee-side body is lower than that for the delta wing alone by about 8%. Of course, the interference is much higher at lower incidence. Variation of the pitching moment C_m about 2/3 chord point with incidence is shown in figure 9b. As expected, C_m for the wing with lee-side body is positive (nose up) at zero incidence and is opposite to that of the plain wing. The large amount of interference due to the lee-side body is obvious from this figure also. The variation of the axial force C_A with incidence is, shown in figure 9c. Increased C_A due to the lee-side body is clearly seen.

It is thus obvious that the claim made by some earlier workers that the lee-side balance housing body has no effect once it is in the aerodynamic shadow of wing is not at all correct and without the special balance, there is no way of getting proper data for delta wing alone at low incidences.

THIN 6-COMPONENT DELTA WING BALANCE

Details of the Thin 6-Component Balance are shown in figure.10. This balance is made of maraging steel.. This balance was designed with the objective of measuring the effectiveness of trailing edge flaps on delta wings. Therefore the design loads viz. N.F.=10 kg and axial force = 8 kg, were higher than that for the 3 component balance. Therefore the thickness of this balance was increased to 4mm. Also, sufficient width was necessary to form the side force S_1 and S_2 bridges. This increased thickness also helps in improving the rigidity for the rolling moment. The rolling moment is measured by using the asymmetric bending of the forward lateral beam. The arrangement for measuring N_1, N_2 and A is very similar to that of the 3 component balance, but with the following modifications. The thickness of the flexures was increased to 1mm. and the axial force flexures were located in between the N_1 & S_1 and N_2 & S_2 load locations. This is expected to reduce the interaction on the axial force output due to normal and side forces. In order to further reduce the interaction of the normal force and side force loads on axial bridge output, the strain gauges forming the axial force bridge were located on both the flexures as shown, with the hope, that opposite type of flexing of the two flexures due to either normal force or side force would tend to cancel and reduce the interaction.

Here only pure loads were applied and it was found, that both direct and interaction outputs were all very linear. Since facility for combined loading for 6-component balance was not available and since the variation of output with load was linear for all cases, only a simple 6x6 matrix for linear coefficients which can be directly inverted to get the loads was used. Here also some typical combinations of loads were applied and the work back loads from the outputs was calculated. It was found that the work back loads were within 1% of the applied loads.

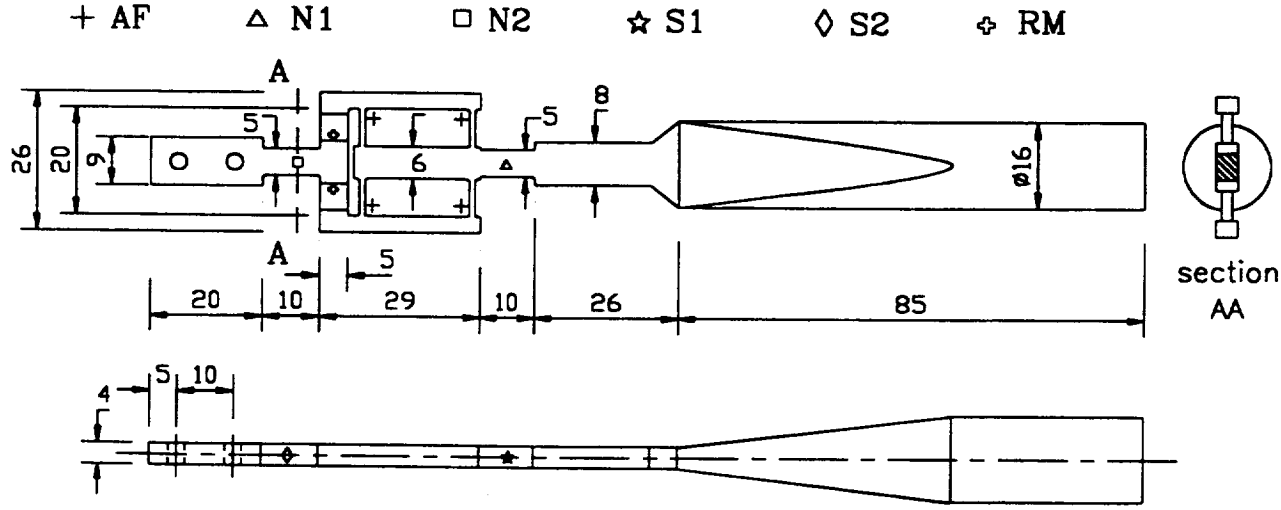

Figure 10. Details of thin six-component balance.

Model Details

Dimensional-details of the 76° sweep, 8 mm thick, delta wing model with trailing edge flaps are shown in figure.11. The arrangement for deflecting the flaps to any desired angle and clamping it in that position is shown in figure 12. The rod on which the flap is clamped is prevented from rotating by the square head located snugly in the corresponding recess in the main model. Note that the model design in this case is also different from that shown in figure 7. In order to accomodate the flap, we cannot have a wide cut out in the wing as was done for the model in conjunction with the 3 component balance. Therefore it is not possible to introduce the 6-component balance from the back as was done in the case of the 3-component balance. Therefore the cut-out in the model is shaped in such a manner that with the cut-out open, the 6-component balance can be brought in from the top and fixed to the model. Afterwards, the cut-out is covered by a cover plate and fixed by screws. In the case of the model used in conjuction with 3-component balance, the cover plates were permanently glued to the model.

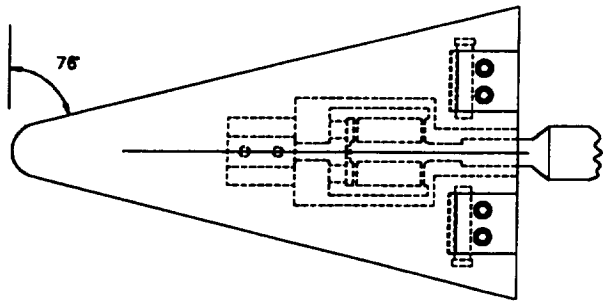

Figure 11. Details of slab delta wing model with flaps.

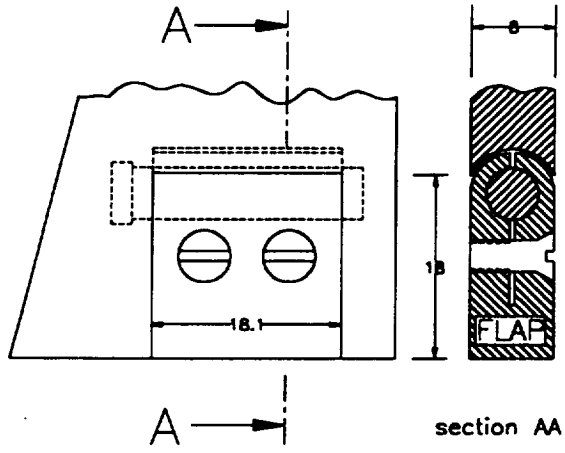

Figure 12. Arrangement for deflecting the flaps to desired angle

Results & discussion

The aerodynamic characteristics of this model at M=8.0 obtained in IISc hypersonic wind tunnel for zero flap deflection, symmetric deflection of both flaps wind ward (δ_f = +20°), leeward (δ_f = -20°), and antisymmetric, (δ_f = ±20°) are shown in figure 13. From this figure, the following inferences can be drawn. The flap effectiveness increases with incidence for windward deflection, whereas its effectiveness decreases rapidly with incidence for leeward deflection. The longitudinal characteristics with δ_f = ±20°, as expected, lies mid way between that for δ_f = +20° and that for δ_f = -20°. The yawing moment and rolling moment variation with incidence for antisymmetric deflection case of δ_f = ± 20° is shown in figures 12d and 12e.

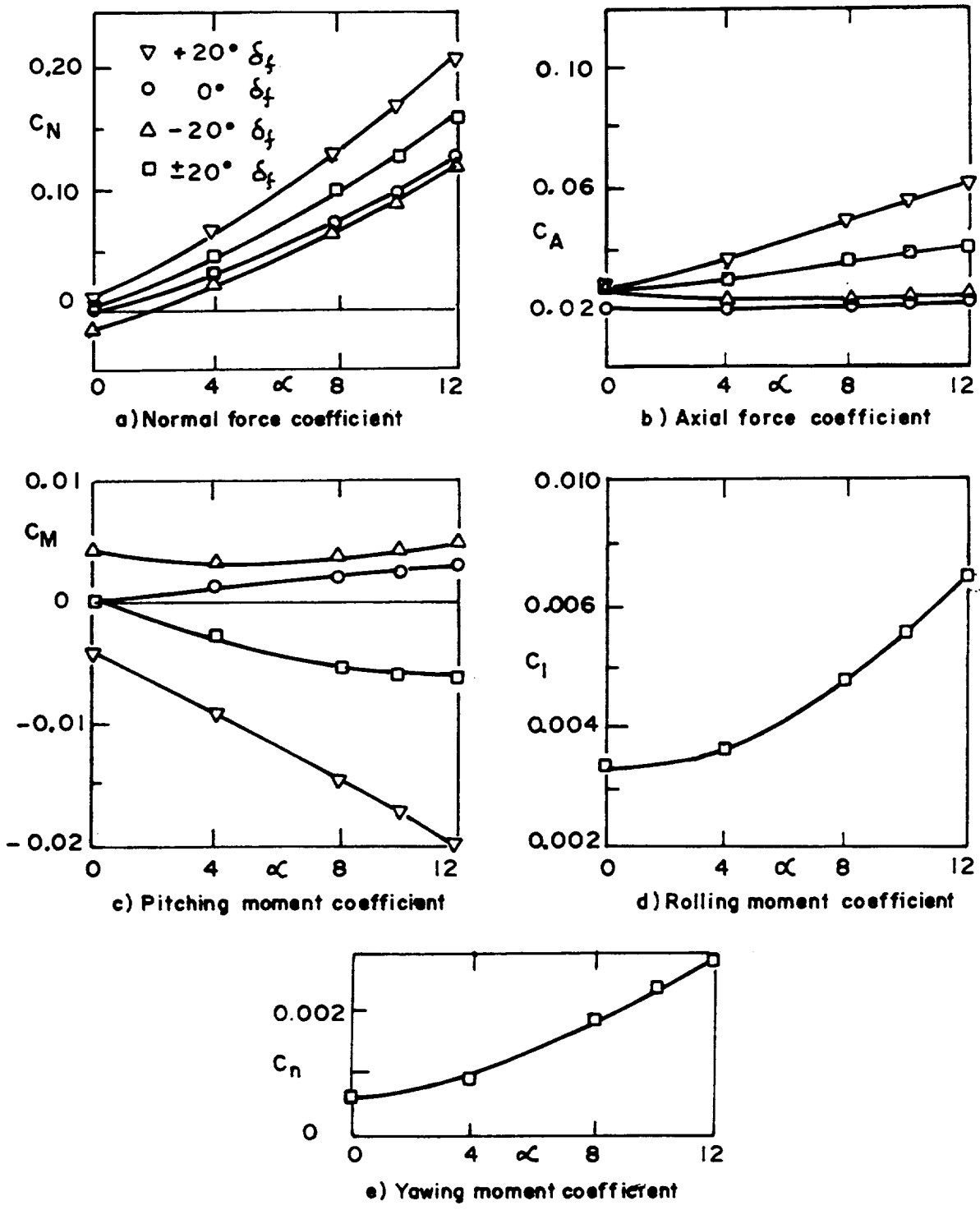

Figure 13. Aerodynamic characteristics of slab delta wing model with symmetric and assymmetric flap deflection

SPECIAL CAGE TYPE 5 COMPONENT BALANCE

A 5 component cage type balance to measure the normal force (NF), side force (SF) pitching moment (PM), yawing moment (YM) and Rolling moment (RM), due to both aerodynamic and inertia forces, acting on the rotating model mounted on the rotary Derivative Rig of the 14'x 9' low speed wind tunnel has been designed. The loads for which the balance has been designed is given below.

NF = 100 kg, SF = 50 kg, PM = 10 kgm , YM = 8 kgm , RM = 2 kg m.

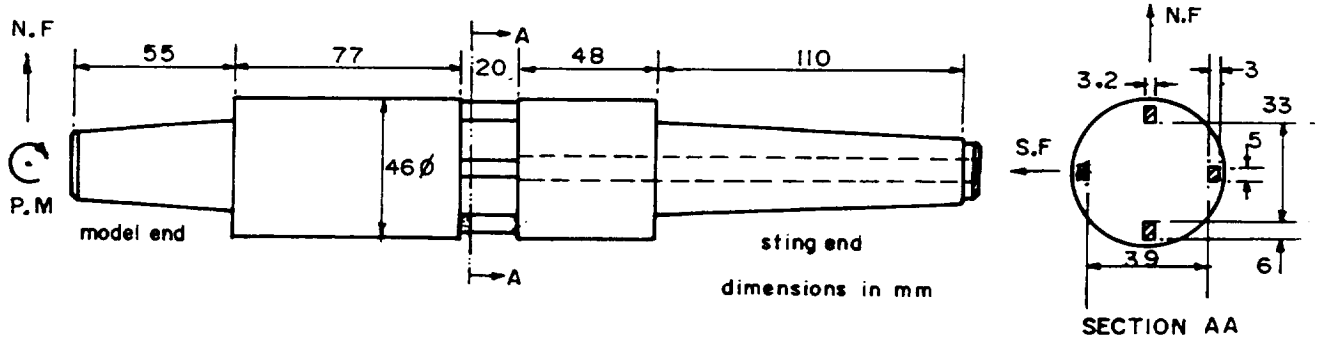

Figure 14. Details of the 5 component cage type balance

The details of the balance are given in figure 14. To arrive at the dimensions of the elements of the cage so that the output of the strain gauge bridges measuring the various loads and moments are of the same order, several interations were required. The special feature of the design lies in the fact, that though all the elements of the cage gets stressed due to all the components, the bridge formation to measure the various components are so made that, when properly located as per design, the bridges are sensitive to their corresponding components and not to the other components. This becomes obvious from figure 15, where the direction of positive loads and moments, the gauge locations and bridge formation for various components, the type of stresses introduced in the arms of each of the bridges for all the components are shown. Therefore theoritically interactions have to be negligible. However, due to errors in gauge locations, same amount of interactions were noticed duing calibration, but they were found to be small. Both the direct and interaction outputs were found to be quite linear.

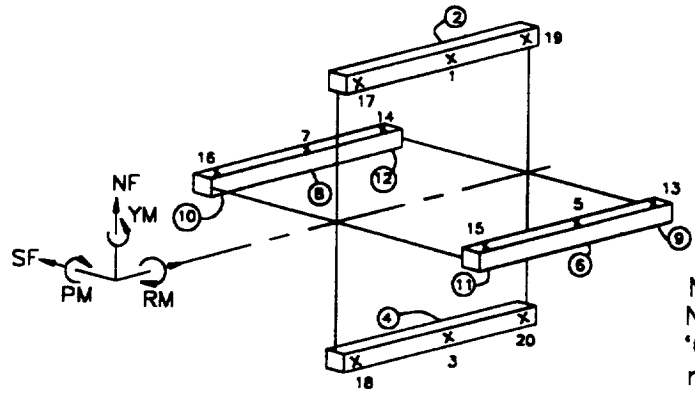

Gauge locations on the cage (ends removed for clarity)

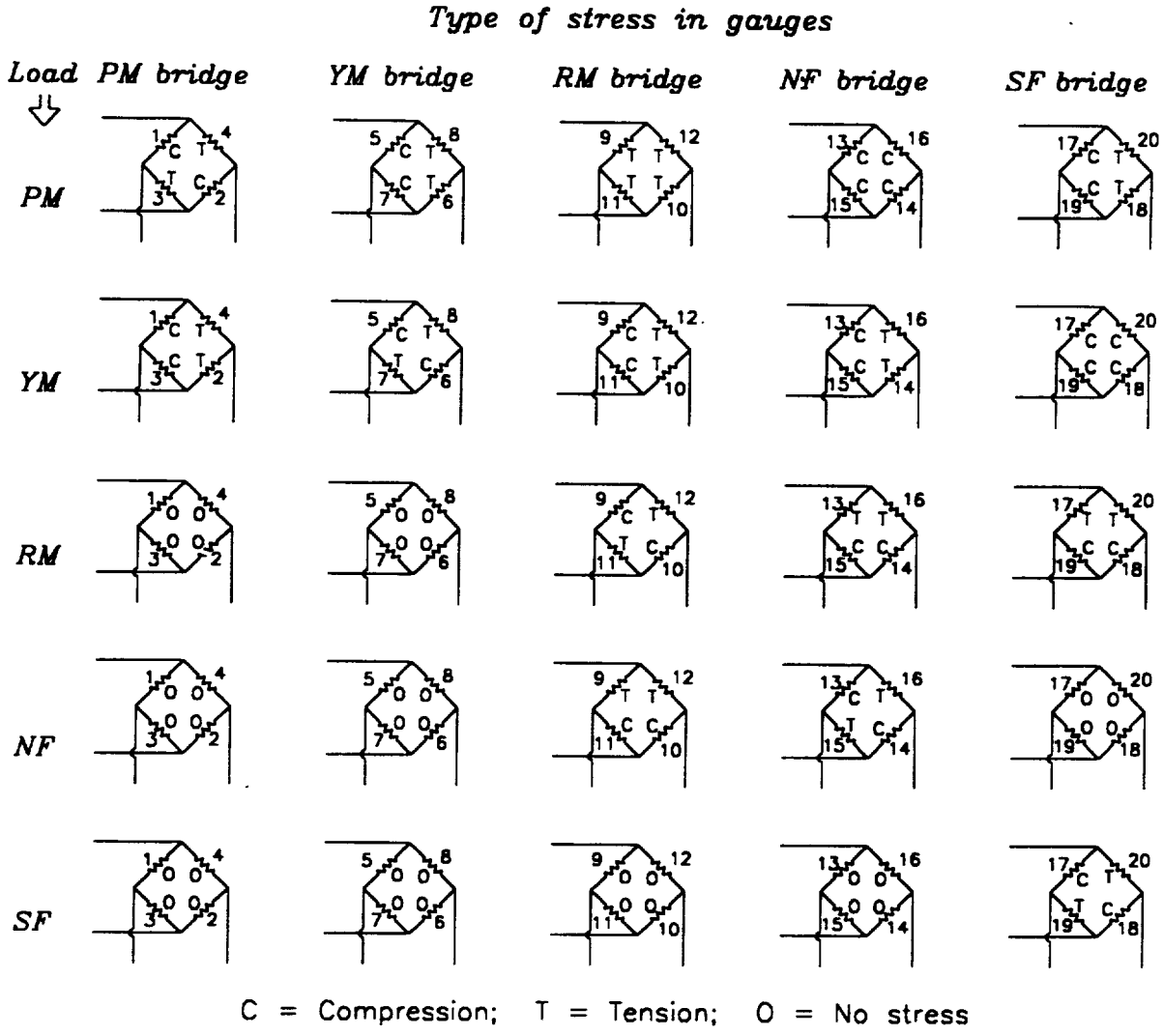

Figure 15. Formation of bridges to minimise interaction.

NOVEL BELLOW TYPE BALANCE FOR WATER TUNNEL

Complete details regarding this balance are covered in another paper being presented in this conference (reference 3). Therefore, only the main features would be touched upon.

Since water proofing of strain gauges of the balance for water tunnel application did not work and since the size of the balance did not permit using encapsulated water proof gauges, it was thought the balance could be covered with a flexible rubber bellow as shown in figure 16, and the hole at the rear end through which the wires are led out is sealed so that the gauges do not come into contact with the water. If the space between the bellow and balance contains trapped air, then as the ambient pressure outside the balance is varied in the water tunnel, the following problems arise. If the ambient pressure is lower than the initial pressure of the trapped air, then, the bellow bulges and touches the model in which it is mounted. If the ambient pressure is higher than the initial trapped pressure of the air, then the bellow collapses and may interfere with the functioning of the balance, particularly for axial force measurement. Apart from these problems, the difference between the inside equillibrium pressure reached and the ambient pressure results in an axial force on the balance which can be of the same order of magnitude as the axial force due to hydrodynamic load. Also one needs to measure both the trapped air pressure and the outside ambient pressure to account for this axial force.

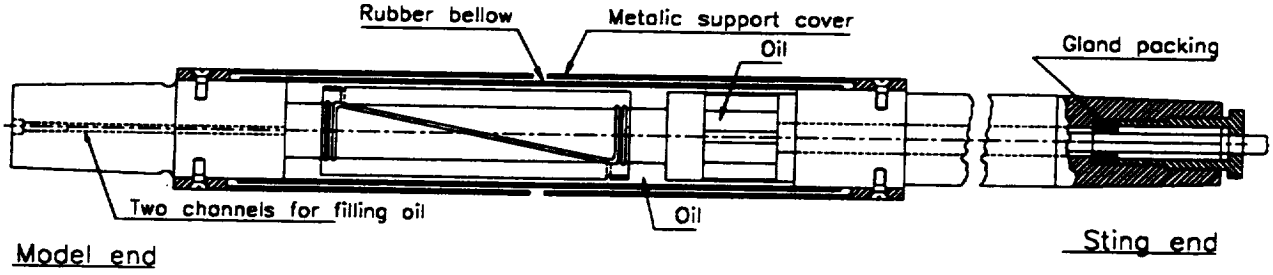

Figure 16. Novel bellow type balance for water tunnel

To overcome these problems, a novel idea of filling up the space between the balance and the bellow with insultig transformer oil was thought off. Note that, since the bellow is flexible and filling it with fluid would end to make the bellow sag, support covers as shown in figure 16 are used to limit this sagging. It was found that these covers do not interfere with the measuring system. Because of nearly incompressible nature of the liquid, the pressure inside will be nearly equal to that of the ambient and no significant bulging or collapsing of the bellow would occur. It was found that, unless all the dissolved gases in the oil was removed before it was filled into the cavity between the bellow and balance, the difference in the pressure between inside and ambient was not small enough to be neglected. However, if proper care is taken in removing the dissolved gases, the pressure difference was negligible and the correspondig axial force output was less than 0.5%, being worst when the ambient conditions went to vacuum conditions of

0.2 bar absolute. The balance output can be calibrated against the ambient pressure and perhaps, even this small effect can be taken into account. A balance using this concept has been successfully developed. As already stated more details of this balance are given in reference 3.

CONCLUDING REMARKS

Many special balances to meet the varied requirement of special tests have been successfully designed, and developed indigenously, at the Department of Aerospace Engineering, Indian Institute of Science, Bangalore.

REFERENCES

1. Ramesh, R.; Ramaswamy, M.A.; and Vasudevan, B.: *Thin Flat Internal Strain Gauge Balances for Testing slab Delta Wing Models at Hypersonic Speeds.* ICIASF - 95, July 1995.

2. Ramaswamy, M.A.; Srinivas, T.; and Holla, V.S.: *A Simple Method for Wind Tunnel Balance Calibration Including Non-linear Interaction Terms.* ICIASF - 87, June 1987

3. Vasudevan, B.; and Ramaswamy, M.A.: *A Novel Oil Filled Bellow Type Internal Strain Gauge Balance for Water Tunnel Applications.* International Symposium on Strain gauge Balances, NASA CP 19

NASA LaRC STRAIN GAGE BALANCE DESIGN CONCEPTS

Ray D. Rhew
NASA Langley Research Center
Hampton, Virginia

ABSTRACT

The NASA Langley Research Center (LaRC) has been designing strain-gage balances for more than fifty years. These balances have been utilized in Langley's wind tunnels, which span over a wide variety of aerodynamic test regimes, as well as other ground based test facilities and in space flight applications. As a result, the designs encompass a large array of sizes, loads, and environmental effects. Currently Langley has more than 300 balances available for its researchers. This paper will focus on the design concepts for internal sting mounted strain-gage balances. However, these techniques can be applied to all force measurement design applications. Strain-gage balance concepts that have been developed over the years including material selection, sting, model interfaces, measuring sections, fabrication, strain-gaging and calibration will be discussed.

BACKGROUND

A strain-gage balance is: *a transducer used to measure the aerodynamic loads encountered by a wind tunnel model during a wind tunnel test.* Figure 1 is a schematic of a typical strain-gage balance installation within a wind tunnel model. There are six degrees of freedom that the balance has to measure and they are depicted in figure 1 with LaRC's naming and sign convention. Although the balance's task to measure these six degrees of freedom appears simplistic, it has proven to be one of the more challenging transducer development technology areas. In addition, as the emphasis increases on improving aerodynamic performance of all types of air and spacecraft the demand for improved balances is at the forefront. This is due to the balances fundamental purpose: as the most important and critical measurement (coupled with angle-of-attack) used to determine the performance of a model undergoing aerodynamic characterization.

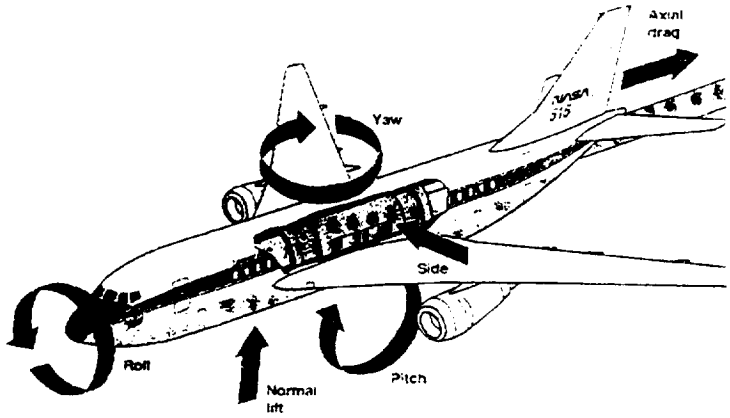

Figure 1. Strain-gage balance location in a wind tunnel model

LaRC's long history as a leader in the aerodynamic community has been in part due to its commitment to high quality transducers. Without quality instrumentation a wind tunnel test result will not be very useful. Therefore, due to its importance in aerodynamic testing results, LaRC has been designing balances and related sensors and test equipment for many years. The earliest balances were constructed out of multiple pieces of material and bolted, screwed and sometimes welded together in order to provide the measurement of six degrees of freedom necessary to characterize a test article. Figure 2 displays one of LaRC's earliest internal strain-gage balances. These multi-piece designs were state-of-the-art at the time, based on design and manufacturing techniques available, but were susceptible to problems such as hysteresis and zero shift as a result of "slop" or movement of the jointed regions. Figure 3 is a depiction of hysteresis and zero shifts that occurs during calibration of a balance.

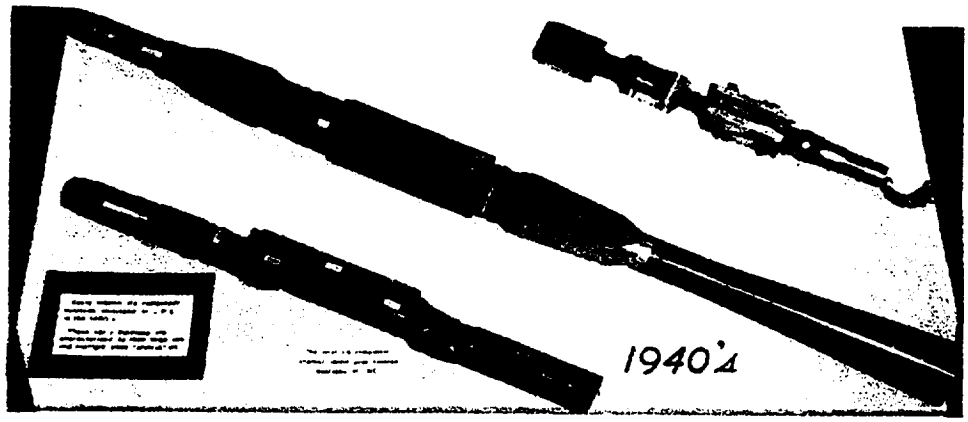

Figure 2. LaRC's First Internal Balance

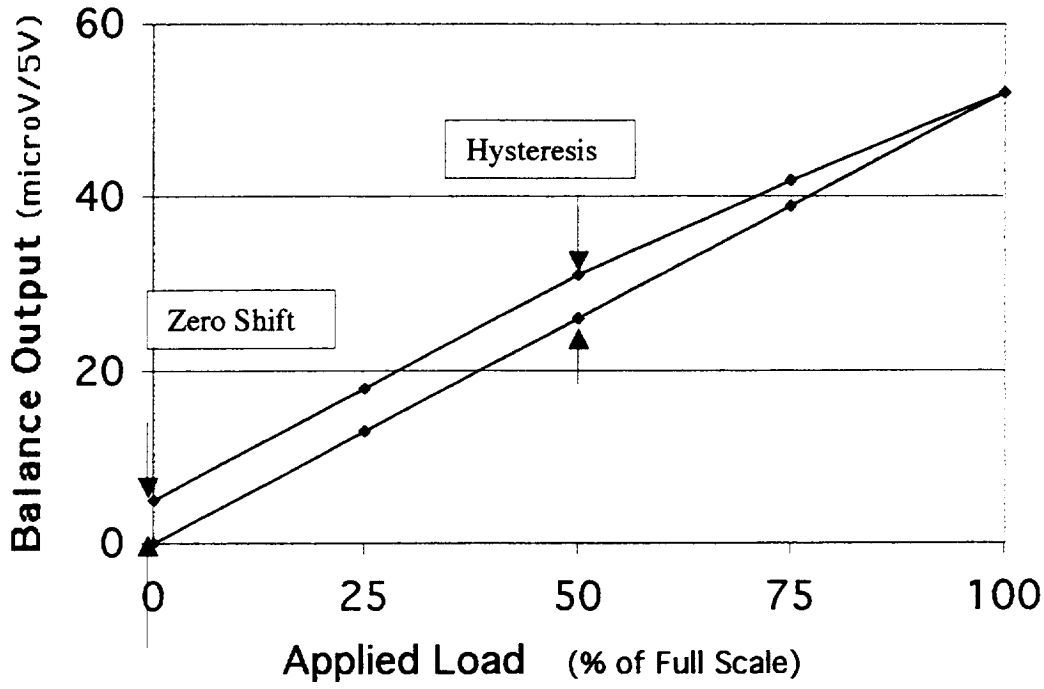

Figure 3. Example of Hysteresis and Zero Shift

One major change in the design of strain-gage balances at LaRC was the incorporation of electrical discharge machining (EDM) into the manufacturing process. This machining technique (circa 1958) allowed balance design to be a single piece of material that greatly reduced the hysteresis and zero shift issues of multi-piece designs. This is the same philosophy employed by our balance design engineers today of utilizing a single piece of material or monolithic design at all times for a quality balance.

Additional background information that has shaped the development of balances at LaRC is the environmental parameters imposed by LaRC test facilities, mainly temperature and load capacity. The major facilities at LaRC that are used for force testing have balance temperature ranges from -250°F to +250°F. In addition, the range of balance sizes is from 0.3 in to 4.5 in. in diameter with load capacities from 1 pound to 12,000 pounds of normal force. Although many of these facilities have tests that require special balances such as flow through types for powered model testing, this paper will focus on typical internal balances.

INTRODUCTION

One of the most important practices of LaRC's research staff, that is highly recommended by the balance group, is to match as closely as possible the expected loads of a test with the full scale loads of the balance. This will ensure that the maximum resolution of the instrument is obtained. Therefore, the best results from a test program

will be attained from designing a balance for each particular test regime such as performance or stability and control (two balances).

As discussed in the background section, the philosophy of our balance engineers is to design the balance from a single piece of material. This is the starting point of the design and the remainder of the information is provided by the researcher preparing for a test program, or possibly by a balance engineer investigating a new design concept. Listed below are the parameters required for designing a new balance.

1. Expected loads in all six degrees of freedom
2. Location of the balance within the model
3. Maximum balance dimensions (typically given in diameter and length)
4. Environmental parameters (temperature, pressure, moisture conditions, dynamics, possible exposure to airflow or corrosive substances)
5. Interface requirements within the model (metric end of the balance) and to the support structure (non-metric end of the balance)
6. Required accuracy and resolution
7. Electrical interfaces available (data signal)
8. Data acquisition system specifications
9. Data analysis software specifications
10. Special set-up and checkout equipment

Once this information is provided the actual design can begin. The initial task is to review past designs and utilize a balance design of similar specifications. From here the balance design engineers at LaRC utilize custom software to iterate through the design and converge to the best solution. This software is based upon textbook mechanics of solids as well as LaRC developed analysis methods. Finite element analysis is beginning to be evaluated as a tool to possibly help in the areas of reducing stress concentration factors, improving thermal characteristics and optimizing the design. Reviews of the design are held with the balance group, researcher, and all personnel involved in the production of the balance to ensure a quality and timely product. The following sections will discuss in more detail the process, and technical attributes of designing LaRC strain-gage balances. Figures 4 and 5 are pictures of two LaRC balances with the main features labeled.

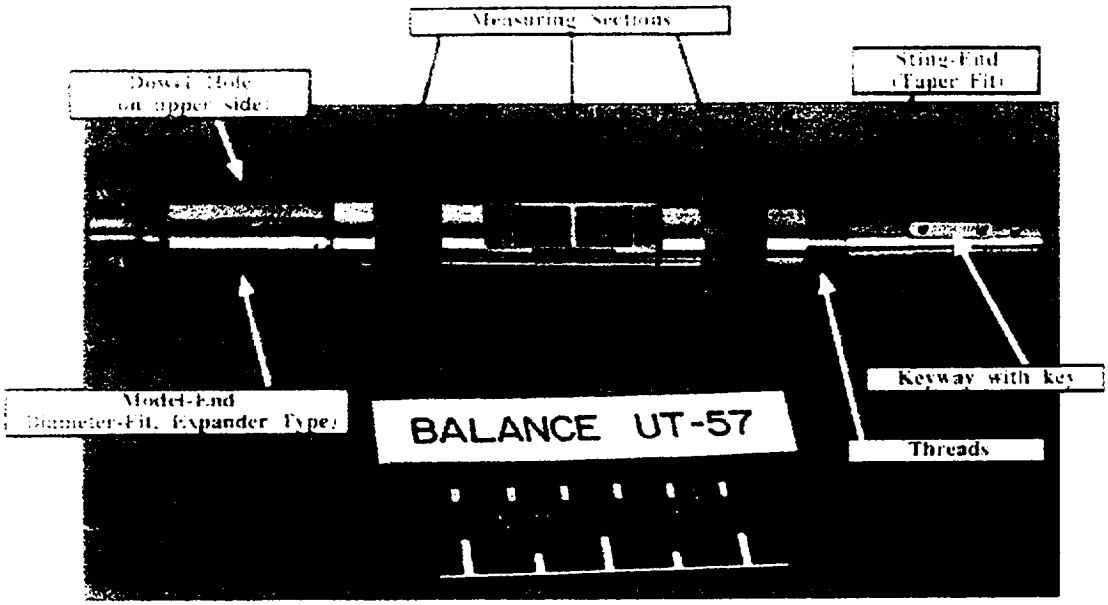

Figure 4. NASA LaRC Internal Strain-Gage Balance (Unitary Tunnel Configuration)

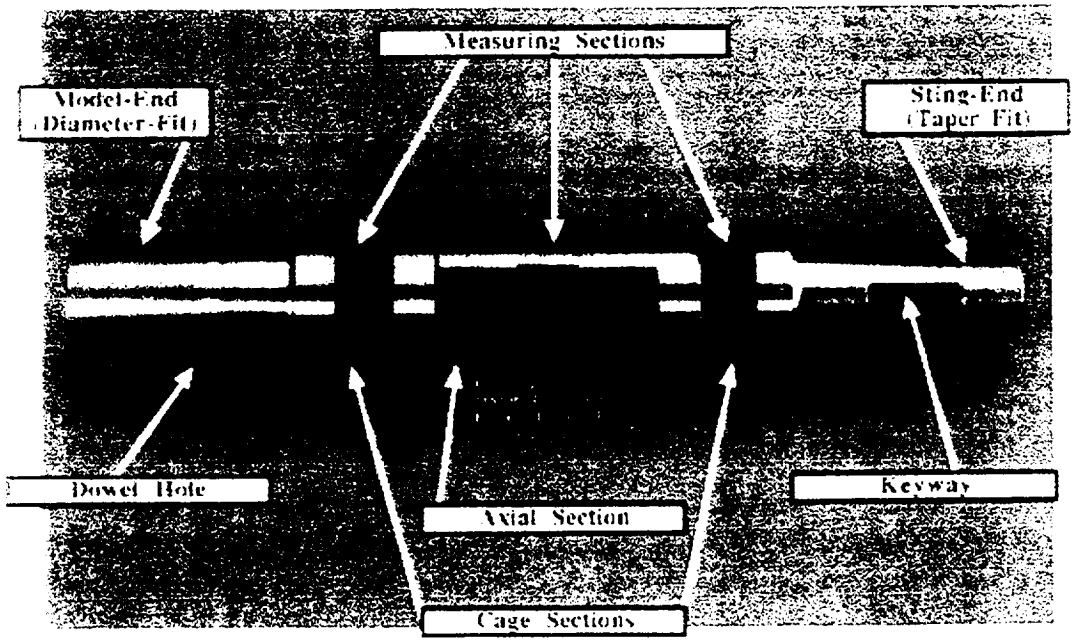

Figure 5. NASA LaRC Internal Strain-Gage Balance (NTF Configuration)

MATERIAL SELECTION

LaRC balances are fabricated from a select group of materials. They must exhibit "transducer quality" characteristics. Based on supplier generated test data and our own research programs the following materials are utilized for LaRC balances with the majority coming from the first three selections.

1. 17-4 PH or 15-5 PH stainless steel (H925; Rc = 40-42)
2. C-200 18% Ni maraging steel (H900; cryogenic applications; Rc = 41-45)
3. C-300 18% Ni maraging steel (H900; high capacity applications; Rc = 52-55)
4. 2024-T4 Aluminum
5. 7075-T6 Aluminum
6. Beryllium Copper (Be-Cu) (extreme temperature applications)

The material selection is typically determined at the outset of the balance design. Reviewing past designs and performing a few very simple diameter to load calculations the strength, toughness and hence the material required for the balance can be selected. However, there are times when some detailed analyses must be performed before final selection when a more ductile lower strength material is preferred.

Other considerations must be given to the selection process such as the environment (moisture, corrosive substances,...). In addition, strain-gage application and interaction with the material under load and test conditions must be thoroughly evaluated.

STING AND MODEL INTERFACES

The typical sting (non-metric or ground-side) interface for LaRC balances is a tapered cylinder (taper). The advantage of this design is its ease of installation especially if the model is required to be assembled to the balance prior to insertion into the sting. In addition, to the taper joint securing feature, all of these joints incorporate either a double-nut or set screw configuration for added security. The double-nut is used as the standard and set screws are employed on balances that are either: 1) too small or lack clearance for a threaded section; or 2) are required to operate cryogenically where the stress concentrations imposed by the threads are not acceptable. Also, a keyway is cut into the taper for roll load reaction. Figure 6 shows the typical configuration of tapered sting end attachments for LaRC balances. The maximum diameter of the tapers range from 0.3125 inches to 5.0 inches.

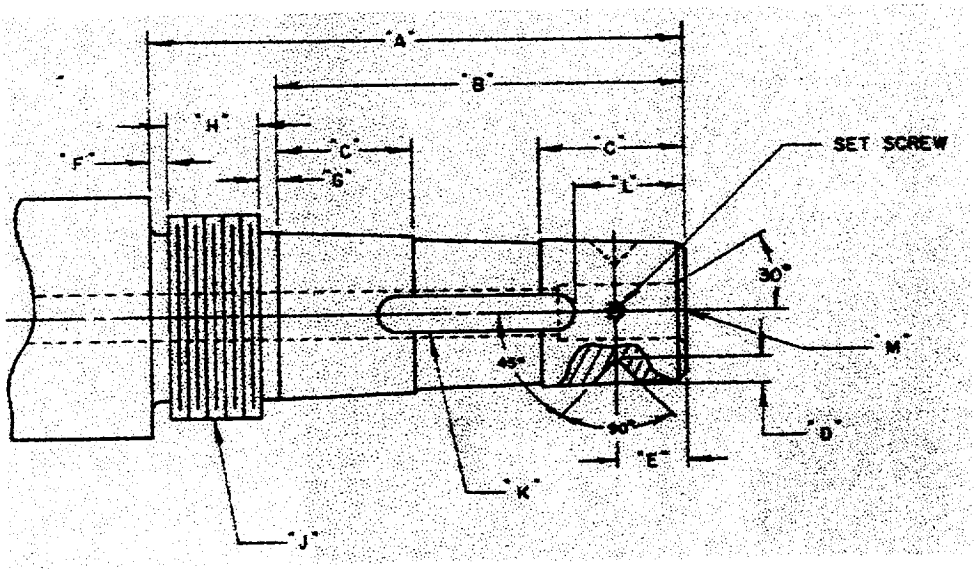

Figure 6. Balance taper (all tapers are 1inch/foot)

There are some disadvantages of the tapered sting-end attachments such as difficulty to machine to rigid specifications and maintain due to wear and high load requirements. Due to the recent increased demand on minimizing motion between balance joints, the tapered keyway design is limited. One characteristic that limits its ability to minimize roll motion is the fact that it requires some clearance for assembly because it is a sliding fit. Also, roll motion is very difficult to control when the largest securing factor is the key that is bearing on a small area.

Difficulties associated with these tapered sting-end attachments have led LaRC to utilize other methods when geometry of the balance/sting interface allows. One type is a flange fit that requires a larger diameter. The majority of semi-span balances utilize this attachment method on both the sting or support structure and model side. These joints are easier to machine, maintain and in some instance easier to assemble. Other interface designs are constantly being researched. However, implementation is a difficult aspect because of the large inventory of balances and stings.

Model interfaces are typically cylindrical fits with a location securing interference fit dowel pin. The model to balance connection is the most critical within the wind tunnel test because this fit determines the axes of the loads to be measured relative to the balance axis. If the balance is not aligned properly and the misalignment is not accounted for, errors will be present. This type of interface has the advantage of providing almost no motion between the balance and model (when properly machined and assembled). A modification of this design is the LaRC front-end expander. The front-end expander provides the same cylindrical fit but with a more adaptable design. By expanding a sleeve on the balance front-end to fit the model bore, an easier installation is provided. This expander front-end is not used for cryogenic applications or with high load to diameter ratios for performance purposes. Figure 7 shows a typical expander front-end fit design. The sizes of the expander front ends range from 0.625 to 3.1 inches.

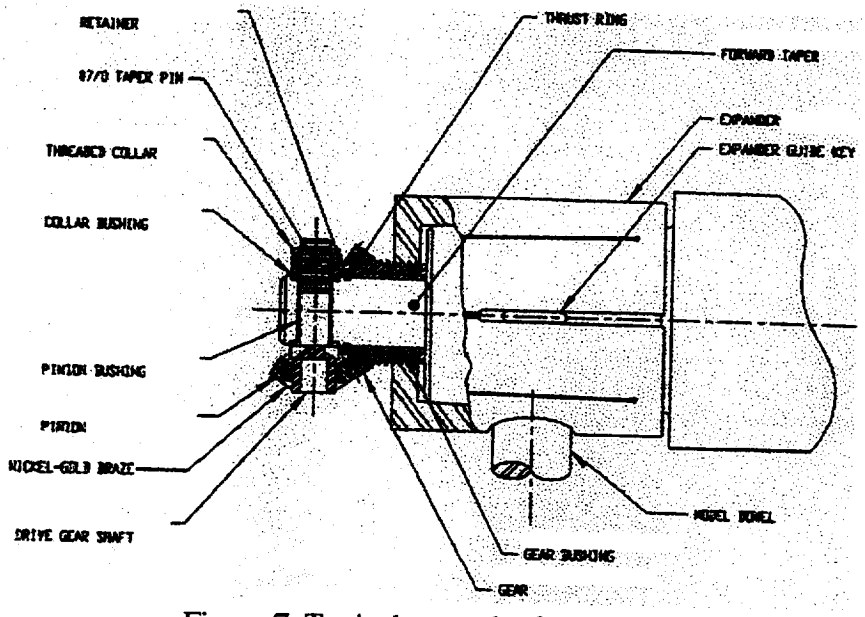

Figure 7. Typical expander front-end

There are some difficulties associated with these designs. Machining is very critical in the areas of roundness and cylindricity as well as true position of the dowel hole. Assembly is critical, can cause wear and requires a detailed procedure. In conclusion, alternative methods are being researched and designs such as the flange-type mentioned above are utilized when possible.

MEASURING SECTIONS

The measuring sections are strain-gaged areas of the balance that have been optimized for a given balance design based on the full scale load of the balance. There are typically three sections, one for measuring axial force and two for measuring the other five components. A typical NTF balance is shown in figure 8 with the measuring sections labeled. Classical strength of materials and internally generated analysis techniques are utilized to optimize the design of the balance measuring sections. Finite element analysis is being evaluated for use in final optimization and in some cases may be utilized for thermal predictions. The target design criteria is 1 to 1.5 milliVolts output voltage per Volt of input or excitation voltage. The equation below shows how this output voltage translates into strain (or stress) on the balance. Therefore, an iterative process is performed to produce this magnitude of strain-gage output while maintaining a safe level of strain on the balance when all six components of load are applied simultaneously. The ultimate goal is to produce a balance that contains strain gages strategically located that are sensitive to the desired measurement and insensitive to all others. This is achieved through design and proper strain-gage location as well as bridge wiring techniques.

$$\text{Strain} = \left(\frac{\text{Bridge Output Voltage (Volts)}}{\text{(Bridge Input Voltage (Volts)*Gage Factor of strain gages)}} \right)$$

Note: This is for a four-arm active strain-gage Wheatstone bridge configuration

The axial section design is centered on producing a target output voltage to assure adequate measurement resolution while minimizing interaction effects (outputs from the axial strain-gage bridge caused by the other five components). The features noted in figure 8 are the measuring beam (axial slotted-T beam) which is the strain-gaged beam, and the flex beams. This configuration provides the following benefits and many more: 1) Locates the measuring beam as close to the centerline of the balance as possible to minimize moment loading effects; 2) Utilizes the slotted configuration to provide a single bending beam effect and reduce the beams strain due to a normal force loading; 3) Reduces the loads transferred to the measuring beam by having flex beams on either side for support.

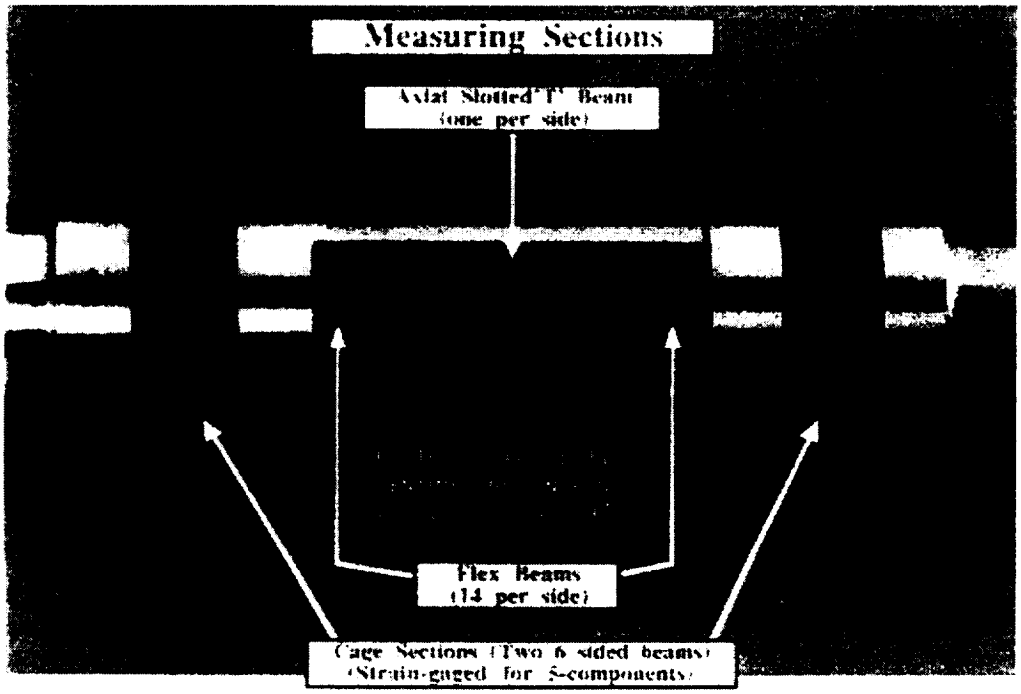

Figure 8. NASA LaRC NTF Balance Measuring Sections

The cage sections take on many different configurations based on the loads to be measured and the ratios of the six components. Figure 9 shows some various designs optimized for the loadings listed. The same philosophy for the axial section holds for these sections, that sensitivity is maximized while interactions are minimized. The typical cross sections of the beams are rectangular. However, notched beams as well as stress riser beams are employed to increase sensitivity when necessary. Other techniques are considered during the design such as stiffening end shoulders which transition the beams to other section of the balance (the model or sting attachment sections) to minimize nonlineraities.

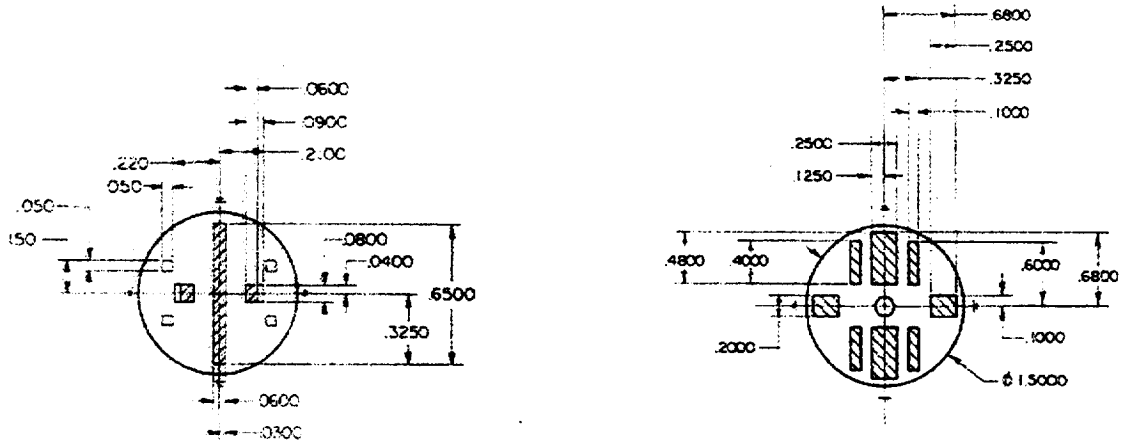

Balance Loads		
Normal Force	50 lbs (220 N)	800 lbs (3,560 N)
Axial Force	10 lbs (45 N)	60 lbs (270 N)
Pitch Moment	100 in-lbs (11 Nm)	2,000 in-lbs (225 N)
Roll Moment	10 in-lbs (1 Nm)	800 in-lbs (90 Nm)
Yaw Moment	15 in-lbs (1.7 Nm)	1,000 in-lbs (110 Nm)
Side Force	15 lbs (65 N)	400 lbs (1,780 N)

Figure 9. Cage Sections

FABRICATION

The fabrication of LaRC balances is a delicate process requiring high precision and patience. Since the balance is constructed from a single piece of material, it is a series process that relies heavily on the Electrical Discharge Machining (EDM) technique (reference 1) and can be separated into the following phases.

- The material certification phase is used to certify the material and ensure it does not contain voids over a pre-determined size for fatigue and fracture requirements. The material undergoes a material certification and an ultrasonic inspection, which is detailed in NASA TM 84625.
- The preliminary machining phase consists of conventional machine shop operations such as turning, milling and grinding. An in process quality assurance (QA) inspection is completed on the balance prior to sending it to step 3, heat treatment, to ensure proper sizing before proceeding.
- The heat treatment phase involves heat treating the material to vendor specifications as listed in the material selection chart. A heat treat certification is issued as well as a hardness test (performed utilizing the Rockwell C scale).
- The final phase of machining is in the EDM process. This consists of wire and plunge type EDM machines. The wire is utilized as much as possible in cutting flats and through holes (typically in the cage sections and on the outline of the axial section). Figure 10 shows a balance in the plunge EDM. Tolerances for the measuring beams are on the order of 0.0005 inches to 0.0002 inches. Therefore, this machining process is very time consuming and critical. The method of either the wire or plunge EDM

requires multiple stages of machining to maintain the tight tolerances and to minimize the EDM effects on the material which are known to reduce the fatigue life. Consequently, there are typically three phases of cutting with the EDM. One is called rough, which gets within approximately 0.050 in of the final dimensions and is performed with the machine in a fast cut mode. The final two steps are called finishing which are performed at much lower cut rates for control as stated above.

- In the QA phase, inspections are performed to tolerances in the range of 0.0002 inches, which require specialized measurement tools and procedures to ensure the measurements are performed correctly. The combination of a coordinate measuring machine (CMM), precision height gages, bore gages, ring, plug and taper gages are typically utilized. This is the final check before proceeding to strain-gaging and is critical for evaluating the final product. A report of actual dimensions verses designed is generated and any deviations noted for review. An internal LaRC document titled "Standardized Model Support System Assembly" lists typical manufacturing fit tolerances and procedures for inspections.

Figure 10. Balance in "plunge type" EDM Machine

Strain-Gaging

Once the balance has completed the final QA inspection it moves into strain-gaging. This step in the production of a balance is very critical to the final performance.

Due to the attention to detail required, usually an experienced technician is required (>5 years experience in transducer quality gaging).

The strain-gaging or wiring diagram, which details the strain-gage layout on the balance, is reviewed by the engineer and strain-gage technician for any possible improvements. The balance undergoes a complete microscopic examination for sharp edges, surface imperfections, and any other areas that may influence the gaging procedures. Reference 2 details the gaging procedures utilized at NASA LaRC. Listed below are typical strain-gages, adhesives, moisture protections and associated materials.

- Strain gages: C-891113-A or B (Micro-Measurements), 350 ohm gages
- Adhesive: M-BOND 610 (Micro-Measurements)
- Moisture Protection: GageCoat 8 (JP Technologies); M-COAT B (Micro-Measurements)
- Solder: 361A (Micro-Measurements)
- Wire: stranded silver-clad copper wire with Teflon insulation (AWG#30 to 44)
- Temperature sensors: type J and T thermocouples, EL-700T (Hy-Cal) platinum resistance temperature detectors

For harsh environments such as elevated temperatures or excessive moisture other techniques are applied and detailed in reference 2.

Following the installation of the strain-gages, a QA inspection is performed to ensure proper location and alignment. The strain-gages are then wired into a bridge configuration as shown in figure 11.

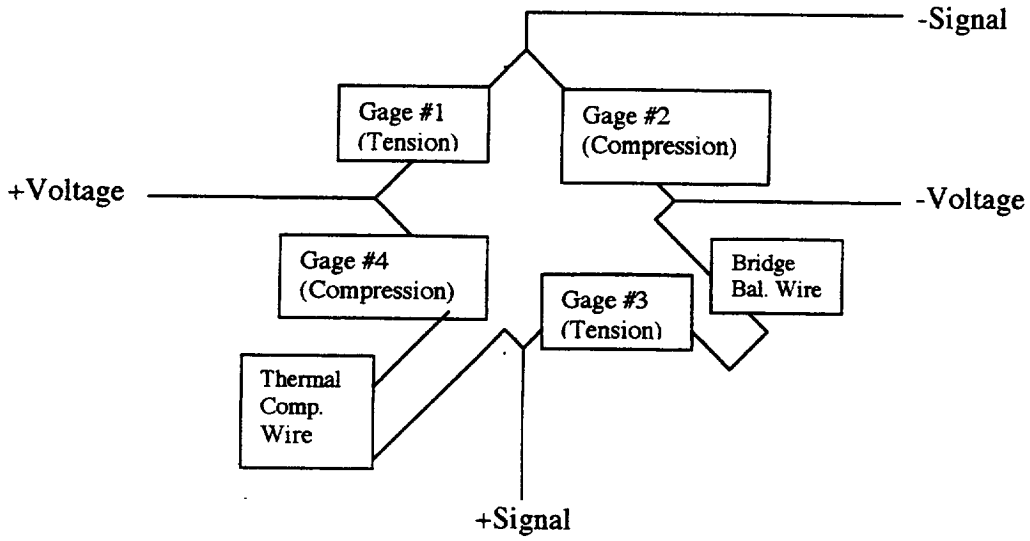

Figure 11. Wheatstone bridge configuration

The bridges must be zero balanced within 0.4 mV/V using Manganin wire to offset the resistance difference between the gages. The balance bridges go through

temperature compensation to minimize the output due to steady state temperature changes. Nickel (and silver-clad copper) wire is placed in the bridge (see figure 11) to counteract the response of the bridge to temperature change in a constant load condition. Figure 12 shows a typical temperature run for a balance to be used in a conventional tunnel (80°F to 180°F to 80°F) and the accepted tolerance. Additional sensors are installed on the balance as needed for monitoring temperature. A list of standard temperature sensors is in the bullet list above. When possible, the lead wires are in twisted pairs, signal and power, with a shield to ensure minimum interference and an outer protective sleeving is installed that is nylon or fiberglass. Once the strain-gage bridge wiring is completed, the balance is temperature cycled through its expected operational temperature range plus 50°F where possible. This ensures that all of the wiring has been relieved.

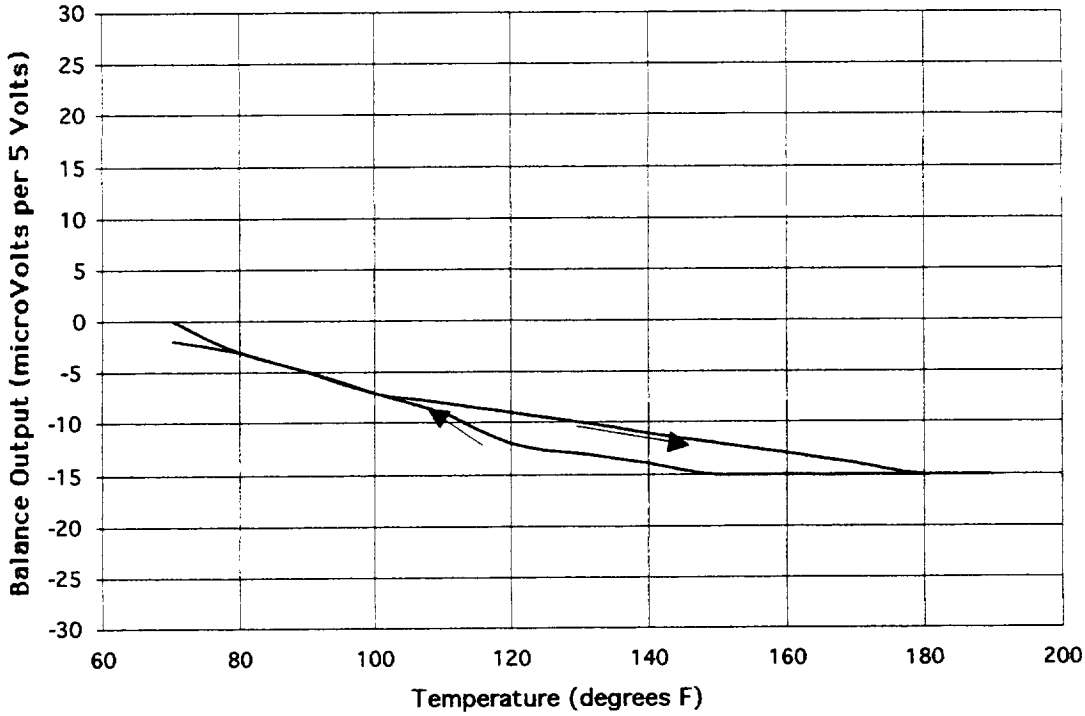

Figure 12. Balance temperature compensation run (test)

Calibration

Balance calibration is the final major step before delivery to the customer. The methods utilized are critical to characterizing the balance and the data is the only deliverable other than the balance itself. The best calibration is achieved when the balance is subjected to the same environmental conditions in the calibration laboratory as the research facility or wind tunnel where the balance will be used. Currently the majority of balances are calibrated at room temperature and to full scale balance loads. While this

approach has been acceptable in the past, certain applications, such as cryogenic, have required more in depth calibration at simulated tunnel conditions to improve accuracy. This section will briefly discuss LaRC's current calibration techniques and touch on future developments. References 3, 4, 5 and 6 discuss these techniques in more detail.

LaRC's traditional calibration approach is to use the 6x27 (matrix) second order iterative math model (illustrated below) to characterize a balance.

Balance output (θ) = $k_{I,1}F_N + k_{I,2}F_A + k_{I,3}M_Y + \ldots + k_{I,6}F_Y + k_{I,7}F_{N\wedge 2} + k_{I,8}F_NF_A + k_{I,9}F_NM_Y + \ldots k_{I,27}F_{Y\wedge 2}$

This equation is rearranged, for each component, to present the form utilized to convert balance output to engineering units.

$$F_N = (F_N)_u - (K_{I,2}F_A + K_{I,3}M_Y + \ldots + K_{I,6}F_Y + K_{I,7}F_{N\wedge 2} + K_{I,8}F_NF_A + K_{I,9}F_NM_Y + \ldots K_{I,27}F_{Y\wedge 2})$$

or

Corrected Balance Load = Uncorrected Load (output*sensitivity) - Σ(interaction effects)

Where, F_N is normal force, F_A is axial force, M_Y is pitching moment, and F_Y is side force.

It is assumed that a balance has all of the possible first and second order interaction terms prior to calibration. Therefore, the loading schedule is tailored around this approach and contains 729 loading points with three proof loadings (2 three component and one six component loading to verify the matrix generated from the calibration data). The accuracy of the balance is determined by statistically analyzing back calculated errors using two standard deviation as the result. The balances are calibrated in manual dead weight stands (figure 13 displays a dead weight stand during calibration). LaRC has a variety of stands ranging from a normal force capacity of 3,000 pounds to 20,000 pounds. All loadings are transferred to the balance through a double-knife edge arrangement to minimize unwanted moments and to ensure accurate locations. All applied moment loadings are generated using the long arm technique (whenever possible) to minimize inaccuracies in the position of the load and isolate interaction effects. After each loading, the balance is releveled before data is acquired. When a pure gravity load can not be achieved, for example, loading normal force and side force simultaneously, cable loads are applied (cable refers to what is used to transfer the load in a plane perpendicular to gravity). Also, these cable loads are applied over a bell crank (LaRC developed) as opposed to a pulley. The bell cranks minimize the frictional effects that are commonly found in pulleys. The loading or calibration hardware such as fixtures, moment arms and adapters are precision machined to state-of-the-art tolerances since this equipment is used for ensuring proper balance performance.

Figure 13 is a typical balance calibration set-up. The data acquisition system is made up primarily of a digital voltmeter with a custom written software operation system. The results of a calibration are the sensitivities and interactions for all six components. In some cases temperature loadings are performed to characterize the balance's behavior in those environments. Resistive strip heaters and liquid nitrogen are utilized for varying

balance temperature during calibration. Figure 14 is a cover sheet and interaction sheet from the results of a balance calibration. The full report contains other balance related information including all of the interaction terms.

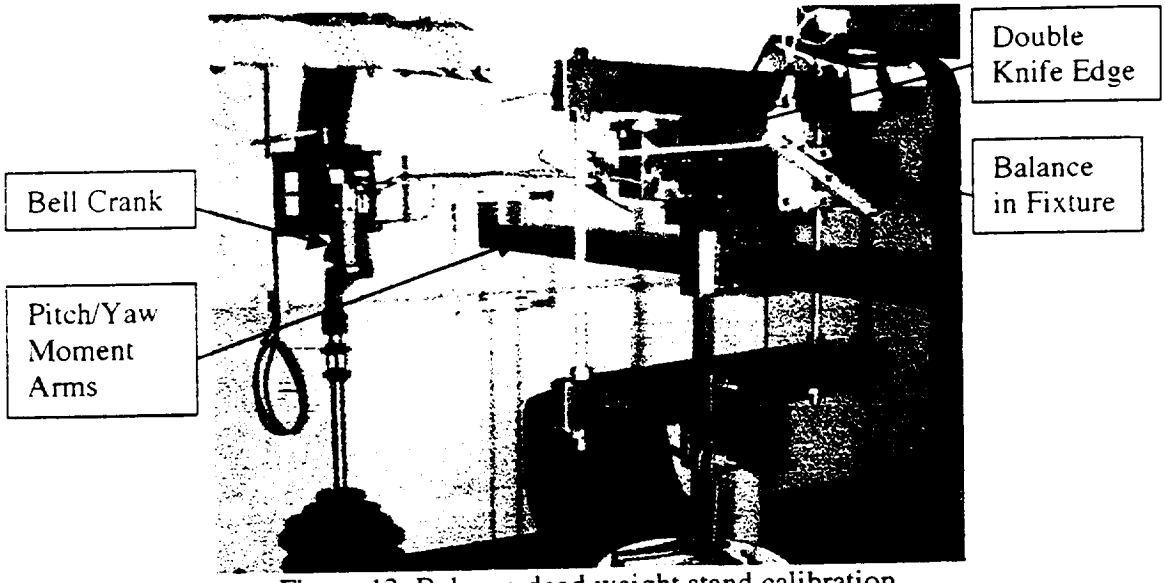

Figure 13. Balance dead weight stand calibration

* N A S A * * * * * * * * * * * * * * * * * * *
* * * * * * * * * * * * * * * * Langley Research Center * * * * * * * * * * * * * * * * * *

STRAIN GAGE BALANCE CALIBRATION RESULTS

FINAL FINAL

Engineer: RHEW

Balance: DT62A
Calibration Date: 11/10/93

Component	Calibration Range		Full Scale Output	Sensitivity Constant		Accuracy
				(lb/mV/V) or (in-lb/mV/V)	(N/mV/V) or (Nm/mV/V)	% F.S.
	(lb or in-lb)	(N or Nm)	(mV/V)			(±2σ)
1 NORMAL	600.0 -600.0	2668.933 -2668.933	1.214	494.1910	2198.2714	0.06
2 AXIAL	60.0 0.0	266.893 0.000	1.003	59.8110	266.0526	0.17
3 PITCH	1800.0 -1800.0	203.373 -203.373	1.548	1163.0000	131.4014	0.06
4 ROLL	400.0 -400.0	45.194 -45.194	1.032	387.5260	43.7848	0.14
5 YAW	600.0 -600.0	67.791 -67.791	1.258	476.9520	53.8883	0.16
6 SIDE	200.0 -200.0	889.644 -889.644	0.996	200.8660	893.4966	0.24

MOMENT CENTER =3.253 INCHES AFT OF CENTERLINE OF FORWARD DOWEL
BALANCE VOLTAGE = 5 VOLTS
DELTA W =.111E+00
SPECIAL REMARKS

Figure 14. Calibration cover sheet example

* * * * * * * * * * * * * * * * * NASA * * * * * * * * * * * * * * * * *
* * * * * * * * * * * * * Langley Research Center * * * * * * * * * * * * *

STRAIN GAGE BALANCE CALIBRATION RESULTS

NORMAL NORMAL

Balance: UT62A
Calibration Date: 11/10/93 Engineer: RHEW

Card Sequence	Components Operated On	Value English	S.I.D.	Effect % of Full Scale
	Linear Interaction Coefficients:			
1	normal	1.0000E+00	1.0000E+00	100.00
2	axial			
3	pitch	4.2737E-03	1.6826E-01	1.28
4	roll	-1.7146E-02	-6.7504E-01	-1.14
5	yaw			
6	side	-2.5882E-03	-2.5882E-03	-0.09
	Nonlinear Coefficients:			
7	normal squared			
8	normal x axial	1.0005E-05	2.2492E-06	0.06
9	normal x pitch			
10	normal x roll			
11	normal x yaw			
12	normal x side	2.6804E-06	6.0257E-07	0.05
13	axial squared			
14	axial x pitch	-3.8468E-06	-3.4047E-05	-0.07
15	axial x roll			
16	axial x yaw			
17	axial x side			
18	pitch squared			
19	pitch x roll			
20	pitch x yaw			
21	pitch x side			
22	roll squared			
23	roll x yaw	-2.1150E-06	-7.3697E-04	-0.08
24	roll x side	-9.0392E-06	-8.0004E-05	-0.12
25	yaw squared			
26	yaw x side			
27	side squared			

Figure 15. Calibration interaction sheet example

Recent advances in automatic balance calibration system technology have caused LaRC to review these techniques in more detail. These systems allow balances to be efficiently calibrated in the expected load and temperature environment of the wind tunnel and thus provide the best calibration.

Summary

NASA LaRC strain-gage balance design concepts have been discussed from initial balance request information to final calibration. All of these areas must be considered during balance design to produce a state-of-the-art balance. However, once a balance is delivered to the customer another process must be executed. This process involves consultation, troubleshooting and maintenance to ensure the balance is used and maintained properly. There are current projects underway or under review to make technological advances in each of the disciplines covered.

References

1. Rhew, Ray: "A Fatigue Study of Electrical Discharge Machine (EDM) Strain-Gage Balance Materials," ICIASF, Gottingen, West Germany, September, 1989.
2. Moore, Thomas C.: "Recommended Strain Gage Application Procedures for Various Langley Research Center Balance and Test Articles," NASA TM 110327, March 1997.
3. Guarino, J: "Calibration and Evaluation of Multicomponent Strain-Gage Balances," NASA Interlaboratory Force Measurements Meeting, Jet Propulsion Laboratory, April, 1964.
4. Smith, Dave: "An Efficient Algorithm Using Matrix Methods to Solve Wind-Tunnel Force Balance Equations," GWU Thesis, December 1971.
5. Ferris, Alice T.: "An Improved Method for Determining Force Balance Calibration Accuracy," Proceeding of the 39th International Instrumentation Symposium, Paper #93-093, May 1993
6. Ferris, Alice T.: "Strain-Gauge Balance Calibration and Data Reduction at NASA Langley Research Center," Proceedings of the First International Symposium on Strain Gauge Balances, NASA LaRC, October 1996.

AN EASY-TO-USE CALIBRATION AND READOUT SYSTEM FOR SMALL INTERNAL BEAM-TYPE WIND TUNNEL BALANCES

Bo R. Fagerström and Pasi P. Kemppainen
Laboratory of Aerodynamics
Helsinki University of Technology
FIN-02150 Espoo, Finland

SUMMARY

A calibration system based on dead weight loads in a simple and relatively inexpensive calibration rig was developed. Interactive software based on a graphical environment and running on a standard low-cost PC plays a central role in this system. Off-the-shelf data acquisition hardware is utilised. The system is intended for small balances with load ranges small enough to make manual handling of dead weights practical.

The scheme used allows a full set of second-order interference terms. To account for possible rollover errors, unsigned first order (absolute value) terms are included, as are some third order terms to improve the handling of main non-linearity. This leads to a maximum of 39 calibration coefficients for each component. Not all of these are of significance in all cases, and individual coefficients can be disabled by the operator. Attention is paid to ergonomics in the user interface (visual and logical clarity, support for correct procedures, autodocumentation). Due to the nature of the platform software, it is easy to integrate auxiliary measurement and control functions (such as the control and measurement of attitude angles in tunnel tests).

INTRODUCTION

An internal six-component balance is typically a relatively slender highly stressed structure. Deformation changes the balance geometry and will introduce relatively strong higher-order interactions between the individual components. For good accuracy the mathematical model of the balance must include second-order calibration coefficients – and possibly even higher order terms. To determine these the calibration must incorporate a relatively large number of combined loads.

This is easily accomplished with a computer-controlled calibration machine typically used by larger wind tunnel laboratories. Such a machine is, however quite expensive, and may not be affordable for a small laboratory with one or a few small tunnels. Then the remaining options are to buy a calibration service from a laboratory equipped with a suitable calibration machine or to resort to traditional dead weight calibration. In every laboratory a certain calibration ability is desirable, as one often wants to make a calibration check to verify that no calibration shifts have taken place e.g. due to tunnel start-up loads.

MATHEMATICAL MODEL OF THE BALANCE

A wind tunnel balance may be perceived as an array of analogue transducers. To interpret the output signals of the balance it is necessary to calibrate them using known forces and moments. The magnitudes of the forces or the moments are calculated from the geometry of the set-up. If the balance behaves in a linear manner, the output signals would be

$$\{U\} = [A] \cdot \{P\} \tag{1}$$

where U is the signal vector (changes from the null level), A is a linear coefficient matrix (typically 6x6) and P is the load component vector. The coefficient matrix A is determined by the calibration. Due to unavoidable signal errors in the calibration a least square method is applied to estimate the coefficient matrix A.

The least square method is a linear estimation method, but it may be used also for the non-linear estimation if a load combination vector is used instead of a pure load vector. For a balance with linear, absolute, second order and third order terms this lead to a coefficient matrix with 39 coefficients for each component. For a non-linear 6-component balance the equation (1) turns into /1/

$$\underset{(6x1)}{\{U\}} = \underset{(6x6)(6x1)}{[L] \cdot \{P\}} + \underset{(6x33)(33x1)}{[G] \cdot [Q]} \tag{2}$$

where L is the linear part of the A-matrix (first 6 rows), G is the non-linear part of the A-matrix and Q is the non-linear load combination vector.

In wind tunnel tests the signals U are measured and the loads are determined by solving the system of equations in (1) or (2). For a linear balance the solution is

$$\{P\} = [A]^{-1} \cdot \{U\} \tag{3}$$

For the non-linear balance it is not possible to solve the system of equations analytically for the components of P, because the same components form the non-linear Q-vector. Therefore an iterative method of successive substitutions is applied. In this method a linear approximation is first calculated. That approximation is then corrected by the non-linear terms calculated in the previous iteration step. Rearranging the equation (2), we get the iterative equation system

$$\{P\}_n = [L]^{-1}\{U\} - [L]^{-1}[G][Q]_{n-1} \tag{4}$$

The first part of the equation (4) is the linear balance approximation. The non-linear load vector Q_{n-1} is calculated in the previous iteration step using P_{n-1}. The iteration converges rapidly.

HARDWARE AND PLATFORM SOFTWARE

The Calibration Rig

The calibration rig used in this work was designed by Rollab of Sweden. For simplicity, all loads are vertical, except for axial load. The loading procedure is described by Fristedt /2/. All components, again except axial force, can be loaded in one direction by direct application of dead weights without the use of pulleys. Negative loads are obtained by rolling the balance 180 degrees. Side force and yawing moment loading is effected by turning the balance 90° and 270° for positive and negative loading. Other roll angles will give any combination of normal force and side force. This scheme maximises simplicity and minimises loss of accuracy due to pulley friction. Some limitations are inherent in this scheme:

- pure moment loads are not possible, a moment load is always accompanied by a normal force or side force.

- the weight of the calibration model (dummy) can not be balanced out and is therefore always present as a tare load.

The dummy model is kept horizontal by means of tilting the support sting to compensate for bending of the balance, twist is compensated by the use of the roll angle mechanism. These angle adjustments will affect the height of the balance, thus the axial force pulleys are adjustable in height to maintain load system orthogonality.

Data Acquisition Hardware

Since a low-cost calibration and measurement system was the goal of the work, a PC-based measurement system was a natural choice. The LabVIEW (National Instruments) measurement software had been successfully used earlier for other projects. Based on this experience LabVIEW was considered very suitable for the present task. A single supplier for both the hardware and software components was desirable in order to minimise the interface problems. Thus the measurement hardware (data acquisition card and signal conditioning equipment) was procured from the same vendor.

In a this PC-based measurement system a data acquisition card is the heart of the system. This alone could be used to measure the balance signals. However, to minimise electrical noise, external pre-amplifiers are employed. The complete hardware set-up is shown in Figure 1.

Platform Software

The sting balance software is created by using a graphic programming language LabVIEW. As a program development environment LabVIEW differs from traditional computer languages like C or FORTRAN in one important respect. Conventional programming languages are text-based;

applications are created by writing blocks of code. The blocks are then compiled and linked together. LabVIEW is based on a graphical programming language and the programs are created in the form of a wire diagram. The code behind the diagram and its symbols is transparent to the programmer/user, but it is compiled and linked by the environment just like any conventional source code

Programming problems are solved by expressing the relations and actions using graphical symbols. Little programming experience is needed. LabVIEW also has efficient program development tools for debugging etc. Many libraries of functions and subroutines for most programming tasks, e.g. for data acquisition, data analysis and data presentation are included. An example of a LabVIEW-program is shown in Figure 2.

LabVIEW programs are called virtual instruments (VIs) because their appearance and operation imitate actual instruments, like meters or analysers. VIs are analogous to the functions in conventional programming languages. VIs have both an interactive user interface and a source code equivalent, a wire diagram.

The interactive user interface is called a front panel because it simulates the panel of a physical instrument. Knobs, push-buttons, graphs and other controls and indicators can be included in the front panel. Each VI receives instructions/data from other VIs as defined by the wire diagram which describes the solution to the programming problem in a graphical form. VIs are hierarchical and modular so it is possible to create a VI inside another VI (subVI). The subVI accepts parameters from higher level VIs. Thus, the programming problem can be divided into several tasks, which can further be divided into subtasks until the problem is built up from simple subtasks. Due to modularity the efficiency of the development process increases, and since any VI can be executed alone, the debugging becomes much easier.

STING BALANCE SOFTWARE

The Sting Balance Software is used to calibrate and use internal bending-beam wind tunnel balances. They can have from 2 to 6 load components (degrees of freedom). The Sting Balance Software consists of five main programs:

1. Rig Loading Program
2. Data Limiting Program
3. Matrix Calculation Program
4. Data Reduction & Matrix Checking Program
5. Wind Tunnel Measuring Program for the Balance.

The programs 1, 2, 3 and 4 are used for the calibration of the balance and programs 4 and 5 for the wind tunnel measurement.

Program Hierarchy

Figure 3 shows the program hierarchy and the flow of data between the program components. All data exchange between the programs occurs via the input and output text files. By nature the programs are interactive. However, for some data used to control calculations it turned out to be more practical to store them in files made manually by the user.

First, the user calibrates the balance using the calibration rig and the Rig Loading Program. The Rig Loading Program is designed for the calibration rig CAR015 by Rollab, or equivalent. This program saves the load data and the corresponding balance signals into an ASCII-file called the calibration load file. This file can be viewed with a text editor or a spreadsheet program.

Next, the calibration load file is read by the Matrix Calculation Program. This program calculates calibration matrices for the balance. The program uses the least square method to determine up to 39 calibration coefficients per balance component. These include linear, absolute linear, second order and third order terms. This program also calculates and inverts the linear matrix, which may be used to make a first approximation of a linear balance.

The calibration matrices are then read into the Data Reduction & Matrix Checking Program. This program also reads the calibration load file and calculates the loads from the signals in the calibration matrices. These calculated loads are compared to the original loads and an error report is created. In the case of a linear balance, the calculation is a straightforward matrix multiplication. In the case of a non-linear balance an iterative method must be used.

When the user is satisfied with the calibration, the balance is ready for the wind tunnel. The Wind Tunnel Program measures the balance signals during the wind tunnel run. The measured values are stored into a run file as raw voltages. The run file is then fed to the Data Reduction & Matrix Checking Program, which converts the signals into forces and moments.

Rig Loading Program

The Rig Loading Program is used to produce a calibration data file. The most important aspect of this program is that it should minimise human errors in the calibration. It is important to be able to monitor the balance signals during the measurement. The program should be easy to use and provide means to detect obvious errors and to correct them.

There are two main sources of human errors in the calibration. One is the possibility to record loads in the calibration file different from those hanging on the rig. The chance to make this kind of mistake is minimised by the use of an interface with an appearance as similar as possible to the physical rig (see Figure 4). The calibration weights are identified by Weight ID-numbers, which are printed on each weight. The selection of the weights is made from a Weight ID Menu (a pre-stored table) upon which forces and moments are calculated by the program. Thus it is not necessary to type the exact weight into the computer eliminating clerical mistakes.

The second type of human error is failure to re-align the balance or the axial load pulleys after a load change. The weights are hanging from the dummy model on the balance, and the model should be exactly level in order to have the loads acting on the balance as intended. The program reminds the user of levelling the balance, but it has no means to verify this was actually done.

A beam type balance loaded with dead weights is very sensitive to vibrations. It is essential to know the level of fluctuation in the signal before any average is calculated from it. Therefore, a panel showing the fluctuation level of the signals is needed in the program (see Figure 5). Swinging load pans cause a low frequency fluctuation of the balance signals. The fluctuation due to swinging weights can be significant even if the movement is not readily visible. Using the signal panel it is possible to minimise the fluctuation in the acceptable level before recording the data. The recorded values are averages over the certain time period, typically 15 seconds.

The calibration is accomplished by loading the balance from the zero load up to a maximum range load of one or more components. Several loads are recorded between zero and maximum. These points (including zero and maximum values) make one half-sweep. When one half-sweep is ready, it is viewed against the loads (Figure 6). A well-made balance should be fairly linear and any large deviations from linearity implies an error; either a wrong load recording or a bad signal measurement. This kind of large errors can be detected here and removed from the data before storing to the calibration data file.

It is not possible to see a complete sweep (consisting of a positive and a negative half-sweep) in the program, because only a half-sweep is recorded in one loading sequence. The checking of the complete sweep (roll-over errors, non-symmetries over the zero) can be done e.g. in a spreadsheet program. This is straight forward since the calibration data file is stored in an ASCII-text file.

Data Limiting Program

The calibration load file can be manipulated before the Matrix Calculation Program. If it is known prior a wind tunnel run that a only limited part of the balance load envelope will be used, a limited calibration matrix may be calculated. Before the matrix calculation, the signals and loads greater than a given limit load are sorted out from the file. A matrix made from the limited calibration data may have better accuracy for the small loads than the matrix which is calculated from the full data.

Matrix Calculation Program

This program is used together with the Data Reduction & Matrix Checking Program to form a calibration matrix and a calibration report. The Matrix Calculation Program calculates the coefficient matrix A using the least square method. The more redundant the data the higher accuracy is gained with the matrix. This program also inverts the linear part of the A-matrix to make a B-matrix for a linear balance approximation. This approximation may be used when some results are required before the whole calibration work is done.

The calculation of the matrices is controlled by control files. The program can calculate the matrices for a balances with 2 to 6 components and 2 to 39 calibration coefficients per component. Sometimes a smaller set of coefficients than the maximum number of 39 is required. The calculation is controlled by a special matrix called the Balance Effect Matrix (BEM). This matrix tells the program whether a certain coefficient or component is active or not. Inactive coefficients are set to zero. This allows the user to choose the set of coefficients he wants to use.

Data Reduction & Matrix Checking Program

The Data Reduction & Matrix Checking Program is used to check the calibration result and for reduction of balance data from wind tunnel tests. When the calibration checking mode is utilised, the program prints an error report for the calibration. All measured load cases used in the calibration are checked against the loads calculated from the corresponding signals using the calibration matrix. The report lists a comparison table and statistics to depicting the overall accuracy of the balance and the calibration matrix. An example of the statistics is shown in Table 1.

In the wind tunnel data reduction mode the input to this program is the run file, which includes all the signals measured during the run. The Data Reduction Program converts the balance signals to forces and moments. It may also convert the other signals measured during the run according to their calibration functions (e.g. thermocouple or pressure transducer readings). The conversion to aerodynamic coefficients may also be included in this program.

Wind Tunnel Measuring Program

The whole measurement chain is calibrated as a whole. Therefore the same hardware (cables, preamplifiers etc.) and data files must be used in the wind tunnel to measure the balance signals as was used to construct the calibration matrix.

The use of the programs may differ for different type of the wind tunnels. For a blow-down wind tunnel it is necessary to use a high data acquisition rate. Usually it is not practical to make any calculations during the run. The conversion of the signals to forces and moments is iterative and takes some time. It may also prove necessary to limit the amount of data shown on the computer screen in real time.

For a continuous-run wind tunnel, and especially for low-speed tunnels, it may be more important to see some results in real time (or pseudo-real time). This leads to a slower data acquisition rate and to the balance calculations during the run. The current work was directed primarily towards blow-down tunnel measurements. Run time performance of the programs has not been tested.

Conclusions

A calibration system based on dead weight loads in a simple and relatively inexpensive calibration rig was developed. Manual dead weight loading is practical only for relatively small balances. Universities and other operators of small wind tunnels with only occasional need for balance calibration often find dedicated calibration machines too expensive and do not require the greater productivity associated with such machines. Dead weight calibration is a viable option for such operators.

Modern low-cost PC:s, associated data acquisition accessories and advanced programming tools have been utilised in this work to make the calibration task as simple and easy as possible. Calibration verification and readout procedures are important parts of a calibration system.

The scheme used allows a full set of second-order interference terms. To account for possible rollover errors, unsigned first order (absolute value) terms are included, as are some third order terms to improve the handling of main non-linearity. This leads to a maximum of 39 calibration coefficients for each component. Not all of these are of significance in all cases, and individual coefficients can be disabled by the operator. Recalculation of the calibration matrix takes only seconds on an up-to-date PC; thus it is easy to experiment with different coefficient sets to find a good one for a particular test.

The software for the system was implemented in LabVIEW – a special measurement oriented graphical programming environment. In the system the computer screen acts as a control panel for the task in progress. Due to the nature of the platform software, it is easy to integrate auxiliary measurement and control functions (such as the control and measurement of attitude angles in tunnel tests).

REFERENCES

1. Fristedt, Knut. A Calibration Model of a Six-Component Internal Wind-Tunnel Balance of the Bending-Beam Type, Measurement 11 (1993), pp 107 - 118.

2. Fristedt, Knut: A Loading Procedure For The Calibration Rig CAR015. Rollab Report RR058, Stockholm, Sweden, 1996.

TABLES AND FIGURES

Table 1. Statistics of the Test Results for the Rollab I6B116 Balance

The calibration data includes 950 x 6 signals and loads. The error-% is the absolute difference between the measured and the calculated load divided by the nominal load of the component.The distribution of the absolute error%s:

From	To	Times	Times(%)	Cumulative	Cumulative(%)
0,00	0,10	4135	72,47	4135	72,47
0,10	0,20	897	15,72	5032	88,19
0,20	0,30	294	5,15	5326	93,34
0,30	0,40	128	2,24	5454	95,58
0,40	0,50	86	1,51	5540	97,09
0,50	0,60	44	0,77	5584	97,86
0,60	0,70	18	0,32	5602	98,18
0,70	0,80	23	0,40	5625	98,58
0,80	0,90	15	0,26	5640	98,84
0,90	1,00	7	0,12	5647	98,97
1,00	1,10	6	0,11	5653	99,07
1,10	1,50	40	0,70	5693	99,77
1,50	2,00	10	0,18	5703	99,95
2,00	100,00	3	0,05	5706	100,00

The maximum error is -2,04 in the load case 694, component C.

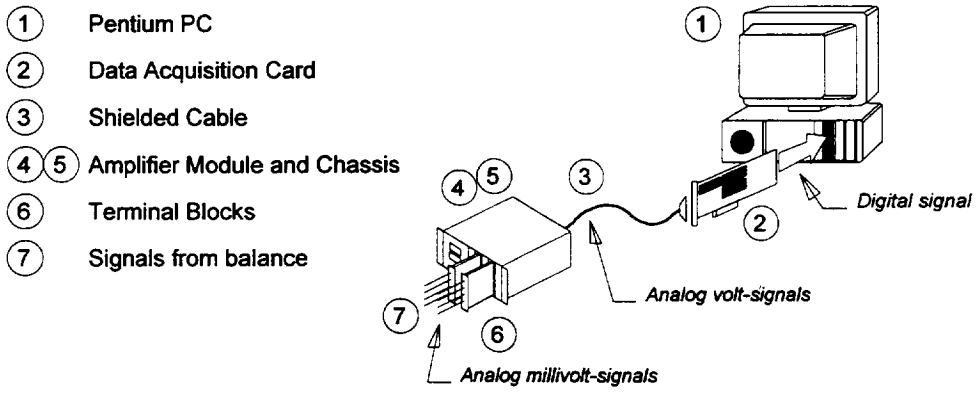

Figure 1. A schematic view of the hardware components of the data acquisition system.

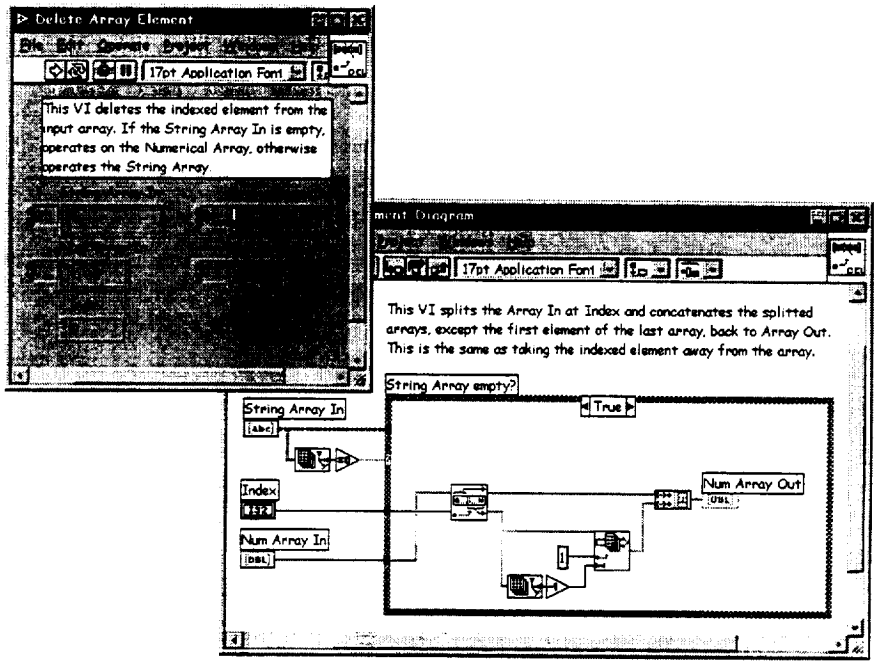

Figure 2. An example of the LabVIEW code and the user interface panel.

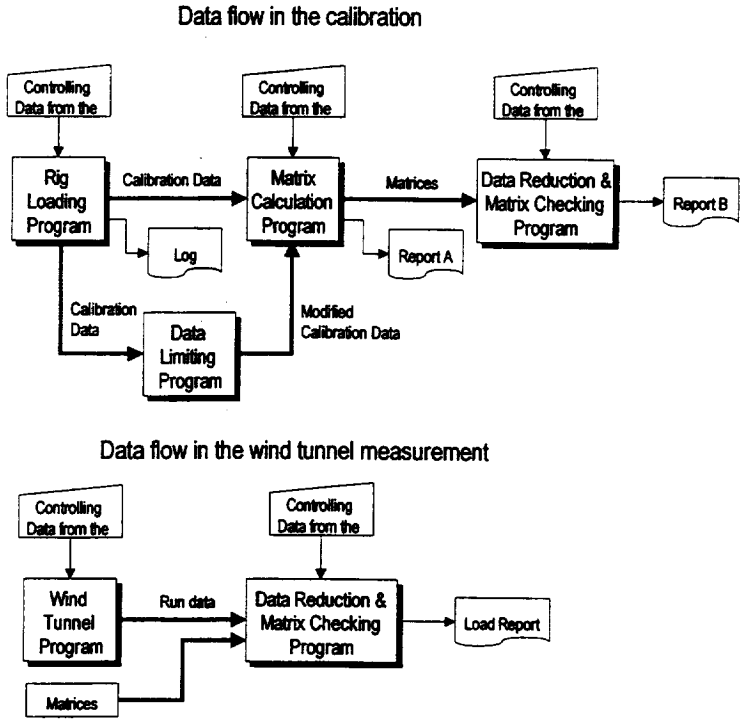

Figure 3. The Sting Balance Software general lay-out and data flow. The input and output files are also shown.

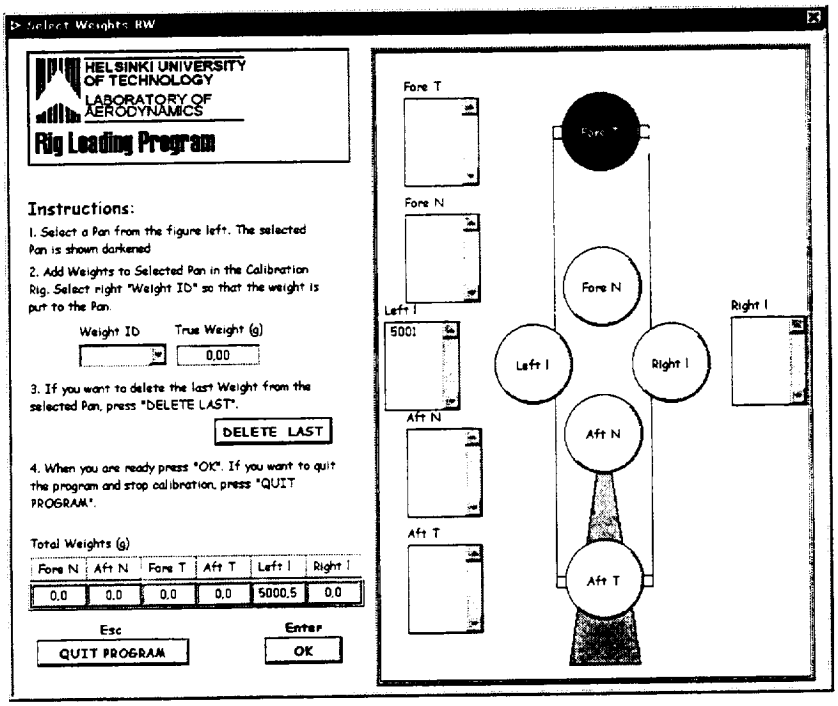

Figure 4. Weight selection panel for the Rig Loading Program.

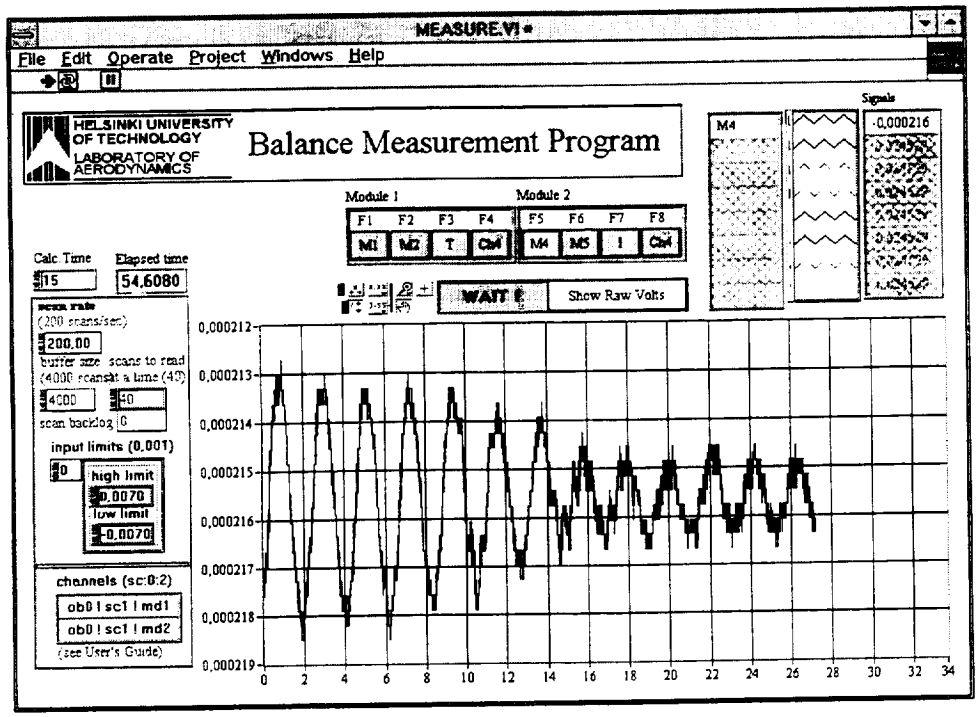

Figure 5. Signal monitoring panel for the Rig Loading Program.

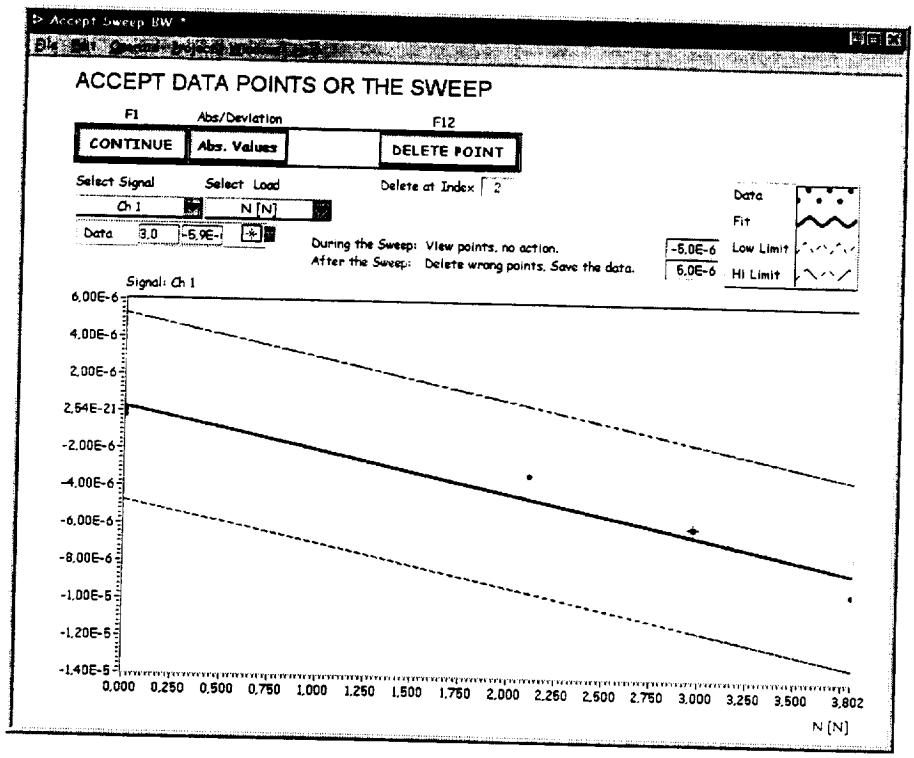

Figure 6. Error detecting and sweep acceptance panel for the Rig Loading Program.

DEVELOPMENT OF BFH SERIES STRAIN GAGES

Gu Xingruo Hu Jinqing
China Aerodynamics Research and Development Center
Mianyang, Sichuan ,P.R.of China

SUMMARY

BFH-series strain gages are specially developed for wind tunnel strain gage balances. It can be cured without being pressed so as to easy the operation of strain gage installation on wind tunnel balance.

This article concentrates on some techniques in the development of BFH-series strain gages, the test result and the application. The test results include the appraisal opinions and the dynamic calibration situations of balances with BFH-series strain gages being used. All that has reached the expected development goal.

INTRODUCTION

The structure of wind tunnel strain gage balance is considerably complex and small. As to the resistance strain gage--sensing element of strain gage balance, miniaturization and easy installation are required. The difficult is that the curing of common strain gage is required being pressed. To meet the requirements of foil strain gage used in balances, BFH-series foil strain gages cured without pressing have been developed and they are mainly used for wind tunnel balances in CARDC.

SELECTION OF RAW MATERIALS

The factors effecting quality and characteristics of foil strain gage mainly have two kinds. One is the raw materials of strain gage element such as sensitive grid, base and adhesive. The other is the materials such as formwork, photoetching glue and corrodent used in processing technology. The high quality strain gage can not be produced unless these materials are selected properly.

Sensitive Grid

Constant alloy is selected as the material of sensitive grid of BFH-series strain gages. Its temperature coefficient of resistance is very small, and the coefficient value covers a wide range from negative to positive through different process of heat treatment. Its machinability of photoetching is good also. Therefore it is an excellent material of sensitive grid of the strain gage used in conventional temperature.

Base

The base of BFH-series strain gages is made of adhesive called JP-M. JP-M is a solvent adhesive of phenolic-eposy type with cyclohexanone. BFH-series strain gages need only "finger pressing" at installing, and can be cured without being pressed. It has good self-adhesive ability so that it can used as adhesive of BFH-series strain gages after diluting also. Its other characteristics are small mechanical hystersis and creep, excellent forming foil performance, and low toxicity.

JP-M's curing requirement is kept 2 hours in constant temperature at 80, 140 and 170 ℃ , respectively. The recommended heating rate from room temperature to 170 ℃ is 3 ℃ per minute.

Photoetching Glue

The positive photoresist called BP-212 is used as photoetching glue of BFH-series strain gages. The advantages are high distingushablity, smooth patter line after being developed, and thorough removing glue easily, as well as being able to use a harmless alkalinity solution as developer.

Corrodent

The quality of corrosion may effect the long-term stability of strain gage, and the different corrodent directly effects the corrosion quality. The solution of ferric chloride is used as corrodent of BFH-series strain gages. The advantages are fast corrosion rate and no corrosion phenomenon for photoetching glue, as well as low transverse corroding rate.

Main Technical Measures

Surface Preparation of Foil Material

There are oil, organism, ash and moisture on the surface of the foil material. The cleaning and surface treatment of foil are first important step in strain gage production.

The new cleaning technology and abrading treatment are put into use in development of BFH-series strain gages. After that the peel strength between foil and base is more than $0.6N / cm^2$. The sensitive grid of strain gage has no come unglued and its performance is stable through the verification of consequent photoetching and corrosion processing.

Positive Photoetching Technique

The key to photoetching technique of BP-212 is how to control thickness and uniformity of the glue layer, and the exposure time should be properly prolonged.

Etch Technology

Two ferric chloride solutions of different density are used for etching. The key here is to hold the temperature and etching time of the corrodent.

Resistance Adjustment

The resistance of a batch strain gages produced scatter always. However, the resistance of strain gages used in same Whetstone bridge must be of less difference. The method combining mechanical way and chemical one is used in adjusting resistance's, which makes the difference less than $\pm$ 0.05 Ω.

Protection of Surface Adhesive

For assuring the sensitive grid of strain gage being adhered to the base firmly, there are two

methods. One is surface treatment of the foil material before coating adhesive as mentioned above so as to increase adhesion between them. The other is that a surface adhesive is coated on the surface of strain gage made and making cure treatment, the sensitive grid is adhered to base depending on the adhesion between adhesive.

The surface adhesive of BAH-series strain gages is same as base adhesive, it is applied soon after diluting.

Pre-Screen for Temperature

The foil material bought is annealing state with large dispersity of temperature coefficient of resistance. BFH-series strain gages must be screened for temperature, the temperature curve of each strain gage is drawn, then the strain gages with same temperature regularity are matched to compose a Whetstone bridge.

Strict Quality Check

BFH-series strain gages are made checking at all levels before being used. The checking consists of primary election, inspection of the weld spot and resistance, as well as self-testing by user.

TEST RESULT

Appraisal

Two samples of BFH-series strain gages have been tested by Shenyang Instrument Technology Institute--national appraisal department. The test reports recognize that BFH-series strain gages are products of grade A according to China Nation Standard of 《 *Resistance Strain Gauge* 》 (GB/T13992-92). The test results are shown in Table 1.

Test Installed on Balance

The performance of strain gages used in balance is not only related to the quality of the strain gages themselves, but also the state of the balance or wind tunnel. To measure performance three

samples of BFH-series strain gages are installed on four balances during trial-producing. The results are shown in Table 2.

The zero-load drift of the balances are measured at room temperature. The maximum value is 3μV in 30 minutes, this value is corresponding to 0.02% of maximum output volt at the design load of that balance.

The thermal drift of the balances are measured in a oven. When no compensation, the maximum value of thermal drift is 0.05μV per volt per degree Centigrade, this is corresponding to 0.035% of maximum output volt at the design load of that balance during working temperature.

After static calibration attaining qualified data three of these balances are calibrated dynamically in M=1.2 and 2.0, respectively. The standard deviations of thermal drift of aerodynamic coefficients are shown in Table 3. As to the axial force aerodynamic coefficient, one of the balances is 0.0001 in 5 minutes, the other is 0.00005 in 50 seconds.

Balance 2N6-28A and 2N6-28B have been dynamically calibrated for two periods to test long-term stability of BFH-series strain gages, both the periods last for nine months. The tests show that both of aerodynamic derivative curves are almost the same, which means the BFH-series strain gages possesses excellent long-term stability. And furthermore the curves are almost the same comparing with the curves achieved by applying other kinds of strain gages, which are shown in Figure 1-3. There are a translation between the curves in Figure 1 and a crossing in Figure 2, which are respectively result from the modifying error for attack angle and the measuring error for reference center position, according to the analysis in Reference 2.

All of these measurement data meet the needs of China Nation Standards of 《 *Specifications of Force-Test Precision for High and Low Speed Wind Tunnels* 》 (GJB1061-91) and 《 *Specification for Wind Tunnel Strain Gage Balances* 》 (GJB2244-94).

APPLICATION

The specifications of BFH-series strain gages are listed in Table 4. They can be changed according to user's requirements. The photograph of BFH-series strain gages is shown in Figure 4.

BFH-series strain gages have been put into batch production. They are not only applied on inside and outside balances in CARDC, but also a few foreign ones. Until now BFH-series strain gages have already applied on more than 100 balances.

The application result indicates the utilization factor of BFH-series strain gages in use have reached more than 90%, and the success rate of one time installation is 100%.

Table 1. Test Report of BFH-series Strain Gages

Characteristics	Explanation		Samples Tested		Target of Grade A
			BFH350-3AA	BFH350-4AA	Defined GB/T13992-92
Resistance	Deviation of Nominal Value	± %	0.28	0.27	0.5
Gage Factor	Scattering for Average Value	± %	0.5	0.6	1
Mechanical Hystersis	at Room Temperature	με/m	2.1	1	3
Creep	1 Hour at Room Temperature	με/m	2.3	2.6	3
Strain Limit	at Room Temperature	με/m	2×10^4	2×10^4	2×10^4
Isolation Resistance	at Room Temperature	MΩ	10^4	10^4	10^4
Transverse Sensitivity Ratio	at Room Temperature	± %	1.2	1.3	0.5
Fatigue Life	at Room or Extreme Operating Temperature	Number of Cycles	10^7	10^7	10^7
Base Thickness	Deviation for Average Value	με	+0.8 ~ -1.1	+0.7 ~ -0.6	–

Table 2. Zero and Thermal Drift of Balances Applied BFH-Series Strain Gages

Balance Mark No.	Zero Drift [*μV/30min*]						Thermal Drift [*μV/V/℃*]					
	Y	Mz	X	Mx	Z	My	Y	Mz	X	Mx	Z	My
1N5-14	1	0	–	0	1	2	0.15	0.35	–	0.10	0.17	0.08
1N3-18A	0	1	0	–	–	–	0.16	0.53	-.20	–	–	–
1N3-18B	0	1	1	–	–	–	0.01	0.18	0.13	–	–	–
2N6-28A	3	0	1	1	0	2	0.38	0.37	0.38	0.03	0.33	0.05
2N6-28B	0	3	1	1	1	1	0.04	0.48	0.09	0.13	0.22	0.13

Table 3. Thermal drift of Balances Applied BFH-Series Strain Gages During Dynamic Calibration Under Room Temperature

Balance Mark No.	Condition	Standard Deviation of Thermal Drift					
		σ_{cy}	σ_{mz}	σ_{cx}	σ_{mx}	σ_{cz}	σ_{my}
1N5-14	M=2.0 α=12°	0.0004	0.0003	–	0	0.0002	0.0001
1N3-18A	v=30° 5 minutes	0.0005	0.0001	0.0001	–	–	–
2N6-28A	M=1.2 α=4°	0.0001	0.0001	0.00005	0.00006	0.00005	0.00002
	50 seconds	0.0003	0.00007	0.00005	0	0.00007	0.00006

Table 4. BFH-Series Foil Strain Gages

Designation	Resistance [*Ohms*]	Sensitive Grid [*mm*]		Base Dimension [*mm*]	
		L	W	L	W
BFH200-1AA	200	1	0.8	3	1.5
BFH350-1AA	350	1	0.8	3	1.5
BFH200-1.2AA	200	1.2	1	3	2
BFH300-1.2AA	300	1.2	1	3	2
BFH150-2AA	150	2	1	4	4
BFH300-2AA	300	2	1	4	4
BFH200-3AA	200	3	2	6	3
BFH300-3AA	300	3	2	6	3
BFH350-3AA	350	3	2	6	3
BFH600-3AA	600	3	2	6	3
BFH350-4AA	350	4	2.5	7	4
BFH600-4AA	600	4	2.5	7	4
BFH350-6AA	350	6	4.2	10	6
BFH600-6AA	600	6	4.2	10	6
BFH1000-6AA	1000	6	4.2	10	6
BFH150-0.9HA	150	0.9	2	2.5	2.5
BFH250-0.9HA	250	0.9	2	2.5	2.5
BFH300-1.4HA	300	1.4	6	4	7
BFH500-1.4HA	500	1.4	6	4	7
BFH250-2HA	250	2	4.2	6	6
BFH400-2HA	400	2	4.2	6	6

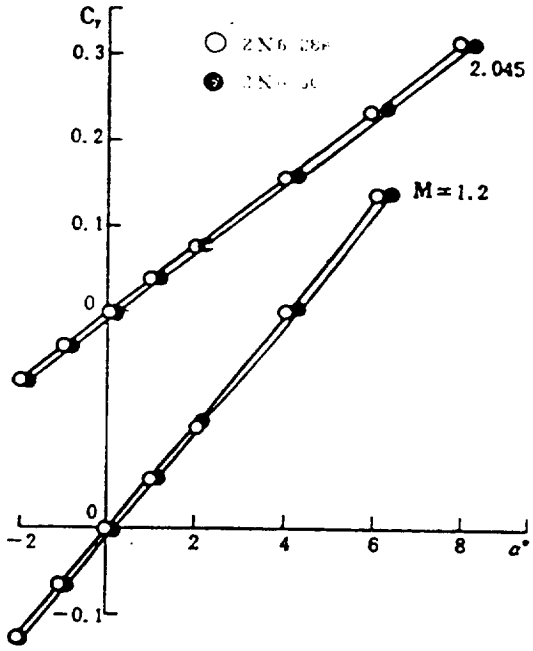

Fig.1 Comparison of Curves Cy–α for Standard Model GBM-04.

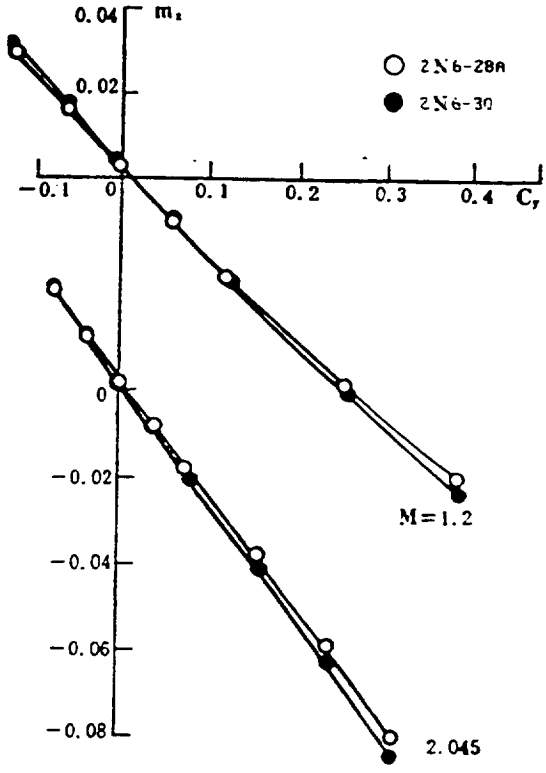

Figure 2.. Comparison Curves m_z–c_y for Standard Model GBM–4

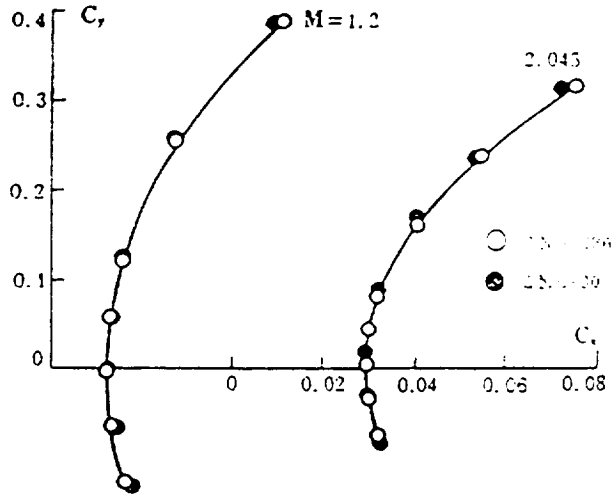

Figure 3. Comparison of Curves Cy–Cx for Standard Model GBM-04.

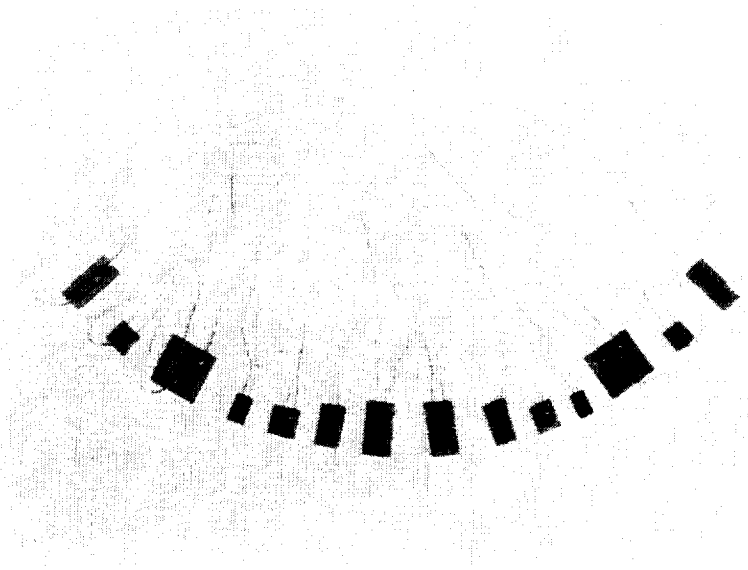

Figure 4 . The photograph of BFH–Series Strain Gages.

Strain Gauge Balance Calibration And Data Reduction at NASA Langley Research Center

A. T. (Judy) Ferris
NASA Langley Research Center
Hampton, VA

Abstract

This paper will cover the standard force balance calibration and data reduction techniques used at Langley Research Center. It will cover balance axes definition, balance type, calibration instrumentation, traceability of standards to NIST, calibration loading procedures, balance calibration mathematical model, calibration data reduction techniques, balance accuracy reporting, and calibration frequency.

Balance Axes

The balance coordinate systems used for force and moment measurement at LaRC are defined as shown in Figure 1. The balance coordinate axes usually coincide with the body axes of the wind tunnel model.

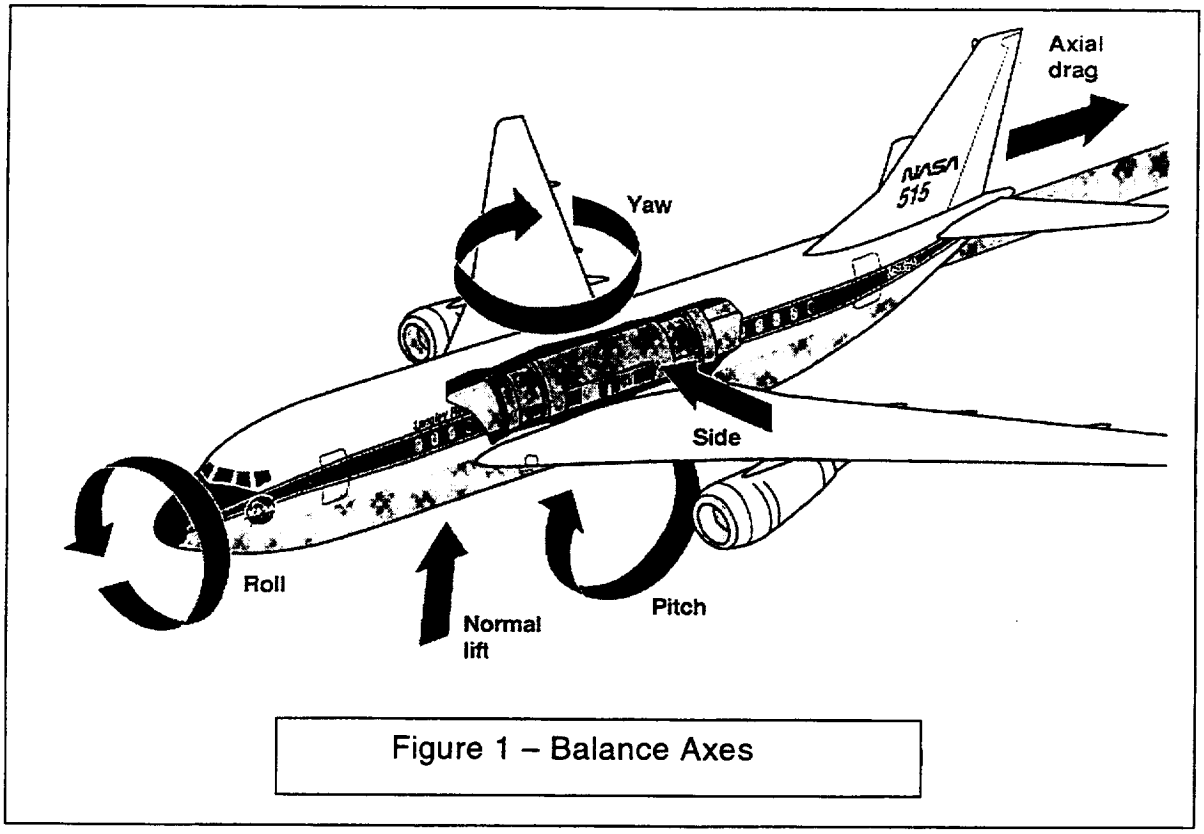

Figure 1 – Balance Axes

Balance Type

All LaRC internal strain-gage balances are custom designed to meet the load ranges, physical size, thermal environment, and accuracy requirements for given research projects. LaRC balance design philosophy is to use single piece construction techniques whenever possible. Multiple piece construction is used only in unique cases such as flow-through balances. LaRC often calibrates and uses multi-piece "Task/Able" type balances furnished by private industrial customers. LaRC also currently operates three external-balance systems and has several side-wall (semi-span) balances. Most LaRC balances are of the direct-reading type. To accommodate better thermal compensation some balances are gaged in such a manner that they require that bridge outputs must be summed and differenced. These balances are used in extreme thermal conditions such as the cryogenic environment at the National Transonic Facility (NTF).

All LaRC balances employ modulus-compensated transducer-quality strain-gages. Where extreme thermal environments are anticipated, an apparent-strain gage-matching technique patented by LaRC is used. Thermal compensation is provided by pure nickel wire placed in each balance bridge circuit to reduce temperature effects on the bridge output to less than 0.005% FS/°F. Balance temperatures and gradients are measured by means of thermocouples or RTD'S. These temperature measurements allow linear corrections to be applied for thermal sensitivity shifts and second-order corrections for apparent strain. Three types of mechanical model-to-balance attachments are employed; namely, diameter fits, expandable diameter fits, and flange fits. Mechanical balance-to-ground attachments include tapered fits, diameter fits, and flange fits.

Calibration Instrumentation

Balances are calibrated in an environmentally-controlled calibration laboratory. The calibration data are acquired using a Hewlett-Packard 3457A Digital Multimeter with ten-channel multiplexer, Option 44492. For a typical balance 5 mV full-scale output, the meter range is set to 30 mV, with an accuracy specification of 0.004% of reading + 3.65 μV. The multiplexer thermal offset specification is less than 3 μV. The data is transferred to a micro-computer (PC) using an IEEE 488 interface. For each of the six balance channels the data acquisition software acquires 50 readings at approximately 30 samples per second. To prevent corruption of the balance data by any swinging motion of the applied weights, the peak-to-peak variations of the fifty readings are monitored. If the total variation is less than ±20 μV the 50 readings are averaged; if the variation is out of tolerance, an additional fifty readings are taken on every channel and the tolerance check is repeated. If the second check fails, the calibration operator is alerted by the program to steady the weights and repeat the data point. Typically, the overall repeatability of the instrumentation system averaged over 50 data points is about 1 μVolt. LaRC employs a single 5 volt DC supply to power all six balance bridges. The input voltage leads for the six bridges are paralleled at the taper (aft end) of the balance. The input voltage is monitored for each data point. The six balance outputs are normalized to a nominal 5.000 V input voltage. The data is displayed, printed, and then stored on magnetic media for later data reduction.

Traceability of Standards to NIST

All of LaRC balance calibrations are performed using dead weight loadings. The laboratory calibration weights are checked and maintained within tolerance at least every two years. Two different weight calibration procedures are employed depending on the magnitudes of the weights. Dead weights in excess of 1,000 pounds are calibrated against Interface Gold Standard Load Cells which have overall accuracies of better than 0.01% FS (typically 0.006% nonlinearity and 0.002% hysteresis.) Every five years the load cells, and the associated power supplies and digital read-out instrumentation are sent to NIST for recalibration. Dead weights less than 1,000 pounds are calibrated on electronic scales (models Metler PC4400, Metler H51, A&-D 60, or Metler PC30.) These scales are maintained annually in the calibration laboratory with Tromner Class M and Class S mass standards. Only trained calibration technicians have access to these mass standards which are calibrated by NIST every five years.

Calibration Loading Procedures

The loading procedure for the LaRC full calibration is designed to fully determine both first and second order interactions. The procedure includes the application of all six primary loads and all two-load combinations. There are 82 loading sequences of nine loading steps each, as given in Table 1. For each sequence, loadings are applied in four equal increments to full scale and are then decremented to zero.

Assorted custom designed hardware is are used for balance calibration. The calibration equipment includes a calibration block or fixture, knife edges, symmetrical moment arms, weight hangers, and precision levels for simple gravity loadings; cables, knife edge pivoting bell cranks, and associated cable alignment equipment for the orthogonal loadings. The loading fixture, affixed to the balance metric end, is precision bored and ground to allow the use of its four orthogonal faces for balance releveling. The precision levels are Spectron electrolytic levels with a repeatability specification of 6 arc seconds. The fixture has longitudinal knife edge grooves and a screw/dowel pattern at the moment center of each face for the attachment of the moment arms. Double knife edges enable the load application point to be accurately placed to within 0.0005 inch. The orthogonal loads are applied through the use of double knife edges and a cable over a "frictionless" bell crank to a weight hanger. The alignment of the cable for orthogonal loads is obtained by first applying a gravity loading and recording the balance output on all components. The same load is then applied, and an iterative cable alignment is performed until the dead weight output is duplicated on all components, indicating that the load is now orthogonal as it was during the gravity loading. This alignment is maintained through the use of a transit and light rig to ensure that the load is kept orthogonal to the balance during the incremental loading sequence.

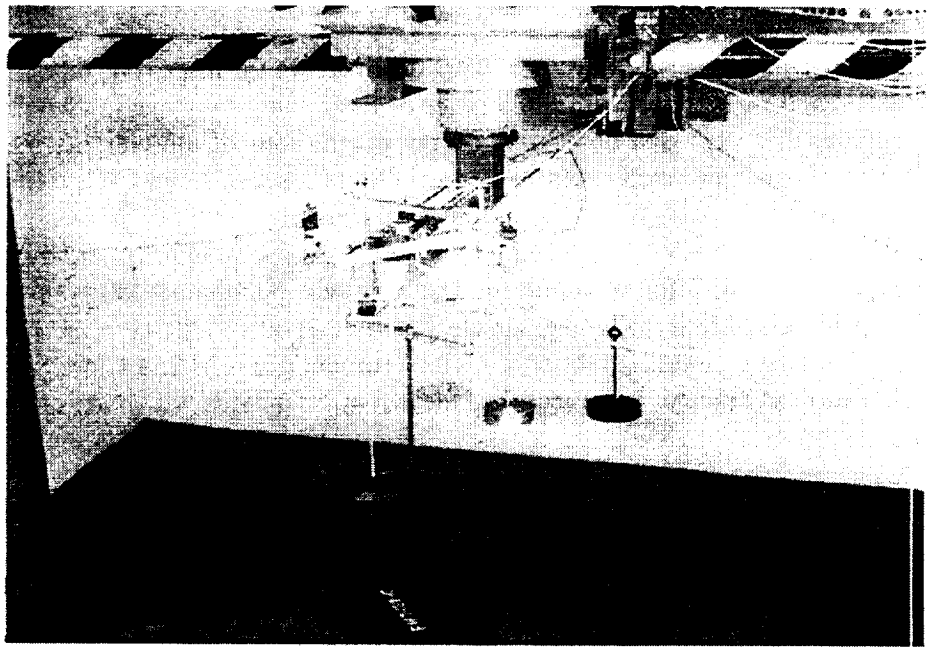

Figure 2. Multicomponent Loading

Balance Calibration Mathematical Model

The term "calibration mathematical model" used at LaRC denotes the multivariate polynomial which represents the functional relationship between the applied loads and die observed strain-gage bridge output voltages of the aerodynamic balance. The form of the polynomial model is specified by the following:

1) The physical parameters selected as independent and dependent variables including forces and moments, and output voltages;
2) The order (degree) of the polynomial;
3) The interaction terms, including quadratic terms and cross-product terms;
4) The rectangular array of muitivariate polynomial coefficients ordered into a matrix format, typically 6 x 27; and
5) The direction of the model, i.e., the choice of independent and dependent variables.

The traditional *forward* model, used at LaRC, characterizes the true physical process in which the independent variables, i.e., the applied loads, produce strains within the balance measuring beams, which in turn manifest voltage variations in the corresponding bonded strain-gage bridges, thereby producing the observed dependent variables, i.e., the output voltages, which vary as functions of applied loads. The forward model has been also designated as the *iterative model.* Computation of the applied loads corresponding to the observed voltage outputs requires iterative inversion of the system of nonlinear multivariate polynomial equations.

The forward mathematical model used at LaRC is a second order muitivariate polynomial function f of the six force-moment components including six linear terms, six quadratic terms, and 15 cross terms. The coefficients of these terms are established by the calibration procedure described in Section G

entitled "Calibration Data Reduction Techniques." Function f is continuous everywhere with continuous partial derivatives. A theorem from advanced calculus shows that a unique inverse function f′ does exist in some open region R about the solution, provided that the Jacobian matrix of f is nonsingular. Moreover, f′ is also continuous with continuous partial derivatives in region R. One cannot find, in general, a closed-form algebraic expression for f′ in terms of radicals or elementary functions.

Calibration Data Reduction Techniques

The loading procedure of LaRC balances allows data reduction to be performed by grouping the loadings to break out the data necessary to compute each sensitivity and interaction. There are 27 groupings which are arranged into sets of sensitivities, linear interactions, quadratic terms, and cross terms respectively. For each grouping, the corresponding coefficient for each component is obtained by second-order least-squares estimation. In most instances the interactions are linear and the initial loads do not adversely affect the computation of the interaction. However, corrections for initial loads are made on the quadratic interactions. The resultant 6 by 27 matrix of coefficients is normalized with respect to the corresponding full scale loads of each component and a standard format print-out and standard format electronic data file is made and stored for the users of force balances at LaRC. The calibration data reduction computations are performed on personal computers.

Balance Accuracy Reporting Method

The calibration of wind tunnel balances at LaRC is a lengthy and labor-intensive process requiring fixture leveling, cable alignment, and dead weight application at each of 738 loading steps. The first description of strain gage balance calibration methods at LaRC was reported in 1956, followed by a refinement of these methods reported in 1964. These two reports described the rationale for including all first and second order interaction coefficients for accurate balance characterization and devised a comprehensive calibration procedure to individually estimate each of the coefficients. This calibration procedure was also valuable in identifying error sources in balance design, strain gage installation, and inaccurate calibration load application. The 1964 reference also presents a scalar iterative data reduction method, which was upgraded by a more efficient muitivariable iterative matrix technique in 1972.

The concept of proof loadings in which multiple loads are simultaneously applied was reported in the 1956 report as a means to verify balance accuracy. The overall accuracy of the balance was cited in the 1964 reference as the worst-case error among all components from the proof loadings. In 1993 an alternative method for reporting balance accuracy was developed which cites the accuracy of each of the six balance components. Each accuracy term is computed as two standard deviations of the residuals of all the 738 loading obtained during the calibration, expressed as a percentage of the full-scale load of the corresponding component. A sample error plot is included in Figure 3.

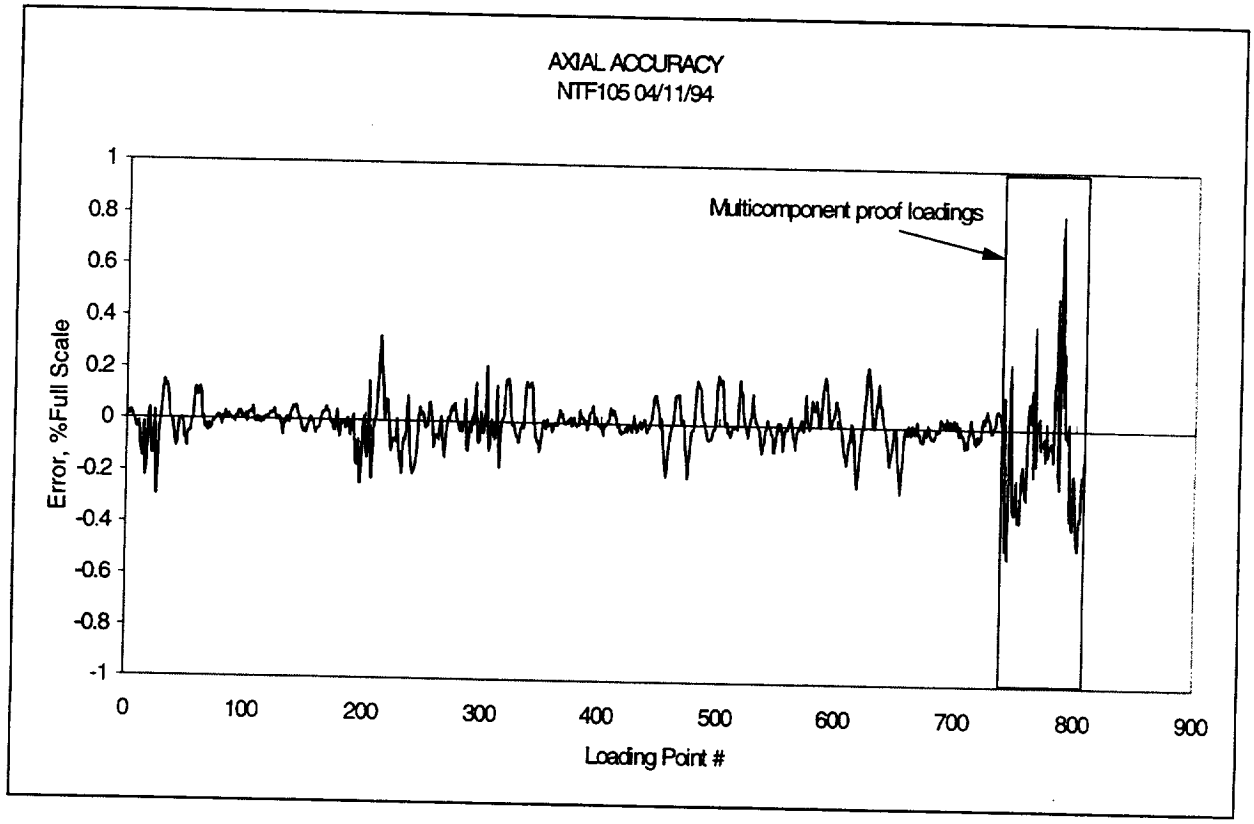

Figure 3. Error Plot

An effort is underway at LaRC to develop a new technique to ascertain the uncertainties of the forces and moments measured by the balance. This technique is an enhanced improvement over the existing procedure in which accuracies were cited as percentages of the full scale loads. It allows error bands to be quoted for each computed force and moment as functions of the actual measurands. The new method has been verified using data obtained from calibration.

LaRC maintains an active balance inventory of over 250 internal strain-gage balances. A two-year calibration update is recommended by the force measurement group. However, complete calibrations are lengthy and labor intensive, and it is not feasible to recalibrate each balance every two years. The frequency of calibration at LaRC is based on the balance usage rate and the needs of the researchers. Frequently used balances are recalibrated on a two-year calibration update cycle. Other balances are recalibrated at user request. Balances are also be recalibrated at the discretion of the staff of the force measurement group as the calibration schedule permits. All new balances receive full calibration. A full calibration consists of the application of 738 dead weight loads in two categories: primary and secondary loadings over all six components to establish the balance sensitivity and interaction coefficients. The calibration coefficients are next validated by application of 123 proof loadings with three to six components loaded simultaneously at 50% and FS levels. Users are furnished a calibration report detailing the balance specifications, wiring codes, calibration coefficients, accuracies, deflections, and other pertinent data. Update recalibrations, which include primary component loadings only, are conducted routinely following the complete calibration.

Table 1

PRECISION DEAD WEIGHT CALIBRATION LOADING SCHEDULE
(LOADING ORDER IS TYPICAL BUT NOT REQUIRED)
LOADING AT EACH CODE IS IN 1/4 FULL SCALE INCREMENTS
TO FULL SCALE AND BACK DOWN TO ZERO LOAD

CODE	PRIMARY LOAD	AUXILIARY #1	AUXILIARY #2	AUXILIARY #3
10	AXIAL			
20	NORMAL			
30	PITCH	NORMAL		
1030	- PITCH	NORMAL		
1040	- ROLL	NORMAL		
40	ROLL	NORMAL		
50	-NORMAL			
1060	- PITCH	-NORMAL		
60	PITCH	-NORMAL		
70	ROLL	-NORMAL		
1070	- ROLL	-NORMAL		
80	SIDE			
90	YAW	SIDE		
1090	- YAW	SIDE		
100	- SIDE			
1110	- YAW	- SIDE		
110	YAW	- SIDE		
120	ROLL	- SIDE		
1120	- ROLL	- SIDE		
130	ROLL	- SIDE		
1130	- ROLL	- SIDE		
1140	- YAW	ROLL	- SIDE	
140	YAW	ROLL	- SIDE	
1150	- YAW	- ROLL	- SIDE	
150	YAW	- ROLL	- SIDE	
1160	- YAW	- SIDE		
160	YAW	- SIDE		
170	YAW	SIDE		
1170	- YAW	SIDE		
1180	- ROLL	SIDE		
180	ROLL	SIDE		
1190	- ROLL	SIDE		
190	ROLL	SIDE		
200	YAW	ROLL	SIDE	
1200	- YAW	ROLL	SIDE	
210	YAW	- ROLL	SIDE	
1210	- YAW	- ROLL	SIDE	
220	PITCH	NORMAL		
1220	- PITCH	NORMAL		
1230	- ROLL	NORMAL		
230	ROLL	NORMAL		
240	PITCH	ROLL	NORMAL	
1240	- PITCH	ROLL	NORMAL	
250	PITCH	- ROLL	NORMAL	
1250	- PITCH	- ROLL	NORMAL	
1260	- PITCH	-NORMAL		

Table 1 (Cont)

60	PITCH	-NORMAL		
270	ROLL	-NORMAL		
1270	- ROLL	-NORMAL		
1280	- PITCH	ROLL	-NORMAL	
280	PITCH	ROLL	-NORMAL	
1290	- PITCH	- ROLL	-NORMAL	
290	PITCH	- ROLL	-NORMAL	
1300	- PITCH	AXIAL	-NORMAL	
300	PITCH	AXIAL	-NORMAL	
310	ROLL	AXIAL	-NORMAL	
1310	- ROLL	AXIAL	-NORMAL	
320	-NORMAL	AXIAL		
330	NORMAL	AXIAL		
340	PITCH	AXIAL	NORMAL	
1340	- PITCH	AXIAL	NORMAL	
1350	- ROLL	AXIAL	NORMAL	
350	ROLL	AXIAL	NORMAL	
360	SIDE	AXIAL		
370	YAW	AXIAL	SIDE	
1370	- YAW	AXIAL	SIDE	
1380	- YAW	AXIAL	- SIDE	
380	YAW	AXIAL	- SIDE	
390	- SIDE	AXIAL		
400	NORMAL	SIDE		
420	NORMAL	YAW	SIDE	
430	PITCH	SIDE	NORMAL	
1430	- PITCH	SIDE	NORMAL	
440	PITCH	YAW	SIDE	NORMAL
1440	- PITCH	YAW	SIDE	NORMAL
460	-NORMAL	SIDE		
470	-NORMAL	YAW	SIDE	
1490	- PITCH	SIDE	-NORMAL	
490	PITCH	SIDE	-NORMAL	
1510	- PITCH	YAW	SIDE	-NORMAL
510	PITCH	YAW	SIDE	-NORMAL
1010	- AXIAL			

Table 1. Calibration Loading Schedule

AN INVESTIGATION ON TEMPERATURE EFFECTS OF STRAIN GAUGE BALANCES FOR CONVENTIONAL HYPERSONIC WIND TUNNELS

Liu Wei
China Aerodynamics Research and Development Center
Mianyang, shichuan, P.R of China

ABSTRACT

In hypersonic wind tunnels, it is needed to heat the air in the upstream of the nozzle so as to avoid air condensation. When Mach number increases,the heated air temperature increases rapidly. In the (0.5m hypersonic wind tunnel, the stagnation temperature in the settling chamber is up to 800 ℃ at Mach number 10. Therefore, the temperature effects of balance on test results can't be ignoredduring 60 ~ 200 seconds' running time.

This paper gave a brief introduction to the performance of balances in hypersonic wind tunnels. It mainly analyzed the factors causing temperature effects of balances in the (0.5m hypersonic wind tunnel and introduced the temperature characteristics calibration equipment, temperature compensation methods and the relevant results .

INTRODUCTION

In the factors affecting static and dynamic performance index of balances, the balance temperature effect is an important factor. Since the settling chamber temperature is up to 800 ℃ at Mach number 5,6,7,8,9,10 in the (0.5m conventional hypersonic wind tunnel of CARDC, if we don't take effective heat-prevention measures and good temperature compensation to balances, the temperature effects of balances will be several or more than ten times static calibration errors, even do damage to the strain gauges.

To the characteristics of the hypersonic wind tunnel, we relief temperature effects of balances mainly from two sides. One is to take effective heat-prevention measure and choose the strain gauge with good temperature characteristics; the other is to make compensation for balance measurement electric bridges so as to make performance of balances meet requirements of the hypersonic wind tunnel testing.

HEAT-PREVENTION OF THE BALANCE

In the (0.5m hypersonic wind tunnel, according to heat-prevention ways, we can divide balances into two types, water cooled internal balances and medium temperature internal balances.

The water cooled internal balance makes water cooling and heat insulation to balance components using water cooling and heat insulation devices. Its structural drawing and components are shown in Fig.1.

After water cooling and heat insulation is taken to the balance by the device, we can control the temperature on balance components within 60 ℃. Therefore, we may use normal temperature strain gauge for this kind of balance.

The medium temperature internal balance chooses the medium temperature strain gauge with the working temperature range reaching 150 ℃. In the meantime, we use fine insulating material to make a nearly closed heat insulation system on balance components so as to make the balance measurement bridge keep in a working condition with relatively stable and well-distributed temperature field. consequently, when Mach number is 10, the total temperature of settling chamber is 800 ℃, and the running time is nearly 100 seconds, the temperature on balance components is kept in the range of working temperature of strain gauges. The medium temperature balance structural drawing is shown in Fig.2.

Although above two types of balances take different heat insulation to balance components, there will be still some changes on temperature of balance components. The former type may be changed tens of degrees, while the latter may be changed even one hundred degrees. If we don't take the measures such as temperature compensation etc. the measurement bridge will still produce bigger temperature effects.

FACTORS CAUSING BALANCE TEMPERATURE EFFECTS

According to the result analysis of ground tests and wind tunnel tests, there are many reasons causing balance temperature effects. Its main factors are shown in Fig.3. Several measure reducing balance temperature effects:

⊙ Shorten the running time of test. As we know, the longer the running time of test is, the higher the temperature of balance becomes. Consequently, projection mechanism and test techniques

in continuos angle-of-attack changing are used in many hypersonic wind tunnels to shorten the running time of test effectively and reduce temperature effects of balance.

⊙ Design the balance rationally, eliminate heat structure deformation, and reduce temperature gradient of balance.

⊙ Choose high-quality strain gauges. Choose foil of strain gauge rationally, coefficient α g and dispersing degree need to be small, β g and β s should be close, meanwhile, choose basis material, binding agents and wire reasonably, use correct parameter of paste treatment technology.

⊙ Strengthen cooling (heat insulation) effect. Use different forms to make cooling and heat insulation to balance components, let balance measuring system be in a working condition with relatively small temperature variation and relatively well-distributed temperature field.

⊙ Make temperature compensation. Use computer or series "Critesistor" with bigger resistance temperature coefficient in the measuring line to reduce or eliminate temperature effects of balances.

TEMPERATURE CHARACTERISTICS CALIBRATION AND TEMPERATURE COMPENSATION

Temperature Characteristics Calibration

Since the temperature characteristics of balance for hypersonic wind tunnel is one of the important indexes of this kind of balances, it is an important work content how to make the balance have good temperature characteristics, make them be calibrated correctly, and have reliablesupports for temperature compensation and aerodynamic tests.

In (0.5m hypersonic wind tunnel, we developed special high and low temperature calibration device of wind tunnel balance. The temperature range of the device is from -40 ℃ to+25 ℃ temperature fluctuation is equal to or less than 1 ℃. Meanwhile, we install multi-component loading system in the test chamber to make loading calibration to balance components on any temperature point in the range of temperature. As this device can increase or decrease temperature rapidly in a wide range, and simulate temperature variation and force-acting in the wind tunnel test as soon as possible, it is possible to correctly measure temperature characteristics of balance components under different temperature conditions, and give curves or function relationship between thermal output and temperature so that we can make more correct compensation or correction for balance components.

Temperature Compensation

There are two general ways of temperature compensation. One way is to input the temperature characteristics of balance to computer. In wind tunnel testing, revise output signal of balance according to temperature variation of thermocouples on the balance. The second way is to use "thermosensitive resistor" to make temperature compensation. The second one is widely used in many wind tunnels because it is effective, simple and convenient. The following is mainly to introduce ways and results of using "thermosensitive resistor" to make temperature compensation in (0.5m hypersonic wind tunnel..

Compensation for Variation Resistance Value in Measuring Circuit

Suppose that temperature variation of former electric bridge is (T ℃, thermal output of electric bridge is (U. It is possible to determine the position of compensation resistance in the bridge circuit according to positive or negative sign of output signals. The functional relationship of compensation resistance Rp with thermal output:

$$Rp=\frac{4Rg}{\alpha_P \bullet U \bullet \Delta T} \bullet \Delta U \qquad (1)$$

Actually Rp is a little different from evaluation. This is mainly because of dispersing degree and nonlinearity of resistance temperature coefficient and welding, which often needs microadjustment.

Use adjustable minitype temperature compensation wires and paste them on nonforce-acting surface near strain gauge, and make compensation wire temperature and strain gauge temperature the same. It is possible to make one-way graded microadjustment to resistance value RP of compensation wire according to test results in the ground test.

Table 1 lists maximum thermal output of each component around the ground temperature compensation when the bridges of a medium temperature balance are in actual bridge voltage. The air temperature in calibrated chamber is from room temperature to 150 ℃,while the temperature of balance elements is from room temperature to 130 ℃. Table 2 lists maximum dynamic temperature effect deviation of each bridge of another medium temperature balance.

Compensation for Variation of Sensitivity Coefficient of Measurement Bridge

As we known, elastic modules E of component material of strain gauge balance in general wind tunnel decreases as the temperature increases, making output signal of balance increase while the load is the same. Nevertheless, sensitivity coefficient K of strain gauge also decreases slightly as the temperature increases, making output signal decrease a little. In most circumstances, (E/E-(K/K>0. A simple but common method is taken in (0.5m hypersonic wind tunnel, which is that eries"thermosensitive resistor" in the charging line of measurement bridge can make actual power supply of electric bridge change with the different variations of temperature to keep the output signal unchangeable.

The compensated "thermosensitive resistor" can be calculated by the following formula:

$$Rm=\frac{Rg \bullet (\Delta E / E - \Delta K / K)}{[\alpha_M + (\Delta E / E - \Delta K / K)]} \qquad (2)$$

where: R_m-compensated resistance value;

α_m --temperature coefficient of compensate resistance;

$\Delta E/E$--variation per degree of balance material E;

$\Delta K/K$--variation per degree of sensitivity K of strain gauges.

During the actual operation, compensated resistance is divided into two parts, which were compensated symmetrically at the voltage input ends of the electric bridge. They were made into structure in the form of strain gauge, and pasted on non-measurement surface near the elastic elements, keeping them in the same temperature with the strain gauge.

Table 3 lists sensitivity variation of longitudinal components of two balances vs temperature variation, in which, 5N6-24A balance does not make elastic modules compensation, but C-5N6-24A1 balance does.

CONCLUSION

Balance temperature effect in hypersonic wind tunnel is an important factor affecting accuracy of force-measuring test. There were many reasons causing balance temperature effects . Therefore, to relief the balance temperature effects needs multiple routes. Only by this can we keep its effects lowest. However, on the ground, we can't completely simulate the thermal effects of balance and there existed uncertain factors in the wind tunnel test, so balance temperature effects can't be eliminated completely. Some work is still in research. For example, compensation of temperature gradient effects for small-scale balance at large temperature gradient is still more difficult. Therefore, the further development of balances of hypersonic wind tunnel is still an important task of ours in the future.

Table 1. Maximum thermal output of D-5N6-20A balance

Bridge Name	M_1	M_2	M_3	M_4	X_1	X_2	M_{X1}	M_{X2}
Before Compensation	0.110	0.148	0.024	0.066	0.170	0.116	0.042	0.031
After Compensation	0.005	0.017	0.009	0.008	0.024	0.025	0.018	0.007

Table 2. Maximum Dynamic Temperature Deviations of C-5N6-24A1 Balance

Mach Number and Stagnation temperature	Y	Mz	X	Mx	Z	My
M=7, To=330 ℃	0.01	0.17	0.04	0.10	0.03	0.19
M=8, To=480 ℃	0.19	0.17	0.16	0.10	0.05	0.12
M=9, To=590 ℃	0.01	0.03	0	0	0.05	0.04
M=10, To=800 ℃	0.01	0.04	0.02	0.10	0	0.04

Table 3. Coefficients Variation with Temperature

Unit : N or N.m/mV/V

Name of Balance	Components	T=20 ℃		T=70 ℃		T=120 ℃	
		Coefficient	Relative Deviation	Coe.	R · D (%)	Coe.	R · D (%)
5N6-24A (not ompensated)	Y	511.8	-	503.5	-1.62	498.6	-2.58
	Mz	38.76	-	38.15	-1.57	37.75	-2.61
C-6N6-24A1 (compensated)	Y	219.2	-	219.6	+0.18	219.3	+0.05
	Mz	5.543	-	5.540	-0.05	5.538	-0.09
	X1	556.5	-	555.6	-0.16	555.4	-0.20
	X2	1111.6	-	1110.3	-0.12	1111.2	-0.04
	Mx	9.630	-	9.633	+0.03	9.649	+0.20

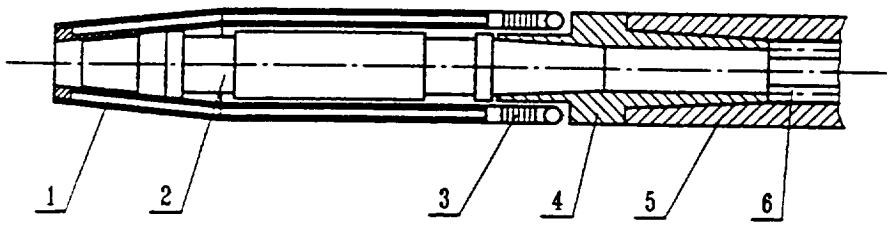

1. water cooling/insulation cover; 2. balance component;
3. bellows; 4. cooling/insulation adapter;
5. sting 6. cooling water tube.

Figure 1. Structural Drawing of Water Cooled Internal Balance.

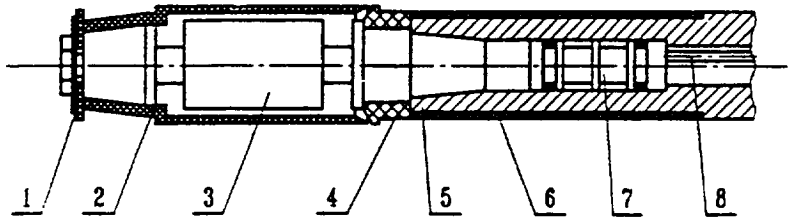

1. Insulation pad; 2. component insulation cover;
3. balance component; 4. Insulation ring;
5. sting; 6. sting insulation cover;
7. cooling cover; 8. cooling water tube.

Figure 2. Structural Drawing of Medium Temperature Balance.

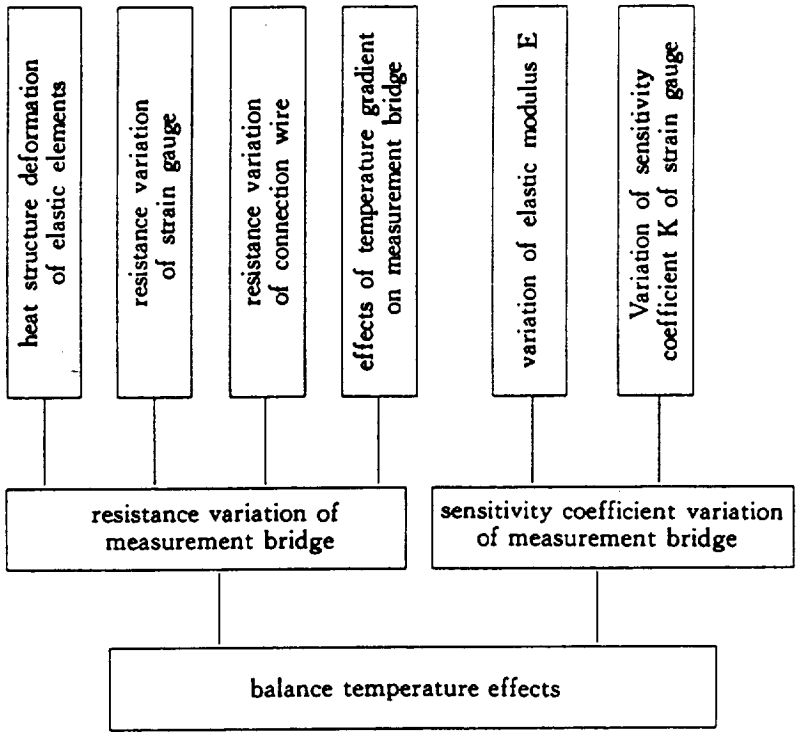

Figure 3. Factors Causing Balance Temperature Effects

ONERA BALANCES AND DYNAMOMETERS

Maurice BAZIN, Francis MILLIAT and Daniel GIRARD
Office National d'Etudes et de Recherches Aérospatiales, BP 72
29, Avenue de la Division Leclerc, 92322 Châtillon Cedex, France

1. INTRODUCTION

The quality of most wind tunnel tests depends directly on the quality of the balances and other experimental dynamometric elements. In this paper, there is not enough room to review in detail all the techniques and know-how acquired at ONERA over the years, not only in its research laboratory, but also throughout a long experience, sanctioned by a mass of test data using many different balances. The most important principles we have developed are now general knowledge, and can be found in many published papers. The authors here have placed their emphasis on synthesizing this knowledge, sometimes in a somewhat didactic form, especially as far as the structural and mastery of the thermal effects are concerned. As manufacturers' requests for accuracy are always increasing [1], especially as concerns the drag count (1×10^{-4}), the balance definition and the manufacturing techniques have changed, drawing from benefits of powerful design optimization systems (CAD and finite elements), of the quality of commercially available components, and of the development of methods for selecting and associating these components.

The mastery of thermal effects, which already appeared to be a major quality factor for conventional wind tunnels, is now an unavoidable one for cryogenic wind tunnels, for certain tests involving hot jet simulations or requiring supply of hot compressed air to the model, and to some extent it is unavoidable for hot hypersonic blowdown wind tunnel tests as well. For balances subjected to dynamic forces, the latest developments concern the use of semiconductor gages and inertial effect correction techniques.
The major progress made in wind tunnel model powerplant simulations, with nacelles to wing integration for civil aircraft and afterbody optimization for military aircraft, and so forth, has required the use of compressed air decoupling devices with the balances, along with the corresponding exhaust devices for turboprop simulators. These devices are placed in a balance bypass configuration, and must induce no mechanical nor thermomechanical effects that would deteriorate the precision of the instruments. This is a new technology that had to be developed and fully managed.

Many other parameters, which may just crop up from time to time in the discussion, have an effect on the measurement quality and user's satisfaction with the wind tunnel balances. These are the moisture protection; balance locking devices so that work can be done safely on the model and for transport purposes; the determination of stress levels under the gages to minimize creep and hysteresis effects, and safety coefficients, including dynamic stresses and monitoring methods. Calibration methods (which are changing now with the emergence of automatic calibration machines) and checking methods are also essential success factors, as are the associated instrumentation (bridge supply stability, amplification, filtering, and so forth), without underestimating the importance of the test control methodology itself.

2. DIFFERENT TYPES OF BALANCES

Force balances and transducers, which differ in their dimensions and capacities and by the structure and/or extensometric equipment, are commonly used in Onera's wind tunnels [2]. There is a total investment of some 100 instruments, including the balances and their replacement units, available for the various wind tunnels and types of tests. Nearly all of them have been designed and manufactured by ONERA, and ONERA also provides balances for test facilities outside the organization.

The balances are generally considered in the following groups and subgroups:

2.1. Sting Balances

These are mainly single piece structures, the central portion of which is used for the drag measurement, and is finely machined by electro-erosion for the six-component balances (Fig. 1, 2).

Exceptionally, the balance may consist of several parts, but which are welded together by electronic beam welding (192 mm balance, with a central passage for the compressed air supply, Fig. 3).
Our own experience also includes a design with removable dynamoters (Able-Task type) for two balances, one of them being 230 mm in diameter (Fig. 4), for the S1MA tunnel. In our opinion, this type of design is limited to « large » sting balances because, when high acuracy is called for, the manufacturing tolerances entailed at the level of the internal fittings are tight to avoid zero pass-through and hysteresis effects, and because of the difficulties in compensating the thermomechanical effects. But this solution to the problem does have advantages, even for small balances, for certain tests on missiles with highly elongated fuselage, where the drag accuracy is not the main criterion. The advantage it has over monoblock balances is its peripheral attachment, which helps stiffen the model, and the fact that, for a similar angular deformation at a given load, it reduces the risk of contact at the bottom. This is because the deformations of the non metric part are essentially internal to the balance.

For certain rare monoblock type balances, the central portion is removable, so that the drag capacity can be changed if necessary. This was initially tried as a means of repair (Fig. 5). The results were satisfactory, and the coming sharp decrease in calibration costs indicates that there may be some future for this type of concept.

The sting balances used for dynamic measurements (dynamic stability studies) may be of conventional design (forced oscillations), or they may use crossed blades (for free oscillations). The extensometric equipment used for these may be very sensitive semiconductor gages requiring special bonding procedures, with a silica deposit as base layer or a thin insulator, and special glues. These gages are very sensitive to thermal effects, but these effects do not disturb the dynamic measurements (for slow temperature variations). This type of gage can be used for the brief, steady measurements in hypersonic wind tunnels, because the intense thermal effects do not have time to affect the balance. The balance equipment then includes accelerometers for compensating the inertial effects that arise during startup (F4 balance and results [3]).

ONERA's balances range in diameter from 8 to 250 mm; in lift measurement capacity from 60 to 90,000 N; and in drag from 100 to 17,000 N.

2.2. Plateau Balances

These are mostly balances consisting of six dynamometers assembled between two rigid plates, one of which is weighed and the other not. Depending on how the dynamometers are arranged, the interactions between the various force components are variable; but the nonlinear interaction terms are small, compared with the monoblock sting balances. The fact that the decoupling between the dynamometers is good is also a factor that lowers the thermal gradient sensitivity between the metric and non metric parts.

The balance capacities are adapted by simply changing the dynamometers. This change calls only for a calibration check for the main interactions. For very large balances (F1 wall), a balance component is equipped with two different sensitivity dynamometers, the most sensitive one being locked in the high-capacity range (Fig. 6-7).

This type of balance is used for tests on wall-mounted half-models, but also for tests on large-scale rotary wings, propellers and helicopter rotors. In this latter case, the balance is fixed and provided with an engine shaft passage and roll bearings. The torque is measured on the shaft with a separate rotary transducer, placed between two flectors.

The combination of sting and plateau balances can be found in the form of a plateau-monoblock balance inside a model mounted on a vertical mast, as in combat aircraft balance used at the S1MA (Fig. 8).

ONERA balances of plateau type range in diameter from 280 to 2,000 mm, with lift capacities from 8,000 to 145,000 N, and drag from 350 to 25,000 N.

2.3. Special Balances

These are generally monoblock balances adapted for weighing different model elements, such as air intakes, fuselage boattail, propeller torque and thrust, lifting surface hinge moments, and so forth.

2.4. Dynamometers

These are single-component measurement instruments with tapered, crossed tips, to decouple the component being measured from the other forces.

They are of variable sizes and capacities, and are used in removable dynamometer balances (Fig. 9).

ONERA has provided the French national metrology laboratory (BNM) with standard dynamometers ranging from 50 to 300 KN in capacity, for use in comparison among European calibration benches. Their precision is better than 1×10^{-4} their capacity (Fig. 10).

3. DESIGN PRINCIPLES OF A SIX-COMPONENT MONOBLOC STING BALANCE

Many different approaches are possible for designing a balance, and many different architectures for the central portion, which is the most delicate part with its decoupling blades and the dynamometric element itself. The blades and drag dynamometer could form a single unit in some commercially available balances. These are generally for small balances or when the desired accuracy makes it necessary to do away with a more complex central portion.

The first approach we adopt, because it is the most effective at the time, is to apply geometry similarity rules to the capacities and strain configuration of an existing balance [4], whenever possible. This is satisfactory, and we are thus able to create « homothetic » balances. When extrapolating to a larger balance, though, we must be careful not to amplify any thermomechanical problems resulting from thermal gradient effects.

To meet special specifications, or to upgrade an existing « family », a new design has to be addressed.
The initial sizing, before the finite element approach is used, concerns the characteristics of the central portion where the longitudinal (drag) component will be measured. Attention to thermomechanical properties of the device is essential in this design phase.

3.1. Decoupling Ratio

The decoupling longitudinal ratio, $Rd = R_D/R_L$, *i.e.* the dynamometer over the decoupling blade rigidities, has to be adapted to the intended use of the balance. In practice, this ratio ranges from 0.2 to 9.

For fine drag measurements, such as when civil aircraft are weighed without consideration of butteting or stall phenomena, high values of Rd are desired.

For a stiff balance that has to take large and sometimes sudden force variations, we want the lowest values of Rd so that the dynamometer will react to only a small part of the force. The low-Rd balances are used for fighter planes and missiles up to very high angles of attack, and for civil aircraft in stall testing.

Historically speaking, we have tried to cover as broad a domain as possible with the same balance, for economic reasons, and of course we have also tried not to have to change balances in the course of the same test, which is often still an economic requirement. The best compromise is found at about Rd = 1. But as soon as the customers called for improved repeatibility we saw that the balances were subjected to thermal effects and we had to recognize it was necessary to overcome thermomechanical effects. This thermal sensitivity increases with

the size of the balance (*i.e.* the thermal inertias do increase very quickly with size).

Our first step was to imagine a method for correcting these effects, which consists of gaging the blades with additional X_L bridges [8]. This method will be recalled in the section on thermal corrections. Our analysis of the thermomechanical behaviour and experience with many different arrangements over the last ten years has now told us that, except for particular applications, decoupling ratios between Rd = 0.4 and 3 should be avoided. Though we have not come up with a concrete realization as yet, our feeling is that there is no way of entirely compensating the thermal gradient effects in this range around Rd = 1, even by adopting a push-pull dynamometer, the theory and advantages of which will also be described below, because of small manufacturing defects.

3.2. Decoupling Blades

For a given transverse force strength and a given longitudinal rigidity ratio, the number and position of the blades used affects the thermomechanical and structural properties of the central portion.

The optimum depends on the performance sought, and especially on the ratio between the transverse and longitudinal forces. A moderate increase in the number of blades with respect to the necessary minimum, defined by a quick material strength computation, seems to improve the thermomechanical properties; but in practice, this also quickly reaches a limit because of the stiffness of the main beams supporting the blades, and for economic reasons too. (Figure 11 shows a balance with 56 blades).
Once the dynamometer is chosen the finite element method is used to optimize the height, width, and thickness of the various blades to reach as uniform as possible a stress level in each of them.

3.3. Drag Dynamometer

There is no absolute principle for guiding the designer in choosing the dynamometer type, except for general geometric considerations concerning the central portion, and the stress level resulting from the desired decoupling ratio. But it should be remembered that, when looking for the optimum tradeoff between sensitivity, on the one hand, and creep and hysteresis on the other (Fig. 12), we should avoid ranging beyond $1 \times 10^{-3}\ \Delta l/l$ (20 hbar under the gages).

The various types of drag dynamometers are (Fig. 13):
- "frog's legs", which operate in semicircular bending mode, and which are going out of style nowadays;
- bending beams, which are tapered at the loading point;
- tensile-compressive beams, also tapered at the ends;
- shear-mode "membranes", also decoupled.

The push-pull arrangement, which can be used whenever the balance dimension so justify, and which raises no cost obstacles, offers a mechanical self-compensation for the thermal gradient effects. Here (Fig. 14), the thermomechanical effects impart stresses of the same sign to each of the two dynamometers, while stresses of opposite sign are imparted by the force to be measured. The gage bridge signals can therefore be subtracted in order to get the data signal we want, with the same sensitivity as with a single dynamometer.

Here again, the final architecture, whether it be a single push-pull in the center or a push-pull in the lateral faces, depends on the designer's experience and also on the difficulties involved in manufacturing and gaging the device. But we are in all cases looking for the greatest symmetry in the central portion of the balance, and as much compactness as possible, too (Fig. 15).

3.4. Transverse Force Measurements and Attaching Parts

The dynamometers designed for lift and pitch and for lateral force and sideslip, consist of of simple flat-faced portions of the structure, sometimes with openings. Their initial dimensioning is determined by a simple materials strength computation. The bridge gages are combined between the two ends of the balance (Fig. 16) in such a way as to make the thermal compensation easier. The output signals will be processed somewhat differently, depending on the half-bridges of a given orientation are combined at M_1, M_2, ($L = M_1+M_2$; $P = M_1 - M_2$ in the signal computation) or directly in lift L and pitch P (the same being true for lateral force and moment).

The definitions of the flanges, cylindrical or conical recesses (and, for the last, of the gradual extraction devices to avoid shocks during disassembly), depends on the model to be fitted. Whatever type of attachment design is used, it is absolutely necessary to locate them and the transverse force measurement gages sufficiently away from each other, to avoid "clamping" effects. A specific computation is also made for the tightening conditions. Lastly, the balance section variations are checked to ensure a proper routing of thermal fluxes.

3.5. Finite Elements Computations

After the balance has been appropriately modeled, finite element computations are performed to check the balance behavior in the main loading configurations, for single and combined loads. This verification process has been developed since 1975 for many ONERA balances, and only the smallest balances still get by the process. These simulation results concern primarily the stresses and strains, and are used to optimize and validate the design (Fig. 17-18). They are also used to determine influence coefficients for various critical points on the balance. Once confirmed by calibration, these coefficients will be used in the real-time calculation of the combined stresses (static and weighted rms dynamic) at these points, at which the balance is monitored during the test. The person responsible for the test has a gradual alarm system and a monitor showing the instantaneous loading ratio, displayed as a point in a stress-strain diagram with the authorized operation envelope.

Except for cryogenic balance studies, finite element simulation of thermal loads was never really used intensively at ONERA before 1992, when the SAMCEF f.e. code was introduced. This code checks more easily the thermomechanical stress levels corresponding to given thermal gradients. The experimental data for the balance delivered to ETW shows (Fig. 19) that this balance, which was specially optimized, is insensitive to the effects of gradients of up to 10 K in the central portion (the calculation check was for 15 K).

Since ref. [5] was produced, data obtained in ETW gave the confirmation that drag cross checkings better than 1.10^{-4} are possible even without waiting, often for more than half an hour, the thermal equilibrium inside the balance after a change of the tunnel temperature.
Time and energy consumption could then significantly decrease.

4. GAGING AND THERMAL COMPENSATIONS [6] (Fig. 20)

It is important to keep a number of well-known dynamometric principles in mind:
In a metal beam of cross-sectional area S. Hooke's law applies:
$\varepsilon = \Delta l/l = \eta/E = F/S.E$,
where ε is the relative strain, η the stress, E the metal's Young's modulus, and F the applied force.

A Wheatstone bridge consists of four gage resistors, R, such that:
$\Delta R/R = k \times \Delta l/l$ with gage factor k,
$\Delta V/U = \Sigma.\Delta R/4R$, where ΔV is the output voltage variation, U the bridge supply voltage, and ΔR the resistor variation due to the measured phenomenon.
The sensitivity $d = \Delta V/F$, and the rigidity $F/\Delta l$ characterize the transducer at a given temperature.

Considering a temperature variation Dq, the metal substrate expands linearly by $\Delta l = \alpha \, . \, l \, . \, \Delta\theta$, and its Young's modulus varies by $\Delta E = C_{TE} \, E \, \Delta\theta$, where a is the substrate expansion coefficient, C_{TE} is its thermoelastic coefficient, while $\Delta R = C_{TR}.R \, \Delta\theta$ and $\Delta k = C_{TK} \, k \, \Delta\theta$ for the gages, where C_{TR} is the gage's thermal sensitivity coefficient, and C_{TK} the gage factor thermal coefficient.

– The zero variations (*i.e.* the bridge output when F = 0) with global temperature changes in the balance are evidenced by small difference in the gage C_{TR} due either to intrinsic homogeneity defects (even after carefully combining the gages) or to unsymmetries caused by the bonding and wiring. Preferably, they are compensated on each half of the bridge (Fig. 21). This is because the two half-bridges are generally far away from each other and may thus be at different temperature levels. The balance is done by introducing additional resistors with high and/or low C_{TR}. This process involves iterative measurements in a thermal chamber with dedicated instrumentation for determining the values of the resistors to be introduced in the circuit. It also includes a linearization process, to improve the result for very large temperature variations (cryogenic balances). Thermal characteristics of compensation resistors have been measured in the range 100-300 K (Fig. 22). Copper and platinium have linear variations which allow slope correction but without any effect on curvature. Manganin, Balco, and Nickel, with different C_{TR}, have non linear behaviour (f of opposite sign) which make possible curvature corrections. The resistor types and values to be inserted inside each half-bridge to correct slope δ and curvature f are computed from the three equations of the figure 22. The residual variation of the zero after compensation currently reach 0.1 10^{-6} $\Delta R/R/K$ (Kelvin) within the temperature domain considered.

Figure 23 shows the results, obtained for the T2 24 mm balance and the 100 mm balance delivered for ETW, in the range 100-300 K from the beginning to the end of the zero compensation process for a drag bridge. As the iterative process is long and costly, it was interrupted as soon as the specifications were reached, without trying to reach perfection.

– The sensitivity may vary with temperature level, because of a difference between the thermoelastic coefficient of the substrate and the gage thermal sensitivity coefficient.
From $C_{TD} = \Delta d/d/\Delta\theta$ and $d = \Delta V/F = kV/S.E$:
$C_{TD} = C_{TK} - 2\,\alpha - C_{TE} + \Delta U/U$, and for a constant voltage supply, as $2\,\alpha$ could be neglected comparatively to C_{TK} or C_{TE}:
$C_{TD} = C_{TK} - C_{TE}$.
The C_{TE} of a metal is often negative, except for certain Fe-Ni alloys, while the C_{TK} of the gage may be negative or positive, depending on the type of gage. One way of getting good sensitivity compensation is to minimize the C_{TD} by choosing an appropriate gage type for the substrate material selected [7]. Many experiments have been performed to determine the strength and elastic characteristics of different materials in a wide temperature range, in order to select the material, and then try various associations of substrate and gages to find the best combination for the targeted temperature domain with the selected material (Fig. 24).

However, this best possible initial compensation absolutely must be improved by introducing thermal resistors in the bridge supply circuit. This is to compensate any remaining sensitivity variation by an automatic supply voltage variation at the bridge level entailing a slight loss with respect to the initial sensitivity. This result calls for another iterative process, including linearization, if a wide temperature variation is expected.

Figure 25 shows the final result obtained on the same bridge as in the previous figure 23.

– The temperature gradient effect, mainly concerning the drag element, can be overcome by additional bridges in the elastic blade parallelogram. The differential expansions within the general structure generate internal forces in opposite directions in the figure 26, which balance each other in the dynamometer and in the parallelogram, while a drag force induces forces in the same direction. An X_L bridge is formed by bonding gages on the symmetrical front and rear blades on each side. The calibration shows (Fig. 27) that a relation of $XD + k\,X_L$ can be established independtly of a temperature gradient, to yield the correct drag. k is a constant that depends on the rigidity ratio and the number of blades [8].

5. COMPRESSED AIR SUPPLY [9]

The following three examples illustrate how compressed air decoupling systems for engine simulations are added to the balance (for pressures from 35 bar to 100 bar and flow rates up to 16 kg/s).

5.1. Sting Balance

In the first example, we consider a complete model setup on a mast, where the monoblock sting balance (diameter 192 mm, length 620 mm) was specially designed with a compressed air inlet. The balance (see Fig. 3) consists of two concentric tubes interconnected by six dynamometric elements cut into the solid material of the inner cylinder, which is the unweighed part. The weighed outer cylinder was initially made of two half-shells,

welded together and to the lateral dynamometers by electron beam welding.

The air supply passes through the center of the balance, and the decoupling is provided by a double series of four transverse bellows operating in opposition (radial arrangement) (Fig. 28). The air flow passage is improved at the level of the bellows by an internal jacket. The annular decoupling enclosure is weighed. The bellows have an axial rigidity of 60 N/mm (260 N/mm transversely), which is small compared with the longitudinal rigidity of the balance itself (650 N/mm).

The pressure forces cancel out at the level of the bellows by matching pairs, to ensure equivalent cross-section. The flow adjustment and measurement system, consisting of sonic throats, provides a separate supply for two nacelles (Fig. 29).

5.2. Donahue System and Improvements

Many setups (both sting and wall mounts) use an existing balance with symmetrical lateral air supplies or a central supply. The decoupling is provided by inserting a « Donahue » [10] device in the circuit. This eliminates nearly all the background effects and makes it possible not to pre-load the balance with a large pressure effect, which varies in accordance with test conditions. In practice, devices like these can also be used on air supplies at the level of the unweighed portions because, by minimizing the internal stresses, this avoids the small structural deformations that might affect the neighboring dynamometric elements.

Donahue devices use bellows having the smallest possible rigidity. The idea is based on a demonstration that proves that an enclosure subjected to a given pressure generates no background effect if its internal volume does not vary during its deformation. By combining three bellows in an appropriate interconnecting design, with one of the bellows having an effective cross section twice that of the other two, this result is successfully achieved with appropriate rigidities and sections (Fig. 30). The same result can be obtained with four identical bellows.

In the latest devices of ONERA patent, buckling safety is ensured with minimum bellows stiffness by applying the pressure to the outside of the bellows. A reduced diameter assembly can also be achieved this way, using a concentric arrangement of bellows and a somewhat complex architecture for connecting them.

These decouplers are used both on the air flow supply and exhaust lines (turboprop simulation) with both sting and plateau balances. For a given flow rate, their size increases inversely with the pressure.

The axial and transverse stiffness of the decoupling devices are of the order of a few tenths of the sting balance stiffness at most, in the setup with two supplies and two exhausts.

5.3. Plateau Balance

Wall balance (plateau) design makes possible a central air passage.

To do this, we can also use Donahue type decouplers to eliminate the background effect, with a long, transversely flexible supply line that contributes to the low parasitic rigidity of the balance. An other possibility presented Figure 31 shows that an external supply line following two opposing paths will cancel out both the background effect and the momentum effects, as in the first case above.

The natural flexibility of the resulting banjo design is enhanced by inserting bellows in the line perpendicular to the drag axis.

For a balance drag capacity of 3,500 N and a stiffness of 110,000 N/mm, the decoupling has a stiffness of 400 N/mm using two supply systems in parallel to control four different channels.

5.4. Calibration

Because of the parallel rigidities of these decoupling devices (the stiffness of which varies a little with the pressure), additional force and pressure calibration is needed, mainly to check the quality of the manufactured elements and proper decoupling device alignments.

Six simple loading configurations and a few representative force combinations to be expected during the test are applied to correct the coefficients [11] initially generated in the full calibration of the balance alone. Experience shows that, especially for the three examples above, the main linear coefficients vary only by 0.1 to 0.4 percent, and the variation in the quadratic and cross-product coefficients are null, except for the pressure effects.

Any residual pressure effects (due to manufacturing defects) are evaluated throughout the pressure domain and in all the expected test combinations. Correction laws are then established. These corrections never exceed 0.5 %. The momentum effects on the drag, which depend on the mass flow rate, are evaluated by analogous procedures. They are zero for those balances having perpendicularly placed bellows (as in the wall balance above).

For the sake of precision in those tests that require compressed air simulator supply, special procedures are also called for. Ordinarily, the operation of the complete setup is checked in the test section, under no-wind conditions. The nacelles in these tests are replaced by standard nozzles. This test also provides a way of qualifying the transposition of the calibrations of the motorized nacelle and even of the same standard nozzles, which is done on a specific stand sometimes equipped with its own balance and different decoupling devices.

Reference [9] gives the results obtained for different balances in different process phases. Figure 33 shows the repeatability of the results obtained at S1MA on a wall balance for a half-model including two jet simulators. The drag measurement scatter comes to about 1×10^{-4}.

6. CONCLUSION

The methods and means ONERA uses in designing, constructing, and operating its wind tunnel balances offer users a drag measurement accuracy of 1×10^{-4}, even under very difficult cryogenic wind tunnel conditions, and for measurements requiring a supply of compressed air to the model.

The instrument process complexity and the high level of precaution needed for constructing it may seem frightening, but the cost of taking these precautions is quickly amortized by the gains in testing time and the quality of results.

7. REFERENCES

[1] B. EWALD and G. KRENZ. The accuracy problem of airplane development force testing in cryogenic wind tunnels. AIAA Paper 86-0776.

[2] M. DUBOIS. Fabrication of high precision strain gauge dynamometers and balances at the ONERA Modane Center. TP ONERA no. 1196 (1973). Institute of Physics and Physical Society, Teddington, February 1973.

[3] A. BUGEAU and E. CASTAN. Hermes first force measurement in ONERA F4 wind tunnel. TP ONERA no. 1996-68. European Symposium on Aerothermodynamics for Space Vehicles, Nordwijk, November 1994.

[4] M. BAZIN. Sting line feasibility study for force measurement in the European wind tunnel. TP no. 1982-90. Symposium on Cryogenic Technology, Amsterdam, September 1982.

[5] M. BAZIN, C. BLANCHET, F. DUPRIEZ. Instrumentation for cryogenic wind tunnels. AGARD FDP VKI Special Course Advance in Cryogenic Wind Tunnel Techniques, DLR, Köln, May 1996.

[6] M. BAZIN and M. DUBOIS. Balance and sting design for cryogenic wind tunnels. TP ONERA no. 1979-40. Symposium on Cryogenic Wind Tunnels, Southampton, April 1979.

[7] M. BAZIN. Instrumentation for cryogenic wind tunnels. TP ONERA no. 1985-29. AGARD FDP VKI Special Course on Cryogenic Technology Applied to Wind Tunnels, Rhode-Saint-Genese, April 1985.

[8] M. DUBOIS. Six component strain-gage balance for large wind tunnels. Experimental Mechanics, Vol. 21, no. 11, 401-407, November 1981.

[9] J.P. BECLE and D. GIRARD. Development of strain-gage balance with flow-through system for ONERA wind tunnels. TP ONERA no. 1989-55.

[10] J.E. DONAHUE. Analysis of pipe systems with special expansion features. ASME Paper no. 54 SA70. (Chaleur Industrie n° 412, novembre 1959).

[11] M. DUBOIS. Calibration of six component dynamometric balances. TP ONERA no. 1976-79. 7th IMECO, May 1976.

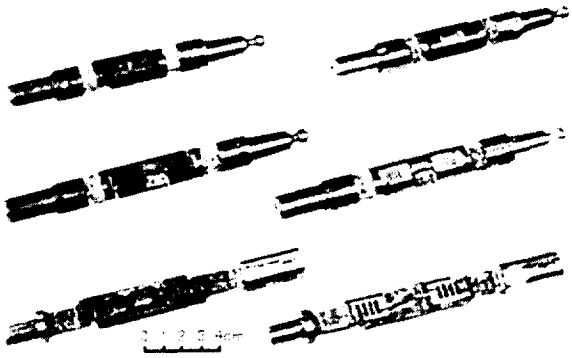

Fig. 1. Example of balances Ø 20 - Ø 22 mm.

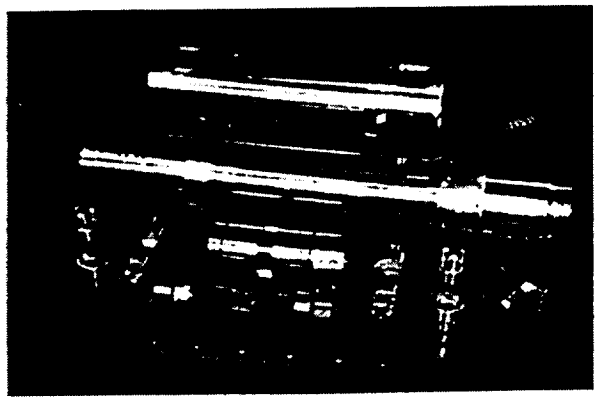

Fig. 4. Assembled balance type Ø 230 mm.

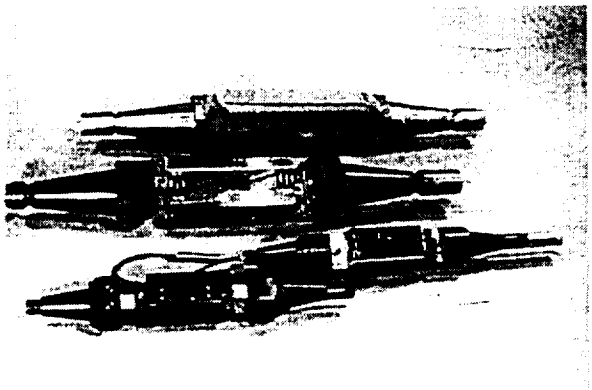

Fig. 2. Example of balances Ø 120 - Ø 190 mm.

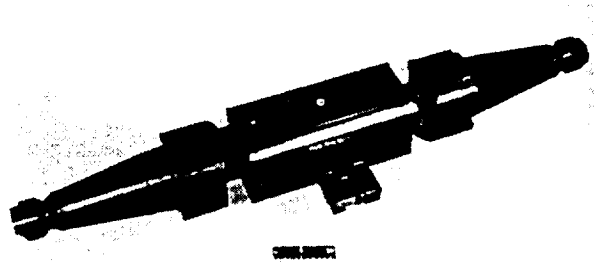

Fig. 5. Removable drag element (balance Ø 180 mm).

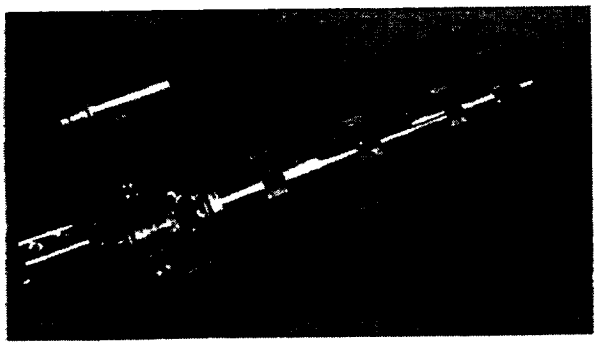

Fig. 3. Electron beam welded balance with air flow through system (Ø 192 mm).

Fig. 6. Assembled wall balance of F1 WT.

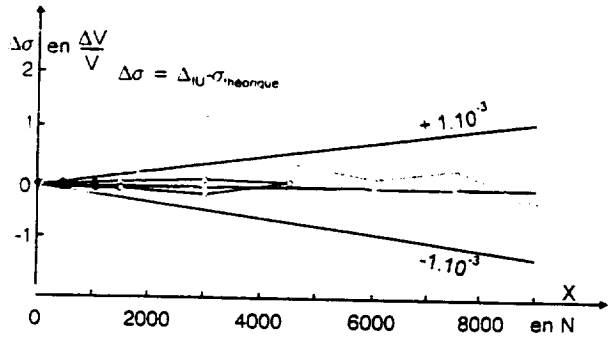

Fig. 7. Accuracy for drag measurement with the « small capacity » dynamometer. Wall balance F1.

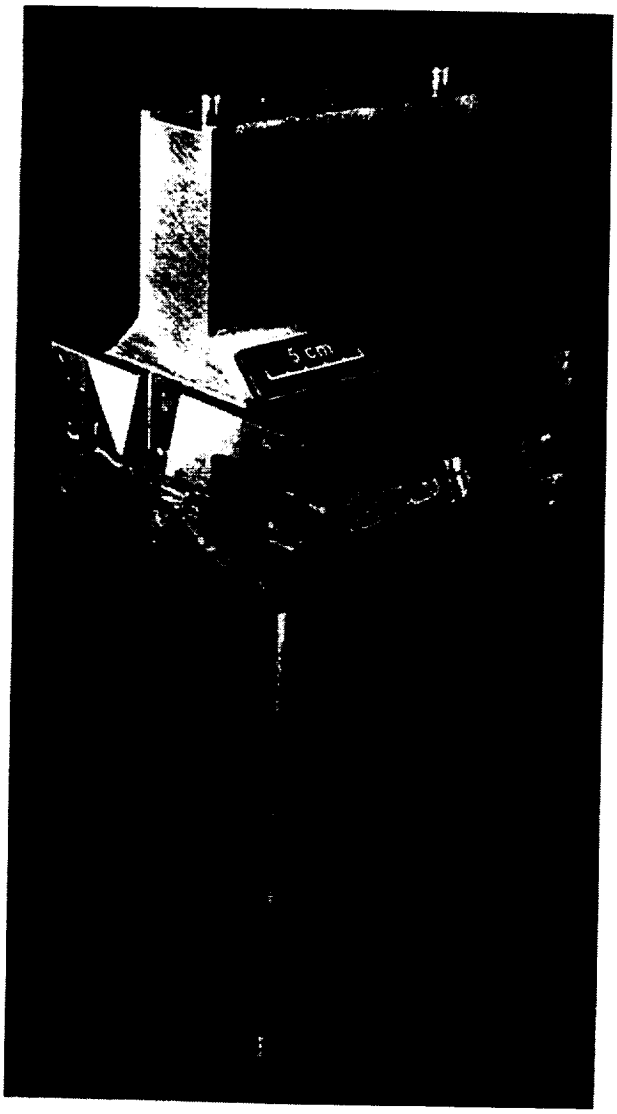

Fig. 8. One piece « sting » balance of two plates type.

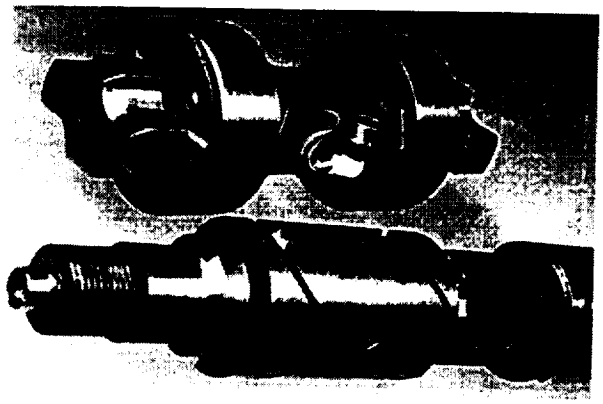

Fig. 9a. Dynamometers: long and short crossed thins.

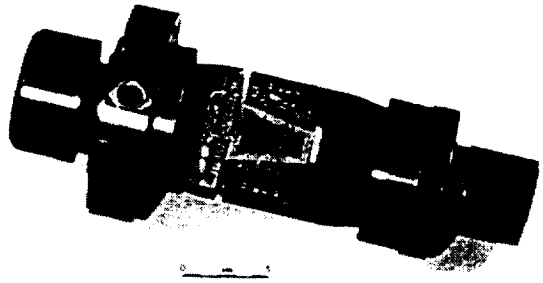

Fig. 9. b. Dynamometer: shear element.

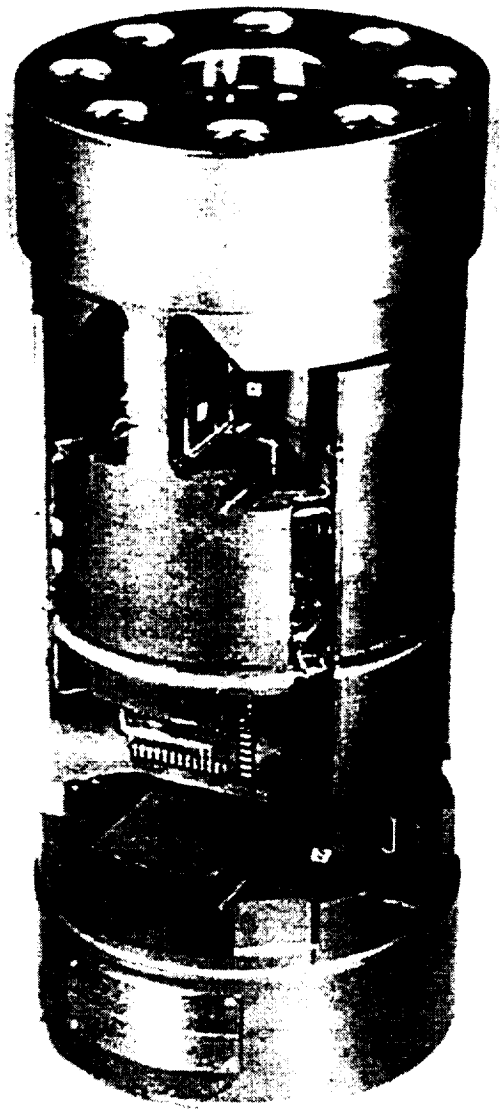

Fig. 10. BNM master dynamometer.

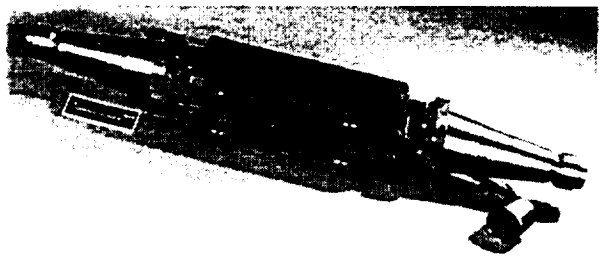

Fig. 11. A 56 blades balance (Ø 190 mm).

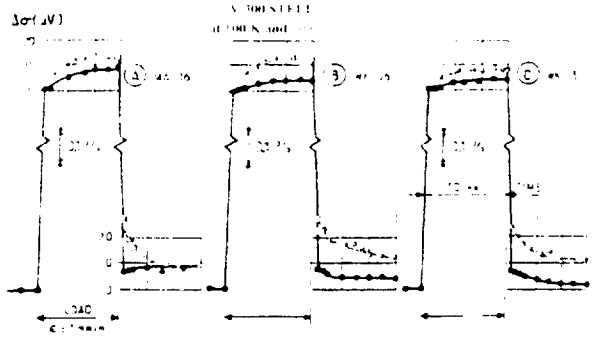

Fig. 12. Creep measurements.

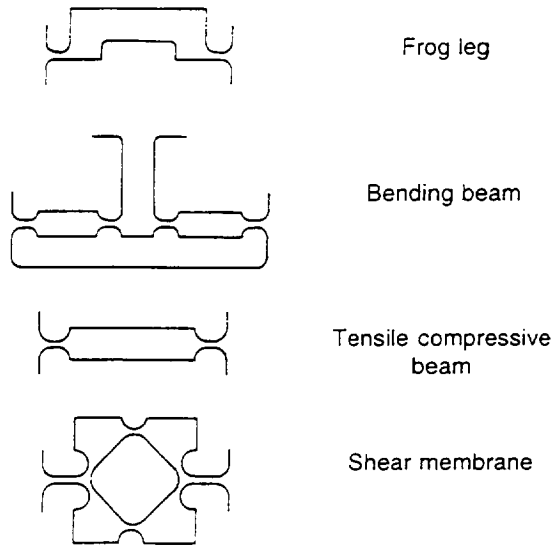

Fig. 13. Types of drag dynamometers.

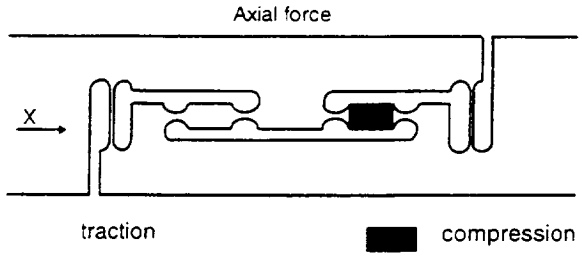

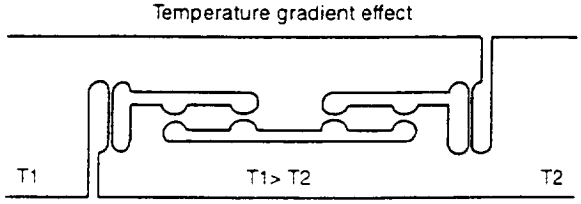

Fig. 14. Traction-compression push pull arrangement.

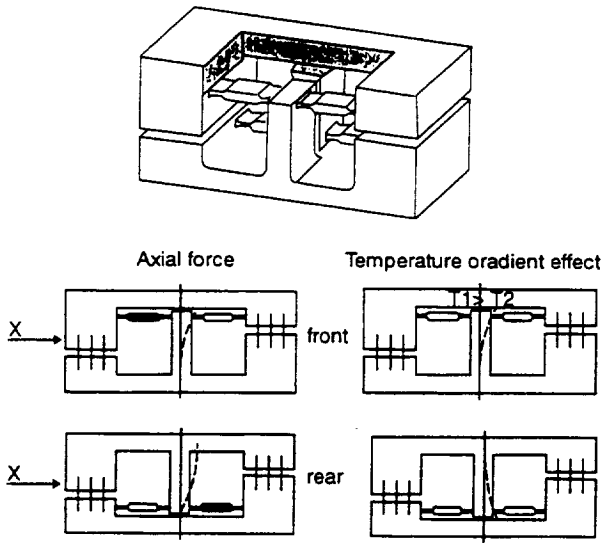

Fig. 15. Bending push pull arrangement.

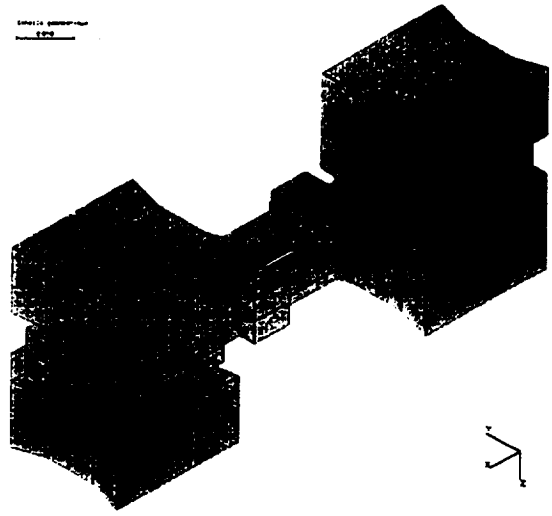

Fig. 17. Finite element: detail of the mesh for drag element.

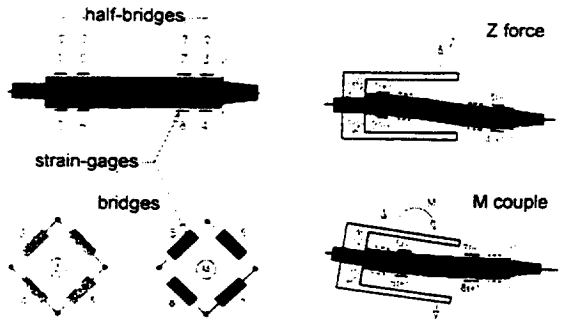

Fig. 16. Half bridge gaging for direct measurement of normal force and pitch moment.

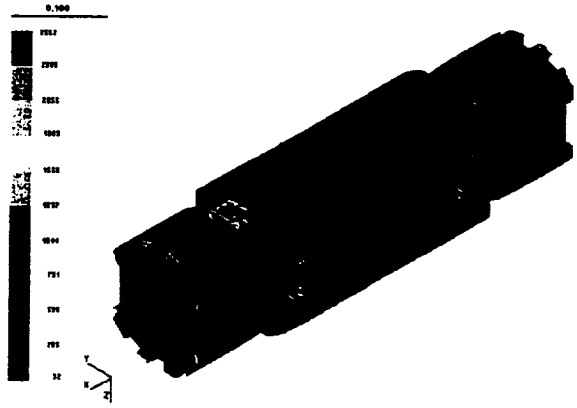

Fig. 18. Finite element: general mesh and Von Mises stress under normal force.

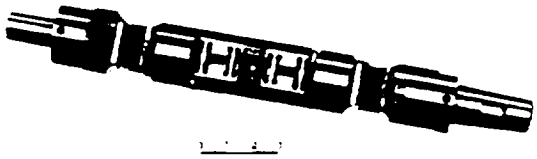

Fig. 19Aa ONERA T2 balance (Ø 24 mm)

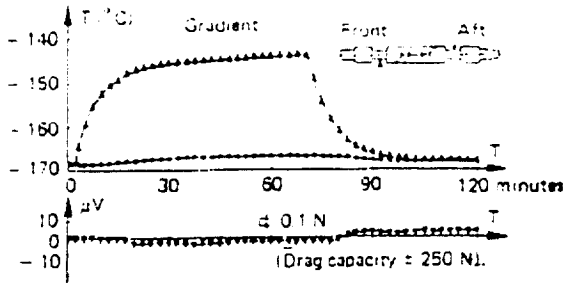

Fig. 19Ab T2 balance experimental result.

	DYNAMOMETRIC PRINCIPLES	THERMAL COEFFICENTS
SUPPORT	$\frac{V}{U} = \frac{I}{\epsilon} = \frac{\epsilon}{SE}$	$\alpha = \frac{V_1}{I} / \Delta\theta$ $CTE = \frac{\Delta E}{E} / \Delta\theta$
GAGES	$\frac{\Delta V}{U} = \frac{\Sigma \Delta R}{4R}$ $\frac{\Delta R}{R} = K \frac{\Delta l}{l}$	$CTR = \frac{\Delta R}{R} / \Delta\theta$ $CTK = \frac{\Delta R}{R} / \Delta\theta$

ZERO	$\neq \Delta R$ (CONSTANT θ) $\neq$ CTR	RESISTORS (LOW CTR, HIGH RESISTIVITY INSERTS (HIGH CTR, LOW RESISTIVITY
SENSITIVITY $d = \frac{\Delta V}{F}$	CTD $\neq$ CTK - CTE (CONSTANT POWER SUPPLY)	APPROPRIATE ASSOCIATION SUPPORT TYPE OF GAGE, RESISTORS INSERTS IN THE BRIDGE VOLTAGE SUPPLY
GRADIENTS	- INTERNAL STRESSES DUE TO DIFFERENTIAL EXPANSIONS (α) - SAME BRIDGES GAGES TEMPERATURE DIFFERENCES - JOULE EFFECT	DESIGN (SYMMETRY, STIFFNESS RATIO, DRAG DYNAMOMETER CONCEPT, GAGES LOCATION) INCREASE INSIDE CONDUCTIVITY EFFECTS INSULATION

Fig. 20. Summary of thermal compensation.

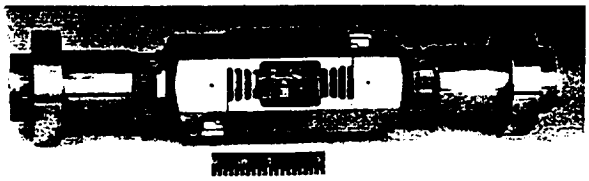

Fig. 19Ba ETW balance (Ø 100 mm).

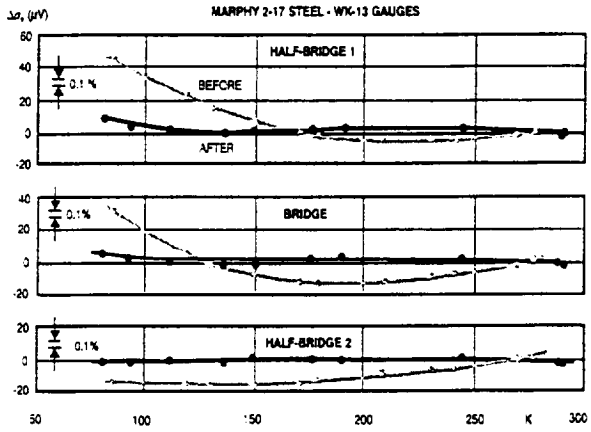

Fig. 21. Zero drift vs temperature.

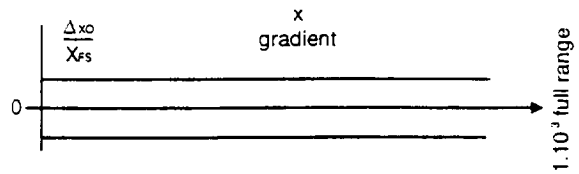

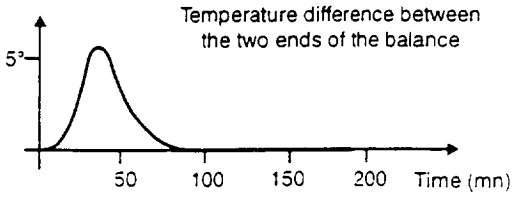

Fig. 19Bb ETW balance - Experimental result.

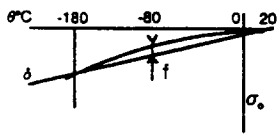

	δ 10^{-6} ΔR/R/°C	f 10^{-6} ΔR/R
	-	+
	-	-
	+	-
	+	+

Materials	TCR = average α in 10^{-6} ΔR/R/°C	f at -80°C in 10^{-3} ΔR/R
Copper	+ 3.97	~ 0
Platinum	+ 3.60	~ 0
Manganin	+ 0.27	- 16
Balco	+ 2.7	- + 60
Constantan	+ 0.06	- 4.4
Nickel	+ 4.3	+ 60

Manganin	Balco	Copper	Unit
$\Delta\sigma_m = \frac{rm}{R}$	$\Delta\sigma_b = \frac{rb}{R}$	$\Delta\sigma_c = \frac{rc}{R}$	10^{-6} ΔR/R
$\Delta\delta_m = TCRm\frac{rm}{R}$	$\Delta\delta_b = TCRb\frac{rb}{R}$	$\Delta\delta_c = TCRc\frac{rc}{R}$	10^{-3} ΔR/R/°C
$\Delta f_m = fm.\frac{rm}{R}$	$\Delta f_b = fb.\frac{rb}{R}$	0	10^{-3} ΔR/R/°C

$f = \Delta f_m + \Delta f_b + 0$
$\delta = \Delta\delta_m + \Delta\delta_b + \Delta\delta_c$
$\sigma_0 = \Delta\sigma_m + \Delta\sigma_b + \Delta\sigma_c$

Fig. 22. Linearization process.

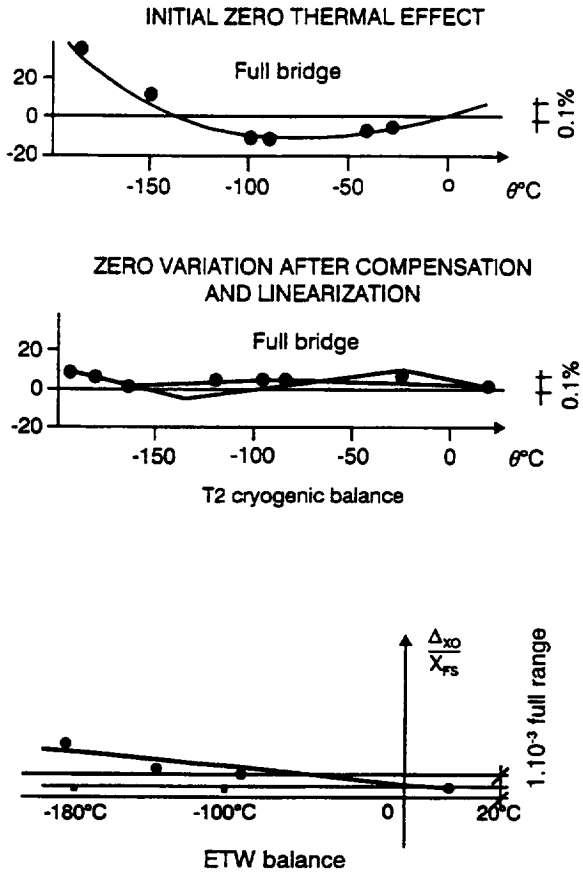

Fig. 23. Zero compensation.

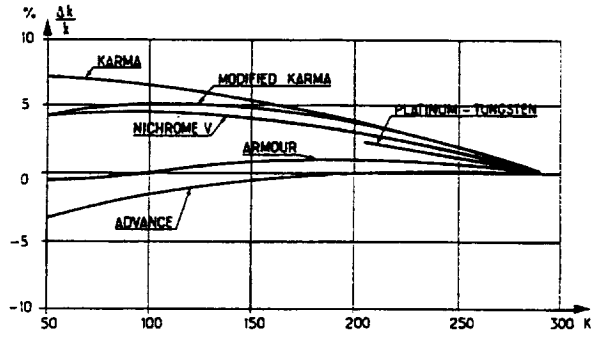

Fig. 24. Thermal gage factor coefficient.

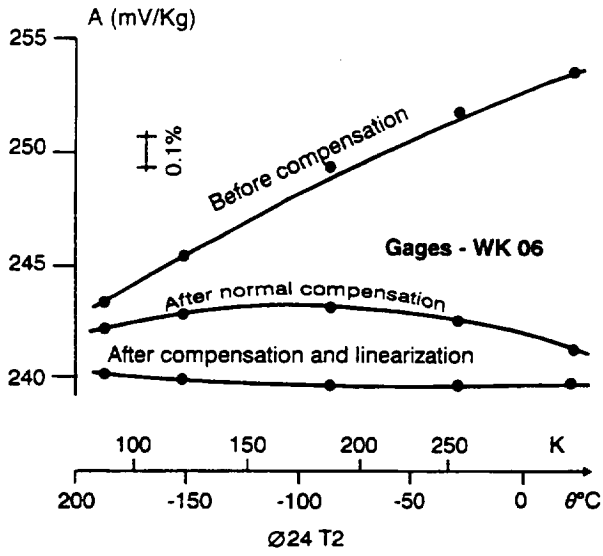

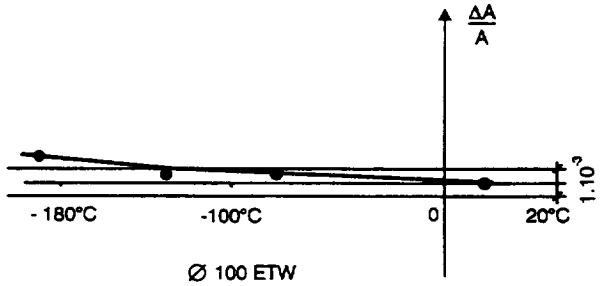

Fig. 25. Sensitivity compensation.

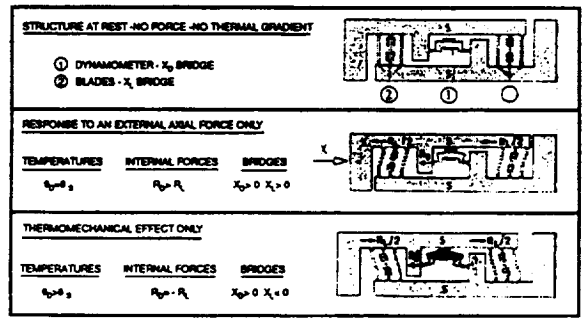

Fig. 26. Axial structure deformation.

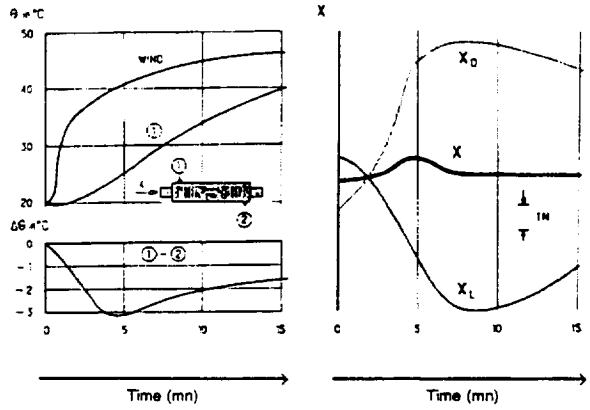

Fig. 27. Thermomechanical effect compensation.

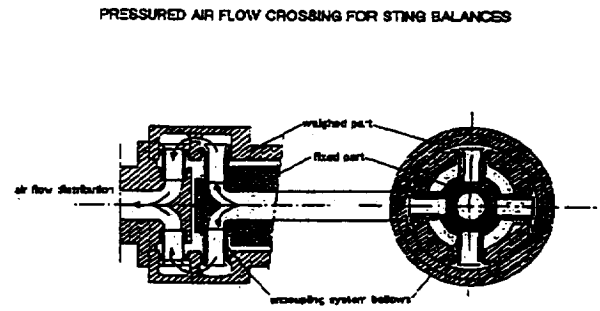

Fig. 28. Pressured air flow crossing for sting balances

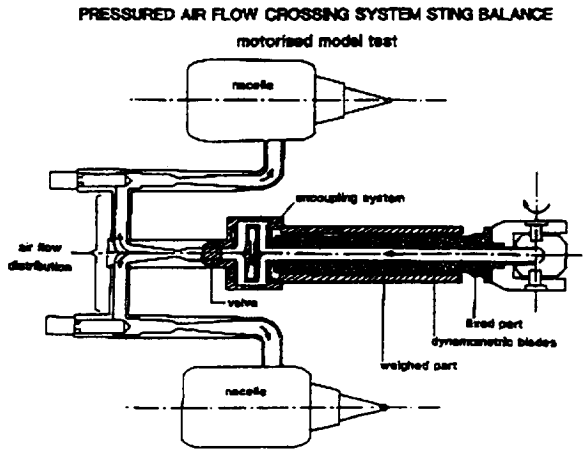

Fig. 29. Pressure air flow crossing system sting balance.

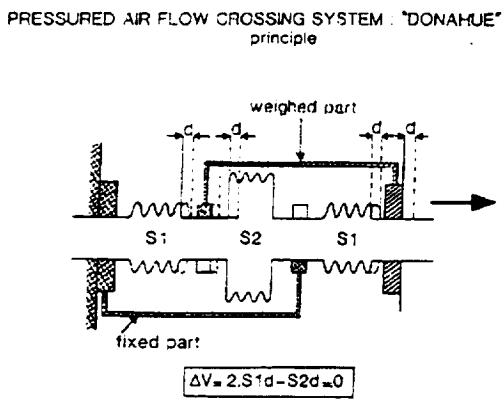

Fig. 30. Pressure air flow crossing system: « Donahue » type.

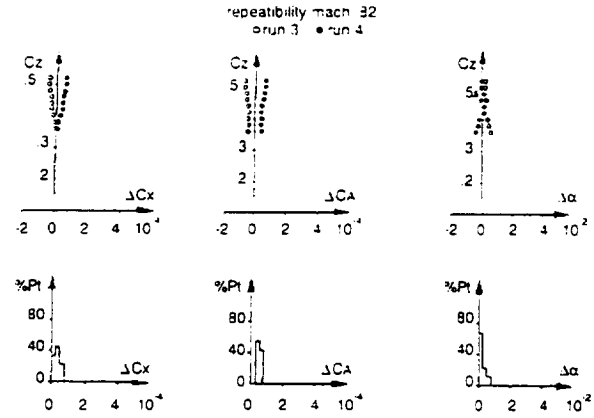

Fig. 32. Half model with two motorised nacelles: repeatability.

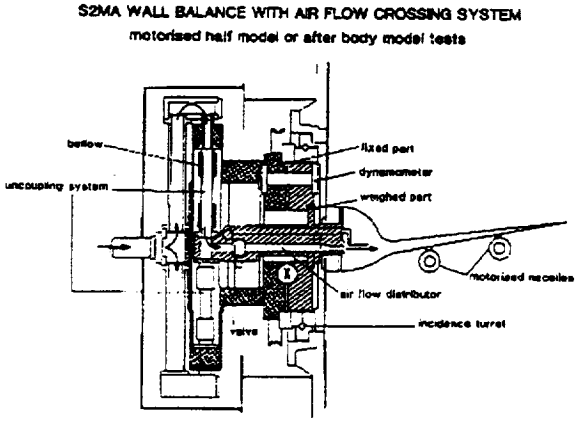

Fig. 31. S2MA wall balance with air flow crossing system.

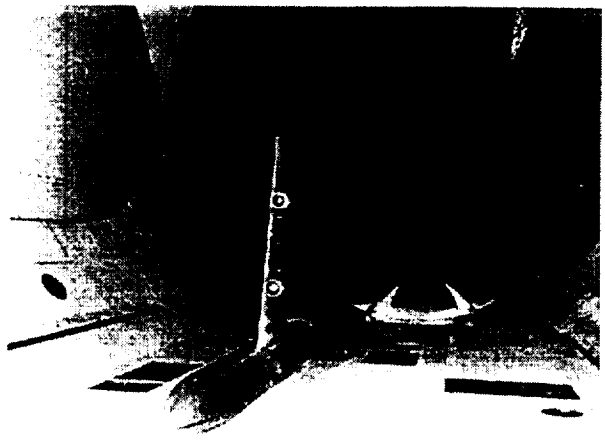

Fig. 33. Half model with two TPS in S1MA WT.

FINITE ELEMENT ANALYSIS OF A NASA NATIONAL TRANSONIC FACILITY WIND TUNNEL BALANCE

Michael C. Lindell
NASA Langley Research Center
Hampton, VA

SUMMARY

This paper presents the results of finite element analyses and correlation studies performed on a NASA National Transonic Facility (NTF) Wind Tunnel balance. In the past NASA has relied primarily on classical hand analyses, coupled with relatively large safety factors, for predicting maximum stresses in wind tunnel balances. Now, with the significant advancements in computer technology and sophistication of general purpose analysis codes, it is more reasonable to pursue finite element analyses of these balances. The correlation studies of the present analyses show very good agreement between the analyses and data measured with strain gages and therefore the studies give higher confidence for using finite element analyses to analyze and optimize balance designs in the future.

INTRODUCTION

Until recent years computer software and hardware limitations have hindered the detailed analysis of strain-gage balances by finite element methods. Due to the intricate design features of balances conventional h-element finite element codes were not practical because extremely fine meshes would be required to adequately capture stress gradients within the intricate geometric regions. If such models were produced the hardware required to run a solution (memory and disk space) would typically be unavailable. Even if the hardware was available to run the solution, several runs with varying mesh size would be required for each load case to gain confidence that stress gradients were reasonably captured. Such a process would be very time-consuming. The emergence of p-element finite element codes coupled with advances in computer technology has brought the detailed analysis of strain-gage balances within the reach of desktop workstations.

The balance under investigation is shown in Figure 1 as a Parametric Technology Corporation (PTC) Pro/Engineer part model. The design is an actual balance used in the NTF (balance number NTF-101A) and is also representative of the kind of intricate features found in other types of balances. The balance is fabricated from a single piece of 200 CVM maraging steel. Room temperature material properties for this steel are shown in Table 1. Some key dimensions of the balance are shown in Figure 2.

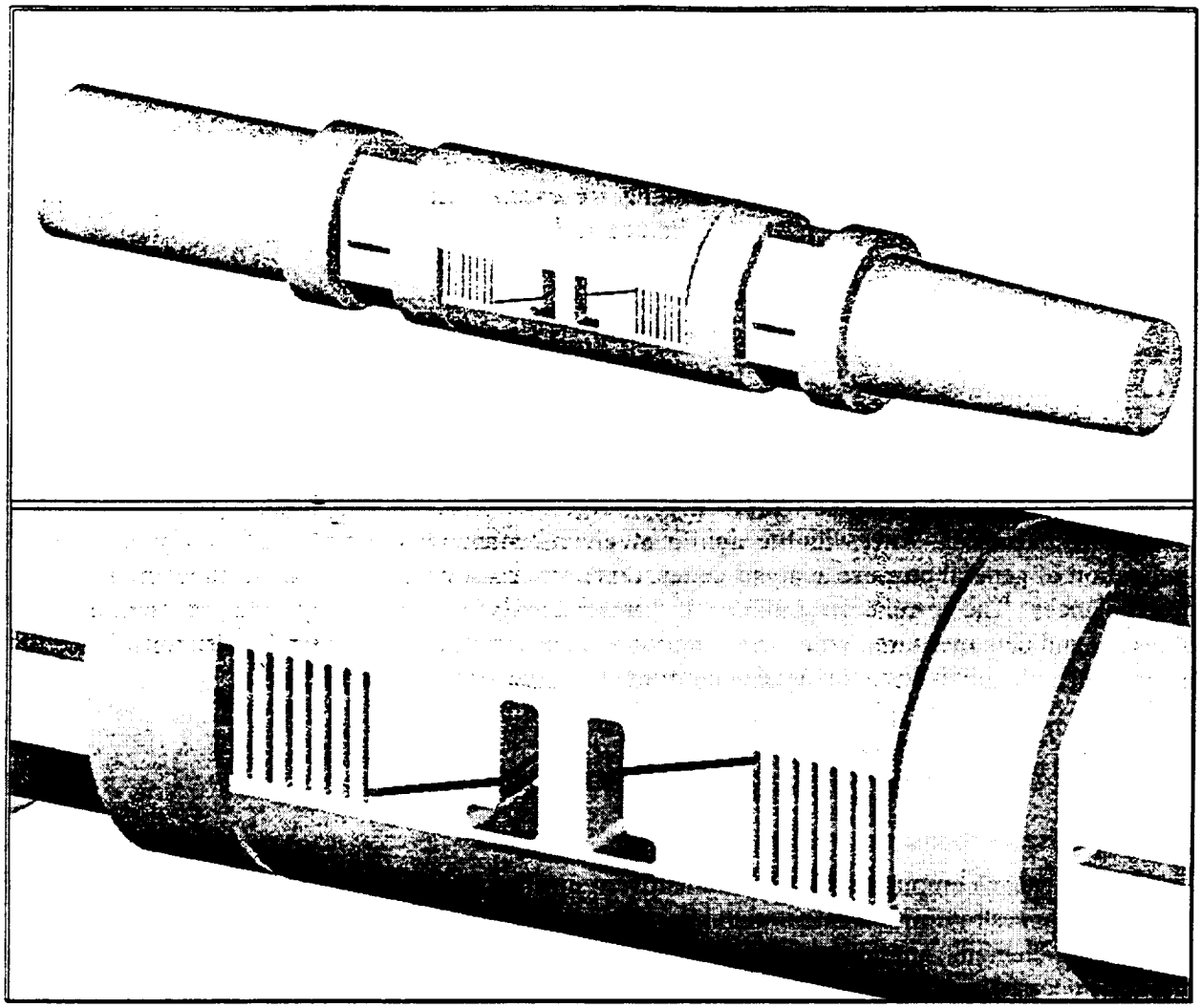

Figure 1. Pro/Engineer geometry model of NTF balance 101A.

Table 1. Room Temperature Material Properties for 200 CVM Maraging Steel

Modulus of Elasticity (psi)	26.2×10^6
Density (lb/in^3)	0.289
Yield Strength (psi)	206,000
Ultimate Strength (psi)	212,000

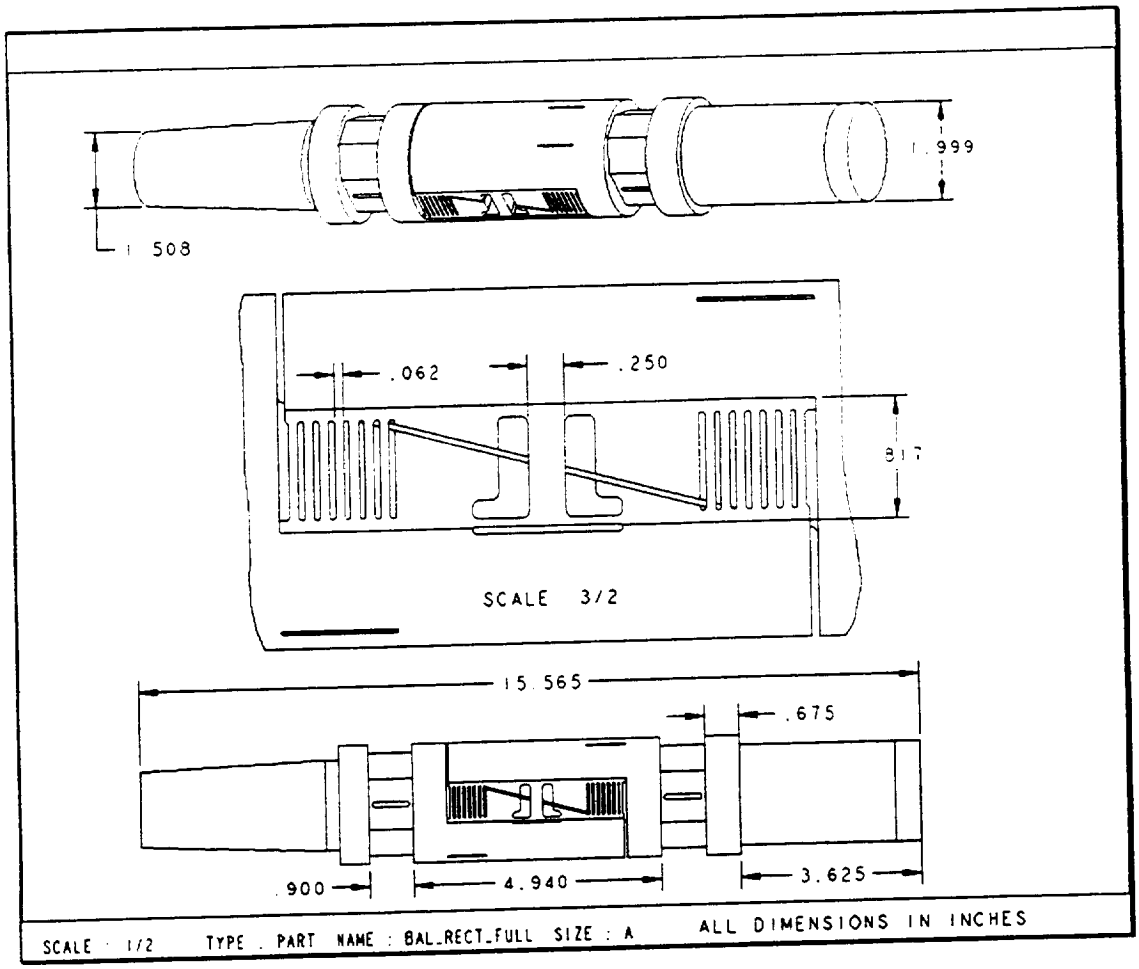

Figure 2. General balance dimensions for NTF 101A.

ANALYSIS AND CORRELATION

The analysis code used in these analyses was PTC Pro/Mechanica, an adaptive p-element technology code. The finite element model created for the balance is shown in Figure 3. The model consists of 8,630 high-order tetrahedral solid elements. The boundary condition on the model, to reflect the test setup, has the outer surface of the tapered end completely restrained. The loads were applied, also reflecting the test setup, by distributing the loads on the surface of the non-tapered end such that the desired resultant load through the balance center was achieved. A total of seven load cases were analyzed, the first six of which were correlated with test data. The seventh load case was a combination of the first six load cases and had no test data with which to correlate. The various load cases applied to the model are shown in Table 2.

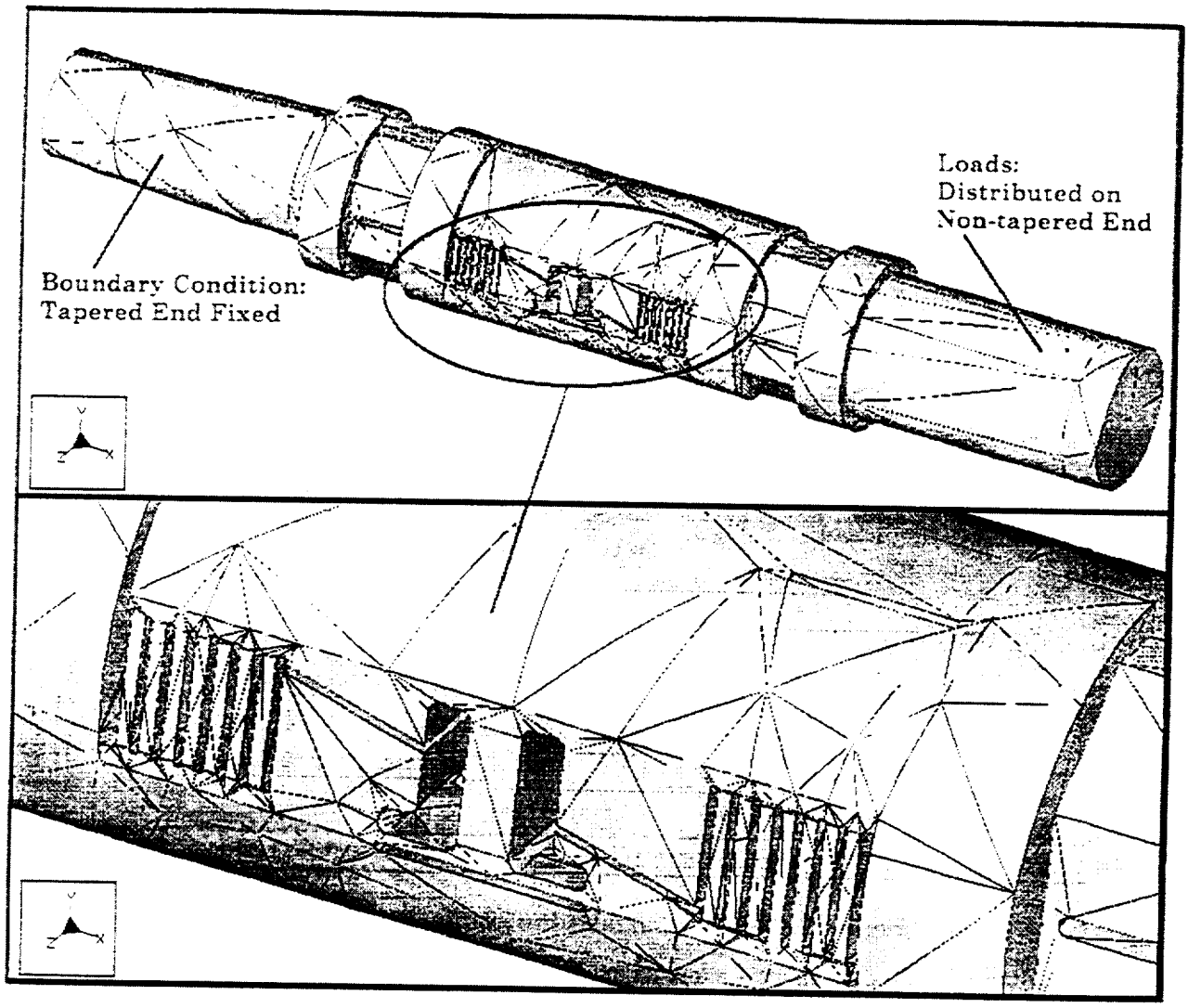

Figure 3. Mechanica model of NTF balance 101A.

Table 2. Applied Load Cases

LOAD CASE	LOAD	AXIS & DIRECTION
1. Axial Force	700 lbs	-X
2. Normal Force	5,000 lbs	-Y
3. Side Force	4,000 lbs	-Z
4. Roll Moment	8,989 in-lbs	RX
5. Yaw Moment	6,480 in-lbs	RY
6. Pitch Moment	13,000 in-lbs	-RZ
7. Combined	Above loads simultaneously	Above axes simultaneously

Load Case 1

The first load case consists of an axial force of 700 pounds applied as a compressive load on the end of the balance. Figure 4 shows a stress (σ_{YY}) fringe plot (see Report Availability section of this report for information on obtaining color versions of these plots) with exaggerated deformation for this load case. Also shown in Figure 4 is the location of the strain gage used for correlation.

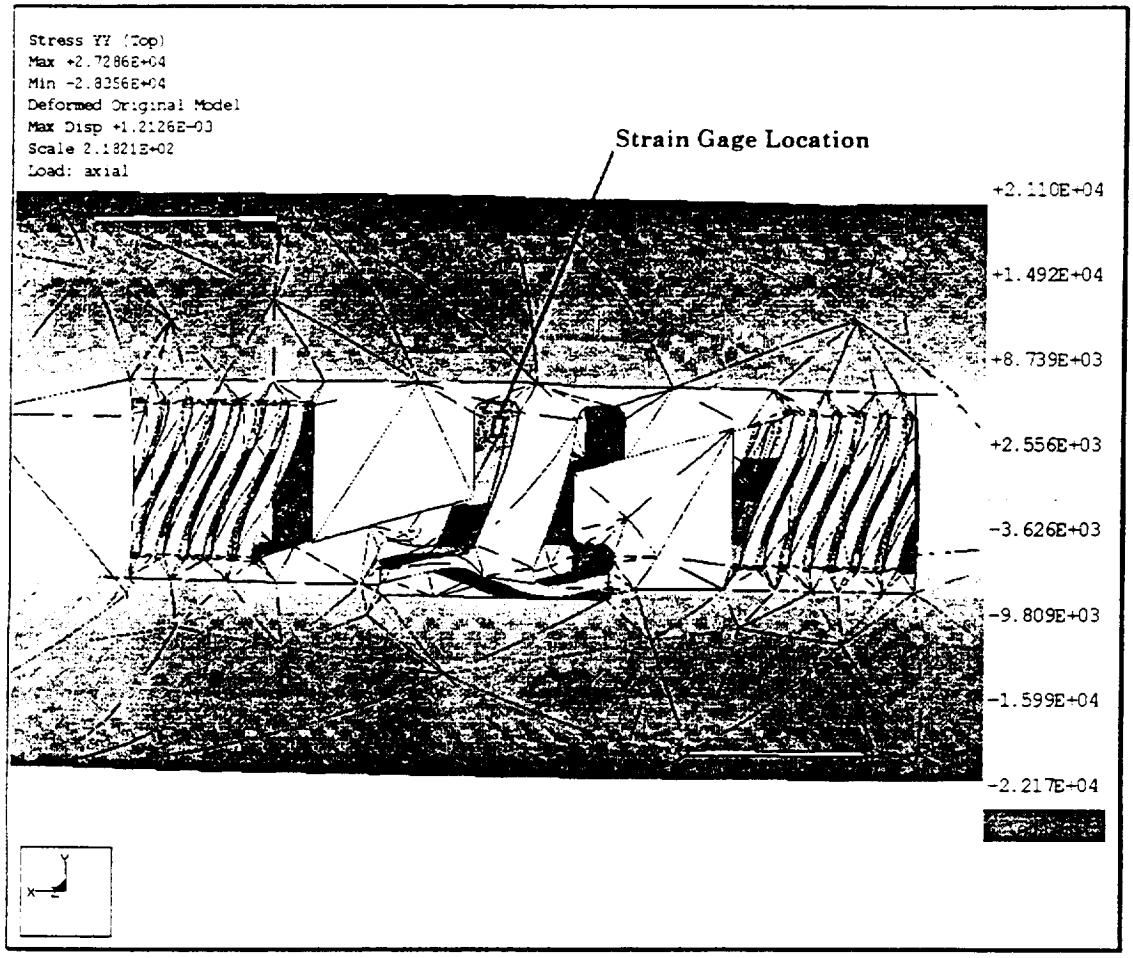

Figure 4. Axial load case stress and deformation.

The measured strain at the gage location for the axial force load condition was 499.5 microstrain (με) (13,090 psi). The strain at the same location from the finite element analysis was 489.3 με (12,820 psi), a difference of -2.0%. There were no excessively high stress regions for this load case.

Load Case 2

The second load case consists of a normal force of 5,000 lbs applied in the -Y axis through the balance center. Figure 5 shows a stress (σ_{XX}) fringe plot with exaggerated deformation for this load case and shows the location of the strain gage used for correlation and also areas of relatively high stress.

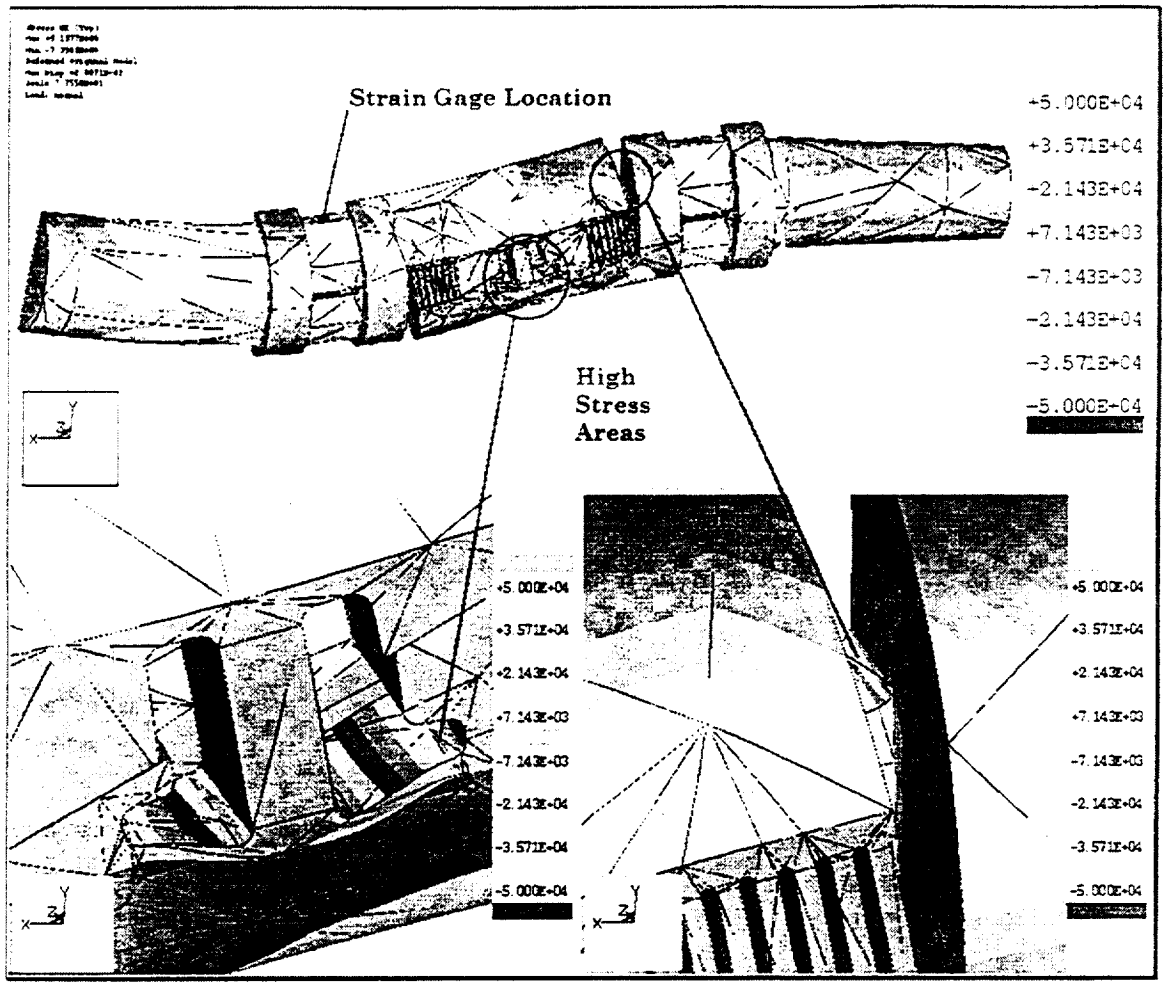

Figure 5. Normal load case stress and deformation.

The measured strain at the gage location for the normal force load condition was 720.4 με (18, 875 psi). The strain at the same location from the finite element analysis was 719.0 με (18,840 psi), a difference of -0.2%. The maximum stress (σ_{xx} stress component) in the high stress area on the right of Figure 5 was between 70,000 and 90,000 psi.

Load Case 3

The third load case consists of a side force of 4,000 lbs applied in the -Z axis through the balance center. Figure 6 shows a stress (σ_{xx}) fringe plot with exaggerated deformation for this load case. Also shown in Figure 6 is the location of the strain gage used for correlation.

The measured strain at the gage location for the side load condition was 767.0 με (20,095 psi). The strain at the same location from the finite element analysis was 774.1 με (20,280 psi), a difference of 0.9%. There were no excessively high stress areas for this load case.

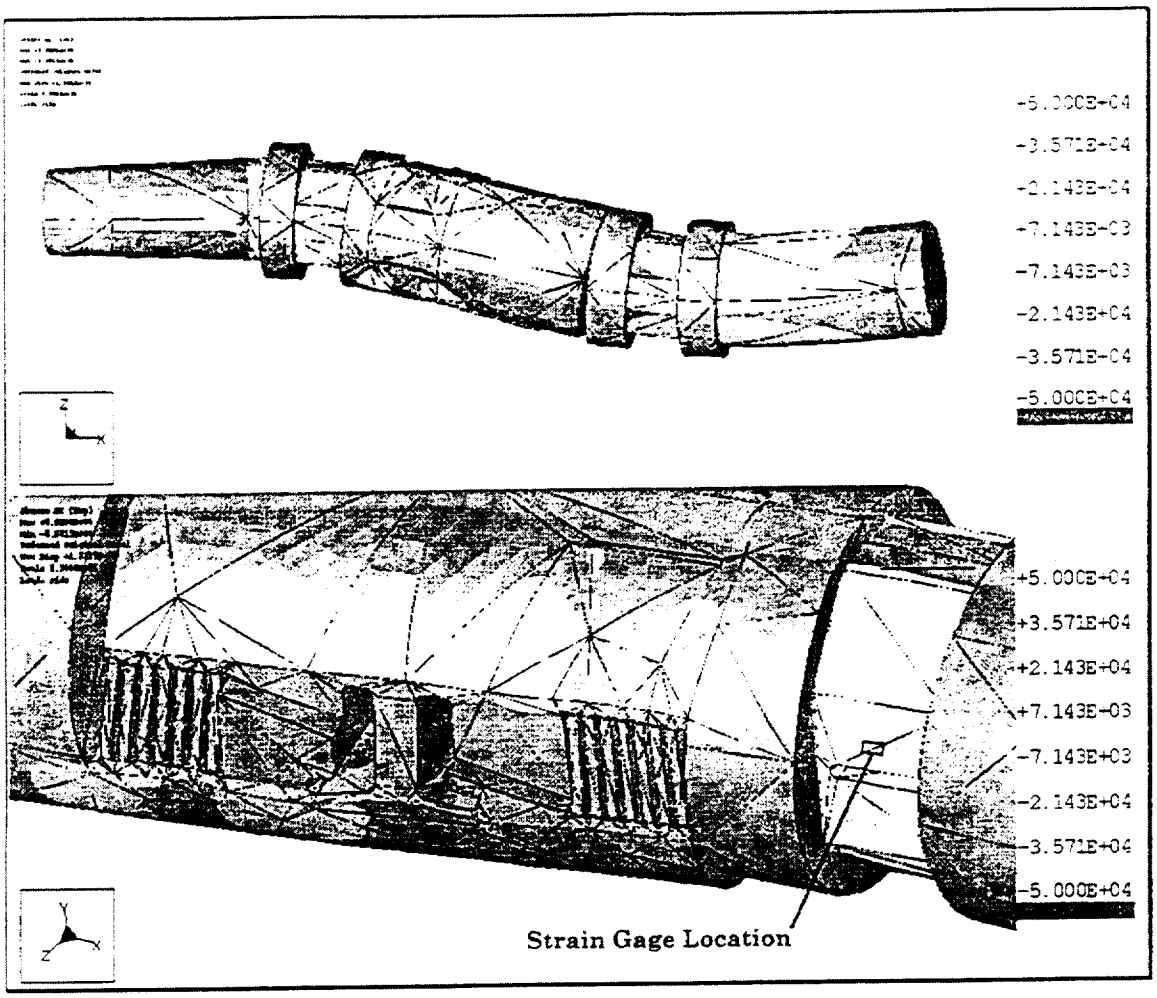

Figure 6. Side load case stress and deformation.

Load Case 4

The fourth load case consists of a roll moment of 8,989 in-lbs applied about the X axis through the balance center. Figure 7 shows a stress (σ_{xx}) fringe plot with exaggerated deformation for this load case and shows the location of the strain gage used for correlation. Also shown in Figure 7 is an area of relatively high stress.

The measured strain at the gage location for the roll moment load condition was 433.3 με (11,350 psi). The strain at the same location from the finite element analysis was 402.3 με (10,540 psi), a difference of -7.2%. The maximum stress (σ_{xx} stress component) in the high stress area was about -70,000 psi.

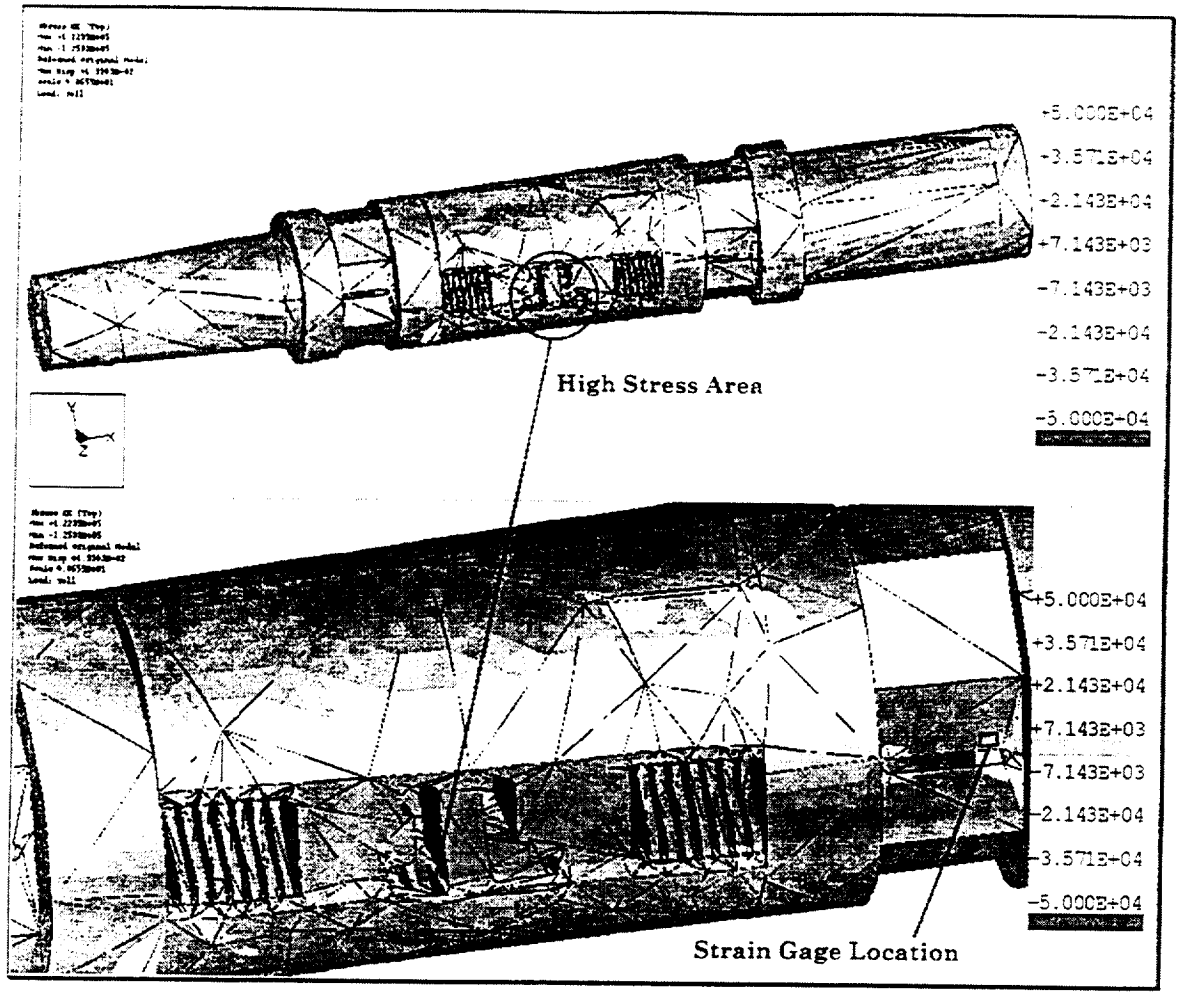

Figure 7. Roll load case stress and deformation.

Load Case 5

The fifth load case consists of a yaw moment of 6,480 in-lbs applied about the Y axis through the balance center. Figure 8 shows a stress (σ_{XX}) fringe plot with exaggerated deformation for this load case. Also shown in Figure 8 are the location of the strain gage used for correlation along with an area of relatively high stress.

The measured strain at the gage location for the yaw moment load condition was 436.1 με (11,425 psi). The strain at the same location from the finite element analysis was 483.1 με (12,660 psi), a difference of 10.8%. The maximum stress (σ_{XX} stress component) in the high stress area was about 55,000 psi.

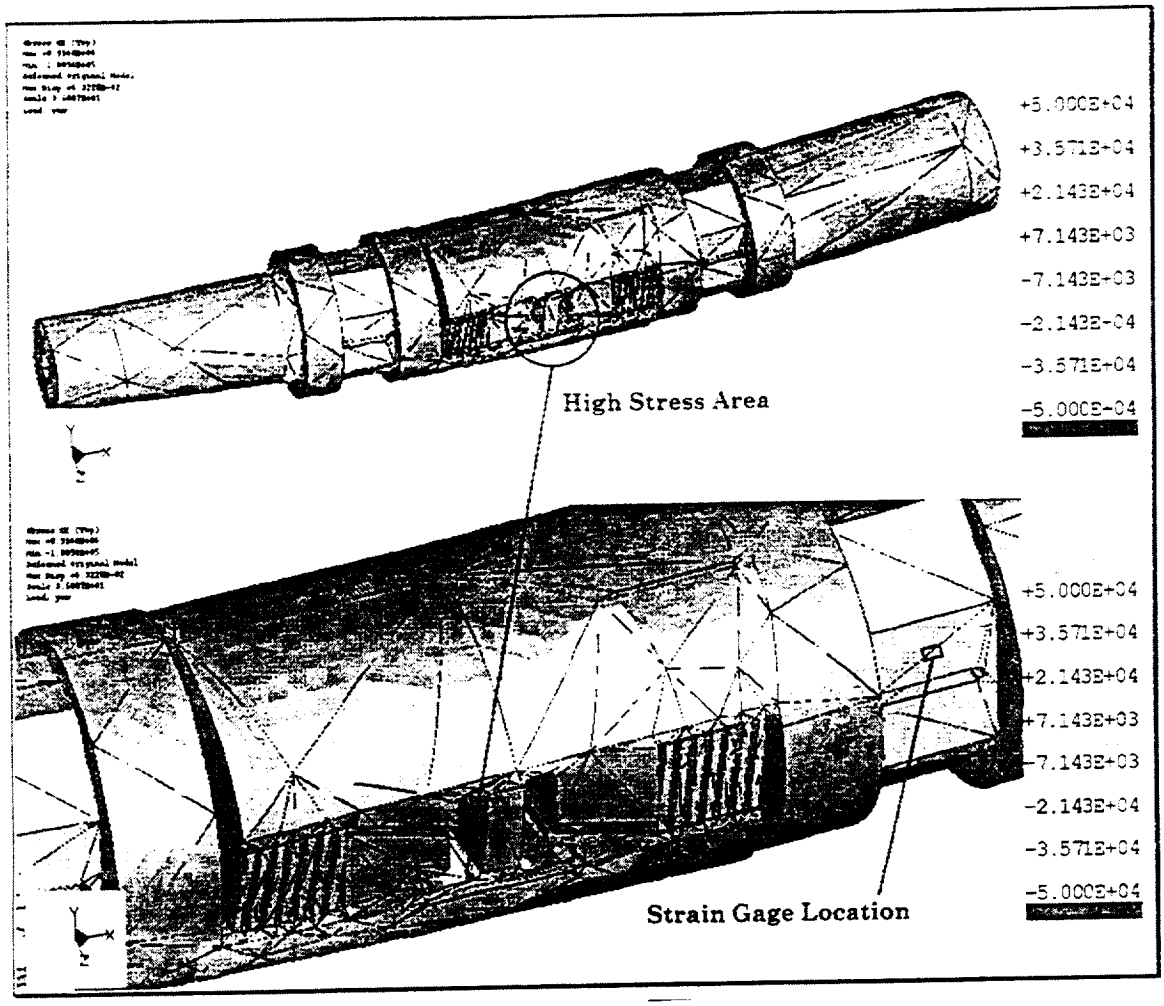

Figure 8. Yaw load case stress and deformation.

Load Case 6

The sixth load case consists of a pitch moment of 13,000 in-lbs applied about the Z axis through the balance center. Figure 9 shows a stress (σ_{XX}) fringe plot with exaggerated deformation for this load case. Also shown in Figure 9 are the location of the strain gage used for correlation along with an area of relatively high stress.

The measured strain at the gage location for the pitch moment load condition was 641.6 με (16,810 psi). The strain at the same location from the finite element analysis was 644.7 με (16,890 psi), a difference of 0.5%. The maximum stress (σ_{XX} stress component) in the high stress area was between 85,000 and 105,000 psi.

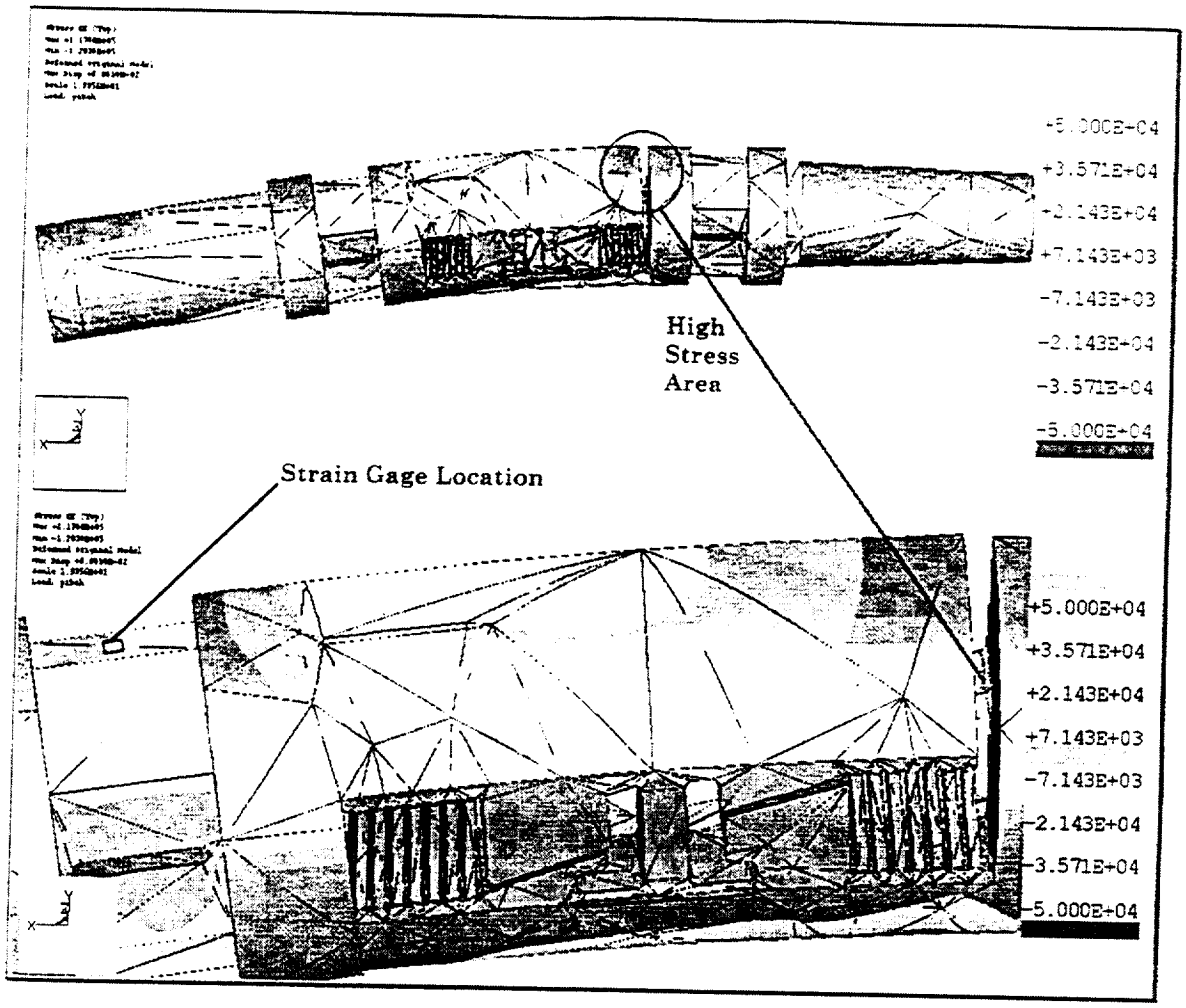

Figure 9. Pitch load case stress and deformation.

Load Case 7

The seventh load case is a combination of the first six load cases (-700 lbs X, -5000 lbs Y, -4000 lbs Z, 8989 in-lbs RX, 6480 in-lbs RY, -13000 in-lbs RZ). Figure 10 shows a stress (Von Mises) fringe plot with exaggerated deformation for this load case. Also shown in Figure 10 are a few areas of high stress.

The maximum stresses (Von Mises) in the high stress areas for the combined load case were in excess of 180,000 psi and approaching yield in some localized areas. A future test is planned with a strain gage in one of these high stress areas to validate this finding.

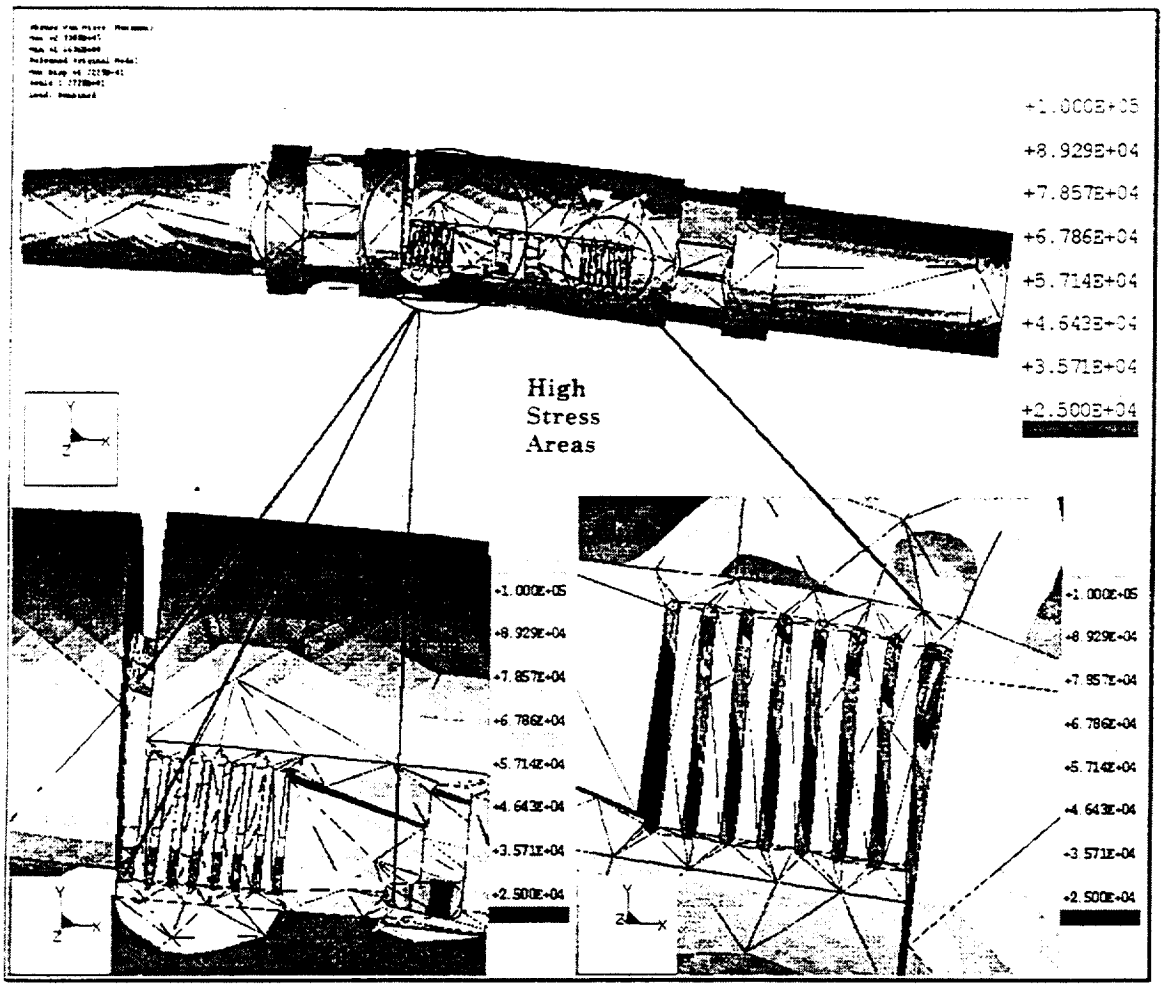

Figure 10. Combined load case stress and deformation.

Summary of Test/Analysis Correlation

Table 3 gives a summary of the degree of correlation between the measured strain and the strain computed from the finite element analyses.

Table 3. Summary of Test/Analysis Correlation

LOAD CASE	APPLIED LOAD	MEASURED STRAIN (με)	ANALYSIS STRAIN (με)	% DIFFERENCE
Axial Force	700 lbs	499.5	489.3	-2.0
Normal Force	5,000 lbs	720.4	719.0	-0.2
Side Force	4,000 lbs	767.0	774.1	0.9
Roll Moment	8,989 in-lbs	433.3	402.3	-7.2
Yaw Moment	6,480 in-lbs	436.1	483.1	10.8
Pitch Moment	13,000 in-lbs	641.6	644.7	0.5

CONCLUSIONS

The results of this study have shown that finite element analyses of strain-gage balances can accurately predict stress levels in the hardware. The results also showed the existence of areas within the balance where stress levels are higher than had previously been anticipated. In the future, results from such finite element analyses can be used to optimize balance designs for higher loads, reduced stress concentrations, lower weight, and reduced safety factors.

FUTURE WORK

Another balance similar to the one analyzed in this report but with more extensive strain gage instrumentation will soon be tested. An analysis and correlation study will also be performed in support of that test and the results will be documented.

ACKNOWLEDGMENTS

The author wishes to thank Susan Palmer of the Model Instrumentation & Systems Branch, NASA Langley Research Center, for providing the Pro/Engineer part file of the balance. Thanks also go to Ray Rhew of the Model Instrumentation & Systems Branch, NASA Langley, and Pete Parker of Modern Machine and Tool Company for their assistance with loads, strain gage data, and strain gage locations.

REPORT AVAILABILITY

This report along with full color versions of the graphics can be found on the internet at http://ixeab3.larc.nasa.gov/ntf/ntf_101a.html.

OPTIMIZATION OF INTERNAL STRAIN-GAGE WINDTUNNEL BALANCES WITH FINITE ELEMENTS COMPUTATION

M.Sc. Junnai Zhai
Dr.-Ing. K. Hufnagel
Technical University of Darmstadt, Germany

1. Abstract

The internal strain gage balance is one of the most important instrumentation in the wind tunnel. The more and more intensive competition in the airplane industry hat set higher demands on the balance. To design and construct such a balance that can meet those demands all aspects of the balance technology must be investigated. In this paper only the structure of the internal strain gage balance is considered.

From the point of view of structure these high demands on the balance can be expressed as:

- Lower interference
- Higher stiffness
- Lower stress level at the strain gage positions and the related parts
- Capability of tolerating errors from the temperature gradients.

Among these demands the interference and stiffness are most important for a transport balance, thus only these two properties are studied in this paper.

For this study the Finite Elements Method (FEM) is best suitable. With this method the various influence factors can be systematically analyzed. Based on the analysis the structure of the balance can be optimized in three levels. At first the balance structure is optimized by choosing the key geometric parameters. Then various shapes for the parts of an internal balance are discussed. Finally different configurations for the internal strain gage balance are studied.

Through a parameter optimization the total linear interference on the drag can be reduced from 6.1% to 3.8% of the F.S. signal. By using the configurations with two symmetrical planes the interference can be reduced to 2.5% of the F.S. signal. By using the point symmetrical configuration the interference on the drag can be reduced to 0.5% of the F.S. signal. This is almost interference-free.

The stiffness in axial direction is mainly affected by the parallelograms. By choosing proper dimensions for the drag measuring beam, the stiffness of the balance in X-axis can be doubled. But the stiffness in other directions is hardly changed.

The stiffness in normal and side direction is mainly affected by the main beams and the moment measuring elements. By using the new main beams, the combined main beams, the stiffness of the balance in Z-axis can be 21% than that of the dove-tail matched form. An further improvement of the stiffness can be achieved by using the shear spring as moment measuring element. A new moment measuring element of this kind is therefore put forward. The FEM computation shows that alone with this element the stiffness in Z-axis can be raised by 65%.

It is to recognize from this study that at the present level of technology there is no structure for a balance that is optimal in all respects. The best solution may be a requirement-oriented design, i.e., to design a balance structure according to the concrete requirements.

2. Introduction

The success of a commercial airplane development is heavily influenced by the accuracy of force measurements during the aerodynamic development in the wind tunnel. One limiting factor of accuracy is the internal strain gage wind tunnel balance.

In order to improve the accuracy all phases in the construction of a balance should be investigated. The phases during the construction of a balance can be summarized as: design, material preparation, manufacturing and strain gage application, signal collection and processing and calibration.

For the purpose of improving the accuracy, large theoretical and experimental work was done in the

past. The elastic characteristic of materials, the performance of strain gages, the method of manufacturing and calibration have been successfully studied. Thus the accuracy of the balance increased continuously. Even in the cryogenic wind tunnel the accuracy of balances arrived at a satisfactory level. But for further improvements of accuracy the phase of design should also be investigated.

The structural factors, which affect the accuracy, can be summarized as interference, stiffness, stress level and the ability to tolerate the temperature gradients in the balance.

The ability to tolerate the temperature gradients is very important for a cryogenic balance, because the formation of temperature gradients is unavoidable during the measurement. This problem has been successfully solved by Prof. Ewald with the concept, to place the drag measuring beams tandem in the parallelogram. It has been proved that under any temperature gradients no error signal for the drag is produced.

The stress level in the balance, especially at the stain gage positions and related positions, should be kept low, since the elastic errors of the balance material increase with the stress. Unlike combat balance, the transport balance is not so heavily loaded. The stress in the transport balance is usually low.

Therefore we have concentrated in this paper on the problem, to reduce the interference and to raise the stiffness of transport balances from the view point of structure.

In order to solve such problems the balance structure is analyzed with FEM. From the result of the analysis the balance structure is optimized in two steps. First, the balance structure is optimized by choosing suitable geometrical dimensions. The configuration stays unchanged. Then various new forms for the balance structure are suggested, and they are checked with FEM.

The most successfully used configuration up to now for the transport balance is shown in Fig. 1. It consists of four parts: two parallelograms and two main beams. The drag measuring elements are arranged tandem in the parallelograms, so that the effects from temperature gradients can be compensated. The two main beams are dove-tail matched. This structure is very stiff, and it is taken as a starting point for this study.

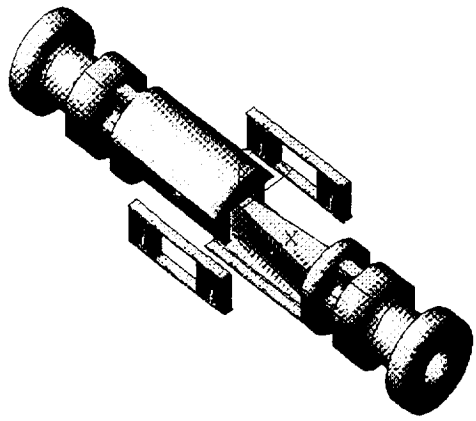

Fig. 1 Components of a transport balance

3 Interference of the Internal Balance

Unlike an external balance the internal balance separates the six components through a symmetrical layout of the structure and flexures. This separation is therefore in practice not complete. The signal caused by components other than the one to be measured is called interference.

The interference can be treated by a careful calibration, but large interference worsens the measuring accuracy. This is because during the measurement all the signals contain errors. The interference signal brings an additional error to the signal to be measured. In addition, the calibration process is also not free of errors, and the algorithm now used in the calibration hat difficulty in treating large interference. Therefore foe an accurate balance the interference must be reduced.

From the calibration practice the relationship between the signal and loads can be described as:

$$S_i = S0_i + \sum_{j=1}^{6} K_{ij} F_j + \sum_{j=1}^{6} \sum_{k=j}^{6} L_{ijk} F_j F_k + \sum_{j=1}^{6} M_i F_i^3 \qquad (1)$$

The nondiagonal elements in the above matrix describe the interference.

From this description one can divide the interference into linear and nonlinear parts. The nonlinear interference can be further divided into cubical (M_i in Eq. 1), product (L_{ijk} , $j \neq k$) and square (L_{ijk} , $j=k$). The nonlinear interference is caused mainly by the deformation of the balance structure and the elastic errors of the material. It can be reduced by a stiffer

construction of the balance and proper heat treatment of the material.

The linear Interference is caused by the asymmetry. This asymmetry comes from the balance structure self, manufacturing errors and strain gages. The Asymmetry from the manufacturing is usually very small and can be neglected. The asymmetry from the strain gages is caused by the *k*-factor deviation, position and direction errors by the application.

In this paper only the linear interference is discussed, and especially the interference on the drag, because the accuracy requirement on it is very high. All the reasons for the linear interference can be simulated with FEM. By the calculation of the interference the *k*-factor deviation is taken as 1%, the position and direction error is taken as 0.1 mm and 0.1 rad separately. The calculated interference is then the maximal possible interference.

3.1 Parameter Investigation

At first we tried to reduce the interference on the drag by choosing suitable dimensions of the internal balance. The dimensions which have a great influence on the influence is the dimensions of the drag measuring beam (the thickness ***d***, width ***b*** and height ***h***), the spacing (***l***) between the two drag beams and the slope of the main beams (α).

After a detailed study it is found out that the interference on the drag can be reduced through:

- Reducing the stiffness of drag measuring beam. This can be achieved by using a thinner, wider and longer beam as measuring element.
- Reducing the spacing between the measuring beams
- Increasing the slope of the main beams, so that the deformation of the main beams can be reduced.

With these measures the balance is optimized. A comparison of the interference on the drag between the initial and the optimized design is shown in Fig. 2.

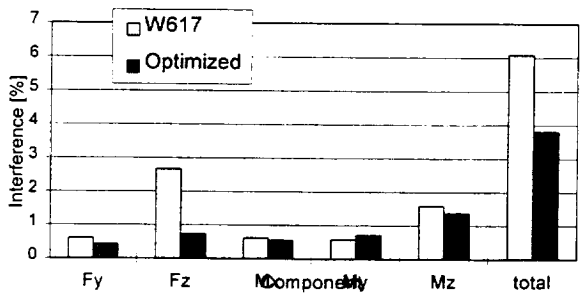

Fig. 2 Comparison of the linear interference on the drag [% F.S. signal]

It is clear from this figure, that the total linear interference on the drag is reduced from 6.6.1% to 3.8% of the F.S. axial signal.

3.2 Investigation of New Shapes

For further reduction of the interference, various shapes for the parts of an internal balance are put forward. The parts, of which the shape has an influence on the interference are drag measuring element and main beams.

During the development of internal balances various drag measuring elements are used. The first used drag measuring element is the decoupled form. In order to reduce the influence from other components on the drag, the drag measuring element is connected by a relative thin beam to the main beam that works like an elastic joint, so that it can only be loaded by an axial force.

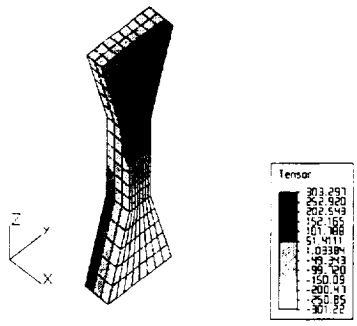

Fig. 3 the refined drag measuring beam

Later it was found that the decoupling is somewhat unnecessary, especially in the case of tandem arrangement of drag elements, because the influence from other components can be compensated by suitable arrangement of drag bridges. In addition this type of measuring elements is difficult to manufacture and has a big heat resistance. Thus it is simplified as a beam with constant cross-section. It is connected directly with the two main beams. Because this

measuring element can be loaded under components other than the drag, it is called the coupled element. In order to reduce the sensibility to the position errors of strain gages, we have used the concept, to form a constant stress distribution in the area of the application. So a double-trapeze beam was developed. A further refinement of this concept leads to a beam shown in Fig. 3. It is clear that the stress in the application area is very constant.

Because these elements have different stiffness and different sensibility to the position errors of strain gages, it is clear that balances using them have different interference on the drag. Under the condition, that the ratio of stiffness between the measuring beam and parallelogram beams and the signal level stay unchanged, a comparison of the interference on the drag among these balances is shown in Fig. 4.

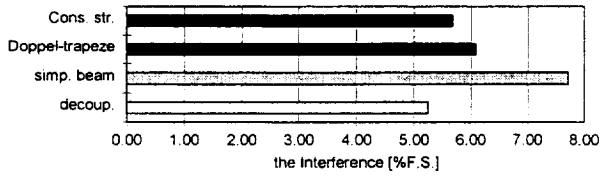

Fig. 4 Comparison of the linear interference on the drag [% F.S. signal

It can be seen from this figure that the decoupled beam has the smallest interference and the beam with constant cross-section has the greatest interference. Considering the other properties, it can be said that the beam with constant bending stress it the best.

3.3 Investigation of New Configurations

All the balances which were constructed till now have only one symmetrical plane. Because the symmetry is very important for the internal balance in separating components, it can be speculated that there would no interference, if the balance structure is more symmetrical.

In order to check this supposition, we have at first designed an internal balance which has two symmetrical planes, plane XZ and XY. The schematic description of this balance is shown in Fig. 5. This balance consists of four parts: two parallelograms and two main beams. The two main beams are similar to that of balance W617, dove-tail matched, only rotated by 90°. The parallelogram has two rows of thin beams. The measuring beam is located in the middle. With this arrangement the measuring beam can be loaded symmetrically.

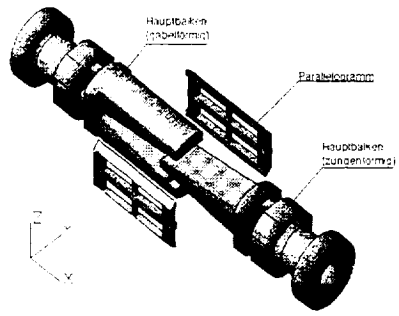

Fig. 5 schematic description of an internal with two symmetrical planes

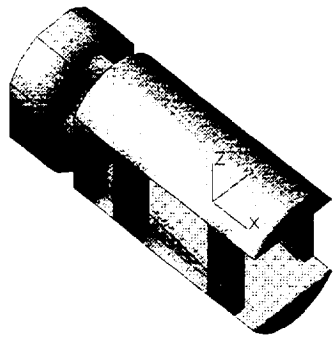

Fig. 6 the improved main beam

Because the stiffness of the main beams is relative low, the measuring beam is highly loaded under the normal force and pitching moment. The structure of the main beams is improved. The new structure for the forked main beam is shown is Fig. 6. The two tenons are strengthened with four plates are placed in the gaps between the parallelogram beam and the measuring beam. With this design the stiffness of the main beams can be enhanced, and the measuring beam is less loaded.

The result of the computation with FEM shows that this balance had no structural interference. The interference from the errors of strain gages is small too. As shown in Fig. 8, the total interference on the drag is reduced to 2.5% of the F.S. signal.

A further development of this idea is then the concept of the point symmetrical balance. One constructive realization of this concept is shown in Fig. 7. This balance consists of four parts: inner and outer main beam, connecting spring and measuring spring. The connecting is „L"-shaped. It has very high load capability in Y- and Z-direction, but flexible in X-direction. This characteristic is very important for this type of balances, since the loads on these springs are

very high. The measuring element is a shear spring. It has a great stiffness.

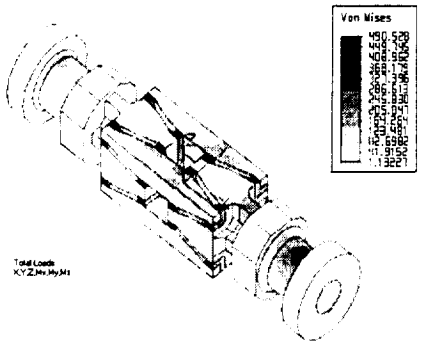

Fig. 7 a balance with point-symmetrical configuration

The computation with FEM shows that the maximal interference on the drag comes only to 0.5% of the F.S. signal. This is almost interference-free.

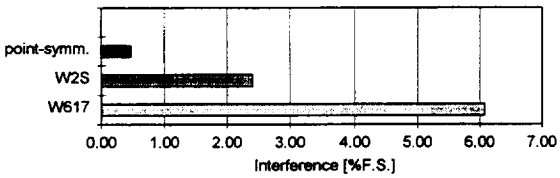

Fig. 8 Comparison of the linear interference on the drag

4 Stiffness of the Internal Balance

The internal balance measures the aerodynamic loads based on the strain caused in the balance body. Thus a deformation of the balance structure is unavoidable. This results in a deviation of the angle of attack of the model during the measurement. A stiffer balance can reduce errors associated with it.

In addition a stiffer balance can raise the nature frequency of the model, balance and sting system, thus the possible vibration of the whole system can be effectively suppressed.

Previous study has shown that the deformation of an internal balance is a direct reason for the nonlinear interference. So a stiffer balance will reduce nonlinear interference too.

From the above discussion it is known that a stiff balance is very desirable. But due to the compact structure of the internal balance there exists often a conflict between the stiffness and other requirements such as sensibility, interference and sensitivity to thermal effect etc. For example, a high sensitivity is of course expected, in order to raise the resolution and suppress the noise signal in the measuring chain. However, a high sensitivity means at the same time for the current balance configuration also a low stiffness. For the requirements on the linear interference and the sensitivity to the temperature gradients it is the same. Previous study shows that a less stiff parallelogram results in a smaller linear interference on the drag component and smaller error signal due to temperature gradients.

4.1 Parameter Investigation

A direct method to raise the stiffness of a balance is to choose suitable dimensions by design. For this purpose the influence of each parameter on the stiffness should be identified.

From Fig. 1 is to see that there are many dimensions needed to define the structure of a balance. These dimensions can be divided into three groups.

The first group defines the geometry of the parallelograms. It includes the thickness (***d***), width (***b***) and height (***h***) of the drag measuring beam and the spacing (***l***) between the two drag beams. The other parameters such as the dimensions of the struts are determined by the signal level.

The second group defines the geometry of the main beams. Most of the dimensions of the main beams are dependent on that of the parallelograms. The only free parameter is the slope of the beams (α).

The third group defines the geometry of the bending moment measuring sections. There are many forms for this section. By different form, the parameters needed are different too.

Due to the complexity of the balance structure the influence of these parameters on the stiffness of the internal balance can only be effectively studied with FEM. For a meaningful comparison the sensitivity stays always constant by variation of the parameters.

4.1.1 The Parallelograms

The dimensions that define the geometry of the parallelograms influence mainly the stiffness in axial direction. The influence on the stiffness in other direction is very small.

A typical result of this study is shown in Fig. 9. In this figure the change of deformation of an internal

balance over the thickness of the drag measuring beam (*d*) is illustrated. It can be seen that the deformation in axial direction sinks with the thickness. But the stiffness in *Y*- and *Z*-direction is almost unchanged.

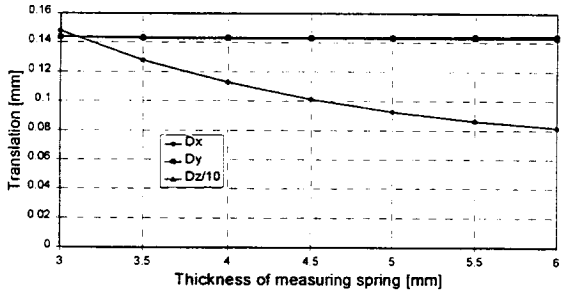

Fig. 9 Deformation of balance over the thickness of drag measuring spring

As a summary it can be said, that the stiffness in axial direction can be raised by using a thicker but shorter and narrower beam as drag measuring element. The spacing between the two drag elements has little influence on the stiffness.

It is worth of noting that with these steps one can raise the stiffness of a balance in the axial direction, but one must put up with the fact, that the interference on the axial component increases, too.

4.1.2 The Main Beams

The geometry of the main beams affects mainly the stiffness in *Y*- and *Z*-direction.

The result of FEM analysis is somewhat contrary to our intuition. The influence of the slope of the main beams (α) on the stiffness is very small. Only a small increment in the stiffness in *Y*-direction with this parameter can be observed.

An analysis of the deformations of each main beam shows, that this is caused by the bending of the tongued beam in transverse direction, as shown in Fig. 10.

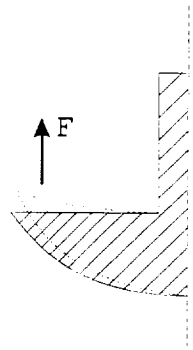

Fig. 10 Deformation of the tongued beam in transverse direction

With the increase of the slope the stiffness of each beam is raised, but the deformation shown in Fig. 3 increases, too. Thus the stiffness of the whole balance is almost unchanged.

4.1.3 The Moment Measuring Element

All the components except the drag are measured at this section. In order to get enough signal for the measurement, this section is weakened. But the deflection of this section has a great influence on the stiffness of the whole balance, because a small slope at this section would cause great deformations at the model flange due to leverage.

In the development of internal wind tunnel balances various forms are used. For the measurement of the bending moment octagon, cross and cage etc. are created. These forms have different sensitivity and stiffness.

Assume that the bending stress is distributed linearly in the cross-section, according to the linear bending theory in mechanics, one can get the relationship between the slope ($\Delta\theta$) and the maximal stress (σ) which is proportional to the signal. This relationship can be written as:

$$\frac{\Delta\theta}{\sigma} = \frac{2L}{Eh} \qquad (2)$$

Where L is the length of this section, h is the height of the cross-section and E elastic module.

It can be seen from this equation (1) that under the condition of a constant signal the slope depends only on the length (L) and height (h) of the cross-section. In order to raise the stiffness one can reduce the length or enlarge the height.

The first possibility, to reduce the length, is limited by the fact that there should exist enough place for the application of strain gages. In addition, if this section is too short, the strain gages may be affected by the notch stress. This would cause nonlinearity in the signal.

For the second possibility, if one enlarges the height, the moment of inertia increases and the signal decreases. To maintain a constant signal the other dimensions of the cross-section must be reduced. Therefore the cross-section which has more possibility in adjusting the moment of inertia can be dimensioned to its maximal height, and thus be stiffer. From this point one can design a stiffer balance by using a cage than using a cross.

4.2 Investigation of New Shapes

It can be seen that with the above steps it is possible to raise the stiffness of an internal balance, but these steps have some disadvantages. First the improvement is relatively small. Second the improvement is achieved at the sacrifice of other important qualities such as interference. Therefore we should investigate new shapes for the internal wind tunnel balance. These shapes may have a bigger influence on stiffness than the dimensions of the common one's.

4.2.1 Drag Measuring Element

Many drag measuring elements have been invented during the development of internal wind tunnel balances. Mostly used are beams of various shapes. According to the interference of other loads they can be divided into coupled and decoupled elements.

Because the coupled element can be loaded by force or moment in all directions, a balance using coupled beam as drag measuring element is stiffer than using decoupled beams.

All these elements have one in common, i.e., the drag is measured through bending stress. The disadvantage of these elements is the low stiffness.

Compared with the bending spring, the shear spring is much stiffer. Therefore a reasonable solution for high stiffness would be to design a shear spring as drag measuring element.

A simple shear spring is designed to measure the drag (Fig. 11). It looks like a coupled beam, only in the middle where the strain gages are to be applied, it is dimensioned very thin, so that in this section there is enough shear stress.

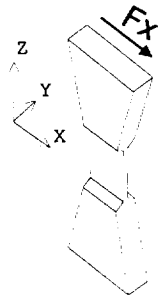

Fig. 11 Shear spring used to measure drag

In order to identify the effect of the shear spring two balances are designed. They have the same dimensions except for the drag measuring elements. One uses a coupled beam and the other uses the shear spring as drag measuring element. The signal stays of course constant.

The two balances are computed with FEM. The calculated stiffness is compared in Fig. 12.

It can be clearly seen from this figure, that by using shear spring as drag element the deformation in axial direction is reduced by 60%. The deformation in *Z*-direction is almost unchanged. The deformation in *Y*-direction is slightly greater (1.5%). This is caused by the small load capability of the shear spring in *Y*-direction.

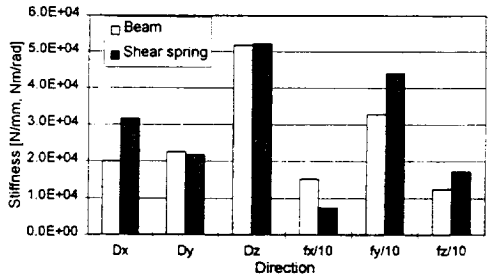

Fig. 12 A comparison of the stiffness of the balance by using beam and shear spring as drag measuring element

Besides high stiffness a balance with shear spring as drag element has a small linear interference too. This is because the shear spring is only sensitive to the force in axial direction, while the bending beam is sensitive to both the force in axial direction and the bending moment in *Y*-direction. In addition, there are shear strain gages where two strain gages are manufactured side by side in one piece of base film.

By application of such strain gages the influence of the position errors is small, and consequently the linear interference from this source is small.

4.2.2 The Main Beams

The shape of the main beams has a great influence on the stiffness. The first form of the main beams was a constant cross-section. Though this is simple to manufacture, the stiffness is very low. Later this form was replaced by the triangular form. In this form the change of cross-section matches the change of moment better, and the stiffness is consequently high.

Due to the invention of electron beam welded balance concept by **Ewald,** there is more freedom in the design of the main beam forms. Thus a form, so-called dovetail matched (Fig. 1) was invented. In this form the cross-section of each beam has the maximal height, so the stiffness of such balances are very high. A computation with FEM has shown that by the same condition the stiffness in *Z*-direction with the dove-tail matched form is 8.8% higher than the triangular form, if only the active part of a balance (Fig. 13) is considered.

The dovetail matched form has high moment of inertia, while the triangular form matches the change of moment good. It seems that a combination of the two forms would result in a stiffer form.

A realization of this idea is shown in Fig. 14. The tongued main beam is formed to look like a triangle, so that the moment of inertia at its root can be raised. The forked main beam can be strengthened at its root correspondingly.

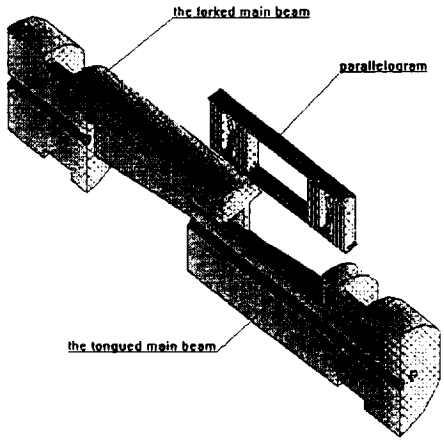

Fig. 13 Balance with main beams of the dove-tail matched is designed for comparison

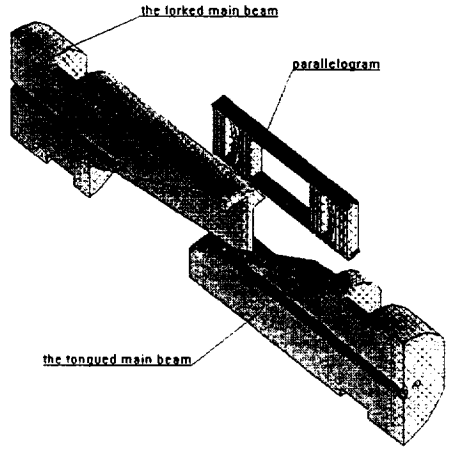

Fig. 14 Balance with main beams of the combined form

In order to prove this idea a balance with main beams of the combined form is designed and computed with FEM. The calculated deformations are shown in Fig. 15. A balance with main beams of the dovetail matched form is used as reference.

It is evident that by using the combined form the stiffness in *Z*-direction is raised by 21%. The stiffness in *Y*-direction is raised by 3%. The stiffness in *X*-direction is unchanged.

The linear interference of this balance is the same as the referenced balance. But the nonlinear interference is smaller due to the higher stiffness.

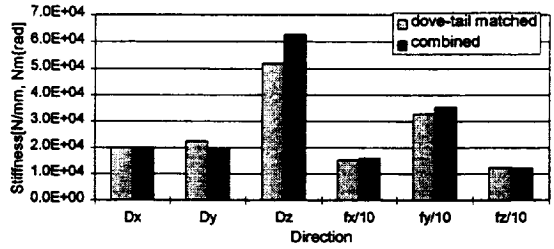

Fig. 15 A comparison of the stiffness of the balance by using dove-tail matched form and the combined form as the main beams

The distribution of von Mises stress in this balance is shown in Fig. 16. Due to the higher stiffness the stress is reduced at the same time. The maximal von Mises stress is 24% smaller than in the reference balance (480 N/mm²).

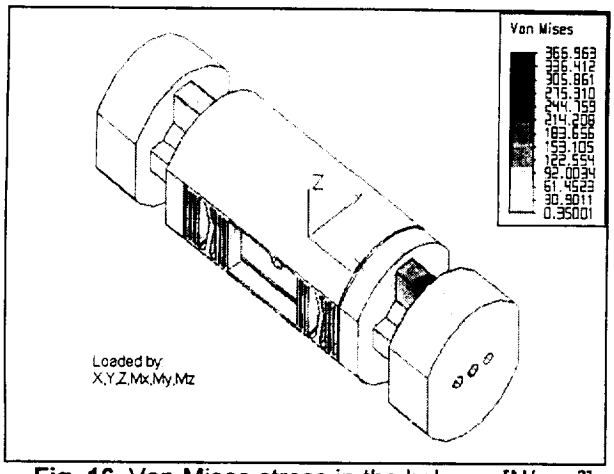

Fig. 16 Von Mises stress in the balance [N/mm²]

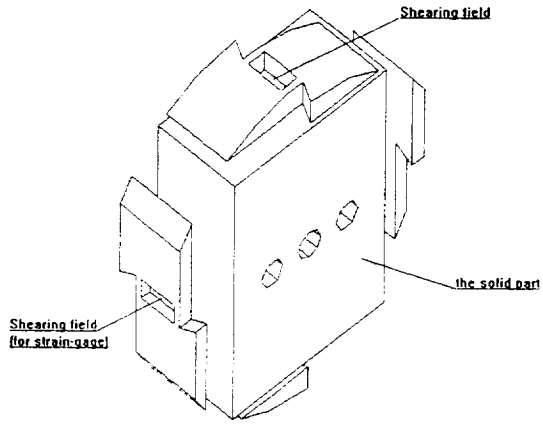

Fig. 17 A moment measuring element using shear springs

4.2.3 The Moment Measuring Element

As stated above this section has a great influence on the stiffness of the whole balance. Up to now there are many forms which can be used to measure the bending moment. But all these forms use the same principle: the moment is measured by bending stress. It is well known that by an equal signal the shear spring is much stiffer than the bending spring. Thus the stiffness of this section can be raised by using a shear element.

A realization of this idea is shown in Fig. 17. It looks like a cage. The inner part is a solid polygon which undertakes the most bending moment and shear force. The outer part consists of four shear stress measuring elements which are arranged around the solid polygon.

Of the two opposite positioned measuring elements, one will be stretched and the other will be compressed under the load of a bending moment. This tension or compression causes a shear stress field. By measuring the shear stress with strain gages one can get the moment to be measured.

A balance using this new bending moment measuring element is designed (Fig. 18). The FEM computation of this balance shows that this balance is very stiff. Under the condition of equal signal the stiffness of this balance in *Z*-direction is 65% higher than that of a balance using a cross as moment measuring element. The stiffness in *Y*-direction is even 88% higher. The stiffness in *X*-direction is almost unchanged. (Fig. 19)

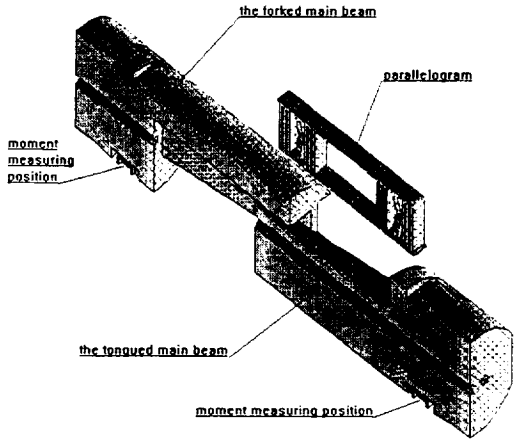

Fig. 18 Balance with shear elements (Detail shown in Fig. 10)

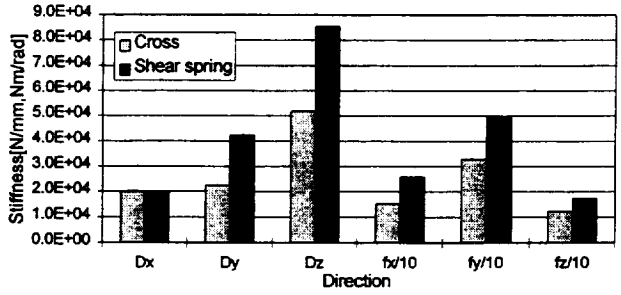

Fig. 19 A comparison of the stiffness of the balance by using cross and shear spring as bending moment measuring element

The von Mises stress in this balance under all loads is shown in Fig. 20. The maximal stress is reduced to 286 N/mm², almost the half of the stress in the reference balance (480 N/mm²).

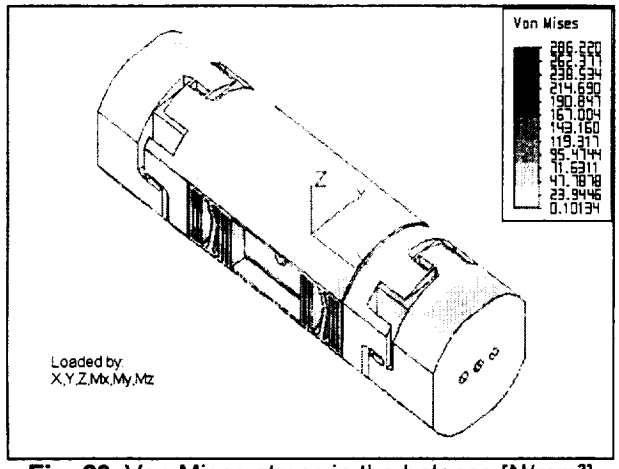

Fig. 20 Von Mises stress in the balance [N/mm²]

5. Conclusions

The stiffness of an internal wind tunnel balance is a decisive factor for quality. In order to get a high stiffness we have tried first choosing the suitable dimensions under the scope of the current balance configuration. With this method the stiffness can be increased, but the improvement is small and it is often achieved by sacrificing accuracy of other properties. Thus we have tried various forms for the balance.

By using shear spring as the drag measuring element the stiffness in *X*-direction can be increased considerably.

By using the form combined from the triangular and dovetail matched form for the main beams the stiffness in *Y*- and *Z*-direction can be increased significantly.

Finally, by using the shear elements to measure the bending moment the stiffness of the whole balance can be improved dramatically.

At least it is worth mentioning, that by these new forms the other qualities of a balance such as interference and stress level are at least unchanged, in some cases they are even improved.

Reference

[1] Ewald, B.: *Development of Electron Beam Welded Strain-Gaged Windtunnel Balances,* Journal of Aircraft Volume 16, May 1 1979

[2] Ewald, B. and Graewe, E.: *Entwicklung einer 6-Komponenten-Waage für den cryo-Bereich,* 3. BMFT-Status-Seminar, Hamburg, May 1983

[3] Ewald, B.: *Grundsatzuntersuchung zum Temperatur-Verhalten von DMS- Axial-Kraftteilen,* BMFT LVW 8420 1 0, Nr. 10185 1985

[4] Ewald, B. and Krenz, G.: *The Accuracy Problem of Airplane Development Force Testing in Cryogenic Wind Tunnels*, AIAA Paper 86-0776, Aerodynamic Testing Conference, March 1986

[5] Ewald, B. and Graewe, E.: *Development of Internal Balances for Cryogenic Wind Tunnels*, .12th ICIASF, Williamsburg, VA, June 1987,

[6] Ewald, B.: *Balance Accuracy and Repeatability as a Limiting Parameter in Aircraft Development Force Measurements in Conventional and Cryogenic Wind Tunnels,* AGARD FDP Symposium, Neapel, September, 1987

[7] Ewald, B., Polanski, L. and Graewe, E.: *The Cryogenic Balance Design and Balance Calibration Methods*, AIAA 'Ground Testing Conference', July 1992, Nashville, Bericht A 99192

[8] Ewald, B., Hufnagel, K. and Graewe, E.: *Internal Strain Gage Balances for Cryogenic Windtunnels*, ICAS- Congress, Sept. 92, Peking, Bericht A 100/92

[9] Ewald, B. and Graewe, E.: *The Development of a Range of Internal Wind Tunnel Balances for Conventional and Cryogenic Tunnels*, European Forum on Wind Tunnels and Wind Tunnel Test Techniques, Sept. 92, Southhampton

[10]Ewald, B., Hufnagel, K. und Graewe, E.: *Internal Strain Gage Balances for Cryogenic Windtunnels*, ICAS- Congress, Sept. 92, Peking, Bericht A 100/92

[11]Ewald, B., Polanski, L. und Graewe, E.: *The Cryogenic Balance Design and Balance Calibration Methods*, AIAA Ground Testing Conference, Juli 1992, Nashville, Bericht A 99192

[12]Ewald, B. and Graewe, E.: *The Development of a Range of Internal Wind Tunnel Balances for Conventional and Cryogenic Tunnels*, European Forurn on Wind Tunnels and Wind Tunnel Test Techniques, Sept. 92, Southharnpton

[13]Ewald, B.: *The Development of a Complete Internal Balance Testing Technology for Cryogenic and Conventional Wind Tunnels*, Pacific International Conference on Aerospace Science and Technology, September, 1993, Bericht A 119/93

[14]Ewald, B. and Viehweger, G.: *Half Model Testing in the Cologne Cryogenic Tunnel (KKK)*, 18 AIAA Ground Testing Conference, Juli 1992, Nashville

[15]Ewald, B: *Advanced Force Testing Technology for Cryogenic and Conventional Wind Tunnels*, ICAS-94-3.5.1, 19th ICAS-Congress, September, 1994, Anaheim, California

[16]Ewald, B.: *Theory and Praxis of Internal Strain Gage Balance Calibration for Conventional and Cryogenic Tunnels*, 18th AIAA Ground Testing Conference, June 1994, Colorado Springs

[17]Ewald, B: *Die Rolle der Aerodynamik und des Windkanals bei der Entwicklung von Verkehrsflugzeugen,* Luft- und Raumfahrt 2/95.

[18]Ewald, B., Hufnagel, K. and Zhai, J.: *'Advanced Force Measuring Technique in Cryogenic and in Conventional Wind Tunnels. Present Status and Further Development'*, the 2nd International Symposium on Aeronautical Science and Technology of Indonesia (ISASTI), Jakarta, Indonesia, June, 1996

[19]Ferris, A. T.: *Cryogenic Strain Gage Techniques used in Force Balance Design for the National Transonic Facility*, NASA TM 87712, May 1986

[20]Graewe, E.: *Development of a Six-Component Balance for Cryogenic Range.* Forschungsbericht W 84-022 BMFT 1984

[21]Hufnagel, K.: *Entwicklung und Optimierung von sechs-Komponenten-DMS-Windkanalwaagen zum Einsatz unter Kryogenen Bedingungen,* Dissertation, 1995, TH Darmstadt

[22]König, K.G.: *Eigenschaften metallischer Meßkörper für die Windkanalmeßtechnik*, Dissertation, 1993, TH Darmstadt

[23]Zhai, J., Ewald, B. and Hufnagel, K.: *An Investigation on the Interference of Internal six-Component Wind Tunnel Balances with FEM*, 16th ICIASF Congress, July, 1995, Dayton, Ohio

[24]Zhai, J., Ewald, B. and Hufnagel, K.: *Shape Optimization of the Internal Wind Tunnel balances Using Simulated Biological Growth Approches*, AIAA-96-2255, 19th AIAA Advanced Measurement and Ground Testing Technology, June, 1996, New Orleans, LA, USA

[25]Zhai, J., Ewald, B. and Hufnagel, K.: *Optimization of the Performance of Internal Six-Component Strain-Gage balances with FEM*, ICAS-96-3.4.3, 20th Congress of ICAS, Sept. 1996, Sorrento, Italy.

NEW DESIGN OF TUBULAR TYPE STRAIN-GAGE BALANCES.

Vyacheslav I. Lagutin
(TSNIIMASH, Russia)

SUMMARY

Widely world used type of strain-gage balances (like the symbol of the Symposium) possesses some imperfections caused mainly by nonsymmetry of the balance structure and difficulties of their fabrication.

Last years new type of the balances based on combination of ring and tubular type dynamometers is successfully used in aerogasdynamic tests provided by TSNIIMASH.

In the article several designs of such types dynamometers and typical designs of tubular aerodynamic strain-gage balances for various application are presented. The balances have a symmetrical structure of springy bodies. As a result it is possible to decrease of loading components interaction and to improve fabrication properties.

INTRODUCTION

At present time a type of six-component strain-gage balance like the Symbol of the Symposium is widely world used in practice of aerogasdynamic tests. Layout of similar balance used in TSNIIMASH is shown on Figure 1 together with Table of general performances of the balance family. Some peculiarities of the balance design concern sensing element of axial (X-force) dynamometer which presents as half of full frame with constant mechanical tension along frame springy plates carrying strain-gages.

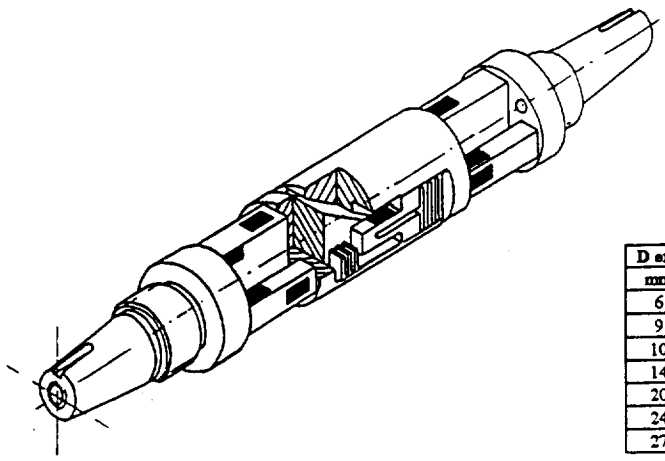

D ext.	X	Y	Z	Mx	My	Mz
mm	N			Nm		
6	50	100	100	0.5	0.3	0.5
9	100	150	150	2	4	4
10	100	200	150	3	2	4
14	300	400	300	15	15	20
20	1000	1500	1000	50	60	100
24	1200	2000	1000	100	80	150
27	1500	3000	2000	120	100	200

Figure 1. Layout of conventional strain-gage balance

An advantage of the balance design is large carrying capacity in relation to transverse load while cross section diameter is small. It is a reason for wide usage of the balance in testing of models with wings or complex models with strap-on blocks when lift force is large (ref. 1).

One of the disadvantages of the design is fabrication difficulty caused by the balance structure having a lot of unthrough cavities and slits with difficulties of accuracy control when manufacturing. Another disadvantage caused by nonsymmetry of X-force dynamometer in relation to axial force is essential influence of bending and rolling moments on the dynamometer output signal.

There are some tubular type balance design with X-force dynamometer elements symmetry in relation to axial force and small non-linear interaction due to the balance structure peculiarities. The floating-frame balance type "TASK"(ref. 2) consists of two coaxial tubes joined by six measuring elements. The screw joints cause a certain hysteresis. Another tubular type balance (ref. 3) is two-shell floating frame balance consists of an external tube which ends are soldered (by special method "fused gold alloy bond") to an internal tube. Measuring elements are formed by several beams milled near ends of the external tube. The measuring elements have mixed functions and linear interaction takes place.

Tubular balances can be used as conventional in the most cases. Internal channel of the balance allows to extend their application for testing tasks concern jet simulation, testing in "hot" wind tunnels and so on because gas or liquid supply pipes for sources of jets or balance cooling, or an in-model mechanism can be mounted inside the channel.

These advantages of tubular balances and considered imperfections of existed tubular balances were the reasons for search of new designs of tubular type dynamometers and complex dynamometrical systems.

Thus the task of new tubular balance creation includes design of one-piece, short extend balance with small hysteresis and component interaction and good fabrication properties.

The creation of new such complex dynamometrical systems was preceeded by development of separate dynamometers.

Figure 2 shows a X-force dynamometer design based on usage of springy parallelograms conjunct in a ring body with springy beams of varying cross section formed by cylindrical undercuts of the beams. Strain-gages are placed opposite the undercuts. Figure 3 shows a construction with half-frame sensing elements built in springy parallelograms.

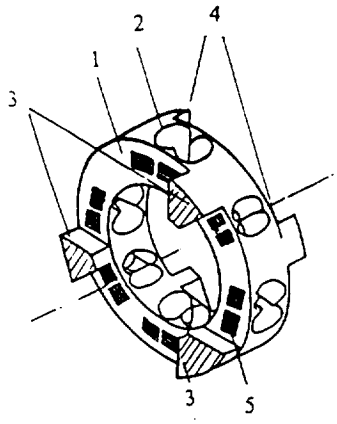

Figure 2. Ring-body X-force dynamometer
1 - ring-body of springy parallelograms; 2 - cylindrical undercut of springy beam; 3, 4 - rigid longitudinal beams; 5 - strain-gage

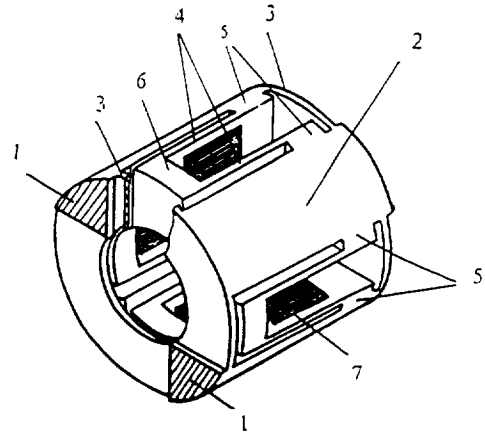

Figure 3. X-force dynamometer with half-frame sensing element.
1, 2 - rigid longitudinal beams; 3 - arch-shaped elements of springy parallelogram; 4 - springy plates of sensing; 5, 6 - firm cross-pieces; 7 - strain-gage

Strain-gages are placed on walls of the frames. Figure 4 shows the similar design with frame type sensing elements. The ring body of the dynamometers may consist of 4; 6; 8 etc. number of springy parallelograms (i.e. more than 2, as it takes place in the designs discussed above). As a result for ring or tubu-

lar type dynamometers it is possible to realize principles of symmetry and integration, which help to provide higher level of selectivity (the influence of bending and rolling moments was found one or two orders less than this one for traditional scheme). In additional the dynamometer design appears more suitable for manufacturing by contemporary machines with numerical control because all slots are through and symmetrical.

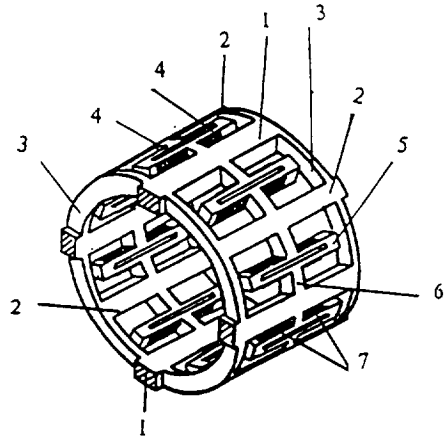

Figure 4. X-force dynamometer with frame sensing element.
1, 2 - rigid longitudinal beams; 3 - arch-shaped elements of springy parallelogram; 4- springy plates of sensing; 5, 6 - firm cross-pieces; 7 - strain-gage

First type construction (Figure 2) is preferable for dynamometers of large loads and sizes. Second type construction (Figures 3, 4) is preferable for dynamometers of relatively small loads and cross sizes which provided by longitudinal orientation of strain-gages.

Measuring load range may be increased using a shear deformed plate as a sensing element.

Figure 5 presents a design of two-component transverse forces (Y, Z) dynamometer based on compact folding of two springy parallelograms with springy beams of varying cross section and strain-gages placed opposite undercuts of the beams. The design provides good combination of rigidity and sensitivity and independence of output signals on varying of input load point position. The dynamometer construction is good entered into ring cross section.

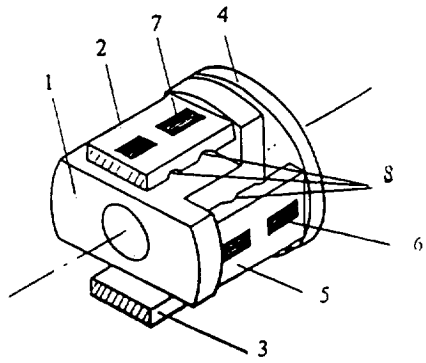

Figure 5. Transverse forces two-component dynamometer
1 - intermediate base; 2, 3 - longitudinal beam of springy parallelogram of Y-force dynamometer; 4 - main base; 5 - longitudinal beam of springy parallelogram of Z-force dynamometer; 6, 7 - strain-gages; 8 - cylindrical undercuts

For designs of moment measuring dynamometer longitudinal beams subjected to bending or twisting were used. Peculiarity of a dynamometer design (intended for measuring of Mx, My, Mz moments) shown on Figure 6 is compact arrangement of all springy elements in one ring cross section.

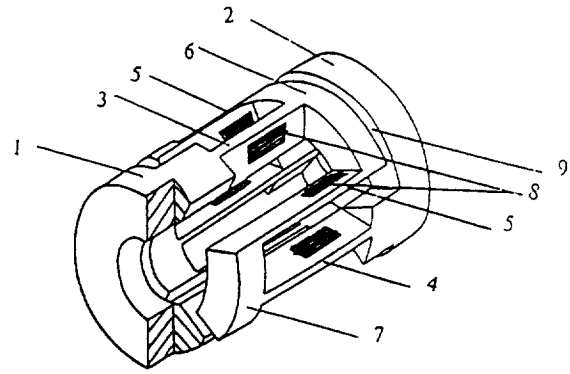

Figure 6. Dynamometer for Mx, My, Mz moment components measuring
1, 2 - main bases; 3, 4 - longitudinal springy beams of My, Mz dynamometers, respectively; 5 - longitudinal springy plates of Mx dynamometer; 6, 7 - intermediate bases; 8 - strain-gages.

In this case it is possible to coincide all electric centers of measuring bridges in one section or even in one point. It is very suitable for special measurements and for provision of required sensitivity for each measuring component. It seems important that compressing load acting on Mx dynamometer (it is a characteristic case for aerodynamic balances) transforms in stretching load for it's springy plates.

Application of a system of springy parallelograms allows to modify the Mx dynamometer design as it shown in Figure 7 and provides possibilities to realize wide opportunities rigidity, sensitivity and selectivity combinations.

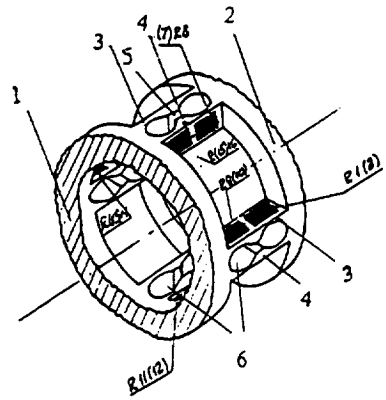

Figure 7. Dynamometer for Mx moment measuring
1, 2 - bases; 3, 4 - longitudinal springy beams; 5 - slot; 6 - cylindrical undercuts; R1 ... R16 - strain-gages.

The dynamometers of considered design are easy combined with each other. It makes possible of various multicomponent strain-gage balances for measuring of transverse forces Y, Z and moment Mx, My, Mz and Figure 8 presents a five-component tubular balance.

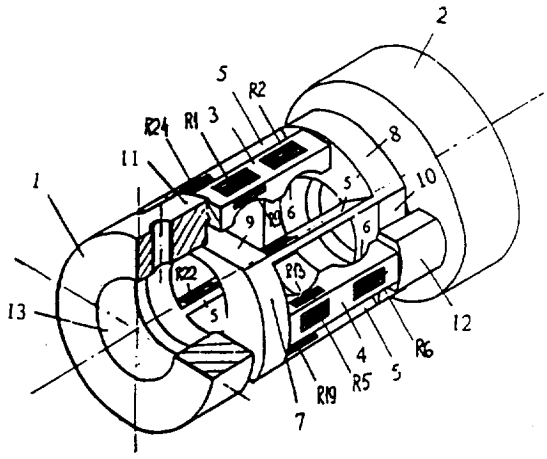

Figure 8. Five-component tubular type dynamometer

1, 2 - main bases; 3 - longitudinal beam of springy parallelogram of Y, My - dynamometer; 4 - longitudinal beams of springy parallelogram of Z, Mz - dynamometer; 5 - springy plates of Mx dynamometer; 6 - cylindrical undercuts of springy beams; 7-12 - rigid element of intermedial bases; 13 - inner channel R1 ... R24 - strain-gages

Layout and general performances of tubular type six-component balances realized in TSNIIMASH are given in Table on Figure 9.

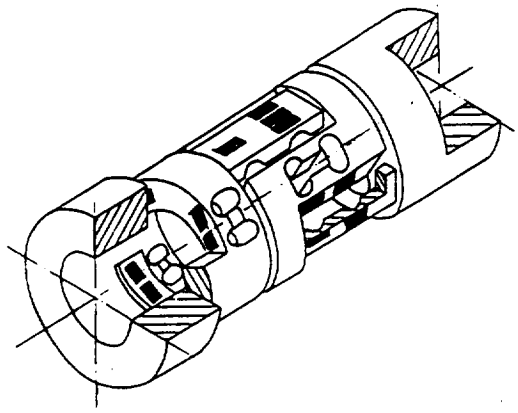

D ext.	X	Y	Z	Mx	My	Mz
mm	N			Nm		
18	500	700	400	5	5	7
20	500	800	500	6	6	8
30	700	800	600	10	20	30
40	1000	1000	800	20	50	70
50	1500	2500	1500	50	100	150

Figure 9. Layout and general performances of tubular type six-component balance

The tubular balance which have individual springy measuring element for each load component can provide a high level of sensitivity, selectivity and accuracy which level is about 0.1 ... 0.25. Owing to short extent of the balances a rather small level of load component interaction can be realized. An additional advantage of the considered balances is good manufacturing properties.

In many cases the tubular balances can be used instead of conventional balances. At the same time testing tasks connected with usage of internal central channel of the balances can be provided. In general balances of short extent are very suitable for many balance testing task provision (e.g. aerodynamic loading measuring of small aspect ratio bodies, control surfaces and model elements, etc. - see ref. 4).

View of a family of tubular balance for various testing tasks is given on figure 10.

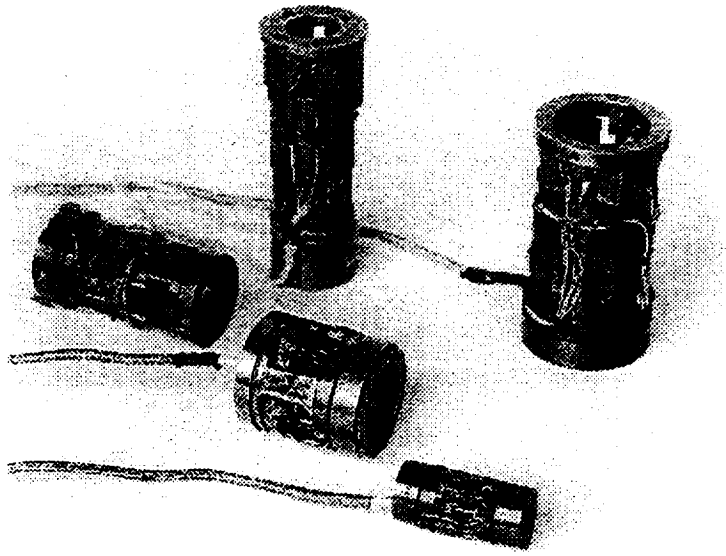

Figure 10. Family of tubular balances

REFERENCES

1. Fristedt, K.: Internal Bending-Beam Strain-Gage Wind-Tunnel Balances. Rollab Rep. 070. 1989
2. Strain-Gage Balances. TASK Brochure.
3. Griffin, S.A.: Study of Six-Component Internal Strain-Gage Balances for Use in the HIRT Facility. AEDC TR-75-63. 1975
4. Lapygin, V.I.; and Lagutin, V.I.: Typical Balance Test Tasks for Aerogasdynamic Facilities of TSNIIMASH (present Proceeding article).

THE DEVELOPMENT OF ADVANCED INTERNAL BALANCES FOR CRYOGENIC AND CONVENTIONAL TUNNELS

Prof. Dipl.-Ing. Bernd Ewald
Dr.-Ing. K. Hufnagel

Darmstadt University of Technology, Germany
Department of Aerodynamics and Measuring Techniques
Faculty for Mechanical Engineering

Abstract

The ever rising accuracy requirements in wind tunnel testing for aeroplane development enforce continuos improvement of force testing technology. The introduction of the cryogenic tunnel is an additional challenge for the force balance, since now even better or at least the same balance accuracy is requested over an operational temperature range of 200 Kelvin.

In more than 12 years of research at the Technical University of Darmstadt all aspects of force testing technology have been dealt with and developed to new standards by the authors in co-operation with Deutsche Aerospace, Airbus GmbH, Bremen. Most of the work was financed by the German Ministry for Research and Technology as a preparation for the ETW Technology..

Basic research on the aspects of metallic spring materials resulted in new understandings about material selection and material treatment for optimum results.

Principal balance design optimisations are done with finite element analysis. For the routine balance design an interactive computer programme was developed.

The very successful technique of the **Electron Beam Welded Balance,** which offers new structural design possibilities, was developed. The balance structure is fabricated from parts, which are welded together by electron beam welding.

For cryogenic balances the main problems are zero shift and sensitivity shift over the large temperature range and false signals especially in the axial force element due to temperature gradients. The problems were overcome by a very careful strain gage matching process, by use of special gages, by application of numerical corrections and by a special design of the axial force system with tandem measuring elements in the flexure groups.

For the calibration of the balance a new third order numerical algorithm was developed. The algorithm works with arbitrary load combinations. This was a requirement for the development of a fully automatic balance calibration machine. The machine (the first specimen is already operational at the ETW) performs a six component calibration including all single loads and all combinations of two loads in one working shift.

So all components of the wind tunnel force testing technology have been developed to new standards with the result of considerable accuracy improvements of the wind tunnel results.

1. INTRODUCTION

The successful design and development of commercial transport aircraft depends (among many other problems !) on excellent aerodynamics. Especially the flight performance reacts very sensitively on aerodynamics. Since flight performance must be guaranteed to potential future customer long before the first flight of the prototype, the success of the aircraft depends heavily on wind tunnel tests with the utmost accuracy. This ever rising requirement for accuracy in wind tunnel testing and especially the challenge of precise force testing in cryogenic wind tunnels gave a strong impetus for strain gage balance research in the recent past. Since accuracy limits for conventional strain gage balances are set mainly by thermal effects, the target to achieve at least the same or possibly even better accuracy with cryogenic balances in cryogenic tunnels is an extremely difficult task. For the research work on cryogenic balances the ambitious target of one drag count repeatability for transonic transport performance testing was set.

To achieve considerable improvements compared to balances known and used today, a single clever balance design idea respectively a single successful detail improvement is not sufficient. A systematic search through all parts and aspects of balance technology and the improvement of all details of this technology to the limits of the available technology is necessary. The important parts of the technology are :

- Design philosophy
- Design computation and optimisation
- Selection of spring material for the balance body
- Material heat treatment
- Balance fabrication methods
- Strain gage selection and wiring method
- Moisture proofing respectively cryogenic environment proofing
- Data acquisition electronics
- Mathematical calibration algorithm
- Calibration equipment
- Strategy of balance use in the wind tunnel

More than twelve years ago we convinced the German Ministry for Research and Technology, that the force measurement technology is perhaps the most important key technology for the success of the new European Transonic Wind Tunnel (ETW), which was in the early planning and design phase at that time. We were happy enough to get a long term funding for the development of the Cryogenic Balance. This put us in a position to do concentrated balance research and development. The aim of this research at the Technical University of Darmstadt was to improve each of these partial aspects of balance technology to the scientific limits available today. Due to this research in Cryogenic Balances many improvements also for balances for conventional wind tunnels resulted. Part of the work was done in close co-operation with the Deutsche Aerospace Airbus GmbH at Bremen with some contributions of the DLR.

2. BALANCE DESIGN PHILOSOPHY

For a successful balance design some essentials must be fulfilled :

1. ***Choose the balance ranges as close as possible to the actual measuring task. In defining the ranges include the consideration, that ranges of the balances can be overloaded, if other ranges are not fully used in the tests. This overload capacity of a balance normally is defined by the 'load rhombus'.***
2. ***Choose the geometric dimensions of the balance as large as allowed by the available space in the model.***
3. ***Design the balance structure for maximum stiffness.***

The first essential requires the design of dedicated and tailored balances for the different tasks of a wind tunnel. As an example for a typical transport configuration model matched in scale to the test section dimensions in a transonic wind tunnel at least three different balances are required for high accuracy testing :

- Very sensitive balance for cruise condition L/D optimisation work.
- Less sensitive balance for cruise condition work including buffet tests, maximum lift tests and M_{DIVE} tests.
- Envelope balance for stability and control tests up to M_{NE} including full control surface deflections and large angles of attack and yaw.

This requirement results in a numerous and expensive numerous balance equipment of a wind tunnel but improves tunnel accuracy very much.

The maximum load capacity of a balance design within a fixed diameter is limited even if an ultra high tensile strength steel (High Grade Maraging Steel) is used. In our balance design method we introduced a balance load capacity parameter S, which is defined as

$$S = \frac{Z \cdot l^* + M_Y}{D^3} \quad [N / cm^2]$$

The characteristic length l^* of the balance is defined as the distance from the reference centre to the end of the active part of the balance, see Figure 1. So this „Balance Capacity Parameter" is a simplified measure of the bending stress in the balance body close to the balance connection to model or sting, which may be a cone or a flange. In most balance designs this is the critical position with respect to stress.

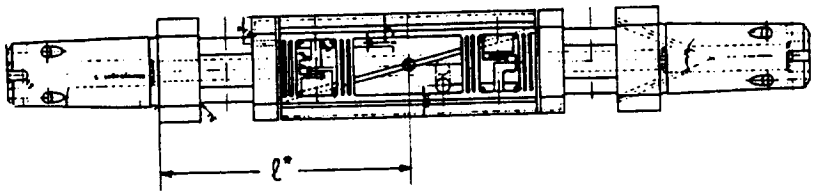

Figure 1 Characteristic Length

Figure 2 shows a load characteristics diagram for a range of balances with diameters between 40 and 110 mm. A group of curves of constant load capacity parameter S is plotted in the diagram. The messages of this figure are :

- Beyond a value of S = 2000 N/cm^2 the design of a precise balance including an axial force system is not possible.
- For a transport performance high precision balance the load capacity parameter should not exceed S = 500 N/cm^2.

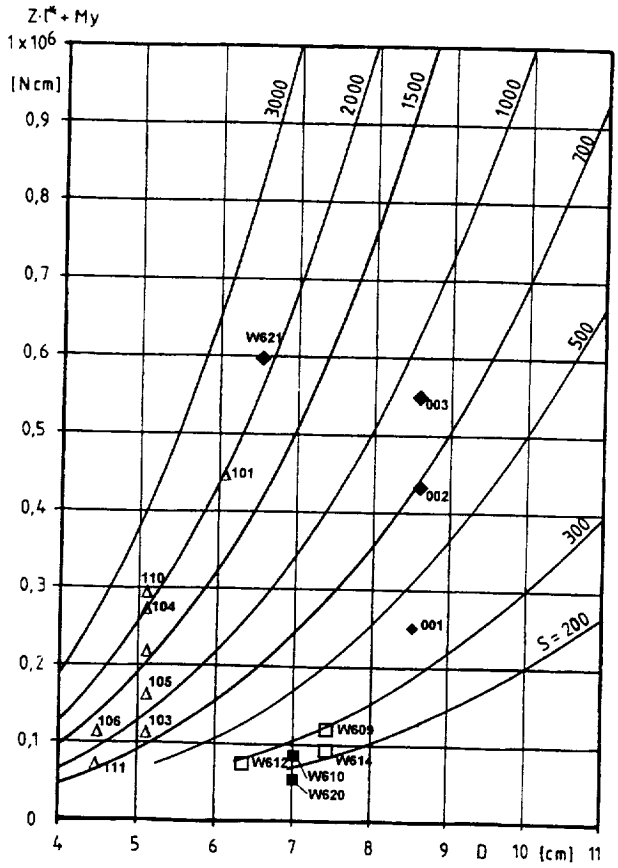

Figure 2 Load Capacity Parameter S

Even lower load capacity parameters are recommended for optimum precision in drag measurement, if the space in the model allows for the larger diameter.

The third essential mentioned above - high stiffness of the balance body - is difficult to achieve with the conventional balance fabrication process by EDM (Electric Discharge Machining). With this method all internal cuts in the balance body must be accessible for the electrode from the outer side of the balance body. This compromises the stiffness requirement. So the fulfilment of the stiffness requirement is mainly a question of the fabrication method.

The ultimate solution of this problem is the Electron Beam Welded Balance concept, which was developed by the author at VFW (now Deutsche Airbus) fifteen years ago. The balance is fabricated from four pieces, which are prefabricated to the final dimensions of all internal surfaces and welded together by electron beam welding. All external machining including opening of the flexure systems is done after welding. The

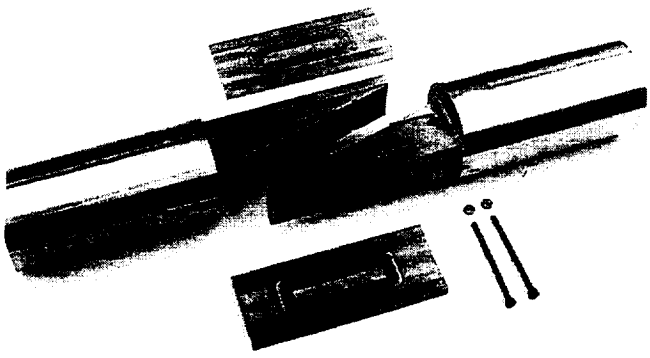

Figure 3a. Prepared Balance Parts

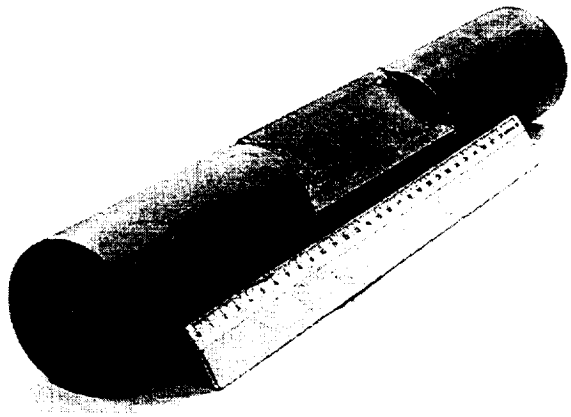

Figure 3b. Welded Balance Body

Figure 3c. Finished Balance Body

production steps are clarified by the Fugures 3.

Provided that a proper material is selected and a sophisticated heat treatment after the welding process is done, full material strength is restored in the welding zone and the finished balance ***is*** a one piece balance and - with respect to strength and hysteresis - definitively behaves like a one piece balance. In a polished cut of the welding seam the welding zone is hardly visibly.

The concept of the Electron Beam Welded Balance turned out to be highly successful and was used since the invention for all balances constructed by the Deutsche Airbus GmbH and by the Technical University of Darmstadt. This fabrication method gives complete freedom in the internal design of the balance structure and allows a much stiffer design of the balance.

3. Balance Design Computation and Optimisation

A strain gage balance is a complicated piece of structure with a very large number of dimensions. So the balance design can not be achieved as a closed solution from the external dimensions and the required component ranges.

At the Technical University of Darmstadt the design computation is done with the interactive computer programme „SEKOWA". With each step this programme completely computes the stress situation at all critical positions of the balance body and some additional characteristic parameters. All results are printed. The user checks the results and according to his experience with the design process he modifies one or several geometric dimensions. Each step is designated as a "RUN". An experienced balance designer needs about 40 to 60 runs for a final satisfying result or for the understanding, that a good balance with the specified ranges can not be designed within given dimensions. This work can easily be done in 2 or 3 hours. The computation is based on basic stress and strain formula for short bending beams and short torsion beams. Provision is made in the programme for notch stress concentration. The computer programme also creates overload diagrams similar to the conventional overload rhombus.

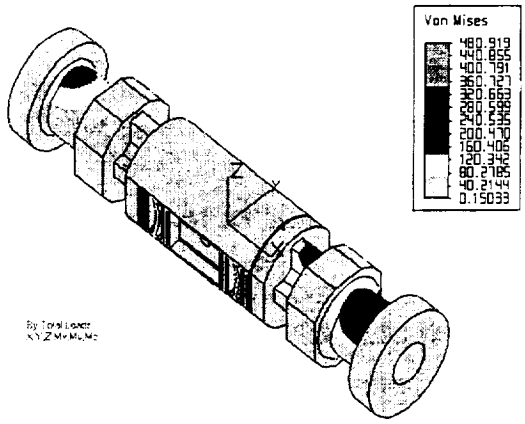

Figure 4. Balance W617, FE Computation

The use of finite element analysis for routine balance design is not possible, since the discretization of the complicated structure with many modifications for the optimised design is to laborious. Nevertheless for principal optimisation of strain gage balance designs finite element analysis proved to be an extremely

valuable tool, this was demonstrated by the work of Junnai Zhai [22] at the Technical University of Darmstadt. Work on balance optimisation with the instrument of finite element analysis is continued at the Technical University of Darmstadt. Figure 4 shows the stress distribution of the balance W 617 under full combined loads computed by finite element analysis.

The analysis of balance structures by the Finite Element Method demonstrated, that the computation and the minimisation of linear and non-linear interference effects is possible by this method. For more details on this work see the paper given by Zhai and Dr. Hufnagel given in this conference.

4. MATERIAL SELECTION

The conventional material for strain gage balances is either maraging steel or precipitation hardening steel like PH 13.8 Mo (1.4534) or 17.4 PH (1.4548). For the welded balance concept we use Maraging 300 (1.6354) for conventional balances resp. Maraging 250 (1.6359) for cryogenic balances. Maraging steel is excellent for electron beam welding; the precipitation hardening steels should be good for welding as well, but no experience was gathered up to now with welded balances from precipitation hardening steels.

A very comprehensive study on force sensor spring materials was performed at the Technical University of Darmstadt. One important result of this study was a general trend of increasing hysteresis with increasing nickel component in the alloy. So the hysteresis quality of the maraging steels is not the best one. With maraging steel hysteresis may be considerably reduced by three provisions :

- Multiple heat treatment for grain refinement as described in [17].
- By deep cooling (77 K, 20 hours) before the ageing treatment the hysteresis is reduced considerably.
- If a lower ultimate strength can be tolerated, underageing reduces the hysteresis of maraging steel considerably.

Additionally at the Technical University of Darmstadt a successful method for numerical correction of force sensor hysteresis was developed. Nevertheless this method was not applied to strain gage balances up to now.

An excellent material for force sensors may be the titanium alloy Ti Al Mg 4 (3.7164). Hysteresis is almost non existing with this material. Nevertheless more experience especially in electron beam welding and in gage application must be gathered before application of titanium as a strain gage balance material.

A very promising material for conventional and cryogenic balances is Copper Beryllium (2 % Beryllium), if the load capacity factor allows for the lower tensile strength of this material compared to maraging steel. Hysteresis is extremely low and electron beam weldability is good. The excellent heat conductivity of copper beryllium will considerably reduce the temperature gradient problems with cryogenic balances. A cryogenic balance for the ETW from copper beryllium was designed and constructed at the Technical University of Darmstadt.

The low corrosion resistance of maraging steel is troublesome for balances especially in the case of cryogenic balances. Nickel plating proved to be an efficient counter-measure. In this case the strain gage positions are covered with a protecting lacquer before the nickel plating process. So the gages are bonded on the uncovered maraging steel.

5. Strain Gauging and Wiring methods.

Up to now we used strain gages exclusively from Micro Measurement (Vishay). From the available range of gages types can be selected, which are very well suited for the cryogenic range and as well for conventional tunnel conditions. For the extreme temperature range of cryogenic balances misadaption of the STC-Factor is recommended. We use SCT-Factors of 11 or 13 for balances constructed from maraging steel.

A more complicated problem is the primary correction of Young's modulus over the extreme temperature range of cryogenic balances. Normal KARMA-alloy is not satisfactory. For a special cryogenic balance production MM has demonstrated, that a special tuning of KARMA gages for extreme temperature range compensation of Young's modulus is possible. Gages of this special type were used for the ETW balance constructed by the Technical University of Darmstadt and Deutsche Airbus.

For a very low zero drift over the temperature range of cryogenic balances misadaption of STC-factor, close coupled arrangement of the gages of one bridge etc. is not sufficient. Even the gages from one pack of five show considerable scatter in thermal behaviour. Gage matching improves this situation very much and was first proposed by Judy Ferris (NASA Langley). Since the thermal behaviour of gages can be evaluated only from the applicated gage, each individual gage is applicated to a common maraging steel sample by cyano cryalate bond. After a measurement of the zero drift of each gage in the cryogenic chamber the arrangement is heated beyond the stability of the cyano cryalate bond and the gages are carefully cleaned. From the results of this process the gages for each bridge are individually selected for minimum bridge zero drift. This procedure is time consuming but reduces bridge zero drift very much.

For final gage application on strain gage balances epoxy hot bonding is used exclusively. Preparing the surfaces, preparing the gages and the bonding procedure must be done with the utmost care, patience and perfect observance of the manufacturers instructions. Even the ut-most care is not sufficient, it must be combined with years of experience in the art of strain gage application.

For conventional balances temperature correction copper wires are integrated in the bridge wiring. For cryogenic balances this procedure is not very successful, since the strong non-linear behaviour of the apparent strain can not be compensated by the copper behaviour with a dif-ferent non-linearity. If for special temperature correction methods the measurement of temperatures on the balance is necessary, a number of temperature sensors (6-10) is installed on the balance. PT 100 sensors are used for the temperature measurement. For very high precision the PT 100 sensors are individually calibrated.

The internal wiring of the bridge circuits is carefully designed for symmetric length and symmetric temperature on all internal bridge wire connections. All bridges are wired separately for excitation lines, excitation voltage sensing lines and signal lines. All circuits are connected to

the tunnel data system via a high quality miniature connector mounted at the sting end of the balance. Normally 80 pin connectors are used.

Very often in wind tunnel testing practice it is necessary to bridge the balance with other electrical signal and power lines as well as pneumatic lines. These lines may deteriorate the balance accuracy due to their stiffness to an extent, that force testing and testing with the use of balance bridging lines must be done separately, So the wind tunnel productivity is reduced very much. At the Technical University of Darmstadt a concept was developed to integrate these bridging lines into the design of the balance. With such an integrated electric or pneumatic line bridging the balance has connectors at the sting and the model end for the lines. Thus any hysteresis due to the bridging is avoided.

6. Moisture Proofing resp. Proofing for Cryogenic Environment

To achieve excellent zero point stability, moisture proofing is most important. For conventional balances a careful observance of strain gage manufacturers instructions may be sufficient. For cryogenic balances moisture proofing is perhaps the most difficult detail of balance construction. Strain gage manufacturers give no sufficient instructions and offer no sufficient materials for these environmental conditions. A very careful application of multiple thin layers of nitril rubber is the best conventional moisture proofing method we found up to now.

7. Data Acquisition Equipment

It stands to reason, that for balance signal acquisition top quality equipment is used only. Nevertheless between wind tunnel instrumentation experts there is a certain disagreement on the basic type of equipment. In most tunnels DC measuring techniques are used in form of specially designed signal conditioning and digitising units or in form of high quality digital multimeters.

In recent years some commercial developments, especially the DMC data acquisition unit (600 Hz carrier frequency) of the German company Hottinger has brought the AC measuring technique back into the field again. This AC equipment is equivalent and in some cases even superior to the best of DC equipment and has the big advantage of blocking any thermal voltage signals. In the case of cryogenic tunnels with their large temperature differences in the test region this may be essential. The disadvantage of the AC measuring method is the limited frequency range, which may cause concern, if dynamic balance stresses shall be monitored. Nevertheless dynamic signals up to 200 Hz can be monitored with this equipment satisfactorily.

The Hottinger measuring system DMC 9012 resp. its successor DMCplus is used successfully in the Aerodynamics Lab and the Wind Tunnel of the Technical University of Darmstadt, the Aerodynamic Department and Wind Tunnel Department of Deutsche Airbus, the Cologne Cryogenic Tunnel (KKK) and the ETW Calibration Machine. The system can be equipped with up to 28 data channels. The maximum speed of this system is 100 000 measurements per second and the resolution is up to 300 000 parts. The system is fully computer controlled;

several systems may be managed in parallel by one PC. The system provides also the excitation for the strain gage bridges.

As a general rule identical electronic measurement hardware or even better the same equipment should be used for balance calibration and for balance use in the wind tunnel.

8. Mathematical Method of Calibration

The field of calibration perhaps includes the largest improvement potential of the balance technology. The first item in this field is the mathematical description of the balance behaviour. The generally used method is the so called second order calibration. Since many years we extended this to a third order approximation of the balance behaviour :

$$S_i = R_{0i} + \sum_{j=1}^{6} A_{ij} F_j + \sum_{j=1}^{6} \sum_{k=j}^{6} B_{ijk} F_j F_k + \sum_{j=1}^{6} C_{ij} F_j^3$$

In this description for the direct component calibration terms a third order term is taken into account. The advantage of this description compared to the conventional second order calibration was often questioned by other experts, nevertheless the use of the third order approximation is simply logical.

Certainly there are physical reasons for a non-linearity of the characteristic line of one component of a strain gage balance (or other Force Sensor) as shown in the positive quadrant of Figure 7. Since a strain gage balance is a symmetrical structure, almost certainly in the third quadrant the non-linearity of the characteristic line should be mirror inverted to the line in the positive quadrant as shown in Figure 7 by the continuous line. There is no reason to expect a monotonic curvature like shown by the dotted line.

The non-linearity of the continuous line in Figure 7 can be described in a polynom by the third order term only. This is the only reason why we use the third order description of the balance behaviour. Applied to actual calibration data the comparison of second and third order calibrations shows that in the case of the third order approximation the third order coefficient have a considerable size and the second order terms come out smaller than in the case of a second order approximation. Nevertheless the quadratic terms should not be neglected. Very often a strain gage force sensor has a slightly different sensitivity in the positive and the negative quadrant. This behaviour is approximated by the quadratic term. Since all the work is done very fast by the computer, the higher mathematical complexity of the third order approximation is no argument against this algorithm.

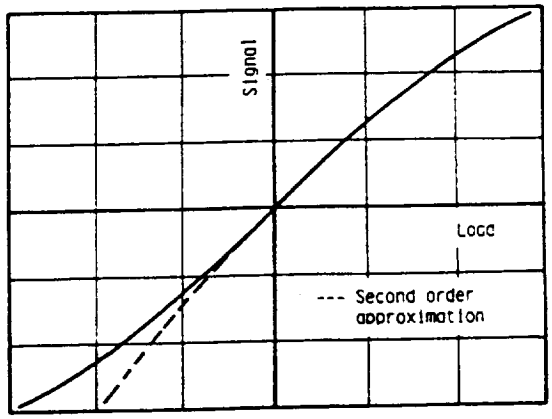

Figure 7. Second/Third Order Approx.

The conventional evaluation of the calibration data is based on the method to apply pure single loads stepwise to the balance plus combinations of two pure single loads. In the latter case one load is constant and the other load is applied stepwise. So a simple evaluation of each loading sequence in the sense of a least square error second or third order polynom approximation is possible. The complete coefficient matrix is successively compiled from such evaluations of loading sequences.

This results in an system of equations

Component Signal = Function (Loads)

which must be converted to a different set of equations

Loads = Function (Signals)

for the use in the wind tunnel. This conversion is not possible in a mathematical sense since a conversion matrix only exists for a linear matrix. So more or less accurate or questionable approximate solutions must be used for the conversion.

The automatic calibration machine invented at the University of Darmstadt produces calibration data, where the desired loads (normally a single component or a combination of two single components) are superimposed by small interfering loads in the other balance components. Though the interfering loads are known precisely since they are measured by the calibration machine, the evaluation of a calibration matrix from such "mixed" loading data sets is not possibly with the conventional evaluation methods. So at the University of Darmstadt we use a different mathematical algorithm, where a system of equations

Loads = Function (Signals)

is extracted in one step from the complete calibration data set (approximately 1000 different loading conditions) as a closed solution in the sense of least square errors. So the questionable conversion of the matrix is no longer necessary and the result is the absolutely best evaluation of the calibration data in a mathematical sense. For more details see [18], [19] and [20].

9. CALIBRATION EQUIPMENT

For information's on modern calibration equipment please see the Paper „Development and Construction of Full Automatic Calibration Machines for Internal Balances" by Ewald, Dr. Hufnagel, Polansky and Badet and the Paper „The Development of a Modern Manual Calibration System and Measuring System for Internal Balances" by Quade and Dr. Hufnagel given in this conference.

10. CRYOGENIC BALANCE DESIGN

A standard design philosophy for cryogenic balances has not yet been established, among the cryogenic community there is even no agreement if unheated or heated balances are to be preferred. The majority of cryogenic balance designs is unheated up to now but the promoters of heated balances argue, that this type will not develop spatial temperature gradients in the body and will not require stabilisation times if tunnel temperature is changed. This is a strong argument, since a necessary stabilisation time will deteriorate the productivity of the tunnel.

Nevertheless the author is pessimistic with respect to the heated balance. The massive joints on model and sting end of the balance will cause considerably large heat flows, so a lot of local heating power will be required to condition the balance to ambient room temperature with no spatial temperature gradients. The result most probably will be even worse temperature gradients in some regions of the balance body. From the authors point of view the more promising solution is a special balance design which tolerates temperature gradients without unacceptable deterioration of the accuracy especially in the axial force measurement.

This was achieved successfully with the concept of the tandem axial force elements, which are integrated in the front and aft flexure groups of the axial force system (see Figure 12 for example). The predominant part of temperature gradient generated axial force errors is proportional to the mean temperature difference in the upper and lower cantilever beams of the axial force system. With the conventional central position of the axial force bending beam the error signals are a function of the arbitrary temperature distribution in the cantilever beams.

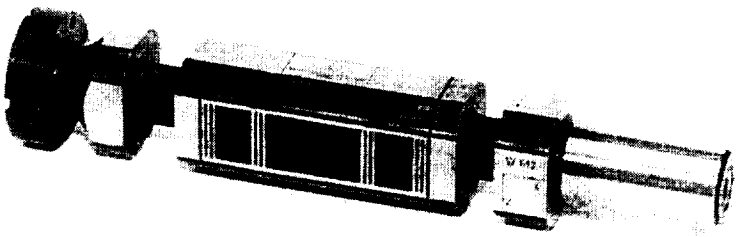

Figure 12. Cryogenic Balance W 612 (KKK) with tandem axial force elements

With the tandem axial force system the error signals due to temperature gradients in the front and in the aft bending beam element have the same magnitude but opposite signs. By adding the signals of the front and the aft sensor the signals due to temperature gradients are cancelled. The unavoidable tolerances in bending beam dimensions and gage position result in a small residual error signal due to temperature gradients. Nevertheless these residual errors may be removed by a simple numerical correction.

The concept of the tandem axial force elements is very successful. For temperature gradients of 5 degrees centigrade along the balance length the gradient induced error of the axial force signal without additional numerical correction is less than 1 µV/Volt in the case of the ETW balance W 618.

The advantage of using copper beryllium as a material for cryogenic balances was mentioned already in chapter 4.

11. THE BLACK BOX BALANCE PRINCIPLE

A distinguished balance expert well known to the author once said : *"You should never hand out a good strain gage balance to the wind tunnel people, they make everything wrong and they will demolish this delicate instrument"*. Obviously this aphorism is not quite correct since also a lot of good measurements have been performed by the "wind tunnel people" using strain gage balances !

Nevertheless there is some truth in it. The use of a balance in the tunnel, that means connecting it to the data acquisition system, adjusting amplifiers, adjusting excitation voltage, programming the signal evaluation (evaluation matrix, numerical corrections etc.), programming axis system transformation etc. offers so many opportunities for human errors, that an actually acting aerodynamic positive yawing moment may well be printed out by the computer as a negative rolling moment multiplied by xx plus a constant yy. To avoid these sources of human errors we propose the 'Black Box Balance' concept.

With this concept a standard electronic hardware for the balance signal conditioning, signal read out and force evaluation for the calibration of the balance and for the use of the balance in the tunnel is specified between client and balance manufacturer or is even delivered by the balance manufacturer. The operating parameters of this balance data acquisition hardware must be fully computer controllable. The balance is delivered by the manufacturer together with a diskette, which contains the standard balance evaluation programme, which sets all parameters of the signal acquisition electronics and converts the balance signals into interference free and corrected forces and moments in physical dimensions.

In the balance itself a miniature memory chip is integrated. This memory chip contains a balance identification code, special corrections to be used with this individual balance and the calibration matrix of this individual balance.

For the use of the balance in the wind tunnel simply the disk is fed into the balance measurement controller (Standard PC) of the wind tunnel computer system and the balance itself is plugged to the measurement system. So always the standard evaluation software is used without the possibility of introducing errors. The balance controller automatically checks the balance identification code and compares it with the identification code of the calibration data. With today's miniature memory chips the calibration data are an integrated part of the balance body at least for conventional tunnel balances. So the balance itself tells the wind tunnels balance computer her calibration data and special corrections to be applied to her results without any additional error source. The calibration data are automatically burned into the memory chip (EPROM) on the balance by the data evaluation system of the Automatic Balance Calibration Machine. The data are refreshed by each recalibration. In the case of a recalibration the calibration software checks for substantial differences between the old calibration matrix and the new one. Such differences may indicate a faulty balance.

Unless the Black Box Balance Concept will simplify the use of internal balances very much and will exclude nearly all possible human errors, it was not realised so far. The main argument of possible clients against the concept was, that a wind tunnel operator is bound to one balance manufacturer with this concept. Nevertheless, if the balance manufacturer is well qualified, this commitment may be not to bad.

12. HALF MODEL BALANCES

For informations on a Half Model balance see the Paper „The Half Model Balance for the Cologne Cryogenic Tunnel (KKK)" presented by Ewald, Dr. Viehweger and Rebstock at this conference.

13. FUTURE DEVELOPMENTS

Some plans for future developments of the balance technology were already indicated in the previous pages. Our most important plans for future developments are :

- Black Box Balance Concept
- Further evaluation of Copper-Beryllium Balance Concept
- Evaluation of Titanium Balance Concept
- Integrated Balance Bridge for signal lines, power lines and pneumatic lines
- On Board Measurement for pressure distribution or other data with light transmission of data into the earth system
- Further optimisation of balance design by finite element analysis
- Further development of the Automatic Calibration Machine

14. SUMMARY

The extensive research on strain gage balances done at the University of Darmstadt in co-operation with Deutsche Airbus demonstrated, that a substantial improvement of the wind tunnel force testing technology requires engineering progresses in any detail of balance design concepts, actual balance designs, material selection, balance fabrication method, gauging methods and calibration equipment and calibration algorithms. So all these details where included into our balance research efforts and any detail was improved to the technological limits available today. The outcome is a balance technology, which leads to much improved balances for conventional tunnels and to cryogenic balances which up to now (this development is not jet finally finished) bring the target of less than one drag count repeatability for transport configuration performance measurements within reach.

Acknowledgements

The author started balance design and fabrication nearly 20 years ago in his position as Head of Experimental Aerodynamics in the VFW Company at Bremen (now Daimler Benz Aerospace Airbus). He has to thank especially Dipl.Ing. Eberhard Graewe from that company for the long co-operation in this field. Valuable contributions to the balance technology originated from the close co-operation with the Deutsch-Niederländischer Windkanal (DNW), the European Transonic Wind Tunnel (ETW) and the Cologne Cryogenic Tunnel (KKK). When the author

moved to the Technical University of Darmstadt in 1983, he continued the work in research and development of balances in co-operation with E. Graewe and now with the untiring scientific work of Dr. Klaus Hufnagel. A most creative co-operation with the Carl Schenck AG, ETW and Deutsche Airbus on the Balance Calibration Machine started. Some contracts with ETW allowed further research on cryogenic balances.

The substantial improvement of the balance technology and especial the cryogenic balance development could only be achieved with this creative teamwork.

Much of the work was funded by the German Ministry for Research and Technology.

REFERENCES

[1] E. Graewe, *"Development of a Six-Component Balance for Cryogenic Range"*. Forschungsbericht W 84-022 BMFT 1984

[2] Prof. B. Ewald, *"Grundsatzuntersuchung zum Temperatur-Verhalten von DMS-Axial-Kraftteilen"*, BMFT LVW 8420 10, Nr. 10/85 1985

[3] B. Ewald , *"Development of Electron Beam Welded Strain-Gage Wind Tunnel Balances"*, Journal of Aircraft Volume 16, May 1979

[4] Prof. B. Ewald, G. Krenz, *"The Accuracy Problem of Airplane Development Force Testing in Cryogenic Wind Tunnels"*, AIAA Paper 86-0776, Aerodynamic Testing Conference, March 1986

[5] Prof. B. Ewald, E. Graewe, *"Entwicklung einer 6-Komponenten-Waage für den Kryo-Bereich"*, 3. BMFT-Status-Seminar, Hamburg, May 1983,

[6] Prof. B. Ewald, E. Graewe, *"Development of Internal Balances for Cryogenic Wind Tunnels"*, 12th ICIASF, Williamsburg, VA, June 1987,

[7] Prof. B. Ewald, *"Balance Accuracy and Repeatability as a Limiting Parameter in Aircraft Development Force Measurements in Conventional and Cryogenic Wind Tunnels"*, AGARD FDP Symposion, Neapel, September 1987

[8] Prof. B. Ewald, P. Giesecke, E. Graewe, T. Balden, *"Feasibility Study of the Balance Calibration Methods for the European Transonic Wind Tunnel"* Report TH Darmstadt A 37/88, January 1988

[9] Prof. B. Ewald, Th. Balden, *"Balance Calibration and Evaluation Software"*, Proc. Second Cryogenic Wind Tunnel Technology Meeting, ETW, Cologne, June 1988

[10] Prof. B. Ewald, T. Preusser, L. Polanski, P. Giesecke, *"Fully Automatic Calibration Machine for Internal Six Component Wind Tunnel Balances Including Cryogenic Balances"*, ISA 35th International Instrumentation Symposium, Orlando, Florida, May 1989

[11] Prof. B. Ewald, P. Giesecke, E. Graewe, TH. Balden, *"Automatic Calibration Machine for Internal Cryogenic Balances"*, Proc. Second Cryogenic Wind Tunnel Technology Meeting, ETW, Cologne, June 1988

[12] Prof. B. Ewald, T. Preusser, L. Polanski, P. Giesecke, *"Fully Automatic Calibration Machine for Internal Six Component Wind Tunnel Balances Including Cryogenic Balances"*, ICIASF Congress, September 1989, Göttingen

[13] Alice T. Ferris, *"Cryogenic Strain Gage Techniques used in Force Balance Design for the National Transonic Facility"*, NASA TM 87712, May 1986

[14] Prof. B. Ewald, L. Polanski, E. Graewe, *"The Cryogenic Balance Design and Balance Calibration Methods"*, AIAA "Ground Testing Conference" July 1992, Nashville, Bericht A 99/92

[15] Prof. B. Ewald, K. Hufnagel, E. Graewe, *"Internal Strain Gage Balances for Cryogenic Wind Tunnels"*, ICAS-Congress, Sept. 92, Peking

[16] Prof. B. Ewald, E. Graewe, *"The Development of a Range of Internal Wind Tunnel Balances for Conventional and Cryogenic Tunnels"*, European Forum on Wind Tunnels and Wind Tunnel Test Techniques, Sept. 92, Southampton

[17] H.F. Rush, *"Grain Refining Heat Treatment To Improve Cryogenic Toughness of High-Strength Steels"*, NASA TM 85816, 1984

[18] Schnabl, *"Entwicklung eines numerischen Algorithmus und eines Rechnerprogramms zur Auswertung der Eichversuche an 6-Komponenten-DMS-Waagen."*, Technical University of Darmstadt, Diploma-Thesis A-D-69/87

[19] Dipl.Ing. T. Balden, *"Ein neues Konzept zur Kalibration von Kry-Windkanal-Waagen"*, Deutsche Airbus Bremen, Proceedings of DGLR Jahrestagung 1993, Göttingen

[20] B. Ewald, *"Theory and Praxis of Internal Strain Gage Balance Calibration for Conventional and Cryogenic Tunnels"*, 18 AIAA Ground Testing Conference, June 1984, Colorado Springs

[21] G. Viehweger, B. Ewald, *"Half Model Testing in the Cologne Cryogenic Tunnel (KKK)"*, 18th AIAA Ground Testing Conference, June 1984, Colorado Springs

[22] Junnai Zhai, Bernd Ewald, Klaus Hufnagel, *„An Investigation on the Interference of Internal Six-Component Wind Tunnel Balances with FEM"*, ICIASF '95, Dayton, Ohio

[23] Bernd Ewald, *„Advanced Force Testing Technology for Cryogenic and Conventional Wind Tunnels"*, ICAS Congress 1994, Anaheim, California

Annex I. Examples of Balances

Some of the six component balances designed and manufactured by the University of Darmstadt and Deutsche Airbus are illustrated here. For a complete overview and for the load ranges see Table 1 in the annex.

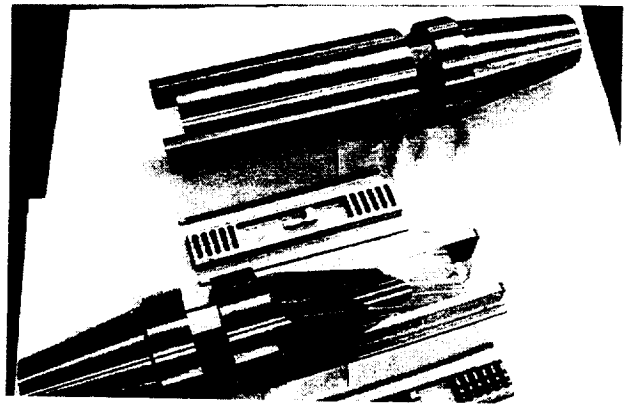

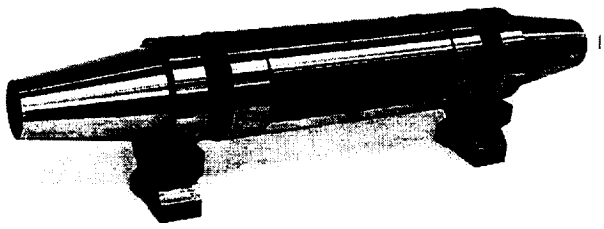

Figure 15. Balance W 605 (DNW-Balance, 3 ton Normal Force Capacity). (Above: Parts before welding.)

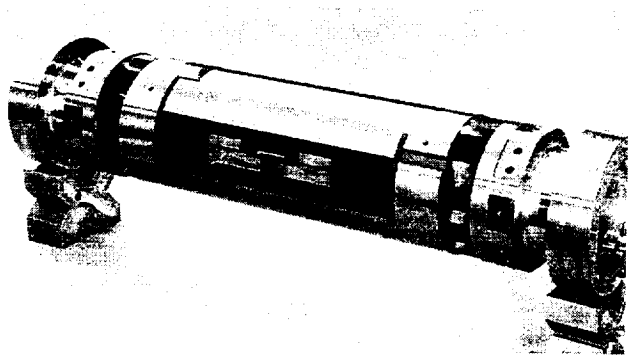

Figure 16. Balance W 608 (DNW-Balance, 3 ton Normal Force Capacity)

Figure 17a : Balance W 607, Prepared Parts

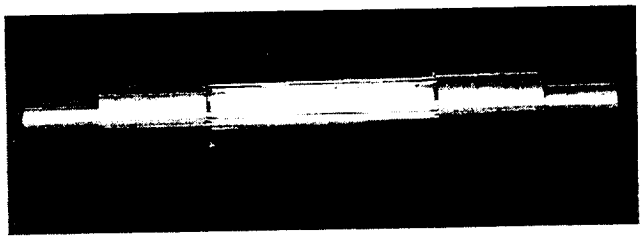

Figure 17b : Balance W 607, Welded Body

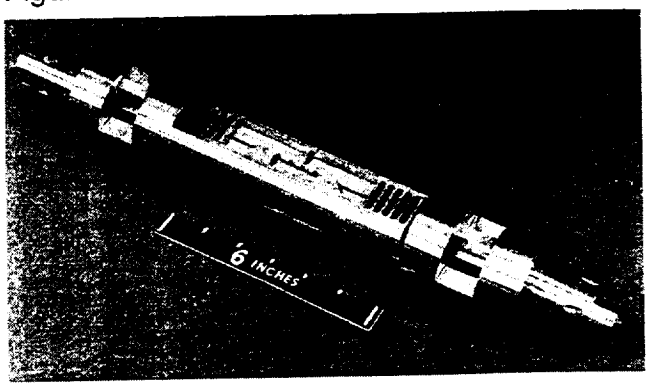

Figure 17c : Balance W 607 ready for gaging

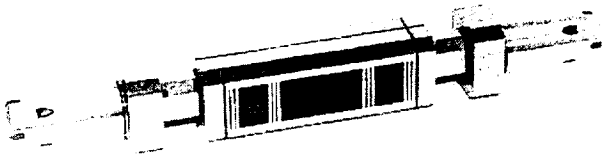

Figure 18 : Cryogenic Balance W 609

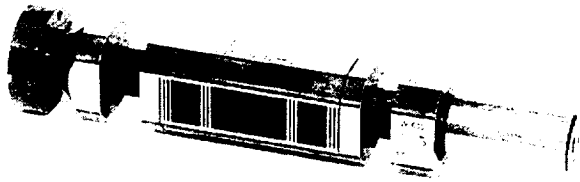

Figure 20 : Cryogenic Balance W 612

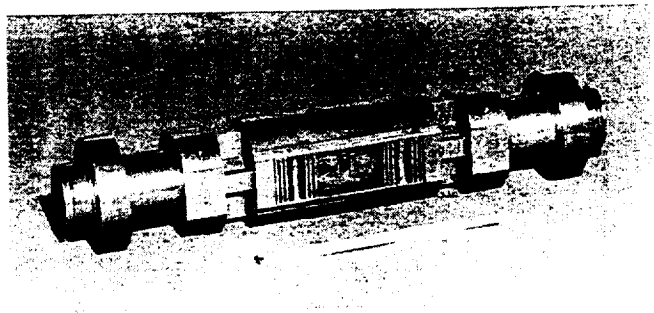

Figure 21 : Copper-Beryllium Balance W 617

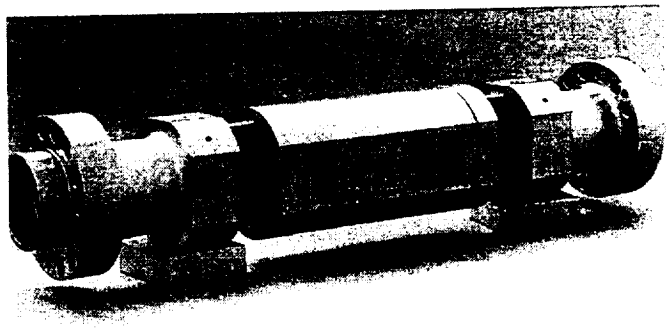

Figure 22 : ETW Balance W 618, Ready for gaging

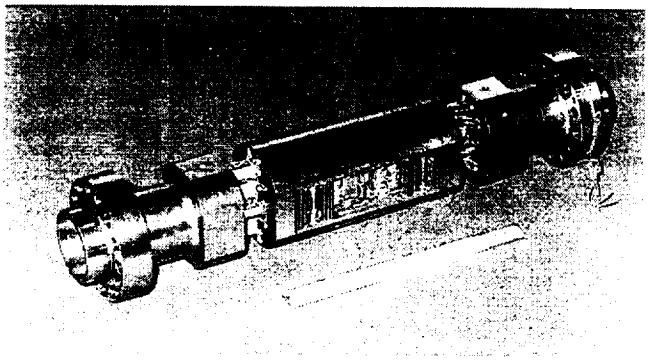

Figure 23 : ETW-Balance W 618, ready for Calibration

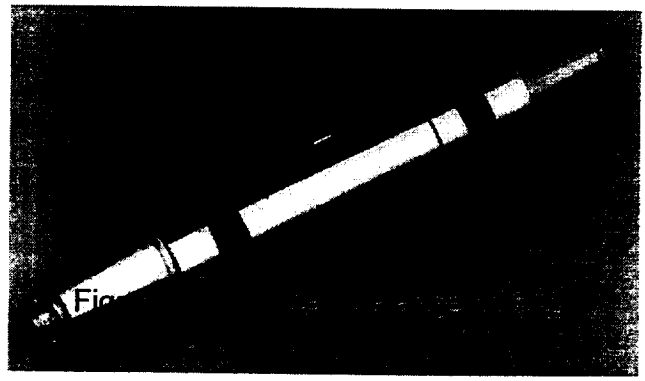

Figure 24 : ETW Combat Balance W 621

Annex 2, Table of Existing Balances

Balance Name and Purpose	Simultaneous Component Ranges					
	X [N]	Y [N]	Z [N]	Mx [Nm]	My [Nm]	Mz [Nm]
W 64 Spin and Roll Balance Constructed for DLR		200	1 500	80	150	100
W 605 General Purpose Balance fabricated for DNW	12 500	12 500	30 000	9 000	11 500	9 000
W 606 First Cryogenic Balance fabricated for KKK	200	500	2 000	120	160	140
W 607 Missile Balance fabricated for AEDC	700	2300	2300	70	460	460
W 608 General Purpose Balance fabricated for DNW	20 000	6 250	50 000	4 500	15 000	4 500
W 609 Second Cryogenic Balance fabricated for KKK	1 400	1 700	4 000	400	500	400
W 610 Darmstadt University Low	800	1 000	2 700	400	450	300

Speed Tunnel. Gen. Purpose						
W 611 **Tech. Univ. of Braunschweig** **Low Speed Tunnel**	120	100	500	10	30	10
W 612 **Third Cryogenic Balance** **fabricated for KKK**	900	400	3 000	200	240	70
	Simultaneous Component Ranges					
Balance Name and Purpose	**X [N]**	**Y [N]**	**Z [N]**	**Mx [Nm]**	**My [Nm]**	**Mz [Nm]**
W 614 **Cryogenic KKK - Balance** **Contract of DLR**	1 400	1 700	4 000	400	400	300
W 615 **Life Dummy Balance for ETW** **Calibration Machine**	-	3 000	20 000	2 000	1 200	1 000
W 616 **Transport Performance Balance for** **DNW**	6 500	10 000	20 000	4 500	7 500	3 000
W 617 **ETW advanced Research Balance.** **Copper-Beryllium**	2 000	1 500	20 000	350	1 250	180
W 618 **ETW Transport Performance** **Balance. Contract ETW**	1 000	1 000	12 000	100	700	80
W 519 **KKK Half Model Balance** **Contract from DLR**	650	-	3 500	2850	350	515
W 620 ***Project for Deutsche Airbus*** ***Low Speed Wind Tunnel***	*700*	*700*	*2 000*	*200*	*200*	*200*
W 621 **ETW High Capacity Balance.** **ETW Contract**	3 500	5 500	30 000	800	2 500	800

File BALLIST.doc , Stand 01.07.1996

A NEW BALANCE CALIBRATION METHODOLOGY FOR LONG SLENDER BODIES IN A BLOWDOWN TUNNEL

G. Rajendra, H. Sundara Murthy, and G. Vijaya Kumar
NATIONAL AEROSPACE LABORATORIES, BANGALORE, INDIA

SUMMARY

Accurate measurement of forces and moments on long slender models in blowdown wind tunnels poses certain special problems at supersonic speeds. While the balances are required to be of high capacity to withstand large starting and stopping loads, the steady loads on the model are usually small fractions of the balance capacity, resulting in reduced measurement accuracies. A large reduction of start and stop loads would permit the use of a sensitive low range balance tailored to the small loads on models. Alleviation methods developed so far have not met with much success to enable this option. The floating frame balances built by ABLE Corporation, USA are able to overcome this problem to some extent due to their inherent ability to provide high accuracy even at very low loads. However there is a strong need to reassess the balance calibration methodologies to be able to achieve acceptable accuracies for measurement of low loads using these high range balances. This paper presents a brief description of the problems faced in obtaining accurate data on long slender models and a new balance calibration method to overcome some of these problems.

INTRODUCTION

Before discussing the new calibration method, it will be useful to briefly indicate the nature of problems encountered due to the use of conventional balance calibration method.

Conventional Calibration

Conventional single component loading (Fig. 1)using standard second order calibration constants gives rise to 144 constants. A typical equation is as shown below

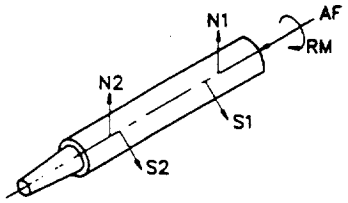

Balance Element Notations

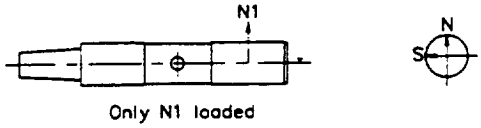

Fig.1 Single Component Loading

$$O_i = \sum a_{ij}F_j + \sum b_{ij}F_j^2\{\pm\}$$

where i = 1 to 6 (no. of elements)

O_i = outputs from each bridge

F_j = 5 loads(N_1, N_2, S_1, S_2, A) and (1 to 6) 1 moment (RM)

The table(1) gives typical standard deviations when several check loads were applied at element stations N_1, N_2, S_1, and S_2.

TABLE 1

TYPICAL STANDARD DERIVATIONS OF WORKED BACK LOADS USING CONVENTIONAL CALIBRATION

Loading method	ΔN_1 lbs	ΔN_2 lbs	ΔS_1 lbs	ΔS_2 lbs
Single component loading	0.48	0.24	0.52	0.26
0.1% of balance capacity	2.0	2.0	0.75	0.75

It is seen that the standard deviations are well within 0.1% of the balance capacity. This fact encouraged us to use such balances for force measurements on launch vehicle models which require very high accuracies to determine their performance characteristics, especially the stability margin and controllability.

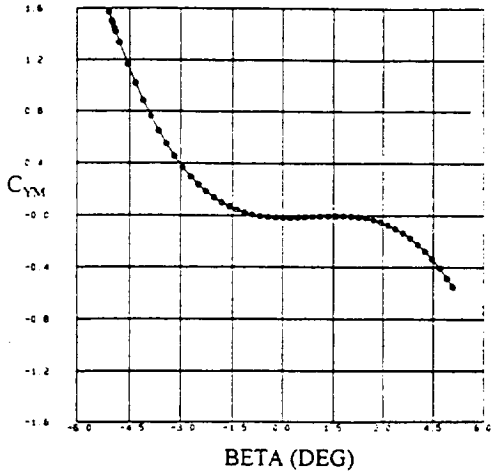

Fig. 2 A typical result using calibration data from single component loading

The results obtained using such a high range balance were not as good as expected. As an example, Figure 2 shows the yawing moment coefficient obtained on a launch vehicle model for a roll orientation of -53°. There exists some asymmetry with respect to β=0° which is not expected from a symmetric configuration. Balance calibration was thought to be the prime source of this discrepancy, especially since the maximum measured load on the model was only 12% of balance capacity. Hence a detailed examination of various aspects of balance calibration and related factors was made.

Differences between Calibration and Test Environment

Major differences between the balance calibration environment and actual conditions under which loads were measured in wind tunnel are:

a) While the model loads act at large distances (upto 20 inches) ahead of balance centre, the balance was loaded at the element stations (Fig.1) during calibration.
b) The model was subjected to a combined loading while single component loading was adopted during calibration.

Both the above factors could have contributed to the observed discrepancy. It was considered necessary to evolve new balance calibration and data reduction procedures to bring down errors due to the above differences. A discussion on two methods tried at NAL is given.

Offset Loading : For calibration of the balance, it would be necessary to load the balance at locations where the loads are expected to act on the model instead of loading only at element stations. This would necessitate inclusion of additional terms such as product terms $N_1 \times N_2$, $S_1 \times S_2$ etc., in the calibration equations.

Before undertaking the offset load calibration on the balance where the loads would be applied atleast 20 inches ahead of balance centre, it was considered worthwhile to carry out a validation exercise to determine the optimum number of loading stations and their locations and other factors. In this exercise appropriate values of all the balance constants including nonlinear terms were initially assumed and the outputs from the balance elements N_1 and N_2 were computed for a series of loadings at selected stations. For a more realistic simulation, random disturbances

were superposed on the computed outputs and the net outputs along with the applied loads were utilized to determine the balance constants using least squares method. From a careful assessment of the standard deviations in the worked back loads it emerged that a minimum of three loading stations ahead of balance centre should be adequate for a satisfactory evaluation of balance constants.

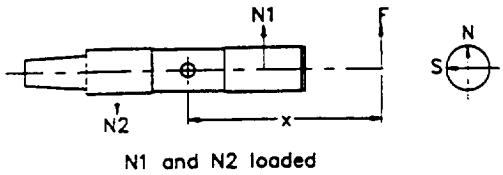

Fig. 3 Offset Loading

Subsequent to the validation exercise a detailed calibration using offset loading in the normal force and the side force plane was undertaken where the loads were applied at a number of stations covering an offset distance of 20 inches (Fig.3). The calibration equations were cast as shown below. The major difference in the equation is the inclusion of product terms N_1xN_2 and S_1xS_2.

$$ON_1 = a_{11}N_1 + a_{12}N_1^2 + a_{13}N_2 + a_{14}N_2^2 + a_{15}N_1xN_2 + b_{11}S_1 + b_{12}S_1^2 + b_{13}S_2 + b_{14}S_2^2 + b_{15}S_1xS_2 + c_{11}A + c_{12}A^2 + d_{11}(RM)^2 + d_{12}(RM)^2$$

Such equations are formed for four combinations of $N_1 \times N_2$ ($+N_1$ & $+N_2$, $+N_1$ & $-N_2$, $-N_1$ & $+N_2$, $-N_1$ & $-N_2$) and four similar combinations of S_1xS_2.

Table(2) lists the standard deviations in the worked back loads obtained from two calibration methodologies i.e single component loading and offset loading. One can see a marked improvement in the accuracies using offset loading as compared to single component loading method of calibration.

TABLE-2

TYPICAL STANDARD DEVIATIONS OF WORKED BACK LOADS USING OFF-SET LOADINGS

Method of Loading	ΔN_1 lbs	ΔN_2 lbs	ΔS_1 lbs	ΔS_2 lbs
Single Component Loading	1.35	0.90	1.60	0.14
Off-set Loading	0.24	0.27	0.08	0.11
0.1% of balance capacity	2.0	2.0	0.75	0.75

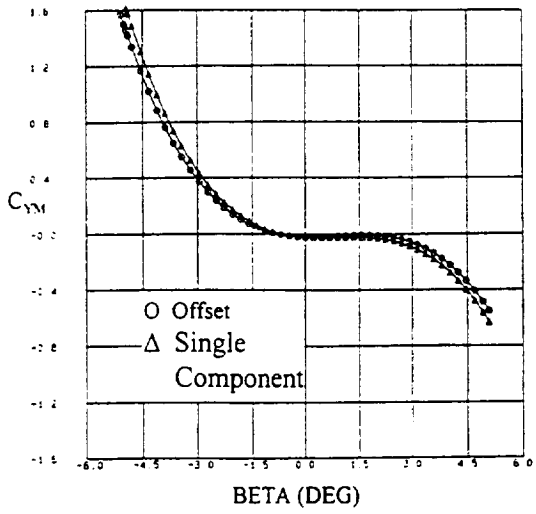

Fig. 4 : Comparison of data from offset loading and single component loading

Combined Loading : Although the offset loading discussed above gives lower standard deviations, it still suffers from insufficient accuracy when combined loads (i.e loads in both normal force and side force planes) act on the model. This is illustrated in fig.4 in which the discrepancy in data shown in fig(2) still exists. A new technique based on local linearization is proposed to handle the cases where loads act simultaneously in normal and side force planes at large distances from balance centre. This technique termed the Local Linearization Technique (LLT) had earlier been successfully adapted for wing load measurements (Ref 1).

In this method the output-load characteristics of the balance is divided into several linear segments. Axial distance of the load from the balance centre line and also the azimuthal direction of the applied load are segmented.

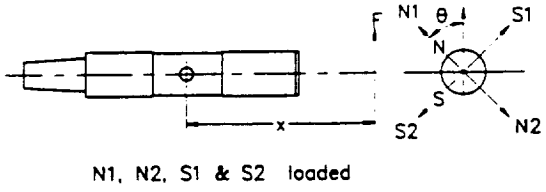

Fig. 5 Combined Loading

Let us say the balance is calibrated by applying loads (F) at various axial distances(x) and also at different orientations (θ) with respect to an identified plane (say normal force plane). From these outputs generated at known values of F, x, θ, additional outputs are evaluated by a robust interpolation scheme at several intermediate grid points in x and θ plane using the following equations.

The interpolated output at x distance is given by

$$O_{i,x} = \frac{F_{i,x} - F_{i,x-1}}{F_{i,x+1} - F_{i,x-1}} O_{i,x+1} + \frac{F_{i,x+1} - F_{i,x}}{F_{i,x+1} - F_{i,x-1}} O_{i,x-1} \quad (i=1,4)$$

Where F_i are the loads in the N_1, N_2, S_1, S_2 elements
and x is the interpolated location of loads for which outputs are desired for a given load and θ

Similarly the interpolated output at a desired θ derived from outputs available from loading at n number of θ stations is given by

$$O_{i,\theta} = \sum_{j=0}^{n} \frac{\prod_{k=0,\neq j}^{n} \sin(\theta - \theta_k)}{\prod_{k=0,\neq j}^{n} \sin(\theta_j - \theta_k)} O_{i,j}$$

Where θ is the interpolated angle for which outputs are desired at a given load and x distance,

n = number of θ stations for which outputs are acquired.

The calibration equations are now written in the following way

$0_i = a_{i1}N_1 + a_{i2}N_2 + a_{i3}S_1 + a_{i4}S_2$

(i = 1,4)

The a_i matrix (4 x 4) is determined for each cuboid as shown in Fig. 5 (F, x, θ space), using only the outputs from loadings applied at 8 corners on the cuboid.

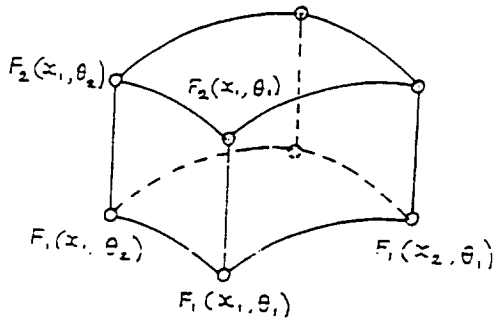

Fig. 6 F,x,θ cuboid

Several such local calibration matrices (amounting to n_f x n_x x n_0) are evaluated. Using the initial estimate of the load vector (F, x, θ) obtained from the global calibration matrix, further refined load vector is determined iteratively by the use of the local calibration matrices.

Table 3 shows a typical standard deviation of worked back loads when loads were applied in the range of 0 to 20 kg, 0 to 20 inches offset distance and eight θ' stations. It is seen that the LLT method yields the lowest value of standard deviation among the three techniques discussed above

TABLE-3

TYPICAL STANDARD DEVIATION OF WORK BACK LOADS

RELATIVE ASSESSMENT

Methodology	Standard deviation in total force (lbs)
1) Single component loading	1.59
2) Offset loading	1.45
3) Combined loading (LLT)	0.62

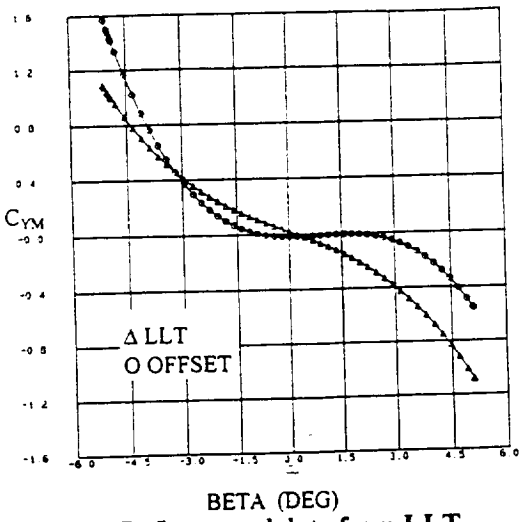

Fig. 7 : Improved data from LLT

Fig (7) illustrates the improvement in the quality of processed data. The asymmetry in C_{YM} noticed when processed using 144 constants (Fig. 1) and offset loading (Fig. 4) is completely eliminated and a symmetric data as expected is obtained using LLT.

Conclusions :

Calibration using offset loading would considerably improve the accuracies as compared to that with single component loading. However, when the model experiences loads in both the normal force and side force planes, combined loading calibration using single component loading rig adapting local linearization technique is found to improve the accuracy further. Based on the above encouraging results, efforts are underway to implement this new technique for routine measurements on long slender models at NAL.

Acknowledgements :

The authors wish to acknowledge the support provided by model shop, 1.2m Tunnel staff for fabricating the calibration body and calibrating respectively. Particular thanks to Dr. S.N. Seshadri, E. Rajagopalan, R. Mahalingam, S.P. Jagadeswarachar, R.U. Rao and P.S. Sridhar for their contribution to this work.

Reference

1. Seshadri S.N, Dutt H.N.V and Gopinath N
'New Calibration Methodology for Measurement of Normal Load on the Lifting surfaces of Aircraft Models. NAL PD NT 9222, Nov, 1992

DEVELOPMENT OF A 5-COMPONENT BALANCE FOR WATER TUNNEL APPLICATIONS*

Carlos J. Suárez, Brian R. Kramer and Brooke C. Smith
EIDETICS CORPORATION

SUMMARY

The principal objective of this research/development effort was to develop a multi-component strain gage balance to measure both static and dynamic forces and moments on models tested in flow visualization water tunnels. A balance was designed that allows measuring normal and side forces, and pitching, yawing and rolling moments (no axial force). The balance mounts internally in the model and is used in a manner typical of wind tunnel balances. The key differences between a water tunnel balance and a wind tunnel balance are the requirement for very high sensitivity since the loads are very low (typical normal force is 90 grams or 0.2 lbs), the need for water proofing the gage elements, and the small size required to fit into typical water tunnel models. The five-component balance was calibrated and demonstrated linearity in the responses of the primary components to applied loads, very low interactions between the sections and no hysteresis. Static experiments were conducted in the Eidetics water tunnel with delta wings and F/A-18 models. The data were compared to forces and moments from wind tunnel tests of the same or similar configurations. The comparison showed very good agreement, providing confidence that loads can be measured accurately in the water tunnel with a relatively simple multi-component internal balance. The success of the static experiments encouraged the use of the balance for dynamic experiments. Among the advantages of conducting dynamic tests in a water tunnel are less demanding motion and data acquisition rates than in a wind tunnel test (because of the low-speed flow) and the capability of performing flow visualization and force/moment (F/M) measurements simultaneously with relative simplicity. This capability of simultaneous flow visualization and for F/M measurements proved extremely useful to explain the results obtained during these dynamic tests. In general, the development of this balance should encourage the use of water tunnels for a wider range of quantitative and qualitative experiments, especially during the preliminary phase of aircraft design.

NOMENCLATURE

YM_1	Yawing moment section #1	YM_2	Yawing moment section #2
PM_1	Pitching moment section #1	PM_2	Pitching moment section #2
RM	Rolling moment section	Co	Root chord
$\bar{c}$	Mean aerodynamic chord	b	Wing Span
α	Angle of attack, deg	α_o	Mean angle of attack, deg
β	Sideslip angle, deg	ϕ	Roll angle, deg
Q_∞	Free stream dynamic pressure	V_∞	Free stream velocity
M	Mach number	Re	Reynolds number
C_N	Normal force coefficient	f	Oscillation frequency, Hz
C_m	Pitching moment coefficient (body axis)	a	Acceleration, deg/sec^2

* Work done at EIDETICS under SBIR Contract NAS2-13571

C_Y	Side force coefficient (body axis)	q	Pitch rate, deg/sec
C_n	Yawing moment coefficient (body axis)	ω	Angular velocity, deg/sec
C_l	Rolling moment coefficient (body axis)	k	Reduced frequency, $\frac{\pi f \bar{c}}{V_\infty}$
ω_{max}	Max. angular velocity, deg/sec	q_o	Non-dim. pitch rate, $\frac{q \bar{c}}{2 V_\infty}$
Ω	Non-dimensional rotation rate, $\frac{\omega\,[rad/sec]\,b}{2 V_\infty}$		

INTRODUCTION

Water tunnels have been utilized in one form or another to explore fluid mechanics and aerodynamics phenomena since the days of Leonardo da Vinci. Many studies (Refs. 1-6) have shown that the flow fields and the hydrodynamic forces in water tunnels are equivalent to the aerodynamic flow fields and forces for models in wind tunnels for the incompressible flow regime (i.e., Mach numbers less than 0.3). Only in recent years, however, have water tunnels been recognized as highly useful facilities for critical evaluation of complex flow fields on many modern vehicles such as high performance aircraft. In particular, water tunnels have filled a unique role as research facilities for understanding the complex flows dominated by vortices and vortex interactions. Flow visualization in water tunnels provides an excellent means for detailed observation of the flow around a wide variety of configurations. The free stream flow and the flow field dynamics are low-speed, allowing real-time visual assessment of the flow patterns using a number of techniques including dye injection, hydrogen bubbles, laser sheet illumination, etc.

Water tunnel testing is attractive because of the relatively low cost and quick turn-around time to perform experiments and evaluate the results. Models are relatively inexpensive (compared to wind tunnel models) and can be built and modified as needed in a relatively short time period. The response of the flow field to changes in model geometry can be directly assessed in water tunnel experiments with flow visualization. One of the principal limitations of a water tunnel, however, is that the low flow speed, which provides for detailed visualization, also results in very small hydrodynamic (aerodynamic) forces on the model, which, in the past, have proven to be difficult to measure accurately. In most cases where force and moment information is essential, wind tunnel tests (usually with a different model) eventually have to be performed. The advent of semi-conductor strain gage technology and devices associated with data acquisition such as low-noise amplifiers, electronic filters, and digital recording has made accurate measurements of very low strain levels feasible. The development of a system to measure the small forces and moments generated in a water tunnel would increase the usefulness of this type of research facility significantly. If the water tunnel could determine forces and moments to some level of accuracy simultaneously with the flow visualization, the interpretation of results would be greatly simplified. Also, it would be possible to quantify the changes produced by configuration modifications, conventional and unconventional control techniques, etc.

In addition to static F/M measurements, the water tunnel balance can also provide a capability for dynamic experiments. The high flow speed typical of wind tunnel tests requires rapid movement of the model in order to simulate a properly scaled dynamic maneuver and the motions are mechanically difficult to implement. The fast model movement also places demanding requirements on the response of the data acquisition system to acquire data at high sample rates. In contrast, the flow speed of water tunnel tests is typically much lower (2 orders of magnitude or more), and consequently, the model motion required to simulate a dynamic maneuver is also very slow. Thus, the response rates for data acquisition required for force and moment measurements during transient and dynamic situations are less demanding than in a wind tunnel.

The specific technical objectives of this research/development project are listed below:

1) Design and fabricate a five-component balance to measure forces and moments in a water tunnel.

2) Calibrate the balance and determine component sensitivities and interactions, i.e., determine the calibration output matrix.

3) Perform static and dynamic experiments on delta wings and F/A-18 models, and compare the results with available wind tunnel or numerical data to assess the performance of the balance.

BALANCE DESCRIPTION

Mechanical Design

Basically, the balance is similar to the sting balances used in wind tunnel tests and is located inside the model (Fig. 1). It consists of a rolling moment section, two pitching moment sections and two yawing moment sections, all 1.91 cm (3/4") in diameter. Five components will provide for the simultaneous measurement of pitching, yawing and rolling moments and normal and side forces. The moment of inertia of each section was carefully calculated in order to obtain the required stress levels that produce the desired sensitivity and resolution when the balance is loaded in the plane of interest and maximum stiffness in the other planes. Each component is attached to the next by means of two screws, and two location pins ensure the perfect alignment between components.

Strain Gages

Semi-conductor strain gages are used to get the desired output, since they are widely acknowledged as being outstanding transduction devices. The change in resistance per unit applied strain results in an output of 50 to 100 times that of either wire or foil strain gages. The gages used have a resistance of 1000 Ω and a gage factor (GF) of 145. They are very small in size, only 0.08 cm (0.03") wide by 0.4 cm (0.16") long. Each section is composed of four gages, connected using a full Wheatstone bridge and of some standard resistors added externally. These resistors are used to compensate for differences in the strain gage resistance and to compensate for temperature changes. The values of the resistors vary for each of the sections and are specified by the gaging company after extensive tests. Temperature compensation for this application is not very critical since the temperature changes during a typical water tunnel test are almost negligible. A 100 Ω potentiometer is used to balance each bridge externally when the internal potentiometer of the signal conditioner is not enough to produce a zero reading under specific loading conditions.

Water Proofing

The fact that the balance has to operate under water complicates the problem significantly, and different water proofing techniques had to be tested until the optimum was found. After the gages, terminals and wires were in place, a layer of silicon rubber was applied over the entire area

where the gages and terminals are located. The balance was later coated with Parylene™, a thin plastic film applied in a vacuum chamber. A rubber sleeve was utilized as a tertiary protection, as seen in Fig. 1.

DATA ACQUISITION/REDUCTION SYSTEM

A multi-channel system was used to provide excitation voltage (5 Volts) to the bridges, and to amplify and condition the output signals. The output lines for each channel were routed both to the digital display of the signal conditioner and to an analog-to-digital (A/D) board inside a Macintosh Quadra 700 computer.

The data acquisition/reduction software was developed specifically for this application using National Instrument's LabView, a graphical programming language. The software provides an interface that is user friendly and is versatile in its ability to reduce and display the balance and tunnel condition data efficiently. The basic methodology for the data reduction system, particularly the treatment of the balance equations, is based on the same approach used for typical wind tunnel data reduction schemes. The data acquisition/reduction software allows to perform a full balance calibration, as well as to acquire and reduce data during static and dynamic experiments. It allows the user to display "on-line" signals, acquire data at specified sampling rates and to reduce the data to coefficient form. Files with raw and coefficient data are created and saved to a disk for later plotting or reprocessing.

BALANCE CALIBRATION

A key to accurately acquiring data from an internal balance is a precise and repeatable calibration. For a multi-component balance, it is important to determine the response of each section to a load in its primary plane of action (sensitivity) and also to loads in other planes (interactions). For example, the output from a pitching moment gage will depend not only on the direct application of a pitching moment (or a normal force) but will also respond to a rolling moment or a yawing moment input. The objective is to minimize these interactive load/response characteristics, but the expense of manufacturing a balance to the tolerance levels to approach zero interactions is not warranted since the interactions can now be accounted for quite easily on modern computers. Therefore, appropriate calibration hardware, software and procedures are essential to obtain the correct sensitivities and interactions.

Calibration Rig

A simple calibration apparatus, shown in Fig. 2, was designed and built to calibrate the five-component balance. Basically, the rig consist of a main aluminum support where the sting mount and balance are attached. Pulleys on each side of the balance can be used to obtain accurate side forces and rolling moments. The pulley system permits the application of a pure rolling moment provided that low friction pulleys are used and the cables are perfectly aligned. Each pulley is mounted on a shaft between two bases that slide along a side rail. The bases can also be moved up and down, so the pulley can be accurately positioned to obtain the desired load. A loading fixture attached to the balance end is used to apply the weights at the desired load points. The loading fixture can be rotated to get the proper configuration according to the desired type of loading. The balance can also be rotated; therefore, the required loading can be obtained either by

rotating the balance or the loading fixture. Levels and stainless steel pins ensure the perfect alignment of the balance and the rig throughout the calibration process.

Calibration Results

A full calibration was performed using the calibration rig and standard procedures typical of wind tunnel sting balances. The balance was loaded at five load points with positive and negative normal and side forces, and at the balance reference center (Load Point 3, LP3) with positive and negative rolling moments. The software developed acquires and graphs the data for the different loading cases, applying a linear curve fit. After all the graphs are created, it automatically builds the calibration input matrix. By inverting the input matrix, the calibration output matrix is obtained. This matrix allows to obtain engineering units from the voltages at each section, applying all the correct sensitivities and interactions.

Figure 3 presents an example of a loading case, i.e., the response of the five channels to a normal force applied at LP4. As expected, the largest response is seen in Channel 1 (CH1), which corresponds to the most forward pitching moment section. Since the load is applied exactly at the location of the second pitching moment section (CH3), this channel does not react to this particular loading. Interactions with the rolling moment and yawing moment sections (CH0, CH2, CH4) are very small.

After all the loading cases were completed, the slopes of the output of each channel at the different load points were plotted versus the distance to said load points. Figure 4 shows one of these plots, in this case, the response of the pitching moment gauges to an applied pitching moment. The slopes of the lines (approximately 0.009 Volts/in-lb) are the sensitivity to pitching moment, while the y-intercepts are the sensitivity of these channels to a normal force. Figure 5 presents, in a similar manner, the sensitivity of the yawing moment gages to an applied yawing moment (0.026 Volts/in-lb).

The rolling moment calibration is presented in Fig. 6. Pure positive and negative rolling moments were applied at LP3, and the output at the gages in Volts is plotted versus moment for the five channels. The response of the rolling moment component (CH2) is linear, both for the positive and negative cases. The slope of this line represents the sensitivity of the section to rolling moment, i.e., -0.0097 Volts/in-lb (average of the slopes of the positive and negative loading cases). Interactions with the other sections are negligible.

Hysteresis was also investigated to complete the calibration. The balance was loaded and then unloaded using the same weight increments. All possible loading cases were investigated, i.e., positive and negative side and normal forces, and positive and negative rolling moments. The balance showed no hysteresis on any of the channels under primary loads.

EXPERIMENTAL SETUP

Water Tunnel

All experiments were conducted in the Eidetics Model 2436 Flow Visualization Water Tunnel. The facility is a continuous horizontal flow tunnel with a test section 0.91 m (3 ft) high x 0.61 m (2 ft) wide x 1.83 m (6 ft) long. The model is mounted inverted, and it is possible to test at angles of attack between 0° and 65°, and at sideslip angles between -25° and 25°.

Models

A 70° flat plate delta wing and F/A-18 models were used for these experiments. The aluminum delta wing (Fig. 7) has a root chord of 15 inches and a double-beveled leading edge. The balance is located at the model centerline and two fiberglass fairings (top and bottom) covered the entire balance. The 1/32nd-scale F/A-18 model is shown in Fig. 8. The reason for choosing the F/A-18 was the availability of data from several wind tunnel tests on this configuration that could be used for direct comparison to evaluate the performance of the balance. The plastic model is equipped with dye ports for flow visualization and the balance is attached to an internal aluminum plate. Control surfaces were fixed at 0° throughout the entire test (leading edge flaps were fixed at 34°). The rotary balance experiments were performed on a 1/48th-scale F/A-18 due to size constraints in the water tunnel. The width of the test section (24 inches) did not allow the use of the 1/32nd-scale F/A-18 model utilized for the other dynamic experiments. The smaller plastic model has a span of 10 inches and a total length of 14 inches. Moments are referenced to the 50% $\bar{c}$ on the delta wing and to the 25% $\bar{c}$ on the F/A-18 models, except when indicated.

STATIC WATER TUNNEL EXPERIMENTS

Methodology And Boundary Corrections

The static tests were performed following standard "wind tunnel procedures". The gages were zeroed at the beginning of each run with the model at $\alpha = \beta = \phi = 0°$. A static tare (or weight tare) was performed before the actual run. This consists of an angle of attack sweep with the tunnel off ($Q_\infty = 0$) to account for gravity effects. After that, the model is always returned to $\alpha = 0°$, a zero point is taken and the tunnel is started.

The water tunnel data were corrected only at high angles of attack. This correction is required as a result of a significant expansion of the wake when the wing stalls and it was developed by Cunningham (Ref. 5). It is a semi-empirical relationship based only on planform blockage and angle of attack. Equations in Ref. 5 are given only for C_N; however, since this is actually a Q_∞ correction, it was also applied to the other components in a similar manner. The correction is applied starting at $\alpha = 38°$ for the delta wings and at $\alpha = 40°$ for the F/A-18 (approximate stall angles for each configuration). Figure 9 shows uncorrected and corrected data for the 70° delta wing at zero sideslip, with the largest changes occurring in the normal and side forces.

Examples of Static Test Results

Most of the static experiments were conducted at velocities ranging from 12.7 cm/sec (0.42 ft/sec) to 17.8 cm/sec (0.58 ft/sec). This range of velocities corresponds to Reynolds numbers from 34,000 to 47,000 per foot. Data were acquired at 100 samples/sec for 25 seconds and were not filtered. The large number of samples acquired permitted to obtain a mean value that represents the average gage reading at that particular loading condition.

The longitudinal characteristics of the 70° delta wing during static conditions are presented and compared to wind tunnel data in Fig. 10. The water tunnel data (obtained at $V_\infty = 0.58$ ft/sec) are compared to similar data obtained in another water tunnel (Ref. 5), and in the KU 3x4' wind tunnel (Ref. 7), the WSU 7x10' wind tunnel (Ref. 8) and the Langley 12' wind tunnel (Ref. 9). The normal force coefficient agrees very well with most of the data, except for the Langley data. The differences between these data and the other wind tunnel data are quite significant and are probably due to the type of corrections applied, mounting system, flow quality, etc. Since the software provided the moments referenced to the 50% $\bar{c}$, the appropriate transformations had to be applied to obtain C_m at other locations. The pitching moment at 30% $\bar{c}$ is compared to two sets of wind tunnel data and the agreement is satisfactory.

Figure 11 shows a comparison between the water tunnel test and other wind tunnel tests for the baseline F/A-18. Angle of attack sweeps at $\beta = 0°$ were performed and the agreement in C_N is very good, both in slope and absolute magnitude. The data obtained in the water tunnel match not only other small-scale wind tunnel tests (Refs. 10-12), but the full-scale test at the NASA Ames 80x120' (Ref. 13) and the F/A-18 Aero Model used in simulation as well. Only one data set (Langley 12', Ref. 12) has much lower values than those obtained in this test. The pitching moment measurements also agree well with other data; small differences are seen between 45° and 55° angle of attack, but trends and slopes are very similar. Lateral/directional characteristics were compared to data from Ref. 11, as seen in Fig. 12, and similarities in the C_Y and C_l curves during β sweeps at $\alpha = 30°$ are evident. It should be noted that corrections due to wall proximity during sideslip sweeps were not introduced in the data reduction scheme, and therefore, small discrepancies can be expected. These comparisons show that the balance can be used effectively to measure five components of the forces and moments experienced by a "real" configuration (as opposed to "generic", as in the case of the delta wing) in this flow regime. For more information and examples on water tunnel static tests, please see References 14 and 15.

DYNAMIC WATER TUNNEL EXPERIMENTS

Methodology And Boundary Corrections

The motion rates selected for the dynamic tests conducted in the water tunnel should, of course, be scaled properly to represent the correct relationship between rotation rate, scale, and free stream velocity. During the dynamic experiments, the data are corrected at high angles of attack with the same technique utilized during the static water tunnel experiments (Refs. 5, 14 and 15). A weight tare ($V_\infty = 0$) is performed to account for gravity effects as in the static tests. The software handles the entire data acquisition and reduction processes, as well as the model motion. In order to correlate the F/M measurements with the model position, the software takes an encoder reading, then acquires the balance data, takes a second encoder reading and assigns the balance values to the average of the two encoder readings. The number of balance samples acquired between each encoder reading can be varied, and the final value for each channel is the arithmetic average of the samples taken. As expected, the larger the number of samples acquired, the better the quality of the data. It was found that by acquiring 800/1,000 per channel, the data obtained are very smooth and repeatable, requiring no post-processing or curve-fitting and clearly indicating the value of the force/moment at the particular model location. Since the A/D board used allows acquiring data very fast (10,000 samples per second), it was possible to take a large number of samples per channel and still obtain an adequate density of points (again, the low motion rates required in the water tunnel facilitate these experiments). For the rotary balance tests, data were acquired and

averaged over two revolutions to avoid excessive twisting of the cables (no slip-ring was used). A weight tare ($V_\infty = 0$), also averaged over exactly two revolutions, was performed at each angle of attack and subtracted from the "tunnel on" data.

Effect Of Inertial Tares

One of the unknowns in dynamic water tunnel experiments was the model inertia effects on the data, i.e., the effect of the resistance to motion due to the model mass moment of inertia. Before actually performing the experiments, it was calculated that the inertia contribution to the aerodynamic values to be measured would be small, because of the low motion rates used in the water tunnel. The inertia effects are determined by measuring the time-variant moment recorded by the balance with the model in motion with the tunnel velocity at zero. This motion must be identical to the motion generated with the tunnel on ($V_\infty > 0$). The aerodynamic contribution is determined by subtracting the measured moment at $V_\infty = 0$ from the moment measured at $V_\infty > 0$.

Results indicate that the inertial contribution is, indeed, very small. Figure 13a shows the measured normal force on the 70° delta wing during a ramp-hold maneuver from 15° to 60° angle of attack. The value of the normal force N (lbs) measured during the pitch-up motion when the water tunnel is off ($V_\infty = 0$) is almost negligible, approximately 1% of the value measured with tunnel speed. Also included in Fig. 13a is the value of the normal force measured during the specified motion with no water in the tunnel. The value of N throughout the dynamic maneuver under the "no water" condition is very similar to the $V_\infty = 0$ case, indicating that there are no major "virtual mass effects" (resistance of the surrounding water to being displaced by the moving model). Similar results were obtained during pitch oscillations with the F/A-18 models (Fig. 13b), and during the other dynamic experiments (yaw and roll oscillations, rotary balance tests). Therefore, depending on the quality of the data required, the inertia effects can be ignored, facilitating the testing and the data reduction process.

Examples of Dynamic Test Results

Pitch Oscillations (70° Delta Wing Model)

The first set of dynamic experiments consisted of large-amplitude pitch oscillations about a mean angle of attack α_0. The purpose of these tests was to directly compare the water tunnel data to results from wind tunnel tests conducted at NASA Langley by Brandon and Shaw, where a 70° wing was investigated for forces and moments produced by these large-amplitude pitch motions (Ref. 16). Figure 14 presents changes in the normal force coefficient produced by oscillating the delta wing ±18° about different α_0's with a reduced frequency k = 0.0376. This k value corresponds to a maximum full-scale pitch rate of approximately 60 deg/sec for a typical fighter aircraft at altitude and at $V_\infty = 200$ ft/sec. The hysteresis loops are evident in the force measurements, with all the cases producing similar values of C_N overshoot. Results from the wind tunnel tests in Ref. 16 are shown in the same figure and the similarities in the two data sets can be clearly identified. The level of C_N is slightly lower in the wind tunnel test, especially above 25°, but the shape of the dynamic loops and the relative increments are very similar in both tests.

Pitch-Up/Down And Hold Maneuvers (F/A-18 Model)

Experiments on the 1/32nd-scale F/A-18 model included pitch-up/down and hold maneuvers. The model rotates about the 25% $\bar{c}$, and the motions are basically constant rate ramps. Figure 15 presents results for pitch-up and hold motions from 15° to 65° angle of attack for different non-dimensional pitch rates q_o. The normal force and pitching moment data show a dependency on pitch rate, as reported by Brandon and Shaw in Ref. 17. This set of experiments was completed with pitch-down and hold maneuvers at different rates. The maneuver consisted of pitching down the F/A-18 model from 65° to 15° angle of attack. The motion profiles for the pitch-up and hold maneuvers, along with the variation of the normal force coefficient with time, are illustrated in Fig. 16. The "persistence" in normal force, defined as the time it takes the force to reach its steady or static value from the moment the motion stopped, is clearly observed. Figure 17 shows the motion profiles and the change in the normal force coefficient versus time for the pitch-down and hold maneuver. It is very interesting to notice that, contrary to the behavior observed during the pitch-up maneuvers in terms of persistence, by the time the model stops after the pitch-down, the value of the normal force is almost the same as the static value, denoting a very small or almost zero persistence. The persistence in C_N, in terms of convective time units, is compared to data from the wind tunnel experiments (Ref. 17) in Fig. 18. A convective time unit is the time it takes one particle in the free stream to travel a distance equal to the mean aerodynamic chord on the model. The similarities between the results from the two experiments are quite evident, indicating similar flows and dynamic force/moment responses.

Rotary-Balance Experiments (F/A-18 Model)

Another important maneuver for present and future aircraft is the "loaded roll" or rolling around the velocity vector at medium to high angles of attack. In the wind tunnel, rotary-balances are used to acquire force and moment data from an internal balance with the model rotating around the velocity vector at varying rotation rates. With the balance, the water tunnel can provide a simplified version of the same type of test capability with the added benefit of being able to observe the behavior of the flow at the same time. The rig consists of an aluminum C-strut that attaches to the roll mechanism and the water tunnel main C-strut (Fig. 19). The angle of attack is changed manually by sliding the arm along the C-strut, allowing testing at angles of attack between 0° and 60°. Once the desired α is obtained, the arm is fixed in position. Sideslip can be varied by rotating the sting in the adapter located at the end of the arm.

As in the other dynamic experiments, it was found that the inertial effects on the data were negligible, and thus, the rotary tare can be performed at any rotation speed. These particular rotary-balance experiments were performed for non-rotational rates Ω up to ± 0.15 and the rotary tares were always conducted at rates corresponding to $\Omega = 0.10$. Data from the water tunnel rotary-balance tests correspond to runs at 0.42 ft/sec and 0.58 ft/sec (Reynolds number of 8,200 and 11,500, respectively). These data are compared to results from a rotary-balance test performed by Eidetics on a 6%-scale F/A-18 in the NASA Ames 7x10' wind tunnel (Ref. 18), and from a test of a 1/10-scale F-18 model at the Langley Spin Tunnel (Ref. 19). Results of F/M measurement at $\alpha = 50°$, presented in Fig. 20, reveal that the normal force coefficient has a similar behavior in all the tests, i.e., a slight increase with rotation rate. The agreement in the lateral/directional coefficients is quite acceptable. Evidently, the forebody vortex flow fields in the water and wind tunnel experiments present opposite asymmetries, as indicated by the side force value at $\Omega = 0$, but the anti-spin slope is similar in both tests. The yawing moment coefficient obtained in the water tunnel presents a smaller slope than that revealed by the wind tunnel results, especially for negative

rotations, denoting again a possible slight shift in the center of pressure. The anti-spin behavior, however, is still present. For more information and examples of water tunnel dynamic experiments, see Ref. 20.

CONCLUSIONS

A five-component balance was designed, built and tested in the Eidetics' water tunnel. The balance was calibrated and showed good linearity and low interactions. Results of static experiments were quite satisfactory, showing good correlation with wind tunnel data of similar configurations (delta wings and F/A-18 models). This research/development project also explored the use of the balance to perform dynamic experiments in the water tunnel. Among the advantages of conducting dynamic tests in a water tunnel are less demanding motion and data acquisition rates than in a wind tunnel test (because of the low-speed flow) and the capability of performing flow visualization and force/moment measurements simultaneously with relative simplicity. Dynamic experiments included pitch, yaw and roll oscillations, pitch-up/down and hold maneuvers and rotary-balance tests. Results obtained in these tests also compared well with wind tunnel data.

In general, results obtained in this research/development project show conclusively that water tunnels can be used effectively for quantitative and qualitative measurements and emphasizes the importance of having the capability of performing simultaneous flow visualization and F/M measurements.

ACKNOWLEDGMENTS

This study was partially supported by NASA Dryden Flight Research Center under SBIR Phase II Contract No. NAS2-13571. The technical monitor was Mr. John Del Frate.

REFERENCES

1. Erickson, G. E., Peake, D. J., Del Frate, J., Skow, A. M., and Malcolm, G. N., "Water Facilities in Retrospect and Prospect - an Illuminating Tool for Vehicle Design", NASA TM 89409, November 1986.

2. Deane J. R., "Wind and Water Tunnel Investigations of the Interaction of Body Vortices and the Wing Panels of a Missile Configuration," AGARD CP-2467, Jan. 1979.

3. Thompson, D. H., "A Water Tunnel Study of Vortex Breakdown Over Wings with Highly Swept Leading Edges," ARL/A-Note-356, Melbourne, May 1975.

4. Davies, A. G., "A Comparative Study of Vortex Flows in Wind and Water Tunnels", presented at the AGARD Fluid Dynamics Panel Symposium on Aerodynamic and Related Hydrodynamic Studies Using Water Facilities, October 1986.

5. Cunningham, A., "Steady and Unsteady Force Testing of Fighter Aircraft Models in a Water Tunnel," AIAA-90-2815, presented at the AIAA 8th Applied Aerodynamics Conference, Portland, Oregon, Aug. 20-22,1990.

6. Malcolm, G.N., Nelson, R.C., "Comparison of Water and Wind Tunnel Flow Visualization Results on a Generic Fighter Configuration at High Angles of Attack," AIAA Paper

87-2423, presented at the AIAA Atmospheric Flight Mechanics Conference, Monterey, CA, Aug. 1987.

7. Wentz, W. H. Jr., "Wind Tunnel Investigations of Vortex Breakdown on Slender Sharp-Edged Wings", Ph.D. Dissertation, University of Kansas, Lawrence, KS.

8. Phillis, D.L., "Force and Pressure Measurements Over a 70° Delta Wing at High Angles of Attack and Sideslip," Master Thesis, Aeronautical Engineering Department, The Wichita State University, 1991.

9. Brandon, J. M. and Shah, G. H., "Effect of Large Amplitude Pitching Motions on the Unsteady Aerodynamic Characteristics of Flat-Plate Wings", AIAA Paper No. 88-4331, presented at the Atmospheric Flight Mechanics Conference, August 15-17, 1988.

10. Kramer, B. R., Suárez, C. J., Malcolm, G. N. and Ayers, Bert F., "F/A-18 Forebody Vortex Control", Eidetics TR-93-003, Volume I (Static Tests), April 1993.

11. Erickson. G. E., Hall, R. M, et. al., "Experimental Investigation of the F/A-18 Vortex Flows at Subsonic Through Transonic Speeds", AIAA Paper 89-2222 (invited), presented at the AIAA 7th Applied Aerodynamics Conference, Seattle, WA, 1989.

12. Brandon, J. M. and Shah, G. H., "Unsteady Aerodynamic Characteristics of a Fighter Model Undergoing Large-Amplitude Pitching Motions at High Angles of Attack", AIAA Paper No. 90-0309, 28th Aerospace Sciences Meeting, January, 1990, Reno, Nevada.

13. Lanser, W. R., Murri, D. G., "Wind Tunnel Measurements on a Full-Scale F/A-18 With Forebody Slot Blowing or Forebody Strakes", AIAA Paper 93-1018, presented at the AIAA/AHS/ASEE Aerospace Design Conference, Irvine, CA, 1993.

14. Suárez, C.J., Ayers, B.F., and Malcolm, G.N., "Force and Moment Measurements in a Flow Visualization Water Tunnel", AIAA 94-0673, presented at the AIAA 32nd Aerospace Sciences Meeting, Reno, Nevada, Jan. 1994.

15. Suárez, C.J. and Malcolm, G.N., "Water Tunnel Force and Moment Measurements on an F/A-18", AIAA 94-1802, presented at the AIAA 12th Applied Aerodynamics Conference, Colorado Springs, CO, June 1994.

16. Brandon, J.M. and Shah, G.H., "Effect of Large Amplitude Pitching Motions on the Unsteady Aerodynamic Characteristics of Flat-Plate Wings," AIAA Paper 88-4331, presented at the Atmospheric Flight Mechanics Conference, August 15-17, 1988.

17. Brandon, J.M. and Shah, G.H., "Unsteady Aerodynamic Characteristics of a Fighter Model Undergoing Large-Amplitude Pitching Motions at High Angles of Attack", AIAA Paper No. 90-0309, 28th Aerospace Sciences Meeting, January, 1990, Reno, Nevada.

18. Kramer, B.R., Suárez, C.J., Malcolm, G.N. and James, K.D., "Forebody Vortex Control on an F/A-18 in a Rotary Flow Field," AIAA Paper 94-0619, presented at the 32nd Aerospace Sciences Meeting, Reno, NV, 1994.

19. Hultberg, R., "Low Speed Rotary Aerodynamics of F-18 Configuration for 0° to 90° Angle of Attack - Test Results and Analysis," NASA Contractor Report 3608, August 1984.

20. Suárez, C.J. and Malcolm, G.N., Dynamic Water Tunnel Tests for Flow Visualization and Force/Moment Measurements on Maneuvering Aircraft", AIAA 95-1843, presented at the AIAA 13th Applied Aerodynamics Conference, San Diego, CA, June 1995.

FIGURES

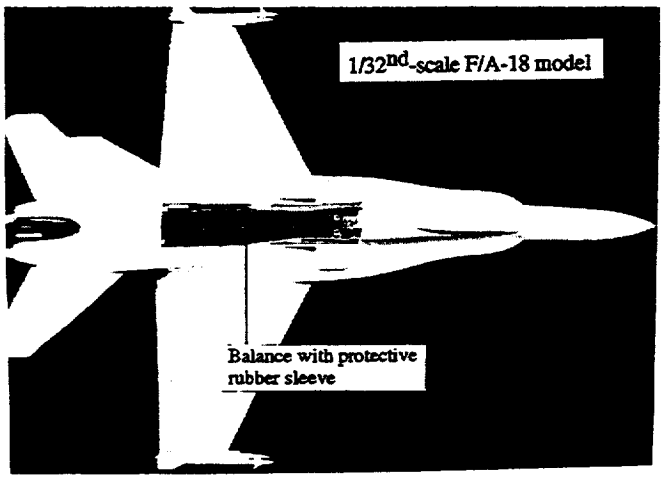

Figure 1 - Water Tunnel Balance Shown in the 1/32nd Scale F/A-18 Model

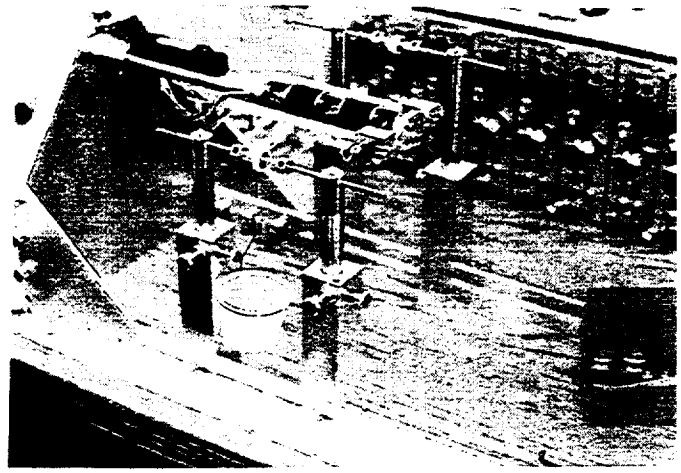

Figure 2 - Calibration Rig

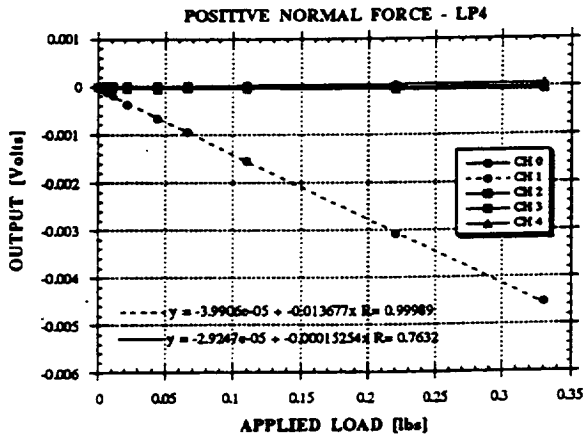

Figure 3 - Balance Response to a Positive Normal Force

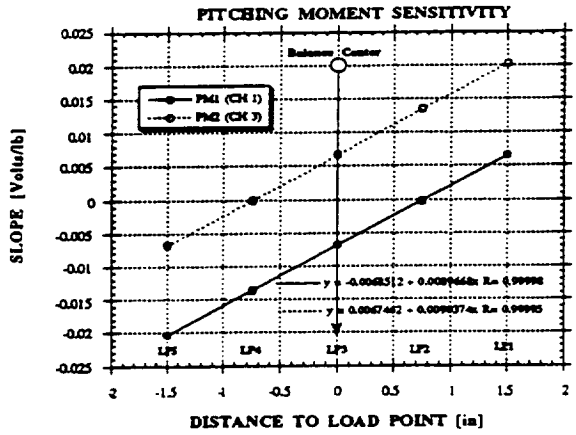

Figure 4 - Pitching Moment Sensitivity

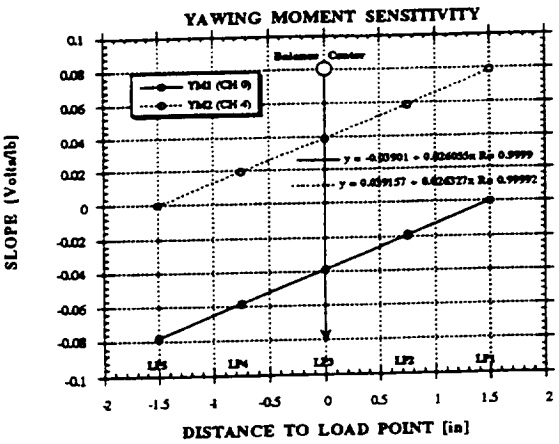

Figure 5 - Yawing Moment Sensitivity

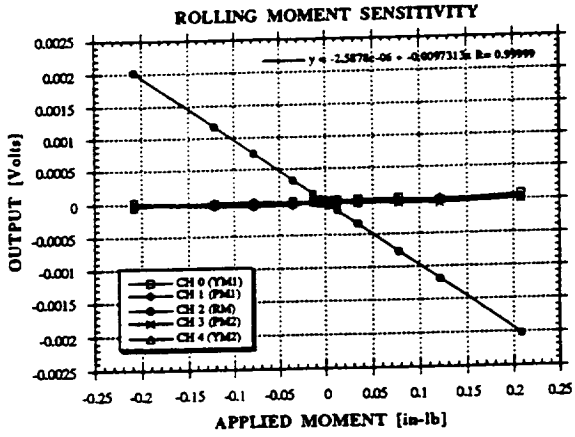

Figure 6 - Rolling Moment Sensitivity

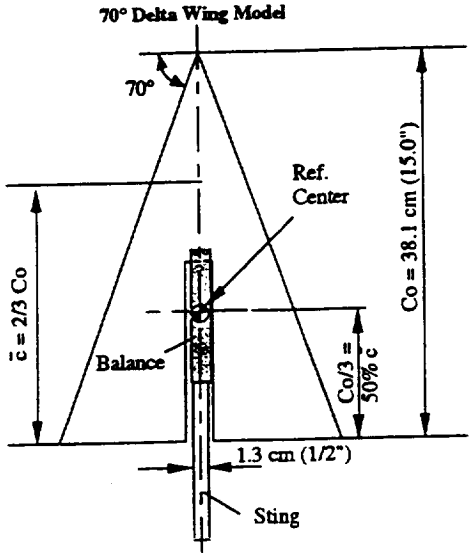

Figure 7 - 70° Delta Wing Model

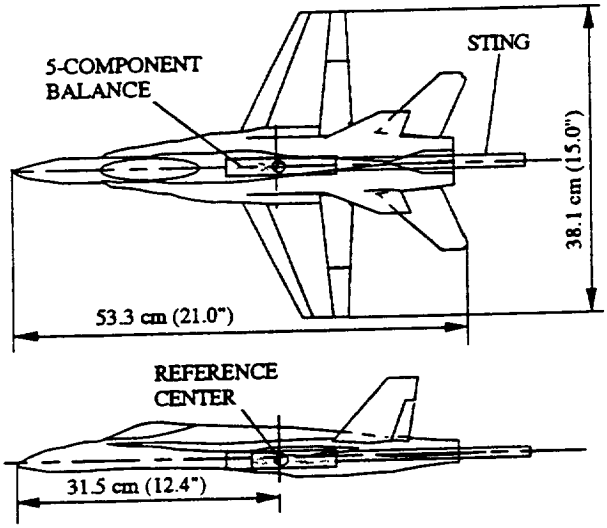

Figure 8 - 1/32nd-Scale F/A-18 Model

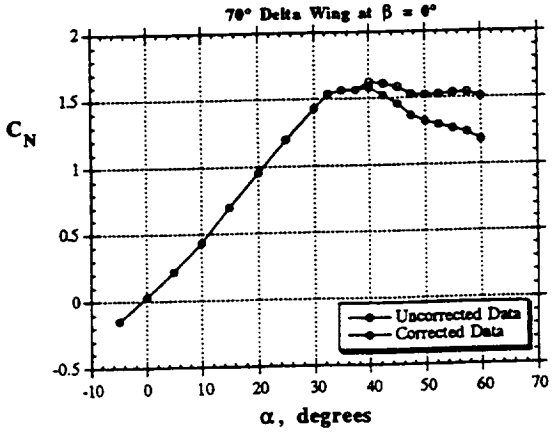

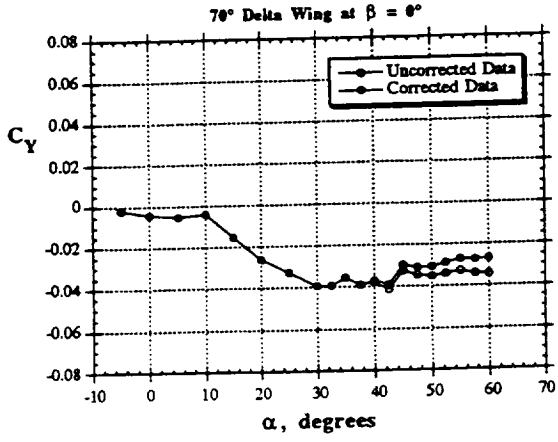

Figure 9 - Effect of Boundary Corrections on Forces (70° Delta Wing)

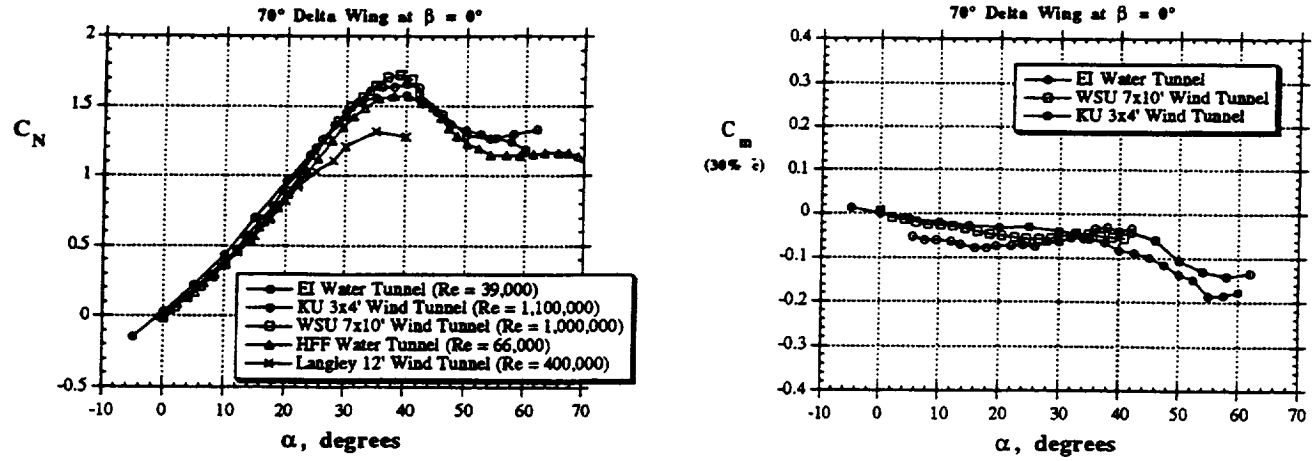

Figure 10 - Longitudinal Characteristics of the 70° Delta Wing

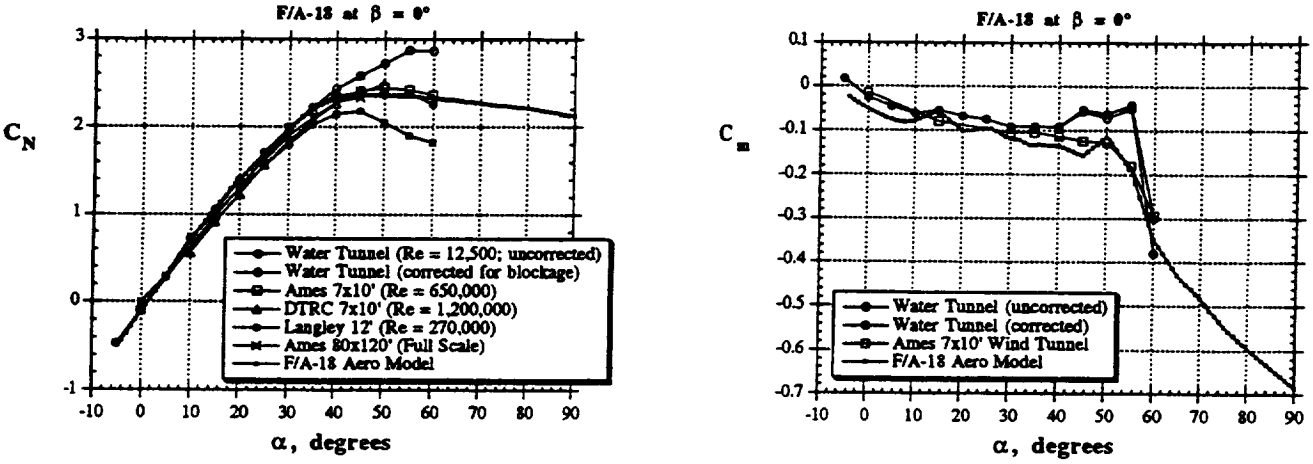

Figure 11 - Longitudinal Characteristics of the F/A-18 Model

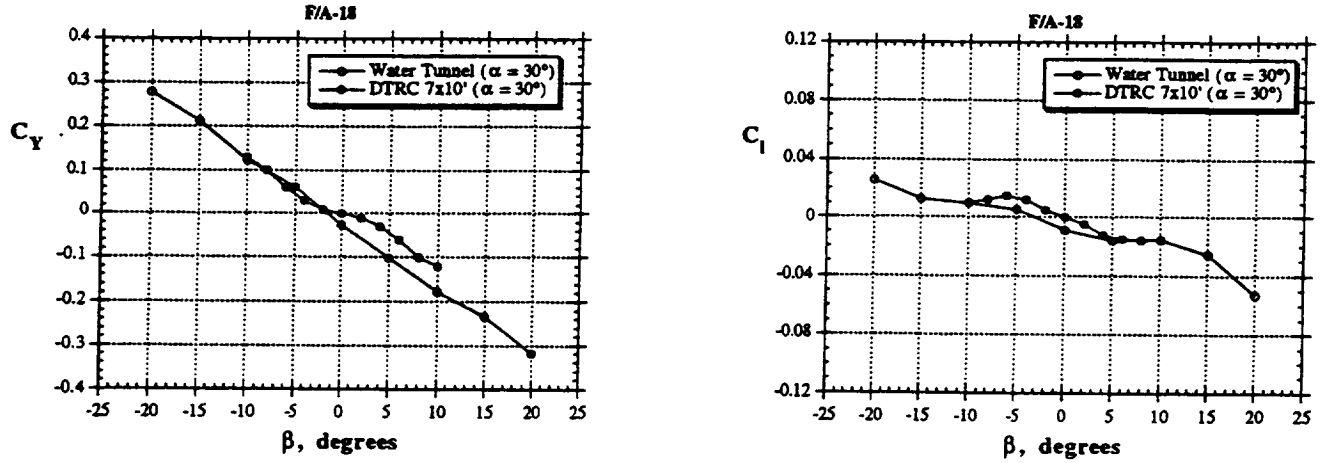

Figure 12 - Lateral/Directional Characteristics of the F/A-18 Model at $\alpha = 30°$

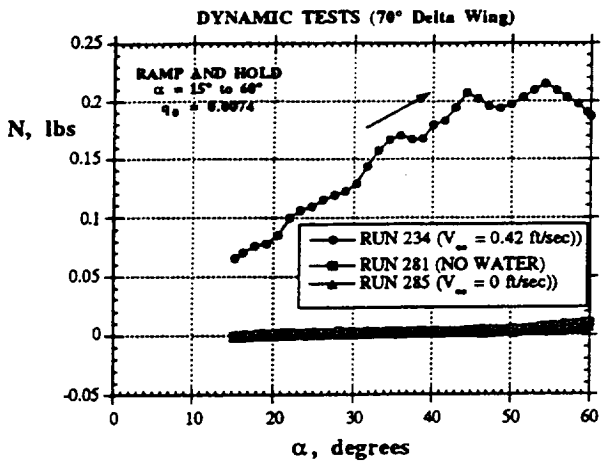

a)

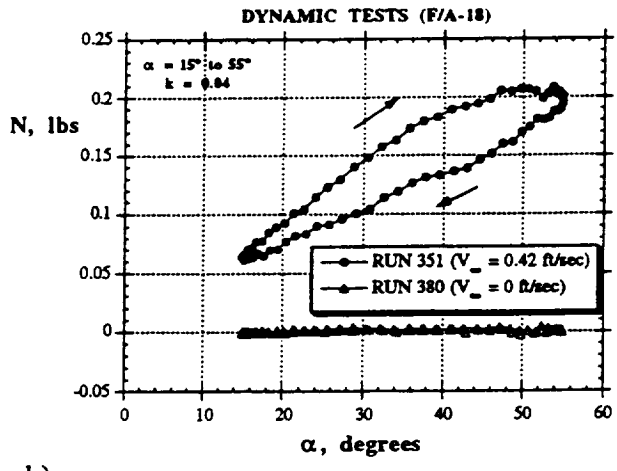

b)

Figure 13 - Inertial Tares During Pitch Maneuvers

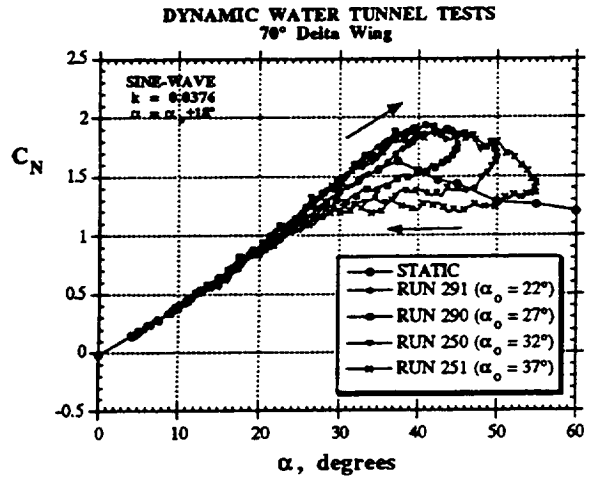

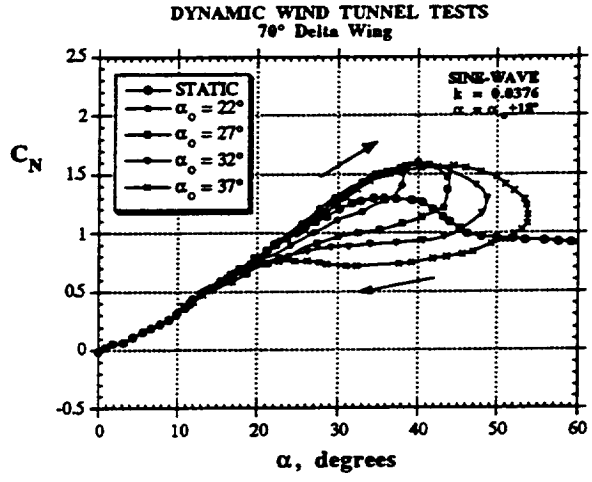

Figure 14 - C_N Variations During Pitch Oscillations about Different Mean Angles of Attack

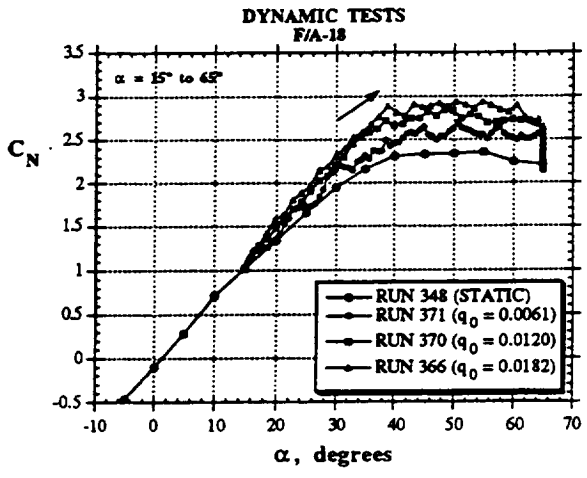

Figure 15 - Pitch-Up and Hold Maneuver

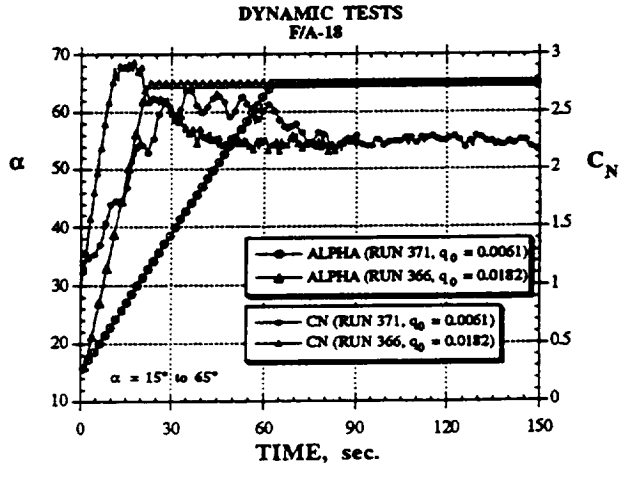

Figure 16 - Pitch-Up and Hold Maneuver

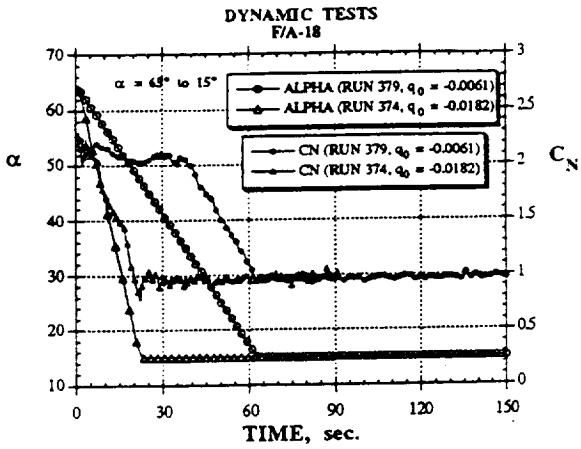

Figure 17 - Pitch-Down and Hold Maneuver

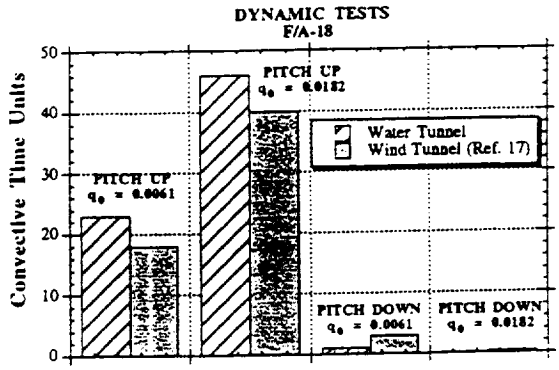

Figure 18 - Persistence of Normal Force

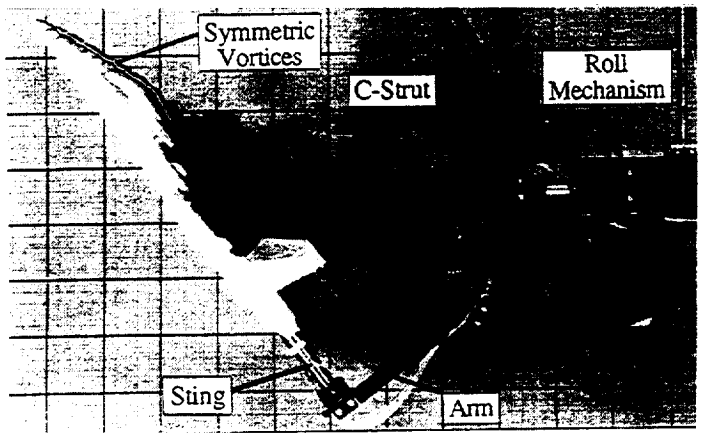

Figure 19 - Rotary-Balance Rig

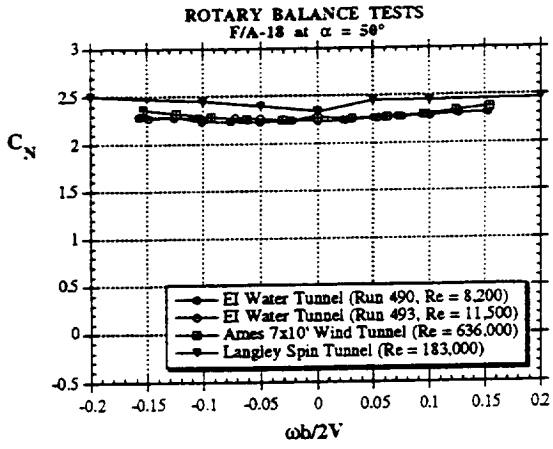

Figure 20 - Rotary-Balance Tests at $\alpha = 50°$

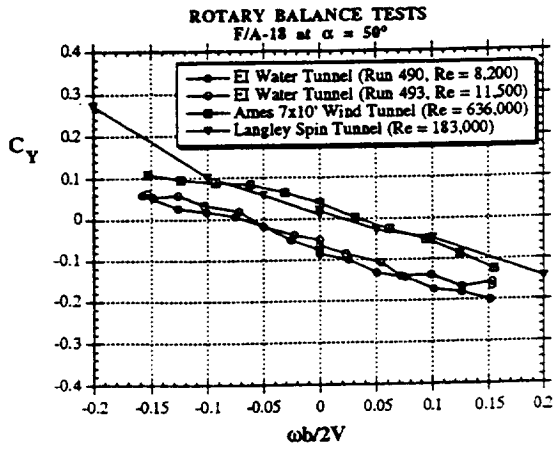

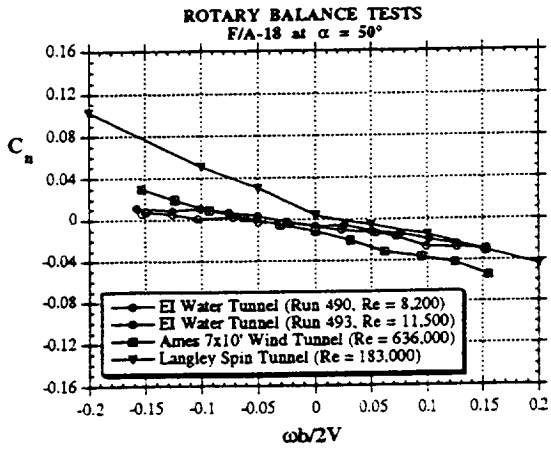

Figure 20 - Continued

DEVELOPMENT AND APPLICATION OF MICROBALANCE IN HYPERSONIC LOW DENSITY WIND TUNNEL

Tang Zhigong Yang Yianguang
China Aerodynamics Research & Development Center

ABSTRACT

This paper summarized the study of aerodynamic measuring technique in Hypersonic Low Density Wind Tunnel (HLDWT) of CARDC, and described the development and application of microbalance, and discussed the directions of development of microbalance in HLDWT.

INTRODUCTION

HLDWT is a effective land facility in simulating the flight status and condition of space vehicle at high altitude and speed. It's mainly use for aerodynamic and aerothermodynamic and testing for space vehicle.

HLDWT in CARDC is the largest of this kind in China, which has a nozzle with it's exit diameter is 300mm. It's applied to simulate the fight statue of vehicle at altitude of 60 ~94 km, Much number ranges from 5 to 24, and the total temperature of front stream may reach 1700K.

There are some kinds of balances and techniques used in HLDWT aerodynamic testing: strain-gauge balance, deferential transfer balance, electric microbalance, free-flight aerodynamic force testing technique and suspension balance assembly.

CHARACTERS OF AERODYNAMIC MEASUREMENT IN HLDWT

The characters of aerodynamic testing in HLDWT are as follows: Small models and small force load, interference of shake, temperature and pressure to the balances are serious. It's requirements to microbalance in test are almost the same in some respects as to that in ordinary hypersonic tunnel and transonic tunnel, such as good characters of linearity, accuracy and repeatability, low hysteresis and low draft and low interference among the components of balance. And especially, it must be more sensitive to aerodynamic load, and have better suppression to various kinds of interference. In this case some special technique must be adapted in the design and calibration of this kinds of microbalances.

High Sensitivity

Because of the low aerodynamic load, small models and wide range of attack angle, the balance used in HLDWT must have high sensitivity. For example, the aerodynamic load in this test of simulating the altitude of 90km on a blunt-nosed conical model with rear diameter of 6mm is only 0.2g. It's due to the small size of the model, low flowing density and low dynamic pressure.

Effects of Interference

Many factors effect the result accuracy of aerodynamic testing in HLDWT: Shake of the tunnel, model support interference and the own weight of the model. To high sensitivity balance, the components should be very flexible to sense the aerodynamic. At the same time, it maybe disturbed by same factors of interference also. It's harmful to the improving of accuracy.

Effects of Ambient Parameters

There are mainly temperature effects and pressure effects in aerodynamic testing. On one hand, the range of total temperature of the free stream in HLDWT of CARDC is 600~900K usually, and maybe as high as 1700K in some testing. On the other hand, the pressure in the test section is below 10^{-2}mmHg usually. Temperature effect and pressure must be considered in the designing of microbalance.

In a word, the following factors must be considered in the designing of microbalance: High sensitivity, accuracy and capability of interference resistance, as well as simple structure, easy to work, calibrate and use.

DEVELOPMENT AND APPLICATION OF MICROBALANCE

The two and three component balance in HLDWT of CARDC are all external balances at present. There are two model supporting methods for two component balance: Standing support and rear support (Fig.2), and the can be changed to each other while all components of balance rotate a certain angle at the same time. It's mainly standing support for three component microbalance (Fig.4). The advantages of standing support method is that the elements of balance are beyond the flow field. It's easy to suppress the effect of temperature, and applicable to aerodynamic testing range of attack angle (0°~180°).

High sensitivity may be achieved by mains of enlarging the strains of microbalance elements. The elements of balance may be more sensitive to aerodynamic load when they get

thinner enough. But it's sensitive to the signal of tunnel shake also and difficult to work. Another method is using semiconductor strain-gauges to improve the sensitivity of balance, but it's hard get rid for the interference of shaking, effects of temperature and pressure.

The two and three components microbalance in HLDWT of CARDC get high sensitivity by adopting lever-multiplied torsion elements which are made of aluminum. The two component balance is made up of two torsion elements by combining them together perpendicularly (Fig.3). The balance measures the aerodynamic load by the force to multiply the actuating arm of the lever. The torsion elements used in this type of balance are typical fore-measuring elements and we can simplify the formula by just considering the displacement strain but ignoring the others:

$$\varepsilon_{max} = -\frac{3NLl}{4Ebhr} \qquad (1)$$

where: E ---- Elastic modules of aluminum;
N ---- Value of aerodynamic load;
r ---- Distance between the beams and the center of element;
L ---- Distance between the model and the center of element;
l ----Length of the elastic beam;
b ----Thickness of the elastic beam;
h ----Width of the elastic beam.

The strain of elements which caused by the action of certain load will be enlarged when L be enlarged and b, h reduced properly, then the sensitivity of balance will be improved. There is less temperature effect because of putting the elements of balance protected by a shell out the flowing field. There are more room on the elastic beams of elements for more strain-gauges. It's convenient to get high output signal and easy to work. There are two mains to prevent the balance being disturbed by the shake of the tunnel: (1)Reduce the moment to the centroid of torsion element which caused by the weight on the ends of the support sting to zero by adjust the additional weight on one end of the sting; (2)Reduce the weight of the balance and models as possible. The three component microbalance is made by adding a torsion element onto the axis and lift elements of a two components balance. The principle is similar to two component balance.

There are some differences in the calibration between microbalance and normal balance. In the calibration of microbalance, the balance be calibrated with model. Model is amounted on the balance, and the loading device is connected to the model directly . It's a friction-free fiber suspension system. In static calibration we get coefficients of the balance by single-component calibration method; And testify the result by the multicomponent loading test to acquired the sensitivity, accuracy of the balance. In dynamic calibration, models of ball, blunt-nosed conical and conical have been used. Table 1 give out the calibration results of two microbalance.

High sensitivity microbalances of CARDC have simple structure, and suitable to testing of wide ranges of attack angle. Fig.5 and Fig .6 give out the testing results for models of ball and sharp conical.

DIRECTIONS OF DEVELOPMENT

The method of standing support is advanced to high sensitivity microbalance in improving sensitivity and resist interference, and it's more convenient to aerodynamic testing of high attack angle. But on the other hand, there are many factors affecting correctness of data acquired in testing. The model support interference is disadvantageous to the aerodynamic testing at low attack angle, and the test result of load must be adjusted by the results of model support interference testing and aerodynamic testing of support sting. For example of drag A:

$$A = 2A_1 - A_2 - A_3 \qquad (2)$$

where: A ---- Adjusted value of drag;
A_1--- Value of drag before adjustment;
A_2--- Value of drag acquired from testing which have a couple of mirroring-stings;
A_3--- Drag of sting.

The certainty of the results acquired from standing-support balance is not so good as from rear-support balance. The result of a series of comparing test in which the same model be used shows that the system error is about 2%. The directions of development of microbalance in HLDWT are high sensitivity, high accuracy and rear-support. Another direction is to develop magnetic suspension balance system.

There are less model support interference when rear-support balance be used. But the structure of balance must be temperature-resisted. There are two methods mainly being used: Water-cooled and heat-insulated, and there are still some problems to be solved.

Table.1 Parameter of Balance

Balance	component	Load Range (g & g mm)	Accuracy of Static Calibration	Accuracy of Dynamic Calibration	Accuracy (g, g mm/mv)
Two Components	Drag A	≥ 0.1	≤ 0.5%	1~2%	0.245
	Lift N	≥ 0.1	≤ 0.5%	1~2%	0.245
Three Components	Drag A	≥ 0.2	≤ 0.5%	1~2%	1.8
	Lift N	≥ 0.2	≤ 0.5%	1~2%	1.1
	Pitching Moment	≥ 5	≤ 1	2%	38.2

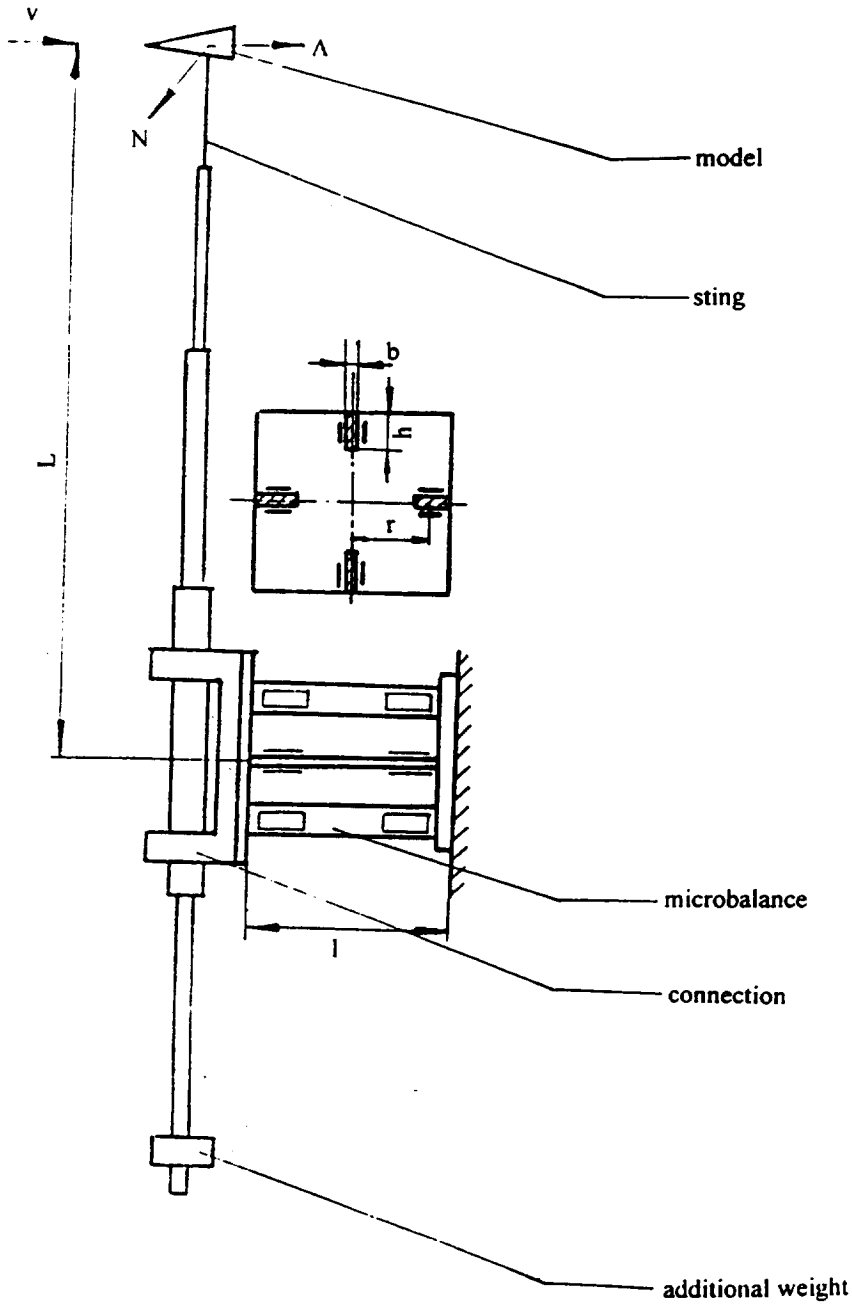

Fig.1 Design of element structure

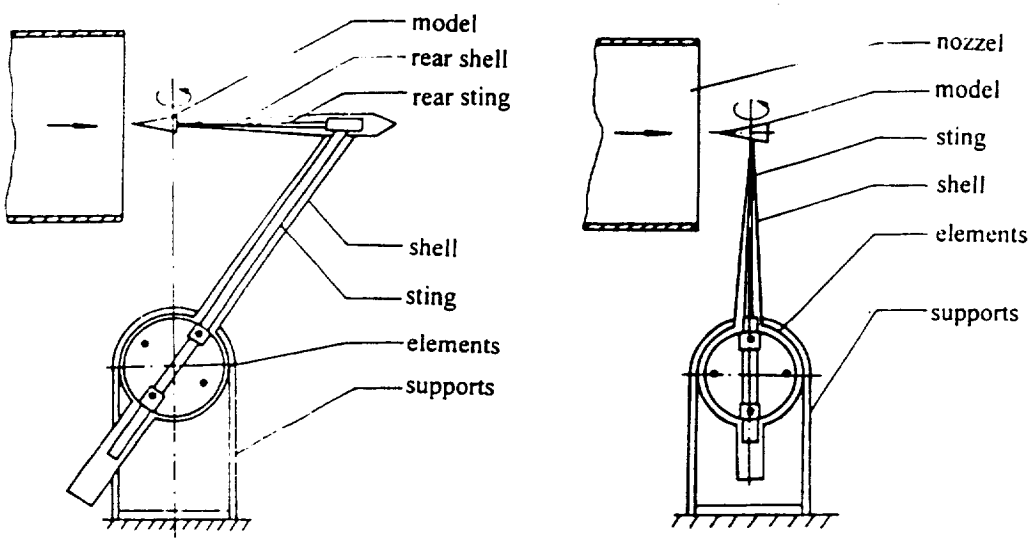

Fig.2 Two methods of support

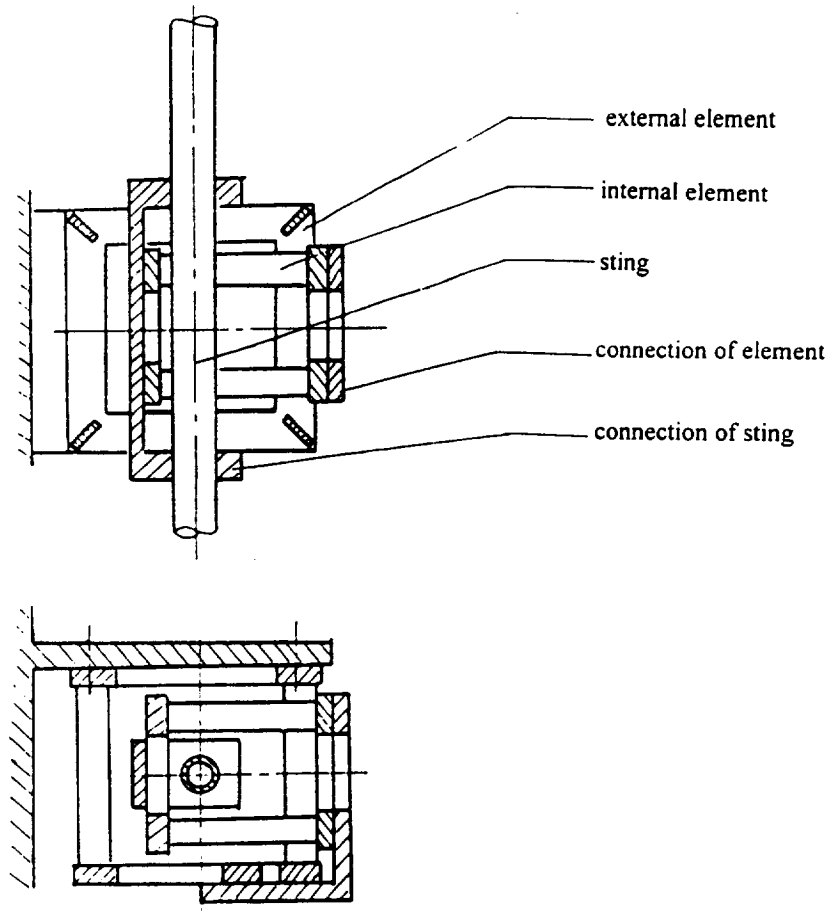

Fig.3 Internal structure of two-components microbalance

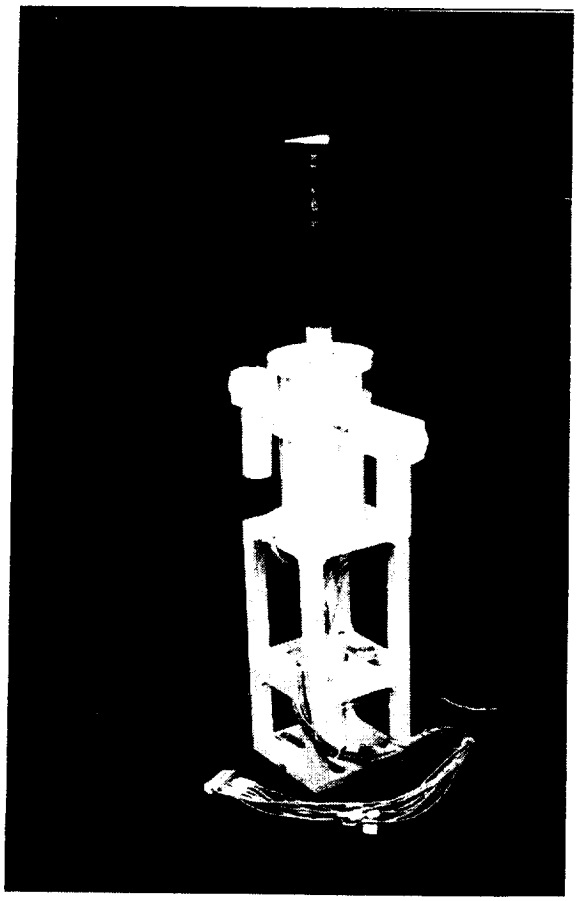

Fig.4 There-components microbalance

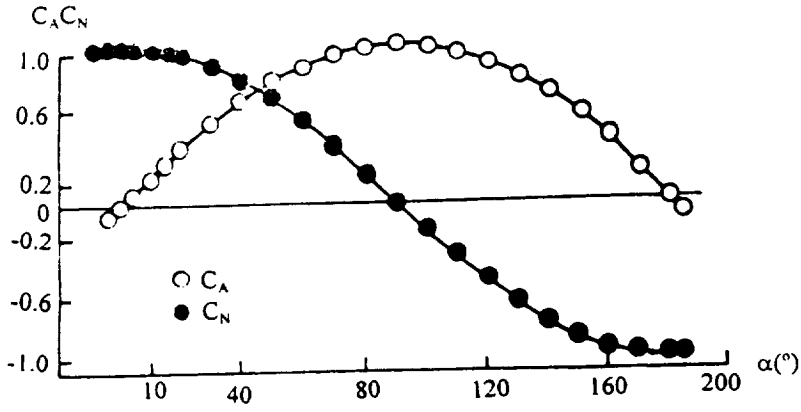

Fig.5 Force testing curves of ball model

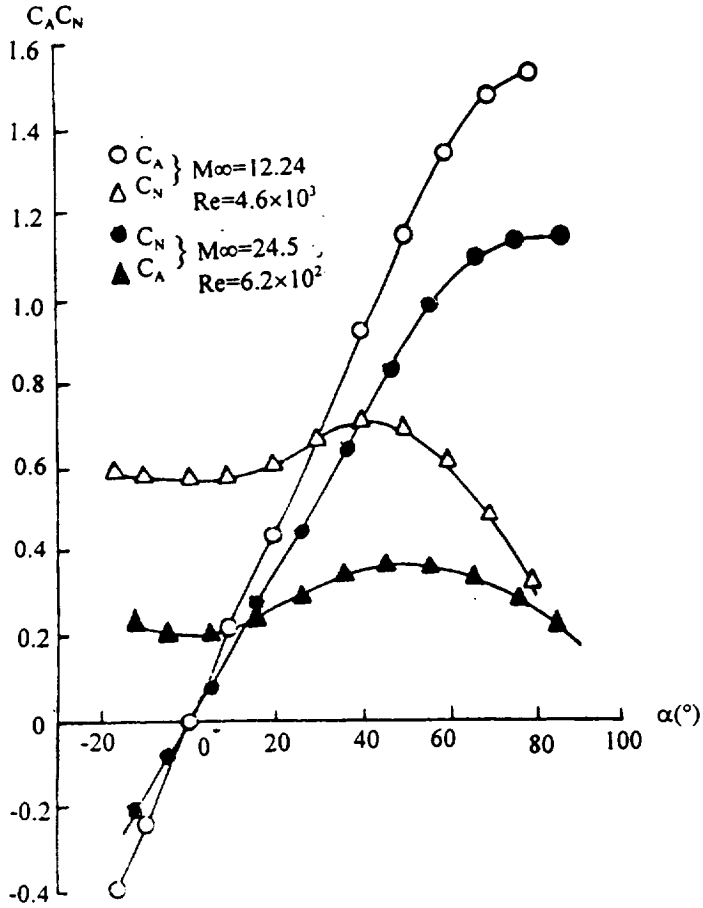

Fig.6 Testing Curves of sharp conical

NOVEL OIL FILLED BELLOW TYPE INTERNAL STRAIN GAUGE BALANCE FOR WATER TUNNEL APPLICATIONS

B. Vasudevan[+] & M.A. Ramaswamy[*]
Department of Aerospace Engineering
Indian Institute of Science
Bangalore 560 012, INDIA

INTRODUCTION

The balance described in this paper was developed in response to a particular need that arose in the measurement of forces and moments over models placed in a return circuit water tunnel facility at the Department of Civil Engineering, Indian Institute of Science, Bangalore. Conventional balances were first tried with several types of water-proofing compounds applied over the foil type strain gages by following the procedures suggested by the manufacturer but over a short period of use, the strain gages failed repeatedly. It was felt that one of the major causes of failure could be due to delamination of the strain gages and the water-proofing coatings due to successive cyclical operations wherein the static pressure in the tunnel was varied in the range -13 psi to + 13 psi with reference to ambient. Large negative pressures were required to simulate the cavitating conditions at different flow velocities and these cyclic operations had presumably caused a rapid deterioration in the functioning of the strain gage sensors resulting in the insulation resistances to drop to alarmingly low values. Over a period of testing, it was realized that no useful result could be obtained even after trying to improve the quality of water proofing as suggested by the international suppliers of strain gages such as Micromeasurements, USA. It was therefore decided to isolate the strain gage sensors from the medium of flow, in this case, water, by the introduction of a suitable bellow. Initially experiments were planned with the sensors being kept in air at ambient pressure inside the bellow with suitable PVC ducting for carrying the electrical lead wires from the strain gauge bridges at the rear end of the balance. However, a simple calculation revealed that such an arrangement would result in large axial loads appearing as balance output even in the absence of any flow at large negative/positive static pressure in the test section. Infact, for the 25 mm dia balance in use, a one atmosphere difference in pressure would give an axial load of about 5 kgs whereas the axial load expected at the maximum flow velocity and angles of incidence was less than 50% of this value. Since this axial load appeared because of the pressure difference between the inside and outside of the bellow, it was decided to introduce an electrically neutral incompressible oil medium inside the bellow and the bellow be made of reasonably thin rubber material such that differential pressure cannot be sustained across it as the tunnel pressure varied from large negative to positive pressures. Also, for the pressure equalization to automatically take place very little volume change of oil is needed for the pressure range under discussion. Thus, the conceptually new, oil filled bellow type balance was expected to give very little output due to a change in tunnel static pressure while completely protecting and giving the same life for the strain

[+] Principal Research Scientist
[*] Professor

gage sensors as that obtained with 'air' as the flow medium. An additional advantage noticed was that the output of the balance kept in an oil bath inside the bellow was extremely steady without any drift unlike in a regular balance where a small drift could be noticed due to ambient temperature changes. This paper describes the Indian Institute of Science water tunnel facility, the experience of using conventional sting type balances in the facility, details of the test rig built to duplicate the absolute pressures obtained in the water tunnel, design details and the performance of the oil filled balance under varying absolute pressures both above and below ambient conditions in this test rig and finally conclusions.

DESCRIPTION OF THE IISC WATER TUNNEL FACILITY

The High Speed Water Tunnel (HSWT) facility at the Department of Civil Engineering, IISc, is a closed circuit type and is equipped with a horizontal resorber. A schematic diagram of the water tunnel is given in Figure 1. Two separate test sections are available, one of which is a closed jet type with a constant inner

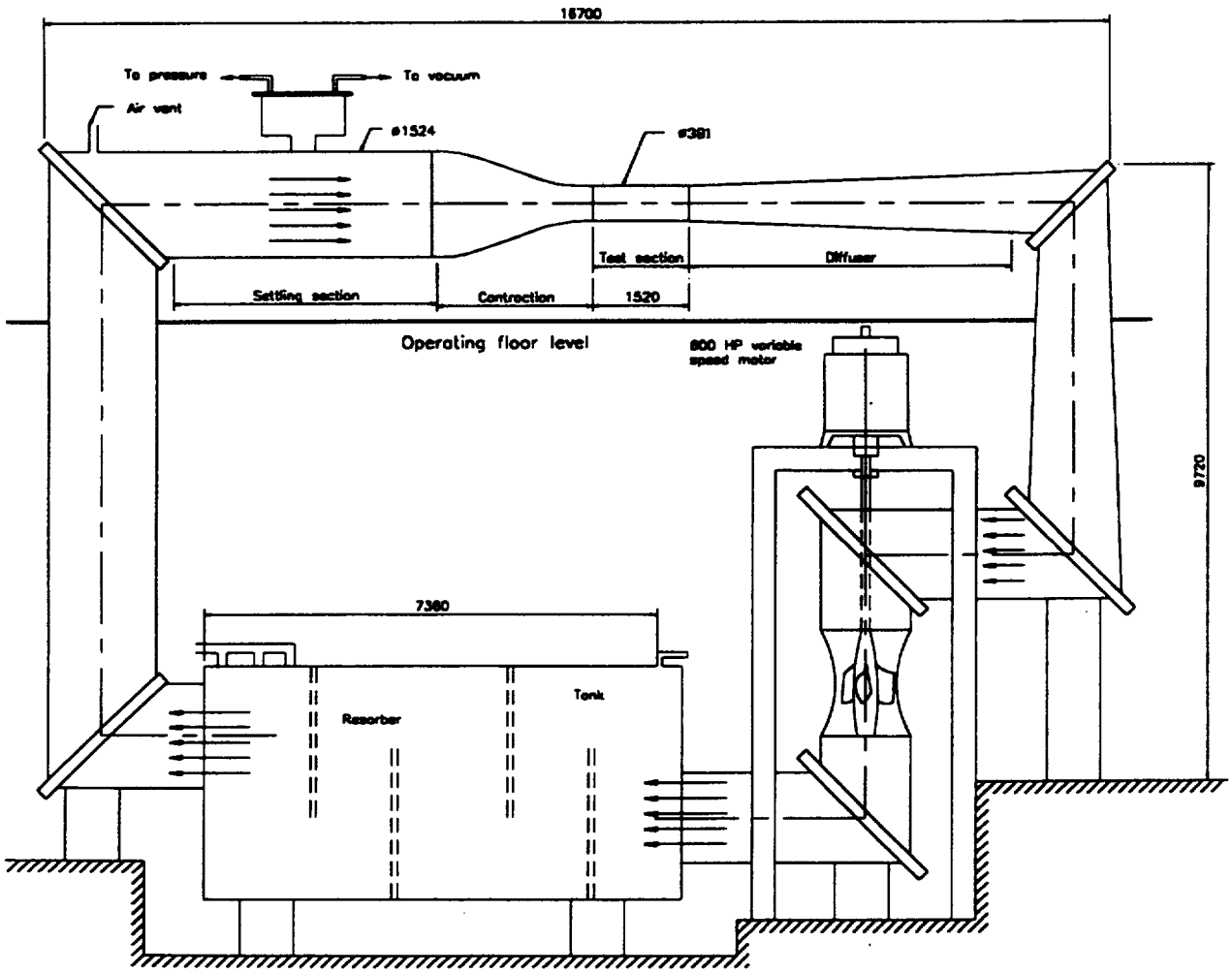

Figure 1. Schematic view of the High Speed Water Tunnel facility.

diameter of 381 mm with an overall length of 1520 mm and is shown in the figure. The other test section is an open-jet with a diameter of 460 mm having a length of 690 mm. Both the test sections are provided with plexiglass windows on all four sides for photographic and observational purpose. Table 1 summarizes the operating parameters of the tunnel and these compare quite favourably with some of the large water tunnel facilities existing in other countries. Mote details of the facility are given elsewhere[1,2].

Table 1. Operating Parameters of Indian Institute of Science Water Tunnel Facility

Parameters	Closed jet	Open jet
1. Test section size	381 mm	460 mm
2. Contraction ratio	16 : 1	11 : 1
3. Maximum velocity	30.3 m/s	20.8 m/s
4. Turbulence level	0.2 - 0.3 %	------
5. Maximum test section pressure (Abs)	2.5 bar	------
6. Minimum test section pressure (Abs)	0.33 bar	------
7. Capacity of the motor	447.4 KW	------

USE OF CONVENTIONAL STRAIN GAUGE BALANCE

It is very common to use sting mounted multi component strain gage balances to measure various loads appearing on any model in a wind tunnel. However, the use of such balances for water tunnel applications has not been reported in literature. The major difficulty in the use of such balances in water medium would be the likelihood of electrical shorting of input and output terminals arising from inadequate water-proofing of the strain gage leads. The major producers of high quality strain gages do manufacture fully encapsulated strain gages for under water use but the sizes of these are rather large and cannot be fitted into the flexures of small balances (25 mm nominal dia). Hence the need for proper sealants for protecting the strain gage terminals under the harsh environments faced in the water tunnel. Initially, several types of water-proofing compunds were used, the most promising one being the application of a black coloured rubber type agent called Hematia R 923T. While some of these lasted only a few cycles of use, the best of them, water-proofed by an expert from a well known international company survived only for a few days leading to a major problem in the measurement of forces in the water tunnel. It was felt that the lower vacuum pressure conditions in the tunnel caused the rapid detoriation of the water proofing of the strain gages. But, the results indicated, that the balance performed reasonably well during the short time the water proofing remained unaffected. It was therefore decided to isolate the strain gauge elements from the medium of flow (water) by introducing a suitable bellow. To test these balances with bellows under simulated conditions, an experimental rig was built.

EXPERIMENTAL TEST RIG

It was felt that a small test rig wherein the balances could be tested under the same pressure conditions existing in the large high speed water facility would greatly facilitate the testing of any new concept. Figure 2 shows the schematic view of the test rig built exclusively for the study. The rig consists of a cylindrical pipe of internal diameter 160 mm and length 1200 mm. The ends are closed with appropriate flanges. Provisions have been made to mount the balance inside the pipe and bring out electrical leads through appropriate leak-proof connectors. The cylindrical pipe could be filled with water so that the balance is kept under water. A transparent tube just outside the pipe shows the level of water inside. The pressure inside the pipe could be varied from -13psi to +15 psi with respect to the ambient by the use of a portable vacuum pump and a compressor unit. A U-tube mercury manometer was used to measure the pressure inside the rig as it went through from high vacuum to positive pressures. A scanivalve type transducer (PDCR 23) was also used at later stages to measure the pressure inside the water chamber and

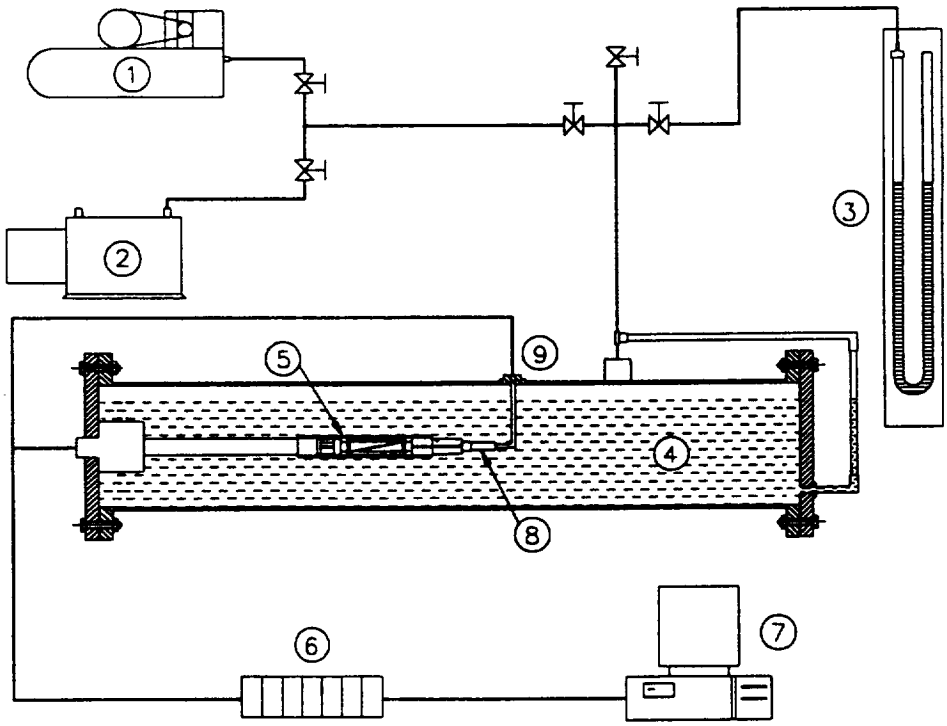

1. Compressor, 2. Vacuum pump, 3. U-Tube manometer
4. Water-Filled rig, 5. Oil-Filled balance, 6. Signal conditioners
7. Intel 486 computer, 8. Scanivalve transducer, 9. Electrical connector.

Figure 2. Schematic view of the test rig and instrumentation.

record the same in an Intel 486 based computer. A standard 12 bit, 16 channel Analog to Digital conversion card with a 10 μsec sampling time was used. The balance was fitted with a differential pressure transducer (Scanivalve PDCR 23, 2.5 PSID) to measure the pressure difference across the bellow (pressure of oil inside the bellow minus water chamber pressure). The electrical lead wires from the balance and the transducers were brought out of the test chamber through leak-proof electrical connectors and taken into the computer through appropriate signal conditioning equipment. The test rig is also provided with appropriate isolation valves to perform either the compressed air experiment or the evacuation experiment or to release air either into the test rig or out of it to the atmosphere to change pressure conditions in the test chamber.

INITIAL EXPERIMENTS WITH METALLIC BELLOW

Figure 3 shows the schematic view of the balance used in the initial stages of this study. This balance is a regular sting type balance with the load rating shown in Table 2. A metallic bellow made of stainless

Table 2 Specification of the 38 mm six-component balance

Normal Force	(max)	.....	120 kgs
Side Force	(max)	.....	40 kgs
Axial Force	(max)	.....	40 kgs
Pitching Moment	(max)	.....	12.0 kg m
Yawing Moment	(max)	.....	4.0 kg m
Rolling Moment	(max)	.....	2.0 kg m

Expected output in each bridge ~ 2 mv/V

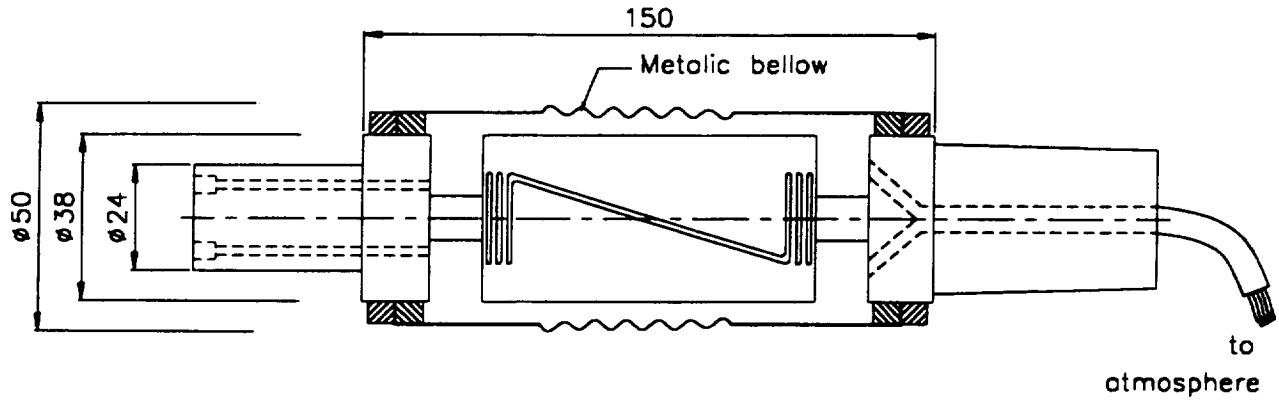

Figure 3. A view of the 38 mm balance with metallic bellow.

steel of thickness 0.3 mm and extremely flexible was used for isolating the strain gages. Initially, the air inside the bellow was kept open to the ambient pressure while being placed in the test rig. This was done by allowing the air from outside to communicate with the inside of the bellow through the tube carrying the electrical leads from the balance to the signal processing equipment placed outside. The pressure in the test rig was then varied from -13 psi to +15 psi (with reference to the ambient pressure) by operating the vacuum pump and the compressor one after the other. The differential pressure introduced across the bellow gives a net resultant force in the axial direction. All the other bridges give very little or negligible output. Figure 4 gives the axial output as a function of the differential pressure applied. The measured axial force agrees very well with the theoretical estimate which is obtained by multiplying the pressure difference by the area across which this pressure acts. It was observed that the actual axial load on the balance due to the pressure change of 1 atm.in the test rig was 20 kgs. This is quite large as compared to the actual hydrodynamic load expected at the maximum flow velocity and angles of incidence for the models which are to be tested with this type of balance. Even if smaller balances and metallic bellows are used, the drag load due to pressure difference across the bellow in the tunnel would exceed the hydrodynamic loads. Hence it was proposed that the balance must use a bellow which is made of thin flexible material and the pressure inside the bellow must follow the outside water pressure as the same is changed in the water tunnel facility. If air is used as the medium inside the bellow, this will call for large volume changes (as air is compressible) for the range of pressure to which the water tunnel will be subjected to. For example, when the water pressure is taken to -13 psi, the flexible bellow material will have to expand to a very large volume (several times its original volume), and the model around the balance will prevent this from happneing and the pressure can never equalize in a practical sense . As the

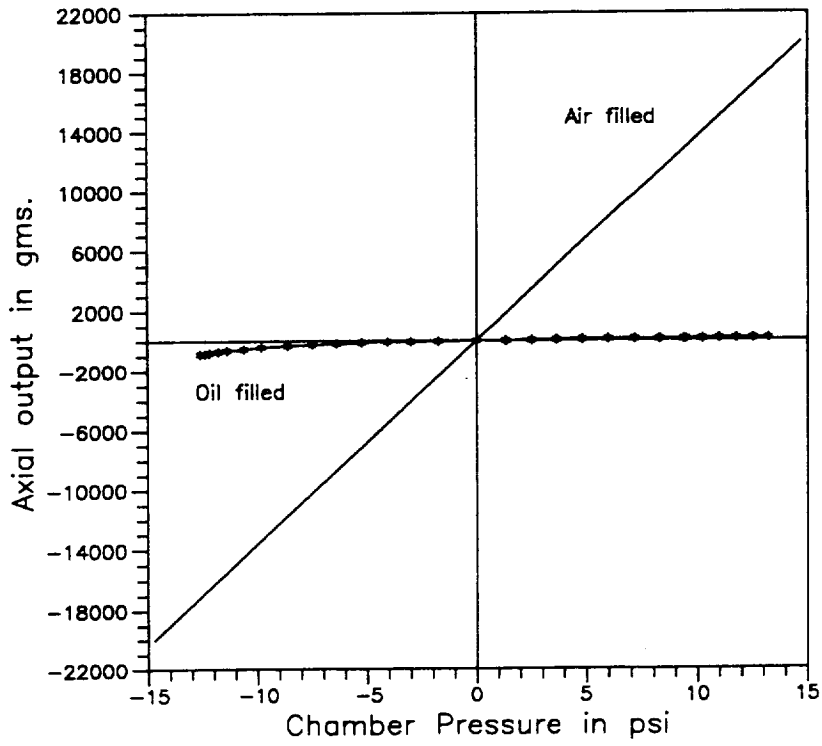

Figure 4. Variation of axial output as a function of test chamber pressure for both oil-filled and air filled cases.

vacuum pressure approaches zero, the volume required will approach infinity. Also, when the bellow starts making contact with the model, proper measurement of loads become impossible. Hence it was decided that the bellow be filled with an electrically neutral incompressible oil medium which will allow pressure equalization to take place with very little change in the bellow volume during the entire range of operational pressures in the water tunnel facility. Modifications were carried out in this balance to fill in oil and remove trapped air by drilling two holes as shown in figure 3 A thin rubber bellow was placed over the balance and two stainless steel cylinders were introduced from either end of the balance to support the 1mm thick rubber bellow from sagging. (not shown in figure 3). A small gap of 1 mm was maintained between these cylinders so that the balance flexures were free to flex and transmit the loads onto the strain gages sensors. Fresh stock of transformer oil normally used in welding transformers was poured into the bellow and after ensuring that no air was trapped inside, the ports were sealed by appropriate allen type screws. Prior to this testing, the balance was immersed in the transformer oil bath for several weeks and the strain gage sensors were kept energized to study any deterioration in the gage bonding as well to observe any drift in the output of the bridges. This study showed practically no change in the output of the balance even after being put in the oil bath for over 1000 hours. This balance was now introduced into the test rig and pressures inside the rig was once again varied from -13 psi to +15 psi. The axial output measured is also shown in figure 4 All the other bridges gave insignificant outputs. The maximum axial output was 800 gms corresponding to the maximum vacuum pressure of -13 psi. This is an order of magnitude less than that obtained with metallic bellows which was 20 kgs as shown in the same figure. It was also found that the axial output for a maximum possible positive water pressure of 15 psi was only 140 gms. This experiment suggested the feasibility of this novel technique and prompted us to build a suitable smaller balance for detailed investigations.

The size of the model restricted the maximum balance size to around 25 mm nominal diameter. Taking into cosideration rigidity and unknown loads that may occur under cavitating conditions, it was decided to design and build a new 24 mm balance, the details of which are given in the next section.

DESIGN DETAILS OF 24 MM DIA SIX-COMPONENT OIL FILLED BALANCE

Table 3 gives the specifications of the six-component balance that is designed and built for the present detailed study. It is observed that the rolling moment is quite low when compared to the other loads which

Table 3 Specification of 24 mm dia Six-Component Balance

Normal Force	(max)	.....	50 kgs
Side Force	(max)	.....	25 kgs
Axial Force	(max)	.....	20 kgs
Pitching Moment	(max)	.....	5.0 kg m
Yawing Moment	(max)	.....	2.5 kg m
Rolling Moment	(max)	.....	0.1 kg m

Expected output in each bridge ~ 2 mv/V

resulted in a multi-element rolling cage design. Figure 5 gives the overall view of the 24 mm balance. The model and the sting ends have a taper of 3° included angle. The diameter of the balance at the flexure location is 24 mm. Both the upstream and downstream sides of the balance have a diameter of 27 mm,

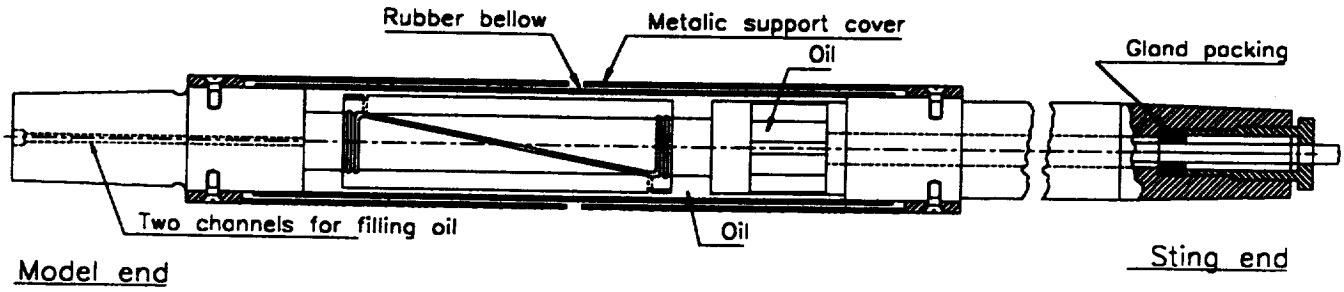

Figure 5. Details of 24 mm six-component oil-filled bellow type balance.

eaving a gap of 3mm between the rubber bellow and the oil-filled balance flexures. Some small gap is required to allow the rubber bellow to bend inwards while trying to equalize the pressure inside with that outside while the chamber pressure in the test rig is increased to +15 psi. The actual volume change required is extremely small for this pressure equalisation to take place. The present design allows a lot more gap than that required to accomodate this volume change, so that the rubber bellow does not interfere with the flexures at the highest positive tunnel pressures. Two,stainless steel cylindrical covers are introduced from either end of the balance to give support and shape to the bellow after it is filled fully with oil. Two 2 mm holes are drilled at the model end of the balance for filling the rubber bellow completely with oil. While oil is poured through one of the holes, the displaced air is driven out through the other. Special care need to be exercised to ensure that the last bubble of air is driven out of the bellow. Two allen type of bolts with teflon washers completely seal the oil filled balance at the model end. At the sting end, an 8 mm stainless steel tube is inserted all the way to the rolling cage. All the teflon coated electrical lead wires are taken out through this tube with a small loop formed near the rolling cage. The entire tube consisting of all these wires is filled with epoxy (Araldite) and sealed preventing any oil leak through the tube. The tube itself could be moved back and forth by about 5 to 10 mm. To prevent the oil from escaping through the gap between the balance and the stainless steel tube as the oil gets pressurized, a gland packing made of asbestos and grease is provided with a suitable gland nut. The same gland packing prevents any water from entering the balance as the water pressure in the tunnel is increased above ambient conditions.

EXPERIMENTS WITH 24 MM BELLOW TYPE BALANCE

The oil-filled and sealed balance is mounted inside the test rig and the electrical leads from the balance are taken out and connected to the signal conditioners and power supply units. The rig is filled with water as shown in figure 2. so that the balance is completely immersed in water. The active bridges of the balance are energised with 3 volts DC and kept for 3 hours before the experiments are started. The test rig was connected to the compressor and the pressure inside was varied from ambient to +15 psi in small

steps. At each step, the output from all the bridges of the balances was noted down. Readings were also taken while the pressure in the chamber was reduced back to ambient conditions. The vacuum pump was switched on after isolating the compressor, the experiment was repeated in the pressure range 0 to -13 psi and then back to ambient conditions. Figure 6 gives the axial output obtained as a function of the applied pressure (case 1). It is seen that the axial bridge gives a maximum output of about 30 gms at a chamber pressure of +13 psi and about 225 gms when the chamber pressure was -13 psi. Change in all the other bridges was negligible. It is obvious that the pressure equalization was much better when the rubber collapses due to increased chamber pressure than when the bellow expanded during the vacuum cycle. It was suggested that expansion of small amounts of water vapour saturated in the oil was resulting in relatively large axial output. In order to remove the saturated water vapour in the oil, the oil was poured into a glass beaker and connected to the vacuum pump. Periodically the beaker was well shaken while the vacuum pump was on to make the process more effective. Initially, one could see large scale bubbling of this saturated water vapour. The maximum vacuum that could be obtained in the present pump was around 30 microns. (0.03 mm Hg). The bubbling completely stopped after about 90 minutes of evacuation. The degassed oil was then poured into the balance and the experiment repeated. The performance dramatically improved as seen in figure 6 (case 2). The experiment was repeated several times to check the repeatability of the results. The repeatability was excellent and the axial bridge gave an output of about 85 gms for -13 psi and about 13 gms for +13 psi. As compared to the design axial load of 20 kgs, this represents 0.425% and 0.065% respectively. If one were to measure the full axial load of 20 kgs in the water tunnel, the output due to the tunnel pressure changes could even be neglected. However, this could result in an error of 4 to 5% if one were to measure an axial load of say, 2 kg. Since the repeatability of the results obtained with varying tunnel pressures was very good, corrections could be

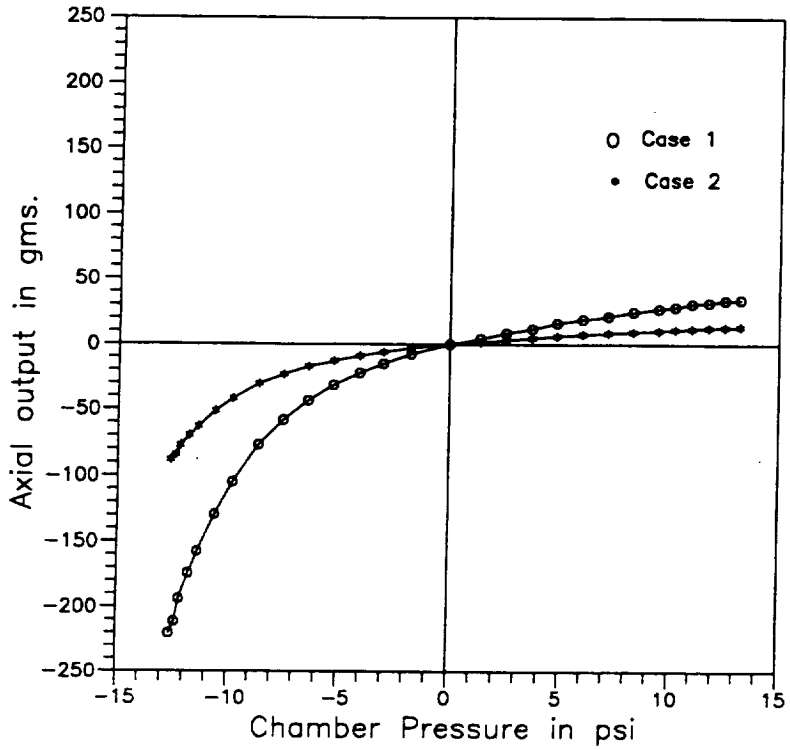

Figure 6. Variation of axial output as a function of test chamber pressure for 24 mm oil filled balance.

applied from figure.6. in the actual experiments conducted in the high speed water tunnel facility improving the overall accuracy of measurements. Figure 7 shows the results of the same experiment with the balance filled and sealed with oil as well as with air inside the bellow and connected to ambient conditions. In the air filled case, as the chamber pressure was varied, the output of the axial bridge gave a very large output which is shown. The axial output of about 5000 gms for a maximum pressure of 14.7 psi corresponds to the theoretically estimatd value (Differential pressure X cross sectional area of the bellow).

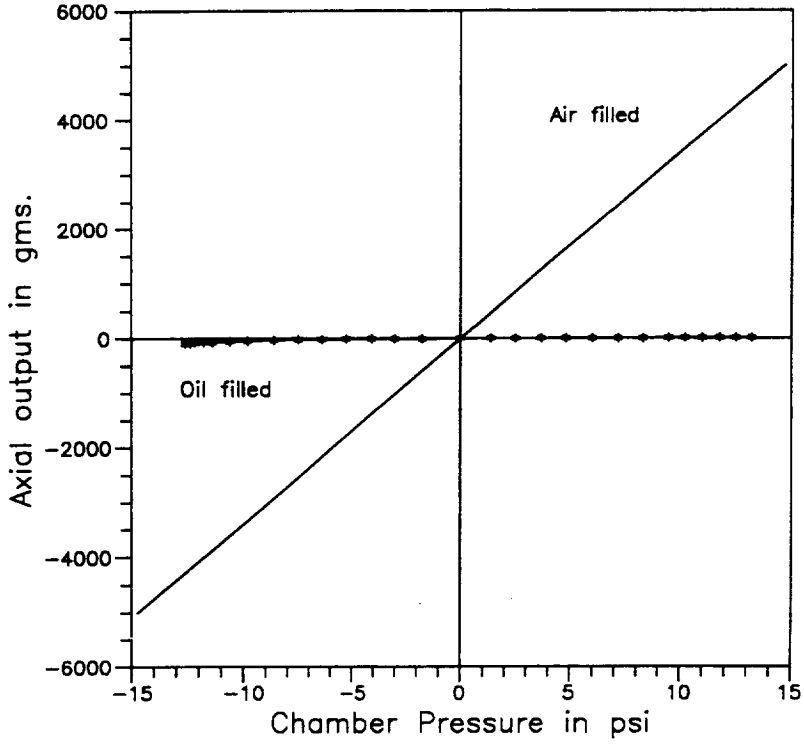

Figure 7. Variation of axial output as a function of test chamber pressure for 24 mm balance for oil filled and air-filled cases.

To further understand the small axial outputs obtained in the oil filled case it was decided to measure the inside oil pressure also, along with the balance outputs, during the experiments. A scanivalve differential transducer (Type PDCR 23) with a range 0 to 2.5 psi was mounted on one of the ports which was earlier used to fill oil ito the balance. Positive pressure port was connected to the oil side and the reference pressure port measured the chamber pressure. The electrical leads from the differential pressure transducer was connected to the signal conditioning equipment and to the ADC of the computer. The experiment was again repeated from -13 psi to + 15 psi in the chamber with reference to ambients and now both the differential pressure output and the axial bridge output were noted. Figure. 8 gives the result. The y-axis gives the differential pressure output in psi as well as an equivalent load in grams when this pressure was multiplied by cross sectional area over which the differential pressure acted (5 cm^2 or 0.8in^2 in the present case). The results in the figure give a clear picture of the events. For a chamber vacuum pressure of say -13 psi, the differential pressure transducer gives 225 gms whereas the axial output is only 85 gms. Since the oil filled bellow changes its shape only marginally during the entire cycle, it is seen that the rubber bellow itself is taking 67% load while passing only 33% of load to the balance. The reason for the bellow taking a large portion of the load due to differential pressure is qalitatively understood from theoritical

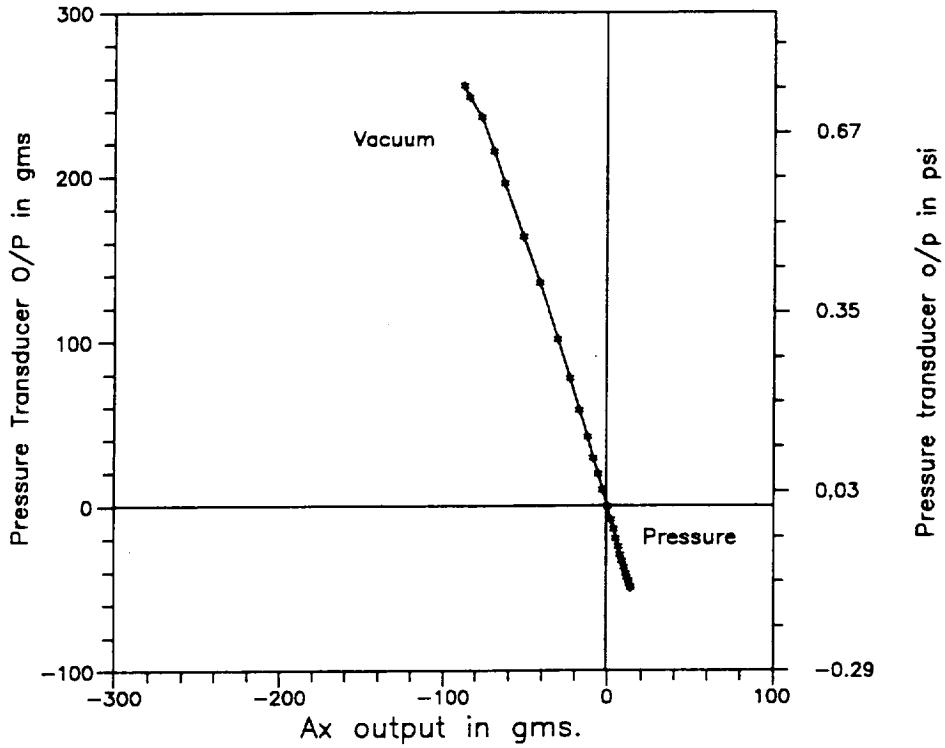

Figure 8. Variation of pressure transducer output as a function of axial output for the 24mm dia balance.

considerations that poisons ratio for rubber is close to 0.5. However to get a quantitative confirmation further study is necessary. However, the results beig highly repeatable,allows the oil-filled balance to be used just like any other balance with almost the same accuracy by giving necessary corrections from the figure.6 discussed earlier.

CONCLUSIONS

Inspite of the best efforts, the conventional sting type balances with different water-proofing compounds failed to perform in the harsh environments of the high speed water tunnel facility. Perhaps the cyclic operations under high pressures and vacuum caused the breakdown of the water-proofing coatings and delamination of strain gages resulting in failure of the balance within a short time. Provision of a metallic bellow to completely isolate the conventional strain gages solved the problem of gage failure but gave very large axial outputs as compared to the hydrodynamic outputs expected in the water tunnel. As this was not acceptable, a thin flexible rubber bellow was introduced and the volume inside the bellow was filled with an incompressible electrically neutral transformer oil. A compact new test rig simulating the various pressure regimes obtained in the actual water tunnel was built as part of this study. The results obtained with the novel oil-filled bellow type balance were very encouraging and the axial outputs due to the pressure changes was reduced to low values (30 gms at a positive chamber pressure of +13 psi and

220 gms at a negative chamber pressure of -13 psi). Degassing of the transformer oil by evacuation and periodic stirring greatly improved the performance. The use of degassed oil in the balance resulted in the pressure equalization to be near perfect as the chamber pressure was varied. Except the axial bridge, the output of all the other bridges was negligible. After degassing, the axial outputs came down to about 85 gms at -13 psi chamber pressure (which is 0.425% of the full scale output) and was only 13 gms at a chamber pressure of +13 psi (0.065%). Even these induced outputs are highly repeatable and can be corrected in the final computation of hydrodynamic loads which will ensure high accuracy of measurement. Finally, measurement of oil pressures inside the bellow gave additional interesting information. The rubber bellow itself was taking a good part of the load (two thirds) arising from differential pressure between the oil and water outside and letting the balance take only the remaining part (one-third). Further studies are being planned to understand this. We conclude that a novel oil filled balance was successfully designed and built and is expected to be the major equipment for accurate study of forces and moments in the high speed water tunnel facility at Indian Institute of Science.

REFERENCES

1. Arakeri, V.H.; Govinda Ram, H.S.; 1978 *Comparative cavitation inception studies on a hemispherically nosed body* WTL Report No.78 - 1, Indian Institute of Science, Bangalore.

2. Mani, K.; 1984; *Design of open jet test section for an existing high speed water tunnel facility*, Report No.DE - NRC/TDP-25/TR-11, Indian Institute of Science, Bangalore.

MEASUREMENT OF FULL-SCALE STOVL PROPULSION LOADS USING MULTIPLE 6-COMPONENT STRAIN GAGE BALANCES*

Duane P. Shelton
Boeing Defense & Space Group
Seattle, WA 98124

Steven F. Lieberg
Boeing Defense & Space Group
Seattle, WA 98124

SUMMARY

A unique approach to measurement of six degree of freedom (DOF) aero-propulsion loads was successfully used at the Boeing Hover Test Facility (BHTF) during hover testing of a full-scale, Advanced Short Take-Off Vertical Landing (ASTOVL) powered model. The force measurement approach was based on the use of three custom designed strain gage balances to measure the six components of force and moment at each of three model attachment points. Details of facility operational features, model/facility interface, balance design & calibration, and force measurement system (FMS) performance issues are discussed. Basic principles and attributes of the shear cell flexure (SCF) for balance design and associated design parameters are covered with reference to previous SCF applications of multi-component balance systems at the Boeing Defense & Space Group.

INTRODUCTION

Complete characterization of the aerodynamic forces resulting from operation of an ASTOVL aircraft in ground effect is a significant concern during design of lightweight, advanced aircraft which utilize new propulsion technologies. Every effort is taken to minimize aircraft weight by reducing the number and/or size of the aircraft engines, with the understanding that this will improve operating performance and minimize cost & complexity. In order to

*Work done on contract at Boeing Defense & Space Group, MDA972-94-2-0011

realize the full potential of the engine and aircraft performance, installed effects on thrust and aerodynamics need to be completely understood.

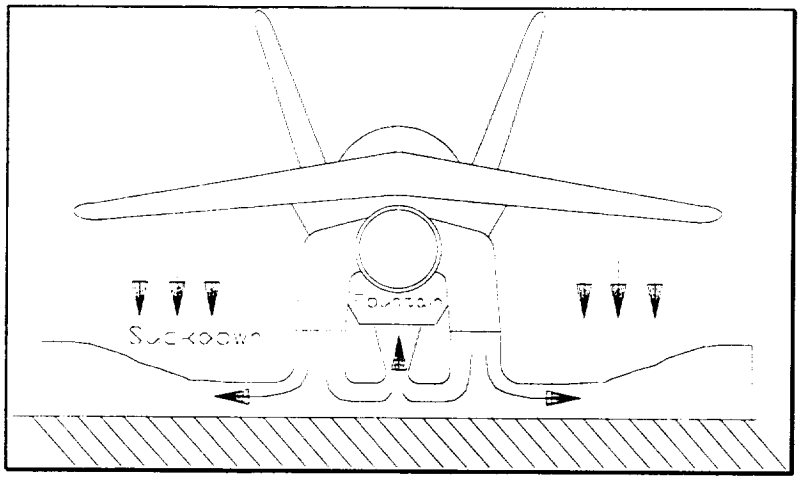

Figure 1. Description of Suckdown and Fountain Effects for A Direct Lift ASTOVL Aircraft

Two types of aero-propulsion forces which can occur when landing an ASTOVL aircraft vertically are aerodynamic suckdown and fountain effects (Figure 1). The suckdown effect is created by the hot exhaust gases from the engine impinging on the landing surface, being redirected parallel to the landing surface, and accelerating toward the wing tips. The high gas velocity reduces the pressure on the lower surface of the wing causing a reduction in lift at a crucial moment. An aerodynamic fountain effect can offset this reduction in lift. The fountain is the component of the exhaust gases that are redirected parallel to the landing surface and accelerated toward the centerline of the aircraft. When the exhaust gases from both nozzles intersect at the aircraft centerline the flow is re-directed upward which increases pressure on the underside of the fuselage.

These competing aero-propulsion effects produce a complex flowfield that is difficult to model mathematically and sensitive to scale effects that occur during aero-propulsion testing. Sub-scale testing, although an efficient method of determining the aero-propulsion phenomenology, results in force and moment data that is questionable when applied to full-scale aircraft performance. This results from the difficulty of matching Reynolds number, exhaust gas temperature, and flowfield mixing with the ambient air. Since the knowledge of the aero-propulsion forces during landing is critical to nozzle design and engine selection, the alternative is to do a near full-scale powered model test where the model height above ground and the model angle of attack can be varied.

TEST FACILITY DESCRIPTION

The Boeing Hover Test Facility (BHTF) is located at the Tulalip Test Site approximately 40 miles North of Seattle, Washington. This unique test facility was designed and built over an 8 month period in 1995 to accommodate ground effects testing of a Large Scale Powered Model

(LSPM). Both the BHTF and the LSPM were designed and fabricated by the BD&SG Aero-Propulsion & Test Support Laboratory located at the Kent Space Center.

The purpose of the BHTF was to provide for remote positioning of the LSPM at specified heights above a smooth ground plane surface without interfering with engine inlet performance or exhaust nozzle flowfields. The basic structure of the BHTF tower, shown in Figure 2, consists of four braced, structural steel columns which support four large steel trusses. The four trusses form an overhead structure from which the model and all its support systems are suspended. The overall structure is 88 feet tall.

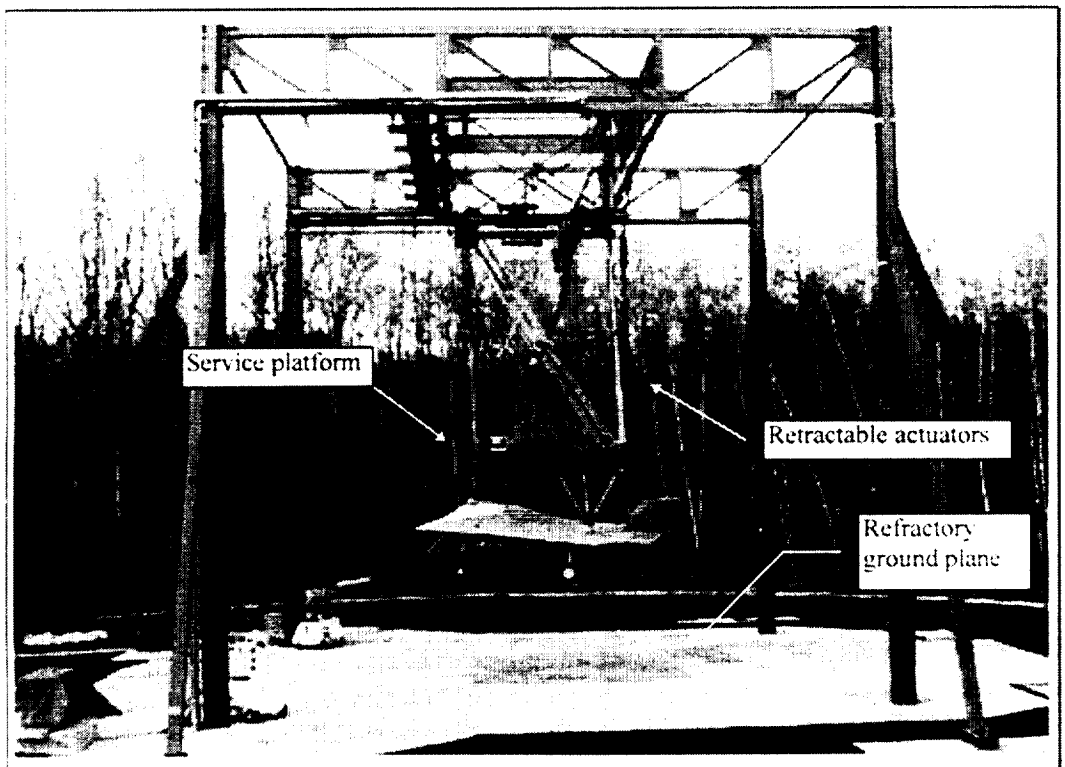

Figure 2. Boeing Hover Test Facility and Large Scale Powered Model

To meet the requirements of the LSPM test program, the facility included a rigid platform immediately above the model for required engine support equipment and reacting of the LSPM thrust loads. The LSPM was suspended from the service platform at three points by five turn barrels and a single gimbaled remotely actuated hydraulic cylinder as shown in Figure 3. Three of the turn barrels were attached to the left wing of the model to position it at a fixed point in space. The other two turn barrels were attached to the right wing in such a way that the model was allowed to expand in the span direction due to any thermal effects during test. The five turn barrels and nose actuator react out the forward, vertical, and lateral thrust. The remote hydraulic actuator was attached to the model on the centerline of the cockpit region and used to set the model pitch attitude using a servoaccelerometer for pitch angle measurement. A spherical

bearing assembly was located at each of the three model attachment points to minimize any local moments. A 6-component balance was rigidly attached to the model below the spherical bearing at each attachment point.

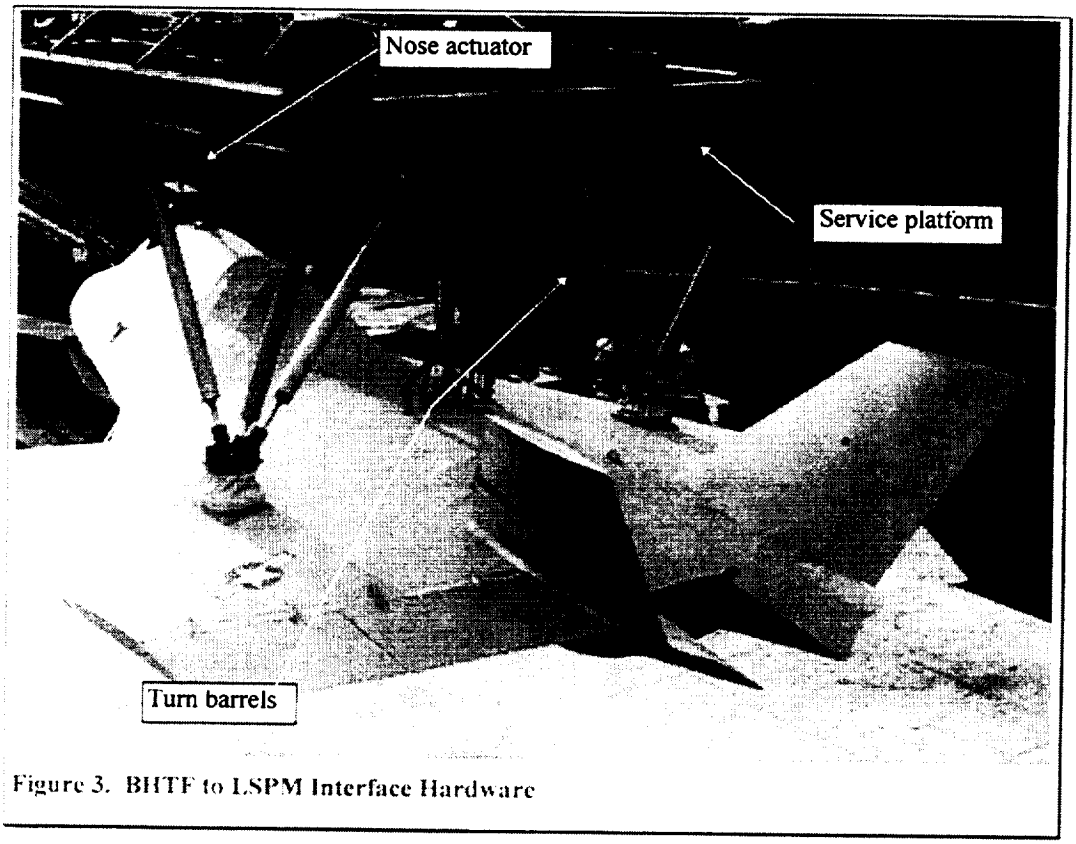

Figure 3. BHTF to LSPM Interface Hardware

The service platform was suspended from the overhead truss structure by six remotely controlled hydraulic actuators as shown in Figure 2. Simultaneous extension and retraction of these actuators resulted in vertical translation of the service platform, model support equipment and the LSPM. The weight of the equipment raised and lowered by the actuator system was on the order of 80,000 lb.

All the standard utilities and services required to operate a high performance gas turbine on an engine thrust stand were also required at the BHTF. High pressure air for starting the engine and cooling of the engine bay & propulsion components was provided by a diesel compressor system. JP-8 fuel was provided from a fixed tank via boost pump at the tank, no fuel was stored on-board the model. Cooling water for instrumentation, heat exchangers and an emergency water deluge system was also pumped to the service platform above the model. Instrumentation and engine control lines were routed to the model separately from AC power lines to minimize noise in low level instrumentation and control lines. The lines for all the support services were required to translate vertically with the service platform. From the service platform, the utility lines were routed to the centerline of the LSPM and, as a result, bridged

across the three balances forming an alternate load path, with the potential to influence overall thrust measurement. The effects of the utility lines on the force measurement system (FMS) data was shown to be negligible during checkout. Prior to each test, balance zeros were taken with all lines pressurized to remove pressure tares from the thrust data.

An important underlying component of the BHTF was the ground plane. The ground plane was required to withstand direct impingement of high temperature, high pressure jet engine exhaust gases while the model remained at a wheels-on-ground condition for several minutes during acquisition of data. A challenging requirement was that the ground plane not spall or otherwise fragment and pose a foreign object damage (FOD) hazard to the engine. Following a series of component tests on various candidates a wire-reinforced, silica based refractory concrete was selected for the 8 ft x 8 ft ground plane panels. The panels were fabricated off-site and fired to over 1000 °F for removal of water and to minimize spalling. This design proved to function satisfactorily with the exception of the ceramic filler material used to fill joints between the panels.

FORCE MEASUREMENT SYSTEM

Shear Cell Flexure (SCF) Balance Background

Applications at BD&SG

The Aero-Propulsion & Test Support Laboratories began developing techniques in 1985 to utilize the SCF in multi-component force measurement applications. The first project consisted of a 6-component aluminum balance with 10 SCFs and was designed for low overall deflection. This single piece balance was used to measure forces and moments on a scale model of the Hard Mobile Launcher in a supersonic wind tunnel. Standard wind tunnel balances had previously been used to support this test but they were found unsatisfactory due to insufficient stiffness and the resultant fouling of the model on the simulated ground plane.

Our next 6-component balance design was based on the requirement to measure high frequency thrust pulses for a Sagittar kinetic energy weapon propulsion system that required 1,000 psi nitrogen at 2 lbm/s to operate. The inherent stiffness of the SCF and integration into a steel, single piece design proved a good choice for the Sagittar balance. Measurement of the high frequency thrust pulses required a resonant frequency of the mechanical system on the order of 5 times greater than the frequency of interest in order to have adequate resolution of the pulse leading edge detail.

Other programs on which SCF balances were utilized include the Starstreak-On-Avenger program to measure blast diffuser impulse loads during first stage booster firing of the shoulder launched Short Brothers Starstreak missile, Royal Ordnance for measuring short duration pulses (pulse width of 10 ms) of their liquid bi-propellant rocket motors, and Hard Mobile Launcher for measurement of the uni-directional shear forces associated with dust laden supersonic flow.

Our experience with SCFs confirms they are reasonably inexpensive to machine and instrument, provide good linear output and result in a low deflection system well suited to high frequency or high load applications. They can be easily arranged in a variety of configurations for measuring various combinations of forces and moments, as is often required by unique tests in the aerospace industry.

Shear Cell Flexure (SCF) Design Principles

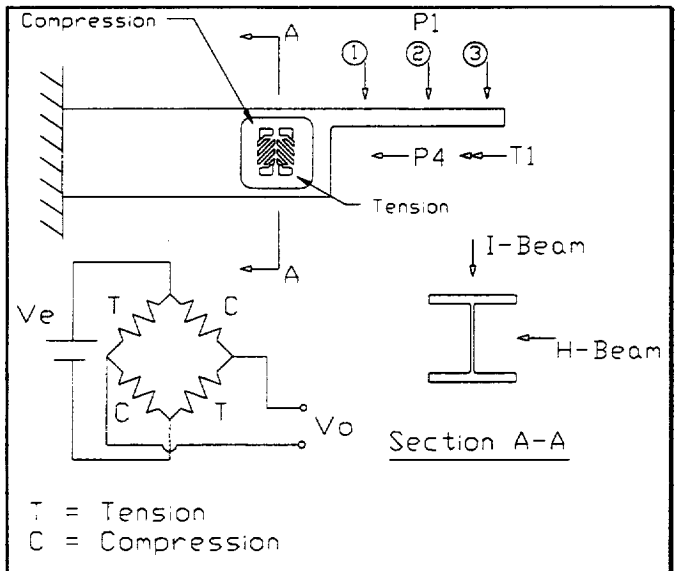

Figure 4. Shear Cell Flexure Description

A simple shear cell is shown in Figure 4. It consists of a milled pocket in a rectangular bar with strain gages oriented at 45° and located about the neutral axis of the cell cross section. Strain gage pairs, located front and back on the shear cell web, are connected into a four arm Wheatstone bridge to provide for temperature compensation and cancellation of interaction loads. The web of the pocket is very thin (~0.030 in) to minimize web load carrying capability and to ensure that the gages are located in an isothermal environment. This minimizes the bridge output due to thermal gradients in the flexure.

Since the gages are mounted on the neutral axis and oriented ±45° to the horizontal centerline, only strains due to shear forces are measured. Figure 4 illustrates the characteristics of the SCF. The force P1 applied in the I-beam direction at different stations (STA. 1, 2, & 3 in Figure 4), will produce nominally the same bridge output since bending strains on the neutral axis are zero. The finite size of the gage does result in some bending moments appearing in the bridge output but the effect is usually less than 2% of shear load and linear with respect to the load. Likewise, with torsion applied to the rectangular bar as shown in Figure 4, very little signal

is produced from the Wheatstone bridge. Most of the torsion is reacted by the section flanges and the small shear strains present on the neutral axis produce no bridge output due to the canceling effects of the bridge arrangement.

Forces applied parallel to the beam are primarily reacted by the significantly thicker flanges of the flexure cross section. The compatible strains at the gage locations are canceled due to the bridge arrangement, since all gages are strained the same amount and in the same direction. Forces applied in the H-beam direction (perpendicular to the plane of the paper in Figure 4) do not effect bridge output significantly. Shear forces perpendicular to the flexure section, in the H-beam direction, are reacted by the thick flange sections and, since the strain gages are located on the neutral axis, the strains due to bending are quite small. Moments do not effect bridge output significantly since the flange sections carry all of the bending moment and the gages are located on the neutral axis.

To summarize, the shear cell is a flexure that is sensitive to loads (not moments) in a single axis only. Interaction forces or moments do not significantly effect bridge output (effects are usually less than 2% of applied force or moment and the effects are linear with load). The flexure exhibits the properties of a good transducer. The question, for most of our applications, is: Can it be made sufficiently stiff and still provide adequate signal levels?

The SCF does produce good signal levels due to the large shear factor ($\frac{\tau_{max} \times A}{V}$) in the short flexure element, with excellent stiffness characteristics due to the compact element design. The relatively constant shear stress on the flexure web allows gages to be used that are large enough to carry high bridge excitation levels (~10 V for foil gages). This results in a large bridge output signal level for a relatively small strain level without adverse gage heating effects and without adversely impacting the overall flexure stiffness. The flexure stiffness is large because the pocket width can be small (essentially, the width of the strain gage). Thus, the displacement is small across the pocket width, and since the stiffness is inversely proportional to displacement, the SCF is characteristically very stiff.

LSPM Balance Design Overview

A force measurement uncertainty goal for normal force was established based on previous experience with shear cell balances and the anticipated complexity of full-scale testing. Normal force measurement was the most critical for the test program due to small force values expected for suckdown and fountain effects. Our design goal of uncertainty for normal force was ±0.5% of the full scale normal force calibration load with a 95% confidence.

The configuration used for each of the three LSPM 6-component balances (Figure 5) was based on experience with our previous designs. Key differences are the significantly higher load range and the use of a geometry which is tailored to the specific needs of the LSPM test program. For each balance, a total of 12 SCFs were machined into 4 flexure assemblies in a single piece of 17-4 PH plate. The load range was high enough that standard foil strain gages were suitable. The requirement was to measure steady state thrust so there was no frequency response requirement for the hover test program; although balance stiffness was an issue since a relatively high natural frequency of the model-balance system was desired. These balances were required to support the hover test program as well as a potential wind tunnel test in the NASA Ames 80 x 120 foot Low Speed Tunnel.

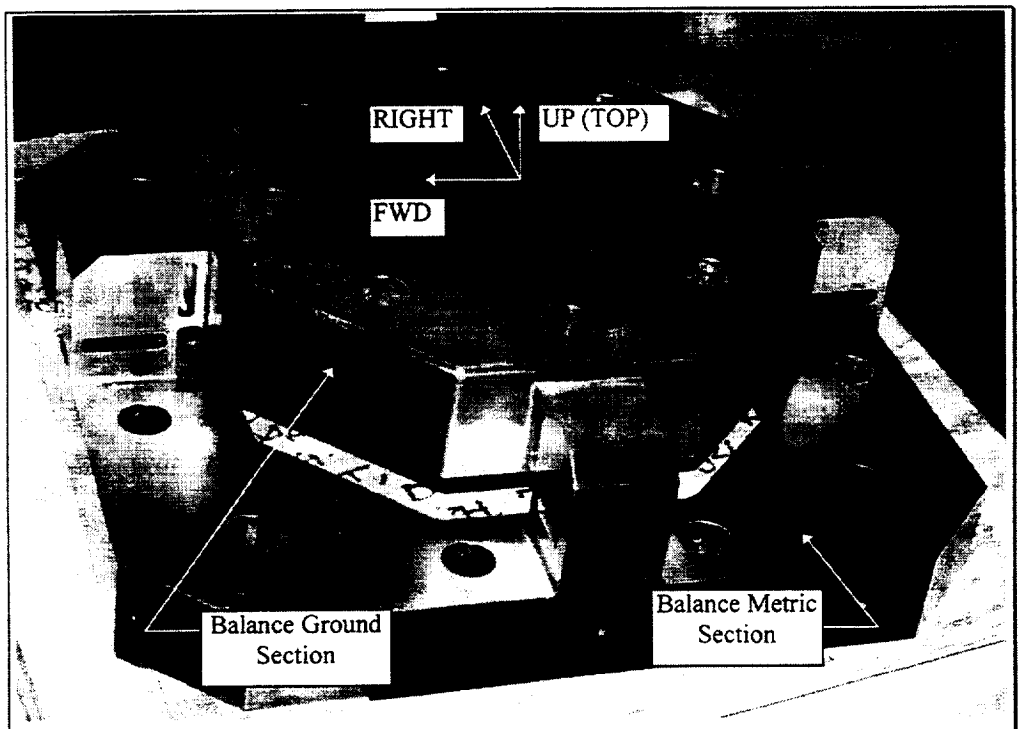

Figure 5. LSPM Wing Balance Configuration

In the case of the hover test program, the model is suspended from the overhead turn barrel system and the interface to the test facility is on the top surface of the balance ground attachment section. For testing in the wind tunnel, the model is supported from below by three struts which are mounted to the turntable in the floor of the wind tunnel test section. Each wind tunnel strut has a spherical bearing assembly which attaches to the lower surface of the balance ground attachment section. This arrangement permits the wing balances to remain installed for both major test programs. The nose balance must be relocated from the top of the canopy to the underside of the cockpit while still remaining in the upright orientation.

Since the balances were going to be used in the wind tunnel, another requirement was to have the balances located completely within the wing cross section at the balance location, with no balance material breaking through the model skin. This required a balance having a low profile (approximately 5.5"). The wing balances ended up protruding slightly outside the loft lines but were judged aerodynamically acceptable to the project engineering staff providing simple fairings over the balances were used.

LSPM Force Measurement System Design Loads

The size of the LSPM presented unique problems when designing the force measurement system. Model weight was a significant design load and represented the largest force applied to the model. The LSPM weight was expected to be approximately 50,000 lb and the maximum estimated force from the engine in the vertical direction was approximately 20,000 lb. Thus, the maximum expected vertical force was approximately 40% of the weight - and the vertical force was the most important measurement for the hover and wind tunnel tests. The balances had to be designed to carry the model weight and be sensitive enough to provide good accuracy and resolution for determining fountain and suckdown forces. A classic "range versus resolution" problem.

Loads were determined for the force measurement system using a finite element model of the LSPM primary structure along with a spreadsheet analysis. The FEM included all stringers, frames, bulkheads, spars, ribs, and skins, as well as representative balance structure. The purpose of the model was twofold: 1) Determine the internal loads for LSPM structural design and 2) Determine balance reaction loads for the overconstrained cases (wind tunnel attachments). The FEM was used to determine influence coefficients that allowed for calculation of balance reaction loads based on external forces and moments as parameters. The influence coefficients were put into a spreadsheet and used to quickly calculate balance reaction loads based on changes in the LSPM external loads.

Twelve test conditions were run to determine the worst case hover and wind tunnel test loading for the balances. Between the hover test and the wind tunnel test, the worst case normal force loading condition would be expected to occur during an inadvertent 1.1G shock loading when translating the service platform and model to a new test position. The worst case loading for axial force occurred during hover test with the lift nozzles oriented 45° to horizontal and the engine operating at maximum test power. Maximum side force exerted on the balances occurred during yawed conditions in the 80'x120' wind tunnel.

Late in the test design program a decision was made to forego the 80'x120' wind tunnel test and to design the LSPM and balances for the loads that would occur only during hover

testing. This decision effected the balance design very little since the worst case loads, except for side force, occurred during hover testing. The design loads for the balance forces are shown in Table 1. Note the wing balance design load that results in the peak stress for the balance occurs with wings-on, lift nozzles at 45° to horizontal, cruise nozzle at 0°, engine at full test power, and 0° model pitch. The nose balance design load that results in the peak stress for the balance occurs with wings-off (uninstalled thrust testing), engine-off, and 7.5° model pitch. Also, note that thrust in our coordinate system was negative axial force and weight was considered negative normal force.

Table 1. Balance Design Loads

	Axial Force (lb)	Side Force (lb)	Normal Force (lb)	Condition
Nose Balance	-1,516	0	-12,437	Wings-on weight
Wing Balance	-758	0	-19,556	Wings-on weight
Nose Balance	4,084	0	-15,790	Wings-off max
Wing Balance	-8,113	5,449	-16,379	Wings-on max

LSPM Balance Flexure Sizing

The detail design consisted of sizing the flexures to produce maximum signal levels and minimum stress in peak stress regions. Maximum von Mises stress was limited to three times the material yield stress to conform to lab policy for dynamic tests. The effects of instrumentation cable line noise on data quality, due to the long cable runs (400-500 ft) at the BHTF, was minimized by designing the axial force and normal force balance bridges to produce signal levels of ~10 mV per bridge, maximizing the signal to noise ratio for the bridges.

The requirements for minimum stress and maximum signal level made sizing the flexures more difficult. The expected signal levels are difficult to estimate using simple beam theories since shear deflection predominates the flexure analysis. Peak stress values and their locations were difficult to assess for this low profile, high capacity balance. The design requirements amounted to designing a balance that could take the distributed dead weight of the model (50,000 lb) while maintaining a factor of safety of 3 on material yield stress and measuring a maximum 20,000 lb distributed normal force while producing ~10 mV per bridge for the 20,000 lb increment. In order to meet these requirements a series of finite element models were created to size the flexures.

The first FEM was mentioned previously for determining balance reaction loads. It consisted of the LSPM primary structure as well as a stiffness representation of the balances.

This model was used for determining the shear and moment in each flexure, in addition to determining balance reaction loads. The second model was used to determine flexure sizes for given unit loads. It consisted of a single flexure assembly of the balance (4 flexure assemblies per balance) with three SCFs per flexure assembly (Figure 6); one to measure normal force, one to measure axial force, and one for side force. The single flexure assembly model was appropriate for sizing the flexures since it was small enough to obtain results quickly, modify the flexure, and rerun the model. Boundary conditions were chosen to be conservative. Once the design was optimized a third detailed FEM of the entire balance was created to verify the design.

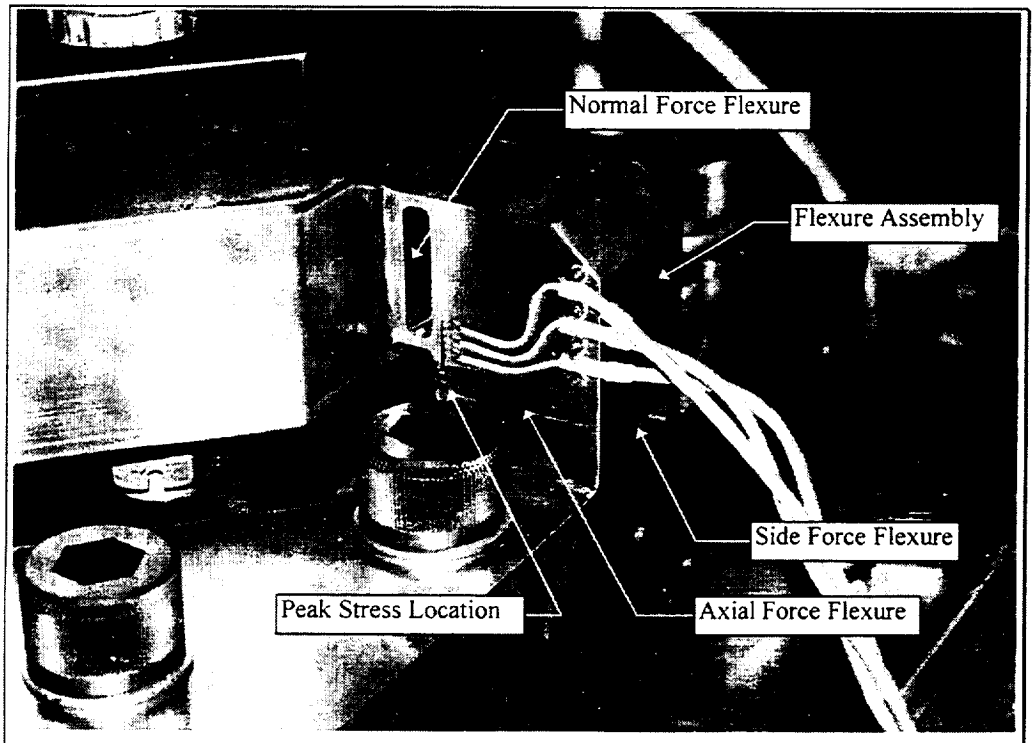

Figure 6. Balance Flexure Assembly Detail

Through the use of this iterative design process the balance goals were met. The peak von Mises stress goal was satisfied with 3.4 factors of safety on material yield stress and the signal levels for normal force and axial force were estimated to be 10 mV. These values were subsequently verified during proof testing and calibration.

LSPM Balance Construction

The hover test at the BHTF required us to use a high strength precipitation hardened steel for the SCF balances. These materials resist corrosion due to moisture, have high strength properties, machine relatively easy, and distort very little after solution heat treating. Their spring material properties are excellent; exhibiting low hysteresis, low creep, and excellent

linearity. Due to availability, 17-4PH was chosen with a H900 solution heat treat, for SCF balance construction.

Magnetic particle inspection, per Boeing specification, was called out for the balances to ensure that no subsurface defects were present in the machined balance material. Unfortunately, the balances failed inspection due to a serious metallurgical problem known as phase segregation. This phenomenon, indicated by the appearance of delta-Ferrite stringers, is described by bands of phase segregated iron particles that are distributed through the plate thickness. Iron has poor crack initiation and fracture toughness properties, which makes it a bad choice to use in any loading application where there are a large number of cycles (>3000)

Due to the compressed test schedule, we had to determine a disposition of the rejected balances that would allow us to use them safely during hover testing at the BHTF. The first requirement of the disposition was that the balances would only be used for the hover test and the number of load cycles would be limited to less than 3000. The second requirement was to proof-load each balance to a minimum of two times the worst case operating load.

All the balances were proof-loaded while measuring the strains at the critical stress location to a factor of 3 times the worst case operating load. All the balances passed the proof-load test and showed no signs of yielding. A consensus decision was reached among laboratory and program personnel to use the balances for the hover test under these limiting conditions.

After completing the proof test, the balances were instrumented with JP TECHNOLOGIES transducer class shear strain rosettes (P/N JK06-062TA-500 L). The rosettes were an etched Karma/Evanohm foil grid with a nominal 500Ω resistance and laminated Kapton backing. The balances were moisture proofed using The Measurements Group M-COAT C, a solvent-thinned RTV silicone rubber.

We experienced problems with the moisture proofing system; water intruded into the gage lead wires prior to FMS checkout which caused spurious readings. There was a significant amount of rain during the test setup and FMS checkout and the LSPM was not covered during these times. The moisture was able to penetrate the coating due to an improper installation of the moisture proofing system. The gage lead wires were laid directly on the metal surfaces of the balance and then covered with the M-COAT C. Recommended procedure at our laboratory is to lay down some of the M-COAT C on the bare metal and then lay the lead wires into the coating. Once the moisture proofing has cured slightly, an additional coating is laid over the lead wire assembly so that the entire wire is encapsulated with the moisture proofing material.

To correct the problem, the coating was removed from the lead wires of all the balances and the lead wires and gage installations were dried using heated air for approximately two days. The bridge outputs were monitored during this time and the FMS performance returned to normal. The gages were recoated with M-COAT C using the above recommended procedure and an additional coating of M-COAT B was applied to the gage and lead wire installation. After this, no other moisture related problems occurred.

LSPM Balance Calibration

The 6-component balances were calibrated individually and assembled into the FMS. The balances were installed on precision ground balance mount blocks in the LSPM and attached to the spherical bearing assemblies mounted to the BHTF turn barrel assembly. Once the mount block misalignment angles in roll, pitch, and yaw were determined the external forces applied to the LSPM could be measured. Using the mount block position information obtained from computer aided theodolite measurements during assembly of the LSPM, the external moments applied to the LSPM could be determined.

Our plan to calibrate the balances individually and then assemble them into the FMS, as opposed to calibrating the overall FMS with the balances installed in the LSPM, required that we use 6-component balances at each attachment point to cancel out any internal forces or moments in the system. The cost of adding additional components to the individual balances to allow for this approach, was more than offset by the cost and schedule reduction of not having to conduct a large scale calibration with the model installed in the BHTF. Measuring the moments at the LSPM attachment points, even though the model was mounted to the balances through spherical bearings, allowed us to determine the level of interaction between moments and forces. The design of the system allowed all external forces and moments to be measured and all internal forces or moments, due to thermal expansion or pressure, to be canceled out.

The calibration block, which had a nine hole pattern on three sides and a center hole on the other two sides, was mounted to the facility attachment surface (ground attachment section) of the balance (Figure 7). Loads were applied to the calibration block through a hanger assembly with an attached spherical bearing. The bearing was used to align the applied load and to ensure no moments were being applied through the attachment. The loads that were applied during calibration, shown in Table 2, were large which required the use of hydraulic actuators and reference load cells. Air driven pumps were used to pressurize the hydraulic oil in the actuators. The hydraulic lines to and from the actuator were then valved off and a calibration load point was taken. This ensured that a steady load was applied to the balance. Reference load cells, used for balance calibration, were calibrated, traceable to NIST, with an overall uncertainty of ±0.13% of the full scale calibration range based on a 95% confidence level.

Table 2. Calibration Range for LSPM 6-Component Balances

Calibration Ranges for ASTOVL LSPM Wind Tunnel Model Balances					
Nose Balance					**Condition**
Axial Force	-500	to	4,500	lb	Wings off, engine off, 7.5 deg pitch
Normal Force	-16,000	to	0	lb	Wings off, engine off, 0 deg pitch
Side Force	-1,400	to	1,400	lb	Wings off, engine off, +/- 5 deg roll
Roll Moment	-1,333	to	1,333	ft-lb	Estimated maximum
Pitch Moment	-1,333	to	1,333	ft-lb	Estimated maximum
Yaw Moment	-750	to	750	ft-lb	Estimated maximum
Wing Balances					**Condition**
Axial Force	-9,000	to	9,000	lb	Wings off/on, nozzles @ 45 deg, full cruise, 0 deg pitch
					Wings on, nozzles @ 110 deg, jet screen on, 7.5 deg pitch
Normal Force	-24,000	to	0	lb	Wings on, engine off, 0 deg pitch
Side Force	-4,000	to	4,000	lb	Wings on, engine on, +/- 5 deg roll +/- addl 2,000 lb SF
Roll Moment	-2,000	to	2,000	ft-lb	Estimated maximum
Pitch Moment	-2,000	to	2,000	ft-lb	Estimated maximum
Yaw Moment	-1,500	to	1,500	ft-lb	Estimated maximum

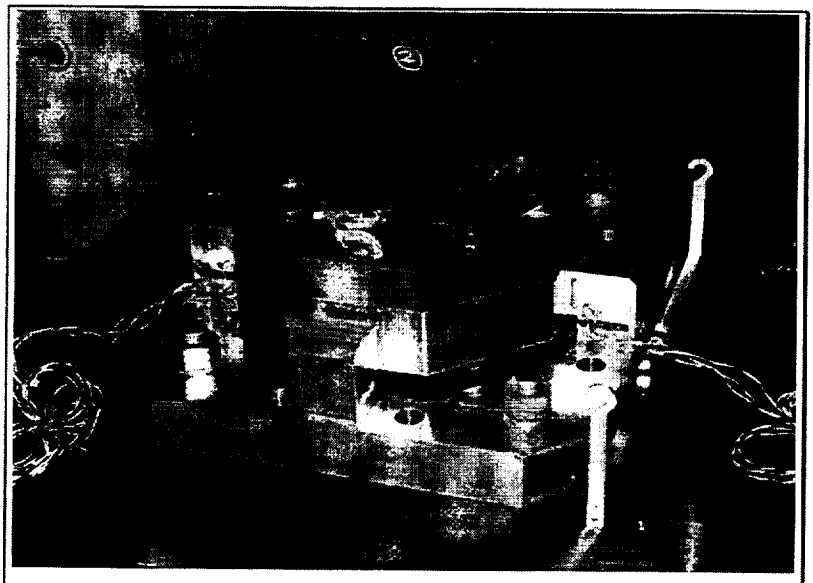

Figure 7. Balance Calibration Block

Structural steel was used to construct a stiff external frame that could securely hold the actuator adjustment hardware. Loads were applied to the balance through steel chain attached to the end of the actuator and hanger assembly. The distance between the end of the actuator and the calibration block was approximately 12 ft for the normal force loads and 6 ft for axial and side force loads. This large distance was used to minimize the error associated with angular alignment. The actuator end points and centers of the calibration block were lined up using a computer aided theodolite. Positions were known with an uncertainty of ±0.010" based on a 95% confidence level which resulted in very small angular biases propagated into the balance calibration of 30 arcseconds for normal force and 60 arcseconds for axial and side force.

After all the data was taken 1st, 2nd, and 3rd order polynomials were fit through the data which included all interactions through 2nd order. The confidence interval was determined using the approach outlined in Reference 1 for each order of polynomial, which consisted of determining the standard error of estimate for the curve as an approximation of the precision index. The differences between 1st and 2nd order residuals are shown for a representative balance (right wing balance) in Figures 8 through 11. The best mathematical model for the SCF balance behavior can be seen by comparing Figures 10 and 11. Figure 11, the 2nd order

polynomial fit, shows a uniform distribution of the residual force over the entire range of applied normal force. Figure 10, the 1st order fit, reveals that the second order effect has not been taken into account and there is a small but significant error associated with this order of curve fit. Thus, for normal force it is clear that the 2nd order polynomial curve fit better models the physical behavior of the balance. Figures 8 and 9 show that the effect of polynomial order is not as significant for axial force as for normal force due to the lower full scale strain levels of the axial force flexures.

Even though the 2nd order polynomials provided a better mathematical model to the balance behavior, the 1st order fits still provided good accuracy and offered additional simplicity during data acquisition and reduction checkout. Thus, linear curve fits with linear interactions were used to reduce the force and moment data during testing. Use of the linear equations simplified the handling of weight tare offsets by using a voltage tare rather than engineering units. This made it more convenient to detect anomalies in bridge operation and was more efficient for data checkout. The use of linear curve fits also allowed us to conservatively and simply determine overall FMS normal force uncertainty - since linear curve fits are insensitive to ± direction - through the use of free weight check loads applied to the model as opposed to the more difficult task of accurately applying a normal force in the upward direction.

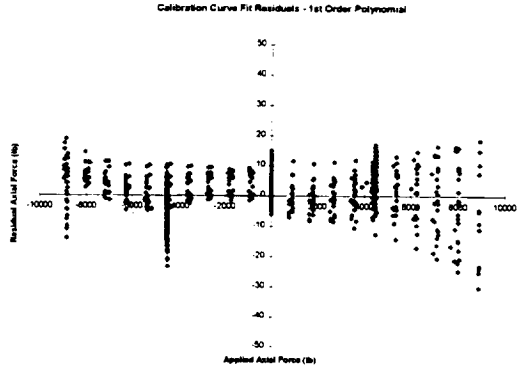

Figure 8. Axial Force Residual - 1st Order

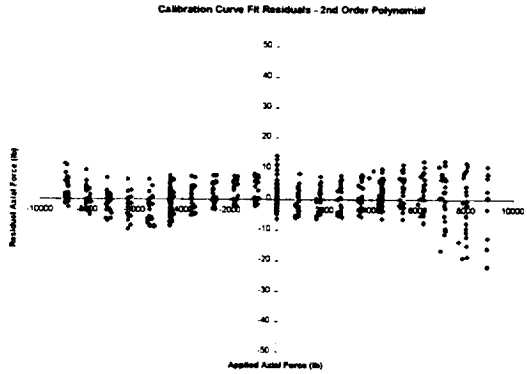

Figure 9. Axial Force Residual - 2nd Order

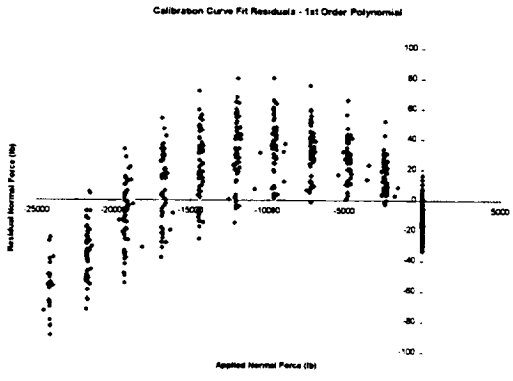

Figure 10. Normal Force Residual - 1st Order

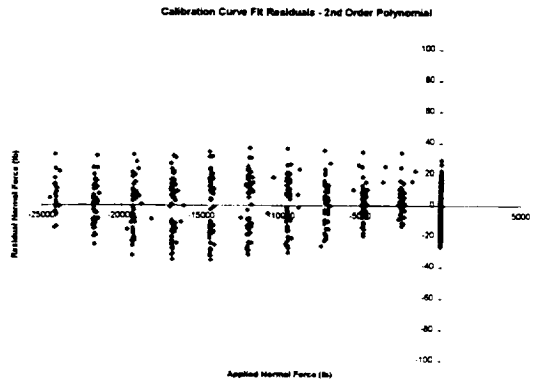

Figure 11. Normal Force Residual - 2nd Order

The calibration curve fit errors and 95% confidence intervals for axial force and normal force are shown for all three balances in Figures 12-17 below. Note that the residuals are plotted versus calibration load point. The normal force data shows small residuals in the beginning of the calibration since only pure normal force or normal force with moment interactions are applied in the beginning of the load schedule. This information will be used to explain why the check load errors are small when applying normal force loads during FMS checkout.

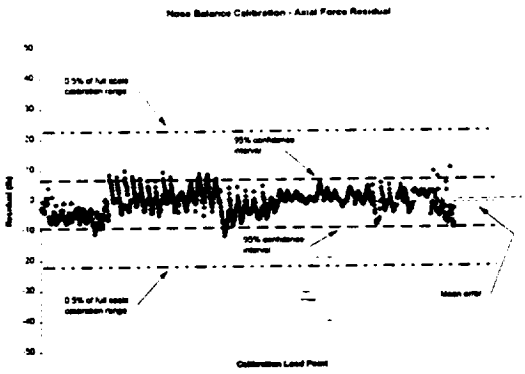

Figure 12. Nose Balance Axial Force Residual

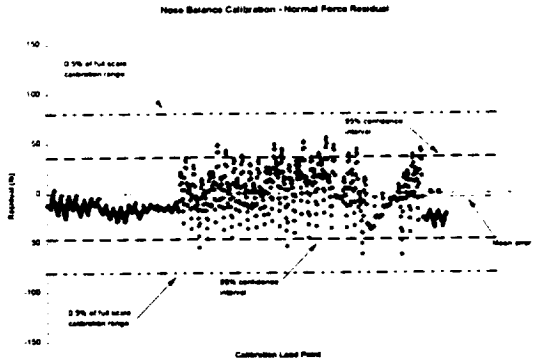

Figure 13. Nose Balance Normal Force Residual

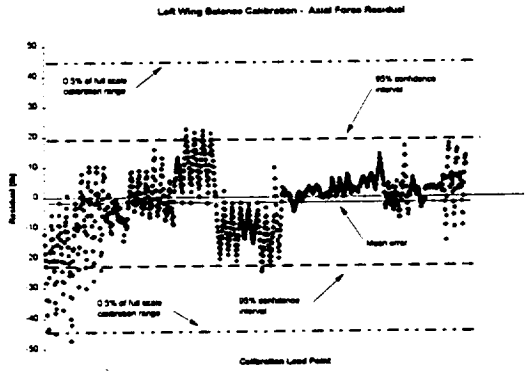

Figure 14. Left Wing Balance Axial Force Residual

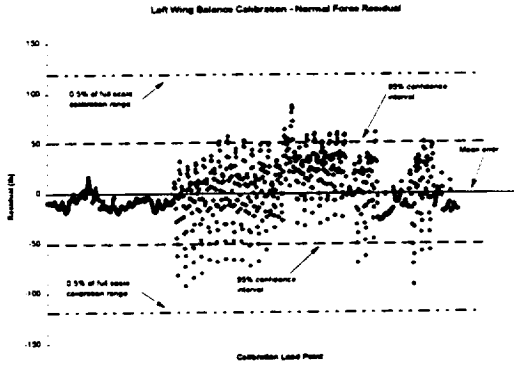

Figure 15. Left Wing Balance Normal Force Residual

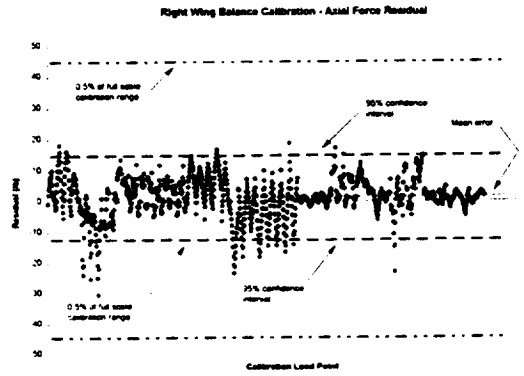

Figure 16. Left Wing Balance Axial Force Residual

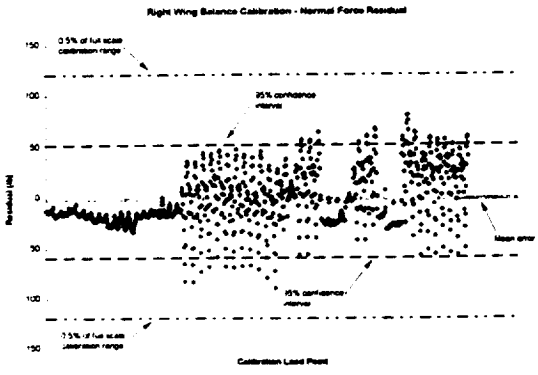

Figure 17. Right Wing Balance Normal Force Residual

LSPM Force Measurement System Performance

FMS performance was determined by performing a detailed elemental uncertainty analysis according to Reference 1 and Reference 2 and comparing the results to those obtained from check loading the system.

Check loading of the FMS was accomplished by applying dead weights to an attachment point on one of the model bulkheads. The weights were certified with a 95% confidence interval uncertainty of ±0.12%. The two check weights (2,576 lb and 6,442 lb) were applied individually through a spherical bearing so no moments would be induced in the model structure. This technique gave us an accurate indication of FMS performance over a limited range.

The technique used for checking the axial force uncertainty (other than the detailed uncertainty estimate) was to pitch the model to a full scale angle of attack of 7.5° and then hang the check weights on the model; which provided a component of the check load in the axial force direction of the aircraft coordinate system.

These techniques for applying check loads were not sufficient for determining full scale uncertainty values. However, these check loads, coupled with the detailed elemental uncertainty analysis described below, allowed us to bound the total expected uncertainty of the FMS with regard to axial force and normal force.

For the detailed uncertainty analysis, the primary contributors to the overall uncertainty in the FMS were the balance calibration errors, correlated biases, and error in the pitch angle measuring device. The correlated biases were due to the same calibration setup and reference load cells being used for each of the three individual balance calibrations.

Errors due to the pitch angle measurement system propagated into the overall FMS uncertainty through the simplified version of the data reduction equations shown below.

$$AF = \left(AF_N + AF_L + AF_R\right)\cos\theta + \left(NF_N + NF_L + NF_R\right)\sin\theta \qquad (1)$$

$$NF = \left(NF_N + NF_L + NF_R\right)\cos\theta - \left(AF_N + AF_L + AF_R\right)\sin\theta \qquad (2)$$

where:

$\theta \equiv$	Angular uncertainty of pitch angle measurement (deg or rad)
$AF \equiv$	Axial Force (lb)
$NF \equiv$	Normal Force (lb)
$AF_N \equiv$	Nose Balance Axial Force (lb)
$AF_L \equiv$	Left Wing Balance Axial Force (lb)
$AF_R \equiv$	Right Wing Balance Axial Force (lb)
$NF_N \equiv$	Nose Balance Normal Force (lb)
$NF_L \equiv$	Left Wing Balance Normal Force (lb)
$NF_R \equiv$	Right Wing Balance Normal Force (lb)

After applying the uncertainty analysis expression, in accordance with Reference 1, to equations (1) and (2) above, it was determined that the error is not independent of the load applied. The normal force is affected by the presence of axial force and the axial force is affected by the normal force as shown below.

$$B_{AF} = \sqrt{NF^2 B_\theta^2 + \left(B_{AF}\right)_{cal} + \left(B_{AF}\right)_{corr}} \tag{3}$$

where:

$B_{AF} \equiv$	Total Axial Force Bias (lb)
$\left(B_{AF}\right)_{cal} \equiv$	Calibration Bias Limit for Axial Force (lb)
$\left(B_{AF}\right)_{corr} \equiv$	Correlated Bias Limit for Axial Force (lb)
$B_\theta \equiv$	Bias Limit for Pitch Measurement System (rad)

$$S_{AF} = \sqrt{NF^2 S_\theta^2 + \left(S_{AF}\right)_{cal}} \tag{4}$$

where:

$S_{AF} \equiv$	Total Axial Force Precision Index (lb)
$\left(S_{AF}\right)_{cal} \equiv$	Calibration Precision Index for Axial Force (lb)
$S_\theta \equiv$	Precision Index for Pitch Measurement System (rad)

$$B_{NF} = \sqrt{AF^2 B_\theta^2 + \left(B_{NF}\right)_{cal} + \left(B_{NF}\right)_{corr}} \tag{5}$$

where:

$B_{NF} \equiv$ Total Normal Force Bias (lb)

$(B_{NF})_{cal} \equiv$ Calibration Bias Limit for Normal Force (lb)

$(B_{NF})_{corr} \equiv$ Correlated Bias Limit for Normal Force (lb)

$$S_{NF} = \sqrt{AF^2 S_\theta^2 + (S_{NF})_{cal}} \tag{6}$$

where:

$S_{NF} \equiv$ Total Normal Force Precision Index (lb)

$(S_{NF})_{cal} \equiv$ Calibration Precision Index for Normal Force (lb)

The elemental uncertainty terms, corresponding to a 95% confidence level, that were used to determine the overall calibration uncertainty and the correlated biases for the axial force and normal force components of the FMS, along with the bias limits and precision index for the pitch angle measuring system, are listed in Tables 2 and 3 below.

Table 3. Elemental Uncertainty Terms for Axial Force Component

Element	Bias Limits	Precision Index	95% confidence t
Reference Load Cell	10.0 lb	0.0 lb	2
Alignment Error	3.5 lb	0.0 lb	2
Deflection Error	Negl	0.0 lb	2
Nose Balance Curve Fit	1.0 lb	3.8 lb	2
Left Balance Curve Fit	1.8 lb	10.2 lb	2
Right Balance Curve Fit	1.3 lb	6.7 lb	2
Model Mount Block Angle	0.01 deg	0.0 deg	2
Pitch Angle Measuring System	0.1 deg	0.02 deg	2

Table 4. Elemental Uncertainty Terms for Normal Force Component

Element	Bias Limits	Precision Index	95% confidence t
Reference Load Cell	30.0 lb	0.0 lb	2
Alignment Error	2.5 lb	0.0 lb	2
Deflection Error	7.1 lb	0.0 lb	2
Nose Balance Curve Fit	4.9 lb	19.9 lb	2
Left Balance Curve Fit	0.5 lb	25.4 lb	2
Right Balance Curve Fit	3.1 lb	27.3 lb	2
Model Mount Block Angle	0.01 deg	0.0 deg	2
Servoaccelerometer	0.1 deg	0.02 deg	2

Using Tables 2 and 3, the fixed calibration uncertainties can be determined. The fixed terms do not vary with either applied normal force or axial force; they consist of the bias and precision errors due to the individual balance calibrations and correlated biases. The last two items in Tables 2 and 3 are used to determine the bias limits and precision index for the pitch angle measuring system used in measurement uncertainty equations (3) - (6).

The overall axial force and normal force uncertainty consists of fixed bias errors due to balance calibration, correlated bias errors due to the reference load cells, alignment error, deflection error, and variable bias & precision limits that are a function of load. The overall uncertainty for the FMS in axial force and normal force are shown in Figures 18 and 19. The results of the dead weight check load test, described below, are included in Figures 18 and 19, as discrete points, to determine the quality of the detailed elemental uncertainty estimate.

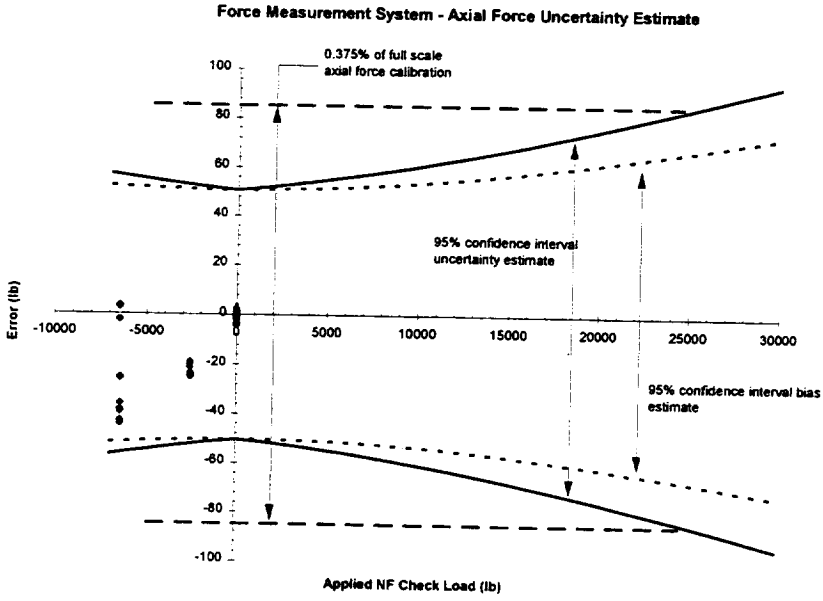

Figure 18. Force Measurement System Axial Force Uncertainty

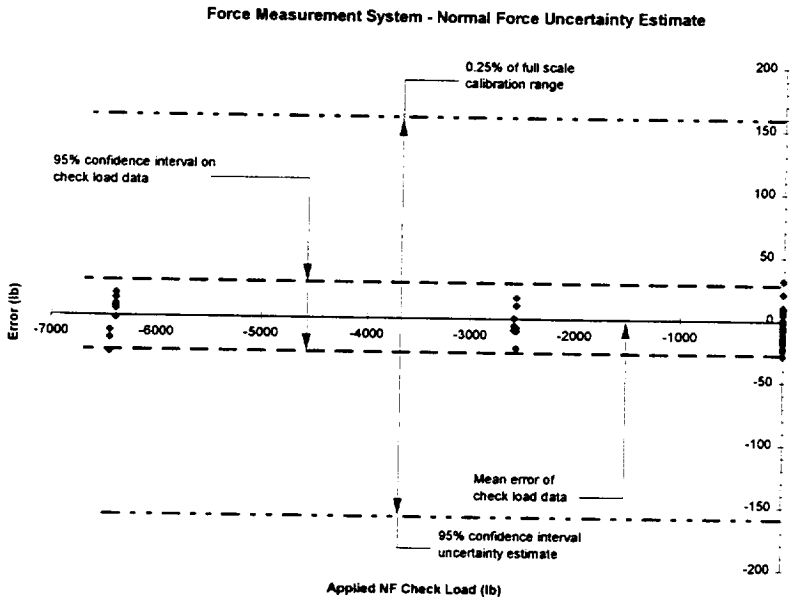

Figure 19. Force Measurement System Normal Force Uncertainty

The quality of the axial force measurement is sensitive to errors in the pitch angle, unlike the normal force which exhibits very little sensitivity to pitch angle error. However, the goal of measuring normal force to within ±0.5% was achieved according to the detailed uncertainty analysis. Note that the check load data points shown in Figure 19 have a 95% confidence precision interval much less than that predicted by the detailed elemental uncertainty analysis. As described earlier in the calibration section and seen in Figures 13, 15, and 17, the individual balance calibrations show small residuals when only the normal force and normal force with moment interactions are considered. Since no large interaction force is applied in the presence of the normal force during the check loads, the larger scatter due to the individual balance interactions is not seen in the normal force check load data.

SUMMARY/CONCLUSIONS

A force measurement system was designed, developed, and fabricated within aggressive schedule and cost constraints for the full-scale LSPM hover test. Shear cell flexure elements have been successfully demonstrated to be an effective element for obtaining balances with high stiffness in a compact design with good force resolution characteristics. Calibration of individual 6-component balances (as opposed to in-situ calibration of the FMS and LSPM) is an effective method for reducing FMS cost and overall calibration time and achieving realistic uncertainty

goals. A detailed uncertainty analysis, along with a limited set of check load data, were used to validate the performance of the BHTF FMS. The goal for the measurement of normal force was an uncertainty of ±0.5% of the full scale calibration range based on a 95% confidence interval. The actual uncertainty limit, based on a 95% confidence level, was better than ±0.25% of the full scale normal force calibration range. The uncertainty limit for the axial force, based on a full scale calibration range and 95% confidence interval, was better than ±0.38%.

Shear cells represent a flexible and cost effective flexure for the design and fabrication of aero-propulsion balances. Excellent linearity, low level interactions, and insensitivity of the flexure to temperature gradients are distinct advantages of this type of flexure over more traditional bending elements. Extensive testing and use over a 10 yr period have validated design techniques for the use of SCFs in propulsion balances. Current efforts are under way to adapt the SCF technique to the design of internal balances for wind tunnel testing. An IR&D effort is providing the means to determine whether or not the stiff SCFs can be integrated to yield an internal balance design that provides for increases in the angle of attack test range for modern wind tunnel fighter models.

REFERENCES

1. Coleman, Hugh W.; Steele, W. Glenn, Jr.: *Experimentation and Uncertainty Analysis for Engineers*. John Wiley & Sons, Inc.,1989.

2. Assessment of Wind Tunnel Data Uncertainty. AIAA S-071-1995.

The Technology Research of 15cm × 15cm Magnetic Suspension and Balance System(MSBS)

Yin Li-ming Shen Long-hua Yang Quan-ling
Department of Automatic Control
Changsha Institute of Technology
Changsha, 410073, Hunan, China

Abstract

The 15cm × 15cm Magnetic Suspension and Balance System (MSBS) is developed in 1995 on the base of research work of MSBS technology since 1987 under the economic support of China CARDC.

The mathematic representations of control model and the principle of the system position control are derived, using the method of the dynamic circuit theory in electro-magnetic system for the MSBS.

The "H" PWM power amplifier, the electro-optical position detector and the 5 component calibration model are introduced tentatively in this paper.

Key words: Magnetic Suspension and Balance System, wind tunnel balance system, PWM power amplifier, electro-optical position sensor, wind tunnel balance system calibration.

Electro-magnetic structure of the 15cm × 15cm MSBS

Since the initiation of the MSBS technology research work in 1987, in our Institute, the 3cm × 3cm and 6cm × 6cm MSBS used for MSBS Principle study are successively developed, investigating some feasible variants of electro-magnetic structures and model position detection. the final 15cm × 15cm MSBS electro-magnetic structure is formed according to the results, obtained in the preceding stages of this research. The MSBS design work is initiated since 1994 and the MSBS is developped in october 1995 after its processing and installation work. Furthermore, some testing results have been obtained now in the preliminary aero-dynamic tests.

The 15cm × 15cm MSBS is equipped with 10 electro-magnetic coils, arranged

symmetrically. The x-directional drag coils are of air cored structure. The z-directional lift coils and the y-directional side force coils are the iron cored coils.

They are divided in two groups: front group and rear group, used to raise the magnetic field intensity in the testing section and to collect the magnetic flux relatively. The arrangement of coils is shown in figure 1.1 (Scheme of twosideviewing of MSBS).

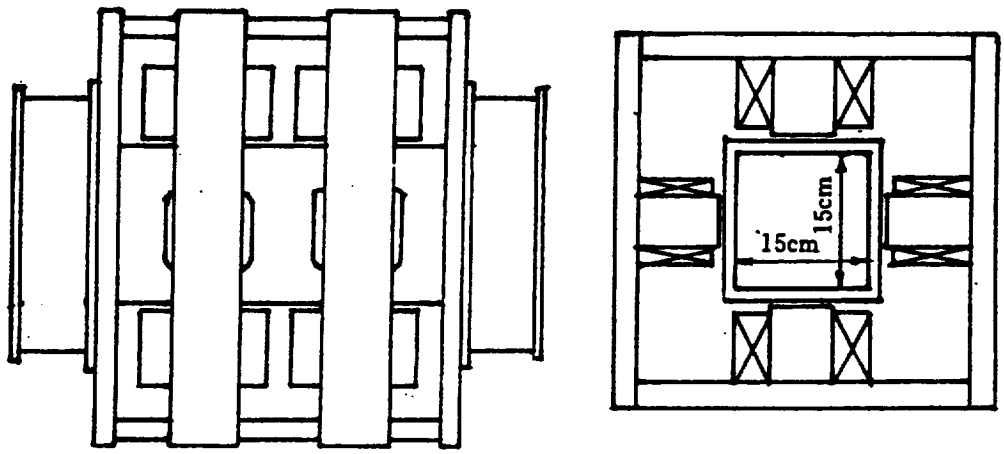

(a) (b)

Fig 1-1: Scheme of two side viewing of MSBS

The coil numbers are shown in figure 1.2

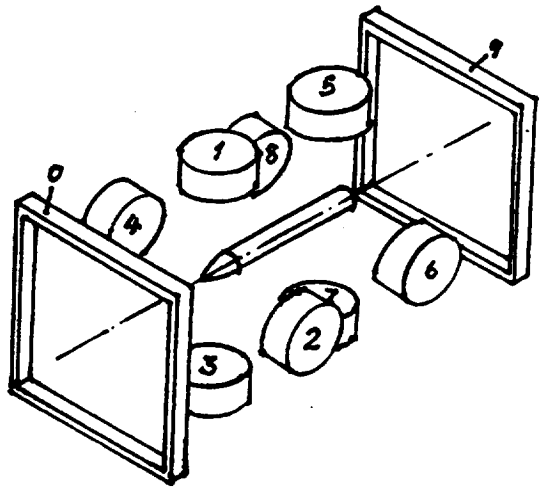

Fig 1-2: Arrangement structure of MSBS coils.

The coils No. 0 and 9, used to generate the x-directional electro-magnetic force Fx are the inversely connected in series coils, represented by Wx. The coils No. 1 and 3, used to generate the z-directional electro-magnetic force $F_{z1}$and the directly connected in series coils, represented by W_{z1}. Similary, the coils No.5 and 7(W_{z2}), the coils No. 2 and 4

(W_{y1}) and the coils No.6 and 8(W_{y2}) are used to generate the electro-magnetic forces F_{z2}, F_{y1} and F_{y2} respectively.

The Nd-Fe-B permanent magnet are selected as inner iron cores of the aero-dynamic testing model. Thus, a very strong secondary magnetic field is obtained and the controlled electro-magnetic force of this model is raisd. Furthermore it is possible to reduce the total control power.

the parameters of the MSBS electro-magnetic coils are listed in table 1.1.

Table 1.1

Coils No.	diameter of enamel-insulated wire (mm)	turns	DC resistance Ω	Self-inductance (H)
0.9	square wire 4 × 2	288	1.29	0.061
1,3	ϕ 2.26	546	1.69	0.206
2,4	ϕ 2.26	295	0.90	0.05
5,7	ϕ 2.26	546	1.70	0.207
6,8	ϕ 2.26	295	0.86	0.051

The iron core of the model is 15mm in diameter and 120mm in length. The Nd-Fe-B material is magnetized in axial dircetion.

Analysis of the dynamic circuit theory of 5 electro-magnetic force components

The 10 electro-magnetic coils of the 15cm × 15cm MSBS constitute the 5 control channels of 5 electro-magnetic forces: Fx, F_{y1}, F_{z1},F_{y2}, F_{z2}.The figure 1-2 shows, that the channel W_{y1}, constituted by two connected in seris coils., should generate the electro-magnetic force F_{y1}. The channel W_{z1} should generate the electro-magnetic force F_{z1}. The F_{y1} and F_{z1} are the front-end y-and z-directional control forces, applied to the model. The iron cores in the coils W_{y1} and W_{z1} share an external magnetic yoke in order to reduce the reluctance of the magnetic circuit. Similarly, the W_{y2} and W_{z2} also share an iron cored magnetic circuit, generating the control forces F_{y2} and F_{z2} in y-and z-directions of the model rear end respectively. The 5 force components bearing on this model are shown schematically in the figure 2-1(a).

According to the situation of mechanical motion the 5 force compronents can apply the constraint to the 5 degree of freedom of the model besides the rolling one.

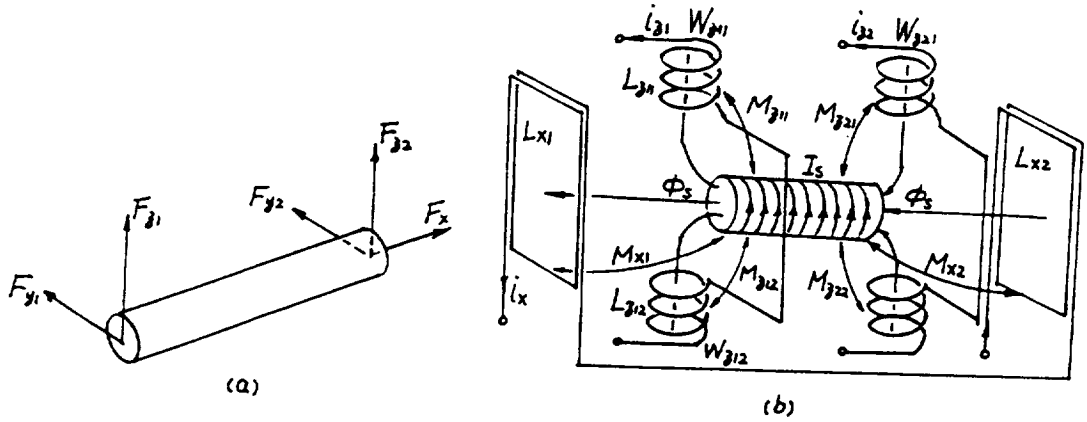

Fig 2-1: Scheme of the force components, bearing on the model iron core and magnetic coupling with control coils.

According to the situation of mechanical motion the 5 force compronents can apply the constraint to the 5 degree of freedom of the model besides the rolling one.

The figure 2-1(b) schematically shows the parameters of MSBS, used to derivate the electro-magnetic forces, bearing on this model by means of the examples of the x-directional control coil channels and of the z-directional front and rear control coil channels. The y-directional coils are not shown in this figure, but the action principle is similary.

Since the selected Nd-Fe-B permanent magnetic material for the model iron core has a very large intensity of its coercive residual magnetism, it is possible to consider that the reluctance in the bar magnet is very large and that the helical coil which make it equivalent surface current I_s generate the distribution of magnetic field similar to the permanent bar magnet. Thus, the control coil current of various channels acting with I_s generate the electro-magnetic force, therefore it is possible to its analysis according to unified theory of dynamic circuit.

When the control voltage U_q applies to one channel coil, it is possible to generate the current i_q, the balance equation of which can be written as following.

$$u_q = R_q i_q + d\Psi_q / dt \quad or \quad u_q = R_q i_q + d(L_q i_q)/dt$$

Taking the preceding group z-directional channel as an example, the magnetic linkage through the coil can be written as:

$$\Psi_{z11} = L_{z11} i_{z1} + M_{z11} I_s, \Psi_{z12} = L_{z12} i_{z1} - M_{z12} I_s$$

Let $L_{z11} = 0.5 L_{z1} = L_{z12}$,

$M_{z11} \approx 0.5 M_{z1} \approx M_{z12}$

All this is led to the nearby balance position. Since the reluctance in the magnetic circuit is larger, the Ψ_{z11}, Ψ_{z12} is related to i_{z1} only, the $M_z I_s$ is related to the model space

$$u_{z1} = R_{z1}i_{z1} + L_{z1}\frac{di_{z1}}{dt} + \frac{\partial M_{z11}}{\partial Z_1} I_s \frac{dZ_1}{dt} + \left(\frac{\partial M_{z12}}{\partial Z_1}\right) I_s \left(-\frac{dZ_1}{dt}\right)$$

$$= R_{z1}i_{z1} + L_{z1}\frac{di_{z1}}{dt} + 2\frac{\partial M_{z1}}{\partial Z_1} I_s \bullet V_{z1} \qquad (2-1)$$

The first term of the equation right side is the resistance voltage drop, the second one is the electric potential of transformer, the third one is the model's kinematic electric potential.

Multiplying the two sides of the equation (2-1) by i_{z1}, it is possible to acquire the relationship of the power balance in this channel as following

$$P_{z1} = u_{z1}i_{z1}$$

$$= R_{z1}i_{z1}^2 + L_{z1}i_{z1}\frac{di_{z1}}{dt} + 2\frac{\partial M_{z1}}{\partial Z_1} \bullet I_s \bullet i_{z1} \bullet V_{z1}$$

$$= P_R + P_L + F_{z1} \bullet V_{z1} \qquad (2-2)$$

There:P_R is the thermal loss of resistance;

P_L is the magnetic energy storage in magnetic circuit;

$F_{z1} \cdot V_{z1}$ is the power of mechanical motion, generated in this channel.

According to the equations (2-1) and (2-2) it is possible to obtain the kinematic electric potential

$$e_v = 2\frac{\partial M_{z1}}{\partial Z_1} \bullet I_s \bullet V_{z1} = C_{ez1} \bullet V_{z1}$$

and the electro-magnetic force:

$$F_{z1} = 2\frac{\partial M_{z1}}{\partial Z_1} \bullet I_s \bullet i_{z1} = C_{fz1} \bullet i_{z1}$$

and there is $C_{z1} = C_{cz1} = C_{fz1}$

It is identical to electro-magnetic relationship of the permanent magnetic DC motor, and it is a linear relationship. Similarly, according to the principle of the electric machine, the C_{z1} can be obtained by experiment.

Synthesizing the principles described above for the 5 channel electro-magnetic system it is necessary to consider all relationships of the inductance and the mutual inductance:

$$L = \begin{bmatrix} L_x \\ L_{y1} \\ L_{z1} \\ L_{y2} \\ L_{z2} \end{bmatrix} = \begin{bmatrix} L_{x0} + M_x & M_{xy1} & M_{xz1} & M_{xy2} & M_{xz2} \\ M_{yx1} & L_{y10} + M_{y1} & M_{yz1} & M_{y12} & M_{yz12} \\ M_{zx1} & M_{zy1} & L_{z10} + M_{z1} & M_{zy12} & M_{z12} \\ M_{yx0} & M_{y21} & M_{yz12} & L_{y20} + M_{y2} & M_{yz2} \\ M_{zx2} & M_{zy21} & M_{z21} & M_{zy2} & L_{z20} + M_{z2} \end{bmatrix} \qquad (2-3)$$

In the linkage magnetic structure the electro-magnetic relationship will became

very complex. In order to reduce the coupling we use a common ironcored magnetic cricuit only for the front and rear y-dircetional and z-directional channels, furthermore the coils are orthogonal. The front and rear y-and z-directional homologous coils have no common magnetic circuit, thus there is a very large air gap, therefore the linkage is very small. The x-directional coil and other coils are orthogonal. All experimental data in the inductance matrix L are listed in table 2.1

table 2.1

L_q(H)	W_x	W_{y1}	W_{x1}	W_{y2}	W_{x2}
W_x	6.1×10^{-2}	1.62×10^{-4}	4.78×10^{-4}	1.58×10^{-5}	3.99×10^{-4}
W_{y1}	1.62×10^{-4}	5.1×10^{-2}	8.08×10^{-5}	9.34×10^{-4}	8.16×10^{-5}
W_{z1}	4.78×10^{-4}	8.08×10^{-5}	2.06×10^{-1}	8.08×10^{-5}	6.87×10^{-4}
W_{y2}	1.58×10^{-5}	9.34×10^{-4}	8.08×10^{-5}	5.1×10^{-2}	6.65×10^{-5}
W_{z2}	3.99×10^{-4}	8.16×10^{-5}	6.87×10^{-4}	6.65×10^{-5}	2.09×10^{-1}

It is clear that the value of the mutual inductance between coils is far smaller than the value of in principal channel, therefore, this value can be neglected

At this time the inductance matrix L can be written as following:

$$L=\begin{bmatrix} L_x \\ L_{y1} \\ L_{z1} \\ L_{y2} \\ L_{z2} \end{bmatrix}=\begin{bmatrix} L_{x0}+M_x & 0 & 0 & 0 & 0 \\ 0 & L_{y10}+M_{y1} & 0 & 0 & 0 \\ 0 & 0 & L_{z10}+M_{z1} & 0 & 0 \\ 0 & 0 & 0 & L_{y20}+M_{y2} & 0 \\ 0 & 0 & 0 & 0 & L_{z20}+M_{z2} \end{bmatrix} \tag{2-4}$$

The voltage balance matrix U can be written as following:

$$U=\begin{bmatrix} U_x \\ U_{y1} \\ U_{z1} \\ U_{y2} \\ U_{z2} \end{bmatrix}=\begin{bmatrix} R_x+pL_{x0} & 0 & 0 & 0 & 0 \\ 0 & R_{y1}+pL_{y10} & 0 & 0 & 0 \\ 0 & 0 & R_{x1}+pL_{z10} & 0 & 0 \\ 0 & 0 & 0 & R_{y2}+pL_{y20} & 0 \\ 0 & 0 & 0 & 0 & R_{z2}+pL_{z20} \end{bmatrix}\begin{bmatrix} i_x \\ i_{y1} \\ i_{z1} \\ i_{y2} \\ i_{z2} \end{bmatrix}+$$

$$+\begin{bmatrix} C_x & 0 & 0 & 0 & 0 \\ 0 & C_{y1} & 0 & 0 & 0 \\ 0 & 0 & C_{z1} & 0 & 0 \\ 0 & 0 & 0 & C_{y2} & 0 \\ 0 & 0 & 0 & 0 & C_{z2} \end{bmatrix}\begin{bmatrix} v_x \\ v_{y1} \\ v_{z1} \\ v_{y2} \\ v_{z2} \end{bmatrix} \tag{2-5}$$

The control electio-magnetic force: $F=(F_{x1},F_{y1},F_{z1},F_{y2},F_{z2})$ can be expressed as

$$F = \begin{bmatrix} C_x & 0 & 0 & 0 & 0 \\ 0 & C_{y1} & 0 & 0 & 0 \\ 0 & 0 & C_{z1} & 0 & 0 \\ 0 & 0 & 0 & C_{y2} & 0 \\ 0 & 0 & 0 & 0 & C_{z2} \end{bmatrix} \bullet \begin{bmatrix} i_x \\ i_{y1} \\ i_{z1} \\ i_{y2} \\ i_{z2} \end{bmatrix} \qquad (2-6)$$

According to the above describing, it is very important to design a reasonable and rational MSBS electro-magnetic structure , permitting change the relationship of electro-mechanical energy conversion of 5 control channels from coupling system to independent relationship.

Principle of the detetion of aero-dynamic model space position

The CCD linear array, used to measure the position of 5 degree of freedom is considered at one time for 15cm × 15 cm MSBS, but for insufficient budget, the matured photo-cell technology is selected for the position detection (see figure 3-1) after testing the monochannel.

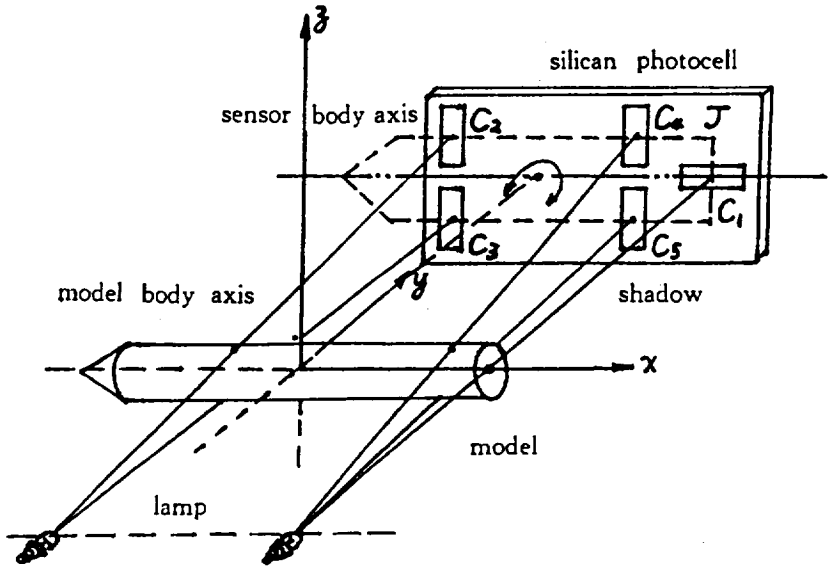

Fig 3-1: The scheme of principle of the silicon photocell position sensor.

These 5 silicon photocells are installed on the connector J. The photocells C_2 and C_3 are used to acquire the pitching and yawing attitudes of the model front end. The photocells C_4 and C_5 are used to acquire the pitching and yawing attitudes of the model rear end. The photocell c_1 is used to acquise the attitude of the x-directional motion. there

are two tungsen iodide lamps, used to generate a shadow of the model on the sensors. The area of the silicon photocell illumination is very closely related to its output voltage strength. In this MSBS the model space position attitude is taking the zero level of the sensor signal as object of control, therefore , the control of attack angle can be carried out by the connector rotation along the y direction. It means that the sensor body axis is coincide with the model body axis on the xz plane projection.

When the model's one end is pitching, the shadow of the model on the two corresponding silicon photocells will move vertically and change differentially, thus the differential changes $U_0 \pm \Delta U$ and $U_0 \mp \Delta U$ are realized on the two photocells as shown on the figure 3-2(a). When this end of the model is yawing, the models shadow on these two photocells will broading and narrowing in form of the conjugate change, causing the change , similar to $U_0 \pm \Delta U$ on photocells as shown in figure 3-2(b). With the two-way processing circuit of the differential amplifier it is possible to separate these two various model motion attitudes. There is a similar principle on the pitching and yawing attitude delection on another end of the model. The processing circuit is shown on figure 3-2(c).

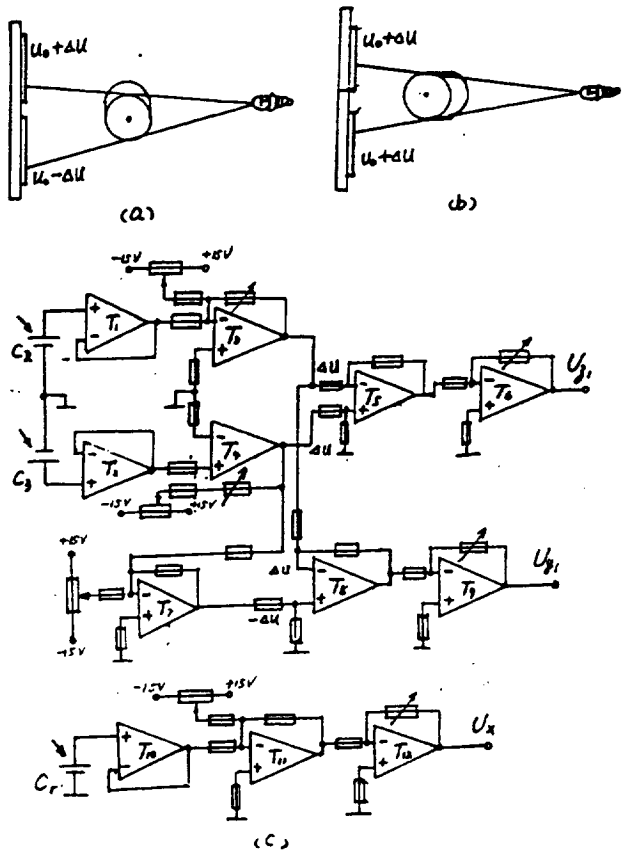

Fig 3-2:The method of the pitching and yawing attitudes and their processing circuit.

If the voltage signal $U_0 \pm \Delta U$ is generated on the photocells C_2 and C_3, the T_3 and

The design of the 5 channel position control system

There are 5 aero-dynamic components F_{Ax},F_{Ay},F_{Az},M_{Ay},M_{Az} bearing on the model at the time of aero-dynamic testing with the MSBS.

In order to maintain the predetermined prosition of this model , the control channels of the 5 magnets of the MSBS shall generate the 5 force components F_x, F_{y1},F_{z1}, F_{y2}, F_{z2} and the dynamic equilibrium, permitting change the control current i_x, i_{y1}, i_{z1}, i_{y2}, i_{z2} in every channel. the value of the aero-dynamic component changes can be acquired indirectly only in case of measuring the 5 changing current value.

By substitution in equation (2-6) the 5 electro-magnetic components corresponding to aero-dynamic components are:

$$\begin{bmatrix} F_x \\ F_y \\ F_z \\ M_y \\ M_z \end{bmatrix} = \begin{bmatrix} C_x & 0 & 0 & 0 & 0 \\ 0 & C_{y1} & 0 & C_{y2} & 0 \\ 0 & 0 & C_{z1} & 0 & C_{z2} \\ 0 & 0 & C_{z1}l^{-1} & 0 & -C_{x2}l^{-1} \\ 0 & -C_{y1}l^{-1} & 0 & C_{y2}l^{-1} & 0 \end{bmatrix} \times \begin{bmatrix} i_x \\ i_{y1} \\ i_{z1} \\ i_{y2} \\ i_{z2} \end{bmatrix} \qquad (4-1)$$

The equation of model motion is :

$$\begin{bmatrix} x_c \\ y_c \\ z_c \\ \theta \\ \Psi \end{bmatrix} = \begin{bmatrix} \frac{C_x}{m} & 0 & 0 & 0 & 0 \\ 0 & \frac{C_{y1}}{m} & 0 & \frac{C_{y2}}{m} & 0 \\ 0 & 0 & \frac{C_{z1}}{m} & 0 & \frac{C_{z2}}{m} \\ 0 & 0 & \frac{C_{z1}}{J_y l} & 0 & -\frac{C_{z2}}{J_y l} \\ 0 & -\frac{C_{y1}}{J_z l} & 0 & \frac{C_{y2}}{J_z l} & 0 \end{bmatrix} \times \begin{bmatrix} i_x \\ i_{y1} \\ i_{z1} \\ i_{y2} \\ i_{z2} \end{bmatrix} - \begin{bmatrix} \frac{F_{Ax}}{m} \\ \frac{F_{Ay}}{m} \\ \frac{F_{Az}}{m} + g \\ \frac{M_{Ay}}{J_y} \\ \frac{A_{Ax}}{J_z} \end{bmatrix} \qquad (4-2)$$

There:m = the model mass ;

J_q = the rolating inertia of the model along its centre of mass.

According to this situation we can build the independent system for control of the position of the 5 electro-magnetic force components and the isochronous first order position control system, placed in space position and used to realize the control object: let the Δ x, Δ y1, Δ z1, Δ y2, Δ z2 tend to zero. Taking the channel F_{z1}as an example the block diagram of the closed loop system is shown in figure 4-1

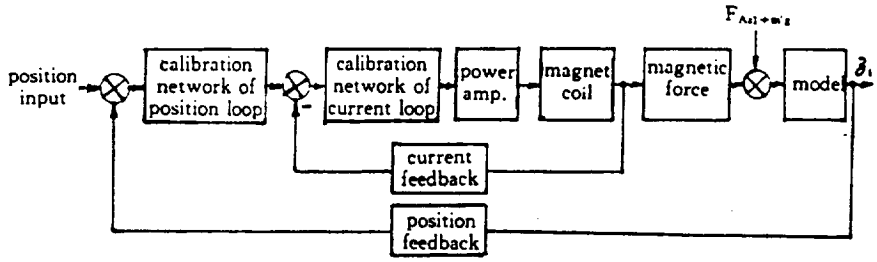

Fig 4-1: The block diagram of the monochannel closed loop system

"H" bidirectional power amplifier used in 5 channel control system

The position of the 15cm × 15cm MSBS dynamic model must be carried out by controlling the individual electro-magnetic force in the 5 independent channel. The force direction or the control current polarity must be adjusted rapidly and the certain linearity must be ensured. In this case the "H" GTR bidirectional power amplifier is selected and the PWM control method is used. The principle of this cricuit is shown schematicaly in figure 5-1.

The control current in all channels of the MSBS is larger. The x-directional coils are the air cored coils, in which the current is more than 30 A. In order to avoid the impact current from the power supply and to unify the chopped wave frequency the signal source of the concentrated crystale oscillator and the 3-position torsion circle distributor are used to generate the 6 constant width square wave signals with 60 ° phase difference, to make the 5 triangle waves after its processing and to generate the PWM control signals after the comparation of various channel circuits. The block diagram of the power amplifier is shown in figure 5-1(b). Considering that the current of the x-directional coils is the maximum,the phase difference of the triangle wave signal in this channel must be 120 °.

If the upper two square wave voltages, shown in the figure 5-2(a) are used to drive the transistors of "H" bridge T_1, T_4 and T_2, T_3, when they alternate the on and the off, the voltage on the magnet winding will change its polarity, (see the third voltage wave form in the figure 5-2(a)). When the on time of the tiansistors T_1, T_4 and T_2, T_3 are equal to each other under the control of the PWM, The positive and negative voltage, applied to the magnet are equal, thus the work current is zero. The chopper frequeney which we selected is 2 KH_z. The relationship of the current and the n time in one cycle t_1 can he written as:

$$I_q = I_{qm}(2\frac{t_1}{T} - 1) \qquad (5-1)$$

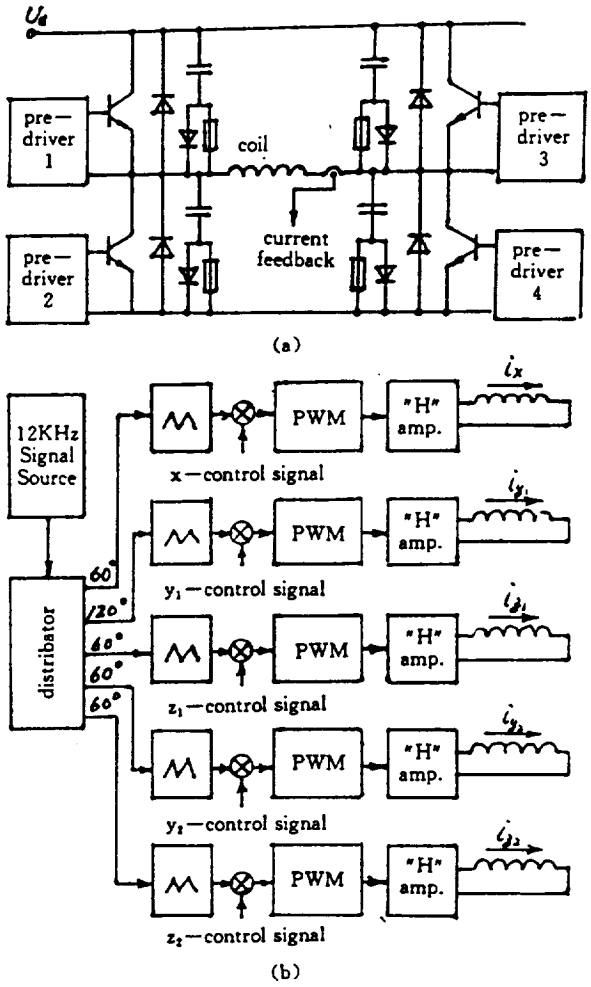

Fig·5-1: "H" power amplifier and its block diagram.

In order to avoid the bridge short circuiting in moment of the alternative work of the transistors T_1, T_4 and T_2, T_3, the dead space of 20 μs is set-up in their predriving voltage. Since the large inductance of the magnet coil,the on time of the transistors T_1, T_4,t_1>0.5T (T is the wave cycle). When the other transistor is powered on, the continuous flow will be generated, an the released energy of this magnetic field permit raise the output efficience of the power amplifier. The wave form of the magnet work current and the input current from DC side are shown in the figure 5-2(b),(c).

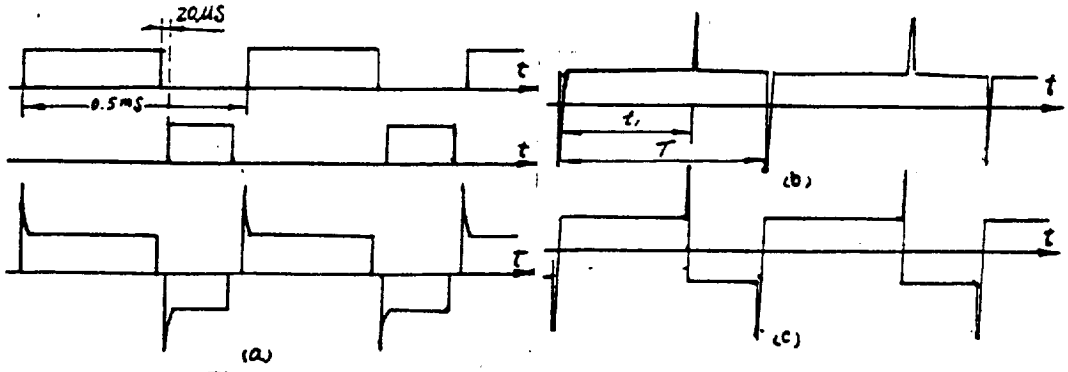

Fig 5-2:Input and output wave form of the "H" amplifier.

According to our practical measurement, the output efficience is more than 85%,and the linear relationship between the control voltage of the magnet and the current is satisfied.

There is a spike with cycle of 0.5T in the current wave form acquired from the magnet coil, therefore, the analog filter and digital filter are used at the time of the current feedback and the sampling by computer.

Static calibration of the MSBS

The particular method of calibration is used for the MSBS with structure and work principle different from the conventional balance system. Because the calibration device must be installed in magnet field, it is necessasy to avoid the use of the ferromagnetic materials in its construction. the scheme of the calibration method is shown in the figure 6-1.

The relationship between the ten weights applied to the MSBS and the 5 components of the MSBS can be written as.

$$\begin{cases} F_x = G_2 - G_1 \\ F_y = F_{y1} + F_{y2} = (G_7 - G_8) + (G_9 + G_{10}) \\ F_z = F_{z1} + F_{z2} = (G_4 - G_3) + (G_6 - G_5) \\ M_y = \dfrac{F_{z1} - F_{z2}}{l_1} = \dfrac{(G_4 - G_3) - (G_6 - G_5)}{l_2} \\ M_z = \dfrac{F_{y1} - F_{y2}}{l_1} = \dfrac{(G_7 - G_8) - (G_9 - G_{10})}{l_2} \end{cases} \qquad (6-1)$$

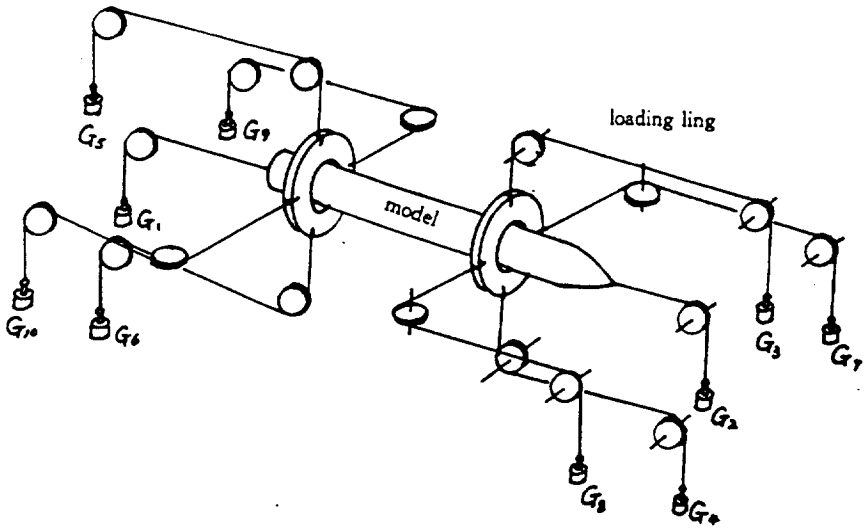

Fig 6-1: Scheme of the MSBS calibration method.

There: l_1 = momental arm lenth of the magnetic force action on the model.

l_2 = momental arm length of the loading weight action on the model.

It is clear from the equation 4-1 that the 5 magnetic components on the MSBS model are corresponding to the 5 channel currents: i_x, i_{y1}, i_{z1},i_{y2},i_{z2}, thus the purpose of the calibration in fact is the measurement of the coefficent of the magnetic force : C_x,C_{y1},C_{z1}, C_{y2},C_{z2}, used to calculate the parameters at the time of the aero-dynamic test.

The Hall current transformer is used in the 15cm × 15cm MSBS. The one of the 5 channel current signals is taking part in the system current feedback, the another one is used to carry-out the A/D conversion in computer. In order to eliminate the interference, the digital filter technology is adopted in the software.

According to national conference of the wind tunnel balance system, we repeated seven times the three loading points: 30%, 50% and 70% of the designed load of the MSBS and obtained the mean value:

$$F_z = \frac{\sum_{j=1}^{7} F_i^j}{7} \qquad (6-2)$$

the deviation:

$$\delta F_i^j = F_i^j - F_i \qquad (6-3)$$

the mean squar error :

$$\varepsilon_i = \sqrt{\frac{\sum (\delta F_i^j)^2}{6}} \qquad (6-4)$$

and the relative error:

$$\delta_i = \frac{\varepsilon_i}{\overline{F}_i} \qquad (6-5)$$

The 20%,40%,60% and 90% of the designed load are taken as the degree of preciseness of the calibration. They are matched correspondingly and divided in 16 groups. In the case of every loading the error of the magnetic force F^j_i and the loading weight is:

$$\delta F_i^j = F_i^j - G_i^j \qquad (6-6)$$

relative error is :

$$\delta_i^j = \frac{\delta F_i^j}{F_i^j} \qquad (6-7)$$

The mean square root difference of every component is:

$$\delta_i = \sqrt{\frac{\sum_{j=1}^{16} \delta_i^j}{15}} \qquad (6-8)$$

The δ_i may be represented as the degree of preciseness of the balance system.

The relationship of the magnetic force F_q and the channel current I_q, obtained after the static calibration may be drawn up by the least square method as a power series polynomial expression and can be processed rapidly at the time of the dynamic tests and became a curve or a data table.

Conclusion

The 15cm × 15cm MSBS is developed by the research group of MSBS in the department of automatic control of changsha Institute of technology, working intensively for 8 years with the preliminary success in the experimentation and testing and with the principle characteristics as following:

1. Model mass: 380 g.;
2. Axial maximam load: ±1.5N;
3. Maximum load along the suspension direction: -4 ~ +8N;
4. Side maximum load: ±2N ;
5. Maximum pitching moment: ±0.2353N.m.
6. Maximum yawing moment: ±0.1176N.m;
7. Maximum attack angle of model: ±18° ;
8. Maximum yawing angle of model: ±20° ;
9. Model calibration precision: 0.5%-4.5%;
10. Model calibration degree of precisenecs: 7%;

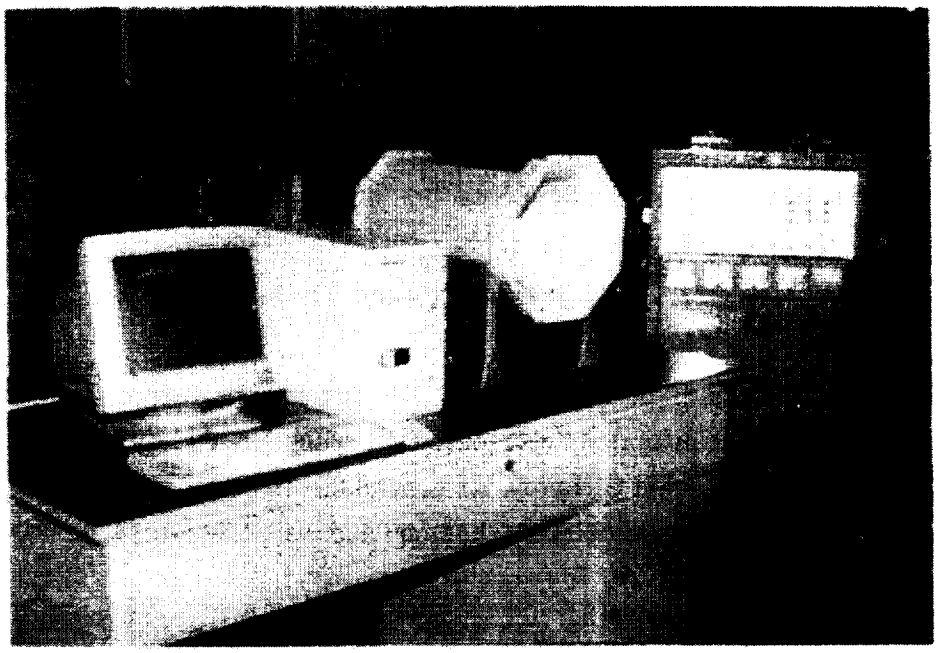

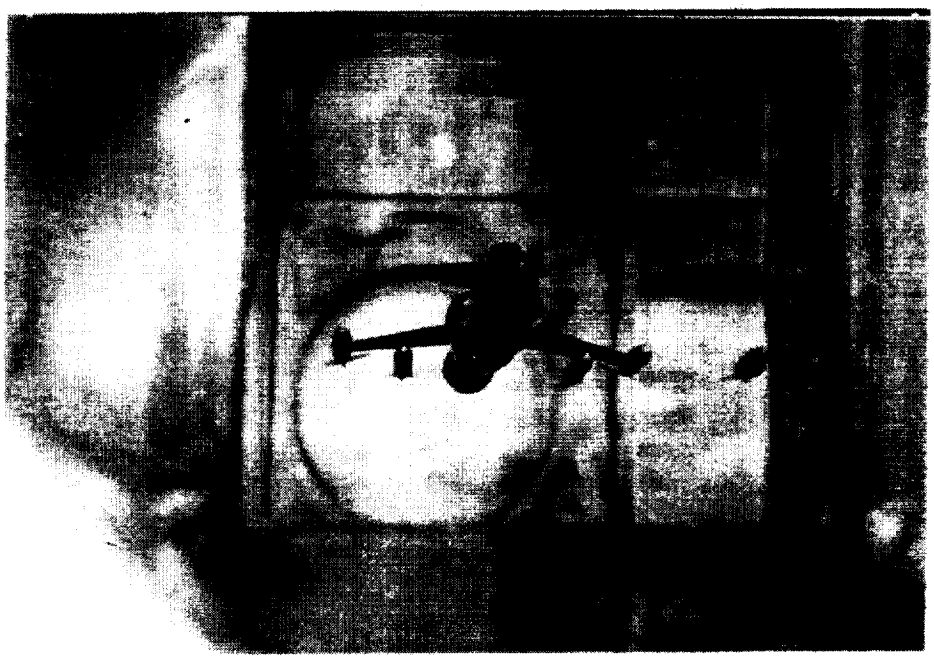

11.Maximum power consumption of the system: less than 1 KW(output power).

This Magnetic Suspension and Balance System can be used now for some aero-dynamic tests. But in order to make it a practical installation,it is necessary to do much research work and to carry-out a great deal of trouble tasks with great force, for example, to use the CCD position sensor of the 5 degree of freedom to realize the precise positioning, to use the rolling control coil to carry-out the active control of the 6 degree of freedom and to design a practical MSBS calibration device and so on and so forth.

References

[1] Sawada Shufu etal, Experimental 0.1m × 0.1m magnetic support installation, The material of the Institute of aerospace technology No. 623.

[2] Bernard, Adkins Ronald G Harley, the general theory of AC machine, Application to practical problems, Chopman and Hall, London 1975.

Summary Report of the First International Symposium on Strain Gauge Balances and Workshop on AoA/Model Deformation Measurement Techniques

John S. Tripp*, Ping Tcheng*,
Alpheus W. Burner#, and Tom D. Finley#
Mail Stop 238
NASA Langley Research Center
Hampton, Virginia 23681
USA

1. SUMMARY

The first International Symposium on Strain Gauge Balances was sponsored under the auspices of the NASA Langley Research Center (LaRC), Hampton, Virginia during October 22-25, 1996. Held at the LaRC Reid Conference Center, the Symposium provided an open international forum for presentation, discussion, and exchange of technical information among wind tunnel test technique specialists and strain gauge balance designers. The Symposium also served to initiate organized professional activities among the participating and relevant international technical communities.

The program included a panel discussion, technical paper sessions, tours of local facilities, and vendor exhibits. Over 130 delegates were in attendance from 15 countries. A steering committee was formed to plan a second international balance symposium tentatively scheduled to be hosted in the United Kingdom in 1998 or 1999.

The Balance Symposium was followed by the half-day Workshop on Angle of Attack and Model Deformation on the afternoon of October 25. The thrust of the Workshop was to assess the state of the art in angle of attack (AoA) and model deformation measurement techniques and to discuss future developments.

2. INTRODUCTION

The concept of an international strain gauge balance symposium was advocated in a technology assessment entitled "A White Paper on Internal Strain Gauge Balances." This internal document, published by LaRC staff members in March 1995, was based on an international survey of internal strain gauge balances conducted under contract in 1994-1995 (ref. 1). The conclusions of the white paper were presented to a peer review panel on wind tunnel testing technology, composed of selected leaders from major commercial and government aeronautical facilities, held in July 1995 at LaRC. The panel strongly endorsed the proposed international strain gauge balance symposium, which is the first of its kind.

Over 130 delegates from 15 countries were in attendance, including Australia, Canada, China, Finland, France, Germany, India, Indonesia, Israel, the Netherlands, Russia, South Africa, Sweden, United Kingdom, and the United States. The program opened with a panel discussion, followed by technical paper sessions, and guided tours of the National Transonic Facility (NTF) wind tunnel, a local commercial balance fabrication facility, and the LaRC balance calibration laboratory. Vendor exhibits were also available.

The opening panel discussion addressed "Future Trends in Balance Development and Applications." The nine panel members included eminent balance users and designers representing eight organizations and five countries. Formal presentation of papers in technical sessions followed the panel discussion. Forty-six technical papers were presented in 11 technical sessions covering the following areas: calibration, automatic calibration, data reduction, facility reports, design, accuracy and uncertainty analysis, strain gauges, instrumentation, balance design, thermal effects, finite element analysis, applications, and special balances. A general overview of the past several years' activities of the AIAA/GTTC (Ground Testing Techniques Committee) Internal Balance Technology Working Group was presented. The group's activities has prompted sufficient interest among the foreign Symposium attendees, that a separate Euro-Asian Inter-Nation Internal Balance Working Group was contemplated. At the conclusion of the Symposium, a steering committee representing most of the nations and several US organizations attending the Symposium was established to initiate planning for a second international balance symposium, to be held within 2 or 3 years in the UK.

The Workshop on Angle of Attack and Model Deformation Measurement Techniques was held immediately following the Symposium for assessment of the state of the art in AOA and model deformation measurement techniques and to discuss future developments. Twelve presentations from industry and government in the United States, Europe, and Asia covered various AOA and model deformation measurement techniques, applications, and concerns. The Workshop concluded with an open panel discussion.

The following summaries of the panel discussion and selected technical papers were obtained orally and from video tape recordings of the presentations. The authors of this report disclaim responsibility for accuracy of the transcribed notes and regret any misinterpretations of the panelists' and symposium authors' intentions. Panelists and symposium authors should be contacted directly for further elaboration; contact information is available from NASA LaRC representatives.

---

* Co-Chairs of the International Balance Symposium

\# Authors of comments on Workshop on AoA/Model Deformation Measurement Techniques

3. PANEL DISCUSSION

The Symposium opened with a panel discussion entitled "Future Trends in Balance Development and Applications." The panel consisted of the following members:

Ron D. Law, Defense Research Agency (DRA), Bedford, UK, Panel Chair

Maurice Bazin, Office National D'Études et de Recherches Aérospatiales (ONERA), France

David M. Cahill, Sverdrup Technology Inc./AEDC Group, USA

Prof. Bernd Ewald, Technische Hochschule Darmstadt (TUD), Germany

Pieter H. Fuykschot, Nationaal Lucht-En Ruimtevaartlaboratorium (NLR), the Netherlands

Steven Hatten, Boeing Commercial Airplane Group, USA

James G. Mitchell, Microcraft, Inc., USA

Lawrence E. Putnam, NASA Langley Research Center (LaRC), USA

Paul W. Roberts, NASA Langley Research Center, USA.

Each panelist briefly presented his views regarding future trends in balance development and applications. Important areas covered included materials, temperature compensation, gauging, analysis methods, and calibration efficiency. The panel members agreed that the existing balance technology will continue to prevail in the foreseeable future, with only evolutionary improvements possible. No radically new basic technologies such as fiber optics techniques are expected to offer any competition in terms of accuracy and reliability. It was agreed that international standards for nomenclature, calibration procedures, accuracy reporting methods, etc. should be adopted in the future following the precedent of the North American Internal Balance Working Group, although agreement is not presently feasible. However, this Symposium is an important first step in establishing formal international discussions about these concerns, especially in regard to agreement on terminology. After the individual presentations a group discussion followed.

Selected observations from the panel discussion follow.

Ron D. Law, DRA Bedford, UK, Panel Chair
Stiffer balances are needed for tests at high angles of incidence under unstable flow conditions. Since the balance forms part of the spring system of the model and its supporting structure, unwanted dynamic oscillations within the balance itself will corrupt test data. Although an infinitely stiff balance would eliminate this problem, it is unrealizable. Stiffer balances are especially needed for half-models and for heavy models. Replacement of strain-gauged flexures with sensitive piezo-electric cells provides greatly increased stiffness with good signal output. The use of high-output platinum strain gauges provides high sensitivity for stiff designs although temperature sensitivity is greater. Composite materials, such as carbon-fiber layered flexures, have been successfully tested in lighter weight balances used for low speed testing. Improved semiconductor strain gauges also offer increased sensitivity. Finite element analysis can be employed during design to predict balance dynamic behavior.

Maurice Bazin, ONERA, France
ONERA has developed balances which provide good drag-count resolution for all wind tunnel applications including cryogenic testing. Future trends are difficult to predict at present. Advanced technology may offer better ways of measuring strain, such as the use of doped materials or micro-laser techniques

David M. Cahill, Sverdrup Technology Inc./AEDC Group.
Analysis of elastic and anelastic hysteresis, and study of fabrication and heat treatment techniques for metallic and non-metallic materials are areas where additional emphasis is needed. Development of alternative techniques for strain measurement would be beneficial. Hardware as well as software compensation techniques for temperature effects are recommended. Calibration techniques need to be examined, including: the number of loadings required for calibration, application of combination loadings including third order and above, and the inclusion of calibration uncertainty analysis. Standardization is needed in the following areas: terminology for forces and moments, and the axis systems; the calibration matrix and the matrix format; treatment of calibration tares; data reduction to forces and moments by the non-iterative mathematical model and the iterative mathematical model; and inclusion of model weight as part of the tares during data reduction.

Prof. Bernd Ewald, TUD, Germany.
TUD has developed a new single-piece balance from copper-beryllium alloy for the European Wind Tunnel (ETW). Although copper-beryllium imposes some inconvenient manufacturing requirements, it is an excellent spring material, has very low hysteresis, and has very high heat conductivity. Tests of titanium alloy at TUD disclosed no detectable hysteresis indicating that it is a promising material for future balance fabrication. Machine calibration is seen as becoming mandatory because of its accuracy and reliability, and because of the excessive manpower requirements for manual calibration. The maximum resolution of the conventional strain gauge is on the order of 25×10^{-9} mm or approximately 1/20000 of the wavelength of visible light. It is unlikely that potential strain measurement alternatives can match this resolution at present. Electric and pneumatic lines bridging the balance in the test model produce measurement bias errors due to unknown residual forces. TUD has considered integrating these lines into the balance structure. The resulting effects of residual forces would then be removed by calibration.

Pieter H. Fuykschot, NLR, the Netherlands.
No major revolution, rather evolution, is seen in balance technology. Two major problem areas are interactions and temperature effects. Balances should be designed for minimum interactions and maximum linearity, rather than using calibration to remove their effects. Nonlinearity can cause bias errors due to rectification effects during dynamic test conditions, which cannot be corrected by calibration. Materials with a low coefficient of thermal expansion, such as titanium, should be considered. Compensation for tempera-

ture gradients is important. Balance convection screens can be installed within the model to reduce heat transfer within the flexures. Dynamic modeling should be done during the design phase to minimize resonant vibrations during tests. Standardized model-to-balance couplings should be adopted for inter-laboratory compatibility. Automatic calibration is an important future trend. The balance should be calibrated through zero load to attain positive and negative loadings rather than by mechanical inversion as usually done during manual calibration. The balance should be calibrated with couplings identical to those used during tests.

Steven Hatten, Boeing Commercial Airplane Group.
Corporate concerns have resulted in an emphasis on reducing the development cycle times for both production aircraft and for test models. Simplified designs and procedures are emphasized, such as parametric spreadsheet design tools. Parametric finite element models are employed to analyze stiffness and dynamic behavior. Older balances in the inventory are being recycled for new testing. External balance calibration is being automated. Balance users at Boeing are demanding improved balance measurement accuracy, especially in drag. Ways to increase drag accuracy are being investigated. Uncertainty due to mechanical hysteresis is being reduced via a redesigned model attachment interface. Effort is also being applied to thermal gradient correction methods for improved accuracy.

James G. Mitchell, Microcraft, Inc.
Progress in strain gauge balances has been slow, with 40-50 year-old strain gauge and design methodology still in use. The strain gauge balance design community should exploit new technology in related fields such as optics, microelectronics, and smart structures. Balance customers, i.e, test facilities and test engineers, are asking for "better, faster, and cheaper." The response is as follows: Better: Uncertainties can be reduced through study of calibration practices, increased load per unit diameter, increased stiffness, improved math models, and calibration using combined loadings. Faster: While balance design, fabrication, and gauging can be accelerated, the large opportunity is in the area of calibration with automated machines. Balance calibration times are reduced from days and weeks to a few hours. Cheaper: Reduced cycle times result in lower costs.

Lawrence E. Putnam, NASA LaRC, USA.
Comments were made from a wind tunnel user's point of view. LaRC balances must function over test environments ranging from cryogenic conditions at the NTF wind tunnel to high temperatures at the eight-foot high temperature structures tunnel. Drag uncertainty provided by LaRC balances, based on calibration laboratory data, is on the order of 0.6 drag counts, which is adequate for customer requirements. However, operational accuracy in the wind tunnel is worse. Temperature gradients during tests are a major source of uncertainty. Multiple calibrations are needed to estimate precision uncertainties which are not currently done with manual calibration. This is feasible only with automated calibration equipment. Improved balance robustness is needed to reduce down time during tests. Problem areas include strain gauges, cement, and moisture proofing.

Paul W. Roberts, NASA LaRC, USA.
Future improvements in balance design and performance can be expected in a number of areas. Areas in calibration include the experimental design, estimation of separate precision and bias uncertainties, and custom calibration for specific wind tunnel tests. The mathematical model will be extended to include higher order interactions. Although interactions and nonlinearities should be minimized, balance physical size constraints dictated by the test facility may preclude this. More complete uncertainty analysis than is now provided will be available. Real-time compensation for thermal gradients and other effects are being developed. More sensitive strain measurement sensors, although not presently feasible, can be expected over the long term. New fabrication methods with shortened production time are possible. Finally, automatic balance calibration systems are an essential need for the future.

4. OVERVIEW OF TECHNICAL PRESENTATIONS

The majority of the three-and-one-half-day symposium was devoted to 46 papers delivered in 11 technical sessions. A list of the scheduled paper presentations and authors is given in the Appendix. Several papers were not presented due to the authors' inability to attend the Symposium. Brief summaries of selected topics representing important areas of the balance technology are now presented.

4.1 Balance Design

Nearly half of the technical papers presented described unique balance design techniques. Several innovative axial section designs for improved sensitivity and reduced thermal effects were discussed. Finite element analysis methods have disclosed unexpected local stress concentrations, approaching yield limits of the material in some cases, which could not be readily predicted by conventional design methods. Varied techniques for thermal gradient characterization and compensation were described. State-of-the-art methods in strain gauge manufacturing and application were described. Other papers were given on conventional and unique balance applications, including unusual balance designs for special applications.

4.1.1 J. Zhai, TUD, Germany, discussed optimization of internal strain gauge balance design using finite element computation. The aim of the TUD study was to improve accuracy by reducing interferences (interactions) and by increasing stiffness. Sources of linear interactions include the structure, strain gauges, and manufacturing tolerance errors. Strain gauge effects include gauge factor, position, and direction. Product interactions result primarily from deformation of the material. Quadratic and cubic interferences arise from nonlinearity of the material. These effects can be reduced by structural redesign. The linear interaction on drag can be reduced by decreasing the stiffness of the measuring spring, decreasing spacing between measuring beams, and increasing the slope of the main beam. The shape of the drag sensing element can be changed to provide additional decoupling. TUD attained a 38% reduction in drag interaction by choosing suitable dimensions and a 92% reduction in drag interaction by use of a point-symmetrical configuration. Low stiffness causes large nonlinear interactions and a lower natural frequency of the model-balance-sting system which, in turn, increases measurement errors during dynamic test conditions. Stiffness in the X direction was increased 60% by changing the drag-sensing element from a bending beam to a

shear spring. Similarly, stiffness in the Z direction was increased 65% by changing the bending moment measuring system from a bending beam to a shear spring. Additionally, stiffness in the Z direction was increased 21% through the use of combined main beams.

4.1.2 Prof. Bernd Evald, TUD, Germany, discussed advanced internal balances for cryogenic and conventional wind tunnels. Only gradual improvements based on careful research and development are anticipated. Three general rules for balance users and designers include the following: selection of the load range to match the test requirements as closely as possible; employment of geometric dimensions as large as possible; and design of the balance structure to be as stiff as possible. Three types of balances are generally needed for industrial aircraft development: very sensitive balances for cruise optimization; less sensitive balances for buffet, maximum lift, and dive testing; and an envelope balance for stability and control, control surface deflection, and large AoA and yaw angle tests. Balances with high stiffness are difficult to fabricate with conventional electric-discharge machining techniques. Now, electron beam welding technology gives the balance designer complete freedom to fabricate any desired internal structure. TUD employs an interactive software package for design via fundamental stress and strain analysis methods. Research and optimization are done via FEA software. Maraging steels, which are good for electron beam welding, are used for cryogenic and conventional balances. Special heat treatment methods are applied to reduce hysteresis. Although some authorities advocate the use of heated balances for cryogenic use, Prof. Evald prefers balance designs which tolerate thermal gradients by mechanical cancellation methods and by electrical compensation. He proposes future development of a "black box" plug-and-play balance concept in which all necessary parameters would be stored in a memory chip integrated into the balance structure. The balance identification, calibration matrix, and electrical connection information would be stored on-board. The proper electrical connections and data reduction would be automatically configured by wind tunnel data systems. Future developments would also provide an optical telemetry link from the balance to the wind tunnel data acquisition system to eliminate mechanical bridging caused by strain gauge conductors.

4.1.3 The design philosophy of a high-quality balance at NASA LaRC is briefly presented. All LaRC balances are custom designed to meet the load ranges, physical size, thermal environment, and accuracy requirements for given research projects. Single-piece construction techniques using high-quality maraging steel are employed whenever possible. Most LaRC balances are of the direct-reading type; moment-type balances are typically used in extreme thermal conditions such as the cryogenic environment at the National Transonic Facility (NTF). All LaRC balances employ modulus compensated transducer quality strain gauges. Where extreme thermal environments are anticipated, a patented apparent-strain gauge-matching technique is used. Thermal compensation is provided by pure nickel wire placed in the Wheatstone bridge circuit to reduce temperature effects on the bridge output to less than 0.005 percent full scale per degree Fahrenheit. Balance temperatures and gradients are measured by means of resistance temperature detectors (RTD). These temperature measurements allow linear corrections to be applied for thermal sensitivity shifts and second-order corrections for apparent strain.

4.2 Automatic Balance Calibration

Presentations were given describing four different automatic calibration machines at DRA-Bedford, CARDC, IAI, and TUD. Significant advantages of automatic calibration include manpower savings, decreased calibration time, expanded experimental loading schedules, the ability to apply multiple loadings, and improved calibration accuracy. However, differing results with respect to loading accuracy and repeatability were reported. Primary sources of calibration inaccuracy are load vector misalignment, force measurement sensor inaccuracy, and precise repeatability of the balance mechanical position within test fixtures. Highlights of reported experience with automatic calibration are summarized

4.2.1 *China Aerodynamics Research and Development Center* (CARDC)

CARDC reports the best calibration accuracy although verification data were not available. It is possible that the cited Chinese calibration accuracy is estimated based on the accuracy of the load cells used and the assumption that the system is perfectly realigned after each load application.

4.2.2 *Israel Aircraft Industries* (IAI)

Michael Levkovitch, IAI, gave an unscheduled presentation describing the IAI automatic calibration machine. He indicated that a new machine with a larger load capacity is under development. The presentation indicated that the IAI machine does not reposition to correct loading deflections, but rather measures deflections. Thus, inaccuracies in measurement of angular alignment may dominate the total machine uncertainty. The authors note that since the machine is not designed to function as a repositioning servomechanism, machine accuracy could be improved with better displacement measurement sensors. Without improved positioning measurement accuracy, the use of expensive highly accurate load cells would produce only marginal improvements in overall calibration machine accuracy at present.

4.2.3 *Technische Hochschule Darmstädt* (TUD)

A first generation automatic calibration machine was designed by TUD and manufactured by Schenk for the European Wind Tunnel (ETW.) A second generation prototype is being developed at TUD. The needs for machine calibration include manpower costs, reduced calibration time, avoidance of human errors, and convenient inclusion of temperature as a calibration parameter. The machine is able to generate loadings in any order in all possible component combinations up to sixth order, thus allowing estimation of third and higher order coefficients. Zero readings are obtained automatically. Loads are generated by actuators and measured independently by load cells, such that the actual applied loads are determined. The balance may be enclosed in a temperature-controlled chamber for cryogenic calibration. The design avoids thermal gradients during temperature-controlled calibration.

4.2.4 *DRA Bedford*

DRA recently developed a six-component precision automatic balance calibration machine for in-house use. Forces are applied using pneumatic actuators and are measured using sensors. Forces are applied such that the need for reposi-

tioning is avoided. An example was given of calibration of a balance to be installed away from its virtual center. Since the measured outputs depend on the moment arm length in this configuration, the balance must be calibrated at two positions to permit correction for positioning at any displacement from center during tests. The automatic machine facilitates the multiple calibrations necessary for this application. A second example illustrated static calibration of a dynamic balance by automatic machine where loads must be applied and removed quickly.

4.2.5 *IAI Balance Calibration Consortium*
In 1995 Microcraft established a consortium to calibrate selected balances using the IAI automatic calibration machine at the San Diego, California facility. Two papers related to this effort were given. A paper containing some of the calibration results is summarized in Section 4.3. A summary of the other paper is now presented.

4.2.6 *IAI Machine Calibration of NASA LaRC Balance*
Ping Tcheng, NASA LaRC, presented a comparison of machine calibration accuracy versus manually loaded calibration accuracy. The paper contained a general discussion covering primarily data reduction and uncertainty analysis. Uncertainty analyses of eight sets of machine calibration data indicated that its calibration accuracy is adequate for many applications, providing better than 0.5 percent full-scale accuracy. The authors believe that manual calibration, albeit time consuming and labor intensive, is necessary to attain the best calibration accuracy at present. The IAI machine was user-friendly, easy to operate, with sophisticated supporting software providing immediate data reduction following calibration.

Inconsistencies noted among the eight calibration data sets were traced to poor repeatability of the balance center position caused by slack in the balance-to-test-fixture attachments following removal and re-installation of the balance. It was of interest to note that comments were received describing "spatial relocation error" problems with the Schenk automatic calibration machine at ETW similar to those observed by LaRC during IAI automatic machine calibrations at San Diego.

4.2.7 *Comments by Participants in IAI Calibration Consortium*
Additional comments were received from other Consortium participants regarding the consistencies of the automatic calibration machine. It was agreed by all participants that further improvements would be desirable. Boeing indicated that, in hindsight, a balance with larger interactions should have been selected for test calibration on the IAI machine. This would have better discriminated between the performance of the machine calibration and that of manual calibration. Moreover, the performance of higher order mathematical models and expanded loading schedules could have been better investigated and evaluated. In addition, during the consortium tests, LaRC engineers attempted to evaluate an enhanced calibration experimental design and mathematical model intended for balances experiencing significant third order interactions. Inasmuch as the test balance possessed only second order interaction effects with no apparent third order effects at all, the test of the enhanced calibration design and expanded mathematical model was not well-posed. Therefore, the results were inconclusive.

4.3 Mathematical Modeling
Several presentations covered the interdependent areas of mathematical modeling, calibration experimental design, and calibration uncertainty analysis. It is clear that potentially significant improvements in balance accuracy lie in improved mathematical modeling and in the calibration experimental design. Additional resources may be profitably allocated to further development effort in this area.

4.3.1 Richard S. Crooks, Microcraft San Diego, presented a paper on the limitations of balance calibration mathematical models. This paper, of a general philosophical nature, was illustrated by comparative studies of the robustness, or predictive accuracy, of various polynomial-based mathematical models for three differently sized calibration experimental designs. The calibration data sets were obtained using the IAI automatic machine to calibrate a single balance. It was seen that the largest and most comprehensive experimental design (1322 points) produced the lowest calibration residuals and, consequently, the least overall standard error.

In order to investigate balance model robustness Crooks has taken advantage of the "proof-load" technique. He found that proof-load residuals were significantly reduced by the addition of a single third-order cross-interaction (non-cubic) term to the standard second-order polynomial model. The particular third-order term was selected by trial and error balance coefficient estimation with proof-load test data appended to the normal calibration data set. However replicated calibrations had not yet been conducted to estimate the uncertainty of the significant third-order term and to verify that it is not merely a spurious effect due to random errors, i.e., fitting data to measurement noise.

4.3.2 The authors believe that the practice of attaching proof-load data to calibration data prior to coefficient estimation invalidates subsequent tests for calibration design and model robustness based on proof-load data. Indeed, predictive validation of the model should be based on independent proof-load data acquired at loading combinations and levels absent from the calibration experimental design.

4.4 Uncertainty Analysis
Frank L. Wright, Boeing, discussed how balance accuracy requirements are specified by balance designers and users. In the past accuracy has been imprecisely defined in widely varying ways. Now AGARD Standard 304 is coming into use wherein bias and precision uncertainties, and their combined uncertainty are specified at a given confidence level. The user must clearly state the factors such as test conditions, the coordinate system being used, units, etc. at which the accuracy is being quoted. In the commercial aircraft industry the most important wind tunnel quantity is drag coefficient. Customers now ask for ½ drag count uncertainty at a 95 percent confidence level. Computations for a typical wind tunnel test show that uncertainties of ±0.002° in angle-of attack, ±2.5 lb in normal force, and ±0.8 lb in axial force are necessary to attain this requirement, which is probably not currently possible. Normal force and axial force precision uncertainties during tunnel tests may be estimated from balance calibration data by the following rules of thumb: tunnel re-

peat-point uncertainty is estimated from repeated back-to-back component calibrations; uncertainty within a Mach number run is estimated from multiple component calibrations interspersed over a five-day calibration; uncertainty over a complete test is estimated from the overall calibration standard error at the desired confidence level; and long term balance bias shift is estimated from zero shifts observed over a four-year period.

John S. Tripp, NASA LaRC, presented an overview of strain gauge balance uncertainty analysis techniques developed at LaRC. A second-order multivariate polynomial direct model is employed; i.e., balance voltage outputs are represented as functions of the applied input loads in accordance with the physical process being modeled. A Newton-Raphson iterative inversion method is employed for data reduction. The uncertainty analysis employs a global regression technique for least-squares estimation of the polynomial coefficient matrix. Equations are obtained therefrom for computation of calibration confidence intervals and prediction intervals as functions of the applied loadings. This is an extension of the previous method of reporting balance uncertainty as simple percentages of the full scale per component. It is noted that the calibration confidence intervals become fossilized bias errors subsequent to calibration. Additional sources of calibration bias uncertainties include calibration standard errors and mathematical modeling errors. Concepts for selection of calibration experimental design based on analytic methods developed by G. E. P. Box were presented for minimization of overall precision uncertainty and overall bias uncertainty. Statistical techniques for detection and estimation of calibration bias errors have been developed. It was pointed out that present procedures of lumping calibration bias and precision errors together in a single computation may significantly underestimate total calibration uncertainty. If the contributions of highly-correlated systematic errors are additive, then for the large calibration experimental designs typically used for balance calibration the usual RMS standard error underestimates the total uncertainty. Methods for separate estimation of bias and precision uncertainties are being developed.

Mark E. Kammeyer, formerly of the Naval Surface Weapons Center, Dahlgren Division, Silver Spring, MD presented an uncertainty analysis for force testing in production wind tunnels. It is an overview of a complete uncertainty analysis to provide bias and precision limits for computed model attitude and force coefficients inferred from measurements in Hypervelocity Wind Tunnel 9 at Dahlgren. Calibration and measurement uncertainties were propagated through the data reduction equations in accordance with the standard procedures specified by ASME, AIAA, and IOS. A jitter approach using computer software rather than analytical computation was used to propagate the bias and precision limits into the inferred reduced data in order to keep the computational requirements manageable. Results using actual test data show that balance load uncertainties are by far the dominant contributors to overall uncertainties in the reduced parameters. It was also found that precision errors in balance axial force measurements are dominant, whereas bias errors in the other balance components are dominant. These results are helpful in pinpointing areas wherein balance measurement accuracy improvements are needed.

The Dahlgren approach is similar to that reported in an uncertainty study conducted by Batill of Notre Dame (ref. 2) for the NTF wind tunnel in 1993. However, Dahlgren's analysis was more manageable because of the lower complexity of the Dahlgren facility compared to NTF.

4.5 Finite Element Analysis

Three agencies reported activities in finite element analysis (FEA): LaRC, NLR, and TUD. Notable progress in the application of FEA to balance stress analysis has been made recently. The technique is especially suited to determination of stress concentrations, to which conventional stress analysis techniques are not generally applicable. TUD reported using the technique for optimizing stress beam design as described above in Section 4.1.1. The consensus seems to be, however, that FEA is not yet sufficient to replace conventional stress analysis techniques. None of the above agencies report temperature effect analysis using FEA techniques. However, papers have previously been published at ONERA, France, on this topic by Bazin, et al. (ref 3).

Michael C. Lindell, NASA LaRC, presented an FEA study of an existing LaRC cryogenic balance. The purpose was to correlate FEA predicted strain levels with experimental values obtained from loadings, and to identify high-stress concentrations within the balance structure. The FEA software, which is adaptive, does not require prior knowledge of stress concentrations. Strain levels for a single full-scale load in each of the six components were computed and compared with measured values. Differences varied from 0.2% in predicted normal force to 11% in yawing moment. Maximum predicted stress was as large as 40% of yield under a full-scale normal force load, and 50% of yield under a full-scale pitching moment load. The analysis predicted maximum stress on the order of 100% of yield under simultaneous full-scale six-component loading. It was planned to verify this result experimentally. The study concluded that stress levels are predicted accurately by FEA and that stress concentrations can be predicted. Thus, FEA can improve the balance design cycle, and can be used to optimize the design to accommodate higher loads with lower weight and higher safety factors.

4.6 Thermal Gradient Compensation

Maurice Bazin, ONERA, France, discussed methods for balance thermal compensation. ONERA follows multiple approaches, namely bridge resistive compensation, mechanical design to minimize thermal effects, and numerical correction. Mechanical design methods to minimize thermal gradient effects are emphasized since error correction is very difficult compared to error prevention. Design methods to reduce temperature gradient effects include a traction-compression push-pull arrangement and a bending push-pull arrangement. Conventional gauging methods are used.

4.7 Facility Reports

Several presentations provided general descriptions of internal balance development and applications at major facilities.

Henk-Jan Alons, NLR, the Netherlands, gave a presentation co-authored with H. B. Vos describing balance development at NLR. NLR has investigated the performance of model-to-balance and balance-to-sting attachments. A hysteresis angle of 0.01° produces a 0.17% FS error in normal force, which is

excessive. In an effort to minimize attachment hysteresis NLR investigated taper joint, cylindrical tap, and end face flange attachments. The hysteresis angle of each of these attachments was measured under load by means of a precision inclinometer. The advantage of the taper joint is its small dimension in comparison to its high bending moment capacity. Its disadvantage is hysteresis under bending due to the unavoidable mating between the sting and the attachment socket. Typical taper joint angle hysteresis of ±0.05° was measured. The cylindrical tap, previously thought to exhibit lower hysteresis, was found to be comparable to the taper joint. The tests disclosed, however, that the end face flange exhibits minimal hysteresis. Currently NLR employs the end face flange on the model end of the balance. Integral Wheatstone bridge strain gauges are provided to insure correct installation pre-stress levels. A taper joint is still employed on the balance sting end to maintain compatibility with existing wind tunnel stings.

5. STATUS REPORT ON NORTH AMERICAN INTERNAL BALANCE USERS WORKING GROUP

David M. Cahill, Sverdrup/AEDC, presented a general overview of the past several years' activities of the AIAA/GTTC Internal Balance Technology Working Group. Numerous areas of progress were cited: an increased willingness to exchange information freely among the participants; a survey of members' balance usage and methods of engineering practice; preliminary agreement on definitions of technical terms; and a 6 × 96 generalized matrix representation of balance calibration parameters. It was noted that a standardized method of computing and reporting balance measurement uncertainties will be developed and accepted soon.

6. FUTURE ACTIVITIES OF THE STRAIN GAUGE BALANCE COMMUNITY

6.1 Second International Symposium on Strain Gauge Balances

A steering committee representing most of the nations and several US organizations attending the Symposium was established to initiate planning for a second international balance symposium. Ron D. Law, DRA-Bedford, announced that DRA might be able to host a second symposium within 3 years. It was agreed that steering committee meetings in the interim should be scheduled in conjunction with other international aerospace conferences to enable as many members as possible to participate. Such an opportunity will arise at the Supersonic Tunnel Association (STA) meeting scheduled to be hosted by ARA and DRA in 1999. It was agreed that Japan should be invited to participate in future symposia. Additional discussion is needed to select a theme for the second Symposium.

6.2 International Round-Robin Balance Calibration

R. W. Galway, National Research Council, Canada, discussed the inter-facility balance calibration project proposed within STA in the fall of 1992. A round-robin test of a single balance by participating facilities had been suggested to provide an opportunity for comparison of different calibration techniques, experimental loading procedures, equipment, data reduction methods, and accuracy reporting methods. It would also provide some insight into the contribution of balance calibration uncertainty in tunnel-to-tunnel comparisons. The round-robin test results would be assembled into a data set to allow investigation of the effects of the various calibration experimental loading designs used by the participants. This data set would be closely controlled in terms of what was measured and how.

STA contains approximately 45 participating organizations of whom about 25 were interested in the round-robin test, and of those about 15 were definitely interested. The Boeing #661 balance had been selected for testing. The STA proposal has remained inactive since the inception of the AIAA/GTTC North American Balance Working Group, the 1995 IAI automatic balance calibration consortium at Microcraft, San Diego, and this Symposium. Galway inquired whether the Symposium delegates considered a round-robin calibration of a single balance to be a "useful exercise." He volunteered to serve as the point of contact through which interested parties may register their interest in participation.

6.3 Euro-Asian Internal Balance Working Group

David M. Cahill proposed the establishment of a separate Euro-Asian Inter-Nation Balance Working Group as a result of interest indicated by several European Symposium attendees in participating in the North American Internal Balance Working Group. He also proposed that the Euro-Asian group should be established under the auspices of AIAA. He suggested that the solidarity of the new group should become established before its eventual merge with the North American Internal Balance Working Group. The feasibility of establishing a Euro-Asian group would depend upon its reception by the proposed membership.

7. CONCLUDING REMARKS ON STRAIN GAUGE BALANCES

The Symposium was very successful in the free open exchange of information, in establishing an international community for future communication on balance usage and technology, and in setting a precedent for future Symposia. It is expected that the professional relationships established during the Symposium pave the way for future international cooperation in the strain gauge balance field. The Symposium provided a previously unavailable technical forum for the exchange of information for users, designers, and manufacturers of strain gauge balances.

The Symposium augmented and extended the results gleaned from the international balance users survey conducted by LaRC in 1995. It is clear that no aerospace agency holds a commanding lead in all technical areas. NASA LaRC is the world's major strain gauge balance user in terms of existing inventory, the number of units used in tests annually, and the number of new balances fabricated annually. Automatic calibration machines, although not yet equivalent to manual calibration with respect to loading accuracy, are an increasingly significant factor in realizing time and manpower savings. They are also an important tool for developing improved mathematical models and calibration experimental designs, and for establishing balance calibration and measurement uncertainties.

Publication of the symposium proceedings is pending.

8. BALANCE SYMPOSIUM REFERENCES

Contractor Reports

1 Kilgore, R. A.: *Internal Strain-Gage Balances: An International Survey.* VigYAN, Inc., Hampton, VA 23666, March 1995.

2 Batill, S. M.: *Experimental Uncertainty and Drag Measurements in the National Transonic Facility.* NASA Contractor Report 4600, June 1994.

Other Reports

3 Bazin, M.; Blanche, C.: and Dupriez, F.: *Instrumentation for Cryogenic Tunnels.* ONERA, France.

9. WORKSHOP ON ANGLE OF ATTACK AND MODEL DEFORMATION

A workshop on angle of attack (AoA) and model deformation measurement techniques was held on the afternoon of the last day of the Symposium. Short review papers were requested covering AoA and model deformation requirements and needs, thoughts for the future, and problem areas, in addition to papers covering actual applications and developments. The thrust of the workshop was to assess the state of the art in AoA and model deformation measurement techniques and discuss future developments in an informal but informative atmosphere. A panel discussion on AoA and model deformation was held in conjunction with the Workshop. Co-chairs of the Workshop were Tom D. Finley and Alpheus W. Burner, NASA LaRC.

9.1 Presentations

Twelve presentations were made at the Workshop. The presenters, affiliation, country, and presentation titles are listed below.

Tom D. Finley, NASA LaRC, USA: "AoA Overview"

Alpheus W. Burner, NASA LaRC, USA: "Model Deformation Overview"

Frank L. Wright, Boeing, USA: "Comparison of Model Attitude systems: Active Target Photogrammetry, Precision Accelerometer, and Laser Interferometry"

Maurice Bazin, ONERA, France: "AoA and Model Deformation at ONERA"

Peter Bauman, DLR, Germany: " DLR Model Deformation Measurement System"

Peiter H. Fuykschot, NLR, the Netherlands: "Vibration Compensation of Gravity Sensing Inclinometers in Wind Tunnels"

J. R. Hooker, McDonnell Douglas, USA: "Static Aeroelastic Analysis of Transonic Wind Tunnel Models Using Finite Element Methods"

YuFu Liu, CARDC, China: "The Model Real Time Angle of Attitude Measurement in 4m X 3m Low Speed wind Tunnel"

Sergi Fonov, TsAGI, Russia: "Model Deformation Measurements in TsAGI's T-128 Wind Tunnel by Videogrammetry System"

Gregory M. Buck, NASA LaRC, USA: "In-Situ Calibration of Sting Bending Using Optical Measurements"

Anton R. Gorbushin, TsAGI, Russia: "Angular, Linear Model Displacements, and Model Deformation During Wind Tunnel Tests"

Ralph D. Buehrle, NASA LaRC, USA: "Summary of Inertial Model Attitude Correction Techniques"

9.2 Panelists

The panel included the following members:

Frank L. Wright, Boeing, USA, Moderator
Pieter Fuyschot, NLR, the Netherlands
Tom D. Finley, NASA LaRC, USA
Richard A. Wahls, NASA LaRC, USA
Alpheus W. Burner, NASA LaRC, USA
John S. Tripp, NASA LaRC, USA

9.3 Summary of Presentations

Tom D. Finley, NASA LaRC, USA, opened the Workshop with an overview of angle of attack (AoA) measurement. He described the history of AoA measurement at LaRC, which has been based primarily on the use of precision accelerometers. He described the current state of the art of LaRC inertial AoA measurement systems including components and implementation. Specially selected high performance sensors are obtained from the manufacturer. Each unit is packaged with special output temperature compensation circuitry and mechanical isolation pads to reduce the effects of high frequency vibration.

Alpheus W. Burner, NASA LaRC, USA, presented an overview of the development of model deformation measurement capability at the Langley Research Center. Aeroelastic model deformation in wind tunnels was defined. Some fundamental questions and concerns about model deformation measurements in general were presented. The approach, described as a single camera, single view video photogrammetric technique, used to make model deformation measurements at three NASA LaRC facilities, was described. An example of the change in wing twist induced by aerodynamic loading as a function of angle-of-attack at the National Transonic Facility at various dynamic pressures was presented as a typical data example.

Frank L. Wright, Boeing, USA, presented a wind-on comparison among three independent model attitude measurement systems: the traditional inertial accelerometer measurement system, a Boeing designed and built laser interferometer system, and a commercially available photogrammetric system. Test data for the three systems, obtained at various Mach numbers, showed prediction intervals lying between 0.005 and 0.01 degrees. Two other applications of the photogrammetric system were described: flap position measurement during an aircraft flight test, and wing twist measurement of a wind tunnel model

Maurice Bazin, ONERA, France, described developments at ONERA in AoA and model deformation measurement techniques. Precision accelerometers are used for AoA as well as the MAMS system due to Bertin (AGARD VKI-1996) which is somewhat similar to the Boeing Laser Angle of Attack (LAM) system. Potentiometers and encoders are used as well. Model deformation measurements have been made with stereo observation with the RADAC (ONERA T.P. n° 1990-57) and ROHR (ONERA Activities 1996). The RADAC system uses special cameras that contain crossed linear arrays. The ROHR system employs two conventional cameras. The uses of optical fibers and quadrant light detectors and a polarization torsionometer for model attitude and deformation measurements are described in ONERA T.P. n° 1982-91.

Peter Bauman, DLR, Germany, discussed the use of moiré interferometry for the measurement of model deformation and hinge moments. DLR selected moiré interferometry as the technique with greatest potential over others such as coded light, holographic interferometry, and speckle interferometry. The technique currently requires diffusely reflecting surfaces that may necessitate the painting of highly polished models. Bending and twist measurements have been made in wind tunnels. Expected accuracies are 0.01° for flap angles, 0.03° for twist, and 0.1 mm for bending. Future applications in the automotive industry and for laboratory measurements on helicopter rotor blades are anticipated.

Peiter H. Fuykschot, NLR, the Netherlands, described a correction technique given in a paper presented at an Instrument Society of America conference in May 1996. The technique reduces bias errors in model AoA measurements due to centrifugal forces developed during high tunnel dynamic test conditions. He showed that this inertial error, termed a "sting whip" error, is corrected by measuring the model's linear and angular velocities and multiplying them together. The technique, which requires multiple sensors for correction in both pitch and yaw planes, provides a real-time correction without knowledge of the vibrational modes of the model. He instrumented a model and demonstrated the ability of the technique at two single frequency modes and one multi-frequency mode.

J. R. Hooker, McDonnel-Douglas, USA, discussed the use of experimental measurements to calibrate computational methods used to predict wind tunnel model aeroelastic deformations. A wind-off static loading experiment conducted in the National Transonic Facility (NTF) test section was used to calibrate both the optical technique and the finite element analysis (FEA) technique. Optical wing twist data from the NTF were presented, which were used to calibrate the FEA results with wind on. It was found that one-dimensional FEA analyses are sufficient to generate wind tunnel model jig wing definition, but that advanced three-dimensional solid FEA analyses may be required to generate wing definition suitable for computational fluid dynamic (CFD) analyses. Hooker recommended utilization of CFD methods to define the required accuracy of model deformation measurements for a given configuration and noted that the required accuracy may vary from configuration to configuration. Generally a 5% variation in wing twist is expected to result in acceptable accuracy for low wing transport configurations.

YuFu Liu, CARDC, China, described real-time attitude measurement and side-slip angle measurement systems used in the CARDC 4 by 3 meter low-speed wind tunnel. The pitch measurement system employs a QFlex accelerometer with an added temperature sensor which corrects the accelerometer output as a function of temperature. This system, used over a range from –30 degrees to 110 degrees by offsetting the accelerometer, a provides a measurement precision of 0.005 degrees. The side-slip system employs a laser and dual CCD linear scanning camera to measure yaw from –2.5 degrees to 2.5 degrees with a measurement precision of 0.005 degrees.

Sergi Fonov, TsAGI, Russia, presented examples of wing twist and bending measurements as functions of lift force and AoA at the T-128 wind tunnel using a CCD camera and reference targets with the single camera, single view videometric technique. He also presented results of flap torsion and displacement for which fluorescent strips were illuminated with a nitrogen laser. A prototype deformation measurement system was described for a full-scale helicopter rotor blade using a camera in the rotating hub with connection to the recording system by slip rings. Deformation measurements using projection moiré were also mentioned.

Gregory M. Buck, NASA LaRC, USA, presented results of tests conducted to study sting bending and model injection during wind-on and wind-off conditions at the 20-Inch Mach 6 CF_4 Tunnel. Angle and displacement measurements were made on a small section of the model that was in the field of view of a camera when the model is fully injected into the test section. A back illuminated ground glass view screen was placed in the field of view of the camera to yield a very high contrast edge from which the slope angle and intercept can be found by least squares estimation.

Anton R. Gorbushin, TsAGI, Russia, briefly discussed angle measurements using accelerometers that are manufactured in Russia. He also described a research and development project based on the development of a magnetic system to measure angular and linear model displacements and model deformations during wind tunnel tests. The purpose is to develop a prototype system for the simultaneous measurements of full angular orientation, coordinates, and deformations of a model, including wings, control surfaces, etc., during wind tunnel testing. High-sensitivity three-axis magnetometers on one-domain film structures will serve as transducers for navigation and orientation in an artificial low-frequency electromagnetic field.

Ralph D. Buehrle, NASA LaRC, USA, summarized several sting whip correction techniques proposed over the last few years. Time-domain and frequency-domain methods were not successful in extracting the small signals necessary to determine error. A modal correction technique was tested with limited success. This method requires measurement of all model vibration modes in pitch and yaw prior to wind tunnel testing. The model must be excited in both vertical and lateral directions; modal analysis of the acquired vibration data provides corrective information. During tests corrections at each mode are summed to provide a total correction. This technique requires considerable pre-test and post-test computation. The linear-angular technique of Pieter H.

Fuykschot described above has the ability to provide real time corrections without modal analysis.

9.4 Panel Discussion

Frank L. Wright, Boeing, USA, served as panel moderator. He opened the discussion with comments on the need to properly define AoA measurement accuracy requirements. Force measurement using internal strain gauge balances requires accurate AoA measurement to properly resolve normal and axial force to obtain lift and drag forces. However, Wright stressed that AoA measurement accuracy requirements vary depending on the test configuration. For instance AoA accuracy requirements are better defined at cruise conditions and are more stringent for climb-out than for approach conditions. The AoA accuracy requirements at maximum lift are also not well defined. Although ±0.01° AoA accuracy may not be required for every test, better than ±0.1° accuracy is probably always necessary. A comment from the audience noted that the wind tunnel user often requests "the best accuracy you can give me". Wright also stressed that repeatability is of the greatest importance during increment testing at a fixed AoA_n. The point was made that the confidence level is often not specified when stating a numerical accuracy requirement.

The topic turned to aeroelastic model deformation. Measurement of aerodynamic twist is needed for comparison with CFD results. As model size increases, wall interference effects become more significant while deformations may increase as well. Both effects must be accounted for. It was asked when ±0.05° experimental wing twist measurement accuracy would be available in wind tunnels. It was pointed out that such measurement accuracies are now possible at the LaRC Unitary Plan Wind Tunnel and are also possible at the NTF wind tunnel at somewhat reduced accuracy. The required accuracy for measurement of the change in wing twist induced by aerodynamic loading is still an open question.

Uncertainty issues in general were then discussed. The uncertainty of CFD results is needed along with the uncertainty of experimental results. The CFD community is just starting to assess uncertainty.

The discussion then returned to AoA where it was stated that AoA should be separated from angle of incidence. To obtain drag, the AoA is needed, not angle of incidence. This led to the question of how well flow angularity can be measured. It was recommended that uncertainty analyses be conducted on the computation of flow angularity from upright and inverted tests. A question was then asked about the Optotrak system in use at Boeing and several other aeronautical establishments. Wright stated that the number of and position of optical markers required for wind tunnel testing with the Optotrak system had not been optimized.

The effect of high-pressure tunnel operation on testing was raised. Wright stated that drag data taken at 4 atm in the NTF wind tunnel was as accurate as data taken at 1 atm in the Boeing wind tunnel; in addition, the 4 atm drag data was as useful for predicting flight behavior as the 1 atm data.

The fragility of precision quartz flexure accelerometers was discussed. Tom D. Finley stated that the typical lifetime of quartz accelerometers is five years. Most problems with accelerometers are due to mishandling rather than excessive model vibration during tests. It was also stated that the quartz flexure is not subject to loss of response as with metal flexures. It was recommended from the audience that accelerometers be powered during transit for protection. Finley pointed out that such protection would occur only in the axial direction. Several people commented that accelerometer manufacturer's specifications are reliable and that they therefore perform no additional calibration. Frank L. Wright stated that accelerometer output data corrected for temperature using manufacturer-furnished data agrees well with temperature-controlled accelerometer output data, as commonly used at the NTF. Pieter H. Fuyschot recommended the use of precision wedges to spot-check angle measurement accuracies. The importance of the use of the local value of the gravitational constant was mentioned.

The discussion turned to the problem of setting the model to zero angle in the facility. Leveling fixtures and tooling balls combined with a bubble level may possibly be used to level horizontal models; however, fundamental leveling problems exist with floor-mounted half models. The importance of the reference surface on which the accelerometer is mounted was also mentioned.

An AGARD uncertainty document published in 1982 was mentioned as an excellent reference. However, Wright cautioned that the individual uncertainty values cited in that reference, which are associated with one drag-count uncertainty, account for the entire one drag-count error. If all of the component uncertainties are combined, approximately 2.8 drag-count uncertainty results as opposed to one drag count. A member of the audience suspected that load resistor variation caused accelerometer output drift. Finley noted that LaRC employs precision load resistors located in the AoA signal conditioning electronics package rather than resistors installed in the accelerometer package. With this arrangement no significant output drift has been observed.

The panel discussion ended with a brief discussion on the problem of measuring yaw. There appears no clear solution. However, the Optotrak system offers promise in solving the yaw measurement problem.

APPENDIX: STRAIN GAUGE BALANCE PAPER TITLES AND AUTHORS

Session 1 CALIBRATION & DATA REDUCTION		
Authors	**Title**	**Organization**
V. Crivoruchenko & I. Panchenko	Calibration of Multi-Component Aerohydrodynamic Balances with Application of Optimal Planning Tests Methods	TsAGI, Russia
M. Quade & K. Hufnagel	The Development of a Modern Manual Calibration and Measuring System for Internal Balances	Technical University of Darmstadt, Germany
I. N. Panchenko	Transformation of Aerodynamic Balances Formulas to the Resolved Respecting To Loading Form	TsAGI, Russia
R. S. Crooks	Limitations of Internal Balance Calibration Math Models for Simulating Multicomponent Interactions	Micro Craft Technology, San Diego, USA
Session 2 FACILITY REPORTS		
E. Graewe, B. Ewald, & D. Eckert	Design and Development of Internal Balances for the German/Netherlands Low Speed Wind Tunnel (DNW)	Technical University of Darmstadt, Germany
D. X. He, & X. R. Gu	Recent Advances in Strain-gage Balances at CARDC	CARDC, China
D. Cahill	AIAA/GTTC Internal Balance Technology Working Group	Sverdrup/AEDC,USA
H. B. Vos	Strain Gauge Balance Development at NLR	NLR, the Netherlands
P. W. Roberts	NASA LaRC Force and Strain Measurement Capabilities	NASA LaRC, USA
Session 3 SPECIAL BALANCES I		
B. Ewald, K. Hufnagel, G. Viehweger, & R. Rebstock	The Half Model Balance for the Cologne Cryogenic Low Speed Tunnel (KKK)	Technical University of Darmstadt, Germany
K., Fristedt	Internal Bending Beam Strain-Gauge Wind-Tunnel Balances	AKTIEBOLAGET ROLLAB, Sweden
K. K. Guo	Hinge Moment Balance for Complete Models	Beijing Institute of Aerodynamics, China
A. Kuzin, G. Shapovalov, & N. Prohorov,	Strain-Gage Balance for Magnetic Suspension and Balance System	Moscow Aviation Technological Institute, Russia
Session 4 ACCURACY AND UNCERTAINTY ANALYSIS		
A. J. Day, & N. Corby	Developments to Improve the Accuracy of Half-Model Balance Measurements in the AEA 9ft x 8ft Transonic Wind Tunnel	Aircraft Research Association, Ltd., UK
P. H. Fuykschot	Looking for the Last Drag Count: Model Vibrations Vs Drag Accuracy	NLR, the Netherlands
M. E. Kammeyer	Uncertainty Analysis for Force Testing in Production Wind Tunnels	Naval Surface Weapons Center, USA
F. L. Wright	Experiences Relative to the Interaction Between the Balance Engineer and the Project Engineer with Regard to Measurement Uncertainty	Boeing Commercial Airplane Group, USA
J. S. Tripp	Strain Gauge Balance Uncertainty Analysis at NASA Langley - A Technical Overview	NASA LaRC, USA
Session 5 AUTOMATIC CALIBRATION		
Ewald K., Hufnagel, L. Polansky, & L. Badet	Development and Construction of Fully Automatic Calibration Machines for Internal Balances	Technical University of Darmstadt, Germany
R. D. Law	The Application of an Automatic Precision Balance Calibration Machine to the Calibration of Wind Tunnel Strain-gauged Balances	DRA-Bedford, UK
Y. P. Zhang	Fully Automatic Calibration System of the Six Component Balance for High Speed Wind Tunnels	CARDC, China
P. Tcheng & J. S. Tripp	Statistical Analysis of the NASA LaRC Evaluation of the IAI Automatic Balance Calibration Machine	NASA LaRC, USA

Session 6 APPLICATIONS		
Authors	**Title**	**Organization**
D. Booth	Development of a Six Component Unitized Flexured Force Balance	Micro Craft Technology, USA
V. Lapygin	Typical Balance Test tasks for Aerodynamic Facilities of TSNIIMASH	TSNIIMASH, Russia
D. Levin & M. Ringel	Accurate Axial Force Measurement with Small Diameter Balances under High Normal Loads	Technion, Israel
A. R. Gorbushin	Some Peculiarities of Balance Tests in the Transonic TsAGI T-128 Wind Tunnel	TsAGI, Russia
T. C. Moore	Strain Gages in Service at NASA Langley - A Technical Review	NASA LaRC, USA
Session 7 SPECIAL BALANCES II		
L. X. Liao & Y. Tao	A Water-cooled Six-Component Internal Balance	Beijing Institute of Aerodynamics, China
G. S. Liu, Z. G. Lu, & X. Q. Qi	Single Load and Multicomponent Balance Calibration System (SL&MBCS) of Piezoelectric Balance in Shock Tunnel	CARDC, China
P. Parker	Free Oscillation Dynamic Stability Balance System	Modern Machine & Tool Company Inc., USA
Session 8 BALANCE DESIGN		
G. Drouin, B. Girard, & K. Mackay	A Stiff Monopiece Wind Tunnel Balance	Defence Research Establishment, Canada
G. I. Johnson	A New Master Balance for the MK15 Calibration Rig at FFA	FFA, Sweden
N. R. Patel	Development of A Five-Component Balance As an Integral Part of a Control Surface	Modern Machine & Tool Company Inc., USA
M. A. Ramaswamy	Design Features of Some Special Strain Gage Balance	India Institute of Science, India
R. D. Rhew	NASA LaRC Strain Gage Balance Design Concepts	NASA LaRC, USA
Session 9 INSTRUMENTATION, STRAIN GAUGES, & THERMAL EFFECTS		
B. Fagerstrom & P. Kemppainen	An Easy-to-use Calibration and Readout System for Small Internal Beam-Type Wind Tunnel Balances	Helsinki University of Technology, Finland
X. R. Gu & J. Q. Hu	Development of BFH-series Strain Gages	CARDC, China
A. T. Ferris	Strain Gauge Balance Calibration and Data Reduction at NASA Langley Research Center	NASA LaRC, USA
W. Liu	Temperature Effect Research on Strain-gage Balances in a Conventional Wind Tunnel	CARDC, China
M. Bazin	ONERA Balances and Dynamometers	ONERA, France
Session 10 FINITE ELEMENT ANALYSIS & NEW TECHNOLOGY		
M. Lindell	Finite Element Analysis of a NASA National Transonic Facility Wind Tunnel Balance	NASA LaRC, USA
J. Zhai & K. Hufnagel	Optimization of the Internal Strain Balances with Finite Elements Computation	Technical University of Darmstadt, Germany
V. Lagutin	New Design of Tubular Type Strain-gage Balances	TSNIIMASH, Russia
B. Ewald, K. Hufnagel, & E. Graewe	The Development of Advanced Internal Balances for Cryogenic and Conventional Tunnels	Technical University of Darmstadt, Germany
V. Bogadanov & V. S. Volobuev	The Status and Prospects for the Further Development of Load Measuring Devices for Wind Tunnel Tests	TsAGI, Russia
Session 11 SPECIAL BALANCES III		
G. Rajendra, H. S. Murthy, & G. V. Kumar	A New Balance Calibration Methodology for Long Slendered Bodies in a Blowdown Tunnel	National Aerospace Laboratories, India
C. J. Suarez, & G. N. Malcolm	Development of a 5-component Strain Gage Balance for Water Tunnel Application	Edidetics Corporation, USA
Z. G. Tang	Development of Microbalance in Low Density Wind Tunnel	CARDC, China
B. Vasudevan & M. A. Ramaswamy	Novel Oil Filled Bellow Type Internal Strain Gauge Balance for Water Tunnel Applications	India Institute of Science, India

Group Photograph

REPORT DOCUMENTATION PAGE

Form Approved
OMB No. 07704-0188

1. AGENCY USE ONLY *(Leave blank)*	2. REPORT DATE	3. REPORT TYPE AND DATES COVERED
	March 1999	Conference Publication

4. TITLE AND SUBTITLE
First International Symposium on Strain Gauge Balances

5. FUNDING NUMBERS
992-35-12-18

6. AUTHOR(S)
John S. Tripp and Ping Tcheng, Editors

7. PERFORMING ORGANIZATION NAME(S) AND ADDRESS(ES)
NASA Langley Research Center
Hampton, VA 23681-2199

8. PERFORMING ORGANIZATION REPORT NUMBER
L-17809B

9. SPONSORING/MONITORING AGENCY NAME(S) AND ADDRESS(ES)
National Aeronautics and Space Administration
Washington, DC 20546-0001

10. SPONSORING/MONITORING AGENCY REPORT NUMBER
NASA/CP-1999-209101/PT 2

11. SUPPLEMENTARY NOTES

12a. DISTRIBUTION/AVAILABILITY STATEMENT
Unclassified–Unlimited
Subject Category 35 Distribution: Standard
Availability: NASA CASI (301) 621-0390

12b. DISTRIBUTION CODE

13. ABSTRACT ***(Maximum 200 words)***

The first International Symposium on Strain Gauge Balances was sponsored and held at NASA Langley Research Center during October 22-25, 1996. The symposium provided an open international forum for presentation, discussion, and exchange of technical information among wind tunnel test technique specialists and strain gauge balance designers. The Symposium also served to initiate organized professional activities among the participating and relevant international technical communities. Over 130 delegates from 15 countries were in attendance. The program opened with a panel discussion, followed by technical paper sessions, and guided tours of the National Transonic Facility (NTF) wind tunnel, a local commercial balance fabrication facility, and the LaRC balance calibration laboratory. The opening panel discussion addressed "Future Trends in Balance Development and Applications." Forty-six technical papers were presented in 11 technical sessions covering the following areas: calibration, automatic calibration, data reduction, facility reports, design, accuracy and uncertainty analysis, strain gauges, instrumentation, balance design, thermal effects, finite element analysis, applications, and special balances. At the conclusion of the Symposium, a steering committee representing most of the nations and several U.S. organizations attending the Symposium was established to initiate planning for a second international balance symposium, to be held in 1999 in the UK.

14. SUBJECT TERMS
Proceedings; Symposium; Strain gauge balance; Wind tunnel instrumentation; Aerodynamic testing

15. NUMBER OF PAGES
322

16. PRICE CODE
A14

17. SECURITY CLASSIFICATION OF REPORT	18. SECURITY CLASSIFICATION OF THIS PAGE	19. SECURITY CLASSIFICATION OF ABSTRACT	20. LIMITATION OF ABSTRACT
Unclassified	Unclassified	Unclassified	UL

NSN 7540-01-280-5500

Standard Form 298 (Rev. 2-89)
Prescribed by ANSI Std. Z39-18
298-102